

# UPDATE ON VASCULAR CONTRIBUTIONS TO AGE-RELATED NEURODEGENERATIVE DISEASES AND COGNITIVE IMPAIRMENT - RESEARCH OF ISNVD 2020 MEETING

EDITED BY: Yulin Ge, Mark Haacke, Meiyun Wang, Robert Zivadinov and  
Andreas Charidimou  
PUBLISHED IN: Frontiers in Neurology





# frontiers

## Frontiers eBook Copyright Statement

The copyright in the text of individual articles in this eBook is the property of their respective authors or their respective institutions or funders. The copyright in graphics and images within each article may be subject to copyright of other parties. In both cases this is subject to a license granted to Frontiers.

The compilation of articles constituting this eBook is the property of Frontiers.

Each article within this eBook, and the eBook itself, are published under the most recent version of the Creative Commons CC-BY licence.

The version current at the date of publication of this eBook is CC-BY 4.0. If the CC-BY licence is updated, the licence granted by Frontiers is automatically updated to the new version.

When exercising any right under the CC-BY licence, Frontiers must be attributed as the original publisher of the article or eBook, as applicable.

Authors have the responsibility of ensuring that any graphics or other materials which are the property of others may be included in the CC-BY licence, but this should be checked before relying on the CC-BY licence to reproduce those materials. Any copyright notices relating to those materials must be complied with.

Copyright and source acknowledgement notices may not be removed and must be displayed in any copy, derivative work or partial copy which includes the elements in question.

All copyright, and all rights therein, are protected by national and international copyright laws. The above represents a summary only. For further information please read Frontiers' Conditions for Website Use and Copyright Statement, and the applicable CC-BY licence.

ISSN 1664-8714

ISBN 978-2-88971-764-4

DOI 10.3389/978-2-88971-764-4

## About Frontiers

Frontiers is more than just an open-access publisher of scholarly articles: it is a pioneering approach to the world of academia, radically improving the way scholarly research is managed. The grand vision of Frontiers is a world where all people have an equal opportunity to seek, share and generate knowledge. Frontiers provides immediate and permanent online open access to all its publications, but this alone is not enough to realize our grand goals.

## Frontiers Journal Series

The Frontiers Journal Series is a multi-tier and interdisciplinary set of open-access, online journals, promising a paradigm shift from the current review, selection and dissemination processes in academic publishing. All Frontiers journals are driven by researchers for researchers; therefore, they constitute a service to the scholarly community. At the same time, the Frontiers Journal Series operates on a revolutionary invention, the tiered publishing system, initially addressing specific communities of scholars, and gradually climbing up to broader public understanding, thus serving the interests of the lay society, too.

## Dedication to Quality

Each Frontiers article is a landmark of the highest quality, thanks to genuinely collaborative interactions between authors and review editors, who include some of the world's best academicians. Research must be certified by peers before entering a stream of knowledge that may eventually reach the public - and shape society; therefore, Frontiers only applies the most rigorous and unbiased reviews.

Frontiers revolutionizes research publishing by freely delivering the most outstanding research, evaluated with no bias from both the academic and social point of view. By applying the most advanced information technologies, Frontiers is catapulting scholarly publishing into a new generation.

## What are Frontiers Research Topics?

Frontiers Research Topics are very popular trademarks of the Frontiers Journals Series: they are collections of at least ten articles, all centered on a particular subject. With their unique mix of varied contributions from Original Research to Review Articles, Frontiers Research Topics unify the most influential researchers, the latest key findings and historical advances in a hot research area! Find out more on how to host your own Frontiers Research Topic or contribute to one as an author by contacting the Frontiers Editorial Office: [frontiersin.org/about/contact](https://frontiersin.org/about/contact)

# UPDATE ON VASCULAR CONTRIBUTIONS TO AGE-RELATED NEURODEGENERATIVE DISEASES AND COGNITIVE IMPAIRMENT - RESEARCH OF ISNVD 2020 MEETING

Topic Editors:

**Yulin Ge**, New York University, United States

**Mark Haacke**, Wayne State University, United States

**Meiyun Wang**, Henan Provincial People's Hospital, China

**Robert Zivadinov**, University at Buffalo, United States

**Andreas Charidimou**, Harvard Medical School, United States

**Citation:** Ge, Y., Haacke, M., Wang, M., Zivadinov, R., Charidimou, A., eds. (2021). Update on Vascular Contributions to Age-Related Neurodegenerative Diseases and Cognitive Impairment - Research of ISNVD 2020 Meeting. Lausanne: Frontiers Media SA. doi: 10.3389/978-2-88971-764-4

# Table of Contents

- 05 Editorial: Update on Vascular Contributions to Age-Related Neurodegenerative Diseases and Cognitive Impairment - Research of ISNVD 2020 Meeting**  
Yulin Ge, Robert Zivadinov, Meiyun Wang, Andreas Charidimou and E. Mark Haacke
- 08 Age-Related Alterations in Brain Perfusion, Venous Oxygenation, and Oxygen Metabolic Rate of Mice: A 17-Month Longitudinal MRI Study**  
Zhiliang Wei, Lin Chen, Xirui Hou, Peter C. M. van Zijl, Jiadi Xu and Hanzhang Lu
- 17 Parietal Perfusion Alterations in Parkinson's Disease Patients Without Dementia**  
Laura Pelizzari, Sonia Di Tella, Federica Rossetto, Maria Marcella Laganà, Niels Bergsland, Alice Pirastru, Mario Meloni, Raffaello Nemni and Francesca Baglio
- 26 Cortical and Deep Gray Matter Perfusion Associations With Physical and Cognitive Performance in Multiple Sclerosis Patients**  
Dejan Jakimovski, Niels Bergsland, Michael G. Dwyer, John Traversone, Jesper Hagemeyer, Tom A. Fuchs, Deepa P. Ramasamy, Bianca Weinstock-Guttman, Ralph H. B. Benedict and Robert Zivadinov
- 35 Quantitative Cerebrovascular Reactivity in Normal Aging: Comparison Between Phase-Contrast and Arterial Spin Labeling MRI**  
Kamil Taneja, Peiying Liu, Cuimei Xu, Monroe Turner, Yuguang Zhao, Dema Abdelkarim, Binu P. Thomas, Bart Rypma and Hanzhang Lu
- 44 Multimodal Evaluation of Neurovascular Functionality in Early Parkinson's Disease**  
Maria Marcella Laganà, Alice Pirastru, Laura Pelizzari, Federica Rossetto, Sonia Di Tella, Niels Bergsland, Raffaello Nemni, Mario Meloni and Francesca Baglio
- 53 Relationships Among Circulating Levels of Hemostasis Inhibitors, Chemokines, Adhesion Molecules, and MRI Characteristics in Multiple Sclerosis**  
Nicole Ziliotto, Robert Zivadinov, Dejan Jakimovski, Marcello Baroni, Niels Bergsland, Deepa P. Ramasamy, Bianca Weinstock-Guttman, Murali Ramanathan, Giovanna Marchetti and Francesco Bernardi
- 62 Association Between Motor and Cognitive Performances in Elderly With Atrial Fibrillation: Strat-AF Study**  
Emilia Salvadori, Francesco Galmozzi, Francesca Uda, Carmen Barbato, Eleonora Camilleri, Francesca Cesari, Stefano Chiti, Stefano Diciotti, Samira Donnini, Benedetta Formelli, Silvia Galora, Betti Giusti, Anna Maria Gori, Chiara Marzi, Anna Melone, Damiano Mistri, Francesca Pescini, Giovanni Pracucci, Valentina Rinnoci, Cristina Sarti, Enrico Fainardi, Rossella Marcucci and Anna Poggesi
- 71 Early Post-stroke Cognition: In-hospital Predictors and the Association With Functional Outcome**  
Richa Sharma, Dania Mallick, Rafael H. Llinas and Elisabeth B. Marsh



- 80 Cerebral Vessels: An Overview of Anatomy, Physiology, and Role in the Drainage of Fluids and Solutes**  
Nivedita Agarwal and Roxana Octavia Carare
- 88 Comparison of Longitudinal Changes of Cerebral Small Vessel Disease Markers and Cognitive Function Between Subcortical Vascular Mild Cognitive Impairment With and Without NOTCH3 Variant: A 5-Year Follow-Up Study**  
Cindy W. Yoon, Young-Eun Kim, Hee Jin Kim, Chang-Seok Ki, Hyejoo Lee, Joung-Ho Rha, Duk L. Na and Sang Won Seo
- 95 Screening for Cognitive Impairment After Stroke: Validation of the Chinese Version of the Quick Mild Cognitive Impairment Screen**  
Yangfan Xu, Lingrong Yi, Yangyang Lin, Suiying Peng, Weiming Wang, Wujian Lin, Peize Chen, Weichao Zhang, Yujie Deng, Suimin Guo, Le Shi, Yuling Wang, D. William Molloy and Rónán O’Caoimh
- 105 An Overview of Venous Abnormalities Related to the Development of Lesions in Multiple Sclerosis**  
E. Mark Haacke, Yulin Ge, Sean K. Sethi, Sagar Buch and Paolo Zamboni
- 122 Severity of Lesions Involving the Cortical Cholinergic Pathways May Be Associated With Cognitive Impairment in Subacute Ischemic Stroke**  
Huo-Hua Zhong, Jian-feng Qu, Wei-Min Xiao, Yang-kun Chen, Yong-lin Liu, Zhi-qiang Wu, Dong-hai Qiu and Wen-cong Liang
- 133 All Central Nervous System Neuro- and Vascular-Communication Channels Are Surrounded With Cerebrospinal Fluid**  
Lara M. Fahmy, Yongsheng Chen, Stephanie Xuan, E. Mark Haacke, Jiani Hu and Quan Jiang
- 144 Spatial Navigation Is Impaired in Elderly Patients With Cerebral Small Vessel Disease**  
Hóngyi Zhào, Liyi Chi, Yanhai Zhang, Yonghua Huang and Hongyan Tian



# Editorial: Update on Vascular Contributions to Age-Related Neurodegenerative Diseases and Cognitive Impairment - Research of ISNVD 2020 Meeting

Yulin Ge<sup>1\*</sup>, Robert Zivadinov<sup>2</sup>, Meiyun Wang<sup>3</sup>, Andreas Charidimou<sup>4</sup> and E. Mark Haacke<sup>5</sup>

<sup>1</sup> Department of Radiology, New York University (NYU) Grossman School of Medicine, New York, NY, United States,

<sup>2</sup> Department of Neurology, Jacobs School of Medicine and Biomedical Sciences, Buffalo, NY, United States, <sup>3</sup> Department of Radiology, Henan Provincial People's Hospital, Zhengzhou, China, <sup>4</sup> Department of Neurology, Boston University Medical Center, Boston University School of Medicine, Boston, MA, United States, <sup>5</sup> Department of Radiology, Wayne State University School of Medicine, Detroit, MI, United States

**Keywords:** MRI, cerebral blood flow, stroke, dementia, neurodegeneration, multiple sclerosis, Parkinson's disease

## OPEN ACCESS

### Edited and reviewed by:

Jean-Claude Baron,  
University of Cambridge,  
United Kingdom

### \*Correspondence:

Yulin Ge  
yulin.ge@nyulangone.org

### Specialty section:

This article was submitted to  
Stroke,  
a section of the journal  
Frontiers in Neurology

**Received:** 18 October 2021

**Accepted:** 22 October 2021

**Published:** 11 November 2021

### Citation:

Ge Y, Zivadinov R, Wang M,  
Charidimou A and Haacke EM (2021)  
Editorial: Update on Vascular  
Contributions to Age-Related  
Neurodegenerative Diseases and  
Cognitive Impairment - Research of  
ISNVD 2020 Meeting.  
Front. Neurol. 12:797486.  
doi: 10.3389/fneur.2021.797486

## Editorial on the Research Topic

### Update on Vascular Contributions to Age-Related Neurodegenerative Diseases and Cognitive Impairment - Research of ISNVD 2020 Meeting

Vascular pathologies are among the most common contributors to neurodegenerative changes along the spectrum of normal aging to dementia. Cerebral small vessel disease (SVD) in particular represents a diverse range of neuropathological conditions that affect capillaries, small arteries, arterioles and small veins in the brain and have a prominent role as vascular contributions to cognitive impairment and dementia (VCID) (1, 2), even in patients considered to have Alzheimer's disease. These cerebrovascular abnormalities are associated with imaging based biomarkers, including white matter hyperintensities, lacunes, cerebral microbleeds, enlarged perivascular spaces, cerebral microinfarcts, and cortical atrophy. As such, SVD currently causes 20% of ischemic strokes, are the underlying cause of spontaneous intracerebral hemorrhage and constitutes a main source of cognitive decline or VCID, particularly in the elderly (3). It has been reported that with one in three people having clinical ischemia or stroke during their lifetime, dementia occurs in an estimated 30% of post-stroke patients; the effects on public health impact is enormous. However, apart from risk containment, efforts to prevent or to treat SVD are ineffective; much remains to be learned about the underpinnings of vascular pathophysiology, regional vulnerability, and disease progression over time. Along this line, MRI plays an important role due to its potential of revealing *in vivo* pathophysiology, early detection and clinical correlations.

In this Research Topic, we aim to gather recent research to better understand vascular contributions to age-related neurodegenerative diseases and cognitive impairment. This special issue includes 2 reviews, 2 brief research reports, and 11 original research articles. The articles cover a number of neurodegenerative diseases including stroke, Alzheimer's disease (AD), Parkinson's

disease (PD), and multiple sclerosis (MS) and give insight into ongoing topics on both arterial (e.g., ischemia) and venous (e.g., inflammation) systems as well as the glymphatic system. We also aim to promote research exchange across different fields (e.g., imaging, vascular anatomy, brain physiology, clinical symptom monitoring and treatment). Most papers in this special issue applied MRI studies to better understand disease mechanisms, to help differential diagnosis, and to develop imaging biomarkers for evaluating disease progression. New technical developments of advanced neurovascular imaging in age-related cognitive impairment are also included.

Currently, there is still a significant knowledge gap of how the vascular pathophysiological underpinnings initiate the long-term neurodegeneration processes in age-related cognitive impairment. There are seven papers on this topic from researchers with diverse expertise. Post-stroke cognitive impairment (PSCI) occurs in over 80% of acute stroke survivors and represents one of the major causes of vascular dementia, however, its underlying mechanism is unknown. Zhong et al. reported that in patients with early subacute ischemic stroke, the lesion volume in the cortical cholinergic pathways (CCP) was associated with cognitive impairment. The disruption of the cholinergic pathways might contribute to newly developed dementia in patients with PSCI. Sharma et al. (4) further demonstrated that the PSCI changes can occur 4-8 weeks post-infarct, and patients with high-risk of early PSCI development should be identified for targeted rehabilitation and counseling to improve longer-term outcomes. Savadori et al. (5) assessed a cohort of elderly who had atrial fibrillation (AF), a condition associated with reduced physical performance and increased risk of cognitive decline, suggesting a possible link between motor and cognitive performance. Cerebral SVD is commonly seen in the elderly. One study by Zhao et al. investigated whether spatial navigation performance is impaired in elderly SVD patients. Compared to healthy controls, only severe SVD or patients with higher Fazekas scores exhibited significantly worse performance on simulated navigation tasks, suggesting spatial navigation decline may be one of manifestation in severe SVD. To study the genetic role in subcortical vascular cognitive impairment (svMCI), Yoon et al. compared the longitudinal changes in SVD markers and cognitive function between svMCI patients with and without NOTCH3 variant, and they showed NOTCH3(+) svMCI group had much greater increases in the lacune and cerebral microbleed counts than the NOTCH3(-) svMCI group. Over 5 years follow up, however, no significant differences were found between the two groups regarding dementia conversion rate in these patients.

Regarding screening for cognitive impairment after stroke, Xu et al. (6) compared the diagnostic accuracy of a Chinese version of the Quick Mild Cognitive Impairment (Qmci-CN) with a widely-used Chinese version of Montreal Cognitive Assessment (MoCA-CN) and Mini-Mental State Examination (MMSE-CN). They showed that the Qmci-CN is accurate in identifying post-stroke dementia and separating PSD from no-dementia PSCI. This test was comparable to MoCA-CN but with a significantly shorter administration time. However, the Qmci-CN is relatively poor in differentiating no-dementia PSCI patients from controls.

One animal study by Wei et al. investigated the age effects on cerebrovascular and physiological parameters by characterizing the longitudinal time courses across the adult lifespan in mice. The results revealed an age-related increase in oxygen consumption without decrease of cerebral perfusion (unlike human studies), which is consistent with the absence of white matter hyperintensities (WMHs) in aged mice. A more relevant implication from this study is that using animal models to study human aging process has limitations.

Recently there is substantial interest regarding the role of the glymphatic system in AD. Agarwal and Carare (7) provided a novel overview of the role of cerebral vessels and their connection with cerebrospinal fluid (CSF) and interstitial fluid (ISF) in brain waste clearance. Emerging evidence shows damage to macro/microvasculature or their dysfunction will compromise the fluid movement and alter the homeostasis of the brain, which in turn leads to neuronal cell loss and dementia. Since the central nervous system (CNS) is completely submerged in CSF, it is critical to map out its clearance pathway from peri-neural and peri-vascular space to bulk flow in subarachnoid space. Using several fluid-sensitive MRI techniques, Fahmy et al. (8) successfully demonstrated the presence of CSF within all peri-neural (cranial and spinal nerves) and peri-vascular spaces *in vivo* human brain and spinal cord. These findings suggest that anatomically, substance exchange neural tissue and outside glymphatic space can only occur through CSF and vascular pathways although further investigations are warranted to study their specific role in waste clearance and immunity.

Two papers focused on brain perfusion changes in Parkinson's disease. Laganà et al. applied a multimodal MRI approach to investigate early PD with resting state functional MRI (rsfMRI) and arterial spin labeling (ASL). They found reduced functional connectivity (FC) in patients within a sensory-motor network and visual networks accompanied by a decreased CBF compared to controls. Another study by Pelizzari et al. investigated CBF within the regions associated with fronto-parietal network in PD patients without dementia. They found significantly lower CBF in the left superior and inferior parietal lobes in patients who also performed poorer on MoCA tests. The decreased perfusion in parietal regions may be associated with lower visuomotor skills and has potential for longitudinal studies investigating cognitive decline in PD.

Haacke et al. reviewed over 200 papers and provided an in-depth discussion of the evidence for vascular pathogenesis in MS lesions. They put together multiple key pieces of information from the literature regarding vascular remodeling, venous collagenosis, abnormal venous flow, perfusion, endothelial dysfunction and vascular endothelial growth factors. After combining their own findings using ultra-small superparamagnetic iron oxide or USPIO-enhanced MRI, they raised one possible theory on MS lesion etiology that is associated with locally disrupted blood flow, which in turn leads to remodeling of the medullary veins followed by endothelial damage with the subsequent cascade of inflammatory and demyelinating events. Two other papers reported cerebrovascular abnormalities in MS. Jakimovski et al. (9) investigated the associations between cerebral

perfusion and disease outcomes in MS patients with and without comorbid cardiovascular diseases (CVD). They found decreased brain perfusion in both cortical and deep GM is associated with poorer MS outcomes, but not with the presence of CVD. By combining plasma and MRI biomarkers of MS, Ziliotto et al. (10) investigated the link between microvascular abnormalities and immune inflammatory changes and their role in neurodegeneration. They showed that higher protein C (PC) levels were associated with large brain volume loss in relapsing remitting but not in progressive MS. Higher chemokine C-C motif ligand 18 (CCL18) levels were associated with higher T2-lesion volumes in all MS patients, and higher CCL18 levels were associated with lower volumes of the GM in progressive MS. These results will help us to better understand the disease heterogenous nature of MS.

Regarding the novel cerebrovascular imaging techniques for aging and dementia studies, Taneja et al. (11) compared two quantitative CBF techniques, phase-contrast (PC)- and ASL-based hypercapnia MRI that were used to assess cerebrovascular reactivity (CVR). CVR is a relatively new marker for assessing

vasomotor function and has shown great promise in predicting age-related neurodegeneration. The results suggest that PC-based CVR is a more sensitive method for aging effects despite being a global measure and lacking spatial information. This voxel-wise ASL-based method tends to underestimate CVR.

In summary, this is an exciting time in neurovascular and aging research. In this Research Topic, we hope to provide a comprehensive collection to cover the latest advances with a wide range of cross-disciplinary topics on neurovascular research in neurodegenerative diseases.

## AUTHOR CONTRIBUTIONS

YG took the lead in writing this editorial. All authors provided critical feedback and helped shape the manuscript.

## FUNDING

This work is supported by National Institute of Health grants (RF1 NS11041, R01 NS108491, and R13 AG067684). This study is also supported by Alzheimer's Association (AARG-17-533484).

## REFERENCES

- Corriveau RA, Bosetti F, Emr M, Gladman JT, Koenig JJ, Moy CS, et al. The Science of vascular contributions to cognitive impairment and dementia (VCID): a framework for advancing research priorities in the cerebrovascular biology of cognitive decline. *Cell Mol Neurobiol.* (2016) 36:281–8. doi: 10.1007/s10571-016-0334-7
- Zlokovic BV, Gottesman RF, Bernstein KE, Seshadri S, McKee A, Snyder H, et al. Vascular contributions to cognitive impairment and dementia (VCID): A report from the 2018 National Heart, Lung, and Blood Institute and National Institute of Neurological Disorders and Stroke Workshop. *Alzheimers Dement.* (2020) 16:1714–33. doi: 10.1002/alz.12157
- Caruso P, Signori R, Moretti R. Small vessel disease to subcortical dementia: a dynamic model, which interfaces aging, cholinergic dysregulation and the neurovascular unit. *Vasc Health Risk Manag.* (2019) 15:259–81. doi: 10.2147/VHRM.S190470
- Sharma R, Mallick D, Llinas RH, Marsh EB. Early post-stroke cognition: in-hospital predictors and the association with functional outcome. *Front Neurol.* (2020) 11:613607. doi: 10.3389/fneur.2020.613607
- Salvadori E, Galmozzi F, Uda F, Barbato C, Camilleri E, Cesari F, et al. Association between motor and cognitive performances in elderly with atrial fibrillation: strat-AF study. *Front Neurol.* (2020) 11:571978. doi: 10.3389/fneur.2020.571978
- Xu Y, Yi L, Lin Y, Peng S, Wang W, Lin W, et al. Screening for cognitive impairment after stroke: validation of the chinese version of the quick mild cognitive impairment screen. *Front Neurol.* (2021) 12:608188. doi: 10.3389/fneur.2021.608188
- Agarwal N, Carare RO. Cerebral vessels: an overview of anatomy, physiology, and role in the drainage of fluids and solutes. *Front Neurol.* (2020) 11:611485. doi: 10.3389/fneur.2020.611485
- Fahmy LM, Chen Y, Xuan S, Haacke EM, Hu J, Jiang Q. All central nervous system neuro- and vascular-communication channels are surrounded with cerebrospinal fluid. *Front Neurol.* (2021) 12:614636. doi: 10.3389/fneur.2021.614636
- Jakimovski D, Bergsland N, Dwyer MG, Traversone J, Hagemeyer J, Fuchs TA, et al. Cortical and deep gray matter perfusion associations with physical and cognitive performance in multiple sclerosis patients. *Front Neurol.* (2020) 11:700. doi: 10.3389/fneur.2020.00700
- Ziliotto N, Zivadinov R, Jakimovski D, Baroni M, Bergsland N, Ramasamy DP, et al. Relationships among circulating levels of hemostasis inhibitors, chemokines, adhesion molecules, and MRI characteristics in multiple sclerosis. *Front Neurol.* (2020) 11:553616. doi: 10.3389/fneur.2020.553616
- Taneja K, Liu P, Xu C, Turner M, Zhao Y, Abdelkarim D, et al. Quantitative cerebrovascular reactivity in normal aging: comparison between phase-contrast and arterial spin labeling MRI. *Front Neurol.* (2020) 11:758. doi: 10.3389/fneur.2020.00758

**Conflict of Interest:** The authors declare that the research was conducted in the absence of any commercial or financial relationships that could be construed as a potential conflict of interest.

**Publisher's Note:** All claims expressed in this article are solely those of the authors and do not necessarily represent those of their affiliated organizations, or those of the publisher, the editors and the reviewers. Any product that may be evaluated in this article, or claim that may be made by its manufacturer, is not guaranteed or endorsed by the publisher.

Copyright © 2021 Ge, Zivadinov, Wang, Charidimou and Haacke. This is an open-access article distributed under the terms of the Creative Commons Attribution License (CC BY). The use, distribution or reproduction in other forums is permitted, provided the original author(s) and the copyright owner(s) are credited and that the original publication in this journal is cited, in accordance with accepted academic practice. No use, distribution or reproduction is permitted which does not comply with these terms.



# Age-Related Alterations in Brain Perfusion, Venous Oxygenation, and Oxygen Metabolic Rate of Mice: A 17-Month Longitudinal MRI Study

Zhiliang Wei<sup>1,2\*</sup>, Lin Chen<sup>1,2</sup>, Xirui Hou<sup>3</sup>, Peter C. M. van Zijl<sup>1,2</sup>, Jiadi Xu<sup>1,2</sup> and Hanzhang Lu<sup>1,2,3</sup>

<sup>1</sup> Russell H. Morgan Department of Radiology and Radiological Science, Johns Hopkins University School of Medicine, Baltimore, MA, United States, <sup>2</sup> F. M. Kirby Research Center for Functional Brain Imaging, Kennedy Krieger Research Institute, Baltimore, MA, United States, <sup>3</sup> Department of Biomedical Engineering, Johns Hopkins University School of Medicine, Baltimore, MA, United States

## OPEN ACCESS

### Edited by:

Yulin Ge,  
New York University, United States

### Reviewed by:

Bo Gao,  
Affiliated Hospital of Guizhou Medical  
University, China  
Mark S. Bolding,  
University of Alabama at Birmingham,  
United States

### \*Correspondence:

Zhiliang Wei  
zhiliang.wei@jhu.edu

### Specialty section:

This article was submitted to  
Applied Neuroimaging,  
a section of the journal  
Frontiers in Neurology

**Received:** 15 March 2020

**Accepted:** 15 May 2020

**Published:** 12 June 2020

### Citation:

Wei Z, Chen L, Hou X, van Zijl PCM,  
Xu J and Lu H (2020) Age-Related  
Alterations in Brain Perfusion, Venous  
Oxygenation, and Oxygen Metabolic  
Rate of Mice: A 17-Month Longitudinal  
MRI Study. *Front. Neurol.* 11:559.  
doi: 10.3389/fneur.2020.00559

**Background:** Characterization of physiological parameters of the aging brain, such as perfusion and brain metabolism, is important for understanding brain function and diseases. Aging studies on human brain have mostly been based on the cross-sectional design, while the few longitudinal studies used relatively short follow-up time compared to the lifespan.

**Objectives:** To determine the longitudinal time courses of cerebral physiological parameters across the adult lifespan in mice.

**Methods:** The present work examined longitudinal changes in cerebral blood flow (CBF), cerebral venous oxygenation ( $Y_v$ ), and cerebral metabolic rate of oxygen (CMRO<sub>2</sub>) using MRI in healthy C57BL/6 mice from 3 to 20 months of age. Each mouse received 16 imaging sessions at an ~1-month interval.

**Results:** Significant increases with age were observed in CBF ( $p = 0.017$ ) and CMRO<sub>2</sub> ( $p < 0.001$ ). Meanwhile,  $Y_v$  revealed a significant decrease ( $p = 0.002$ ) with a non-linear pattern ( $p = 0.013$ ). The rate of change was 0.87, 2.26, and  $-0.24\%$  per month for CBF, CMRO<sub>2</sub>, and  $Y_v$ , respectively. On the other hand, systemic parameters such as heart rate did not show a significant age dependence ( $p = 0.47$ ). No white-matter-hyperintensities (WMH) were observed on the T<sub>2</sub>-weighted image at any age of the mice.

**Conclusion:** With age, the mouse brain revealed an increase in oxygen consumption. This observation is consistent with previous findings in humans using a cross-sectional design and suggests a degradation of the brain's energy production or utilization machinery. Cerebral perfusion remains relatively intact in aged mice, at least until 20 months of age, consistent with the absence of WMH in mice.

**Keywords:** aging, cerebral blood flow, cerebral metabolic rate of oxygen, longitudinal, C57BL/6



## INTRODUCTION

Characterization of neurobiological changes in the aging brain is important in understanding brain function, neurodegeneration, and possibly dementia (1–3). While brain anatomical and structural measures have been studied extensively and generally reveal degradations with age (4–8), functional and physiological changes are more complex and have yielded more intriguing observations (9–12). For example, many studies on human brain aging have shown that fMRI signals in response to tasks are paradoxically greater in old than in young participants (13–16). Furthermore, when measuring basal brain oxygen metabolic rate as a surrogate marker of neural activity at rest, several studies have suggested that the brain of an older individual consumes more oxygen (per unit volume tissue) compared to younger individuals (10, 17). These findings have led to several interesting hypotheses such as a compensatory increase in neural activity in older individuals (10, 18), a diminishment of specificity in brain activation (19), or a reduced computational efficiency in neural circuits (20).

However, a shared limitation of these reports lies in their cross-sectional experimental design without the tracking of same subjects over time. There are also concerns related to potential sampling bias, in that the older participants may represent a group of “supernormals” who can stay healthy and participate in research even at an advanced age. While a few other studies have been conducted in a longitudinal fashion, the follow-up duration was relatively short compared to the lifespan (21–23), which may hamper their ability to estimate changes over longer periods of time.

In preclinical studies, mouse has been a popular species due to its genetic pliability to develop mutant strains and availability for surgery to build disease models (24). In particular, its proximity of genome and physiology to human and short lifespan (1–3 years) make it an excellent candidate for aging investigations (25, 26). Therefore, a longitudinal study on age-related changes in brain physiological parameters of mice will shed new light on neurobiological alterations in aging.

Brain relies on aerobic metabolism to provide energy for neuronal activities (27), thus the oxygen consumption constitutes an interesting parameter to understand the neurobiology of the aging brain. In this study, we examined longitudinal changes in physiological parameters of oxygen supply (i.e., cerebral blood flow, CBF), venous oxygenation ( $Y_v$ ), and oxygen consumption (i.e., cerebral metabolic rate of oxygen, CMRO<sub>2</sub>). These physiological parameters were evaluated with quantitative MRI techniques in C57BL/6 mice from 3 to 20 months old at an approximately 1-month interval. To allow the mice to survive the large number of imaging sessions, no MRI contrast agents were used and all measures were based on non-contrast-agent MRI sequences. In addition to the physiological measures, T<sub>2</sub>-weighted images were also collected for the assessment of potential white-matter hyperintensities, which are thought to be associated with insufficient blood supply (28).

## MATERIALS AND METHODS

### General

The experimental protocols involved in this study were approved by the Johns Hopkins Medical Institution Animal Care and Use Committee, and conducted in accordance with the National Institutes of Health guidelines for the care and use of laboratory animals. Five C57BL/6 mice (female, Charles River Laboratories) were scanned longitudinally from 3 to 20 months old at an interval of 1 month. Two of the monthly scans were not completed due to the unavailability of scanner caused by technical problems. Thus, 16 time points (3–9, 11–14, and 16–20 months old) were collected.

One mouse was euthanized after the 16-month-old time point for ethical reasons due to the animal's suffering from a rectal prolapse. Behavioral test using a Y-maze was performed in the remaining mice at ~20 months of age (i.e., the last time point) to investigate the spatial memory as a representative for cognition status at this advanced age. A spontaneous-alternating-performance score in percent was obtained from the test (29).

### MRI

All MRI experiments were performed on an 11.7T Bruker Biospec system (Bruker, Ettlingen, Germany) equipped with a horizontal bore and actively shielded pulsed field gradients (maximum intensity of 0.74 T/m). Images were acquired using a 72-mm quadrature volume resonator as a transmitter and a four-element (2 × 2) phased-array coil as a receiver. The B<sub>0</sub> field over the mouse brain was homogenized by a global shimming (up to 2nd order) based on a pre-acquired subject-specific field map.

Respiration rate was monitored during the experiment to ensure the survival of the mouse. Anesthesia was administered under following regimen: 1.5% vaporized isoflurane was used for 15 min as the induction followed by a continuous 1.0% isoflurane for maintenance until the end of experiments; during the experiment, the maintenance dosage would be increased slightly to ~1.2% in case that a mouse breathed at a rate >150 breaths per minute. At the 10th minute under 1.5% isoflurane inhalation, the mouse was immobilized with a bite bar and ear pins, and placed onto a water-heated animal bed with temperature control before entering the magnet.

Each MRI session consisted of MRI measurements detailed below.

### Cerebral Venous Oxygenation ( $Y_v$ )

$Y_v$  was assessed non-invasively from the confluence of sagittal sinuses with a T<sub>2</sub>-relaxation-under-spin-tagging (TRUST) technique, which was originally developed on human scanners and recently optimized for animal MRI systems (30–32). In order to visualize the confluence of sagittal sinuses, an axial time-of-flight (TOF) sequence was first performed with the following parameters: TR/TE = 20/2.6 ms, field of view (FOV) = 16 × 16 mm, matrix size = 256 × 256, 35 axial slices, slice thickness = 0.5 mm, and scan duration = 2.2 min. The TRUST scan was then positioned based on the TOF images (31), and was repeated three times to improve precision. The TRUST sequence

used the following parameters: TR/TE = 3500/6.5 ms, FOV = 16 × 16 mm, matrix size = 128 × 128, slice thickness = 0.5 mm, EPI factor = 16, inversion-slab thickness = 2.5 mm, post-labeling delay = 1000 ms, eTE = 0.25, 20, 40 ms, echo spacing of eTE = 5.0 ms, and scan duration = 2.8 min.

Data processing of TRUST MRI was conducted with a custom-written graphic-user-interface (GUI) tool built on MATLAB (MathWorks, Natick, MA) and followed procedures detailed previously (30, 31). Briefly, for each TRUST dataset, subtraction between the control and labeled images was performed to obtain difference images (**Figure 1A**). A region of interest (ROI) was manually drawn on the difference image to encompass the sinus confluence. Four voxels within the ROI with the largest difference signals were selected for spatial averaging. Then, venous blood signal intensities at three different eTEs were fitted into a monoexponential function to obtain  $T_2$  (**Figure 1A**). Finally,  $T_2$  was converted into  $Y_v$  using a  $T_2$ - $Y_v$  calibration plot (**Figure 1A**) reported by Li et al. (33).

## Cerebral Blood Flow (CBF)

Global CBF was evaluated with phase-contrast (PC) MRI covering four major feeding arteries (**Figure 1B**), i.e., left internal carotid artery (LICA), right internal carotid artery (RICA), left vertebral artery (LVA), and right vertebral artery (RVA), in separate scans to collect corresponding through-plane velocity maps (**Figure 1B**) (34, 35). Prior to the PC scans, we first performed a coronal TOF angiogram (7 slices, slice thickness = 0.5 mm, no inter-slice gap, TR/TE = 45/2.6 ms, scan duration = 2 min) to visualize the feeding arteries. Then, a sagittal TOF (single slice, tilted to contain the target artery identified from coronal TOF images, thickness = 0.5 mm, TR/TE = 60/2.5 ms, scan duration = 0.4 min) was applied to visualize the in-plane trajectory of the target artery. PC MRI was then positioned using both TOFs and performed using following parameters: TR/TE = 60/3.2 ms, FOV = 15 × 15 mm, matrix size = 300 × 300, slice thickness = 0.5 mm, number of average = 4, dummy scan = 8, receiver bandwidth = 100 kHz, flip angle = 25°, partial Fourier acquisition factor = 0.7, and scan duration = 2.4 min.

Processing of PC dataset was performed with custom-written MATLAB scripts (MathWorks, Natick, MA). The artery of interest was first manually delineated on the complex-difference image (**Figure 1B**), which shows an excellent contrast between vessel and surrounding tissue. The mask was then applied to the phase velocity map and the integration of arterial voxels yields blood flow through that targeted artery in ml/min. Summation of blood-flow values across the four major feeding arteries yields total blood flow to the brain. To further account for the brain-size differences and to obtain unit-mass CBF values, the total blood flow was divided by the brain weight, which was calculated as the product of brain volume and density [1.04 g/ml (36)]. The global CBF value is written in the unit of milliliters per 100 g brain tissue per minute (ml/100 g/min). Inter-rater reproducibility of PC MRI processing has previously been assessed and reported an interrater correlation of >95% (34).

## Cerebral Metabolic Rate of Oxygen (CMRO<sub>2</sub>)

CMRO<sub>2</sub> was computed from  $Y_v$  and CBF using the Fick principle (37–39), i.e.,  $CMRO_2 = C_a \cdot (Y_a - Y_v) \cdot CBF$ , where  $C_a$  denotes the molar concentration of oxygen in a unit volume of blood and was assumed to be 882.1 μmol O<sub>2</sub>/100 ml blood based on previous literature (40, 41).  $Y_a$  represents arterial oxygen saturation fraction.  $Y_a$  is generally close to unity, and is assumed to be 0.99 in this study (42). CMRO<sub>2</sub> is written in the unit of μmol oxygen per 100 g brain tissue per min (μmol O<sub>2</sub>/100 g/min).

## Additional Anatomical MRI Sequence

A T<sub>2</sub>-weighted fast spin-echo MRI protocol was utilized to collect anatomical MRI images. The imaging parameters were: TR/TE = 4000/26 ms, FOV = 15 × 15 mm, matrix size = 128 × 128, slice thickness = 0.5 mm (without inter-slice gap), echo spacing = 5 ms (8 spin echoes per scan), 35 axial slices, and scan duration = 1.1 min (43, 44).

In humans, microvascular insults to the brain are often assessed by white matter hyperintensities (WMH) on T<sub>2</sub>-weighted images (45–47). We therefore visually inspected the T<sub>2</sub>-weighted images to examine the potential presence of hyperintensities. Z.W. (>5 years of experience) and J. X. (>10 years of experience) performed independent image assessments and reached a consensus.

Additionally, the T<sub>2</sub>-weighted images were analyzed manually by delineating the brain boundary on a slice-by-slice basis (by Z.W.) while referencing to a mouse brain atlas (<https://atlas.brain-map.org/>). Voxels inside the masks were summed to yield the total brain volume in mm<sup>3</sup>. The total brain volume was used in the estimation of unit-mass CBF as described above.

## Heart Rate Measurement

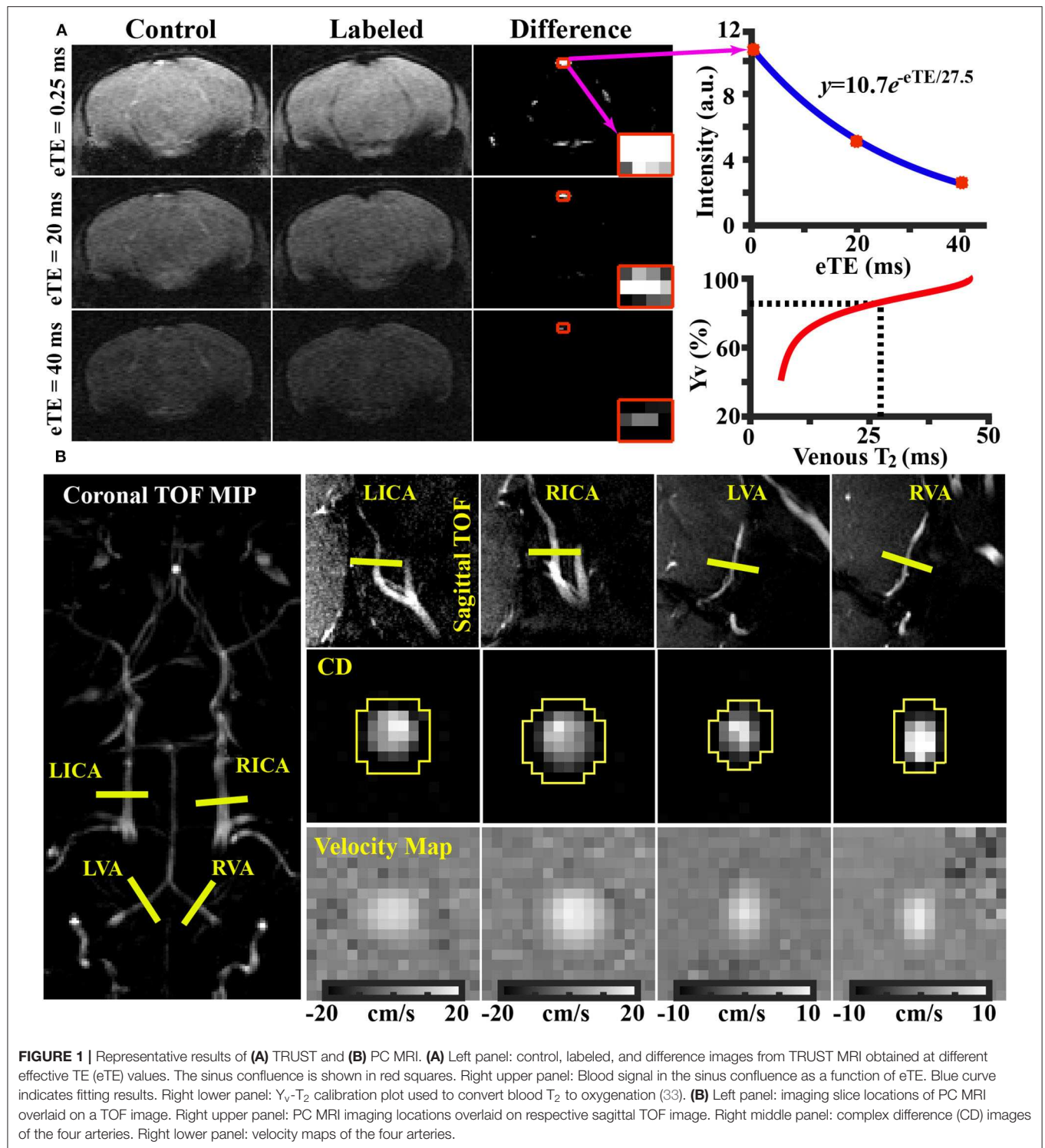
It is known that heart rate is inversely related to the dosage of isoflurane anesthesia in rodents (48). We therefore utilized a MRI sequence to perform in-scanner measurement of heart rate during each session. The sequence acquired the center  $k$ -space repeatedly at an interval of 8.0 ms, thereby yielding a time course of MR signal intensity, the period of which is the R-R interval (49). Two measurements were performed in each session and the values were averaged. This allowed us to examine whether there is an age-dependent change in anesthesia level and how this may affect the interpretation of the physiological data.

## Statistical Analyses

All statistical analyses were performed with SPSS v23 (IBM Corporation, Armonk, NY). A linear mixed-effect model was utilized to analyze longitudinal measurements (i.e.,  $Y_v$ , CBF, CMRO<sub>2</sub>, and heart rate), in which age was a fixed effect and individual mouse was a random effect. An age<sup>2</sup> term was also tested in the model to determine any non-linear effect of age. A  $p$ -value < 0.05 was considered significant.

## RESULTS

**Figure 1A** shows representative data from TRUST MRI, which consisted of control, labeled, and difference images acquired

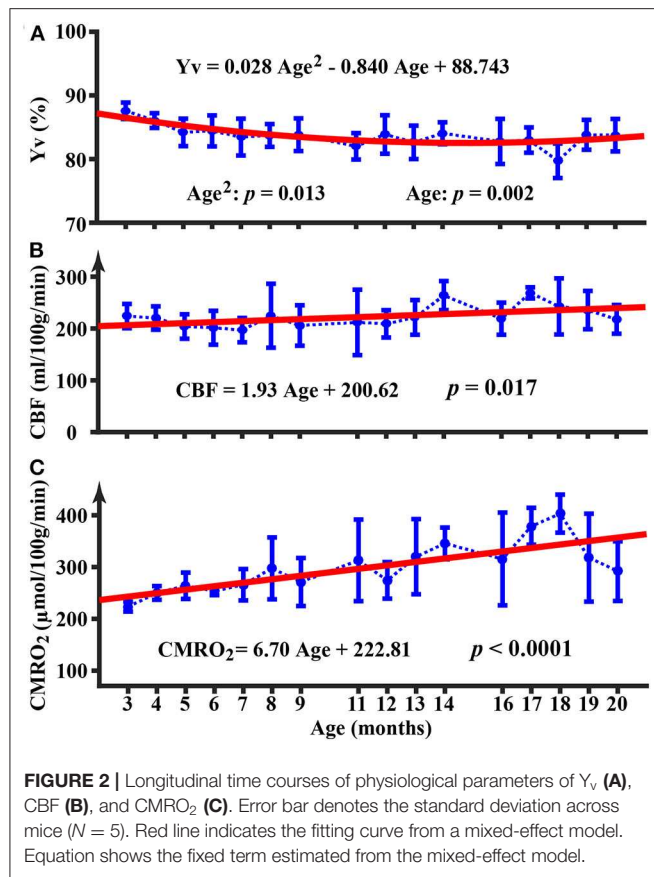


at different eTE values. **Figure 1B** illustrates representative PC images. Both complex difference (CD) and velocity map images are shown. ROIs (yellow polygons in **Figure 1B**) delineating the target vessels are also displayed.

The longitudinal time course for  $Y_v$  is shown in **Figure 2A**. There was an age-related decrease in  $Y_v$  ( $p = 0.002$ ) from 3 to

20 months of age. Furthermore, the quadratic term of age was also significant ( $p = 0.013$ ), suggesting that the age-dependence of  $Y_v$  was non-linear ( $Y_v = 0.028\text{Age}^2 - 0.840\text{Age} + 88.743$ ). **Figure 2B** displays the longitudinal time courses of CBF, which exhibited an increase with age ( $p = 0.017$ ) ( $\text{CBF} = 1.93\text{Age} + 200.62 \text{ ml/100g/min}$ ). There was not a quadratic effect of age on





CBF measure ( $p = 0.64$ ). Longitudinal time course of  $CMRO_2$  is shown in **Figure 2C** and exhibited an increase with age ( $p < 0.0001$ ) ( $CMRO_2 = 6.70\text{Age} + 222.81 \mu\text{mol}/100\text{g}/\text{min}$ ). The  $\text{Age}^2$  term was not significant for  $CMRO_2$  ( $p = 0.12$ ). At 19 and 20 months of age, there appeared to be a decrease in  $CMRO_2$ ; but these values were not significantly different from  $CMRO_2$  at 18 months of age ( $p = 0.11$  and  $0.09$ , respectively).

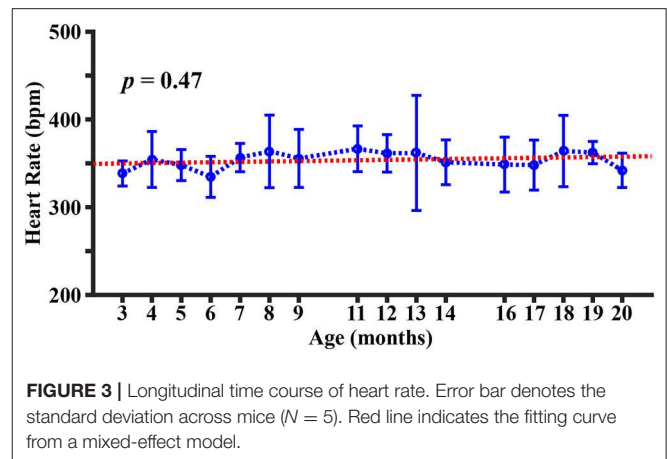
**Figure 3** shows the longitudinal time course of heart rate. It can be seen that the heart rate is within the range of 300–400 beats per minute (bpm), which is consistent with those reported in the literature under similar anesthetic conditions (50). There was no significant change in heart rate with age ( $p = 0.47$ ).

The Y-maze test revealed an average spontaneous-alternating-performance score of  $62 \pm 20\%$ . These scores are within the normal range of wild-type mice (29, 51), indicating that the utilized mice did not exhibit obvious cognitive decline throughout the study period.

Visual inspection of  $T_2$ -weighted images revealed no WMH in the brain, even at 20 months of age (**Figure 4**).

## DISCUSSION

To the best of our knowledge, the present work is the first longitudinal study to characterize brain energy homeostasis across the adult lifespan of mice. Our findings suggested that brain perfusion and oxygen metabolic rate both increased within



the age range of 3 to 20 months in C57BL/6 mice, consistent with the notion of flow-metabolism coupling (52). On the other hand, systemic parameters such as heart rate did not show a significant change with age. Results from the present study also provide normative data on these important brain physiological parameters of C57BL/6 mice, which is the most widely-used mouse strain for developing disease models (53, 54).

Our data suggested that  $CMRO_2$ , an index of the brain's energy budget and a surrogate marker of aggregated brain cell activity, is in the range of 250–350  $\mu\text{mol}/100 \text{ g}/\text{min}$  in mice. These values are in good agreement with reports in the literature using  $^{17}\text{O}$  magnetic resonance spectroscopy (55, 56) or Doppler/spectroscopic OCT methods (40), and are higher than human  $CMRO_2$  values of 120–200  $\mu\text{mol}/\text{min}/100 \text{ g}$ , showing consistency with reports that mouse brain consumes more energy (per unit volume tissue) compared to humans (57, 58). Our longitudinal data also confirmed previous cross-sectional observations in humans that  $CMRO_2$  does in fact increase with age (10, 17). In terms of the reason for age-related increase in oxygen metabolism, it could be a compensatory response to reduced efficiency in neural computation and/or cellular machinery of oxidative metabolism and energy production chain. It has been reported that 24 month-old rats reveal  $\geq 30\%$  (59) synapse losses in comparison with 3-month-old young controls. Therefore, it is plausible that escalated neural computation is needed in the presence of synaptic loss.

Quantification of CBF in mice is not trivial. The present study revealed, for the first time, that unit-volume CBF increases with age in mice. Compared to the literature, our CBF values of 200–250  $\text{ml}/100 \text{ g}/\text{min}$  in mice are in good agreement with those obtained with arterial-spin-labeling (ASL) MRI, which showed values of  $\sim 200 \text{ ml}/\text{min}/100 \text{ g}$  for mice at 3 months of age (60, 61). However, previous ASL studies in mice have generally failed to observe an age effect on CBF. For example, Maier et al. performed a longitudinal ASL study (1.5, 2.5, 5, 7, 13, and 18 months old) in mice and found that CBF was constant across age (62). Similarly, Hirschler et al. reported in a cross-sectional ASL study that no CBF difference was observed between mice 6 and 26 months of age (63). Note that the ASL technique relies on the spin tagging principle to generate perfusion information

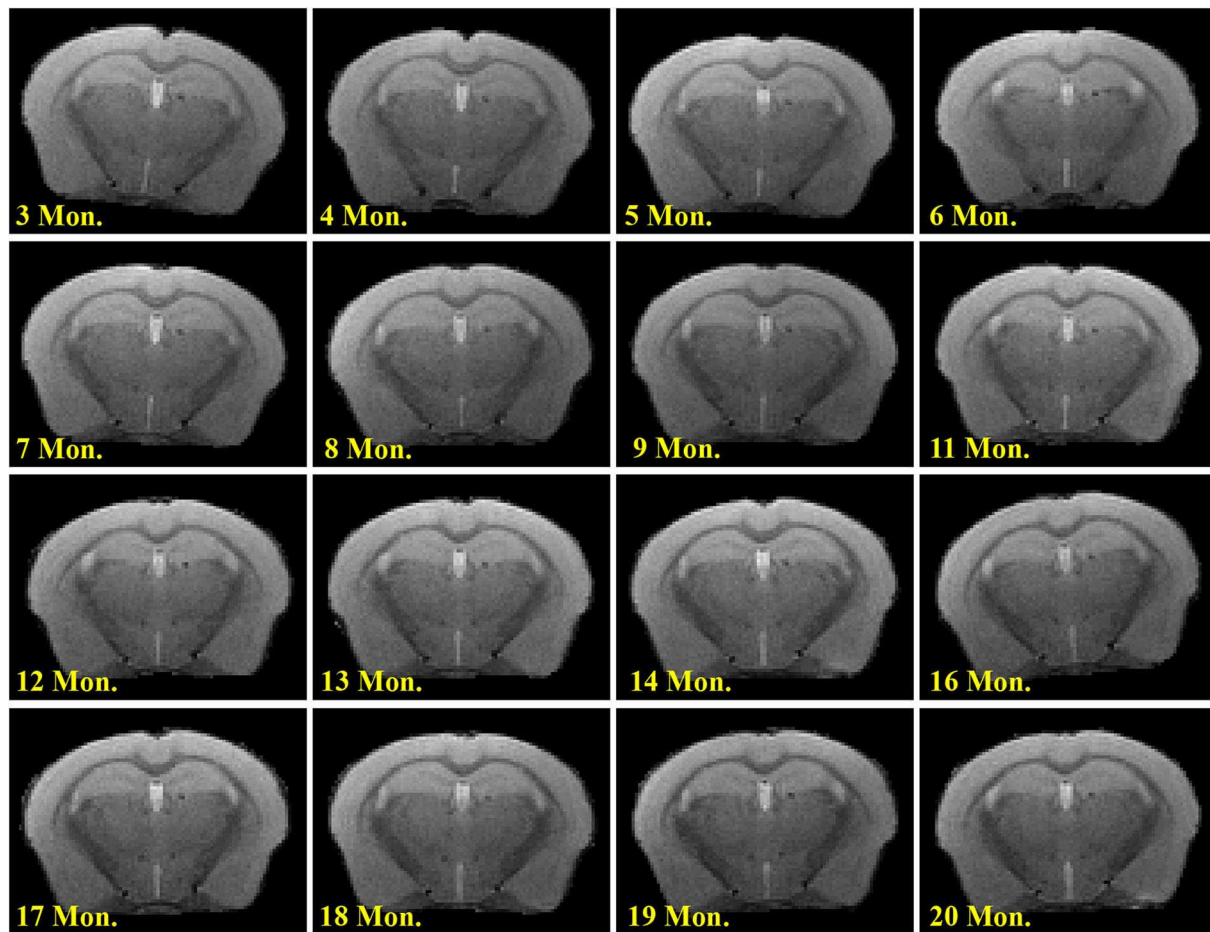


**FIGURE 4 |** Longitudinal T<sub>2</sub>-weighted images in a representative mouse.

after pair-wise subtraction (64). A limitation of ASL MRI is that the SNR of this signal is relatively low, thus it is typically used in a lower resolution setting in humans. In the mouse brain, spatial resolution has to be increased for delineation of structures, which results in a further decrease in SNR in mouse ASL data. In addition, ASL MRI also suffers from multiple confounding factors, e.g., bolus arrival time, labelling efficiency, and vessel contributions, in terms of its quantification. On the other hand, PC MRI utilizes the principle that flowing spins can accumulate a phase proportional to its velocity through the use of a pair of bipolar gradients (65). Two separate scans with inverted gradient polarities can be performed to cancel phases due to spurious field inhomogeneities and thereby allows the calculation of a flow map. The quantification of blood flow in PC is more straightforward with fewer confounding factors. Moreover, the coefficient of variation (CoV) of PC (5.3%) (34) was found to be smaller than that in ASL (~10%) (66), suggesting that PC is more reproducible. Therefore, the present study used the PC MRI technique to quantify global CBF, and the sequence has been extensively characterized previously for quantitative flow measurement (34, 67). CBF measurement using PC MRI presents a new approach for hemodynamic assessment in mice.

In humans, it has been suggested that CBF decreases with age (10, 68, 69). This decrease is thought to be attributed to increased arterial stiffness, thickening of basement membrane, stenosis or narrowing of vessel lumen, and development of arteriolosclerosis (70, 71). The present observation of an age increase in CBF of mice is apparently different from the human findings. One possible explanation is species differences. Humans have a much longer lifespan and thus vascular degradation may be substantial in older individuals. In contrast, it is possible that cerebral vessels are still in good health in aged mice. This is consistent with the histology study where cerebral capillary density was not significantly different between 24-month-old and 7-month-old C57BL/6 mice (72), and the notion that aged mice rarely have strokes (73) or WMH as shown in the present study. Therefore, when brain metabolic rate increases with age, mouse brain is able to garner more blood flow to meet its demand, following the flow-metabolism coupling principle (52). It is also interesting to compare CBF time-pattern in mice to that in humans for the same absolute time period. Previous studies that investigated CBF changes in neonates and young children have shown that, the first few months of humans, CBF exhibited an increase from ~20 ml/100 g/min to ~70 ml/100 g/min from 30 to 120 gestational

weeks (i.e., 7 to 28 months) (74). Thus, it is plausible that CBF can increase in the first two years of life, and this occurs in both humans and mice.

One potential confounding factor in animal studies like ours is the anesthetic effect on physiological parameters. In this study, the anesthetic regimen used was the same throughout the study period. To further confirm that the age changes observed in this work were not attributed to variations in anesthetic level, we measured heart rate as an index of anesthetic depth. As shown in **Figure 3**, the heart rate did not reveal a dependence on age, indicating that the anesthetic level was not a contributor to the physiological alternations observed in the present study. This is consistent with literature that resting heart rate does not change with age (75). Isoflurane is known to induce an increase in CBF and a decrease in CMRO<sub>2</sub> (76). Therefore, absolute values of metabolic parameters during awake state may be different from those reported here. Based on the relationship among CBF, CMRO<sub>2</sub>, and OEF, Y<sub>v</sub> measured under isoflurane is expected to be greater than that under awake state. Additionally, it should be pointed out that different anesthetic agents may induce different physiological alterations. For example, dexmedetomidine has been reported to be associated with decreases in both CBF and CMRO<sub>2</sub> (77). Therefore, absolute values of physiological parameters under different anesthesia are not directly comparable; however, the age pattern is expected to be valid when a consistent anesthetic scheme is used.

Human studies have reported that Y<sub>a</sub> is minimally affected by age with a 1~2% decrease across the lifespan (10). On the other hand, noninvasive measurement of Y<sub>a</sub> in mouse is not trivial, and the measurement error could easily exceed the systematic error in Y<sub>a</sub>. Regarding C<sub>a</sub>, it is related to the hemoglobin level, which is not significantly different between young and older age according to the literature (78). Therefore, the assumptions on Y<sub>a</sub> and C<sub>a</sub> are not expected to alter the major conclusions in the current study.

Findings in current study should be interpreted in the context of several limitations. First, brain perfusion and oxygen consumption were measured in a global manner without spatial information. Regional maps can further enhance our understanding of spatial distributions of oxygen metabolism across the brain. Second, arterial oxygenation was based on an assumed value (99%) instead of subject-specific measurements, e.g., with pulse oximeter. The CMRO<sub>2</sub> estimation is thus based upon such assumptions. However, we should point out that our study used a longitudinal design thus inter-subject variations in Y<sub>a</sub> should not affect our conclusion. Finally, this study has only used female C57BL/6 mice. Thus potential sex effects on our findings require further studies. The number of mice used in this study was relatively small. However, we would like to point out

that, when it comes to study power, one should also consider the number of data points from each mouse. In the present study, each mouse underwent 16 sessions (one with 12 sessions). Thus the total number of experimental sessions was 76, which is considered large compared to many studies in the literature. As a result, the statistical power of our findings was satisfactory, with a *p*-value of 0.002 for Y<sub>v</sub> and <0.0001 for CMRO<sub>2</sub>. In addition, there are limitations of using animal models to study human conditions. In this case, the aging process in humans is expected to be different from that in mice in many aspects (79–81). Aged mice often do not develop neurodegeneration and have low prevalence of cardiovascular disease, possibly due to species differences in physiology, disparity in maximal lifespan, diet, and environmental factors. Thus caution should be used when generalizing these observations to other mouse strains.

## CONCLUSIONS

We conducted a longitudinal assessment of brain physiological parameters in C57BL/6 mice, and observed an age-related increase in brain perfusion and oxygen consumption within 3 to 20 months of age. While the age increases in oxygen metabolic parameters are consistent with findings in humans and suggest a compensatory hypermetabolism of brain tissue, the continuous increase in perfusion suggests that cerebrovascular function remains relatively intact in aged C57BL/6 mice and is consistent with an absence of WMH, in contrast to human elderly individuals.

## DATA AVAILABILITY STATEMENT

The datasets generated for this study are available on request to the corresponding author.

## ETHICS STATEMENT

The animal study was reviewed and approved by Johns Hopkins Medical Institution Animal Care and Use Committee.

## AUTHOR CONTRIBUTIONS

ZW and HL designed the study. ZW, LC, and JX performed the experiments and collected the data. XH helped with the statistical analyses. PZ and HL helped with the data interpretation. ZW and HL wrote the manuscript with editing from all other authors.

## FUNDING

This work was supported by the Grant Sponsors: NIH R01 MH084021, NIH R21 AG058413, and NIH P41 EB015909.

## REFERENCES

- Mattay VS, Goldberg TE, Sambataro F, Weinberger DR. Neurobiology of cognitive aging: insights from imaging genetics. *Biol Psychol.* (2008) 79:9–22. doi: 10.1016/j.biopsycho.2008.03.015
- Wyss-Coray T. Ageing, neurodegeneration and brain rejuvenation. *Nature.* (2016) 539:180–6. doi: 10.1038/nature20411
- Irwin K, Sexton C, Daniel T, Lawlor B, Naci L. Healthy aging and dementia: two roads diverging in midlife? *Front Aging Neurosci.* (2018) 10:275. doi: 10.3389/fnagi.2018.00275



4. Fletcher MA, Low KA, Boyd R, Zimmerman B, Gordon BA, Tan CH, et al. Comparing aging and fitness effects on brain anatomy. *Front Hum Neurosci.* (2016) 10:286. doi: 10.3389/fnhum.2016.00286
5. Smith CD, Chebrolu H, Wekstein DR, Schmitt FA, Markesbery WR. Age and gender effects on human brain anatomy: a voxel-based morphometric study in healthy elderly. *Neurobiol Aging.* (2007) 28:1075–87. doi: 10.1016/j.neurobiolaging.2006.05.018
6. Fjell AM, Walhovd KB. Structural brain changes in aging: courses, causes and cognitive consequences. *Rev Neurosci.* (2010) 21:187–221. doi: 10.1515/revneuro.2010.21.3.187
7. Gu T, Fu C, Shen Z, Guo H, Zou M, Chen M, et al. Age-Related whole-Brain structural changes in relation to cardiovascular risks across the adult age spectrum. *Front Aging Neurosci.* (2019) 11:85. doi: 10.3389/fnagi.2019.00085
8. Guo H, Siu W, D'Arcy RC, Black SE, Grajauskas LA, Singh S, et al. MRI assessment of whole-brain structural changes in aging. *Clin Interv Aging.* (2017) 12:1251–70. doi: 10.2147/CIA.S139515
9. Tomasi D, Volkow ND. Aging and functional brain networks. *Mol Psychiatry.* (2012) 17:471:549–58. doi: 10.1038/mp.2011.81
10. Lu H, Xu F, Rodrigue KM, Kennedy KM, Cheng Y, Flicker B, et al. Alterations in cerebral metabolic rate and blood supply across the adult lifespan. *Cereb Cortex.* (2011) 21:1426–634. doi: 10.1093/cercor/bhq224
11. Liang Z, Liu X, Zhang N. Dynamic resting state functional connectivity in awake and anesthetized rodents. *Neuroimage.* (2015) 104:89–99. doi: 10.1016/j.neuroimage.2014.10.013
12. Liu X, Duyn JH. Time-varying functional network information extracted from brief instances of spontaneous brain activity. *Proc Natl Acad Sci USA.* (2013) 110:4392–7. doi: 10.1073/pnas.1216856110
13. Li HJ, Hou XH, Liu HH, Yue CL, Lu GM, Zuo XN. Putting age-related task activation into large-scale brain networks: a meta-analysis of 114 fMRI studies on healthy aging. *Neurosci Biobehav Rev.* (2015) 57:156–74. doi: 10.1016/j.neubiorev.2015.08.013
14. Sala-Llanch R, Bartres-Faz D, Junque C. Reorganization of brain networks in aging: a review of functional connectivity studies. *Front Psychol.* (2015) 6:663. doi: 10.3389/fpsyg.2015.00663
15. Park DC, Reuter-Lorenz P. The adaptive brain: aging and neurocognitive scaffolding. *Annu Rev Psychol.* (2009) 60:173–96. doi: 10.1146/annurev.psych.59.103006.093656
16. Turner GR, Spreng GR. Executive functions and neurocognitive aging: dissociable patterns of brain activity. *Neurobiol Aging.* (2012) 33:826 e1–13. doi: 10.1016/j.neurobiolaging.2011.06.005
17. Peng SL, Dumas JA, Park DC, Liu P, Filbey FM, McAdams CJ, et al. Age-related increase of resting metabolic rate in the human brain. *Neuroimage.* (2014) 98:176–83. doi: 10.1016/j.neuroimage.2014.04.078
18. Cabeza R. Hemispheric asymmetry reduction in older adults: the hAROLD model. *Psychology and Aging.* (2002) 17:85–100. doi: 10.1037/0882-7974.17.1.85
19. Ferando I, Faas GC, Mody I. Diminished kCC2 confounds synapse specificity of ITP during senescence. *Nat Neurosci.* (2016) 19:1197–200. doi: 10.1038/nn.4357
20. Samson RD, Barnes CA. Impact of aging brain circuits on cognition. *Eur J Neurosci.* (2013) 37:1903–15. doi: 10.1111/ejn.12183
21. Liu W, Wei D, Chen Q, Yang W, Meng J, Wu G, et al. Longitudinal test-retest neuroimaging data from healthy young adults in southwest china. *Sci Data.* (2017) 4:170017. doi: 10.1038/sdata.2017.17
22. De Vis JB, Peng SL, Chen X, Li Y, Liu P, Sur S, et al. Arterial-spin-labeling (ASL) perfusion MRI predicts cognitive function in elderly individuals: a 4-year longitudinal study. *J Magn Reson Imaging.* (2018) 48:449–58. doi: 10.1002/jmri.25938
23. Vetter NC, Steding J, Jurk S, Ripke S, Mennigen E, Smolka MN. Reliability in adolescent fMRI within two years - a comparison of three tasks. *Sci Rep.* (2017) 7:2287. doi: 10.1038/s41598-017-02334-7
24. Vandamme TF. Use of rodents as models of human diseases. *J Pharm Bioallied Sci.* (2014) 6:2–9. doi: 10.4103/0975-7406.124301
25. Yue F, Cheng Y, Breschi A, Vierstra J, Wu W, Ryba T, et al. A comparative encyclopedia of dNA elements in the mouse genome. *Nature.* (2014) 515:355–64. doi: 10.1038/nature13992
26. Dutta S, Sengupta P. Men and mice: relating their ages. *Life Sci.* (2016) 152:244–8. doi: 10.1016/j.lfs.2015.10.025
27. Magistretti PJ, Allaman I. A cellular perspective on brain energy metabolism and functional imaging. *Neuron.* (2015) 86:883–901. doi: 10.1016/j.neuron.2015.03.035
28. Pantoni L. Cerebral small vessel disease: from pathogenesis and clinical characteristics to therapeutic challenges. *Lancet Neurol.* (2010) 9:689–701. doi: 10.1016/s1474-4422(10)70104-6
29. Liu N, Wang Y, An AY, Banker C, Qian YH, O'Donnell JM. Single housing-induced effects on cognitive impairment and depression-like behavior in male and female mice involve neuroplasticity-related signaling. *Eur J Neurosci.* (2019) doi: 10.1111/ejn.14565
30. Lu H, Ge Y. Quantitative evaluation of oxygenation in venous vessels using t2-Relaxation-Under-Spin-Tagging MRI. *Magn Reson Med.* (2008) 60:357–63. doi: 10.1002/mrm.21627
31. Wei Z, Xu J, Liu P, Chen L, Li W, van Zijl P, et al. Quantitative assessment of cerebral venous blood t2 in mouse at 11.7T: implementation, optimization, and age effect. *Magn Reson Med.* (2018) 80:521–8. doi: 10.1002/mrm.27046
32. Watchmaker JM, Juttukonda MR, Davis LT, Scott AO, Faraco CC, Gindville MC, et al. Hemodynamic mechanisms underlying elevated oxygen extraction fraction (OEF) in moyamoya and sickle cell anemia patients. *J Cereb Blood Flow Metab.* (2018) 38:1618–30. doi: 10.1177/0271678X16682509
33. Li W, van Zijl PCM. Quantitative theory for the transverse relaxation time of blood water. *NMR Biomed.* (2020) 2020:e4207. doi: 10.1002/nbm.4207
34. Wei Z, Chen L, Lin Z, Jiang D, Xu J, Liu P, et al. Optimization of phase-contrast MRI for the estimation of global cerebral blood flow of mice at 11.7T. *Magn Reson Med.* (2019) 81:2566–75. doi: 10.1002/mrm.27592
35. Zheng G, Wen J, Yu W, Li X, Zhang Z, Chen H, et al. Anemia rather than hypertension contributes to cerebral hyperperfusion in young adults undergoing hemodialysis: a phase contrast MRI study. *Sci Rep.* (2016) 6:22346. doi: 10.1038/srep22346
36. Bothe HW, Bodsch W, Hossmann KA. Relationship between specific gravity, water content, and serum protein extravasation in various types of vasogenic brain edema. *Acta Neuropathol.* (1984) 64:37–42. doi: 10.1007/bf00695604
37. Kety SS, Schmidt CF. The effects of altered arterial tensions of carbon dioxide and oxygen on cerebral blood flow and cerebral oxygen consumption of normal young men. *J Clin Invest.* (1948) 27:484–92. doi: 10.1172/jci101995
38. Bulte DP, Kelly M, Germuska M, Xie J, Chappell MA, Okell TW, et al. Quantitative measurement of cerebral physiology using respiratory-calibrated MRI. *Neuroimage.* (2012) 60:582–91. doi: 10.1016/j.neuroimage.2011.12.017
39. Xu F, Ge Y, Lu H. Noninvasive quantification of whole-brain cerebral metabolic rate of oxygen (CMRO2) by MRI. *Magn Reson Med.* (2009) 62:141–8. doi: 10.1002/mrm.21994
40. Chong SP, Merkle CW, Leahy C, Srinivasan VJ. Cerebral metabolic rate of oxygen (CMRO2) assessed by combined doppler and spectroscopic OCT. *Biomed Opt Express.* (2015) 6:3941–51. doi: 10.1364/BOE.6.003941
41. Ulatowski JA, Oja JME, Suarez JJ, Kauppinen RA, Traystman RJ, van Zijl PCM. In vivo determination of absolute cerebral blood volume using hemoglobin as a natural contrast agent: an MRI study using altered arterial carbon dioxide tension. *J Cereb Blood Flow Metab.* (1999) 19:809–17. doi: 10.1097/00004647-199907000-00012
42. Lin AL, Qin Q, Zhao X, Duong TQ. Blood longitudinal (T1) and transverse (T2) relaxation time constants at 11.7 tesla. *MAGMA.* (2012) 25:245–9. doi: 10.1007/s10334-011-0287-2
43. Nessler S, Boretius S, Stadelmann C, Bittner A, Merkler D, Hartung HP, et al. Early MRI changes in a mouse model of multiple sclerosis are predictive of severe inflammatory tissue damage. *Brain.* (2007) 130(Pt 8):2186–98. doi: 10.1093/brain/awm105
44. Natt O, Watanabe T, Boretius S, Radulovic J, Frahm J, Michaelis T. High-resolution 3D MRI of mouse brain reveals small cerebral structures in vivo. *J Neurosci Methods.* (2002) 120:203–9. doi: 10.1016/s0165-0270(02)00211-x
45. Atwi S, Metcalfe AWS, Robertson AD, Rezmovitz J, Anderson ND, MacIntosh BJ. Attention-Related brain activation is altered in older adults with white matter hyperintensities using multi-Echo fMRI. *Front Neurosci.* (2018) 12:748. doi: 10.3389/fnins.2018.00748
46. Wardlaw JM, Valdes Hernandez MC, Munoz-Maniega S. What are white matter hyperintensities made of? Relevance to vascular cognitive impairment. *J Am Heart Assoc.* (2015) 4:e001140. doi: 10.1161/JAHA.114.001140
47. Knight MJ, McCann B, Tsivos D, Dillon S, Coulthard E, Kauppinen RA. Quantitative T2 mapping of white matter: applications for

- ageing and cognitive decline. *Phys Med Biol.* (2016) 61:5587–605. doi: 10.1088/0031-9155/61/15/5587
48. Yang C-F, Yu-Chih Chen M, Chen T-I, Cheng C-F. Dose-dependent effects of isoflurane on cardiovascular function in rats. *Tzu Chi Med J.* (2014) 26:119–22. doi: 10.1016/j.tcmj.2014.07.005
  49. Piekarski E, Chitiboi T, Ramb R, Feng L, Axel L. Use of self-gated radial cardiovascular magnetic resonance to detect and classify arrhythmias (atrial fibrillation and premature ventricular contraction). *J Cardiovasc Magn Reson.* (2016) 18:83. doi: 10.1186/s12968-016-0306-6
  50. Constantinides C, Murphy K. Molecular and integrative physiological effects of isoflurane anesthesia: the paradigm of cardiovascular studies in rodents using magnetic resonance imaging. *Front Cardiovasc Med.* (2016) 3:23. doi: 10.3389/fcvm.2016.00023
  51. Hakimizadeh E, Jandaghi F, Hajmohammadi M, Fatemi I, Kaeidi A, Shamsizadeh A, et al. Pistachio extract improves neurocognitive behaviors in ovariectomized mice. *Res J Pharmacogn.* (2019) 6:45–51. doi: 10.22127/rjp.2019.93515
  52. Chiarelli PA, Bulte DP, Gallichan D, Piechnik SK, Wise R, Jeppard P. Flow-metabolism coupling in human visual, motor, and supplementary motor areas assessed by magnetic resonance imaging. *Magn Reson Med.* (2007) 57:538–47. doi: 10.1002/mrm.21171
  53. Bryant CD. The blessings and curses of c57BL/6 substrains in mouse genetic studies. *Ann N Y Acad Sci.* (2011) 1245:31–3. doi: 10.1111/j.1749-6632.2011.06325.x
  54. Song HK, Hwang DY. Use of c57BL/6N mice on the variety of immunological researches. *Lab Anim Res.* (2017) 33:119–23. doi: 10.5625/lar.2017.33.2.119
  55. Lou S, Lepak VC, Eberly LE, Roth B, Cui W, Zhu XH, et al. Oxygen consumption deficit in huntington disease mouse brain under metabolic stress. *Hum Mol Genet.* (2016) 25:2813–26. doi: 10.1093/hmg/ddw138
  56. Cui W, Zhu XH, Vollmers ML, Colonna ET, Adriany G, Tramm B, et al. Non-invasive measurement of cerebral oxygen metabolism in the mouse brain by ultra-high field (17)O mR spectroscopy. *J Cereb Blood Flow Metab.* (2013) 33:1846–9. doi: 10.1038/jcbfm.2013.172
  57. Herculano-Houzel S. Scaling of brain metabolism with a fixed energy budget per neuron: implications for neuronal activity, plasticity and evolution. *PLoS ONE.* (2011) 6:e17514. doi: 10.1371/journal.pone.0017514
  58. Karbowski J. Global and regional brain metabolic scaling and its functional consequences. *BMC Biol.* (2007) 5:18. doi: 10.1186/1741-7007-5-18
  59. Chen S, Hillman DE. Dying-back of purkinje cell dendrites with synapse loss in aging rats. *J Neurocytol.* (1999) 28:187–96. doi: 10.1023/a:1007015721754
  60. Xu J, Qin Q, Wu D, Hua J, Song X, McMahon MT, et al. Steady pulsed imaging and labeling scheme for noninvasive perfusion imaging. *Magn Reson Med.* (2016) 75:238–48. doi: 10.1002/mrm.25641
  61. Duhamel G, Callot V, Tachrount M, Alsop DC, Cozzzone PJ. Pseudo-continuous arterial spin labeling at very high magnetic field (11.75t) for high-resolution mouse brain perfusion imaging. *Magn Reson Med.* (2012) 67:1225–36. doi: 10.1002/mrm.23096
  62. Maier FC, Wehr HF, Schmid AM, Mannheim JG, Wiehr S, Lerdkrai C, et al. Longitudinal pET-MRI reveals beta-amyloid deposition and rCBF dynamics and connects vascular amyloidosis to quantitative loss of perfusion. *Nat Med.* (2014) 20:1485–92. doi: 10.1038/nm.3734
  63. Hirschler L, Munting LP, Khmelinskii A, Teeuwisse WM, Suidgeest E, Warnking JM, et al. Transit time mapping in the mouse brain using time-encoded pCASL. *NMR Biomed.* (2018) 31:3855. doi: 10.1002/nbm.3855
  64. Alsop DC, Detre JA, Golay X, Gunther M, Hendrikse J, Hernandez-Garcia L, et al. Recommended implementation of arterial spin-labeled perfusion MRI for clinical applications: a consensus of the ISMRM perfusion study group and the european consortium for aSL in dementia. *Magn Reson Med.* (2015) 73:102–16. doi: 10.1002/mrm.25197
  65. Lotz J, Meier C, Leppert A, Galanski M. Cardiovascular flow measurement with phase-contrast mR imaging: basic facts and implementation. *Radiographics.* (2002) 22:651–71. doi: 10.1148/radiographics.22.3.g02ma11651
  66. Naresh NK, Chen X, Moran E, Tian Y, French BA, Epstein FH. Repeatability and variability of myocardial perfusion imaging techniques in mice: comparison of arterial spin labeling and first-pass contrast-enhanced MRI. *Magn Reson Med.* (2016) 75:2394–405. doi: 10.1002/mrm.25769
  67. Peng SL, Su P, Wang FN, Cao Y, Zhang R, Lu H, et al. Optimization of phase-contrast MRI for the quantification of whole-brain cerebral blood flow. *J Magn Reson Imaging.* (2015) 42:1126–33. doi: 10.1002/jmri.24866
  68. Chen JJ, Rosas HD, Salat DH. Age-associated reductions in cerebral blood flow are independent from regional atrophy. *Neuroimage.* (2011) 55:468–78. doi: 10.1016/j.neuroimage.2010.12.032
  69. Catchlove SJ, Macpherson H, Hughes ME, Chen Y, Parrish TB, Pipingas A. An investigation of cerebral oxygen utilization, blood flow and cognition in healthy aging. *PLoS ONE.* (2018) 13:e0197055. doi: 10.1371/journal.pone.0197055
  70. Head T, Daunert S, Goldschmidt-Clermont PJ. The aging risk and atherosclerosis: a Fresh look at arterial homeostasis. *Front Genet.* (2017) 8:216. doi: 10.3389/fgene.2017.00216
  71. Lee HY, Oh BH. Aging and arterial stiffness. *Circ J.* (2010) 74:2257–62. doi: 10.1253/circj.cj-10-0910
  72. Tucsek Z, Toth P, Tarantini S, Sosnowska D, Gautam T, Warrington JB, et al. Aging exacerbates obesity-induced cerebrovascular rarefaction, neurovascular uncoupling, and cognitive decline in mice. *J Gerontol A Biol Sci Med Sci.* (2014) 69:1339–52. doi: 10.1093/gerona/glu080
  73. Snyder JM, Ward JM, Treuting PM. Cause-of-Death analysis in rodent aging studies. *Vet Pathol.* (2016) 53:233–43. doi: 10.1177/0300985815610391
  74. Liu P, Qi Y, Lin Z, Guo Q, Wang X, Lu H. Assessment of cerebral blood flow in neonates and infants: a phase-contrast MRI study. *Neuroimage.* (2019) 185:926–33. doi: 10.1016/j.neuroimage.2018.03.020
  75. Kostis JB, Moreyra AE, Amendo MT, Di Pietro J, Cosgrove N, Kuo PT. The effect of age on heart rate in subjects free of heart disease. Studies by ambulatory electrocardiography and maximal exercise stress test. *Circulation.* (1982) 65:141–5. doi: 10.1161/01.cir.65.1.141
  76. Oshima T, Karasawa F, Okazaki Y, Wada H, Satoh T. Effects of sevoflurane on cerebral blood flow and cerebral metabolic rate of oxygen in human beings: a comparison with isoflurane. *Eur J Anaesthesiol.* (2003) 20:543–7. doi: 10.1017/s0265021503000863
  77. Drummond JC, Dao AV, Roth DM, Cheng CR, Atwater BI, Minokadeh A, et al. Effect of dexmedetomidine on cerebral blood flow velocity, cerebral metabolic rate, and carbon dioxide response in normal humans. *Anesthesiology.* (2008) 108:225–32. doi: 10.1097/01.anes.0000299576.00302.4c
  78. Li M, Ratcliffe SJ, Knoll F, Wu J, Ances B, Mardini W, et al. Aging: impact upon local cerebral oxygenation and blood flow with acute isovolemic hemodilution. *J Neurosurg Anesthesiol.* (2006) 18:125–31. doi: 10.1097/00008506-200604000-00006
  79. Mitchell SJ, Scheibye-Knudsen M, Longo DL, de Cabo R. Animal models of aging research: implications for human aging and age-related diseases. *Annu Rev Anim Biosci.* (2015) 3:283–303. doi: 10.1146/annurev-animal-022114-110829
  80. Gomes AC, Falcao-Pires I, Pires AL, Bras-Silva C, Leite-Moreira AF. Rodent models of heart failure: an updated review. *Heart Fail Rev.* (2013) 18:219–49. doi: 10.1007/s10741-012-9305-3
  81. Ross CN, Salmon AB. Aging research using the common marmoset: focus on aging interventions. *Nutrition Healthy Aging.* (2019) 5:97–109. doi: 10.3233/nha-180046

**Conflict of Interest:** The authors declare that the research was conducted in the absence of any commercial or financial relationships that could be construed as a potential conflict of interest.

Copyright © 2020 Wei, Chen, Hou, van Zijl, Xu and Lu. This is an open-access article distributed under the terms of the Creative Commons Attribution License (CC BY). The use, distribution or reproduction in other forums is permitted, provided the original author(s) and the copyright owner(s) are credited and that the original publication in this journal is cited, in accordance with accepted academic practice. No use, distribution or reproduction is permitted which does not comply with these terms.



# Parietal Perfusion Alterations in Parkinson's Disease Patients Without Dementia

Laura Pelizzari<sup>1\*</sup>, Sonia Di Tella<sup>1</sup>, Federica Rossetto<sup>1</sup>, Maria Marcella Laganà<sup>1</sup>, Niels Bergsland<sup>1,2</sup>, Alice Pirastru<sup>1</sup>, Mario Meloni<sup>1</sup>, Raffaello Nemni<sup>1,3</sup> and Francesca Baglio<sup>1</sup>

<sup>1</sup> IRCCS, Fondazione Don Carlo Gnocchi, Milan, Italy, <sup>2</sup> Buffalo Neuroimaging Analysis Center, Department of Neurology, Jacobs School of Medicine and Biomedical Sciences, University at Buffalo, State University of New York, Buffalo, NY, United States, <sup>3</sup> Department of Pathophysiology and Transplantation, Università degli Studi di Milano, Milan, Italy

## OPEN ACCESS

### Edited by:

Yulin Ge,  
New York University, United States

### Reviewed by:

Ronald Peeters,  
University Hospitals Leuven, Belgium  
Simon Fristed Eskildsen,  
Aarhus University, Denmark

### \*Correspondence:

Laura Pelizzari  
lapelizzari@dongnocchi.it

### Specialty section:

This article was submitted to  
Applied Neuroimaging,  
a section of the journal  
Frontiers in Neurology

**Received:** 17 March 2020

**Accepted:** 18 May 2020

**Published:** 23 June 2020

### Citation:

Pelizzari L, Di Tella S, Rossetto F, Laganà MM, Bergsland N, Pirastru A, Meloni M, Nemni R and Baglio F (2020) Parietal Perfusion Alterations in Parkinson's Disease Patients Without Dementia. *Front. Neurol.* 11:562. doi: 10.3389/fneur.2020.00562

Fronto-parietal regions are involved in cognitive processes that are commonly affected in Parkinson's disease (PD). The aims of this study were to investigate cerebral blood flow (CBF) and gray matter (GM) volume within the regions belonging to the fronto-parietal circuit in people with PD (pwPD) without dementia, and to assess their association with cognitive performance. Twenty-seven pwPD without dementia (mean [SD] age = 67.4 [8.1] years, 20 males, mean [SD] Montreal Cognitive Assessment, MoCA score = 24.2 [2.9], median [IQR] Hoehn and Yahr scale = 1.5 [1–2]) and twenty-six age- and sex-matched healthy controls (HC) were scanned with arterial spin labeling (ASL) and T1-weighted magnetic resonance imaging (MRI) sequences to investigate CBF and GM volume, respectively. The cognitive performance of the enrolled pwPD was assessed with MoCA, Trail Making Test (TMT, part A, B, B-A), phonemic fluency and semantic fluency tests. The scores were adjusted for age and education. After standard preprocessing, CBF differences between pwPD and HC were tested with a voxel-wise approach. Voxel-based morphometry was used to compare pwPD and HC in terms of GM volume. Both voxel-wise comparisons between pwPD and HC were restricted to regions of the fronto-parietal circuit. The following additional voxel-wise analyses were performed within regions showing either perfusion or GM volume alterations: (1) correlation with neuropsychological test scores; (2) subgroup comparison after median split on each neuropsychological test score. Family-wise error-corrected (FWE) *p*-values lower than 0.05 were considered significant. Significant hypoperfusion was identified in the left inferior parietal lobule (IPL,  $p_{\text{peak}} = 0.037$ ) and in the bilateral superior parietal lobule (SPL, left hemisphere:  $p_{\text{peak}} = 0.037$ ; right hemisphere:  $p_{\text{peak}} = 0.049$ ) of pwPD when compared to HC. No significant GM atrophy was observed. Local hypoperfusion did not correlate with any neuropsychological test scores. However, significantly lower CBF was observed in the left SPL and IPL of the pwPD subgroup who performed poorer on TMT part A in comparison with the pwPD subgroup that performed better. Perfusion alterations may occur in parietal regions of pwPD without dementia, and may be associated with lower visuomotor skills. Parietal CBF may be considered as a suitable early biomarker for longitudinal studies investigating cognitive decline in PD.

**Keywords:** arterial spin labeling, cerebral blood flow, gray matter, cognitive decline, Parkinson's disease, magnetic resonance imaging

## INTRODUCTION

Parkinson's disease (PD) is a neurological disorder that is prominently characterized by motor symptoms, including bradykinesia, rigidity, resting tremor and gait disturbance (1). Besides these hallmarks, cognitive deficits have been identified as an important non-motor manifestation of the disease (2). Cognitive decline typically occurs gradually, after a period of pure motor symptoms (3). Specifically, executive dysfunction may occur in the milder stages of PD, while global dementia can develop as the disease progresses (4).

Alterations in the neural circuits including subcortical structures and frontal and parietal cortices are thought to be associated with PD cognitive deficits (5). Two profiles of neuropsychological deficit were proposed in PD: working memory and executive function deficits, reflecting fronto-striatal dysfunction, and visuospatial function and semantic fluency impairment, indicative of posterior cortical dysfunction (6). Reduced dopamine uptake in the caudate was observed in persons with PD (pwPD) presenting with executive dysfunctions (7), and bilateral caudate involvement was associated with increased risk of developing cognitive impairment (8). In addition, lower functional connectivity in the fronto-parietal network was reported to be associated with mild cognitive impairment (MCI) in pwPD (9). Significantly reduced regional cerebral blood flow (rCBF) in frontal and parietal cortices was detected with single photon emission computed tomography (SPECT) in demented pwPD (10). Furthermore, fluorodeoxyglucose (FDG) positron-emission tomography (PET) studies showed an association between reduced metabolism in prefrontal and parietal cortex and cognitive impairment in PD (11), and a declining metabolism in these brain areas as the disease progresses (12). Besides metabolic deficits, brain atrophy is the most commonly documented imaging correlate of PD with established dementia (13). Gray matter (GM) volume loss in cognitively impaired pwPD was observed in widespread cortical and subcortical structures involved in cognitive functions (3).

Despite the consistent evidence of structural, functional, and metabolic alterations throughout the brain in demented pwPD, it remains unclear whether some changes are present even in absence of frank cognitive deficits and whether some imaging biomarkers can predict cognitive decline in PD. Several studies reported no cortical structural alterations in cognitively preserved pwPD, making GM volume loss less obvious as a prodromal biomarker for cognitive decline in PD. Nevertheless, FDG cortical hypometabolism was reported even in non-demented pwPD, and parietal metabolism was suggested as a risk factor for cognitive decline (14, 15). In addition, arterial spin labeling (ASL) magnetic resonance imaging (MRI) revealed reduced perfusion in a group of pwPD without dementia (16), and Montreal Cognitive Assessment (MoCA) score was reported as a significant predictor of ASL-derived hypoperfusion in posterior parieto-occipital regions, middle, and superior frontal gyri dorsolateral prefrontal cortex and pre- and post-central gyri in pwPD (17).

ASL is an MRI technique that quantitatively assesses brain perfusion in terms of cerebral blood flow (CBF). Due to the

neurovascular coupling, CBF varies in proportion to the local energy consumption and the metabolic needs of the brain (18). For this reason, ASL was suggested as a proxy technique to investigate the patterns of metabolic alterations (19). Compared to FDG PET, ASL has the advantage of not requiring any injection of radiotracers or exogenous contrast agents, making its acquisition more acceptable (20). ASL studies have found evidence of hypoperfusion patterns that mirror those seen with FDG PET in Alzheimer's disease and fronto-temporal dementia (19, 21, 22). Conversely, patterns of ASL-derived hypoperfusion have not yet been confirmed as a valuable biomarker for the risk of developing cognitive impairment in PD.

Our objective was first to assess CBF within the caudate nucleus and fronto-parietal brain regions in a group of non-demented pwPD using ASL MRI, to test whether perfusion is altered in these areas in PD in absence of frank cognitive impairment. Second, we aimed to evaluate GM volume in the same regions and to assess if hypoperfusion is also reflected by atrophy. Finally, this study aimed to test if either CBF or GM volume alterations are associated with the cognitive performance, to probe ASL and structural MRI as possible prodromal biomarkers for cognitive decline in PD.

## MATERIALS AND METHODS

### Participants

Fifty-three subjects [27 pwPD and 26 healthy controls (HC)] participated in this study. PwPD were recruited from the Neurorehabilitation Unit of the IRCCS Fondazione don Carlo Gnocchi in Milan, Italy, while most of HC were volunteers and personnel from our Institute. Being left-handed or presenting with neurological diseases other than PD, psychiatric disorders, cardiovascular and/or metabolic diseases were considered as exclusion criteria for this study. Inclusion criteria for the pwPD participating in the study were: (1) diagnosis of probable PD, according to the Movement Disorder Society (MDS) Clinical Diagnostic Criteria for PD; (23) (2) positive DaT scan; (3) mild to moderate stages of the disease (Modified Hoehn and Yahr-H&Y <3); (23) (4) time spent with dyskinesias assessed with the MDS-sponsored revision of the Unified Parkinson's Disease Rating Scale (MDS-UPDRS), part IV lower than 2; (23) (5) stable dopaminergic therapy for at least 3 months; (6) MoCA score adjusted according to Santangelo et al. (24) higher than 15.5.

All the enrolled pwPD underwent a clinical evaluation by an experienced neurologist, who assessed the severity of motor symptoms with the H&Y Scale (25) and the MDS-UPDRS part III (23). The global cognitive performances of pwPD who participated in the study were assessed by experienced neuropsychologists. Specifically, the cognitive assessment included MoCA, Trail Making Test (TMT, part A, B, B-A), phonemic fluency and semantic fluency tests. The scores of neuropsychological tests were adjusted for age and education (24, 26–28). The levodopa equivalent daily dose (LEDD) was computed for all the pwPD (29).

Body mass index (BMI) was recorded for all the participants.

The study was approved by the Ethics Committee of IRCCS Fondazione don Carlo Gnocchi and it was



performed in accordance with the principles of the Helsinki Declaration. Written and informed consent was provided by all the participants.

## MRI Acquisition

All scans were acquired on the same 1.5T Siemens Magnetom Avanto scanner, with a 12-channel head coil. Each participant was scanned according to the following MRI protocol: (1) dual-echo turbo spin echo proton density PD/T2-weighted sequence [repetition time (TR) = 5,550 ms, echo time (TE) = 23/103 ms, matrix size =  $320 \times 320 \times 45$ , resolution  $0.8 \times 0.8 \times 3 \text{ mm}^3$ ]; (2) 3D high-resolution magnetization-prepared rapid acquisition with gradient echo (MPRAGE) sequence (TR = 1,900 ms, TE = 3.37 ms, TI = 1,100 ms, matrix size =  $192 \times 256 \times 176$ , resolution  $1 \times 1 \times 1 \text{ mm}^3$ ); (3) 2D T1-weighted sequence (TR/TE = 393/12 ms, matrix size =  $128 \times 128 \times 26$ , resolution =  $1.7 \times 1.7 \times 5 \text{ mm}^3$ ); (4) multi-delay pseudo-continuous ASL (pCASL) sequence with background suppressed 3D gradient and spin echo (GRASE) readout (30) (TR/TE = 3500/22.58 ms, labeling duration = 1500 ms, 5 post-labeling delays (PLD) = [700, 1200, 1700, 2200, 2700] ms, 12 pairs of tag/control images for each delay, matrix size =  $64 \times 64 \times 32$ , resolution =  $3.5 \times 3.5 \times 5 \text{ mm}^3$ , distance between the center of imaging slices and labeling plane of 90 mm; 3 M0 images acquired with TR = 5,000 ms).

## MRI Processing

All the MRI processing was performed with FMRIB's Software Library (FSL, <http://www.fmrib.ox.ac.uk/fsl>), unless otherwise specified.

White matter (WM) T2-hyperintensities were segmented on the PD/T2-weighted images by an experienced operator with Jim 6.0 software package (<http://www.xinapse.com/>). The T2-hyperintensity masks were registered to the respective MPRAGE T1-weighted image with Advanced Normalization Tools (ANTs—<http://stnava.github.io/ANTs>). The registered masks were thresholded at 0.5 and binarized.

N3 bias field correction was applied to MPRAGE T1-weighted images, then lesion filling tool was used to correct for WM T1-hypointensities concurrent to the T2-hyperintensities (31). Brain extraction was performed (32) and SIENAX software tool was used to derive WM, GM, and cerebrospinal fluid (CSF) masks for each subject (33).

Partial volume GM maps were non-linearly registered to Montreal Neurological Institute (MNI) standard space with ANTs (<http://stnava.github.io/ANTs>). The Jacobian determinant image of the transformation was derived with ANTs (<http://stnava.github.io/ANTs>). Each registered GM map was multiplied by the respective Jacobian determinant image, and then smoothed with a Gaussian kernel ( $\sigma = 3 \text{ mm}$ ).

ASL data were realigned with ANTs (<http://stnava.github.io/ANTs>) to correct for movements. Once realigned, the 12 pairs of tag/control images for each delay were averaged, and the tag images were subtracted by the respective control ones. The obtained perfusion-weighted images were used to compute the CBF map with `oxford_asl` tool (34) (tissue T1 = 1.2 s, T1 of blood = 1.36 s, tagging efficiency = 0.8) (30, 35). CSF magnetization was estimated from the M0 image and CBF maps were calibrated

accordingly, with `asl_calib` tool (34). Partial volume effect (PVE) correction was performed, assuming a perfusion ratio between GM and WM of 2.5, as described in Marshall et al. (36) and Pelizzari et al. (37). GM CBF maps were registered to MNI standard space with ANTs (<http://stnava.github.io/ANTs>), by applying a concatenation of transformations, as follows: (1) linear, from ASL space to the respective 2D T1-weighted image (presenting with the same slice thickness of ASL data); (2) linear, from 2D T1-weighted image to the respective MPRAGE; (3) non-linear, from MPRAGE to MNI standard space.

## Statistical Analysis

The assumption of normality of data distribution was tested with Shapiro-Wilk test. Parametric or non-parametric statistics were used, as appropriate. Demographic characteristics were compared between pwPD and HC groups.

Voxel-wise comparisons between pwPD and HC in terms of both CBF and GM volume were performed with randomize tool (5,000 permutations, cluster detection with threshold-free cluster enhancement) (38). Age was included as a covariate in both the general linear models (GLM). Given that the Jacobian determinants derived with ANTs include the linear registration component, voxel-based morphometry (VBM) analyses were controlled also for the scaling factor derived with SIENAX (33). Both CBF and GM volume voxel-wise comparisons between pwPD and HC were restricted to specific ROIs. The region of interest (ROI) mask used for this study included the caudate nucleus [defined according to the Harvard-Oxford subcortical structural atlas (39)], Brodmann area (BA) 9, BA 10, and BA 46 [defined according to the Sallet's dorsal frontal parcellation atlas (40), thr = 50%], superior parietal lobule (SPL) regions [defined and labeled according to the Mars' parietal cortex atlas (41), thr = 75%] and inferior parietal lobule (IPL) regions [defined and labeled according to the Mars' parietal cortex atlas (41), thr = 75%].

If either perfusion or GM volume alterations were detected in pwPD with respect to HC, voxel-wise correlations between neuropsychological test scores (NPS) and either CBF or GM volume were assessed in pwPD with randomize tool (5,000 permutations, threshold-free cluster enhancement for cluster detection) (38), to assess if the observed MRI alterations were mirrored by the cognitive performance. NPS-CBF and NPS-GM volume voxel-wise correlations were restricted to the regions showing either perfusion or GM volume alterations, respectively. A specific GLM was defined for each neuropsychological test (i.e., MoCA, TMT part A, TMT part B, TMT part B-A, phonemic fluency and semantic fluency); scores adjusted for age and education were used.

In order to further assess the association between cognitive performance and either CBF or GM volume alterations, pwPD were split into two subgroups according to the median score at each neuropsychological test (i.e., median split in the pwPD group). CBF within areas of hypoperfusion and GM volume within atrophic regions, if any, were compared between each pair of pwPD subgroups with randomize tool (5,000 permutations, cluster detection with threshold-free cluster enhancement) (38).



**TABLE 1 |** Demographic and clinical characteristics of the recruited pwPD and HC groups.

	pwPD (n = 27)	HC (n = 26)	pwPD vs. HC p-value
Males, n (%)	20 (74)	17 (65)	0.491 <sup>a</sup>
Age in yrs, mean (SD)	67.4 (8.1)	66.1 (7.5)	0.527 <sup>b</sup>
BMI, mean (SD)	25.3 (2.6)	24.2 (3.6)	0.118 <sup>b</sup>
HandY, median (IQR)	1.5 (1–2)	-	-
MDS-UPDRS III, mean (SD)	19.7 (12.1)	-	-
Disease duration in yrs, median (IQR)	3 (2–5)	-	-
Clinical onset laterality, left n (%)	12 (44.4)	-	-
Onset symptoms		-	-
Tremor, n (%)	12 (44.4)		
Bradykinesia, n (%)	7 (25.9)		
Motor deficits, n (%)	5 (18.5)		
Others, n (%)	3 (11.1)		
LEDD, mean (SD)	209.5 (128.6)	-	-
Education in years, median (IQR)	13 (8–17)	-	-

Mean and SD were reported in case of normal distribution, while median and IQR were reported in case of non-normal distribution.

BMI, body mass index; HC, healthy controls; HandY, Modified Hoehn and Yahr; IQR, interquartile range; LEDD, Levodopa daily dose equivalent; MDS-UPDRS, Movement Disorder Society-sponsored revision of the Unified Parkinson's Disease Rating Scale; n, number; pwPD, persons with Parkinson's disease; SD, standard deviation; yrs-years.

Chi-squared test <sup>a</sup> and independent samples Student's t-test <sup>b</sup> were used to evaluate differences between pwPD and HC groups, as appropriate. P-values lower than 0.05 were considered significant.

The results of all the voxel-wise analyses were Family-Wise Error (FWE) corrected to account for multiple comparisons (38, 42). FWE-corrected *p*-values lower than 0.05 were considered significant. Significant clusters in the cortex were mapped according to Sallet's dorsal frontal parcellation atlas (40) and Mars's parietal cortex atlas (41).

## RESULTS

### Demographic and Clinical Characteristics of the Participants

Demographic and clinical information of pwPD and HC groups are reported in **Table 1**. The groups were age-matched (mean age [SD] = 67.4 [8.1] years vs. 66.1 [7.5] years for pwPD and HC respectively, *p* = 0.527) and sex-matched (20 males vs. 17 males in pwPD and HC groups respectively, *p* = 0.491). Although the pwPD group presented with a mean BMI within the overweight range, no differences in terms of BMI were found between pwPD and HC groups (mean BMI [SD] = 25.3 [2.6] vs. 24.2 [3.6], in pwPD and HC respectively, *p* = 0.118). The recruited pwPD presented with a median (IQR) H&Y of 1.5 (1–2) and mean (SD) MDS-UPDRS III score of 19.7 (12.1). The score from the neuropsychological examination of pwPD, adjusted for age and education, are shown in **Table 2**. The pwPD had a mean (SD) MoCA score adjusted for age and education of 24.2 (2.9). For the TMT, the pwPD performed as follows: median (IQR) TMT

**TABLE 2 |** Neuropsychological test scores of the pwPD group.

	pwPD (n = 27)	Cut-off defining pathological condition
MoCA, mean (SD)	24.2 (2.9)	15.5 (≤)
TMT part A, median (IQR)	42 (30–56)	94 (≥)
TMT part B, median (IQR)	73 (58–139)	283 (≥)
TMT part B-A, median (IQR)	40 (18–68)	187 (≥)
Phonemic fluency, mean (SD)	35.4 (9.5)	17.35 (≤)
Semantic fluency, mean (SD)	42.9 (8.5)	25 (≤)

Reported scores have been adjusted for age and education. Mean and SD were reported in case of normal distribution, while median and IQR were reported in case of non-normal distribution. The respective pathological cut-off scores are also shown.

IQR, interquartile range; MoCA, Montreal Cognitive Assessment; n, number; pwPD, persons with Parkinson's disease; SD, standard deviation; TMT, Trail Making Test; yrs-years.

MoCA scores were adjusted according to Santangelo et al. (24), TMT according to Giovagnoli et al. (28), phonological fluency according to Carlesimo et al. (27) and semantic fluency according to Novelli (26). The respective cut-off scores for pathological condition are reported.

A score of 42 (30–56), median (IQR) TMT B score of 73 (58–139), and median (IQR) TMT B-A score of 40 (18–68). The pwPD mean (SD) phonemic and semantic fluency scores at were 35.4 (9.5) and 42.9 (8.5), respectively.

### CBF and GM Volume Comparison Between pwPD and HC

Significantly lower CBF in pwPD with respect to HC was found within the SPL bilaterally and in the left IPL (**Figure 1**, in red). Specifically, hypoperfusion was present within the following clusters defined in the Mars's parietal cortex atlas: (41) left SPL C (16 mm<sup>3</sup>, *p*<sub>peak</sub> = 0.049), right SPL C (64 mm<sup>3</sup>, *p*<sub>peak</sub> = 0.049), left SPL D (896 mm<sup>3</sup>, *p*<sub>peak</sub> = 0.037), left SPL E (936 mm<sup>3</sup>, *p*<sub>peak</sub> = 0.038), left IPL D (552 mm<sup>3</sup>, *p*<sub>peak</sub> = 0.037) and left IPL E (816 mm<sup>3</sup>, *p*<sub>peak</sub> = 0.037) (**Table 3**).

No significant GM volume differences were detected between pwPD and HC.

### Association With Neuropsychological Test Scores

No significant correlation between the local CBF and the neuropsychological test scores was found within the regions of hypoperfusion. Significantly lower CBF in the left SPL and IPL was found for the subgroup of pwPD who performed poorer on TMT part A (i.e., higher TMT A score) with respect to the pwPD subgroup that performed better (**Figure 2**). Specifically, according to the Mars' parietal cortex atlas (41), the areas of significant difference were located within left SPL C (8 mm<sup>3</sup>, *p*<sub>peak</sub> = 0.049), left SPL D (808 mm<sup>3</sup>, *p*<sub>peak</sub> = 0.037), left SPL E (912 mm<sup>3</sup>, *p*<sub>peak</sub> = 0.038), left IPL D (544 mm<sup>3</sup>, *p*<sub>peak</sub> = 0.037) and left IPL E (640 mm<sup>3</sup>, *p*<sub>peak</sub> = 0.035). The two pwPD subgroups obtained from the median split on TMT A score were matched for age (*p* = 0.239), sex (*p* = 0.546), H&Y (*p* = 0.981), MDS-UPDRS III (*p* = 0.720), LEDD (*p* = 0.519), MoCA (*p* = 0.720), phonemic fluency (*p* = 0.259), semantic fluency (*p* = 0.583)

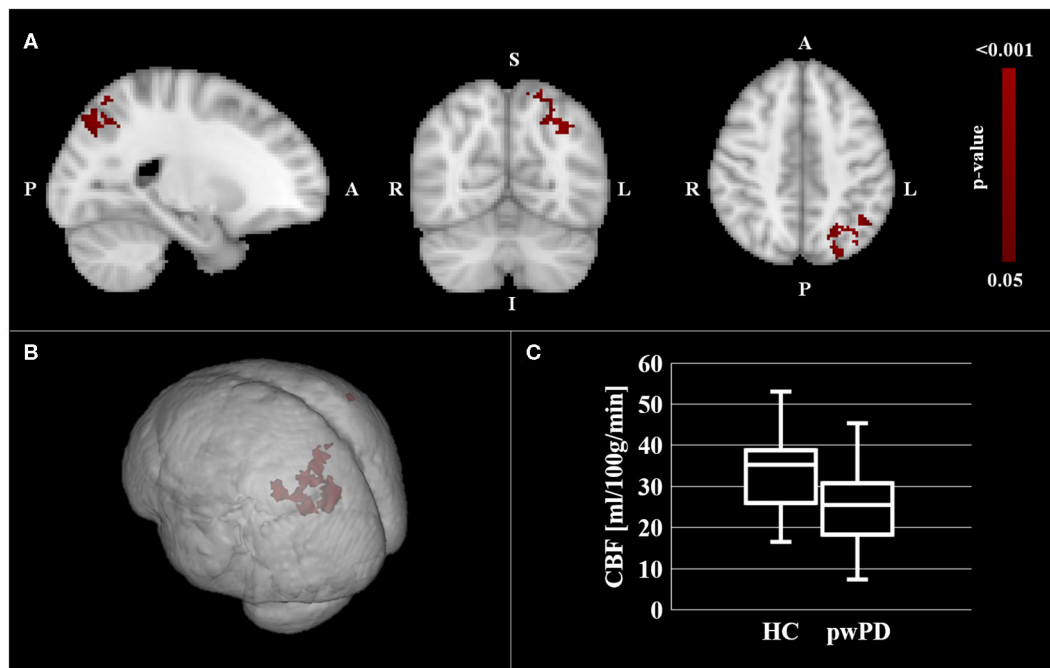


**FIGURE 1 |** CBF comparison between pwPD and HC. The areas showing significantly lower CBF ( $p_{FEW} < 0.05$ ) in pwPD with respect to HC are represented in MNI standard space (in red, **A,B**). The comparison of mean CBF within these areas between pwPD and HC is shown in **(C)**. CBF, cerebral blood flow; FEW, family wise error; HC, healthy controls; pwPD, people with Parkinson's disease.

while presenting significant differences in terms of TMT B score ( $p = 0.006$ , with the subgroup performing poorer on TMT A performing poorer also to TMT B).

No significant CBF differences were observed when splitting the recruited pwPD group into subgroups according to the other neuropsychological test scores.

## DISCUSSION

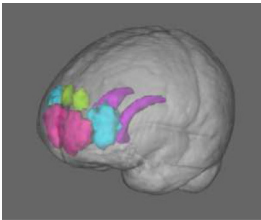
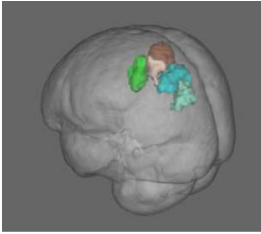
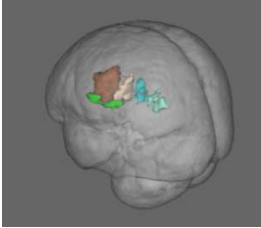
In the current study, CBF and GM volume were assessed with a voxel-wise approach in a group of early PD patients without dementia, focusing on the brain regions belonging to the visuospatial and executive systems, that are known to be affected in PD. The presence of parietal hypoperfusion in absence of parietal GM atrophy and its association with the TMT A score are the main findings that were observed.

Although the majority of PD studies that have previously detected parietal hypoperfusion or hypometabolism included cognitively impaired cohort of subjects (11, 15, 43–45), few works reported alterations in SPL (14, 16) and IPL (14, 46) even in absence of frank cognitive impairment. Cortical hypometabolism was detected in the posterior parietal cortex of non-demented PD patients with both phosphorus-31 magnetic resonance spectroscopy and FDG-PET (14). More recently Gonzalez-Redondo and colleagues showed small cortical areas of hypometabolism, including the angular gyrus, in cognitively normal pwPD (46). This result is in agreement with the hypoperfusion that we observed in left IPL D and IPL E

in our pwPD cohort. The same PET-based study assessed brain metabolism also in MCI-pwPD and demented pwPD, and revealed hypometabolism in more extended brain areas in these two groups of subjects in comparison with the group of cognitively normal PD patients (46). Declining metabolic activity in the parietal cortex was further reported in a 2-year longitudinal PET study assessing an early stage PD cohort of subjects (12), indicating that reduced metabolism is a relatively early PD feature that gradually evolves as the disease progresses. Despite the several PET-based evidences of parietal hypometabolism in PD, ASL failed in consistently showing parietal hypoperfusion in early PD as of yet. However, CBF patterns were proposed as an accessible method to characterize and track progression of both motor and cognitive status in PD (17). Parietal perfusion changes may be subtle at the early stage of the disease, when dementia is not commonly established yet. However, focusing the analysis on specific ROIs that are known to be involved in cognitive processes typically altered in PD may increase the statistical power and may help to detect early perfusion changes occurring in pwPD in these areas. Due to the tight coupling of perfusion and metabolism in the brain, ASL has already been proposed as a non-invasive alternative to FDG-PET to assess metabolic abnormalities during cognitive decline in Alzheimer's disease (19). Our results support the assumption that this MRI technique might be useful to investigate the signature of cognitive impairment even in PD (17).

Interestingly, perfusion changes that were found in the pwPD enrolled in this study were not owing to parietal GM volume loss. This suggests that hypoperfusion in these regions may

**TABLE 3 |** Classification of areas of significant hypoperfusion in pwPD group with respect to HC according to Mars' parietal atlas (41) and Sallet's dorsal-frontal atlas (40).

	ROI	Associated functions	Left mm <sup>3</sup> (p <sub>peak</sub> )	Right mm <sup>3</sup> (p <sub>peak</sub> )
	CN	Involved in procedural and associative learning, inhibitory control	-	-
	BA 9	Involved in attention, working memory and motor planning	-	-
	BA 10	Involved in working memory and multiple-task coordination	-	-
	BA 46	Involved in attention and working memory	-	-
	SPL A	Involved in motion processing using visual, tactile and auditory stimuli	-	-
	SPL B	Involved in reaching movements and adjustments when following a moving target	-	-
	SPL C	Involved in visually guided hand movements and adjustments when intentions are updated	16 (0.049)	64 (0.049)
	SPL D	Involved in mechanisms of attention or task-switching related to the execution of manual responses	896 (0.037)	-
	SPL E	Involved in the allocation of visual attention and in memorizing targets for intended eye movements	936 (0.038)	-
	IPL A	Involved in tool use	-	-
	IPL B	Involved in object manipulation	-	-
	IPL C	Involved in exploratory decisions and changes of response strategy	-	-
	IPL D	Involved in reorienting of attention and reorienting of saccades (anterior part of the angular gyrus)	552 (0.037)	-
	IPL E	Involved in recognition memory (posterior part of the angular gyrus)	816 (0.037)	-

The cluster dimension in mm<sup>3</sup> and the most significant FWE-corrected *p*-value within the cluster (*p*<sub>peak</sub>) are reported.

BA, Brodmann area; CN, Caudate Nucleus; FWE, family wise error; HC, healthy controls; IPL, inferior parietal lobule; pwPD, people with Parkinson's disease; ROI, region of interest; SPL, superior parietal lobule.

precede atrophy and exacerbate the neurodegenerative process by promoting oxidative stress and neuronal energy crisis (47). A previous cross-sectional study investigating both metabolism and atrophy in cognitively impaired and cognitively preserved pwPD concluded that hypometabolism may precede GM volume loss and may be progressively replaced by atrophy during cognitive worsening (46). The greater ability of FDG-PET to reveal significant PD-related alterations compared to MRI-VBM is in line with this hypothesis (45). Parietal GM atrophy may be a feature that is mainly associated with late stage of PD, when cognitive impairment is already established. Since functional changes seem to be already present (48) and more relevant than cortical atrophy in early PD (49), GM volume in these ROIs might not be the best option as a prodromal marker for PD itself and for the risk of developing PD-related dementia.

In the current study perfusion and GM volume were investigated specifically in the fronto-parietal circuit, known to be associated with cognitive impairment in PD (11). The prefrontal cortex is critical for many high-level cognitive abilities, including executive functions, while the parietal cortex is involved in lower level functions. Specifically, the SPL is commonly activated by visuomotor tasks requiring shifting spatial attention, engaging spatial working memory, reaching a visual target or making

saccadic eye movements (50), whereas the IPL is critical for stimulus-driven reorienting of attention, self-perception, introspection and memory (51). In this framework, the here reported association between the TMT A score and CBF in some regions of the SPL and IPL of pwPD is noteworthy. Although no significant correlation was observed between the TMT A score and CBF locally, the subgroup of pwPD that performed poorer on TMT A showed lower CBF compared to the other subgroup. A similar finding was reported in a SPECT-based perfusion study in Alzheimer's disease (52). Specifically, lower SPL perfusion levels were found in Alzheimer's disease patients with poorer performance on TMT A in comparison with the subgroup performing better on the test (52), suggesting that functional activity in SPL is highly associated with performance at TMT A. TMT A primarily tests visual-perceptive skills and graphomotor speed. It is thus not surprising that the main SPL and IPL clusters showing lower CBF associated with poorer TMT A performance are specifically involved in allocation of visual attention, reorienting of saccades, memorizing targets for intended eye movements and attention-switching related to the execution of manual responses. As lower parietal CBF was associated with poorer TMT-A performance, parietal CBF may be an early MRI marker for cognitive decline in PD.

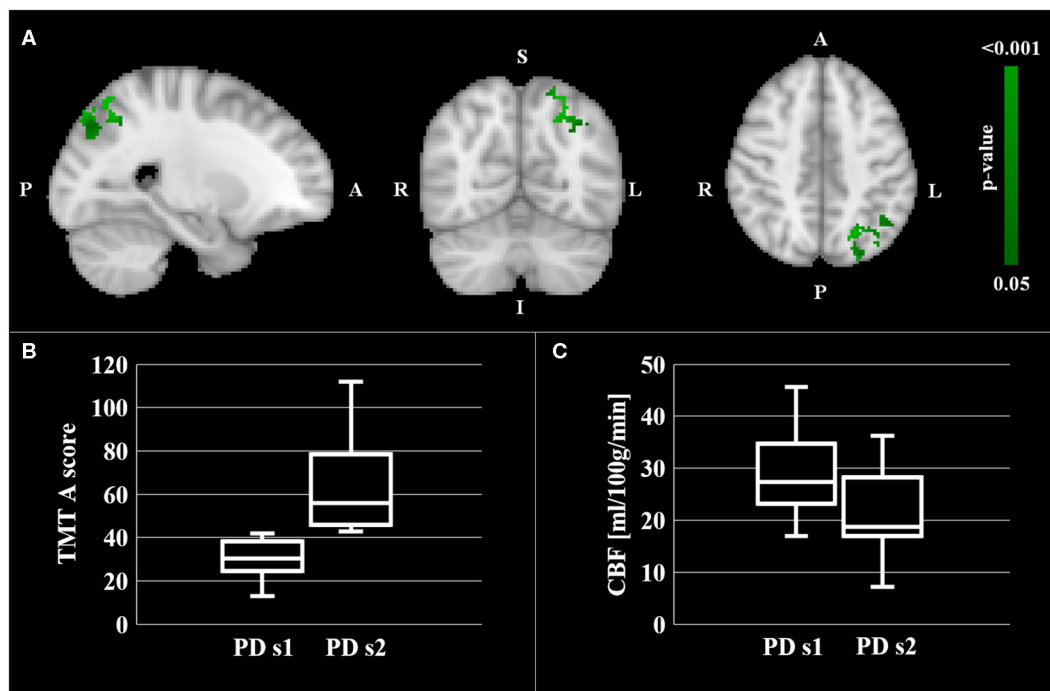


**FIGURE 2 |** CBF comparison between pwPD with a TMT A score below the median TMT A value (PD s1 subgroup) and pwPD with a TMT A score over the median TMT A value (PD s2 subgroup). Areas showing significantly lower CBF ( $p_{FWE} < 0.05$ ) in PD s2 subgroup are represented in MNI standard space (in green, **A**). The comparison of TMT A scores and mean CBF within these areas between the two pwPD subgroups are shown in the boxplots in (**B,C**), respectively.

Neither GM volume nor perfusion alterations were observed in the caudate nucleus and in the prefrontal cortex of the enrolled group of pwPD. Parietal CBF alterations may precede gross caudate denervation and changes in the prefrontal cortex, and may be an earlier predictor of cognitive decline. Although PD pathophysiology is characterized by striatal dopaminergic denervation, caudate dysfunction is generally observed in pwPD at advanced stages (53). In an FDG-PET study comparing brain metabolism of cognitively preserved pwPD, MCI-pwPD and demented pwPD with HC, caudate hypometabolism was observed only in the group of demented pwPD (46), indicating that metabolic changes in this region unlikely occur prior to the onset of cognition-related functional decline. Similar considerations can be made about our findings within the prefrontal ROIs. Frontal hypoperfusion and hypometabolism were observed in pwPD presenting with established dementia. GM atrophy in these areas was also reported (54, 55). Our findings of no perfusion and GM changes in the caudate and in the prefrontal ROIs could suggest that the dopaminergic pathways that project from the substantia nigra into BA 9, 10, and 46, passing through the caudate, may be still relatively spared in our patient sample.

The main limitation of this study is the relatively limited neuropsychological evaluation of pwPD. Assessing the cognitive performance with scales that are validated for use in PD (56) is warranted to detect possible MCI and to clarify the role of CBF as a predictor of cognitive decline in pwPD.

Furthermore, weaknesses of the study include the relatively limited sample size and the heterogeneity of the pwPD group. Different clinical phenotype and laterality onset were suggested to influence the disease severity and its patterns of progression (57, 58). Therefore, these aspects should be considered as confounding factors in future analysis performed in larger groups of subjects. Finally, this study is cross-sectional in nature. A longitudinal study would allow to better understand the link between perfusion alterations and cognitive decline. In addition, extending the analysis to other subcortical brain areas that are known to be associated with PD (e.g., putamen, globus pallidus, thalamus) is warranted.

In conclusion, our findings suggest that ASL MRI may be sensitive to parietal changes associated with cognitive decline in PD, even in absence of concurrent established GM atrophy. Reduced perfusion in the parietal cortex may be associated with the risk of developing cognitive impairment, but longitudinal studies in a larger cohort of pwPD are needed to confirm this hypothesis. Knowledge of the risk of cognitive decline, particularly at early phases of the disease, is crucial to define prompt pharmacological and rehabilitation treatments. Since engaging in physical activity and cognitive activities were proposed as strategies to attenuate neurodegeneration by promoting neurovascular health and brain plasticity (59), investigating the impact of multi-factorial rehabilitation on parietal CBF in early pwPD would be a further interesting future development.



## DATA AVAILABILITY STATEMENT

The datasets generated for this study are available on request to the corresponding author.

## ETHICS STATEMENT

The studies involving human participants were reviewed and approved by Fondazione Don Carlo Gnocchi Ethics Committee. The patients/participants provided their written informed consent to participate in this study.

## AUTHOR CONTRIBUTIONS

LP, SD, ML, NB, AP, and FB contributed conception and design of the study. RN and MM recruited PD patients. ML and FR enrolled HC. FB and MM performed the clinical evaluation of PD patients. SD and FR performed the neuropsychological evaluation of PD patients. LP performed the image processing, the statistical analysis, and wrote the first draft of the manuscript.

## REFERENCES

- Kalia LV, Lang AE. Parkinson's disease. *Lancet*. (2015) 386:896–912. doi: 10.1016/S0140-6736(14)61393-3
- Hoogland J, Boel JA, de Bie RMA, Gekus RB, Schmand BA, Dalrymple-Alford JC, et al. Mild cognitive impairment as a risk factor for Parkinson's disease dementia. *Mov Disord*. (2017) 32:1056–65. doi: 10.1002/mds.27002
- Aarsland D. Cognitive impairment in Parkinson's disease and dementia with Lewy bodies. *Parkinsonism Relat Disord*. (2016) 22 (Suppl. 1):S144–8. doi: 10.1016/j.parkreldis.2015.09.034
- O'Callaghan C, Lewis SJG. Cognition in Parkinson's Disease. *Int Rev Neurobiol*. (2017) 133:557–83. doi: 10.1016/bs.irn.2017.05.002
- Hall JM, Ehgoetz Martens KA, Walton CC, O'Callaghan C, Keller PE, Lewis SJ, et al. Diffusion alterations associated with Parkinson's disease symptomatology: a review of the literature. *Parkinsonism Relat Disord*. (2016) 33:12–26. doi: 10.1016/j.parkreldis.2016.09.026
- Kehagia AA, Barker RA, Robbins TW. Cognitive impairment in Parkinson's disease: the dual syndrome hypothesis. *Neurodegener Dis*. (2013) 11:79–92. doi: 10.1159/000341998
- Bruck A, Portin R, Lindell A, Laihin A, Bergman J, Haaparanta M, et al. Positron emission tomography shows that impaired frontal lobe functioning in Parkinson's disease is related to dopaminergic hypofunction in the caudate nucleus. *Neurosci Lett*. (2001) 311:81–4. doi: 10.1016/S0304-3940(01)00214-3
- Pasquini J, Durcan R, Wiblin L, Gersel Stockholm M, Rochester L, Brooks DJ, et al. Clinical implications of early caudate dysfunction in Parkinson's disease. *J Neurol Neurosurg Psychiatry*. (2019) 90:1098–104. doi: 10.1136/jnnp-2018-320157
- Amboni M, Tessitore A, Esposito F, Santangelo G, Picillo M, Vitale C, et al. Resting-state functional connectivity associated with mild cognitive impairment in Parkinson's disease. *J Neurol*. (2015) 262:425–34. doi: 10.1007/s00415-014-7591-5
- Sawada H, Uda K, Kameyama M, Seriu N, Nishinaka K, Shindou K, et al. SPECT findings in Parkinson's disease associated with dementia. *J Neurol Neurosurg Psychiatry*. (1992) 55:960–3. doi: 10.1136/jnnp.55.10.960
- Huang C, Mattis P, Perrine K, Brown N, Dhawan V, Eidelberg D. Metabolic abnormalities associated with mild cognitive impairment in Parkinson disease. *Neurology*. (2008). 70:1470–7. doi: 10.1212/01.wnl.0000304050.05332.9c
- Huang C, Tang C, Feigin A, Lesser M, Ma Y, Pourfar M, et al. Changes in network activity with the progression of Parkinson's disease. *Brain*. (2007) 130:1834–46. doi: 10.1093/brain/awm086
- Weintraub D, Dietz N, Duda JE, Wolk DA, Doshi J, Xie SX, et al. Alzheimer's disease pattern of brain atrophy predicts cognitive decline in Parkinson's disease. *Brain*. (2012) 135:170–80. doi: 10.1093/brain/awr277
- Hu MT, Taylor-Robinson SD, Chaudhuri KR, Bell JD, Labbe C, Cunningham VJ, et al. Cortical dysfunction in non-demented Parkinson's disease patients: a combined (31)P-MRS and (18)FDG-PET study. *Brain*. (2000) 123:340–52. doi: 10.1093/brain/123.2.340
- Firbank MJ, Yarnall AJ, Lawson RA, Duncan GW, Khoo TK, Petrides GS, et al. Cerebral glucose metabolism and cognition in newly diagnosed Parkinson's disease: ICICLE-PD study. *J Neurol Neurosurg Psychiatry*. (2017) 88:310–6. doi: 10.1136/jnnp-2016-313918
- Fernandez-Seara MA, Mengual E, Vidorreta M, Aznarez-Sanado M, Loayza FR, Villagra F, et al. Cortical hypoperfusion in Parkinson's disease assessed using arterial spin labeled perfusion MRI. *Neuroimage*. (2012) 59:2743–50. doi: 10.1016/j.neuroimage.2011.10.033
- Melzer TR, Watts R, MacAskill MR, Pearson JF, Rueger S, Pitcher TL, et al. Arterial spin labelling reveals an abnormal cerebral perfusion pattern in Parkinson's disease. *Brain*. (2011) 134:845–55. doi: 10.1093/brain/awq377
- Iadecola C. The neurovascular unit coming of age: a journey through neurovascular coupling in health and disease. *Neuron*. (2017) 96:17–42. doi: 10.1016/j.neuron.2017.07.030
- Haller S, Zaharchuk G, Thomas DL, Lovblad KO, Barkhof F, Golay X. Arterial spin labeling perfusion of the brain: emerging clinical applications. *Radiology*. (2016) 281:337–56. doi: 10.1148/radiol.2016150789
- Duncan GW, Firbank MJ, O'Brien JT, Burn DJ. Magnetic resonance imaging: a biomarker for cognitive impairment in Parkinson's disease? *Mov Disord*. (2013) 28:425–38. doi: 10.1002/mds.25352
- Vercllytte S, Lopes R, Lenfant P, Rollin A, Semah F, Leclerc X, et al. Cerebral hypoperfusion and hypometabolism detected by arterial spin labeling MRI and FDG-PET in early-onset Alzheimer's Disease. *J Neuroimaging*. (2016) 26:207–12. doi: 10.1111/jon.12264
- Anazodo UC, Finger E, Kwan BYM, Pavlosky W, Warrington JC, Gunther M, et al. Using simultaneous PET/MRI to compare the accuracy of diagnosing frontotemporal dementia by arterial spin labelling MRI and FDG-PET. *Neuroimage Clin*. (2018) 17:405–14. doi: 10.1016/j.nicl.2017.10.033
- Postuma RB, Berg D, Stern M, Poewe W, Olanow CW, Oertel W, et al. MDS clinical diagnostic criteria for Parkinson's disease. *Mov Disord*. (2015) 30:1591–601. doi: 10.1002/mds.26424
- Santangelo G, Siciliano M, Pedone R, Vitale C, Falco F, Bisogno R, et al. Normative data for the montreal cognitive assessment in an Italian population sample. *Neurol Sci*. (2015) 36:585–91. doi: 10.1007/s10072-014-1995-y
- Goetz CG, Poewe W, Rascol O, Sampaio C, Stebbins GT, Counsell C, et al. Movement disorder society task force report on the Hoehn and Yahr staging scale: status and recommendations. *Mov Disord*. (2004) 19:1020–8. doi: 10.1002/mds.20213

All authors contributed to manuscript revision, read, and approved the submitted version.

## FUNDING

This study was in part funded by a grant awarded by the Annette Funicello Research Fund for Neurological Diseases and the Italian Ministry of Health (Ricerca Corrente 2019–2021).

## ACKNOWLEDGMENTS

We acknowledge the receipt of multi-delay pCASL sequence from the University of Southern California's Stevens Neuroimaging and Informatics Institute. We also acknowledge The Regents of the University of California, on behalf of its Los Angeles campus as a source of portions of the Licensed Technology. Finally, we acknowledge that Dr. DJJ Wang and SIEMENS Healthineers helped in setting the sequence on our scanner.

26. Novelli GPC, Capitani E, Laiacina M, Vallar G, Cappa SF. Tre test clinici di ricerca e produzione lessicale. Taratura su soggetti normali. *Arch Psicol Neurol Psichiatr.* (1986) 4:477–506.
27. Carlesimo GA, Caltagirone C, Gainotti G. The mental deterioration battery: normative data, diagnostic reliability and qualitative analyses of cognitive impairment. The group for the standardization of the mental deterioration battery. *Eur Neurol.* (1996) 36:378–84. doi: 10.1159/000117297
28. Giovagnoli AR, Del Pesce M, Mascheroni S, Simoncelli M, Laiacina M, Capitani E. Trail making test: normative values from 287 normal adult controls. *Ital J Neurol Sci.* (1996) 17:305–9. doi: 10.1007/bf01997792
29. Tomlinson CL, Stowe R, Patel S, Rick C, Gray R, Clarke CE. Systematic review of levodopa dose equivalency reporting in Parkinson's disease. *Mov Disord.* (2010) 25:2649–53. doi: 10.1002/mds.23429
30. Wang DJ, Alger JR, Qiao JX, Gunther M, Pope WB, Saver JL, et al. Multi-delay multi-parametric arterial spin-labeled perfusion MRI in acute ischemic stroke - Comparison with dynamic susceptibility contrast enhanced perfusion imaging. *Neuroimage Clin.* (2013) 3:1–7. doi: 10.1016/j.nicl.2013.06.017
31. Battaglini M, Jenkinson M, De Stefano N. Evaluating and reducing the impact of white matter lesions on brain volume measurements. *Hum Brain Mapp.* (2012) 33:2062–71. doi: 10.1002/hbm.21344
32. Lutkenhoff ES, Rosenberg M, Chiang J, Zhang K, Pickard JD, Owen AM, et al. Optimized brain extraction for pathological brains (optiBET). *PLoS ONE.* (2014) 9:e115551. doi: 10.1371/journal.pone.0115551
33. Smith SM, Zhang Y, Jenkinson M, Chen J, Matthews PM, Federico A, et al. Accurate, robust, and automated longitudinal and cross-sectional brain change analysis. *Neuroimage.* (2002) 17:479–89. doi: 10.1006/nimg.2002.1040
34. Chappell MA, Groves AR, Whitcher B, Woolrich MW. Variational bayesian inference for a nonlinear forward model. *IEEE J MagazineIEEE Trans Signal Processing.* (2009) 57:223–36. doi: 10.1109/tsp.2008.2005752
35. Lagana MM, Mendozzi L, Pelizzari L, Bergsland NP, Pugnetti L, Cecconi P, et al. Are cerebral perfusion and atrophy linked in multiple sclerosis? Evidence for a multifactorial approach to assess neurodegeneration. *Curr Neurovasc Res.* (2018) 15:282–91. doi: 10.2174/1567202616666181123164235
36. Marshall O, Chawla S, Lu H, Pape L, Ge Y. Cerebral blood flow modulation insufficiency in brain networks in multiple sclerosis: a hypercapnia MRI study. *J Cereb Blood Flow Metab.* (2016) 36:2087–95. doi: 10.1177/0271678X16654922
37. Pelizzari L, Lagana MM, Rossetto F, Bergsland N, Galli M, Baselli G, et al. Cerebral blood flow and cerebrovascular reactivity correlate with severity of motor symptoms in Parkinson's disease. *Ther Adv Neurol Disord.* (2019) 12:1756286419838354. doi: 10.1177/1756286419838354
38. Winkler AM, Ridgway GR, Webster MA, Smith SM, Nichols TE. Permutation inference for the general linear model. *Neuroimage.* (2014) 92:381–97. doi: 10.1016/j.neuroimage.2014.01.060
39. Frazier JA, Chiu S, Breeze JL, Makris N, Lange N, Kennedy DN, et al. Structural brain magnetic resonance imaging of limbic and thalamic volumes in pediatric bipolar disorder. *Am J Psychiatry.* (2005) 162:1256–65. doi: 10.1176/appi.ajp.162.7.1256
40. Sallet J, Mars RB, Noonan MP, Neubert FX, Jbabdi S, O'Reilly JX, et al. The organization of dorsal frontal cortex in humans and macaques. *J Neurosci.* (2013) 33:12255–74. doi: 10.1523/JNEUROSCI.5108-12.2013
41. Mars RB, Jbabdi S, Sallet J, O'Reilly JX, Croxson PL, Olivier E, et al. Diffusion-weighted imaging tractography-based parcellation of the human parietal cortex and comparison with human and macaque resting-state functional connectivity. *J Neurosci.* (2011) 31:4087–100. doi: 10.1523/JNEUROSCI.5102-10.2011
42. Smith SM, Nichols TE. Threshold-free cluster enhancement: addressing problems of smoothing, threshold dependence and localization in cluster inference. *Neuroimage.* (2009) 44:83–98.
43. Kamagata K, Motoi Y, Hori M, Suzuki M, Nakanishi A, Shimoji K, et al. Posterior hypoperfusion in Parkinson's disease with and without dementia measured with arterial spin labeling MRI. *J Magn Reson Imaging.* (2011) 33:803–7. doi: 10.1002/jmri.22515
44. Madhyastha TM, Askren MK, Boord P, Zhang J, Leverenz JB, Grabowski TJ. Cerebral perfusion and cortical thickness indicate cortical involvement in mild Parkinson's disease. *Mov Disord.* (2015) 30:1893–900. doi: 10.1002/mds.26128
45. Albrecht F, Ballarín T, Neumann J, Schroeter ML. FDG-PET hypometabolism is more sensitive than MRI atrophy in Parkinson's disease: a whole-brain multimodal imaging meta-analysis. *Neuroimage Clin.* (2019) 21:101594. doi: 10.1016/j.nicl.2018.11.004
46. Gonzalez-Redondo R, Garcia-Garcia D, Clavero P, Gasca-Salas C, Garcia-Eulate R, Zubieta JL, et al. Grey matter hypometabolism and atrophy in Parkinson's disease with cognitive impairment: a two-step process. *Brain.* (2014) 137:2356–67. doi: 10.1093/brain/awu159
47. Wolters FJ, Zonneveld HI, Hofman A, van der Lugt A, Koudstaal PJ, Vernooij MW, et al. Cerebral perfusion and the risk of dementia: a population-based study. *Circulation.* (2017) 136:719–28. doi: 10.1161/CIRCULATIONAHA.117.027448
48. Baglio F, Blasi V, Falini A, Farina E, Mantovani F, Olivetto F, et al. Functional brain changes in early Parkinson's disease during motor response and motor inhibition. *Neurobiol Aging.* (2011) 32:115–24. doi: 10.1016/j.neurobiolaging.2008.12.009
49. Saeed U, Compagnone J, Aviv RI, Straffella AP, Black SE, Lang AE, et al. Imaging biomarkers in Parkinson's disease and Parkinsonian syndromes: current and emerging concepts. *Transl Neurodegener.* (2017) 6:8. doi: 10.1186/s40035-017-0076-6
50. Husain M, Nachev P. Space and the parietal cortex. *Trends Cogn Sci.* (2007) 11:30–6. doi: 10.1016/j.tics.2006.10.011
51. Igelstrom KM, Graziano MSA. The inferior parietal lobule and temporoparietal junction: a network perspective. *Neuropsychologia.* (2017) 105:70–83. doi: 10.1016/j.neuropsychologia.2017.01.001
52. Shindo A, Terada S, Sato S, Ikeda C, Nagao S, Oshima E, et al. Trail making test part a and brain perfusion imaging in mild Alzheimer's disease. *Dement Geriatr Cogn Dis Extra.* (2013) 3:202–11. doi: 10.1159/000350806
53. Kish SJ, Shannak K, Hornykiewicz O. Uneven pattern of dopamine loss in the striatum of patients with idiopathic Parkinson's disease. Pathophysiologic and clinical implications. *N Engl J Med.* (1988) 318:876–80. doi: 10.1056/NEJM198804073181402
54. Burton EJ, McKeith IG, Burn DJ, Williams ED, O'Brien JT. Cerebral atrophy in Parkinson's disease with and without dementia: a comparison with Alzheimer's disease, dementia with Lewy bodies and controls. *Brain.* (2004) 127:791–800. doi: 10.1093/brain/awh088
55. Nagano-Saito A, Washimi Y, Arahata Y, Kachi T, Lerch JP, Evans AC, et al. Cerebral atrophy and its relation to cognitive impairment in Parkinson disease. *Neurology.* (2005) 64:224–9. doi: 10.1212/01.WNL.0000149510.41793.50
56. Litvan I, Goldman JG, Troster AI, Schmand BA, Weintraub D, Petersen RC, et al. Diagnostic criteria for mild cognitive impairment in Parkinson's disease: movement disorder society task force guidelines. *Mov Disord.* (2012) 27:349–56. doi: 10.1002/mds.24893
57. De Pablo-Fernandez E, Lees AJ, Holton JL, Warner TT. Prognosis and Neuropathologic Correlation of Clinical Subtypes of Parkinson Disease. *JAMA Neurol.* (2019) 76:470–9. doi: 10.1001/jamaneuro.2018.4377
58. Pelizzari L, Di Tella S, Lagana MM, Bergsland N, Rossetto F, Nemni R, et al. (2020). White matter alterations in early Parkinson's disease: role of motor symptom lateralization. *Neurol Sci.* 41:357–64. doi: 10.1007/s10072-019-04084-y
59. Jackson PA, Pialoux V, Corbett D, Drogos L, Erickson KI, Eskes GA, et al. Promoting brain health through exercise and diet in older adults: a physiological perspective. *J Physiol.* (2016) 594:4485–98. doi: 10.1113/JP271270

**Conflict of Interest:** The authors declare that the research was conducted in the absence of any commercial or financial relationships that could be construed as a potential conflict of interest.

Copyright © 2020 Pelizzari, Di Tella, Rossetto, Lagana, Bergsland, Pirastru, Meloni, Nemni and Baglio. This is an open-access article distributed under the terms of the Creative Commons Attribution License (CC BY). The use, distribution or reproduction in other forums is permitted, provided the original author(s) and the copyright owner(s) are credited and that the original publication in this journal is cited, in accordance with accepted academic practice. No use, distribution or reproduction is permitted which does not comply with these terms.



# Cortical and Deep Gray Matter Perfusion Associations With Physical and Cognitive Performance in Multiple Sclerosis Patients

## OPEN ACCESS

### Edited by:

Itamar Ronen,  
Leiden University Medical  
Center, Netherlands

### Reviewed by:

Govind Nair,  
National Institutes of Health (NIH),  
United States  
Jan Petr,  
Helmholtz-Zentrum  
Dresden-Rossendorf,  
Helmholtz-Gemeinschaft Deutscher  
Forschungszentren (HZ), Germany

### \*Correspondence:

Robert Zivadinov  
rzivadinov@bnac.net

### Specialty section:

This article was submitted to  
Applied Neuroimaging,  
a section of the journal  
Frontiers in Neurology

**Received:** 17 March 2020

**Accepted:** 09 June 2020

**Published:** 17 July 2020

### Citation:

Jakimovski D, Bergsland N,  
Dwyer MG, Traversone J,  
Hagemeier J, Fuchs TA,  
Ramasamy DP, Weinstock-Guttman B,  
Benedict RHB and Zivadinov R (2020)  
Cortical and Deep Gray Matter  
Perfusion Associations With Physical  
and Cognitive Performance in Multiple  
Sclerosis Patients.  
Front. Neurol. 11:700.  
doi: 10.3389/fneur.2020.00700

Dejan Jakimovski<sup>1</sup>, Niels Bergsland<sup>1,2</sup>, Michael G. Dwyer<sup>1</sup>, John Traversone<sup>1</sup>,  
Jesper Hagemeier<sup>1</sup>, Tom A. Fuchs<sup>1,3</sup>, Deepa P. Ramasamy<sup>1</sup>, Bianca Weinstock-Guttman<sup>3</sup>,  
Ralph H. B. Benedict<sup>3</sup> and Robert Zivadinov<sup>1,4\*</sup>

<sup>1</sup> Department of Neurology, Buffalo Neuroimaging Analysis Center, Jacobs School of Medicine and Biomedical Sciences, University at Buffalo, State University of New York, Buffalo, NY, United States, <sup>2</sup> IRCCS, Fondazione Don Carlo Gnocchi, Milan, Italy, <sup>3</sup> Department of Neurology, Jacobs Multiple Sclerosis Center, Jacobs School of Medicine and Biomedical Sciences, University at Buffalo, The State University of New York, Buffalo, NY, United States, <sup>4</sup> Center for Biomedical Imaging at Clinical Translational Science Institute, University at Buffalo, State University of New York, Buffalo, NY, United States

**Background:** Reports suggest presence of cerebral hypoperfusion in multiple sclerosis (MS). Currently there are no studies that examine if the cerebral MS perfusion is affected by presence of cardiovascular comorbidities.

**Objective:** To investigate associations between cerebral perfusion and disease outcomes in MS patients with and without comorbid cardiovascular diseases (CVD).

**Materials:** One hundred three MS patients (75.7% female) with average age of 54.4 years and 21.1 years of disease duration underwent 3T MRI dynamic susceptibility contrast (DSC) imaging and were tested with Expanded Disability Status Scale, Multiple Sclerosis Severity Score (MSSS), Timed 25-Foot Walk (T25FW), 9-Hole Peg Test (9HPT) and Symbol Digit Modalities Test (SDMT). Structural and perfusion-based normalized measures of cerebral blood flow (nCBF), cerebral blood volume (nCBV) and mean transit time (MTT) of global, tissue-specific and deep gray matter (DGM) areas were derived. CBV and CBF were normalized by the normal-appearing white matter counterpart.

**Results:** In linear step-wise regression analysis, age- and sex-adjusted, MSSS ( $R^2 = 0.186$ ) was associated with whole brain volume (WBV) ( $\beta = -0.244$ ,  $p = 0.046$ ) and gray matter (GM) nCBF ( $\beta = -0.22$ ,  $p = 0.035$ ). T25FW ( $R^2 = 0.278$ ) was associated with WBV ( $\beta = -0.289$ ,  $p = 0.012$ ) and hippocampus nCBV ( $\beta = -0.225$ ,  $p = 0.03$ ). 9HPT ( $R^2 = 0.401$ ) was associated with WBV ( $\beta = 0.195$ ,  $p = 0.049$ ) and thalamus MTT ( $\beta = -0.198$ ,  $p = 0.032$ ). After adjustment for years of education, SDMT ( $R^2 = 0.412$ ) was explained by T2-lesion volume ( $\beta = -0.305$ ,  $p = 0.001$ ), and GM nCBV ( $\beta = 0.236$ ,

$p = 0.013$ ). No differences in MTT, nCBF nor nCBV measures between patients with ( $n = 42$ ) and without CVD ( $n = 61$ ) were found. Perfusion-measures were also not able to distinguish CVD status in a logistic regression model.

**Conclusion:** Decreased GM and deep GM perfusion is associated with poorer MS outcomes, but not with presence of CVD.

**Keywords:** MS, cerebral arterial blood flow, cognition, cardiovascular disease, hypertension, hyperlipidemia, heart disease, perfusion

## INTRODUCTION

Multiple sclerosis (MS) is a chronic inflammatory and demyelinating autoimmune disease of the central nervous system (CNS), characterized by episodes of neurological worsening, followed by either complete or partial restoration and concurrent neurodegeneration (1). Furthermore, varying proportion MS patients (from 35% in relapsing-remitting, up to 60% in secondary progressive MS) exhibit a significant cognitive impairment, particularly within the domain of cognitive processing speed (2). New and improved disease modifying treatments (DMTs) and greater access to specialized MS healthcare have led to a substantial increase in overall MS prevalence, as a result of decreased mortality rate while maintaining steady incidence rate (3). With an aging MS population, clinicians and researchers alike have raised concerns regarding an increased risk and frequency of vascular comorbidities like myocardial infarction, stroke, hypertension, heart failure, and abnormal lipid profiles when compared to healthy controls (4). Presence of these pathological vascular abnormalities have the potential to decrease overall quality of life, worsen cerebral perfusion and may additionally contribute to greater disease progression (5). Furthermore, patients affected by cerebrovascular diseases are associated with worse cognitive performance and MRI-derived MS outcomes (5).

To assess changes in cerebral perfusion and its implications on pathological MS processes, multiple studies have used various MRI methods including dynamic susceptibility contrast (DSC), dynamic contrast-enhanced (DCE) and arterial spin labeling (ASL) perfusion-weighted imaging (PWI) (6). As such, these methods can provide valuable quantitative measures like total cerebral blood volume (CBV) and cerebral blood flow (CBF) (6). The processes of MS lesion formation and repair are dependent on continuous influx of inflammatory cells, successful debridement, and delivery of oxygenated blood. A large perfusion-based study showed discrepancies between greater lesion formation occurring in highly perfused white matter (WM) compared to greater accumulation of chronic MS lesion in physiologically hypoperfused areas (7). Moreover, perfusion measures are able to expose previously undetected widespread changes in the otherwise normal-appearing brain tissue and supplement the classically monitored MS lesions. In similar manner, hypoperfusion of the thalamus, a deep gray matter (DGM) region highly implicated in MS, has been associated with worse disability and composite clinical scores (8). Lastly, MS patients with cognitive impairment demonstrate greater

cortical perfusion deficits despite any evidence of structural abnormalities or significant brain atrophy (9). The changes in DSC and ASL-based perfusion measures within the cortical and DGM in MS patients and their association with clinical outcomes have been recently reviewed elsewhere (6). These findings were supplemented by a study showing associations of decreased total cerebral extracranial blood inflow and lower cognitive performance (10). However, no MS studies have previously investigated changes in cerebral perfusion in regards to presence of comorbid cardiovascular diseases (CVD).

Based on this background, we hypothesized that presence of cerebral perfusion abnormalities within the GM are associated with MS-specific clinical and cognitive performance of a large sample of heterogeneous MS population, and that perfusion measures are associated with presence of CVD.

## MATERIALS AND METHODS

### Study Population

Patients were recruited within a larger, prospective, longitudinal study that aimed to determine association between MRI and cardiovascular, genetic and environmental characteristics of MS patients (CEG-MS) (11, 12). The inclusion criteria for the MS patients were: (1) age between 18 and 75 years old, (2) being diagnosed with MS per 2010-revised McDonald criteria (13) or being clinically isolated syndrome (CIS) patients, (3) have MRI examination within 30 days of the clinical visit, (4) presence of PWI-based sequences in the MRI protocol, (5) availability of cognitive testing. Contrarily, MS patients were excluded if: (1) having clinically-defined relapse or have received intravenous corticosteroids within 30 days of the MRI examination, (2) pregnant or nursing mother, (3) having anatomical extracranial or intracranial vascular malformation like Parkes-Weber, Servedio-Martorell, Klippel-Trenaunay-Weber, or Budd-Chiari syndromes, (4) major depressive disorder or any other psychiatric comorbidities that can potentially influence cognitive performance and (5) presence of other major neurological disorders. An experienced neurologist examined the MS patients. Expanded Disability Status Scale (EDSS) and Multiple Sclerosis Severity Score (MSSS) were used to characterize disability levels (14, 15). Furthermore, timed 25-foot walk (T25FW) and 9-hole peg test (9HPT) were additionally administered (16, 17). Longer test times indicate worse walking and hand function, respectively. Symbol Digit Modalities Test (SDMT) determined cognitive processing speed performance, where higher raw scores indicated better performance (18). The MS phenotypes of



relapsing-remitting MS (RRMS) and progressive MS (PMS) were determined based on medical history and clinical presentation as per 2013 Lublin criteria (19). Clinical information regarding disease duration, 5-year relapse rate, presence of CVD was collected by structured in-person questionnaire and further corroborated with electronic medical records, as previously reported (5, 10, 20). Diagnosis of heart disease, hypertension, diabetes, and hyperlipidemia and body-mass-index (BMI) were assessed. BMI  $\geq 30$  was considered as obesity. Lastly, the use of disease modifying treatment (DMT) was determined and categorized. All participants signed written consent form and local Institutional Review Board (IRB) approved the study.

## MRI Acquisition and Analysis

The MS patients underwent an MRI examination on a 3T Signa Excite HD 12 Twin-Speed scanner (GE, Milwaukee, WI, USA) equipped with 8-channel head and neck coil. Sequences/acquisitions used in this analysis included: (1) 3D spoiled-gradient recalled (SPGR) high-resolution T1w(weighted) sequence with echo time(TE)/inversion time(IR)/repetition time(TR) of 2.8/900/5.9 ms, flip angle (FLIP) of 10 degrees, voxel size of  $1 \times 1 \times 1 \text{ mm}^3$  and no gaps, (2) Fluid attenuated inversion recovery (FLAIR) sequence with TE/IR/TR of 120/2,100/8,500 ms, FLIP = 90 degrees and same voxel size of  $1 \times 1 \times 1 \text{ mm}^3$  with no gap, (3) Dynamic susceptibility contrast (DSC) was acquired with a single-shot echo-planar imaging sequence with TR/TE of 2,275/45 ms, FLIP = 90 degrees, echo train length = 1, bandwidth = 250 kHz,  $1 \times 1 \times 4 \text{ mm}^3$  without gap which was acquired during and after injection of during and after injection of 15 ml of 0.1 mM/kg gadolinium-diethylenetriamine penta-acetic acid by power injector at speed of 5 ml/s. A total of 40 volumes were acquired.

T2 lesion volume (LV) was determined by an experienced clinical neuroimager (13 years of experience) using a validated semi-automated contouring/thresholding procedure conducted with Java Imaging Manipulation (JIM) software (Xinapse Systems, version 6.0, Essex, UK) on FLAIR sequence. Intra-rater agreement is evaluated annually with good agreement (ICC  $\geq 0.8$ ). Global volumes of whole brain (WBV; WBV = GMV + WMV + cerebellar volume), WM (WMV), gray matter and (GMV; GMV = cortical + deep gray matter) were derived by SIENAX software (FMRIB, Oxford, UK) and scaled for differences in skull size (by using the SIENAX scaling factor) (21). FMRIB's Integrated Registration and Segmentation Tool (FIRST) software derived the regional, nuclei-specific volumes of total DGM, thalamus, caudate, putamen, globus pallidus, and hippocampus. In order to prevent tissue misclassification, both global and nuclei specific volumes were derived after inpainting for T1 hypointense lesions which were semi-automatically segmented on the T1w sequence.

The PWI-derived measures of cerebral blood volume (CBV), cerebral blood flow (CBF), and mean transit time (MTT) were calculated with the JIM Perfusion tool. To obtain the arterial input function, we utilized the automatic arterial input (AIF) function detection feature, which searches for voxels that have AIF-like behavior. For all analyses, the selected voxels were visually inspected to ensure accurate identification.

By utilizing the first steady-state volume before contrast arrival, FMRIB's Linear Image Registration Tool (FLIRT) was used to bring other images into DSC space with a rigid body registration. Mean values for CBV, CBF, and MTT were calculated in the SIENAX and FIRST-based ROIs. (Supplement Figure 1). As an absolute quantification of CBV and CBF could not be performed due to technical limitations of the DSC sequence

**TABLE 1 |** Demographic, clinical, and cognitive characteristics of the study population.

Demographic and clinical characteristics	MS (n = 103)	CIS+RRMS (n = 63)	PMS (n = 40)	RRMS vs. PMS p-value
Female, n (%)	78 (75.7)	47 (74.6)	31 (77.5)	0.738
Age, mean (SD)	54.5 (11.7)	49.9 (11.8)	61.5 (7.3)	<b>&lt;0.001</b>
Disease duration, mean (SD)	21.1 (10.9)	17.1 (9.6)	27.4 (9.9)	<b>&lt;0.001</b>
EDSS, median (IQR)	3.0 (1.5–6.0)	2.0 (1.5–2.63)	6.5 (4.0–6.5)	<b>&lt;0.001</b>
MSSS, median (IQR)	2.26 (1.0–5.6)	1.28 (0.78–2.49)	5.6 (3.4–6.7)	<b>&lt;0.001</b>
BMI, mean (SD)	27.3 (5.3)	27.0 (5.3)	27.9 (5.4)	0.42
Obese, n (%)	27 (26.2)	13 (20.6)	14 (35.0)	0.115
At least one CVD, n (%)	42 (40.7)	22 (34.9)	20 (50.0)	0.129
Hypertension, n (%)	18 (17.5)	5 (7.9)	13 (32.5)	<b>0.001</b>
Hyperlipidemia, n (%)	24 (23.3)	12 (19.0)	12 (30.0)	0.2
Heart disease, n (%)	14 (13.6)	10 (15.9)	4 (10.0)	0.397
Diabetes, n (%)	2 (1.9)	0 (0)	2 (5.0)	-
5-year relapse rate, mean (SD)	0.155 (0.377)	0.232 (0.459)	0.031 (0.088)	<b>0.008</b>
T25FW, median (IQR)	5.4 (4.5–7.7)	4.8 (4.3–5.8)	7.7 (6.2–13.5)	<b>&lt;0.001</b>
9HPT, median (IQR)	23.4 (19.9–30.4)	20.9 (18.9–24.5)	29.4 (24.5–41.3)	<b>&lt;0.001</b>
SDMT, mean (SD)	49.5 (14.8)	53.8 (13.3)	42.6 (14.5)	<b>&lt;0.001</b>
<b>DMT use, n (%)</b>	<b>31 (30.1)</b>	<b>23 (36.5)</b>	<b>8 (20)</b>	<b>0.742</b>
Interferon-beta				
Glatiramer acetate	28 (27.2)	15 (23.8)	13 (32.5)	
Natalizumab	3 (2.9)	2 (3.2)	1 (2.5)	
Oral medications	10 (9.7)	6 (9.5)	4 (10)	
Off-label medications	5 (4.9)	3 (4.8)	2 (5)	
No DMT use	26 (25.2)	14 (22.2)	12 (30)	

MS, multiple sclerosis; CIS, clinically isolated syndrome; RRMS, relapsing remitting MS; PMS, progressive MS; EDSS, expanded disability status scale; MSSS, multiple sclerosis severity score; BMI, body mass index; T25FW, timed 25-foot walk; 9HPT, 9-hole peg test; SDMT, symbol digit modalities test; DMT, disease modifying treatment; CVD, cardiovascular disease; SD, standard deviation; IQR, interquartile range. Oral medications included dimethyl fumarate, teriflunomide, and fingolimod, whereas off-label medications included intravenous immunoglobulins, azathioprine, rituximab, mitoxantrone. Comparisons between the groups were performed by Student's t-test,  $\chi^2$  and Mann-Whitney U-test, accordingly.  $P < 0.05$  were considered statistically significant and shown in bold.

utilized, we normalized all derived perfusion parameters to the normal-appearing WM (NAWM) (22). On the other hand, MTT is an absolute measure and was quantified in seconds. Only the

WBV was utilized as a structural volumetric measure in the models described hereafter.

## Statistical Analysis

The statistical analyses were performed using SPSS version 25.0 (IBM, Armonk, NY, USA). The data distribution was assessed by Kolmogorov-Smirnov test and by visual inspection of Q-Q plots. EDSS and MSSS were normalized by natural logarithmic transformation. For normalization of T25FW and 9HPT, two-step approach was utilized. After initial transformation of the data into fractional ranks, an inverse distribution function utilized the mean and standard deviation and returned the values into normal distribution where the cumulative probability is  $\text{Prob}(X < x)$ . For demographic, clinical, and cognitive comparisons between the RRMS and PMS groups,  $\chi^2$ , Student's *t*-test, Mann-Whitney *U*-test, and age- and sex-adjusted analysis of covariance (ANCOVA) were used. Five linear regression models assessed associations between each specific clinical or cognitive outcomes with the MRI-derived measures. The models were constructed by initial block that adjusted for effects derived from age, sex, and years of education. The second block utilized step-wise hierarchical inclusion of scalar WBV and perfusion-based variables (independent) with an increasing explanatory power of respective outcome variance (dependent). Regression-based  $R^2$ , standard error of the estimate, standardized  $\beta$ , and *t*-statistics were reported.  $P < 0.05$  were considered statistically significant. The significant predictors in the models were also adjusted for multiple comparisons using false discovery rate (Benjamini-Hochberg procedure). Differences in MTT between MS patients with and without at least one of the aforementioned cardiovascular disease were determined by age-adjusted ANCOVA analysis. Logistic regression model determined MRI-based predictors of CVD presence. Lastly, the absolute values derived by automatic arterial input (AIF) are compared between patients with and without CVD.

## RESULTS

### Demographic, Clinical, Cognitive, and MRI-Based Characteristics

Demographic, clinical and cognitive characteristics of the study population are shown in Table 1. A total of 103 MS patients was composed of 63 CIS/RRMS (6 CIS and 57 RRMS) and 40 PMS individuals and had an average age of 54.5 years, disease duration of 21.1 years, 5-year relapses rate of 0.155, median disability EDSS score of 3.0 and median MSSS score of 2.26. In particular, the median T25FW and 9HPT performance were 5.4 s and 23.4 s, respectively. Similarly, the average SDMT performance was 49.5. Use pattern of DMT is also shown in Table 1. Forty two MS patients (40.7%) had a diagnosis of at least one CVD. In particular, 18 (17.5%) MS patients had hypertension, 24 (23.3%) hyperlipidemia, 14 (13.6%) heart disease, 27 (26.2%) were obese, and 2 (1.9%) diabetes. As expected, the PMS population was older (Student's *t*-test,  $p < 0.001$ ), had longer disease duration (Student's *t*-test,  $p < 0.001$ ), had greater disability scores (Mann Whitney *U*-test,  $p < 0.001$  for

**TABLE 2 |** Association between clinical MS scores (EDSS and MSSS) and MRI-derived measures.

EDSS	$R^2$	SE of estimate	<i>t</i> -statistics	Standardized $\beta$	<i>p</i> -value
Block 1	0.325	0.55			
Sex	–	–	0.318	0.029	0.751
Patients' age	–	–	6.142	0.566	<b>&lt;0.001*</b>
<b>Block 2</b>					
+WBV	0.409	0.52	–3.366	–0.345	<b>0.001*</b>
<b>MSSS</b>					
Block 1	0.115	0.92			
Sex	–	–	–0.499	–0.052	0.619
Patients' age	–	–	3.285	0.343	<b>0.001*</b>
<b>Block 2</b>					
+ GM nCBF	0.155	0.89	–2.14	–0.22	<b>0.035</b>
+ WBV	0.186	0.87	–2.027	–0.244	<b>0.046</b>
<b>T25FW</b>					
Block 1	0.161	20.6			
Sex	–	–	3.635	0.078	0.459
Patients' age	–	–	0.744	0.381	<b>&lt;0.001*</b>
<b>Block 2</b>					
+ WBV	0.232	19.9	–2.582	–0.289	<b>0.012*</b>
+ Hippocampus nCBV	0.278	19.4	–2.214	–0.225	<b>0.03</b>
<b>9HPT</b>					
Block 1	0.333	20			
Sex	–	–	3.656	0.367	<b>&lt;0.001*</b>
Patients' age	–	–	2.22	0.198	<b>0.029*</b>
<b>Block 2</b>					
+ Thalamus MTT	0.371	19.6	–1.992	–0.198	<b>0.032</b>
+ WBV	0.401	19.2	2.177	0.195	<b>0.049</b>
<b>SDMT</b>					
Block 1	0.276	12.6			
Sex	–	–	–0.831	–0.078	0.408
Patients' age	–	–	–5.068	–0.477	<b>&lt;0.001*</b>
Years of education	–	–	1.992	0.186	0.05
<b>Block 2</b>					
+ T2 LV	0.364	11.9	–3.364	–0.305	<b>0.001*</b>
+ GM nCBV	0.412	11.5	2.546	0.236	<b>0.013*</b>

MS, multiple sclerosis; EDSS, Expanded Disability Status Scale; MSSS, Multiple Sclerosis Severity Score; T25FW, Timed 25-foot walk; 9HPT, 9-hole peg test; SDMT, Symbol Digit Modalities Test; WBV, whole brain volume; GM, gray matter; nCBF, normalized cerebral blood flow; nCBV, normalized cerebral blood volume; MTT, mean transit time; LV, lesion volume; SE, standardized error. Higher EDSS and MSSS score indicate greater disability. Longer T25FW time (in seconds) indicates worse walking ability. Longer 9HPT time (in seconds) indicates poorer hand performance. Higher SDMT score indicates better cognitive processing speed.

The regression models were constructed by initial block which force entered and adjusted for effects derived from age and sex (regardless of their significance). The second block utilized step-wise hierarchical inclusion of variables (independent) with an increasing explanatory power of respective outcome variance (dependent). Only significant predictors that provide additional power outside of block 1 are included in this block. In the case of SDMT model, years of education is additionally added in the first force entered block.

$P < 0.05$  were considered statistically significant and shown in bold. \* - Survives false discovery rate (FDR) correction with Benjamini-Hochberg procedure.

both EDSS and MSSS), had poorer walking, hand and cognitive processing speed performance (Mann-Whitney *U*-test, all  $p < 0.001$ ) and had significantly lower 5-year relapse rate (Mann-Whitney *U*-test,  $p = 0.008$ ). PMS patients had numerically greater number of CVD and significantly higher percent of them were hypertensive ( $\chi^2$ ,  $p = 0.001$ ).

The specific global, regional and lesion brain volumes of the study population are shown in **Supplement Table 1**.

## Associations Between Clinical, Cognitive, and Perfusion-Based Measures

The association between clinical scores, walking performance, hand performance and cognitive processing speed performance with MRI-derived measures are shown in **Table 2**. After adjustment for age and sex, greater EDSS scores were associated with smaller WBV ( $R^2$  increase from 32.5 to 40.9%, WBV standardized  $\beta = -0.345$ ,  $t$ -statistics =  $-3.366$ , and  $p = 0.001$ ). On the other hand, in addition to age and sex, the MSSS variance was additionally explained by GM nCBF ( $R^2$  increase of 4.0%, standardized  $\beta = -0.22$ ,  $t$ -statistics =  $-2.14$ ,  $p = 0.035$ ) and WBV ( $R^2$  increase of 2.9%, standardized  $\beta = -0.244$ ,  $t$ -statistics =  $-2.027$ , and  $p = 0.046$ ). When WBV was introduced in the first initial correction regression step, the GM nCBF was retained in the step-wise model.

Age and sex explained a total of 16.1% of T25FW performance variance. Both WBV ( $R^2$  increase of 7.1%, standardized  $\beta = -0.289$ ,  $t$ -statistics =  $-2.582$ , and  $p = 0.012$ ) and hippocampus nCBV (additional  $R^2$  increase of 4.6%, standardized  $\beta = -0.225$ ,  $t$ -statistics =  $-2.214$ , and  $p = 0.03$ ) were able to further explain greater variance.

In a similar manner, age and sex were able to explain 33.6% of hand dexterity (9HPT) performance variance. Two additional variables were included in the step-wise hierarchical modeling. First, the thalamus MTT provided an additional 3.8%  $R^2$  increase (standardized  $\beta = -0.198$ ,  $t$ -statistics =  $-1.992$ ,  $p = 0.032$ ). Furthermore, WBV explained 3.0% more  $R^2$  variance (standardized  $\beta = 0.195$ ,  $t$ -statistics =  $2.177$ ,  $p = 0.049$ ). Similarly to the MSSS analysis, when the WBV variable was in the first block of controlling variables, the thalamus MTT was also retained in the model.

Finally, 27.6% of cognitive processing speed performance variance was initially explained by sex, age, and years of education alone. Further  $R^2$  increases were noted by adding T2-LV ( $R^2$  increase of 8.8%, standardized  $\beta = -0.305$ ,  $t$ -statistics =  $-3.364$ ,  $p = 0.001$ ) and GM nCBV ( $R^2$  increase of 4.8%, standardized  $\beta = 0.236$ ,  $t$ -statistics =  $2.546$ ,  $p = 0.013$ ). GM nCBV was the only significant perfusion-based predictor after multiple comparison correction for all regression models. Scatter plot representation for the final regression-based prediction models for 9HPT, T25FW, and SDMT are shown in **Figure 1**.

## Cardiovascular Diseases and Differences in Perfusion Measures

The demographic and clinical characteristics of MS patients with and without at least one CVD diagnosis are shown in **Table 3**.

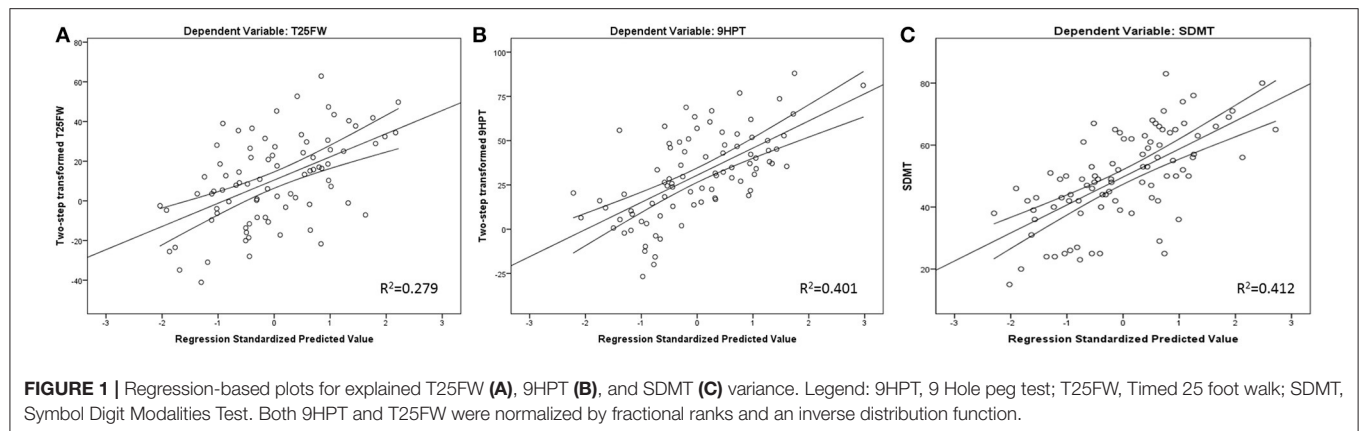
**TABLE 3 |** Differences in MTT between MS patients with and without at least one CVD.

Demographic and clinical characteristics	MS CVD + ( <i>n</i> = 42)	MS CVD – ( <i>n</i> = 61)	CVD + vs. CVD – <i>p</i> -value
Female, <i>n</i> (%)	32 (76.2)	46 (75.4)	0.928
Age, mean (SD)	58.7 (9.3)	51.5 (5.4)	<b>0.002</b>
BMI, mean (SD)	28.5 (5.1)	26.6 (5.4)	0.08
Obese, <i>n</i> (%)	16 (38.1)	11 (18.0)	<b>0.039</b>
CIS/RRMS/PMS	2/20/20	4/37/20	0.357
Disease duration, mean (SD)	23.5 (11.1)	19.4 (10.5)	0.065
EDSS, median (IQR)	3.25 (1.88–6.5)	2.0 (1.5–6.0)	0.177
MSSS, median (IQR)	2.28 (1.28–6.0)	2.23 (0.92–5.1)	0.408
5-year relapse rate, mean (SD)	0.113 (0.364)	0.184 (0.385)	0.356
T25FW, median (IQR)	5.7 (4.6–8.2)	5.2 (4.5–6.9)	0.343
9HPT, median (IQR)	25.2 (21.7–32.7)	21.6 (19.1–29.1)	<b>0.028</b>
SDMT, mean (SD)	48.1 (14.8)	50.5 (14.8)	0.44
<b>DSC measures, mean (SD)</b>	<b>Age-adjusted ANCOVA</b>		
NABT MTT	3.47 (0.7)	3.44 (0.7)	0.802
NAWM MTT	3.52 (0.7)	3.5 (0.7)	0.836
GM MTT	3.44 (0.8)	3.42 (0.7)	0.721
DGM MTT	3.3 (0.8)	3.21 (0.7)	0.903
Thalamus MTT	3.25 (0.9)	3.1 (0.8)	0.768
GM nCBV	1.79 (0.15)	1.8 (0.25)	0.725
DGM nCBV	1.57 (0.1)	1.56 (0.17)	0.566
Thalamus nCBV	1.57 (0.16)	1.54 (0.19)	0.482
GM nCBF	1.95 (0.35)	1.9 (0.28)	0.209
DGM nCBF	1.89 (0.38)	1.83 (0.26)	0.258
Thalamus nCBF	1.72 (0.29)	1.71 (0.29)	0.414

MS, multiple sclerosis; CVD, cardiovascular disease; BMI, body mass index; MTT, mean transit time; nCBV, normalized cerebral blood volume; nCBF, normalized cerebral blood flow; EDSS, Expanded Disability Status Scale; MSSS, Multiple Sclerosis Severity Score; T25FW, timed 25-foot walk; 9HPT, 9-hole peg test; SDMT, Symbol Digit Modalities Test; NABT, normal-appearing brain tissue; NAWM, normal-appearing white matter; GM, gray matter; DGM, deep gray matter.

Comparison between the MS patients with (CVD +) and without (CVD –) at least one CVD disease were done by Student's *t*-test,  $\chi^2$  and Mann-Whitney *U*-test, accordingly. Analysis of covariance (ANCOVA) was used to compare perfusion-based MTT/nCBV/nCBF measures. Normalized CBV and CBF are calculated as a ratio of the respective measure in NAWM.  $P < 0.05$  were considered statistically significant and shown in bold.

Although the CVD+ group had numerically more PMS patients (47.6 vs. 32.8%), this did not reach statistical significance ( $\chi^2$ ,  $p = 0.357$ ). In terms of perfusion-based measures, there were no significant differences between the MS patients with or without at least one CVD. Apart from age, presence of CVD was not predicted by any DSC measure in a step-wise logistic regression model [age Exp(B) = 1.087,  $p = 0.008$ ]. Exploratory analysis of the logistic regression model showed that higher thalamic MTT



was the only trending variable (stand-alone main effect of higher thalamic MTT values and presence of CVD with  $p = 0.052$ ) Lastly, comparison of raw CBV and CBF (i.e., not normalized to NAWM) values were compared between MS patients with and without CVD and are shown in **Supplement Table 2**.

## DISCUSSION

In this study, we demonstrated significant associations between clinical and cognitive processing speed performance of MS patients with decreased cerebral perfusion as measured by DSC-PWI. These associations were independent of T2-LV and WBV effects and explained additional physical and cognitive disability variance. There were no differences in PWI-derived MTT between patients with at least one CVD when compared to patients without cardiovascular comorbidities.

Previous MS perfusion studies have reported mixed results with most studies demonstrating cerebral hypoperfusion and its effect on MS outcomes. As such, our results fall in line with the majority of the literature, which highlights the importance of cortical perfusion and its effect on MS outcomes including physical disability, cognitive impairment, and fatigue. For example, a small study of 22 MS patients and 11 age- and sex-matched healthy controls demonstrated associations between lower DGM CBV and CBF measures with patient-reported fatigue severity (23). Another recent MS voxel-based morphometry report demonstrated presence of significant reduction of both GM and DGM perfusion despite the lack of structural pathology (24). In addition, hypoperfusion was associated with impaired cognitive processing speed and lower performance on memory tests (24, 25). On the contrary, few studies were not able to replicate the perfusion findings reported in the literature finding lack of associations (26). A recent comprehensive summary of all previous perfusion studies and their results has been published elsewhere (4).

The importance of sufficient cerebral perfusion in maintaining proper cognitive functioning is recently highlighted in both cross-sectional and longitudinal studies of otherwise cognitively intact healthy population. For an example, a recent 2-year long longitudinal ASL study showed that healthy individuals with decline in GM CBF present with concurrent decline

in other markers of brain aging including lower cortical volume, worse WM microstructural integrity, and greater appearance of WM hyperintensities (27). More importantly, the longitudinal GM CBF decline was associated with worsening of the cognitive processing speed (27). Reduction in cerebral perfusion has been also hypothesized as early marker of multiple neurodegenerative diseases, greater cerebral protein accumulation, and as a predictor of dementia development (28). As such, a population-based study has demonstrated that lower cerebral perfusion is associated with 31% greater risk of Alzheimer's disease development and accelerated decline in cognition (29). Lastly, presence of cardiovascular and cardiovascular-driven inflammation can expedite the cerebral vascular control and lead to greater cognitive decline (30). Given that MS patients present with greater prevalence of cardiovascular comorbidities when compared to the general population, lifestyle-based modification and appropriate CVD treatment may alleviate some of the perfusion-driven cerebral pathology (20). However, in our sample of 103 MS patients, the presence of CVD did not influence the MRI-derived perfusion measure. These findings may be explained by the low sample size and relatively low prevalence of CVDs. Furthermore, the CVD effect on MS perfusion may be more significant within an older MS population that presents with greater number of CVD comorbidities (3). Moreover, potential changes in cerebral perfusion due to persistent chronic NAWM inflammation and/or significant cortical lesions activity may be more prevalent within active MS population which is generally younger and have lower prevalence of CVD diagnoses. Lastly, since the recent hypertension guidelines have lowered the threshold to  $>130/80$  mmHg, some hypertension-perfusion interactions may be present within our non-CVD MS population (31). Future studies should aim at determining whether the MS cerebral hypoperfusion has primary or secondary etiology, its relationship with cardiovascular comorbidities and a potential additive effect on disability accrual.

In a previous work, we demonstrated that cognitively impaired MS patients present with lower total extracranial arterial blood flow (10). The smaller amount of blood entering the cranium may be directly associated with lower cerebral perfusion measures including lower CBV, CBF, and prolonged MTT. In



order to compensate for the variable extracranial blood flow, the neurovascular unit is responsible for adjusting the overall CBV by triggering vasodilatory or vasoconstrictory responses. However, recent reports suggest that MS patients present with impaired functional cerebrovascular reactivity where they are not able to compensate during hypercapnic stimuli and result with neurodegenerative changes and brain atrophy (32). Therefore, the relative inability of the cerebral circulation to adapt will result in greater dependence on the cardiac output and on systematic arterial pressure to deliver the necessary brain blood flow. Presence of cardiovascular comorbidities will further exacerbate the extracranial arterial pathology and may result with even lower blood output to the brain (33). Contrarily, intact cerebrovascular reactivity processes can sufficiently compensate for early CVD-based hypoperfusion and attempt at maintaining sufficient blood flow. Therefore, future studies should aim at assessing the multifaceted nature of cerebral perfusion control and the consequences when one or more processes start to fail.

The study presents with several limitations. The perfusion measures derived from DSC are typically relative in nature and specific to the patient's hematocrit and relaxivity of the contrast agent (6). More advanced acquisitions and post-processing can be utilized to account for such factors, but were unavailable in the present study. Although significantly affected by partial volume effects, we utilized deconvolution with arterial input function and compared the absolute CBV and CBF (6). Moreover, the normalization of  $r$  CBV and  $r$ CBF with the respective NAWM perfusion rates can be influenced by varying rate of NAWM pathology. Furthermore, MS may present with spatially discrepant GM/WM pathology ratio, where some patients exhibit significantly more affected WM and other exhibit greater GM pathology. Such examples of exclusive myelocortical pathology distribution have been recently described (34). MS patients also demonstrate variable and undetectable NAWM pathology which can alter NAWM perfusion and in this case significantly influence the nGM CBF calculation. Studies can utilize MRI sequences that are able to provide absolute blood measure quantifications like ASL or book-end DSC method together with sequences that allow GM lesion quantification. The significant variability within the physiological brain perfusion can be attributed to more than 58 different perfusion modifiers divided into four large groups (physiological, blood components, mental state and caffeine/recreational drugs) (35). In particular controlling for age, blood gases and caffeine consumption can significantly decrease the inconsistency in the perfusion literature (35). Another limitation is the lack of healthy control population. A longitudinal, case-controlled design would provide better understanding of the temporal associations between changes in perfusion and their effect on clinical or cognitive outcomes.

In conclusion, decreased GM and DGM perfusion is independently associated with poorer clinical and cognitive

outcomes in MS patients. These findings further corroborate the concurrent GM dependence of physical and cognitive functioning. Presence of cardiovascular comorbidity did not affect the perfusion-based MTT measure in this particular MS population.

## DATA AVAILABILITY STATEMENT

All datasets generated for this study are included in the article/supplementary material. The data is further available from the corresponding author upon reasonable request.

## ETHICS STATEMENT

The studies involving human participants were reviewed and approved by University at Buffalo IRB. The patients/participants provided their written informed consent to participate in this study.

## AUTHOR CONTRIBUTIONS

DJ: study concept and design, analysis and interpretation, drafting of the manuscript, critical revision of the manuscript for important intellectual content, and study supervision. RZ: study concept and design, analysis and interpretation, critical revision of the manuscript for important intellectual content, and study supervision. RB and BW-G: analysis and interpretation, critical revision of the manuscript for important intellectual content, and study supervision. DR, TF, JT, MD, NB, and JH: analysis and interpretation, critical revision of the manuscript for important intellectual content. All authors contributed to the article and approved the submitted version.

## FUNDING

Research reported in this publication was funded by the National Center for Advancing Translational Sciences of the National Institutes of Health (NIH) under award Number UL1TR001412. The content is solely the responsibility of the authors and does not necessarily represent the official views of the NIH.

## ACKNOWLEDGMENTS

We thank both Reviewers that have significantly contributed in improving the overall quality of the manuscript.

## SUPPLEMENTARY MATERIAL

The Supplementary Material for this article can be found online at: <https://www.frontiersin.org/articles/10.3389/fneur.2020.00700/full#supplementary-material>

## REFERENCES

- Thompson AJ, Baranzini SE, Geurts J, Hemmer B, Ciccarelli O. Multiple sclerosis. *Lancet*. (2018) 391:1622–36. doi: 10.1016/S0140-6736(18)30481-1
- Jakimovski D, Weinstock-Guttman B, Roy S, Jaworski M III, Hancock L, Nizinski A, et al. Cognitive profiles of aging in multiple sclerosis. *Front Aging Neurosci*. (2019) 11:105. doi: 10.3389/fnagi.2019.00105
- Vaughn CB, Jakimovski D, Kavak KS, Ramanathan M, Benedict RHB, Zivadinov R, et al. Epidemiology and treatment of multiple sclerosis in elderly populations. *Nat Rev Neurol*. (2019) 15, 329–42. doi: 10.1038/s41582-019-0183-3
- Jakimovski D, Topolski M, Genovese AV, Weinstock-Guttman B, Zivadinov R. Vascular aspects of multiple sclerosis: emphasis on perfusion and cardiovascular comorbidities. *Expert Rev Neurother*. (2019) 19:445–58. doi: 10.1080/14737175.2019.1610394
- Jakimovski D, Gandhi S, Paunkoski I, Bergsland N, Hagemeyer J, Ramasamy DP, et al. Hypertension and heart disease are associated with development of brain atrophy in multiple sclerosis: a 5-year longitudinal study. *Eur J Neurol*. (2019) 26:e87–8. doi: 10.1111/ene.13769
- Lapointe E, Li DKB, Traboulsee AL, Rauscher A. What have we learned from perfusion MRI in multiple sclerosis? *AJNR Am J Neuroradiol*. (2018) 39:994–1000. doi: 10.3174/ajnr.A5504
- Holland CM, Charil A, Csapo I, Liptak Z, Ichise M, Khoury SJ, et al. The relationship between normal cerebral perfusion patterns and white matter lesion distribution in 1,249 patients with multiple sclerosis. *J Neuroimaging*. (2012) 22:129–36. doi: 10.1111/j.1552-6569.2011.00585.x
- Doche E, Lecocq A, Maarouf A, Duhamel G, Soulier E, Confort-Gouny S, et al. Hypoperfusion of the thalamus is associated with disability in relapsing remitting multiple sclerosis. *J Neuroradiol*. (2017) 44:158–64. doi: 10.1016/j.neurad.2016.10.001
- Vitorino R, Hojjat SP, Cantrell CG, Feinstein A, Zhang L, Lee L, et al. Regional frontal perfusion deficits in relapsing-remitting multiple sclerosis with cognitive decline. *AJNR Am J Neuroradiol*. (2016) 37:1800–7. doi: 10.3174/ajnr.A4824
- Jakimovski D, Benedict RH, Marr K, Gandhi S, Bergsland N, Weinstock-Guttman B, et al. Lower total cerebral arterial flow contributes to cognitive performance in multiple sclerosis patients. *Mult Scler*. (2019) 26:201–9. doi: 10.1177/1352458518819608
- Jakimovski D, Ramanathan M, Weinstock-Guttman B, Bergsland N, Ramasamy DP, Dwyer MG, et al. Higher EBV response is associated with more severe gray matter and lesion pathology in relapsing multiple sclerosis patients: a case-controlled magnetization transfer ratio study. *Mult Scler*. (2019) 26:322–32. doi: 10.1177/1352458519828667
- Jakimovski D, Topolski M, Kimura K, Pandya V, Weinstock-Guttman B, Zivadinov R. Decrease in secondary neck vessels in multiple sclerosis: a 5-year longitudinal magnetic resonance angiography study. *Curr Neurovasc Res*. (2019) 16:215–223. doi: 10.2174/1567202616666190612111127
- Polman CH, Reingold SC, Banwell B, Clanet M, Cohen JA, Filippi M, et al. Diagnostic criteria for multiple sclerosis: 2010 revisions to the McDonald criteria. *Ann Neurol*. (2011) 69:292–302. doi: 10.1002/ana.22366
- Kurtzke JF. Rating neurologic impairment in multiple sclerosis: an expanded disability status scale (EDSS). *Neurology*. (1983) 33:1444–52. doi: 10.1212/WNL.33.11.1444
- Roxburgh RH, Seaman SR, Masterman T, Hensiek AE, Sawcer SJ, Vukusic S, et al. Multiple sclerosis severity score: using disability and disease duration to rate disease severity. *Neurology*. (2005) 64:1144–51. doi: 10.1212/01.WNL.0000156155.19270.F8
- Feys P, Lamers I, Francis G, Benedict R, Phillips G, Larocca N, et al. The nine-hole peg test as a manual dexterity performance measure for multiple sclerosis. *Mult Scler*. (2017) 23:711–20. doi: 10.1177/1352458517690824
- Motl RW, Cohen JA, Benedict R, Phillips G, Larocca N, Hudson LD, et al. Validity of the timed 25-foot walk as an ambulatory performance outcome measure for multiple sclerosis. *Mult Scler*. (2017) 23:704–10. doi: 10.1177/1352458517690823
- Benedict RH, Deluca J, Phillips G, Larocca N, Hudson LD, Rudick R, et al. Validity of the symbol digit modalities test as a cognition performance outcome measure for multiple sclerosis. *Mult Scler*. (2017) 23:721–33. doi: 10.1177/1352458517690821
- Lublin FD, Reingold SC, Cohen JA, Cutter GR, Sorensen PS, Thompson AJ, et al. Defining the clinical course of multiple sclerosis: the 2013 revisions. *Neurology*. (2014) 83:278–86. doi: 10.1212/WNL.0000000000000560
- Jakimovski D, Guan Y, Ramanathan M, Weinstock-Guttman B, Zivadinov R. Lifestyle-based modifiable risk factors in multiple sclerosis: review of experimental and clinical findings. *Neurodegener Dis Manag*. (2019) 9:149–72. doi: 10.2217/nmt-2018-0046
- Smith SM, Zhang Y, Jenkinson M, Chen J, Matthews PM, Federico A, et al. Accurate, robust, and automated longitudinal and cross-sectional brain change analysis. *Neuroimage*. (2002) 17:479–89. doi: 10.1006/nimg.2002.1040
- Sowa P, Nygaard GO, Bjornerud A, Celius EG, Harbo HF, Beyer MK. Magnetic resonance imaging perfusion is associated with disease severity and activity in multiple sclerosis. *Neuroradiology*. (2017) 59:655–64. doi: 10.1007/s00234-017-1849-4
- Inglese M, Park SJ, Johnson G, Babb JS, Miles L, Jaggi H, et al. Deep gray matter perfusion in multiple sclerosis: dynamic susceptibility contrast perfusion magnetic resonance imaging at 3 T. *Arch Neurol*. (2007) 64:196–202. doi: 10.1001/archneur.64.2.196
- Debernard L, Melzer TR, Van Stockum S, Graham C, Wheeler-Kingshott CA, Dalrymple-Alford JC, et al. Reduced grey matter perfusion without volume loss in early relapsing-remitting multiple sclerosis. *J Neurol Neurosurg Psychiatr*. (2014) 85:544–51. doi: 10.1136/jnnp-2013-305612
- Hojjat SP, Cantrell CG, Carroll TJ, Vitorino R, Feinstein A, Zhang L, et al. Perfusion reduction in the absence of structural differences in cognitively impaired versus unimpaired RRMS patients. *Mult Scler*. (2016) 22:1685–94. doi: 10.1177/1352458516628656
- Ingrisch M, Sourbron S, Herberich S, Schneider MJ, Kumpfel T, Hohlfeld R, et al. Dynamic contrast-enhanced magnetic resonance imaging suggests normal perfusion in normal-appearing white matter in multiple sclerosis. *Invest Radiol*. (2017) 52:135–41. doi: 10.1097/RLI.00000000000000320
- Staffaroni AM, Cobigo Y, Elahi FM, Casaleto KB, Walters SM, Wolf A, et al. A longitudinal characterization of perfusion in the aging brain and associations with cognition and neural structure. *Hum Brain Mapp*. (2019) 40:3522–33. doi: 10.1002/hbm.24613
- Clark LR, Berman SE, Rivera-Rivera LA, Hoscheidt SM, Darst BF, Engelman CD, et al. Macrovascular and microvascular cerebral blood flow in adults at risk for Alzheimer's disease. *Alzheimers Dement*. (2017) 7:48–55. doi: 10.1016/j.dadm.2017.01.002
- Wolters FJ, Zonneveld HI, Hofman A, Van Der Lugt A, Koudstaal PJ, Vernooij MW, et al. Cerebral perfusion and the risk of dementia: a population-based study. *Circulation*. (2017) 136:719–28. doi: 10.1161/CIRCULATIONAHA.117.027448
- Chung CC, Pimentel D, Jor'dan AJ, Hao Y, Milberg W, Novak V. Inflammation-associated declines in cerebral vasoreactivity and cognition in type 2 diabetes. *Neurology*. (2015) 85:450–8. doi: 10.1212/WNL.0000000000001820
- Whelton PK, Carey RM, Aronow WS, Casey DE Jr, Collins KJ, Dennison Himmelfarb C, et al. 2017 ACC/AHA/AAPA/ABC/ACPM/AGS/APhA/ASH/ASPC/NMA/PCNA guideline for the prevention, detection, evaluation, and management of high blood pressure in adults: executive summary: a report of the american college of cardiology/american heart association task force on clinical practice guidelines. *Hypertension*. (2018) 71:1269–324. doi: 10.1161/HYP.0000000000000066
- Marshall O, Lu H, Brisset JC, Xu F, Liu P, Herbert J, et al. Impaired cerebrovascular reactivity in multiple sclerosis. *JAMA Neurol*. (2014) 71:1275–81. doi: 10.1001/jamaneurol.2014.1668
- Jakimovski D, Zivadinov R, Pelizzari L, Browne RW, Weinstock-Guttman B, Ramanathan M. Lipoprotein(a) levels are associated with the size of extracranial arteries in multiple sclerosis. *J Vasc Res*. (2019) 15:16–23. doi: 10.1159/000502115

34. Trapp BD, Vignos M, Dudman J, Chang A, Fisher E, Staugaitis SM, et al. Cortical neuronal densities and cerebral white matter demyelination in multiple sclerosis: a retrospective study. *Lancet Neurol.* (2018) 17:870–84. doi: 10.1016/S1474-4422(18)30245-X
35. Clement P, Mutsaerts HJ, Vaclavu L, Ghariq E, Pizzini FB, Smits M, et al. Variability of physiological brain perfusion in healthy subjects - a systematic review of modifiers. Considerations for multi-center ASL studies. *J Cereb Blood Flow Metab.* (2018) 38:1418–37. doi: 10.1177/0271678X17702156

**Conflict of Interest:** MD has received research grant support from Novartis and Keystone Heart. RB received personal compensation from Veraci, Genentech, Roche, Novartis, Genzyme, Sanofi and Biogen, Bristol Myers Squibb and EMD Serono for speaking and consultant fees. He received financial support for research activities from Genzyme, Genentech, Biogen, Verasci, and Mallinckrodt. BW-G received honoraria as a speaker and as a consultant for Biogen Idec, Teva Pharmaceuticals, EMD Serono, Novartis, Genentech and Mallinckrodt. BW-G received research funds from Biogen Idec, Teva Pharmaceuticals, EMD Serono,

Novartis, Genentech and Mallinckrodt. RZ received personal compensation from EMD Serono, Genzyme-Sanofi, Celgene and Novartis for speaking and consultant fees. He received financial support for research activities from Genzyme-Sanofi, Novartis, Celgene, Mapi Pharma, Protembis, V-Wave Medical, and Keystone Heart.

The remaining authors declare that the research was conducted in the absence of any commercial or financial relationships that could be construed as a potential conflict of interest.

Copyright © 2020 Jakimovski, Bergsland, Dwyer, Traversone, Hagemeyer, Fuchs, Ramasamy, Weinstock-Guttman, Benedict and Zivadinov. This is an open-access article distributed under the terms of the Creative Commons Attribution License (CC BY). The use, distribution or reproduction in other forums is permitted, provided the original author(s) and the copyright owner(s) are credited and that the original publication in this journal is cited, in accordance with accepted academic practice. No use, distribution or reproduction is permitted which does not comply with these terms.



# Quantitative Cerebrovascular Reactivity in Normal Aging: Comparison Between Phase-Contrast and Arterial Spin Labeling MRI

Kamil Taneja<sup>1</sup>, Peiying Liu<sup>1</sup>, Cuimei Xu<sup>1</sup>, Monroe Turner<sup>2</sup>, Yuguang Zhao<sup>2</sup>, Dema Abdelkarim<sup>2</sup>, Binu P. Thomas<sup>3</sup>, Bart Rypma<sup>2,4</sup> and Hanzhang Lu<sup>1,5,6\*</sup>

<sup>1</sup> The Russel H. Morgan Department of Radiology, Johns Hopkins University School of Medicine, Baltimore, MD, United States, <sup>2</sup> School of Behavioral and Brain Sciences, University of Texas at Dallas, Richardson, TX, United States, <sup>3</sup> Advanced Imaging Research Center, University of Texas Southwestern Medical Center, Dallas, TX, United States, <sup>4</sup> Department of Psychiatry, University of Texas Southwestern Medical Center, Dallas, TX, United States, <sup>5</sup> F.M. Kirby Research Center for Functional Brain Imaging, Kennedy Krieger Institute, Baltimore, MD, United States, <sup>6</sup> Department of Biomedical Engineering, Johns Hopkins University School of Medicine, Baltimore, MD, United States

## OPEN ACCESS

### Edited by:

Yulin Ge,  
New York University, United States

### Reviewed by:

Zhongliang Zu,  
Vanderbilt University, United States  
Bo Gao,  
Affiliated Hospital of Guizhou Medical  
University, China  
Lirong Yan,  
University of Southern California,  
Los Angeles, United States

### \*Correspondence:

Hanzhang Lu  
hlu3@jhmi.edu

### Specialty section:

This article was submitted to  
Applied Neuroimaging,  
a section of the journal  
Frontiers in Neurology

**Received:** 06 April 2020

**Accepted:** 19 June 2020

**Published:** 31 July 2020

### Citation:

Taneja K, Liu P, Xu C, Turner M,  
Zhao Y, Abdelkarim D, Thomas BP,  
Rypma B and Lu H (2020) Quantitative  
Cerebrovascular Reactivity in Normal  
Aging: Comparison Between  
Phase-Contrast and Arterial Spin  
Labeling MRI. *Front. Neurol.* 11:758.  
doi: 10.3389/fneur.2020.00758

**Purpose:** Cerebrovascular reactivity (CVR) is an index of the dilatory function of cerebral blood vessels and has shown great promise in the diagnosis of risk factors in cerebrovascular disease. Aging is one such risk factor; thus, it is important to characterize age-related differences in CVR. CVR can be measured by BOLD MRI but few studies have measured quantitative cerebral blood flow (CBF)-based CVR in the context of aging. This study aims to determine the age effect on CVR using two quantitative CBF techniques, phase-contrast (PC), and arterial spin labeling (ASL) MRI.

**Methods:** In 49 participants (32 younger and 17 older), CVR was measured with PC, ASL, and BOLD MRI. These CVR methods were compared across young and older groups to determine their dependence on age. PC and ASL CVR were also studied for inter-correlation and mean differences. Gray and white matter CVR values were also studied.

**Results:** PC CVR was higher in younger participants than older participants (by 17%,  $p = 0.046$ ). However, there were no age differences in ASL or BOLD CVR. ASL CVR was significantly correlated with PC CVR ( $p = 0.042$ ) and BOLD CVR ( $p = 0.016$ ), but its values were underestimated compared to PC CVR ( $p = 0.045$ ). ASL CVR map revealed no difference between gray matter and white matter tissue types, whereas gray matter was significantly higher than white matter in the BOLD CVR map.

**Conclusion:** This study compared two quantitative CVR techniques in the context of brain aging and revealed that PC CVR is a more sensitive method for detection of age differences, despite the absence of spatial information. The ASL method showed a significant correlation with PC and BOLD, but it tends to underestimate CVR due to confounding factors associated with this technique. Importantly, our data suggest that there is not a difference in CBF-based CVR between the gray and white matter, in contrast to previous observation using BOLD MRI.

**Keywords:** phase-contrast, arterial spin labeling, MRI, cerebrovascular reactivity, aging



## INTRODUCTION

Cerebrovascular reactivity (CVR) is an index of the dilatory function of cerebral blood vessels. This index has potential utility in arterial stenosis (1–3), stroke (4–6), neurodegenerative diseases (7–9), and normal aging (10–12). CVR can be measured by applying a vasodilatory challenge, such as CO<sub>2</sub> (13), while recording hemodynamic parameters of the brain, and the change in the hemodynamic parameter per unit dilatory stimulus is quantified as CVR.

The vast majority of prior CVR studies have been based on the Blood-Oxygenation-Level-Dependent (BOLD) MRI signal (2, 10, 12–14), due to its straightforward pulse sequence, high sensitivity, high spatial, and temporal resolution (13). However, BOLD signal reflects a complex interplay between many physiological parameters such as cerebral blood flow (CBF), venous cerebral blood volume (vCBV), cerebral metabolic rate of oxygen (CMRO<sub>2</sub>), and hematocrit (Hct) (14), thus this signal is often considered as a semi-quantitative measure of brain hemodynamics and its interpretation is sometimes difficult (15–17).

CBF-based CVR is generally considered a more quantitative measure. This technique has a direct physiological meaning, thus is not dependent on magnetic field strength. Furthermore, such a measure can be compared across imaging modalities such as MRI (18), Positron Emission Tomography (PET) (19), Single Photon Emission Computed Tomography (SPECT) (20), ultrasound (21), and optical imaging (22). Two commonly used MRI approaches to measure CBF are arterial spin labeling (ASL) and phase-contrast (PC) MRI. ASL measures voxel-wise CBF by using labeled water protons as an endogenous tracer (18, 23, 24) and subtraction of label and control images yields a perfusion-weighted image, which can be used for quantification of CBF maps (25, 26). Two major limitations of ASL are that it suffers from low signal-to-noise ratio (SNR) and that there exist several confounding factors in its quantification such as bolus arrival time and labeling efficiency (27). These factors are known to vary with CO<sub>2</sub> levels (28, 29).

PC MRI is a technique to measure blood flow via imaging of flow velocity in blood vessels (28, 30). This method can

be used to measure global CBF through arterial vessels (e.g., internal carotid arteries) or venous vessels (e.g., superior sagittal sinus, SSS). PC MRI does not suffer from variables such as bolus arrival time or labeling efficiency, although it does not provide regional CBF information. CBF measurements from PC and ASL MRI under basal states have been compared previously (13, 27, 28).

The purpose of this study was to compare PC and ASL-based CVR in the context of normal aging. For completeness, BOLD-based CVR data were also collected. CVR was measured in younger ( $N = 32$ ) and older ( $N = 17$ ) participants with all three techniques to determine their sensitivity to age-related cerebrovascular decline. The correlation and magnitude between these CVR techniques were also studied. Basal CBF differences between the younger and older groups were examined using the normocapnic PC data.

## MATERIALS AND METHODS

### Study Participants

Forty-nine participants (27 females, 22 males) were recruited at the University of Texas at Dallas (UTD) and Johns Hopkins University (JHU). The demographic and cognitive information of participants from both institutions is summarized in **Table 1**. The study was approved by the Institutional Review Boards of both institutions. Written informed consent in accordance with the Declaration of Helsinki was obtained before participants were enrolled in the study.

**TABLE 1 |** Demographic and cognitive information for study participants.

	Young	Old	<i>p</i>	<i>t</i> <sub>44</sub>
<b>Demographic Information</b>				
<b><i>N</i></b>	32	17		
UTD	16	10		
JHU	16	7		
<b>Age, years (SE)</b>				
UTD	23.1 (0.6)	59.6 (1.6)		
JHU	20.9 (0.6)	66.0 (3.0)		
<b>Gender (M, F)</b>				
UTD	(5, 11)	(3, 7)		
JHU	(11, 5)	(3, 4)		
<b>Cognitive Measures, z-Score (SE)</b>				
Multiple domains	−0.007 (0.206)	0.038 (0.129)	1	0
Motor speed	0.312 (0.139)	−0.404 (0.198)	0.01	−2.69
Attention	0.118 (0.165)	−0.117 (0.194)	1	0
Short term memory	0.356 (0.162)	−0.543 (0.163)	0.141	−1.50
Working memory	0.233 (0.186)	−0.372 (0.149)	0.692	−0.40
Fluid intelligence	0.328 (0.132)	−0.519 (0.208)	0.019	−2.44
Crystalline intelligence	0.182 (0.117)	−0.336 (0.241)	0.37	−0.91
Processing speed	0.475 (0.112)	−0.767 (0.112)	<0.001	−5.86
Global cognition	0.328 (0.085)	−0.510 (0.111)	<0.001	−4.66

*F*, female; *JHU*, Johns Hopkins University; *M*, male; *N*, number of participants; *SE*, standard error; *UTD*, University of Texas at Dallas.

**Abbreviations:** ASL, arterial spin labeling; *ASL<sub>RA</sub>*, room air arterial spin labeling; *ASL<sub>HC</sub>*, room air arterial spin labeling; BOLD, blood-oxygen-level-dependent; *BOLD<sub>RA</sub>*, room air blood-oxygen-level-dependent; *BOLD<sub>HC</sub>*, hypercapnia blood-oxygen-level-dependent; CBF, cerebral blood flow; CC, cross correlation; CVR, cerebrovascular reactivity; EtCO<sub>2</sub>, end-tidal CO<sub>2</sub>; *EtCO<sub>2ASL, RA</sub>*, end-tidal CO<sub>2</sub> during arterial spin labeling at room air; *EtCO<sub>2ASL, HC</sub>*, end-tidal CO<sub>2</sub> during arterial spin labeling at hypercapnia; *EtCO<sub>2PC, RA</sub>*, end-tidal CO<sub>2</sub> during phase-contrast at room air; *EtCO<sub>2PC, HC</sub>*, end-tidal CO<sub>2</sub> during phase-contrast at hypercapnia; FA, flip angle; *Flux<sub>RA</sub>*, flux at room air; *Flux<sub>HC</sub>*, flux at hypercapnia; FOV, field-of-view; GM, gray matter; HC, hypercapnia; Hct, hematocrit; JHU, Johns Hopkins University; MPRAGE, magnetization-prepared rapid acquisition with gradient echo; PC, phase-contrast; pCASL, pseudo-continuous arterial spin labeling; PET, positron emission tomography; RA, room air; ROI, region-of-interest; SNR, signal-to-noise ratio; SPECT, single positron emission computed tomography; SPM, Statistical Parameter Mapping; SSS, superior sagittal sinus; TE, echo time; TI, inversion time; TR, repetition time; UTD, University of Texas at Dallas; vCBV, venous cerebral blood volume; *V<sub>enc</sub>*, velocity encoding; WB, whole-brain; WM, white matter.

## Experimental Procedures

The MRI scans were performed on two 3T systems (Philips Healthcare, Best, The Netherlands). The two systems have the identical model number (Achieva with QUASAR gradient) and hardware configurations. A body coil was used for transmission and a 32-channel head coil was used for receiving. Before the subject entered the scanner, a nose clip and a mouth piece was attached on the subject to allow for control of inspired air, as detailed previously (31). Once the subject was inside the scanner, we performed MRI scans illustrated in **Figure 1A**. The scan session began with room air breathing. A PC-MRI was performed first followed by a dual-echo ASL/BOLD sequence for 10 min. At 4 min into the ASL/BOLD sequence (green line in **Figure 1A**), the inspired gas was switched to CO<sub>2</sub>-enriched gas mixture (5% CO<sub>2</sub>, 21% O<sub>2</sub>, and 74% N<sub>2</sub>) and the scan continued for another 6 min. The CO<sub>2</sub> gas mixture was stored in a Douglas bag and delivered through a two-way non-rebreathing valve (Hans Rudolph, 2600 series, Shawnee, KS). A research assistant was in the MRI room to change the valve from room-air to 5% CO<sub>2</sub> gas at the appropriate time. After the dual-echo ASL/BOLD sequence, a PC-MRI was performed in the hypercapnic state. End-tidal CO<sub>2</sub> (EtCO<sub>2</sub>) was continuously measured through the duration of the experiment using a capnograph device (NM3 Respiratory Profile Monitor, Model 7900, Philips Healthcare, Wallingford, CT).

PC-MRI used the following parameters: field-of-view (FOV) = 230 × 230 mm<sup>2</sup>, matrix size = 320 × 192, slice thickness = 5 mm, repetition time (TR)/echo time (TE)/flip angle (FA) = 20 ms/7 ms/15°, velocity encoding ( $V_{enc}$ ) =

80 cm/s, scan duration = 30 s. The 2D PC imaging slice was positioned at 20 mm above sinus confluence with the imaging slice parallel to AC-PC line to measure flow through the SSS (**Figure 1B**). The dual-echo ASL sequence used the following parameters: pseudo-continuous ASL (pCASL) labeling, FOV = 220 × 220 × 126 mm<sup>3</sup>, matrix size = 64 × 64 × 22, slice thickness = 6 mm, TR/TE1/TE2/FA = 4,006 ms/13 ms/30 ms/90°, scan duration = 10 min (**Figure 1C**). The sequence was used to obtain simultaneous ASL (the TE1 data) and BOLD (the TE2 data) signals. Note, however, that these BOLD data are slightly different from the traditional BOLD-CVR data which are typically acquired in several CO<sub>2</sub> breathing cycles with a shorter breathing period (13).

A T1-weighted magnetization-prepared rapid acquisition with gradient echo (MPRAGE) scan was performed for tissue segmentation. The MPRAGE sequence had the following parameters: TR of 8.1 ms, TE of 3.7 ms, a flip angle of 12°, a shot interval of 2,100 ms, an inversion time (TI) of 1,100 ms, with a voxel size of 1 × 1 × 1 mm<sup>3</sup>, 160 slices with a sagittal slice orientation.

## Data Processing

Data analysis was performed using Statistical Parameter Mapping (SPM) (University College London, UK) and in-house MATLAB scripts (MathWorks, Natick, MA).

The dual-echo ASL scan yielded both ASL and BOLD data. The ASL (first echo) and BOLD (second echo) images were first preprocessed using a standard pipeline: motion correction by

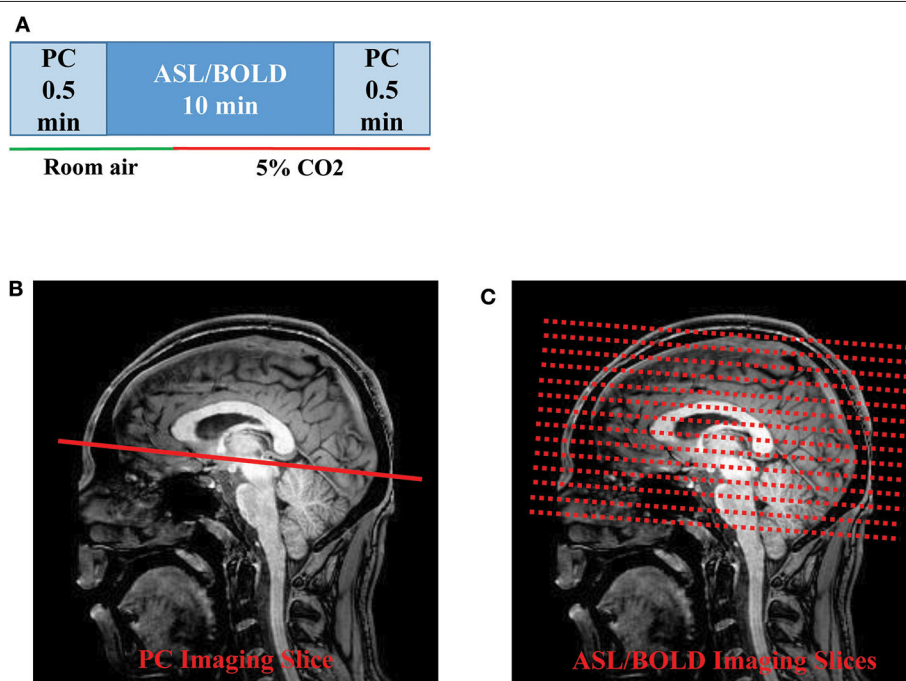


**FIGURE 1 |** Illustration of the MRI scan procedures: **(A)** Timing of the PC and ASL/BOLD MRI scans during normocapnic and hypercapnic states. The timing of the gas switch is shown by the colored bars. The gas switch occurred 4 min into the ASL/BOLD scan. **(B)** Slice positioning of PC and **(C)** ASL/BOLD MRI. ASL, arterial spin labeling; BOLD, blood-oxygenation-level-dependent; PC, phase-contrast.

realignment (to the first dynamic) and spatial smoothing with a Gaussian filter with a full-width-at-half-maximum of 4 mm. A whole-brain (WB) mask was obtained by segmentation of the raw image and used to obtain a WB raw ASL and BOLD time course. The ASL label and control values were subtracted using a surround subtraction algorithm (32, 33) to obtain CBF-weighted time course (**Figure 2A**). The BOLD label and control values were averaged to cancel out the labeling effect (34), yielding a final BOLD time course (**Figure 2A**). Note that the dual-echo ASL scan lasted for 10 min with the switch from room air to CO<sub>2</sub> gas taking place at 4 min into the scan. We averaged the data in the first 4 min as the room air values (ASL<sub>RA</sub> and BOLD<sub>RA</sub>) and the last 4 min as the hypercapnic values (ASL<sub>HC</sub> and BOLD<sub>HC</sub>) (**Figure 2A**). Data during the middle 2 min were not used for CVR calculation as physiology was not in a steady-state.

ASL and BOLD based CVR were then calculated with:

$$\text{ASL CVR} = \frac{100 * \frac{\text{ASL}_{\text{HC}} - \text{ASL}_{\text{RA}}}{\text{ASL}_{\text{RA}}}}{\text{EtCO}_2_{\text{ASL, HC}} - \text{EtCO}_2_{\text{ASL, RA}}} \quad (1)$$

$$\text{BOLD CVR} = \frac{100 * \frac{\text{BOLD}_{\text{HC}} - \text{BOLD}_{\text{RA}}}{\text{BOLD}_{\text{RA}}}}{\text{EtCO}_2_{\text{ASL, HC}} - \text{EtCO}_2_{\text{ASL, RA}}} \quad (2)$$

where EtCO<sub>2HC</sub> and EtCO<sub>2RA</sub> represent end-tidal CO<sub>2</sub> values during the hypercapnia and room air MRI acquisition, respectively.

The EtCO<sub>2</sub> values were extracted from the CO<sub>2</sub> recording. To obtain EtCO<sub>2HC</sub> and EtCO<sub>2RA</sub> that are time-matched to the MRI data acquisitions, the EtCO<sub>2</sub> time course was temporally aligned to the BOLD signal time course by computing cross-correlation (CC) between them at various time-shifts and finding the shift yielding the highest CC (**Figure 2B**). This process allows the correction of the time it takes for the CO<sub>2</sub> to travel from the lungs to the brain (13). Once temporally aligned, the EtCO<sub>2</sub> data points during the corresponding MRI scan were averaged to yield EtCO<sub>2</sub> values room air and hypercapnia, which was used for the calculation of CVR in Equations (1) and (2).

In addition to WB CVR values, which include both gray matter (GM) and white matter (WM), we also separately examined GM and WM CVR. To create GM and WM masks, the T1-weighted MPRAGE image was skull-stripped and segmented using SPM12.

To calculate PC CVR, the flux at room air (*Flux<sub>RA</sub>*) and hypercapnia (*Flux<sub>HC</sub>*) were measured. Region-of-interests (ROIs) encompassing the SSS were manually drawn on complex difference images for both the room air and hypercapnia PC scans (**Figure 3A**). These ROIs were then overlaid onto the respective

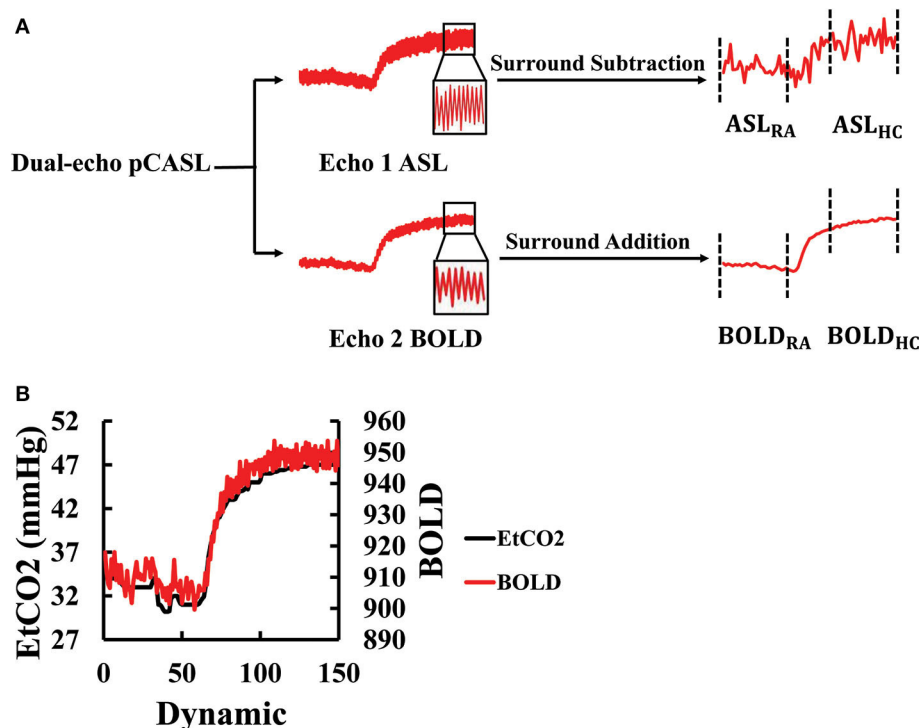


**FIGURE 2 |** Processing of the dual-echo ASL/BOLD MRI data: **(A)** Flowchart of the ASL/BOLD data processing. The dual-echo data were first split into two echoes, the first corresponding to ASL and the second BOLD. The time courses of these raw data reveal high-frequency signal fluctuations in accordance with the control-label alternations. Subtraction and addition of the time courses result in the final ASL and BOLD time courses, respectively. The corresponding time periods were averaged to obtain room-air (RA) and hypercapnic (HC) signal values. **(B)** Illustration of the maximal alignment between EtCO<sub>2</sub> and WB BOLD signal from a representative subject. The EtCO<sub>2</sub> time course was shifted to find the best temporal match with the BOLD. ASL, arterial spin labeling; BOLD, blood-oxygen-level-dependent; EtCO<sub>2</sub>, end-tidal CO<sub>2</sub>; HC, hypercapnia; pCASL, pseudo-continuous arterial spin labeling; RA, room air; WB, whole-brain.

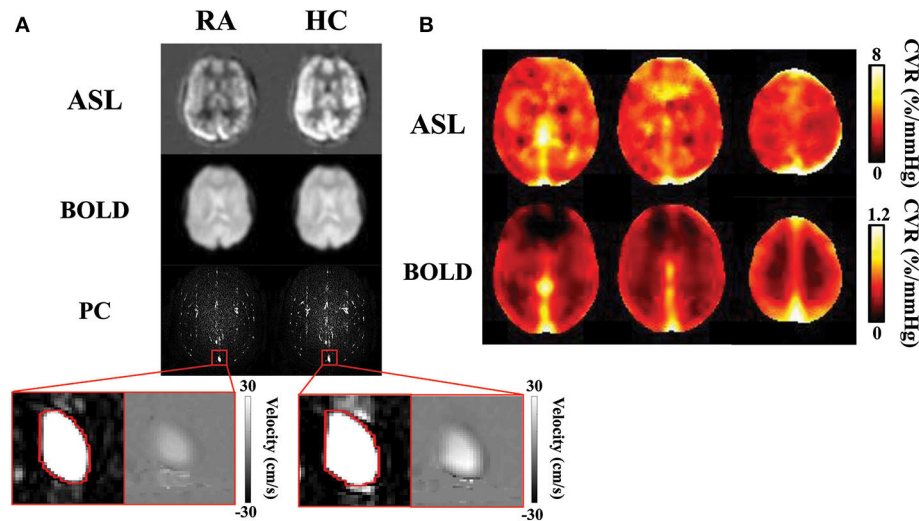


**FIGURE 3 |** CVR results obtained with ASL, BOLD, and PC MRI data: **(A)** Normocapnic and hypercapnic ASL, BOLD, and PC images from a representative subject. For PC MRI, the complex difference images are shown, with a zoom-in version showing the complex difference and velocity map in the superior sagittal sinus. **(B)** Group-average ASL and BOLD CVR maps. Note that the ASL and BOLD CVR values have different ranges. ASL, arterial spin labeling; BOLD, blood-oxygen-level-dependent; CVR, cerebrovascular reactivity; HC, hypercapnia; PC, phase-contrast; RA, room air.

velocity maps, and flux was calculated by the multiplying the ROI area by the mean velocity in the ROI. PC CVR could then be calculated as:

$$\text{PC CVR} = \frac{100 * \frac{\text{Flux}_{\text{HC}} - \text{Flux}_{\text{RA}}}{\text{Flux}_{\text{RA}}}}{\text{EtCO}_{2\text{PC, HC}} - \text{EtCO}_{2\text{PC, RA}}} \quad (3)$$

where  $\text{EtCO}_{2\text{PC, HC}}$  and  $\text{EtCO}_{2\text{PC, RA}}$  represent averaged end-tidal  $\text{CO}_2$  values during hypercapnic and room air PC scan, respectively.

The PC MRI scan during room air breathing was also used to calculate basal CBF (ml/100 g/min):

$$\text{Basal CBF} = \frac{\text{Flux}_{\text{RA}}}{\text{Brain Volume} * 1.06 * 100} * \frac{1}{0.46} \quad (4)$$

where 0.46 represents the ratio between flow in the SSS and that in the whole-brain (35), brain volume was estimated by segmentation of the T1-MPRAGE image using MRICloud (36). 1.06 is the mass density of brain tissue (37), and the number “100” allows the expression of CBF in “per 100 g tissue.”

## Statistical Analysis

All CVR values are reported as mean  $\pm$  standard error. CVR was compared across young and older groups with a linear regression analysis, after adjusting for sex and site. For comparison of CVR across MRI techniques, a Pearson correlation was computed. For within-subject comparison of tissue type effect and imaging method effect, a paired  $t$ -test was used. A  $p$ -value of 0.05 or less was considered significant.

## RESULTS

**Figure 3A** illustrates images of PC, ASL, and BOLD MR images during room air and hypercapnia breathing from a representative subject. Group-averaged ASL and BOLD-based CVR maps are shown in **Figure 3B**. Note that the ASL CVR map is noisier compared to the BOLD CVR map, consistent with a lower SNR of the ASL data. Importantly, the ASL CVR map shows an absence of GM-WM contrast. This is confirmed by region-of-interest analysis which showed that GM and WM CVR were not different in the ASL data (GM ASL CVR =  $5.6 \pm 0.3\%$  /mmHg, WM ASL CVR =  $5.1 \pm 0.4\%$  /mmHg,  $p > 0.05$ ,  $t_{48} = 1.9$ ). This observation suggests that, even though GM contains more blood vessels (thereby higher basal perfusion) than WM, their vascular reactivities in terms of fractional changes in CBF are comparable. On the other hand, the BOLD CVR map shows a higher CVR in the GM than WM, due to the confounding factors (e.g., vCBV) in the BOLD signal (38). Accordingly, GM BOLD CVR was found to be significantly higher than WM BOLD CVR (GM =  $0.33 \pm 0.01\%$  /mmHg, WM =  $0.19 \pm 0.01\%$  /mmHg,  $p < 0.001$ ,  $t_{48} = 15.1$ ). Note that PC CVR is a global measure and does not produce a map.

**Table 2** summarizes the age effect on the three CVR modalities. Only PC CVR demonstrates an age effect, where older participants ( $5.46 \pm 0.32\%$  /mmHg) have a significantly lower PC CVR than younger participants ( $6.59 \pm 0.41\%$  /mmHg,  $p = 0.046$ ,  $t_{45} = -2.06$ ). On the other hand, WB ASL CVR (young =  $5.53 \pm 0.37\%$  /mmHg, old =  $5.03 \pm 0.55\%$  /mmHg,  $p = 0.31$ ,  $t_{45} = -1.03$ ), GM ASL CVR (young =  $5.74 \pm 0.35\%$  /mmHg, old =  $5.31 \pm 0.6\%$  /mmHg,  $p = 0.35$ ,  $t_{45} = -0.95$ ), and WM ASL CVR (young =  $5.27 \pm 0.53\%$  /mmHg, old =  $4.86 \pm 0.58\%$  /mmHg,  $p = 0.52$ ,  $t_{45} = -0.65$ ) did not display a significant age effect. Similarly, WB BOLD CVR (young =  $0.27 \pm 0.01\%$  /mmHg, old =



$0.28 \pm 0.01$  %/mmHg,  $p = 0.72$ ,  $t_{45} = 0.37$ ), GM BOLD CVR (young =  $0.33 \pm 0.01$  %/mmHg, old =  $0.33 \pm 0.01$  %/mmHg,  $p = 0.95$ ,  $t_{45} = 0.07$ ), and WM BOLD CVR (young =  $0.19 \pm 0.01$  %/mmHg, old =  $0.21 \pm 0.02$  %/mmHg,  $p = 0.29$ ,  $t_{45} = 1.07$ ) did not demonstrate a significant age effect.

Since both PC and ASL MRI measures CBF-based CVR, we compared whole-brain values between these two imaging methods. It was found that WB ASL CVR ( $5.37 \pm 0.32$  %/mmHg) was significantly lower than PC CVR ( $6.15 \pm 0.30$  %/mmHg,  $p = 0.045$ ,  $t_{48} = 2.06$ ), consistent with previous suggestions that confounding factors in ASL quantification (e.g., reduced labeling efficiency during hypercapnia) may result in a bias in CVR values when measured with ASL MRI.

We further studied the correlation between different CVR methods across participants. **Figure 4** shows correlations between the different CVR measures. Despite different pulse sequences and different underlying physiological mechanisms, all three CVR methods showed a significant correlation ( $p < 0.05$ ).

We also examined basal CBF, (i.e., CBF without hypercapnia challenge). We found that older subjects revealed a significantly lower CBF compared to the younger group (young =  $68.2 \pm 3.9$  mL/100 g/min, old =  $51.5 \pm 3.5$  mL/100 g/min,

$p = 0.0028$ ,  $t_{44} = 3.17$ , **Figure 5**), consistent with previous reports (10, 38–40).

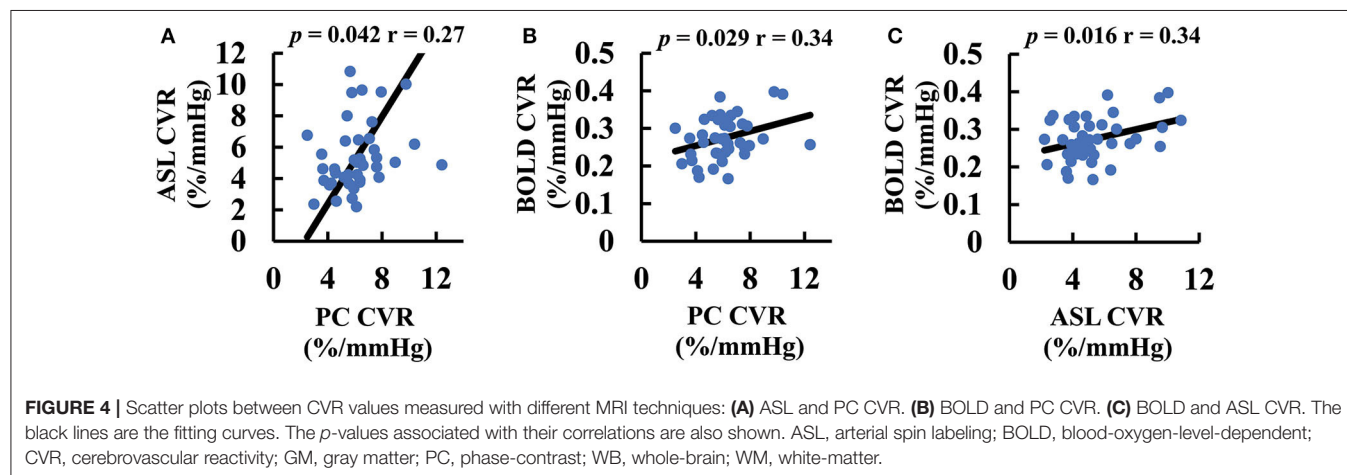
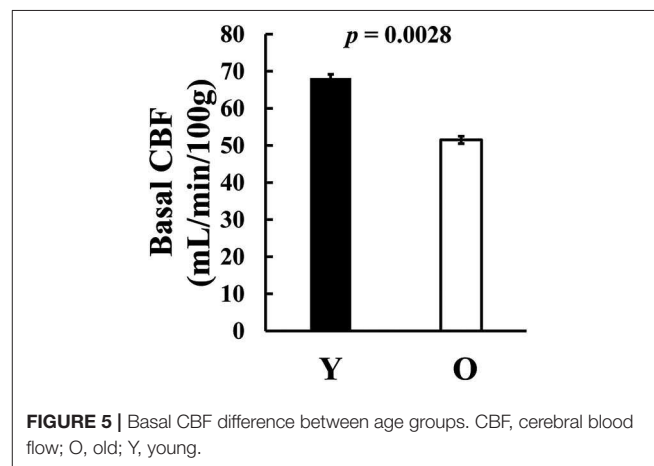
## DISCUSSION

CVR is known to be a sensitive marker in large vessel diseases, such as Moyamoya disease and stroke (1, 6, 41, 42), and small vessel diseases, such as vascular cognitive impairment (43, 44) and dementia (7, 45) and diabetes (46, 47). Because aging is a risk factor for many of these diseases, it is important to characterize age-related changes in CVR. Several studies have investigated this topic using BOLD signal as the readout for hemodynamic responses (10–12, 48). However, BOLD signal reflects a complex interplay between  $vCBV$ , CBF, and  $CMRO_2$ , thus its quantitative interpretation is not trivial, both in terms of brain physiology (13, 14) and age-related physiological changes [e.g., (34)]. Furthermore, there is a non-linear relationship between blood  $CO_2$  content and BOLD signal change (49, 50). Therefore, a more direct and less complex measurement of brain hemodynamics is desirable to deliver more quantitative measurements of CVR. PC MRI and ASL MRI represent two of the most commonly used CBF techniques, both of

**TABLE 2 |** CVR age differences.

	Young (%/mmHg)	Old (%/mmHg)	<i>p</i>	<i>t</i> <sub>44</sub>
<b>WB CVR, (SE)</b>				
PC	6.59 (0.41)	5.46 (0.32)	0.046	−2.06
ASL	5.53 (0.37)	5.03 (0.55)	0.31	−1.03
BOLD	0.27 (0.01)	0.28 (0.01)	0.72	0.37
<b>GM CVR, (SE)</b>				
ASL	5.74 (0.35)	5.31 (0.60)	0.35	−0.95
BOLD	0.33 (0.01)	0.33 (0.01)	0.95	0.07
<b>WM CVR, (SE)</b>				
ASL	5.27 (0.53)	4.86 (0.58)	0.52	−0.65
BOLD	0.19 (0.01)	0.21 (0.02)	0.29	1.07

ASL, arterial spin labeling; BOLD, blood-oxygen-level-dependent; CVR, cerebrovascular reactivity; GM, gray matter; PC, phase-contrast; SE, standard error; WB, whole-brain; WM, white matter.



which require no contrast agent and are suitable for dynamic measurements. ASL measures microscopic perfusion in a region-specific manner. However, ASL has a few disadvantages including lower SNR and its susceptibility to several confounding factors such as bolus arrival time (51) and labeling efficiency (28), which are known to change during hypercapnia. On the other hand, PC MRI measures macroscopic flow velocity in large vessels (e.g., superior sagittal sinus, internal carotid artery) and the pulse sequence is relatively straightforward with few confounding factors. However, this technique provides only a global measure and does not provide spatial information. Data from the present study suggested that, although lacking regional information, PC CVR was able to detect age-related decreases in CVR, which may be attributed to changes such as higher vessel stiffness, increased basement membrane thickness, reduced smooth muscle volume, and impaired astrocyte, or endothelial function (52, 53). It is worth noting that ASL CVR significantly underestimated CVR, presumably due to reduced labeling efficiency during the hypercapnic state (28, 54), and was unable to identify a significant age reduction. Therefore, for global assessment, PC CVR provides a sensitive and reliable measurement of cerebrovascular function. It should also be noted that PC MRI scan only takes 0.5 min for each state, thus is a rapid pulse sequence compared to ASL or BOLD MRI.

An interesting observation of the present study is that we showed, for the first time, a voxel-wise ASL CVR map, which revealed that GM and WM evince similar CVR. It is known that WM has substantially lower vessel density compared to the GM (55), often yielding substantially lower WM hemodynamic parameters than those in GM. This includes vCBV, CBF, and CMRO<sub>2</sub> (39, 56–59). Previous studies of BOLD CVR have also shown a clear gray-white contrast, with GM having a higher CVR than WM (2, 10, 12–14). Our results suggest the hypothesis that this gray-white matter difference might be artifactual, due to the complexity of the physiology from which the BOLD signal arises. The results of the present study suggest that there is not a clear gray-white matter difference in ASL-CVR. Indeed, ROI results confirmed this finding, revealing equivalent CVR values in these two tissue types. This is physiologically plausible in that, although CO<sub>2</sub> induced CBF change is lower in WM, its basal CBF is also lower. Thus, CVR based on fractional changes in CBF is actually similar between GM and WM.

Our conclusions are tempered by some limitations in this study. First, a step-breathing paradigm was used in the BOLD CVR scan instead of the more common block-cycle breathing paradigm. Step-breathing was used because the BOLD CVR data were collected simultaneously with the ASL CVR data. A potential problem with the step breathing paradigm is that it is not possible to correct any BOLD signal drifts due to gradient heating or electronic instabilities (60, 61). Thus, the lack of age effect might be partly attributed to the non-traditional BOLD paradigm used. Another possible reason for the lack of age difference in BOLD CVR is that, due to the nature of the pCASL sequence (e.g., long labeling duration, long post-labeling delay, and the need for one control and one labeled image), the BOLD data in the present study had a temporal resolution of 8 s, which is considerably longer than typical BOLD acquisition of <2 s. This

may have reduced the sensitivity of the BOLD data and resulted in an absence of age effect. Another limitation is that the pCASL sequence used a multi-slice 2D EPI, rather than 3D GRASE or stack-of-spiral, acquisition. This is to allow T2\* contrast to be preserved in the signal which is important for the BOLD signal. However, 3D acquisition would have yielded a higher SNR. A final limitation is that the data presented in this work were collected at two different sites, due to our study design. However, we note that the MRI scanners used at the two sites were identical in terms of hardware and software configurations and that the gas-inhalation apparatus was also identical (31).

## CONCLUSION

This study compared two quantitative CVR techniques in the context of brain aging and revealed that PC CVR is a more sensitive method to detect age differences, despite a lack of spatial information. The ASL method showed a significant correlation with PC and BOLD, but it tends to underestimate CVR due to confounding factors associated with this technique. Importantly, our data suggest that there is not a difference in CBF-based CVR between GM and WM, in contrast to previous observation using BOLD MRI.

## DATA AVAILABILITY STATEMENT

The raw data supporting the conclusions of this article will be made available by the authors, without undue reservation.

## ETHICS STATEMENT

The studies involving human participants were reviewed and approved by Johns Hopkins University IRB; UT Southwestern IRB. The patients/participants provided their written informed consent to participate in this study.

## AUTHOR CONTRIBUTIONS

BT and BR were involved with study design. CX, DA, and YZ were involved with data collection. HL was involved with study design and manuscript writing. KT was involved with data collection, data analysis, and manuscript writing. PL and MT were involved with study design and data collection. All authors commented on the manuscript, read, and approved the final version.

## FUNDING

This work was supported by National Institutes of Health: R01 AG047972, R01 MH084021, R01 NS106711, R01 NS106702, P41 EB015909, and S10 OD021648.

## ACKNOWLEDGMENTS

The authors are grateful to the MR technologists in the imaging centers for their assistance.

## REFERENCES

- Donahue MJ, Ayad M, Moore R, Van Osch M, Singer R, Clemmons P, et al. Relationships between hypercarbic reactivity, cerebral blood flow, and arterial circulation times in patients with moyamoya disease. *J Magn Reson Imaging*. (2013) 38:1129–39. doi: 10.1002/jmri.24070
- Gupta A, Chazen JL, Hartman M, Delgado D, Anumula N, Shao H, et al. Cerebrovascular reserve and stroke risk in patients with carotid stenosis or occlusion: a systematic review and meta-analysis. *Stroke*. (2012) 43:2884–91. doi: 10.1161/STROKEAHA.112.663716
- De Vis JB, Petersen ET, Bhogal A, Hartkamp NS, Klijn CJM, Kappelle LJ, et al. Calibrated MRI to evaluate cerebral hemodynamics in patients with an internal carotid artery occlusion. *J Cereb Blood Flow Metab*. (2015) 35:1015–23. doi: 10.1038/jcbfm.2015.14
- Krainik A, Hund-Georgiadis M, Zysset S, Von Cramon DY. Regional impairment of cerebrovascular reactivity and BOLD signal in adults after stroke. *Stroke*. (2005) 36:1146–52. doi: 10.1161/01.STR.0000166178.40973.a7
- Geranmayeh F, Wise RJS, Leech R, Murphy K. Measuring vascular reactivity with breath-holds after stroke: a method to aid interpretation of group-level BOLD signal changes in longitudinal fMRI studies. *Hum Brain Mapp*. (2015) 36:1755–71. doi: 10.1002/hbm.22735
- Taneja K, Lu H, Welch BG, Thomas BP, Pinho M, Lin D, et al. Evaluation of cerebrovascular reserve in patients with cerebrovascular diseases using resting-state MRI: a feasibility study. *Magn Reson Imaging*. (2019) 59:46–52. doi: 10.1016/j.mri.2019.03.003
- Yezhuvath US, Uh J, Cheng Y, Martin-Cook K, Weiner M, Diaz-Arrastia R, et al. Forebrain-dominant deficit in cerebrovascular reactivity in Alzheimer's disease. *Neurobiol Aging*. (2012) 33:75–82. doi: 10.1016/j.neurobiolaging.2010.02.005
- Glodzik L, Randall C, Rusinek H, De Leon MJ. Cerebrovascular reactivity to carbon dioxide in Alzheimer's disease. *J Alzheimer's Dis*. (2013) 35:427–40. doi: 10.3233/JAD-122011
- Marshall O, Lu H, Brisset JC, Xu F, Liu P, Herbert J, et al. Impaired cerebrovascular reactivity in multiple sclerosis. *JAMA Neurol*. (2014) 71:1275–81. doi: 10.1001/jamaneurol.2014.1668
- Lu H, Xu F, Rodrigue KM, Kennedy KM, Cheng Y, Flicker B, et al. Alterations in cerebral metabolic rate and blood supply across the adult lifespan. *Cereb Cortex*. (2011) 21:1426–34. doi: 10.1093/cercor/bhq224
- Gauthier CJ, Madjar C, Desjardins-Crépeau L, Bellec P, Bherer L, Hoge RD. Age dependence of hemodynamic response characteristics in human functional magnetic resonance imaging. *Neurobiol Aging*. (2013) 34:1469–85. doi: 10.1016/j.neurobiolaging.2012.11.002
- De Vis JB, Hendrikse J, Bhogal A, Adams A, Kappelle LJ, Petersen ET. Age-related changes in brain hemodynamics; A calibrated MRI study. *Hum Brain Mapp*. (2015) 36:3973–87. doi: 10.1002/hbm.22891
- Liu P, De Vis JB, Lu H. Cerebrovascular reactivity (CVR) MRI with CO<sub>2</sub> challenge: a technical review. *Neuroimage*. (2019) 187:104–15. doi: 10.1016/j.neuroimage.2018.03.047
- Chen JJ. Functional MRI of brain physiology in aging and neurodegenerative diseases. *Neuroimage*. (2019) 187:209–25. doi: 10.1016/j.neuroimage.2018.05.050
- Lythgoe DJ, Williams SCR, Cullinane M, Markus HS. Mapping of cerebrovascular reactivity using bold magnetic resonance imaging. *Magn Reson Imaging*. (1999) 17:495–502. doi: 10.1016/S0730-725X(98)00211-2
- Blockley NP, Driver ID, Francis ST, Fisher JA, Gowland PA. An improved method for acquiring cerebrovascular reactivity maps. *Magn Reson Med*. (2011) 65:1278–86. doi: 10.1002/mrm.22719
- Thomas BP, Liu P, Aslan S, King KS, van Osch MJP, Lu H. Physiologic underpinnings of negative BOLD cerebrovascular reactivity in brain ventricles. *Neuroimage*. (2013) 83:505–12. doi: 10.1016/j.neuroimage.2013.07.005
- Williams DS, Detre JA, Leigh JS, Koretsky AP. Magnetic resonance imaging of perfusion using spin inversion of arterial water. *Proc Natl Acad Sci USA*. (1992) 89:212–6. doi: 10.1073/pnas.89.1.212
- Ye FQ, Berman KF, Ellmore T, Esposito G, Van Horn JD, Yang Y, et al. H2150 PET validation of steady-state arterial spin tagging cerebral blood flow measurements in humans. *Magn Reson Med*. (2000) 44:450–6. doi: 10.1002/1522-2594(200009)44:3<450::AID-MRM16>3.0.CO;2-0
- Knutsson L, Börjesson S, Larsson EM, Risberg J, Gustafson L, Passant U, et al. Absolute quantification of cerebral blood flow in normal volunteers: correlation between Xe-133 SPECT and dynamic susceptibility contrast MRI. *J Magn Reson Imaging*. (2007) 26:913–20. doi: 10.1002/jmri.21093
- Sorond FAS, Hollenberg NK, Panych LP, Fisher ND. Brain blood flow and velocity: Correlations between magnetic resonance imaging and transcranial doppler sonography. *J Ultrasound Med*. (2010) 29:1017–22. doi: 10.7863/jum.2010.29.7.1017
- Devor A, Sakadžić S, Srinivasan VJ, Yaseen MA, Nizar K, Saisan PA, et al. Frontiers in optical imaging of cerebral blood flow and metabolism. *J Cereb Blood Flow Metab*. (2012) 32:1259–76. doi: 10.1038/jcbfm.2011.195
- Detre JA, Leigh JS, Williams DS, Koretsky AP. Perfusion imaging. *Magn Reson Med*. (1992) 23:37–45. doi: 10.1002/mrm.1910230106
- Zhang W, Williams DS, Detre JA, Koretsky AP. Measurement of brain perfusion by volume-localized NMR spectroscopy using inversion of arterial water spins: accounting for transit time and cross-relaxation. *Magn Reson Med*. (1992) 25:362–71. doi: 10.1002/mrm.1910250216
- Alsop DC, Detre JA. Reduced transit-time sensitivity in noninvasive magnetic resonance imaging of human cerebral blood flow. *J Cereb Blood Flow Metab*. (1996) 16:1236–49. doi: 10.1097/00004647-199611000-00019
- Detre JA, Zhang W, Roberts DA, Silva AC, Williams DS, Grandis DJ, et al. Tissue specific perfusion imaging using arterial spin labeling. *NMR Biomed*. (1994) 7:75–82. doi: 10.1002/nbm.1940070112
- Dolui S, Wang Z, Wang DJJ, Mattay R, Finkel M, Elliott M, et al. Comparison of non-invasive MRI measurements of cerebral blood flow in a large multisite cohort. *J Cereb Blood Flow Metab*. (2016) 36:1244–56. doi: 10.1177/0271678X16646124
- Aslan S, Xu F, Wang PL, Uh J, Yezhuvath US, Van Osch M, et al. Estimation of labeling efficiency in pseudocontinuous arterial spin labeling. *Magn Reson Med*. (2010) 63:765–71. doi: 10.1002/mrm.22245
- Ho YCL, Petersen ET, Zimine I, Golay X. Similarities and differences in arterial responses to hypercapnia and visual stimulation. *J Cereb Blood Flow Metab*. (2011) 31:560–71. doi: 10.1038/jcbfm.2010.126
- Spilt A, Fricke MA, Van Der Geest RJ, Reiber JHC, Kunz P, Kamper AM, et al. Reproducibility of total cerebral blood flow measurements using phase contrast magnetic resonance imaging. *J Magn Reson Imaging*. (2002) 16:1–5. doi: 10.1002/jmri.10133
- Lu H, Liu P, Yezhuvath U, Cheng Y, Marshall O, Ge Y. MRI mapping of cerebrovascular reactivity via gas inhalation challenges. *J Vis Exp*. (2014) 52306. doi: 10.3791/52306
- Liu TT, Wong EC. A signal processing model for arterial spin labeling functional MRI. *Neuroimage*. (2005) 24:207–15. doi: 10.1016/j.neuroimage.2004.09.047
- Lu H, Donahue MJ, Van Zijl PCM. Detrimental effects of BOLD signal in arterial spin labeling fMRI at high field strength. *Magn Reson Med*. (2006) 56:546–52. doi: 10.1002/mrm.20976
- Hutchison JL, Lu H, Rypma B. Neural mechanisms of age-related slowing: the  $\Delta\text{CBF}/\Delta\text{CMRO}_2$  ratio mediates age-differences in BOLD signal and human performance. *Cereb Cortex*. (2013) 23:2337–46. doi: 10.1093/cercor/bhs233
- De Vis JB, Lu H, Ravi H, Hendrikse J, Liu P. Spatial distribution of flow and oxygenation in the cerebral venous drainage system. *J Magn Reson Imaging*. (2018) 47:1091–6. doi: 10.1002/jmri.25833
- Mori S, Wu D, Ceritoglu C, Li Y, Kolasny A, Vaillant MA, et al. MRICloud: delivering high-throughput MRI neuroinformatics as cloud-based software as a service. *Comput Sci Eng*. (2016) 18:21–35. doi: 10.1109/MCSE.2016.93
- Herscovitch P, Raichle ME. What is the correct value for the brain-blood partition coefficient for water? *J Cereb Blood Flow Metab*. (1985) 5:65–9. doi: 10.1038/jcbfm.1985.9
- Thomas BP, Liu P, Park DC, Van Osch MJP, Lu H. Cerebrovascular reactivity in the brain white matter: magnitude, temporal characteristics, and age effects. *J Cereb Blood Flow Metab*. (2014) 34:242–7. doi: 10.1038/jcbfm.2013.194
- Leenders KL, Perani D, Lammertsma AA, Heather JD, Buckingham P, Jones T, et al. Cerebral blood flow, blood volume and oxygen utilization: normal values and effect of age. *Brain*. (1990) 113:27–47. doi: 10.1093/brain/113.1.27
- Iadecola C, Park L, Capone C. Threats to the mind: aging, amyloid, and hypertension. *Stroke*. (2009) 40:S40–4. doi: 10.1161/STROKEAHA.108.533638

41. Liu P, Li Y, Pinho M, Park DC, Welch BG, Lu H. Cerebrovascular reactivity mapping without gas challenges. *Neuroimage*. (2017) 146:320–6. doi: 10.1016/j.neuroimage.2016.11.054
42. Mandell DM, Matouk CC, Farb RI, Krings T, Agid R, Terbrugge K, et al. Vessel wall MRI to differentiate between reversible cerebral vasoconstriction syndrome and central nervous system vasculitis: preliminary results. *Stroke*. (2012) 43:860–2. doi: 10.1161/STROKEAHA.111.626184
43. Sorond FA, Galica A, Serrador JM, Kiely DK, Iloputaife I, Cupples LA, et al. Cerebrovascular hemodynamics, gait, and falls in an elderly population: MOBILIZE Boston study. *Neurology*. (2010) 74:1627–33. doi: 10.1212/WNL.0b013e3181df0982
44. Glodzik L, Rusinek H, Brys M, Tsui WH, Switalski R, Mosconi L, et al. Framingham cardiovascular risk profile correlates with impaired hippocampal and cortical vasoreactivity to hypercapnia. *J Cereb Blood Flow Metab*. (2011) 31:671–9. doi: 10.1038/jcbfm.2010.145
45. Cantin S, Villien M, Moreaud O, Tropres I, Keignart S, Chipon E, et al. Impaired cerebral vasoreactivity to CO<sub>2</sub> in Alzheimer's disease using BOLD fMRI. *Neuroimage*. (2011) 58:579–87. doi: 10.1016/j.neuroimage.2011.06.070
46. Jor'dan AJ, Manor B, Novak V. Slow gait speed—an indicator of lower cerebral vasoreactivity in type 2 diabetes mellitus. *Front Aging Neurosci*. (2014) 6:135. doi: 10.3389/fnagi.2014.00135
47. Chung CC, Pimentel Maldonado DA, Jor'dan AJ, Alfaro FJ, Lioutas VA, Núñez MZ, et al. Lower cerebral vasoreactivity as a predictor of gait speed decline in type 2 diabetes mellitus. *J Neurol*. (2018) 265:2267–76. doi: 10.1007/s00415-018-8981-x
48. Peng SL, Chen X, Li Y, Rodrigue KM, Park DC, Lu H. Age-related changes in cerebrovascular reactivity and their relationship to cognition: a 4-years longitudinal study. *Neuroimage*. (2018) 174:257–62. doi: 10.1016/j.neuroimage.2018.03.033
49. Bhogal AA, Siero JCW, Fisher JA, Froeling M, Luijten P, Philippens M, et al. Investigating the non-linearity of the BOLD cerebrovascular reactivity response to targeted hypo/hypercapnia at 7T. *Neuroimage*. (2014) 96:296–305. doi: 10.1016/j.neuroimage.2014.05.006
50. Sobczyk O, Battisti-Charbonney A, Fierstra J, Mandell DM, Poublanc J, Crawley AP, et al. A conceptual model for CO<sub>2</sub>-induced redistribution of cerebral blood flow with experimental confirmation using BOLD MRI. *Neuroimage*. (2014) 92:56–68. doi: 10.1016/j.neuroimage.2014.01.051
51. Donahue MJ, Faraco CC, Strother MK, Chappell MA, Rane S, Dethrage LM, et al. Bolus arrival time and cerebral blood flow responses to hypercarbia. *J Cereb Blood Flow Metab*. (2014) 34:1243–52. doi: 10.1038/jcbfm.2014.81
52. D'Esposito M, Deouell LY, Gazzaley A. Alterations in the BOLD fMRI signal with ageing and disease: a challenge for neuroimaging. *Nat Rev Neurosci*. (2003) 4:863–72. doi: 10.1038/nrn1246
53. Abdelkarim D, Zhao Y, Turner MP, Sivakolundu DK, Lu H, Rypma B. A neural-vascular complex of age-related changes in the human brain: anatomy, physiology, and implications for neurocognitive aging. *Neurosci Biobehav Rev*. (2019) 107:927–44. doi: 10.1016/j.neubiorev.2019.09.005
54. Heijtel DFR, Mutsaerts HJMM, Bakker E, Schober P, Stevens MF, Petersen ET, et al. Accuracy and precision of pseudo-continuous arterial spin labeling perfusion during baseline and hypercapnia: a head-to-head comparison with 15O H<sub>2</sub>O positron emission tomography. *Neuroimage*. (2014) 92:182–92. doi: 10.1016/j.neuroimage.2014.02.011
55. Kubíková T, Kochová P, Tomášek P, Witter K, Tonar Z. Numerical and length densities of microvessels in the human brain: correlation with preferential orientation of microvessels in the cerebral cortex, subcortical grey matter and white matter, pons and cerebellum. *J Chem Neuroanat*. (2018) 66:22–32. doi: 10.1016/j.jchemneu.2017.11.005
56. Rostrup E, Law I, Blinkenberg M, Larsson HBW, Born AP, Holm S, et al. Regional differences in the CBF and BOLD responses to hypercapnia: a combined PET and fMRI study. *Neuroimage*. (2000) 11:87–97. doi: 10.1006/nimg.1999.0526
57. An H, Lin W, Celik A, Lee YZ. Quantitative measurements of cerebral metabolic rate of oxygen utilization using MRI: a volunteer study. *NMR Biomed*. (2001) 14:441–7. doi: 10.1002/nbm.717
58. Preibisch C, Haase A. Perfusion imaging using spin-labeling methods: contrast-to-noise comparison in functional MRI applications. *Magn Reson Med*. (2001) 46:172–82. doi: 10.1002/mrm.1173
59. Helenius J, Perkiö J, Soinne L, Østergaard L, Carano RAD, Salonen O, et al. Cerebral hemodynamics in a healthy population measured by dynamic susceptibility contrast MR imaging. *Acta Radiol*. (2003) 44:538–46. doi: 10.1034/j.1600-0455.2003.00104.x
60. Bandettini PA, Jesmanowicz A, Wong EC, Hyde JS. Processing strategies for time-course data sets in functional mri of the human brain. *Magn Reson Med*. (1993) 30:161–73. doi: 10.1002/mrm.1910300204
61. Yan L, Zhuo Y, Ye Y, Xie SX, An J, Aguirre GK, et al. Physiological origin of low-frequency drift in blood oxygen level dependent (BOLD) functional magnetic resonance imaging (fMRI). *Magn Reson Med*. (2009) 61:819–27. doi: 10.1002/mrm.21902

**Conflict of Interest:** The authors declare that the research was conducted in the absence of any commercial or financial relationships that could be construed as a potential conflict of interest.

Copyright © 2020 Taneja, Liu, Xu, Turner, Zhao, Abdelkarim, Thomas, Rypma and Lu. This is an open-access article distributed under the terms of the Creative Commons Attribution License (CC BY). The use, distribution or reproduction in other forums is permitted, provided the original author(s) and the copyright owner(s) are credited and that the original publication in this journal is cited, in accordance with accepted academic practice. No use, distribution or reproduction is permitted which does not comply with these terms.





# Multimodal Evaluation of Neurovascular Functionality in Early Parkinson's Disease

Maria Marcella Laganà<sup>1†</sup>, Alice Pirastru<sup>1\*†</sup>, Laura Pelizzari<sup>1</sup>, Federica Rossetto<sup>1</sup>, Sonia Di Tella<sup>1</sup>, Niels Bergsland<sup>1,2</sup>, Raffaello Nemni<sup>1,3</sup>, Mario Meloni<sup>1</sup> and Francesca Baglio<sup>1</sup>

<sup>1</sup>IRCCS, Fondazione Don Carlo Gnocchi ONLUS, Milan, Italy, <sup>2</sup>Department of Neurology, Buffalo Neuroimaging Analysis Center, School of Medicine and Biomedical Sciences, University at Buffalo, State University of New York, Buffalo, NY, United States, <sup>3</sup>Department of Pathophysiology and Transplantation, Università degli Studi di Milano, Milan, Italy

## OPEN ACCESS

### Edited by:

Yulin Ge,  
Langone Medical Center, New York  
University, United States

### Reviewed by:

Maria Salsone,  
National Research Council (CNR), Italy  
Konstantinos Kalafatakis,  
University of Ioannina, Greece

### \*Correspondence:

Alice Pirastru  
apirastru@dongnocchi.it

<sup>†</sup>These authors have contributed  
equally to this work

### Specialty section:

This article was submitted to  
Applied Neuroimaging,  
a section of the journal  
Frontiers in Neurology

**Received:** 20 March 2020

**Accepted:** 03 July 2020

**Published:** 26 August 2020

### Citation:

Laganà MM, Pirastru A, Pelizzari L,  
Rossetto F, Di Tella S, Bergsland N,  
Nemni R, Meloni M and Baglio F  
(2020) Multimodal Evaluation of  
Neurovascular Functionality in Early  
Parkinson's Disease.  
Front. Neurol. 11:831.  
doi: 10.3389/fneur.2020.00831

Parkinson's disease (PD) is a multisystem neurological condition affecting different neurotransmitter pathways characterized by aberrant functional connectivity (FC) and perfusion alteration. Since the FC, measuring neuronal activity, and cerebral blood flow (CBF) are closely related through the neurovascular coupling (NVC) mechanism, we aim to assess whether FC changes found in PD mirror perfusion ones. A multimodal MRI study was implemented by acquiring resting state functional MRI (rsfMRI) and arterial spin labeling (ASL) datasets on a group of 26 early PD ( $66.8 \pm 8$  years, 22 males, median [interquartile range] Hoehn and Yahr = 1.5 [1]) and 18 age- and sex-matched healthy controls (HCs). In addition, a T1-weighted MPRAGE was also acquired in the same scan session. After a standard preprocessing, resting state networks (RSNs) and CBF maps were extracted from rsfMRI and ASL dataset, respectively. Then, by means of a dual regression algorithm performed on RSNs, a cluster of FC differences between groups was obtained and used to mask CBF maps in the subsequent voxel-wise group comparison. Furthermore, a gray matter (GM) volumetric assessment was performed within the FC cluster in order to exclude tissue atrophy as a source of functional changes. Reduced FC for a PD patient with respect to HC group was found within a sensory-motor network (SMN,  $p_{FWE} = 0.01$ ) and visual networks (VNs, primary  $p_{FWE} = 0.022$  and lateral  $p_{FWE} = 0.01$ ). The latter was accompanied by a decreased CBF (primary  $p_{FWE} = 0.037$ , lateral  $p_{FWE} = 0.014$  VNs), while no GM atrophy was detected instead. The FC alteration found in the SMN of PD might be likely due to a dopaminergic denervation of the striatal pathways causing a functional disconnection. On the other hand, the changes in connectivity depicted in VNs might be related to an altered non-dopaminergic system, since perfusion was also reduced, revealing a compromised NVC. Finally, the absence of GM volume loss might imply that functional changes may potentially anticipate neurodegeneration. In this framework, FC and CBF might be proposed as early functional biomarkers providing meaningful insights in evaluating both disease progression and therapeutic/rehabilitation treatment outcome.

**Keywords:** Parkinson's disease, resting state fMRI, arterial spin labeling, functional connectivity, cerebral blood flow, neurovascular coupling

## INTRODUCTION

Parkinson's disease (PD) is one of the most frequent neurodegenerative disorders affecting over four million people worldwide (1). PD is clinically characterized by both motor symptoms, such as tremor, bradykinesia, and rigidity, and non-motor ones, including cognitive impairment, neuropsychiatric symptoms, and autonomic dysfunction (2, 3). From a neuropathological point of view, PD can be considered as a multisystem brain disorder (4, 5) affecting different neurotransmitter pathways. The dopaminergic denervation of striatal pathways is considered the cardinal signature of PD, and it is often linked to motor symptoms (5). The other pathophysiological feature of PD is the progressive deposition of  $\alpha$ -synuclein in cholinergic and monoaminergic brain neurons, concurrent with the evolution of Lewy body pathology (6).

The scientific community has shown a great interest in trying to identify non-invasive imaging biomarkers that may improve our understanding of the mechanisms underlying PD. In this framework, both resting state functional magnetic resonance imaging (rsfMRI) and arterial spin labeling (ASL) have provided considerable insights into the neural correlates of PD, detecting functional connectivity (FC) and cerebral blood flow (CBF) alterations, respectively.

FC alterations in PD have been extensively reported both in terms of increased and decreased connectivity (7, 8). Increased blood oxygen level dependent (BOLD) signal was found in primary and secondary motor cortices and the middle frontal gyrus of PD patients (9). On the other hand, decreased FC was observed in the supplementary motor area (SMA) (10) and between temporal regions and left occipital cortex and left lingual gyrus (11). Furthermore, reduced FC in posterior cortical regions has been associated with global cognitive decline (12), while the disruption of anticorrelation patterns between the occipito-parietal areas and the default mode network correlated with visuospatial deficits in PD (13).

Besides FC changes, perfusion alterations were also observed in PD (14, 15). Perfusion was found to be reduced in pre-SMA (16). Reduced CBF was also reported in occipital and parietal cortices (14, 17), precuneus and cuneus (17), and frontal cortex (16) bilaterally. Hypoperfusion was hypothesized to be related to the alteration of cholinergic, serotonergic, and noradrenergic neurotransmitter pathways in PD (16, 18, 19). Although several studies reported no perfusion changes in PD (18, 20, 21), in Pelizzari et al. (21), the resulting CBF correlated with symptoms severity, while Al-Bachari et al. (18) revealed a prolonged arterial arrival time confirming an aberrant neurovascular status of PD.

Since BOLD signal reflects changes in the venous oxygenation level (22), rsfMRI contrast is closely dependent on CBF (23). The neuronal activity and cerebral perfusion are strictly related by means of the physiological mechanism known as neurovascular coupling (NVC), which enables the prompt adaptation of brain perfusion to the (local) metabolic demand. Evidence of injury to both neural innervations and capillaries were reported in idiopathic PD (19), suggesting that the neurovascular unit is

affected at different levels in PD. For these reasons, cross-talk between observed FC and CBF alterations in PD cannot be excluded.

In order to better understand the relationship between neural activity and perfusion alterations in PD, we conducted a multimodal MRI study by concurrently assessing FC and CBF by means of rsfMRI and ASL, respectively. We aimed to investigate whether the FC changes found in PD reflect perfusion alterations. Gray matter (GM) volume was also assessed to exclude atrophy as a confounding factor of functional and perfusion changes.

## METHODS

### Demographic and Clinical Evaluation

Twenty-six PD patients and 18 age and sex-matched healthy controls (HC) were enrolled in this study. The inclusion criteria for the PD patients were as follows: (1) a diagnosis of idiopathic PD according to the Movement Disorder Society Clinical Diagnostic Criteria for PD (24); (2) absence of neuropsychiatric disorders beside PD diagnosis at clinical evaluation; (3) absence of neurovascular diseases at clinical evaluation, documented also with previous MRI/CT examination; (4) Positive DaTscan; (5) mild to moderate stage of the disease with a scoring between stages 1 and 3 of the Modified Hoehn and Yahr (H&Y) Scale (25); (6) stable drug therapy with either L-Dopa or dopamine agonists; (7) freezing assessed with UPDRS part II lower than 2; and (8) time spent with dyskinesias assessed with UPDRS part IV lower than 2. HC were included after assessing the absence of any neurological and/or neuropsychiatric disorder and/or neurovascular diseases.

All participants were right-handed.

For PD patients, the clinical evaluation included the quantification of the disease stage with H&Y and the assessment of the symptom severity with UPDRS motor part III (UPDRS III) performed by an experienced neurologist. Moreover, PD patients were classified as either tremor dominant or akinetic-rigid (26). Drug administration was recorded, and levodopa equivalent daily dose (LEDD) was calculated as suggested in Tomlinson et al. (27).

The global cognitive level of all the participants was assessed with the Montreal Cognitive Assessment (MoCA) test.

The study was performed in accordance with the principles of the Helsinki Declaration and by previous approval from the IRCSS Fondazione Don Carlo Gnocchi Ethics Committee. Written informed consent was signed by each participant.

### MRI Acquisition

All the subjects underwent a magnetic resonance imaging (MRI) examination performed on a 1.5T Siemens Avanto scanner (Erlangen, Germany) equipped with a 12-channel head coil. The acquisition comprised: (1) a 3D high-resolution magnetization-prepared rapid gradient echo (MPRAGE) T1-weighted image [repetition time (TR) = 1,900 ms, echo time (TE) = 3.3 ms, inversion time (TI) = 1,100 ms, matrix size =  $192 \times 256 \times 176$ , resolution =  $1 \text{ mm}^3$  isotropic]; (2) a multi-echo resting state fMRI (ME-rsfMRI) sequence (TR = 2,570 ms, TE = 15/34/54 ms, matrix size =  $64 \times 64 \times 31$ , resolution =  $3.75 \times 3.75 \times 4.5 \text{ mm}^3$ , 200 volumes); (3) a double-echo GRE field map (TR =

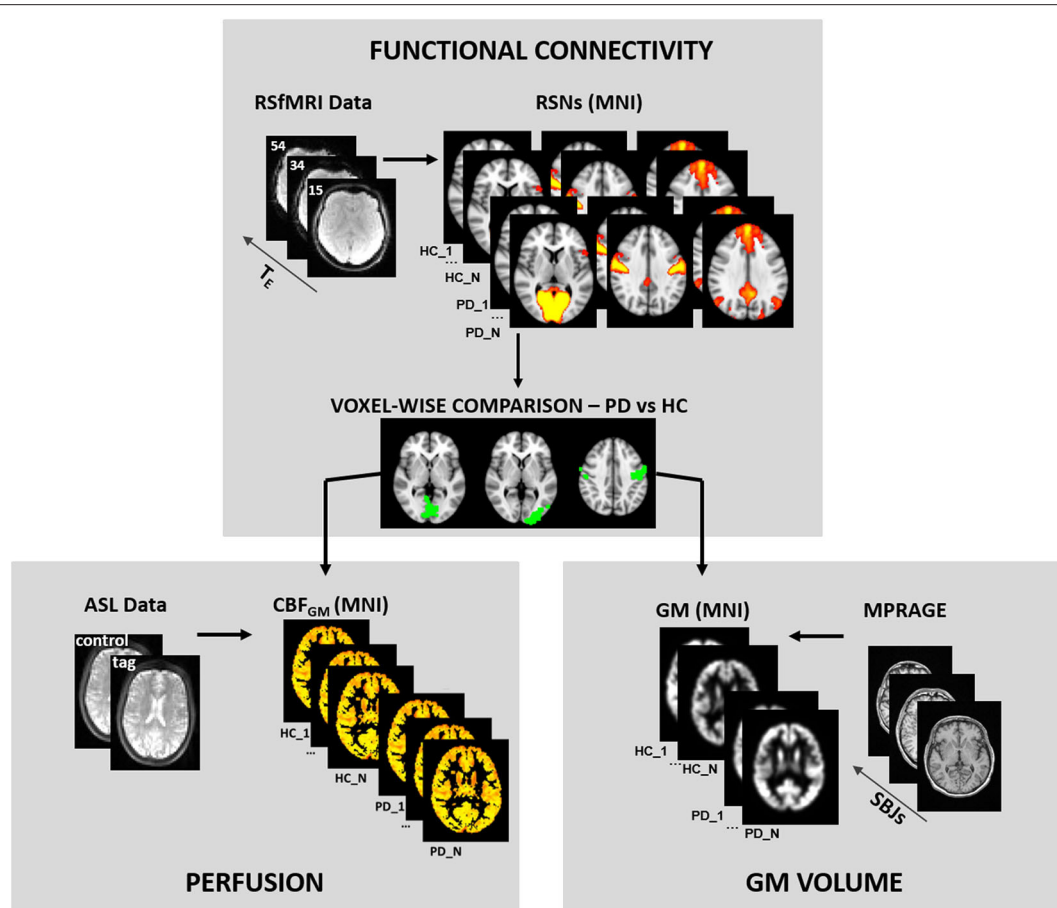


**FIGURE 1 |** MRI analysis pipeline. The figure shows the pipeline of MRI analyses. Briefly, the preprocessing is shown in each panel for the different modalities. The functional results of the comparison between healthy control (HC) and Parkinson's disease (PD) groups were used as masks of the statistical analysis of perfusion and gray matter maps.

528 ms, TE = 4.76/9.52 ms, matrix size =  $100 \times 100 \times 42$ , resolution =  $3.2 \times 3.2 \times 3.3 \text{ mm}^3$ ; and (4) a 3D gradient and spin echo (GRASE) multidelay pseudo-continuous arterial spin labeling (pCASL) with background suppression sequence [TR/TE = 3,500/22.58 ms, labeling duration = 1,500 ms, 5 post-labeling delays (PLD) = 700/1200/1700/2200/2700 ms, 12 pairs of tag/control volumes, matrix size =  $64 \times 64 \times 32$ , resolution =  $3.5 \times 3.5 \times 5 \text{ mm}^3$ , distance between the center of imaging slices and labeling plane = 90 mm].

## MRI Analysis

The image processing was performed by means of FMRIB Software Library (FSL, <http://www.fmrib.ox.ac.uk/fsl>) toolboxes 5.0.6 if not otherwise specified.

The pipeline of MRI processing is schematized in **Figure 1**.

## Pre-processing of MRI Data

### 3D-T1 MPRAGE

The MPRAGE, which was used as an anatomical reference for registration purposes, was skull-stripped by means of bet toolbox (28), then the SIENAX algorithm (29) was run in order

to segment the brain tissues in GM, white matter (WM), and cerebrospinal fluid. A voxel-based morphometry (VBM) analysis (30) was then carried out. Specifically, a symmetrical study-specific template was created in MNI standard space; then, using a non-linear registration, individual GM images were aligned to the study-specific template. Finally, the GM images were spatially smoothed with  $\sigma = 3$ .

### rsfMRI Dataset

Movement parameters were estimated for each subject-specific ME-rsfMRI dataset by means of FEAT (31). Subjects presenting with relative movement  $< 0.5 \text{ mm}$  were excluded from the study. The first 10 volumes (out of 200) were discarded to allow for magnetization stabilization.

The rsfMRI dataset was then preprocessed with the ME-Independent Component Analysis (ICA) algorithm (32, 33). After standard preprocessing comprising motion correction and realignment, the MEICA algorithm performed the estimation of an optimal combination of the three echoes together with a denoising step, based on the TE dependencies, of the ICA-derived components. The denoised volume was then aligned

with the subjects' MPAGE by means of a linear transformation performed using a Boundary-Based registration (BBR) (34, 35). The BBR simultaneously performed the registration and the distortion correction using the acquired field map.

MPAGE images were normalized to the Montreal Neurological Institute (MNI) atlas using the advanced normalization tools (ANTs; <http://stnava.github.io/ANTs>) (36) and subsequently used to align the functional data to standard space.

### ASL Dataset

The preprocessing of the pCASL dataset included realignment and motion correction of the original tag and control volumes, using ANTs software package. The group of 12 tag and control volumes acquired with the same delay was then separately averaged. The estimation and calibration of cerebral blood flow maps were performed by means of `oxford_asl` and `asl_calib` tools (37) respectively, by setting the required parameters as follows: T1 of brain tissue = 1.2 s, T1 of blood = 1.36 s, tagging efficiency = 0.8 accordingly (38, 39). Partial volume correction was performed using GM and WM masks derived from the MPAGE and registered to the ASL space and considering GM perfusion as 2.5 that of WM, as described in Marshall et al. (40). Then, corrected CBF maps were non-linearly registered to the MNI standard space and smoothed with a Gaussian kernel ( $\sigma = 3$ ).

### Group Level Analyses

For group analysis, the rsfMRI datasets were then decomposed in spatial independent components (IC) by means of the MELODIC toolbox (41) setting the dimensionality to 20. The derived IC were visually classified in order to detect the well-defined Smith's resting state networks (RSN) described in Smith et al. (42). Dual regression (43, 44), one on the group spatial maps and one on the subject's time series, was run on the group ICA derived from the functional dataset and allowed to derive subject-specific spatial maps. Then the comparison between the PD and HC groups was implemented through a randomize tool (45) using threshold-free cluster enhancement (TFCE) with 5,000 permutations. Furthermore, in the PD patient group, a partial correlation (age and sex as covariates) between  $z$ -values extracted from the clusters of significant FC differences and UPDRS III was performed.

In order to understand if the FC changes were accompanied by perfusion or volumetric alterations, we also performed a voxel-wise analysis of CBF and GM volume, comparing PD and HC in the areas of FC differences. The statistics were carried out by means of the randomize tool with 5,000 permutations and cluster detection with TFCE (45), and were restricted within the cluster of significant FC difference between the two groups (Figure 1), using them as masks. The percentage of the altered FC cluster that reported CBF differences was also computed. Finally, in the PD group patients, to test the effect of levodopa treatment on our perfusion results, we assessed the correlation between the CBF values of the significant cluster and LEDD.

**TABLE 1 |** Demographic characteristic of HC and PD groups.

	HC ( <i>n</i> = 18)	PD ( <i>n</i> = 26)	<i>p</i> -value
Males <i>n</i> (%)	11 (61%)	22 (85%)	0.077 <sup>a</sup>
Age in years, mean (SD)	65.6 (8.25)	66.85 (8.0)	0.62 <sup>b</sup>
Disease duration in years, median (IQR)	–	3 (2)	–
UPDRS III, mean (SD)	–	21.92 (13.2)	–
Tremor-dominant/Akinetic-rigid <i>n</i> (%)	–	14 (54%)/12 (46%)	–
H&Y, median (IQR)	–	1.5 (1)	–
LEDD, mean (SD)	–	228.2 (139.5)	–
MoCA, median (IQR)	26.43 (3.94)	24.84 (3.73)	<b>0.025<sup>c</sup></b>
Visuo-spatial	3.9 (0.72)	3.3 (1.32)	<b>0.002<sup>c</sup></b>
Executive	3.77 (1)	2.91 (1.46)	0.015 <sup>c</sup>
Memory	5 (1)	3 (3)	<b>0.0004<sup>c</sup></b>
Attention	5.76 (0.89)	5.71 (0.46)	0.892 <sup>c</sup>
Language	5.9 (1.34)	5.27 (0.825)	0.037 <sup>c</sup>
Orientation	6.04 (0.07)	5.99 (0.31)	0.026 <sup>c</sup>

*a* = chi-squared test; *b* = independent sample *t*-test; *c* = Mann-Whitney test. \*MoCA subscores were corrected for multiple comparison using Bonferroni correction resulting in  $\alpha = 0.008$ . MoCA scores were adjusted for age and education when required. SD, standard deviation; IQR, interquartile range; UPDRS III, Unified Parkinson's Disease Rating Scale—Part III; H&Y, Hoehn and Yahr; LEDD, levodopa equivalent daily dose; MoCA, Montreal Cognitive Assessment. Significant *p*-values are highlighted in bold.

## RESULTS

### Sample Demographic and Neuropsychological Evaluation

Demographic data and neuropsychological scores are reported in Table 1 for the two groups. PD patients and HCs were age- and sex-matched at the group level; the clinical phenotype of patients was tremor-dominant in 54% and akinetic-rigid in 46%. Five patients were treated with antidepressant (mirtazapine or escitalopram or duloxetine), and only three patients were taking low dose of benzodiazepine (prazepam or alprazolam). The overall cognitive performance was in the range of normality for both HC and PD. However, the comparison between the MoCA total score of HC and PD revealed a significant reduction in PD (26.4 vs. 24.8,  $p = 0.025$ ) and in the subscores of visuospatial ( $p = 0.002$ ) and memory ( $p < 0.001$ ) functions (Table 1). None of the enrolled subjects was excluded for excessive movements.

### Functional Connectivity Results

Eleven ICs out of 20 were classified as RSN according to Beckmann et al. (46) and are reported in Supplementary Figure 1.

Significantly lower FC was observed for PD patients within the sensory-motor network ( $p_{\text{FWE}} = 0.01$ ) and within the primary ( $p_{\text{FWE}} = 0.022$ ) and lateral ( $p_{\text{FWE}} = 0.01$ ) visual RSNs (Figure 2A). The maximum peak, the extension, and the localization of the clusters of significant FC difference are reported in Table 2.



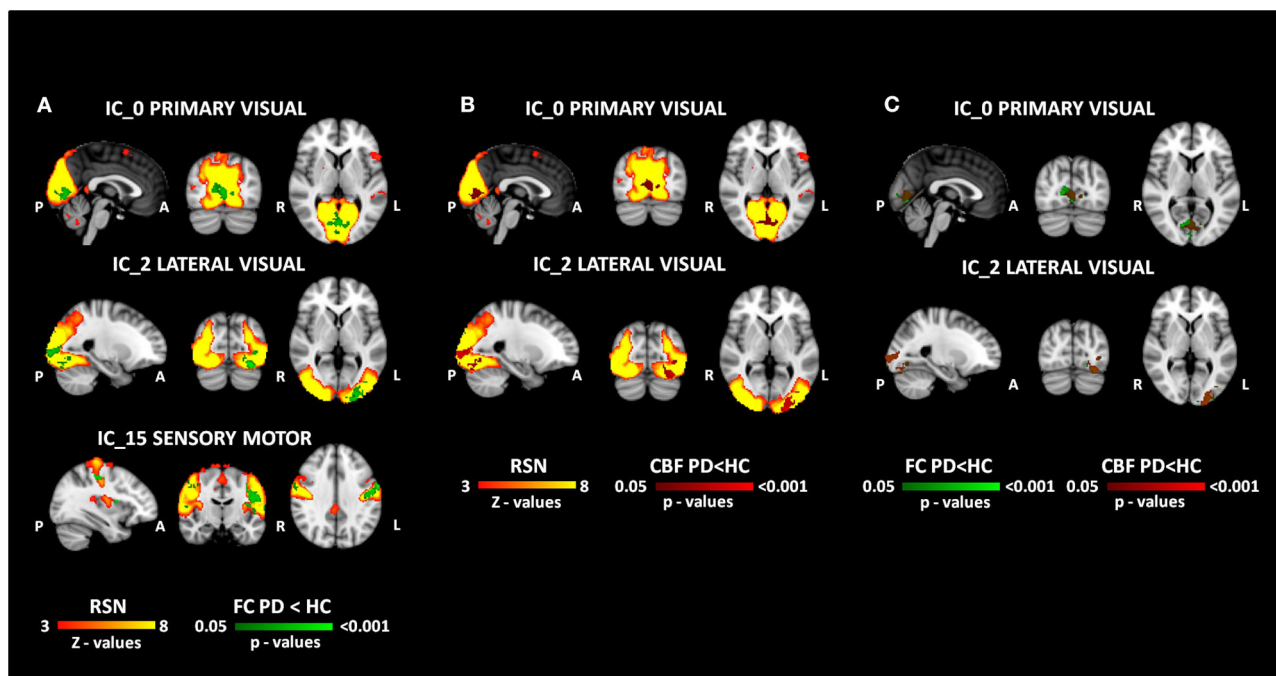


**FIGURE 2 |** MRI results. The results of functional and perfusion MRI analyses are reported in the figure. **(A)** The functional changes (FC HC > FC PD in green) within the resting state networks (red-yellow). **(B)** The perfusion changes (CBF HC > CBF PD in red) overlapped to the functional network (red-yellow). **(C)** The overlap between functional (green) and perfusion (red) clusters of significant differences. All the reported *p*-values are FWE corrected.

Furthermore, the partial correlation showed a negative trend ( $p = 0.06$ ,  $r = -0.38$ ) between the *z*-values of the sensory-motor network and the UPDRS III score for PD patients.

## Perfusion Results

Perfusion alterations were found both within primary ( $p_{\text{FWE}} = 0.037$ ) and lateral ( $p_{\text{FWE}} = 0.014$ ) visual networks, whereas no difference in CBF was detected in the sensory-motor one (**Figure 2B**). The maximum peak, the extension, and the localization of the clusters of CBF significant difference are reported in **Table 3**. The percentage of the overlap resulted in 46% and 74% of voxels for primary and lateral visual components, respectively (**Figure 2C**). The alteration in CBF did not correlate with any clinical variable, and no significant relationship between the CBF values of the significant CBF clusters and LEDD variables was found ( $r = 0.063$ ,  $p = 0.763$  for primary visual network and  $r = 0.141$ ,  $p = 0.502$  for the lateral visual one).

## VBM Results

No GM atrophy was found concurrent with the functional alteration for our cohort of early PD patients when compared to HC.

## DISCUSSION

The present work aimed to study the relationship between changes in FC and altered perfusion reported in PD. To do so, we concurrently assessed FC and CBF in a cohort of early PD

patients and HC by means of rsfMRI and ASL, respectively. FC changes were found in the sensory-motor and visual cortices of our PD patients. Interestingly, the FC alterations within the visual cortex were also accompanied by altered CBF.

The significant FC reduction that we observed in the SMN extended between pre- and post-central gyri and also comprised part of the middle frontal gyrus. Consistently, other studies using an ICA-based approach had previously evidenced changes in FC specific to the SMN in resting conditions. Canu et al. showed a decreased connectivity within the SMA and primary motor cortex, belonging to the SMN, in PD compared to HC (47), confirming previous findings of reduced SMA FC (48). Moreover, the aberrant FC pattern that we detected in our sample was linked to symptom severity measured using MDS-UPDRS III. We hypothesized that the altered SMN FC might be related to a disconnection of the striatal pathways following dopaminergic denervation. In fact, paralleling the neuropathological progression of PD, decreased FC between cortical and subcortical motor areas involving the dopaminergic corticostriatal loop has been reported (49).

In this study a significant FC decrease was also observed in primary (lingual gyrus and intracalcarine cortex) and lateral (inferior lateral occipital cortex, specifically occipital pole, and fusiform gyrus) VNs. The key regions of the primary visual areas are related to visual awareness, whereas the secondary visual network is involved in visual experience (50). Our findings point to dysfunction not only of the primary visual system but also of higher visual processing areas in the extrastriate cortex. The

**TABLE 2 |** Functional connectivity differences.

RSN	Dimension [voxels]	Harvard–oxford atlas	Position (COG)			Minimum <i>p</i> -value	Peak		
			x[mm]	y[mm]	z[mm]		x[mm]	y[mm]	z[mm]
Primary visual	605	Lingual G., intracalcarine C.	2.88	−78.1	3.84	0.022	0	−80	−4
Lateral visual	459	Occipital pole	−21.5	−95.7	−1.99	0.018	−20	−102	−8
	302	Occ. fusiform G.	−25.6	−78.8	−14.7	0.01	−30	−78	−18
Sensory motor	968	Post/Pre-central G.	−48	−12.3	36.8	0.01	−64	0	20
	304	Post/Pre-Central G.	61.3	−3.18	22.5	0.02	64	2	20
	103	Post-central G.	50.9	−15.3	49.3	0.03	52	−20	52
	51	Central opercular C., hescl G.	−50.9	−11.8	8.12	0.032	−50	−14	6
	18	Post/Pre-Central G.	−26.7	−27.2	60.3	0.024	−26	−26	60
	13	Inferior frontal G.	−40	25.2	22.1	0.028	−40	24	20
	11	Post/Pre-central G.	37.6	−20	57.5	0.04	98	−20	58
	10	Precentral G, middle frontal G.	−39.4	−3.2	57.2	0.02	−38	−4	56

Cluster of significant differences (*HC > PD*) in functional connectivity within resting state networks. Only the cluster with an extension  $\geq 10$  voxels are shown in the table. The coordinates reported refer to MNI standard space. RSN, resting state network; COG, center of gravity; G, gyrus; C, cortex.

**TABLE 3 |** Perfusion differences.

RSN	Dimension [voxels]	Harvard–oxford atlas	Position (COG)			Minimum <i>p</i> -value	Peak		
			x[mm]	y[mm]	z[mm]		x[mm]	y[mm]	z[mm]
Primary visual	279	Lingual G., intracalcarine C.	−1.15	−77.5	3.23	0.037	−6	−88	−4
Lateral visual	328	Occipital pole	−24.5	−95.4	−0.58	0.014	−22	−104	0
	247	Occipital fusiform G.	−27.4	−78.6	−15.6	0.019	−34	−78	−16

Cluster of significant differences (*HC > PD*) of perfusion within the cluster of functional connectivity changes. Only the cluster with an extension  $\geq 10$  voxels are shown in the table. The coordinates reported refer to MNI standard space. RSN, resting state network; COG, center of gravity; G, gyrus; C, cortex.

decreased activity of the primary visual network is probably due to specific PD-associated retinopathy targeting the striate visual areas (51). The functional alteration of the extrastriate visual pathways is supported by the significantly lower visuospatial performances (as assessed using MoCA subscales) that were found in our PD patients with respect to HC.

Similar FC changes have already been reported in literature (11, 52). Interestingly, the decreased connectivity within the primary and lateral VNs was accompanied by a significant CBF reduction. Our perfusion results are in line with previous studies quantitatively investigating vascular alteration in PD by means of ASL (16, 17, 53) or other modalities (14). Specifically, Melzer and colleagues reported preserved perfusion in post- and pre-central gyri, while perfusion was reduced in the posterior parieto-occipital cortex, similarly to Syrimi et al. (53). Abe et al. (14) also found reduced CBF in the same region by means of single-photon emission computed tomography.

The functional and perfusion changes were extensively concurrent in the visual RSN, with an overlap ranging from 46% to 74% in our PD sample. The hypoperfusion that we found in occipital areas concurrently to a decrease in FC may be indicative of a possible impairment of the NVC mechanism in PD. It has been previously proposed that CBF reductions might be due to modifications of non-dopaminergic transmitter systems (specifically cholinergic, serotonergic, and noradrenergic) and their neurovascular innervation of the neocortex (16, 18, 19, 54). Contextually, Shimada et al. (55) reported an alteration of the

cholinergic system in PD patients without dementia, which was most significant in the medial occipital cortex. According to Braak staging (56), neuronal cholinergic degeneration occurs at the same stage of nigral pathology, which characterizes relatively early phases of the disease. Thus, we hypothesize that structural and microstructural changes in the noradrenergic and cholinergic system nuclei at this stage of the pathology may be the cause of the alteration of the coupling between neural activity and blood flow observed in visual areas of our early PD patients [H&Y median (IQR), 1.5 (1)].

Furthermore, the FC and CBF alterations in VNs were not accompanied by local GM atrophy, suggesting that functional changes occur prior to tissue loss. Evidence from recent studies reporting CBF reductions at the early stage of the disease in cortical regions without manifested pathology (16, 57) supports this hypothesis. Moreover, Fernandez-Seara et al. (16) demonstrated that there is not a direct correspondence between GM atrophy and hypoperfusion, with the latter being more extensive throughout the brain.

One of the main drawbacks regarding FC studies in PD is the heterogeneity of the results presented in the literature, likely due to clinically variegated samples of patients and different methodological approaches. For these reasons, in the present study, we used a well-established data-driven ICA-approach together with a dual regression analysis. This method investigates all the GM voxels and exploits the simultaneous analysis of several subjects, thus increasing the signal-to-noise

ratio (58). This study is not without limitations. First, a 1.5T field scanner was employed for data acquisition. Despite being extensively used in the clinical setting, 1.5T MRI has relatively low signal-to-noise ratio. For this reason, both the rsfMRI and ASL sequences were set to partially mitigate this problem. Specifically, a multi-echo rsfMRI sequence was employed to improve the image contrast and to reduce image distortions by means of an optimal combination of the volumes acquired at three different echo times (32). For what concerns the ASL sequence, a pseudocontinuous acquisition scheme was used, together with a background suppressed 3D gradient and spin echo readout, aiming to enhance both SNR and signal tagging efficiency, as recommended by international guidelines (59). Another limitation of the study is the relatively small size of the sample, which may have prevented us from showing significant correlations between clinical and neuroimaging parameters. Furthermore, levodopa and benzodiazepines/antidepressants may interfere with fMRI (60, 61) and CBF analysis (62, 63). However, a group of clinically homogeneous patients, under stable pharmacological treatment, was considered, and when we tested the effect of levodopa treatment on our perfusion results, no significant relationship between the variables was found. Finally, only MoCA scores and subscales were available for our sample, so the addition of more precise neuropsychological tests should be considered.

Altogether, our results suggest that MRI-derived measures, such as FC and CBF, may constitute valuable biomarkers to detect early neurovascular dysfunction occurring in PD prior to structural modification in terms of GM atrophy. Since FC and CBF provide complementary information about the neurovascular unit physiology, concurrently assessing both of them is crucial. Multimodal longitudinal studies are warranted to better understand the evolution of neurovascular dysfunction along with PD disease progression and to monitor treatment-related changes due to pharmacological and/or rehabilitative interventions.

## DATA AVAILABILITY STATEMENT

The datasets generated for this study are available on request to the corresponding author.

## REFERENCES

1. Foffani G, Obeso JA. A cortical pathogenic theory of Parkinson's disease. *Neuron*. (2018) 99:1116–28. doi: 10.1016/j.neuron.2018.07.028
2. Kalia LV, Lang AE. Parkinson's disease. *Lancet*. (2015) 386:896–912. doi: 10.1016/S0140-6736(14)61393-3
3. Marras C, Chaudhuri KR. Nonmotor features of Parkinson's disease subtypes. *Mov Disord*. (2016) 31:1095–102. doi: 10.1002/mds.26510
4. Poewe W, Seppi K, Tanner CM, Halliday GM, Brundin P, Volkman J, et al. Parkinson disease. *Nat Rev Dis Primers*. (2017) 3:17013. doi: 10.1038/nrdp.2017.13
5. Papagno C, Trojano L. Cognitive and behavioral disorders in Parkinson's disease: an update. I: cognitive impairments. *Neurol Sci*. (2018) 39:215–23. doi: 10.1007/s10072-017-3154-8
6. Jahanshahi M, Obeso I, Rothwell JC, Obeso JA. A fronto-striato-subthalamic-pallidal network for goal-directed and habitual inhibition. *Nat Rev Neurosci*. (2015) 16:719–32. doi: 10.1038/nrn4038
7. Tessitore A, Giordano A, De Micco R, Russo A, Tedeschi G. Sensorimotor connectivity in Parkinson's disease: the role of functional neuroimaging. *Front Neurol*. (2014) 5:180. doi: 10.3389/fneur.2014.00180
8. Tessitore A, Cirillo M, De Micco R. Functional connectivity signatures of Parkinson's disease. *J Parkinsons Dis*. (2019) 9:637–52. doi: 10.3233/JPD-191592
9. Kwak Y, Peltier SJ, Bohnen NI, Muller ML, Dayalu P, Seidler RD. L-DOPA changes spontaneous low-frequency BOLD signal oscillations in Parkinson's disease: a resting state fMRI study. *Front Syst Neurosci*. (2012) 6:52. doi: 10.3389/fnsys.2012.00052

## ETHICS STATEMENT

The studies involving human participants were reviewed and approved by Fondazione Don Carlo Gnocchi Local Ethics Committee. The patients/participants provided their written informed consent to participate in this study.

## AUTHOR CONTRIBUTIONS

ML, AP, and FB contributed to the conception and design of the study. AP, NB, and LP performed the MRI data analysis. AP and ML performed the statistical analyses. AP wrote the first draft of the manuscript. FR and SD performed the neuropsychological evaluation. RN, FB, and MM recruited subjects and performed the clinical evaluation. All authors participated in reviewing the work, providing important intellectual content, and approving the final form.

## FUNDING

This study was funded by the Italian Ministry of Health (Ricerca Corrente 2018–2020).

## ACKNOWLEDGMENTS

We acknowledge the receipt of multidelay pCASL sequence from the University of Southern California's Stevens Neuroimaging and Informatics Institute. We also acknowledge the Regents of the University of California, on behalf of its Los Angeles campus, as a source of portions of the Licensed Technology. Finally, we acknowledge that Dr. DJJ Wang and SIEMENS Healthineers helped in setting the sequence on our scanner.

## SUPPLEMENTARY MATERIAL

The Supplementary Material for this article can be found online at: <https://www.frontiersin.org/articles/10.3389/fneur.2020.00831/full#supplementary-material>

10. Wu T, Wang L, Chen Y, Zhao C, Li K, Chan P. Changes of functional connectivity of the motor network in the resting state in Parkinson's disease. *Neurosci Lett.* (2009) 460:6–10. doi: 10.1016/j.neulet.2009.05.046
11. Luo C, Guo X, Song W, Chen Q, Yang J, Gong Q, et al. The trajectory of disturbed resting-state cerebral function in Parkinson's disease at different hoehn and yahr stages. *Hum Brain Mapp.* (2015) 36:3104–16. doi: 10.1002/hbm.22831
12. Olde Dubbelink KT, Schoonheim MM, Deijen JB, Twisk JW, Barkhof F, Berendse HW. Functional connectivity and cognitive decline over 3 years in Parkinson disease. *Neurology.* (2014) 83:2046–53. doi: 10.1212/WNL.0000000000001020
13. Baggio HC, Segura B, Sala-Llonch R, Marti MJ, Valldeoriola F, Compta Y, et al. Cognitive impairment and resting-state network connectivity in Parkinson's disease. *Hum Brain Mapp.* (2015) 36:199–212. doi: 10.1002/hbm.22622
14. Abe Y, Kachi T, Kato T, Arahata Y, Yamada T, Washimi Y, et al. Occipital hypoperfusion in Parkinson's disease without dementia: correlation to impaired cortical visual processing. *J Neurol Neurosurg Psychiatry.* (2003) 74:419–22. doi: 10.1136/jnnp.74.4.419
15. Teune LK, Renken RJ, De Jong BM, Willemsen AT, Van Osch MJ, Roerdink JB, et al. Parkinson's disease-related perfusion and glucose metabolic brain patterns identified with PCASL-MRI and FDG-PET imaging. *Neuroimage Clin.* (2014) 5:240–4. doi: 10.1016/j.nicl.2014.06.007
16. Fernandez-Seara MA, Mengual E, Vidorreta M, Aznarez-Sanado M, Loayza FR, Villagra F, et al. Cortical hypoperfusion in Parkinson's disease assessed using arterial spin labeled perfusion MRI. *Neuroimage.* (2012) 59:2743–50. doi: 10.1016/j.neuroimage.2011.10.033
17. Melzer TR, Watts R, Macaskill MR, Pearson JF, Rueger S, Pitcher TL, et al. Arterial spin labelling reveals an abnormal cerebral perfusion pattern in Parkinson's disease. *Brain.* (2011) 134:845–55. doi: 10.1093/brain/awq377
18. Al-Bachari S, Parkes LM, Vidyasagar R, Hanby MF, Tharaken V, Leroy I, et al. Arterial spin labelling reveals prolonged arterial arrival time in idiopathic Parkinson's disease. *Neuroimage Clin.* (2014) 6:1–8. doi: 10.1016/j.nicl.2014.07.014
19. Iadecola C. The neurovascular unit coming of age: a journey through neurovascular coupling in health and disease. *Neuron.* (2017) 96:17–42. doi: 10.1016/j.neuron.2017.07.030
20. Pelizzari L, Lagana MM, Di Tella S, Rossetto F, Bergsland N, Nemni R, et al. Combined assessment of diffusion parameters and cerebral blood flow within basal ganglia in early Parkinson's disease. *Front Aging Neurosci.* (2019) 11:134. doi: 10.3389/fnagi.2019.00134
21. Pelizzari L, Lagana MM, Rossetto F, Bergsland N, Galli M, Baselli G, et al. Cerebral blood flow and cerebrovascular reactivity correlate with severity of motor symptoms in Parkinson's disease. *Ther Adv Neurol Disord.* (2019) 12:1756286419838354. doi: 10.1177/1756286419838354
22. Gagnon L, Sakadzic S, Lesage F, Musacchia JJ, Lefebvre J. Quantifying the microvascular origin of BOLD-fMRI from first principles with two-photon microscopy and an oxygen-sensitive nanoprobe. *J Neurosci.* (2015) 35:3663–75. doi: 10.1523/JNEUROSCI.3555-14.2015
23. Kim T, Kim SG. Quantitative MRI of cerebral arterial blood volume. *Open Neuroimag J.* (2011) 5:136–45. doi: 10.2174/1874440001105010136
24. Postuma RB, Berg D, Stern M, Poewe W, Olanow CW, Oertel W, et al. MDS clinical diagnostic criteria for Parkinson's disease. *Mov Disord.* (2015) 30:1591–601. doi: 10.1002/mds.26424
25. Goetz CG, Poewe W, Rascol O, Sampaio C, Stebbins GT, Counsell C, et al. Movement disorder society task force report on the hoehn and yahr staging scale: status and recommendations. *Mov Disord.* (2004) 19:1020–8. doi: 10.1002/mds.20213
26. Rajput AH, Voll A, Rajput ML, Robinson CA, Rajput A. Course in Parkinson disease subtypes: A 39-year clinicopathologic study. *Neurology.* (2009) 73:206–12. doi: 10.1212/WNL.0b013e3181ae7af1
27. Tomlinson CL, Stowe R, Patel S, Rick C, Gray R, Clarke CE. Systematic review of levodopa dose equivalency reporting in Parkinson's disease. *Mov Disord.* (2010) 25:2649–53. doi: 10.1002/mds.23429
28. Smith SM. Fast robust automated brain extraction. *Hum Brain Mapp.* (2002) 17:143–55. doi: 10.1002/hbm.10062
29. Smith SM, Zhang Y, Jenkinson M, Chen J, Matthews PM, Federico A, et al. Accurate, robust, and automated longitudinal and cross-sectional brain change analysis. *Neuroimage.* (2002) 17:479–89. doi: 10.1006/nimg.2002.1040
30. Douaud G, Smith S, Jenkinson M, Behrens T, Johansen-Berg H, Vickers J, et al. Anatomically related grey and white matter abnormalities in adolescent-onset schizophrenia. *Brain.* (2007) 130:2375–86. doi: 10.1093/brain/awm184
31. Woolrich MW, Ripley BD, Brady M, Smith SM. Temporal autocorrelation in univariate linear modeling of FMRI data. *Neuroimage.* (2001) 14:1370–86. doi: 10.1006/nimg.2001.0931
32. Kundu P, Inati SJ, Evans JW, Luh WM, Bandettini PA. Differentiating BOLD and non-BOLD signals in fMRI time series using multi-echo EPI. *Neuroimage.* (2012) 60:1759–70. doi: 10.1016/j.neuroimage.2011.12.028
33. Kundu P, Brenowitz ND, Voon V, Worbe Y, Vertes PE, Inati SJ, et al. Integrated strategy for improving functional connectivity mapping using multiecho fMRI. *Proc Natl Acad Sci USA.* (2013) 110:16187–92. doi: 10.1073/pnas.1301725110
34. Jenkinson M, Bannister P, Brady M, Smith S. Improved optimization for the robust and accurate linear registration and motion correction of brain images. *Neuroimage.* (2002) 17:825–41. doi: 10.1006/nimg.2002.1132
35. Greve DN, Fischl B. Accurate and robust brain image alignment using boundary-based registration. *Neuroimage.* (2009) 48:63–72. doi: 10.1016/j.neuroimage.2009.06.060
36. Avants BB, Tustison NJ, Song G, Cook PA, Klein A, Gee JC. A reproducible evaluation of ANTs similarity metric performance in brain image registration. *Neuroimage.* (2011) 54:2033–44. doi: 10.1016/j.neuroimage.2010.09.025
37. Chappell M, Groves A, Whitcher B, Woolrich M. Variational bayesian inference for a nonlinear forward model. *IEEE Trans Signal Process.* (2009) 57:223–36. doi: 10.1109/TSP.2008.2005752
38. Wang DJ, Alger JR, Qiao JX, Gunther M, Pope WB, Saver JL, et al. Multi-delay multi-parametric arterial spin-labeled perfusion MRI in acute ischemic stroke - comparison with dynamic susceptibility contrast enhanced perfusion imaging. *Neuroimage Clin.* (2013) 3:1–7. doi: 10.1016/j.nicl.2013.06.017
39. Lagana MM, Mendozzi L, Pelizzari L, Bergsland NP, Pugnetti L, Cecconi P, et al. Are cerebral perfusion and atrophy linked in multiple sclerosis? Evidence for a multifactorial approach to assess neurodegeneration. *Curr Neurovasc Res.* (2018) 15:282–91. doi: 10.2174/1567202616666181123164235
40. Marshall O, Chawla S, Lu H, Pape L, Ge Y. Cerebral blood flow modulation insufficiency in brain networks in multiple sclerosis: a hypercapnia MRI study. *J Cereb Blood Flow Metab.* (2016) 36:2087–95. doi: 10.1177/0271678X16654922
41. Beckmann CF, Smith SM. Probabilistic independent component analysis for functional magnetic resonance imaging. *IEEE Trans Med Imaging.* (2004) 23:137–52. doi: 10.1109/TMI.2003.822821
42. Smith SM, Fox PT, Miller KL, Glahn DC, Fox PM, Mackay CE, et al. Correspondence of the brain's functional architecture during activation and rest. *Proc Natl Acad Sci USA.* (2009) 106:13040–5. doi: 10.1073/pnas.0905267106
43. Nickerson LD, Smith SM, Ongur D, Beckmann CF. Using dual regression to investigate network shape and amplitude in functional connectivity analyses. *Front Neurosci.* (2017) 11:115. doi: 10.3389/fnins.2017.00115
44. Beckmann CF, Mackay CE, Filippini N, Smith SM. Group comparison of resting-state FMRI data using multi-subject ICA and dual regression. *Neuroimage.* (2009) 47:S148. doi: 10.1016/S1053-8119(09)71511-3
45. Winkler AM, Ridgway GR, Webster MA, Smith SM, Nichols TE. Permutation inference for the general linear model. *Neuroimage.* (2014) 92:381–97. doi: 10.1016/j.neuroimage.2014.01.060
46. Beckmann CF, Deluca M, Devlin JT, Smith SM. Investigations into resting-state connectivity using independent component analysis. *Philos Trans R Soc Lond B Biol Sci.* (2005) 360:1001–13. doi: 10.1098/rstb.2005.1634
47. Canu E, Agosta F, Sarasso E, Volonte MA, Basaia S, Stojkovic T, et al. Brain structural and functional connectivity in Parkinson's disease with freezing of gait. *Hum Brain Mapp.* (2015) 36:5064–78. doi: 10.1002/hbm.22994
48. Esposito F, Tessitore A, Giordano A, De Micco R, Paccone A, Conforti R, et al. Rhythm-specific modulation of the sensorimotor network in drug-naïve patients with Parkinson's disease by levodopa. *Brain.* (2013) 136:710–25. doi: 10.1093/brain/awt007
49. Filippi M, Elisabetta S, Piramide N, Agosta F. Functional MRI in idiopathic Parkinson's disease. *Int Rev Neurobiol.* (2018) 141:439–67. doi: 10.1016/bs.irn.2018.08.005



50. Furman M. Visual network. In: Faingold CL, Blumenfeld H, editors. *Neuronal Networks in Brain Function, CNS Disorders, and Therapeutics*. Amsterdam: Elsevier; 1Academic Press (2014). p. 247–59. doi: 10.1016/B978-0-12-415804-7.00019-8
51. Diederich NJ, Fénelon G, Stebbins G, Goetz CG. Hallucinations in Parkinson disease. *Nat Rev Neurol*. (2009) 5:331. doi: 10.1038/nrneurol.2009.62
52. Ma LY, Chen XD, He Y, Ma HZ, Feng T. Disrupted brain network hubs in subtype-specific Parkinson's disease. *Eur Neurol*. (2017) 78:200–9. doi: 10.1159/000477902
53. Syrimi ZJ, Vojtisek L, Eliasova I, Viskova J, Svatkova A, Vanicek J, et al. Arterial spin labelling detects posterior cortical hypoperfusion in non-demented patients with Parkinson's disease. *J Neural Transm*. (2017) 124:551–7. doi: 10.1007/s00702-017-1703-1
54. Toussay X, Basu K, Lacoste B, Hamel E. Locus coeruleus stimulation recruits a broad cortical neuronal network and increases cortical perfusion. *J Neurosci*. (2013) 33:3390–401. doi: 10.1523/JNEUROSCI.3346-12.2013
55. Shimada H, Hirano S, Shinotoh H, Aotsuka A, Sato K, Tanaka N, et al. Mapping of brain acetylcholinesterase alterations in lewy body disease by PET. *Neurology*. (2009) 73:273–8. doi: 10.1212/WNL.0b013e3181ab2b58
56. Braak H, Del Tredici K, Rub U, De Vos RA, Jansen Steur EN, Braak E. Staging of brain pathology related to sporadic Parkinson's disease. *Neurobiol Aging*. (2003) 24:197–211. doi: 10.1016/S0197-4580(02)00065-9
57. Borghammer P, Chakravarty M, Jonsdottir KY, Sato N, Matsuda H, Ito K, et al. Cortical hypometabolism and hypoperfusion in Parkinson's disease is extensive: probably even at early disease stages. *Brain Struct Funct*. (2010) 214:303–17. doi: 10.1007/s00429-010-0246-0
58. Cole DM, Smith SM, Beckmann CF. Advances and pitfalls in the analysis and interpretation of resting-state FMRI data. *Front Syst Neurosci*. (2010) 4:8. doi: 10.3389/fnsys.2010.00008
59. Alsop DC, Detre JA, Golay X, Günther M, Hendrikse J, Hernandez-Garcia L, et al. Recommended implementation of arterial spin-labeled perfusion MRI for clinical applications: a consensus of the ISMRM perfusion study group and the European consortium for ASL in dementia. *Magn Reson Med*. (2015) 73:102–16. doi: 10.1002/mrm.25197
60. Harris JJ, Reynell C. How do antidepressants influence the BOLD signal in the developing brain? *Dev Cogn Neurosci*. (2017) 25:45–57. doi: 10.1016/j.dcn.2016.12.003
61. Frodl T, Scheuerecker J, Schoepf V, Linn J, Koutsouleris N, Bokde AL, et al. Different effects of mirtazapine and venlafaxine on brain activation: an open randomized controlled fMRI study. *J Clin Psychiatry*. (2011) 72:448–57. doi: 10.4088/JCP.09m05393blu
62. Chen Y, Pressman P, Simuni T, Parrish TB, Gitelman DR. Effects of acute levodopa challenge on resting cerebral blood flow in Parkinson's disease patients assessed using pseudo-continuous arterial spin labeling. *PeerJ*. (2015) 3:e1381. doi: 10.7717/peerj.1381
63. Lin WC, Chen PC, Huang YC, Tsai NW, Chen HL, Wang HC, et al. Dopaminergic therapy modulates cortical perfusion in Parkinson disease with and without dementia according to arterial spin labeled perfusion magnetic resonance imaging. *Medicine*. (2016) 95:e2206. doi: 10.1097/MD.0000000000002206

**Conflict of Interest:** The authors declare that the research was conducted in the absence of any commercial or financial relationships that could be construed as a potential conflict of interest.

Copyright © 2020 Laganà, Pirastru, Pelizzari, Rossetto, Di Tella, Bergsland, Nemni, Meloni and Baglio. This is an open-access article distributed under the terms of the Creative Commons Attribution License (CC BY). The use, distribution or reproduction in other forums is permitted, provided the original author(s) and the copyright owner(s) are credited and that the original publication in this journal is cited, in accordance with accepted academic practice. No use, distribution or reproduction is permitted which does not comply with these terms.



# Relationships Among Circulating Levels of Hemostasis Inhibitors, Chemokines, Adhesion Molecules, and MRI Characteristics in Multiple Sclerosis

Nicole Ziliotto<sup>1†</sup>, Robert Zivadinov<sup>2,3</sup>, Dejan Jakimovski<sup>2</sup>, Marcello Baroni<sup>1</sup>, Niels Bergsland<sup>2,4</sup>, Deepa P. Ramasamy<sup>2</sup>, Bianca Weinstock-Guttman<sup>3</sup>, Murali Ramanathan<sup>5</sup>, Giovanna Marchetti<sup>6</sup> and Francesco Bernardi<sup>1\*</sup>

## OPEN ACCESS

### Edited by:

Fabiana Novellino,  
National Research Council (CNR), Italy

### Reviewed by:

Jordi A. Matias-Guiu,  
Hospital Clínico San Carlos, Spain  
Bo Gao,  
Affiliated Hospital of Guizhou Medical  
University, China

### \*Correspondence:

Francesco Bernardi  
ber@unife.it

### † Present address:

Nicole Ziliotto,  
School of Medicine and Surgery,  
University of Milano-Bicocca, Monza,  
Italy

### Specialty section:

This article was submitted to  
Applied Neuroimaging,  
a section of the journal  
Frontiers in Neurology

Received: 19 April 2020

Accepted: 31 August 2020

Published: 15 October 2020

### Citation:

Ziliotto N, Zivadinov R, Jakimovski D,  
Baroni M, Bergsland N,  
Ramasamy DP, Weinstock-Guttman B,  
Ramanathan M, Marchetti G and  
Bernardi F (2020) Relationships  
Among Circulating Levels of  
Hemostasis Inhibitors, Chemokines,  
Adhesion Molecules, and MRI  
Characteristics in Multiple Sclerosis.  
Front. Neurol. 11:553616.  
doi: 10.3389/fneur.2020.553616

<sup>1</sup> Department of Life Sciences and Biotechnology, University of Ferrara, Ferrara, Italy, <sup>2</sup> Department of Neurology, Buffalo Neuroimaging Analysis Center, State University of New York, Buffalo, NY, United States, <sup>3</sup> Center for Biomedical Imaging at the Clinical Translational Science Institute, State University of New York, Buffalo, NY, United States, <sup>4</sup> Istituto di Ricovero e Cura a Carattere Scientifico (IRCCS), Fondazione Don Carlo Gnocchi, Milan, Italy, <sup>5</sup> Department of Pharmaceutical Sciences, State University of New York, Buffalo, NY, United States, <sup>6</sup> Department of Biomedical and Specialty Surgical Sciences, University of Ferrara, Ferrara, Italy

**Background:** Several studies suggested cross talk among components of hemostasis, inflammation, and immunity pathways in the pathogenesis, neurodegeneration, and occurrence of cerebral microbleeds (CMBs) in multiple sclerosis (MS).

**Objectives:** This study aimed to evaluate the combined contribution of the hemostasis inhibitor protein C (PC) and chemokine C-C motif ligand 18 (CCL18) levels to brain atrophy in MS and to identify disease-relevant correlations among circulating levels of hemostasis inhibitors, chemokines, and adhesion molecules, particularly in CMB occurrence in MS.

**Methods:** Plasma levels of hemostasis inhibitors (ADAMTS13, PC, and PAI1), CCL18, and soluble adhesion molecules (sNCAM, sICAM1, sVCAM1, and sVAP1) were evaluated by multiplex in 138 MS patients [85 relapsing-remitting (RR-MS) and 53 progressive (P-MS)] and 42 healthy individuals (HI) who underwent 3-T MRI exams. Association of protein levels with MRI outcomes was performed by regression analysis. Correlations among protein levels were assessed by partial correlation and Pearson's correlation.

**Results:** In all patients, regression analysis showed that higher PC levels were associated with lower brain volumes, including the brain parenchyma ( $p = 0.002$ ), gray matter ( $p < 0.001$ ), cortex ( $p = 0.001$ ), deep gray matter ( $p = 0.001$ ), and thalamus ( $p = 0.001$ ). These associations were detectable in RR-MS but not in P-MS patients. Higher CCL18 levels were associated with higher T2-lesion volumes in all MS patients ( $p = 0.03$ ) and in the P-MS ( $p = 0.003$ ). In the P-MS, higher CCL18 levels were also associated with lower volumes of the gray matter ( $p = 0.024$ ), cortex ( $p = 0.043$ ), deep gray matter ( $p = 0.029$ ), and thalamus ( $p = 0.022$ ). PC-CCL18 and CCL18-PAI1 levels were positively correlated in both MS and HI, PC-sVAP1 and PAI1-sVCAM1 only in MS, and PC-sICAM1 and PC-sNCAM only in HI. In MS patients with CMBs ( $n = 12$ ),

CCL18–PAI1 and PAI1–sVCAM1 levels were better correlated than those in MS patients without CMBs, and a novel ADAMTS13–sVAP1 level correlation ( $r = 0.78$ ,  $p = 0.003$ ) was observed.

**Conclusions:** Differences between clinical phenotype groups in association of PC and CCL18 circulating levels with MRI outcomes might be related to different aspects of neurodegeneration. Disease-related pathway dysregulation is supported by several protein level correlation differences between MS patients and HI. The integrated analysis of plasma proteins and MRI measures provide evidence for new relationships among hemostasis, inflammation, and immunity pathways, relevant for MS and for the occurrence of CMBs.

**Keywords:** multiple sclerosis, neurodegeneration, cerebral microbleeds, hemostasis inhibitors, adhesion molecules

## INTRODUCTION

In multiple sclerosis (MS) pathogenesis, blood–brain barrier (BBB) disruption and vascular changes interact in a vicious cycle with altered immune trafficking and the inflammatory processes, supported by adhesion molecules and chemokines (1–3). Several studies also suggested the cross talk of immunity and inflammation with hemostasis, potentially reflected in MS pathogenesis and progression of neurodegeneration (4).

Plasma levels of protein C (PC) have been associated with neurodegenerative magnetic resonance imaging (MRI) outcomes in MS patients (5). Among hemostasis components, PC has coagulation inhibitor activity and also anti-inflammatory and cell protective properties (6). Activated PC might inhibit leukocyte adhesion and transmigration, downregulating endothelial expression of intercellular adhesion molecule-1 (ICAM1) and vascular cell adhesion molecule-1 (VCAM1) (7, 8). In MS-related vascular changes, circulating soluble (s) forms of cell adhesion molecules (CAMs) can result from activated membranes shedding in response to endothelial damage (9).

Neurodegenerative outcomes in MS patients have been also associated with higher plasma levels of C-C motif ligand 18 (CCL18), a chemokine involved in immune cell chemotaxis (10). To note, inflammatory cytokines favor the expression of plasminogen activator inhibitors-1 (PAI1) (11), the key fibrinolysis inhibitor, which counteracts the dissolution of the fibrin clot and may contribute to perturbed fibrinolysis in MS cerebral tissue (12, 13). Interestingly, significantly higher levels of CCL18 and of PAI1 have been reported in MS patients (10, 14).

Among the main regulators of hemostasis, the disintegrin-like and metalloprotease with thrombospondin type 1 motif 13 (ADAMTS13) has been suggested to support vascular integrity (14–16), and ADAMTS13 function has been reported to be also affected by inflammatory profiles (15, 17).

The progressive failure of BBB integrity might have the pathological features of cerebral microbleeds (CMBs) (18), revealed by MRI analysis and associated with worsening of physical and cognitive disability in MS (19). Lower plasma levels

of ADAMTS13 in MS and particularly in those with CMBs (14) together with higher levels of soluble vascular adhesion protein 1 (sVAP1) (20) have been reported.

Taking advantage of main findings reported in our previous studies, focused on different biological pathways and performed on the same MS cohort, we hypothesized that circulating concentration of hemostasis inhibitors could participate in the immunity and inflammation MS-related network. To assess this hypothesis, in the current study, (i) we evaluated the combined contribution of the main coagulation inhibitor PC and the CCL18 chemokine levels to MS brain atrophy, (ii) we compared PC and CCL18 plasma concentrations for their ability to explain the observed neurodegeneration, and (iii) we investigated the correlations among circulating levels of hemostasis inhibitors (PC, ADAMTS13, and PAI1), CCL18, and adhesion molecules [sICAM, soluble neural CAM (sNCAM), sVAP1, and sVCAM1], particularly in relation to CMBs.

## METHODS

### Study Population

The population used for this analysis included 138 MS patients and 42 healthy individuals (HI) derived from the CEG-MS study. Details on the collection, diagnosis, and demographics of this cohort have been previously described (14). The study protocols were approved by the institutional review boards of the University at Buffalo (USA) (ID:MODCR00000352) and the University/Hospital of Ferrara (Italy) (ID:170585). All participants provided informed consent.

### Plasma Assay

Multiplex magnetic-bead technology (Luminex R&D Systems Inc., Minneapolis, MN, USA; Merck Millipore, Darmstadt, Germany) was used to measure the following panel of hemostasis inhibitors, chemokines, and adhesion molecules: ADAMTS13, PC, PAI1, CCL18, sICAM1, sNCAM, sVAP1, and sVCAM1 (10, 14, 20, 21).

**TABLE 1** | Demographic and clinical characteristics of the cohort.

	<b>N</b>	<b>Female (%)</b>	<b>Age, year</b>	<b>Disease duration, year</b>	<b>EDSS</b>	<b>Annual relapse rate</b>
All MS	138	100 (72.5)	54.3 ± 10.8	21.1 ± 10.6	3.5 (2.0–6.0)	0.2 ± 0.4
RR-MS	85	60 (70.6)	50.1 ± 10.7	17.0 ± 8.8	2.0 (1.5–3.5)	0.2 ± 0.4
P-MS	53	40 (75.5)	60.9 ± 7.2	27.6 ± 10.0	6.0 (4.0–6.5)	0.1 ± 0.3
MS with CMBs	12	6 (50)	60.8 ± 8.8	25 ± 11.3	4.0 (3.5–6)	0.1 ± 0.1
HI	42	31 (73.8)	51.0 ± 14.3	n.a.	n.a.	n.a.
MS vs. HI <i>p</i> -value		0.99	0.11	–	–	–
RR-MS vs P-MS <i>p</i> -value		0.56	<0.001	<0.001	<0.001	0.002

All continuous variables are shown as mean ± standard deviation. The ordinal EDSS is shown as median (interquartile range).

MS, multiple sclerosis; RR-MS, relapsing-remitting multiple sclerosis; P-MS, progressive multiple sclerosis; CMBs, cerebral microbleeds; HI, healthy individuals; N, number; EDSS, Expanded Disability Status Scale; n.a., not applicable.

## Magnetic Resonance Imaging Acquisition and Image Analysis

Brain MRI was performed by 3-T GE Signa Excite HD 12.0 scanner (Milwaukee, WI, USA) with an eight-channel head and neck coil. Details of the acquisition protocol and MRI analyses were previously provided (5, 14) and here reported.

Acquisition of two-dimensional (2D) T2/PD-weighted images (WI), fluid-attenuated inversion recovery (FLAIR), spin-echo T1-WI with and without gadolinium contrast, and a three-dimensional (3D) high-resolution T1-WI was performed. 2D sequences were collected using a 256 × 192 matrix and 256 × 192 mm<sup>2</sup> field of view (FOV), resulting in a nominal in-plane resolution of 1 × 1 mm<sup>2</sup>. For the whole-brain coverage, 48 gap-less 3-mm-thick slices were acquired. The sequence-specific parameters were as follows: dual fast spin echo (FSE) proton density and T2-WI (TE1/TE2/TR = 9/98/5,300 ms; echo-train length = 14), 4:31 min long; FLAIR (TE/TI/TR = 120/2,100/8,500 ms; flip angle = 90°; echo-train length = 24), 4:16 min long; and spin-echo T1-WI (TE/TR = 16/600 ms), 4:07 min long. Last, a 3D high-resolution T1-WI fast spoiled gradient echo sequence with a magnetization-prepared inversion recovery pulse was obtained (TE/TI/TR = 2.8/900/5.9 ms, flip angle = 10°), 4:39 min long, with 184 slices of 1 mm.

For the image analysis, a semi-automated edge detection thresholding technique was used to assess T2- and T1-LV, as previously reported (22). Prior to tissue segmentation, lesion filling was utilized to minimize the impact of T1 hypointensities. SIENAX software (version 2.6) was used to calculate normalized volumes of whole brain (WBV), gray matter (GMV), white matter (WMV), cortex (CV), and lateral ventricles (LVV). Deep GMV (DGMV) and thalamic volume were calculated using FIRST (23) and subsequently normalized using the SIENAX-derived scaling factor (24).

The CMB analysis was performed on susceptibility-weighted imaging (SWI) minimum-intensity projection images and susceptibility maps. CMBs were classified as focal, small, and round to ovoid punctuate areas of signal hypointensity on SWI minimum-intensity projection images, as previously reported (19). Signal voids caused by sulcal vessels, calcifications,

and signal averaging from bone were considered mimics of microbleeds. The presence and number of definite CMBs were determined on SWI minimum-intensity projection images by using the Microbleed Anatomic Rating Scale (25). The CMB volume was calculated on susceptibility maps by using a semiautomated edge detection contouring and thresholding technique (22).

## Statistical Analyses

Analyses were performed using SPSS (version 24, IBM, Armonk, NY, USA). Demographic and clinical variables were compared using  $\chi^2$ , Student's *t*-test, or Mann–Whitney U-test.

To evaluate the contribution of PC and CCL18 to MS brain atrophy, multiple regression analysis was conducted with each MRI characteristic used as the dependent variable while age, sex, body mass index (BMI), and the plasma protein levels were predictor variables. The first block included the forced entry of age, sex, and BMI; and the second block included the stepwise entry of PC and CCL18 natural logarithmic values. To further determine the findings' validity, multivariate regression analysis by enter method with 1000-sample bootstrapping procedure was performed.

Association analysis of logarithmic values of protein levels in MS patients and HI was performed by partial correlation with 1000-sample bootstrapping procedure, using age and sex as covariates. Due to the low number of MS patients with CMBs, Pearson's correlation with 1000-sample bootstrapping procedure was used to assess associations among logarithmic values of protein levels.

All reported *p*-values are based on two-tailed statistical tests, with a significance level of 0.05.

## RESULTS

### Demographic, Clinical, and MRI Characteristics

Table 1 summarizes the demographic and clinical characteristics of the study population. There were no significant differences



**TABLE 2 |** MRI characteristics of the study population.

	T2-LV	T1-LV	WBV	WMV	GMV	CV	LVV	DGMV	Thalamus volume
All MS	15.8 ± 19.0	2.9 ± 6.2	1,438 ± 92.1	710.4 ± 44.5	727.6 ± 61.1	591 ± 48.6	55.1 ± 27.0	53.6 ± 7.1	17.7 ± 2.5
RR-MS	11.8 ± 15.9	2.0 ± 4.6	1,469 ± 82.4	721.8 ± 41	747 ± 56.9	606 ± 44.8	50.7 ± 25.2	55.5 ± 6.5	18.4 ± 2.3
P-MS	22.2 ± 21.9	4.4 ± 8.1	1,387 ± 85.2	691.5 ± 44.1	695.8 ± 54.4	567 ± 44.8	62.3 ± 28.5	50.4 ± 6.9	16.5 ± 2.4
RR-MS vs. P-MS	0.016	0.075	0.001	0.001	0.018	0.028	0.23	0.007	0.008
p-value									

Lesion and brain volumes are expressed in milliliters and reported as mean values ± standard deviation. ANCOVA with age and sex as covariates was used for comparison of MRI volumes. MS, multiple sclerosis; RR-MS, relapsing-remitting multiple sclerosis; P-MS, progressive multiple sclerosis; LV, lesion volume; WBV, whole brain volume; WMV, white matter volume; GMV, gray matter volume; CV, cortical volume; LVV, lateral ventricular volume; DGMV, deep gray matter volume.

in any demographic characteristics between the MS and HI groups.

The progressive (P)-MS group comprised 46 secondary-progressive MS patients and seven primary-progressive MS patients. As expected, P-MS patients were older than relapsing-remitting (RR)-MS patients ( $p < 0.001$ ), and the RR-MS and P-MS groups differed in clinical characteristics and brain MRI measures (Table 2).

## Measures of Protein Levels and Neurodegeneration: An Integrated Model

To evaluate the combined contribution on MRI characteristics of PC and CCL18 levels, previously found to be associated with neurodegeneration in two separate investigations on the same MS patient cohort (5, 10), integrated regression analyses were performed.

To normalize data, regression analyses were conducted using natural logarithmic values of PC and CCL18. In the whole MS population, higher PC levels were associated with lower GMV, CV, DGMV, and thalamic volume (Table 3). PC alone was able to predict 37, 36, 22, and 25% of total variation of GMV, CV, DGMV, and thalamic volume, respectively. In this model, one logarithmic unit ( $\sim 2.7$  ng/ml) increase in PC was associated with decrease in GMV (40.9 ml), in CV (28.9 ml), in DGMV (4.79 ml), and in thalamic volume (1.7 ml). All associations were confirmed by bootstrap analysis (Table 3).

In the whole MS population, higher CCL18 levels were associated with higher T2-lesion volume (LV). CCL18 alone was able to predict the 10% of total variation of T2-LV, and for one logarithmic unit ( $\sim 2.7$  ng/ml) increase in CCL18 was associated with 8.16-ml increase in T2-LV. This result showed a trend for significance in bootstrap analysis ( $p = 0.057$ ).

Sub-analysis of clinical phenotype groups indicated that PC and CCL18 levels were predictors of variation of GM-related volumes in RR-MS and P-MS patients, respectively (Table 3).

In RR-MS patients, one logarithmic unit ( $\sim 2.7$  ng/ml) increase in PC was associated with decrease in GMV (41.2 ml), in CV (30 ml), in DGMV (5.04 ml), and in thalamic volume (1.7 ml).

In P-MS patients, one logarithmic unit ( $\sim 2.7$  ng/ml) increase in CCL18 was associated with decrease in GMV (44.4 ml), in CV (32.4 ml), in DGMV (5.8 ml), and in thalamic volume (2.1 ml) and with increase in T2-LV (25 ml).

## Protein Level Correlations of Protein C and Chemokine C-C Motif Ligand 18 in Multiple Sclerosis and Healthy Individuals

In MS patients and in HI, PC levels were positively associated with CCL18 levels (Table 4).

A focused sub-analysis in clinical phenotype groups showed that PC-CCL18 levels were correlated in RR-MS patients ( $\rho = 0.29$ ,  $p = 0.008$ , CI 95% = 0.08, 0.48) but not in progressive patients ( $\rho = 0.23$ ,  $p = 0.10$ , CI 95% =  $-0.04$ , 0.48).

In both MS patients and HI, CCL18 levels were also positively associated with PAI-1.

PC was associated with sVAP1 only in MS patients, and with sICAM1 and sNCAM only in HI.

## Protein Level Correlations in Patients With Cerebral Microbleeds

In MS patients with CMBs, the correlation between CCL18 and PAI1 ( $r = 0.85$ ,  $p = 0.001$ , CI 95% = 0.74, 0.97) was even stronger than in MS patients without CMBs ( $r = 0.26$ ,  $p = 0.003$ , CI 95% = 0.10, 0.42). Similarly, in MS with CMBs, the correlation between PAI1 and sVCAM1 ( $r = 0.64$ ,  $p = 0.026$ , CI 95% = 0.29, 0.94) was better than in MS patients without CMBs ( $r = 0.21$ ,  $p = 0.022$ , CI 95% = 0.03, 0.36).

Levels of ADAMTS13 were correlated with those of sVAP1 ( $r = 0.78$ ,  $p = 0.003$ , CI 95% = 0.42, 0.96). Correlation between ADAMTS13 and sVAP1 was detectable neither/nor in MS without CMBs ( $r = 0.16$ ,  $p = 0.86$ , CI 95% =  $-0.16$ , 0.20) nor in HI ( $r = 0.26$ ,  $p = 0.12$ , CI 95% =  $-0.10$ , 0.50).

Scatter plots of protein concentrations in MS patients with and without CMBs are shown in Figure 1.

## DISCUSSION

Our study was aimed at providing an integrated analysis of plasma levels of hemostasis inhibitors, chemokines, and adhesion molecules, found associated with MRI findings in an MS cohort.

The main results of this study were (i) the differences between PC and CCL18 levels in the ability to predict neurodegeneration in MS patients and (ii) the positive correlation between PC and CCL18 levels present in diseased and healthy conditions. Both observations support the hypothesis of a relation between the hemostasis and chemokine pathways, which might act in the disease pathophysiology. Our findings in patients are coherent

**TABLE 3 |** Association of PC and CCL18 concentrations with MRI characteristics in multiple sclerosis patients.

	All MS (n = 138)						RR-MS (n = 85)						P-MS (n = 53)					
	PC		CCL18				PC		CCL18				PC		CCL18			
	<i>r<sub>p</sub></i>	<i>P</i>	<i>r<sub>p</sub></i>	<i>p</i>	<i>R</i> <sup>2</sup>	$\beta$ [CI 95%] <i>p</i> <sup>#</sup>	<i>r<sub>p</sub></i>	<i>p</i>	<i>r<sub>p</sub></i>	<i>p</i>	<i>R</i> <sup>2</sup>	$\beta$ [CI 95%] <i>p</i> <sup>#</sup>	<i>r<sub>p</sub></i>	<i>p</i>	<i>r<sub>p</sub></i>	<i>p</i>	<i>R</i> <sup>2</sup>	$\beta$ [CI 95%] <i>p</i> <sup>#</sup>
T2-LV	/	0.241	<b>0.19</b>	<b>0.030</b>	0.106	[0.5, 17.0] 0.057	/	0.088	/	0.952			/	0.802	<b>0.43</b>	<b>0.003</b>	0.209	[10.7, 39.4] 0.003
T1-LV	/	0.421	/	0.214			/	0.313	/	0.357			/	0.522	<b>0.34</b>	<b>0.021</b>	0.182	[1.7, 1.6] 0.089
WBV	<b>-0.27</b>	<b>0.002</b>	/	0.353	0.316	[-90.4, -15.2] 0.006	<b>-0.31</b>	<b>0.006</b>	/	0.803	0.293	[-94.6, -11.7] 0.013	/	0.274	/	0.112		
WMV	/	0.166	/	0.436			/	0.224	/	0.845			/	0.645	/	0.747		
GMV	<b>-0.32</b>	<b>&lt;0.001</b>	/	0.279	0.374	[-63.0, -14.8] 0.006	<b>-0.36</b>	<b>0.001</b>	/	0.760	0.367	[-66.8, -8.0] 0.005	/	0.380	<b>-0.33</b>	<b>0.024</b>	0.200	[-78.0, -2.8] 0.021
CV	<b>-0.28</b>	<b>0.001</b>	/	0.217	0.362	[-48.3, -10.8] 0.002	<b>-0.34</b>	<b>0.003</b>	/	0.922	0.380	[-49.7, -6] 0.009	/	0.606	<b>-0.30</b>	<b>0.043</b>	0.179	[-60.3, -2.3] 0.027
LWV	/	0.381	/	0.105			/	0.226	/	0.430			/	0.758	/	0.109	/	
DGMV	<b>-0.26</b>	<b>0.001</b>	/	0.052	0.219	[-7.6, -1.9] 0.003	<b>-0.35</b>	<b>0.002</b>	/	0.434	0.246	[-8.3, -1.1] 0.008	/	0.452	<b>-0.32</b>	<b>0.029</b>	0.127	[-10.9, -0.03] 0.042
Thalamic volume	<b>-0.29</b>	<b>0.001</b>	/	0.088	0.248	[-2.7, -0.6] 0.003	<b>-0.36</b>	<b>0.002</b>	/	0.724	0.269	[-2.9, -0.4] 0.006	/	0.486	<b>-0.34</b>	<b>0.022</b>	0.152	[-4.0, -0.3] 0.039

Regression model: the first block included the forced entry of age, sex, and BMI; and the second block included the stepwise entry of PC and CCL18 natural logarithmic values.

Partial correlation (*r<sub>p</sub>*) and *p*-value from the regression analysis are shown. *R*<sup>2</sup> of the regression model is reported. Predictor variable excluded from the model (/). The 95% confidence intervals (CIs) of  $\beta$  coefficient and the *p*-value<sup>#</sup> from the 1000-sample bootstrapping are reported.

LV, lesion volume; WBV, whole brain volume; WMV, white matter volume; GMV, gray matter volume; CV, cortical volume; LWV, lateral ventricular volume; DGMV, deep gray matter volume; MS, Multiple Sclerosis; RR-MS, relapsing-remitting multiple sclerosis; P-MS, progressive multiple sclerosis. Significant results are in bold. No significant results are in grey.

**TABLE 4 |** Correlations among protein levels in multiple sclerosis patients and healthy individuals.

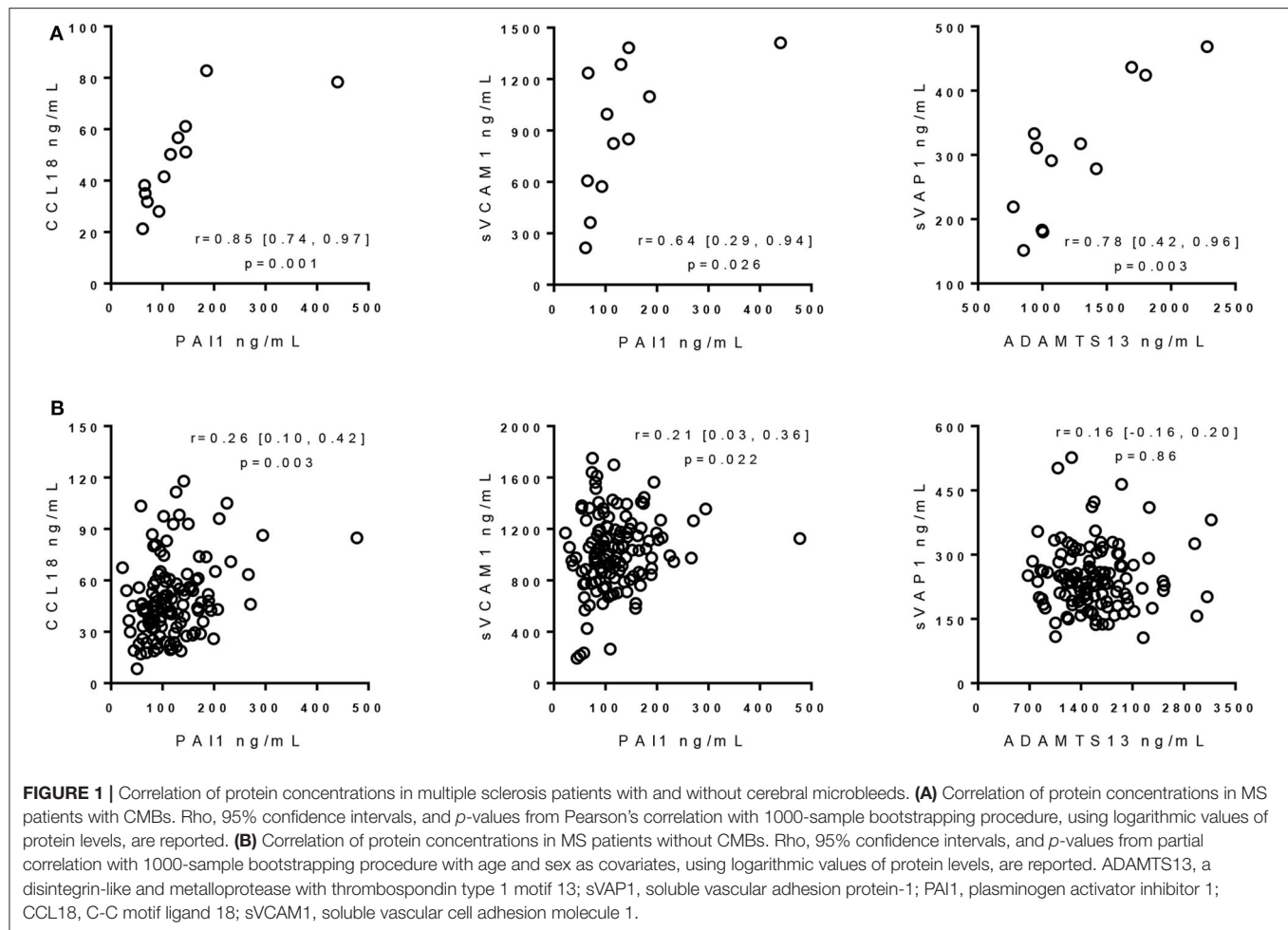
		ADAMTS13	PC	PAI1
<b>All MS (n = 138)</b>				
CCL18	Rho, [CI 95%]	−0.10, [−0.24, 0.06]	<b>0.28, [0.12, 0.44]</b>	<b>0.30, [0.15, 0.44]</b>
	p-value	0.24	<b>0.001</b>	<b>&lt;0.001</b>
sICAM	Rho, [CI 95%]	0.09, [−0.12, 0.28]	0.03, [−0.13, 0.18]	−0.14, [−0.32, 0.03]
	p-value	0.286	0.77	0.11
sNCAM	Rho, [CI 95%]	0.09, [−0.09, 0.25]	0.01, [−0.15, 0.18]	−0.03, [−0.17, 0.09]
	p-value	0.31	0.884	0.700
sVAP1	Rho, [CI 95%]	0.07, [−0.11, 0.25]	<b>0.20, [0.05, 0.36]</b>	0.06, [−0.11, 0.23]
	p-value	0.39	<b>0.018</b>	0.45
sVCAM1	Rho, [CI 95%]	0.00, [−0.14, 0.17]	0.06, [−0.12, 0.22]	<b>0.25, [0.08, 0.38]</b>
	p-value	0.98	0.51	<b>0.004</b>
<b>HI (n = 42)</b>				
CCL18	Rho, [CI 95%]	0.25, [−0.09, 0.52]	<b>0.42, [0.17, 0.64]</b>	<b>0.33, [−0.03, 0.66]</b>
	p-value	0.13	<b>0.008</b>	<b>0.045</b>
sICAM	Rho, [CI 95%]	0.19, [−0.14, 0.41]	<b>0.33, [−0.04, 0.66]</b>	0.30, [0.00, 0.58]
	p-value	0.26	<b>0.040</b>	0.066
sNCAM	Rho, [CI 95%]	0.21, [−0.11, 0.48]	<b>0.35, [0.02, 0.60]</b>	−0.04, [−0.30, 0.24]
	p-value	0.22	<b>0.031</b>	0.83
sVAP1	Rho, [CI 95%]	0.26, [−0.10, 0.50]	0.23, [−0.11, 0.56]	0.27, [−0.09, 0.52]
	p-value	0.12	0.161	0.11
sVCAM1	Rho, [CI 95%]	0.20, [−0.07, 0.45]	0.27, [0.03, 0.48]	0.21, [−0.17, 0.52]
	p-value	0.22	0.097	0.21

Significant correlations are in bold. Correlations present only in MS patients are reported in dark gray cells. Correlations present only in healthy individuals are reported in light gray cells. ADAMTS13, a disintegrin-like and metalloprotease with thrombospondin type 1 motif 13; MS, multiple sclerosis; HI, healthy individuals; PC, protein C; PAI1, plasminogen activator inhibitor 1; CCL5, C-C motif ligand 5; CCL18, C-C motif ligand 18; sICAM1, soluble intercellular adhesion molecule; sNCAM, soluble neural cell adhesion molecule; sVAP1, soluble vascular adhesion protein-1; sVCAM1, soluble vascular cell adhesion molecule 1.

with previous data: (i) PC and CCL18 levels have been positively associated with neurodegeneration (5, 10), (ii) the proteomic profiles within chronic active plaques have detected the presence of the PC inhibitor (26), which binds activated PC, and (iii) high CCL18 gene expression has been found in the rim of chronic active MS lesions (27).

The different results of the regression analysis between the clinical phenotype groups suggest that the circulating levels of PC and CCL18 might be related to different aspects of neurodegeneration. The relation of PC levels with GM-related volumes in whole MS population and RR-MS could be interpreted as an increase of PC expression-associated with inflammation. This might represent the response to diffuse neuronal loss associated with inflammatory and oxidative injuries, which might occur independently of focal lesions (28). Our data suggest that in patients with slightly higher PC concentration, which did not differ from that in HI, the well-known protective effects of this protein (29, 30) are not sufficient to counterbalance the ongoing neurodegeneration. Differently, the association of CCL18 with T2-LV in the whole MS population, and in particular in P-MS, would be mainly involved in the neurodegeneration mediated by focal lesions. Moreover, the association of this cytokine with GM volume loss in P-MS might be explained by both secondary antegrade (Wallerian) and retrograde neurodegeneration (31).

These hypotheses are strengthened by the analysis of level correlation among proteins related to MRI findings in MS patients, which pointed out the noticeable correlation between levels of PC and CCL18, both associated with neurodegeneration. This correlation would suggest factors able to upregulate expression of both PC and CCL18 by mechanisms that are only partially known (32–35). On the other hand, it has been shown that age, sex, BMI, low-density lipoprotein, high-density lipoprotein, and triglycerides can differentially influence concentration and activity of PC (36–38). A limitation of our study is that the plasma sampling conditions prevented the evaluation of PC activity. However, we expect that higher total PC levels measured in our study are proportional to higher PC activity levels. We can only speculate that mechanism underlying neurodegeneration can affect both PC and CCL18 levels with partially different pathological consequences. This novel hemostasis inhibitors–immunity link is further supported by the positive correlation between PAI1 and CCL18 levels, previously found higher in MS patients than HI (10, 14). As a matter of fact, increased CCL18 gene expression has been found in the rim of chronic active MS lesions (27), and increased PAI1 protein in MS lesions has been associated with impaired fibrin clearance (12, 13), which would contribute to the chronic inflammation [reviewed in (4)].



The hemostasis inhibitors–immunity link was even stronger in the low number of patients with CMBs, who displayed high correlation between CCL18 and PAI1 levels. The high association of PAI1 with sVCAM1 extends this molecular relationship to adhesion molecules. Several differences between MS patients and HI in PC correlation with sICAM1, sNCAM, and sVAP1 concentrations support dysregulation, associated with the MS disease, of the adhesion molecules and PC pathways. The absence of correlation between PC and sICAM and sNCAM in MS patients could be reflected in a decreased inhibition of leukocyte adhesion and transmigration (7, 8).

Based on the high correlation between ADAMTS13 with sVAP1 detected only in MS patients with CMBs, and on low ADAMTS13 (14) and high sVAP1 plasma levels (20), previously observed in the same patients, it is intriguing to speculate that the ADAMTS13 function could be correlated to reactive oxygen species (39) produced by VAP1, an inflammatory adhesion molecule endowed with enzymatic properties (40). The contribution of ADAMTS13 to cerebral vascular integrity is supported by finding low ADAMTS13 activity associated with increased risk of dementia (41), ischemic stroke (42), and subarachnoid hemorrhage (43). On the

other hand, intracranial hemorrhages and adverse neurological outcome in stroke have been associated with higher activity of VAP1 (44, 45).

In conclusion, with the limitations of a cross-sectional study and the low number of MS patients with CMBs, the integrated analysis of plasma proteins and MRI measures, here reported, provides evidence for new MS disease-relevant relationships among hemostasis, inflammation, and immunity pathways.

## DATA AVAILABILITY STATEMENT

The datasets presented in this article are not readily available because they are restricted to the Buffalo Neuroimaging Analysis Center. Requests to access the datasets should be directed to Robert Zivadinov, rzivadinov@bnac.net.

## ETHICS STATEMENT

The studies involving human participants were reviewed and approved by The study protocols were approved by the institutional review boards of the University at Buffalo (USA) (ID:MODCR0000352) and the University/Hospital of Ferrara



(Italy) (ID:170585). The patients/participants provided their written informed consent to participate in this study.

## AUTHOR CONTRIBUTIONS

NZ, RZ, MR, GM, and FB substantially contributed to the concept and design of the study. MB contributed to assay setup. NZ contributed to data acquisition, analysis, and interpretation. DJ, MB, NB, DR, BW-G, and RZ contributed to data acquisition. RZ, DJ, NB, and BW-G contributed to data interpretation, discussion, and manuscript preparation. NZ, GM, and FB wrote the manuscript. All authors critically revised the manuscript for important intellectual content and contributed to the article and approved the submitted version.

## REFERENCES

- Marrie RA, Rudick R, Horwitz R, Cutter G, Tyry T, Campagnolo D, et al. Vascular comorbidity is associated with more rapid disability progression in multiple sclerosis. *Neurology*. (2010) 74:1041–7. doi: 10.1212/WNL.0b013e3181d6b125
- D'haeseleer M, Cambron M, Vanopdenbosch L, De Keyser J. Vascular aspects of multiple sclerosis. *Lancet Neurol*. (2011) 10:657–66. doi: 10.1016/S1474-4422(11)70105-3
- Spencer JJ, Bell JS, Deluca GC. Vascular pathology in multiple sclerosis: reframing pathogenesis around the blood-brain barrier. *J Neurol Neurosurg Psychiatry*. (2018) 89:42–52. doi: 10.1136/jnnp-2017-316011
- Ziliotto N, Bernardi F, Jakimovski D, Zivadinov R. Coagulation pathways in neurological diseases: multiple sclerosis. *Front Neurol*. (2019) 10:409. doi: 10.3389/fneur.2019.00409
- Ziliotto N, Zivadinov R, Baroni M, Marchetti G, Jakimovski D, Bergsland N, et al. Plasma levels of protein C pathway proteins and brain magnetic resonance imaging volumes in multiple sclerosis. *Eur J Neurol*. (2020) 27:235–43. doi: 10.1111/ene.14058
- Griffin JH, Zlokovic BV, Mosnier LO. Activated protein C: biased for translation. *Blood*. (2015) 125:2898–907. doi: 10.1182/blood-2015-02-355974
- Frommhold D, Tschada J, Braach N, Buschmann K, Doerner A, Pflaum J, et al. Protein C concentrate controls leukocyte recruitment during inflammation and improves survival during endotoxemia after efficient in vivo activation. *Am J Pathol*. (2011) 179:2637–50. doi: 10.1016/j.ajpath.2011.07.023
- Braach N, Frommhold D, Buschmann K, Pflaum J, Koch L, Hudalla H, et al. RAGE controls activation and anti-inflammatory signalling of protein C. *PLoS ONE*. (2014) 9:e89422. doi: 10.1371/journal.pone.0089422
- Lee SJ, Benveniste EN. Adhesion molecule expression and regulation on cells of the central nervous system. *J Neuroimmunol*. (1999) 98:77–88. doi: 10.1016/S0165-5728(99)00084-3
- Ziliotto N, Bernardi F, Jakimovski D, Baroni M, Bergsland N, Ramasamy DP, et al. Increased CCL18 plasma levels are associated with neurodegenerative MRI outcomes in multiple sclerosis patients. *Mult Scler Relat Disord*. (2018) 25:37–42. doi: 10.1016/j.msard.2018.07.009
- Dellas C, Loskutov DJ. Historical analysis of PAI-1 from its discovery to its potential role in cell motility and disease. *Thromb Haemost*. (2005) 93:631–40. doi: 10.1160/TH05-01-0033
- Gveric D, Herrera B, Petzold A, Lawrence DA, Cuzner ML. Impaired fibrinolysis in multiple sclerosis: a role for tissue plasminogen activator inhibitors. *Brain*. (2003) 126:1590–8. doi: 10.1093/brain/awg167
- Yates RL, Esiri MM, Palace J, Jacobs B, Perera R, Deluca GC. Fibrin(ogen) and neurodegeneration in the progressive multiple sclerosis cortex. *Ann Neurol*. (2017) 82:259–70. doi: 10.1002/ana.24997
- Ziliotto N, Bernardi F, Jakimovski D, Baroni M, Marchetti G, Bergsland N, et al. Hemostasis biomarkers in multiple sclerosis. *Eur J Neurol*. (2018) 25:1169–76. doi: 10.1111/ene.13681
- Bernardo A, Ball C, Nolasco L, Moake JF, Dong JF. Effects of inflammatory cytokines on the release and cleavage of the endothelial cell-derived ultralarge von Willebrand factor multimers under flow. *Blood*. (2004) 104:100–6. doi: 10.1182/blood-2004-01-0107
- Lu K, Liu L, Xu X, Zhao F, Deng J, Tang X, et al. ADAMTS13 ameliorates inflammatory responses in experimental autoimmune encephalomyelitis. *J Neuroinflammation*. (2020) 17:67. doi: 10.1186/s12974-020-1713-z
- Cao WJ, Niiya M, Zheng XW, Shang DZ, Zheng XL. Inflammatory cytokines inhibit ADAMTS13 synthesis in hepatic stellate cells and endothelial cells. *J Thromb Haemost*. (2008) 6:1233–5. doi: 10.1111/j.1538-7836.2008.02989.x
- Fisher MJ. Brain regulation of thrombosis and hemostasis: from theory to practice. *Stroke*. (2013) 44:3275–85. doi: 10.1161/STROKEAHA.113.000736
- Zivadinov R, Ramasamy DP, Benedict RR, Polak P, Hagemeier J, Magnano C, et al. cerebral microbleeds in multiple sclerosis evaluated on susceptibility-weighted images and quantitative susceptibility maps: a case-control study. *Radiology*. (2016) 281:884–95. doi: 10.1148/radiol.2016160060
- Ziliotto N, Zivadinov R, Jakimovski D, Bergsland N, Ramasamy DP, Weinstock-Guttman B, et al. Are plasma levels of vascular adhesion protein-1 associated both with cerebral microbleeds in multiple sclerosis and intracerebral haemorrhages in stroke? *Thromb Haemost*. (2019) 119:175–8. doi: 10.1055/s-0038-1676346
- Ziliotto N, Zivadinov R, Jakimovski D, Baroni M, Tisato V, Secchiero P, et al. Plasma levels of soluble NCAM in multiple sclerosis. *J Neurol Sci*. (2019) 396:36–41. doi: 10.1016/j.jns.2018.10.023
- Zivadinov R, Heininen-Brown M, Schirda CV, Poloni GU, Bergsland N, Magnano CR, et al. Abnormal subcortical deep-gray matter susceptibility-weighted imaging filtered phase measurements in patients with multiple sclerosis: a case-control study. *Neuroimage*. (2012) 59:331–9. doi: 10.1016/j.neuroimage.2011.07.045
- Patenaude B, Smith SM, Kennedy DN, Jenkinson M. A Bayesian model of shape and appearance for subcortical brain segmentation. *Neuroimage*. (2011) 56:907–22. doi: 10.1016/j.neuroimage.2011.02.046
- Smith SM, Zhang Y, Jenkinson M, Chen J, Matthews PM, Federico A, et al. Accurate, robust, and automated longitudinal and cross-sectional brain change analysis. *Neuroimage*. (2002) 17:479–89. doi: 10.1006/nimg.2002.1040
- Gregoire SM, Chaudhary UJ, Brown MM, Yousry TA, Kallis C, Jager HR, et al. The Microbleed Anatomical Rating Scale (MARS): reliability of a tool to map brain microbleeds. *Neurology*. (2009) 73:1759–66. doi: 10.1212/WNL.0b013e3181c34a7d
- Han MH, Hwang SI, Roy DB, Lundgren DH, Price JV, Ousman SS, et al. Proteomic analysis of active multiple sclerosis lesions reveals therapeutic targets. *Nature*. (2008) 451:1076–81. doi: 10.1038/nature06559
- Hendrickx DA, Van Scheppingen J, van der Poel M, Bossers K, Schuurman KG, van Eden CG, et al. (2017). Gene expression profiling of multiple sclerosis pathology identifies early patterns of demyelination surrounding chronic active lesions. *Front Immunol*. (2017) 8:1810. doi: 10.3389/fimmu.2017.01810

## FUNDING

This study was supported by the Annette Funicello Research Fund for Neurological Diseases, the Jacquemin Family Foundation, the National Center for Advancing Translational Sciences of the National Institutes of Health (UL1TR001412), the Emilia Romagna Region-Italy (grant 1786/2012), and internal resources of the BNAC.

## ACKNOWLEDGMENTS

We thank the Italian foundation Fondazione Il Bene Onlus for its support for MS research.

28. Lassmann H. Pathogenic mechanisms associated with different clinical courses of multiple sclerosis. *Front Immunol.* (2019) 9:3116. doi: 10.3389/fimmu.2018.03116
29. Bock F, Shahzad K, Vergnolle N, Isermann B. Activated protein C based therapeutic strategies in chronic diseases. *Thromb Haemost.* (2014) 111:610–7. doi: 10.1160/TH13-11-0967
30. Griffin JH, Zlokovic BV, Mosnier LO. Activated protein C, protease activated receptor 1, and neuroprotection. *Blood.* (2018) 132:159–69. doi: 10.1182/blood-2018-02-769026
31. Fuchs TA, Carolus K, Benedict RHB, Bergsland N, Ramasamy D, Jakimovski D, et al. Impact of focal white matter damage on localized subcortical gray matter atrophy in multiple sclerosis: a 5-year study. *Am J Neuroradiol.* (2018) 39:1480–6. doi: 10.3174/ajnr.A5720
32. Pereira CP, Bachli EB, Schaer DJ, Schoedon G. Transcriptome analysis revealed unique genes as targets for the anti-inflammatory action of activated protein C in human macrophages. *PLoS ONE.* (2010) 5:e15352. doi: 10.1371/journal.pone.0015352
33. Nilsson E, Jansson PA, Perflyev A, Volkov P, Pedersen M, Svensson MK, et al. Altered DNA methylation and differential expression of genes influencing metabolism and inflammation in adipose tissue from subjects with type 2 diabetes. *Diabetes.* (2014) 63:2962–76. doi: 10.2337/db13-1459
34. Dehne N, Brune B. Hypoxic inhibition of JMJD3 reduces H3K27me3 demethylation and induction of the STAT6 target gene CCL18. *Biochim Biophys Acta.* (2016) 1859:1490–501. doi: 10.1016/j.bbagr.2016.10.004
35. Sartain SE, Turner NA, Moake JL. TNF regulates essential alternative complement pathway components and impairs activation of protein C in human glomerular endothelial cells. *J Immunol.* (2016) 196:832–45. doi: 10.4049/jimmunol.1500960
36. Conlan MG, Folsom AR, Finch A, Davis CE, Sorlie P, Wu KK. Correlation of plasma protein C levels with cardiovascular risk factors in middle-aged adults: the Atherosclerosis Risk in Communities (ARIC) Study. *Thromb Haemost.* (1993) 70:762–7. doi: 10.1055/s-0038-1649666
37. Tait RC, Walker ID, Islam SI, McCall F, Conkie JA, Wight M, et al. Protein C activity in healthy volunteers—influence of age, sex, smoking and oral contraceptives. *Thromb Haemost.* (1993) 70:281–5. doi: 10.1055/s-0038-1649566
38. Griffin JH, Kojima K, Banka CL, Curtiss LK, Fernandez JA. High-density lipoprotein enhancement of anticoagulant activities of plasma protein S and activated protein C. *J Clin Invest.* (1999) 103:219–27. doi: 10.1172/JCI5006
39. Lancellotti S, De Filippis V, Pozzi N, Oggianu L, Rutella S, Scaglione GL, et al. Oxidized von Willebrand factor is efficiently cleaved by serine proteases from primary granules of leukocytes: divergence from ADAMTS-13. *J Thromb Haemost.* (2011) 9:1620–7. doi: 10.1111/j.1538-7836.2011.04367.x
40. Salmi M, Jalkanen S. Vascular adhesion protein-1: a cell surface amine oxidase in translation. *Antioxid Redox Signal.* (2017) 30:314–32. doi: 10.1089/ars.2017.7418
41. Wolters FJ, Boender J, De Vries PS, Sonneveld MA, Koudstaal PJ, De Maat MP, et al. Von Willebrand factor and ADAMTS13 activity in relation to risk of dementia: a population-based study. *Sci Rep.* (2018) 8:5474. doi: 10.1038/s41598-018-23865-7
42. Sonneveld MA, De Maat MP, Portegies ML, Kavousi M, Hofman A, Turecek PL, et al. Low ADAMTS13 activity is associated with an increased risk of ischemic stroke. *Blood.* (2015) 126:2739–46. doi: 10.1182/blood-2015-05-643338
43. Kumar M, Cao W, Mcdaniel JK, Pham HP, Raju D, Nawalinski K, et al. Plasma ADAMTS13 activity and von Willebrand factor antigen and activity in patients with subarachnoid haemorrhage. *Thromb Haemost.* (2017) 117:691–9. doi: 10.1160/TH16-11-0834
44. Hernandez-Guillamon M, Garcia-Bonilla L, Sole M, Sosti V, Pares M, Campos M, et al. Plasma VAP-1/SSAO activity predicts intracranial hemorrhages and adverse neurological outcome after tissue plasminogen activator treatment in stroke. *Stroke.* (2010) 41:1528–35. doi: 10.1161/STROKEAHA.110.584623
45. Hernandez-Guillamon M, Sole M, Delgado P, Garcia-Bonilla L, Giralt D, Boada C, et al. VAP-1/SSAO plasma activity and brain expression in human hemorrhagic stroke. *Cerebrovasc Dis.* (2012) 33:55–63. doi: 10.1159/000333370

**Conflict of Interest:** RZ reports personal fees from EMD Serono, Genzyme-Sanofi, Bristol Myers Squibb, and Novartis for speaking and consultant fees, and grants from Genzyme-Sanofi, Novartis, Bristol Myers Squibb, Mapi Pharma, Keystone Heart, Boston Scientific, Protendis, and V-Vawe Medical unrelated to the submitted work. BW-G reports grants and personal fees from Biogen, EMD Serono, Novartis, and Genentech, and personal fees from Mallinckrodt, outside the submitted work. MR reports grants from Otsuka Pharmaceutical Research and Development and grants from National Institute of Neurological Diseases and Stroke, outside the submitted work.

The remaining authors declare that the research was conducted in the absence of any commercial or financial relationships that could be construed as a potential conflict of interest.

Copyright © 2020 Ziliotto, Zivadinov, Jakimovski, Baroni, Bergsland, Ramasamy, Weinstock-Guttman, Ramanathan, Marchetti and Bernardi. This is an open-access article distributed under the terms of the Creative Commons Attribution License (CC BY). The use, distribution or reproduction in other forums is permitted, provided the original author(s) and the copyright owner(s) are credited and that the original publication in this journal is cited, in accordance with accepted academic practice. No use, distribution or reproduction is permitted which does not comply with these terms.



# Association Between Motor and Cognitive Performances in Elderly With Atrial Fibrillation: Strat-AF Study

Emilia Salvadori<sup>1</sup>, Francesco Galmozzi<sup>2</sup>, Francesca Uda<sup>2</sup>, Carmen Barbato<sup>1,2</sup>, Eleonora Camilleri<sup>3,4</sup>, Francesca Cesari<sup>5</sup>, Stefano Chiti<sup>6</sup>, Stefano Diciotti<sup>7</sup>, Samira Donnini<sup>2</sup>, Benedetta Formelli<sup>2</sup>, Silvia Galora<sup>3,4</sup>, Betti Giusti<sup>3,4</sup>, Anna Maria Gori<sup>3,4</sup>, Chiara Marzi<sup>7</sup>, Anna Melone<sup>2</sup>, Damiano Mistri<sup>2</sup>, Francesca Pescini<sup>8</sup>, Giovanni Pracucci<sup>2</sup>, Valentina Rinnoci<sup>1</sup>, Cristina Sarti<sup>2,8</sup>, Enrico Fainardi<sup>9</sup>, Rossella Marcucci<sup>3,4</sup> and Anna Poggesi<sup>1,2,8\*</sup>

## OPEN ACCESS

### Edited by:

Andreas Charidimou,  
Massachusetts General Hospital and  
Harvard Medical School,  
United States

### Reviewed by:

Lina Palaodimou,  
University General Hospital  
Attikon, Greece  
Georgios Tsigoulis,  
National and Kapodistrian University  
of Athens, Greece  
Deren Wang,  
West China Hospital of Sichuan  
University, China

### \*Correspondence:

Anna Poggesi  
anna.poggesi@unifi.it

### Specialty section:

This article was submitted to  
Stroke,  
a section of the journal  
Frontiers in Neurology

Received: 12 June 2020

Accepted: 30 September 2020

Published: 13 November 2020

### Citation:

Salvadori E, Galmozzi F, Uda F, Barbato C, Camilleri E, Cesari F, Chiti S, Diciotti S, Donnini S, Formelli B, Galora S, Giusti B, Gori AM, Marzi C, Melone A, Mistri D, Pescini F, Pracucci G, Rinnoci V, Sarti C, Fainardi E, Marcucci R and Poggesi A (2020) Association Between Motor and Cognitive Performances in Elderly With Atrial Fibrillation: Strat-AF Study. *Front. Neurol.* 11:571978. doi: 10.3389/fneur.2020.571978

<sup>1</sup> IRCCS Fondazione Don Carlo Gnocchi, Florence, Italy, <sup>2</sup> Neuroscience Section, NEUROFARBA Department, University of Florence, Florence, Italy, <sup>3</sup> Department of Experimental and Clinical Medicine, University of Florence, Florence, Italy,

<sup>4</sup> Atherothrombotic Diseases Center, Careggi University Hospital, Florence, Italy, <sup>5</sup> Central Laboratory, Careggi University Hospital, Florence, Italy, <sup>6</sup> Department Health Professions, U.O. Research and Development, Careggi University Hospital, Florence, Italy, <sup>7</sup> Department of Electrical, Electronic, and Information Engineering 'Guglielmo Marconi', University of Bologna, Bologna, Italy, <sup>8</sup> Stroke Unit, Careggi University Hospital, Florence, Italy, <sup>9</sup> Neuroradiology Unit, Department of Experimental and Clinical Biomedical Sciences, Careggi University Hospital, University of Florence, Florence, Italy

**Background/Objective:** Growing evidence suggests a close relationship between motor and cognitive abilities, but possible common underlying mechanisms are not well-established. Atrial fibrillation (AF) is associated with reduced physical performance and increased risk of cognitive decline. The study aimed to assess in a cohort of elderly AF patients: (1) the association between motor and cognitive performances, and (2) the influence and potential mediating role of cerebral lesions burden.

**Design:** Strat-AF is a prospective, observational study investigating biological markers for cerebral bleeding risk stratification in AF patients on oral anticoagulants. Baseline cross-sectional data are presented here.

**Setting:** Thrombosis outpatient clinic (Careggi University Hospital).

**Participants:** One-hundred and seventy patients (mean age  $77.7 \pm 6.8$ ; females 35%).

**Measurements:** Baseline protocol included: neuropsychological battery, motor assessment [Short Physical Performance Battery (SPPB), and walking speed], and brain magnetic resonance imaging (MRI) used for the visual assessment of white matter hyperintensities, lacunar and non-lacunar infarcts, cerebral microbleeds, and global cortical and medial temporal atrophies.

**Results:** Mean Montreal Cognitive Assessment (MoCA) total score was  $21.9 \pm 3.9$ , SPPB total score  $9.5 \pm 2.2$ , and walking speed  $0.9 \pm 0.2$ . In univariate analyses, both SPPB and walking speed were significantly associated with MoCA ( $r = 0.359$ ,  $r = 0.372$ , respectively), visual search ( $r = 0.361$ ,  $r = 0.322$ ), Stroop ( $r = -0.272$ ,  $r = -0.263$ ), short story ( $r = 0.263$ ,  $r = 0.310$ ), and semantic fluency ( $r = 0.311$ ,  $r = 0.360$ ). In multivariate models adjusted for demographics, heart failure, physical activity, and either stroke history (Model 1) or neuroimaging markers (Model 2), both SPPB and walking speed

were confirmed significantly associated with MoCA (Model 1:  $\beta = 0.256$ ,  $\beta = 0.236$ ; Model 2:  $\beta = 0.276$ ,  $\beta = 0.272$ , respectively), visual search (Model 1:  $\beta = 0.350$ ,  $\beta = 0.313$ ; Model 2:  $\beta = 0.344$ ,  $\beta = 0.307$ ), semantic fluency (Model 1:  $\beta = 0.223$ ,  $\beta = 0.261$ ), and short story (Model 2:  $\beta = 0.245$ ,  $\beta = 0.273$ ).

**Conclusions:** In our cohort of elderly AF patients, a direct association between motor and cognitive functions consistently recurred using different evaluation of the performances, without an evident mediating role of cerebral lesions burden.

**Keywords:** elderly, atrial fibrillation, cognition, motor performance, gait speed

## INTRODUCTION

Gait is a complex task involving the integration of several brain regions, and high-order cognitive functions are currently recognized to play a role in coordinating and controlling mobility (1, 2). Aging is known to be related to both cognitive decline and reduced physical performance. Although these processes may occur separately, a growing body of literature suggests the presence of a close relationship between cognitive and motor dysfunction. Evidence also indicates that walking impairment could precede cognitive decline, and thereby it may represent a marker of cognitive status and contribute to an early identification of subjects at risk of cognitive impairment (3–5). Possible shared pathological mechanisms underlying this relationship are not well-established, and most studies investigate the hypothesis of a neural overlap determined by the possible engagement of shared neural circuits (6–8).

Among the cognitive abilities, executive functions and processing speed are the most commonly associated with gait dysfunction, with evidence coming both from studies on healthy older adults and on neurologic patients (9, 10). Both neurodegenerative and vascular processes are well-known neurobiological determinants of cognitive decline and could to some extent contribute to motor impairment. Since gait disturbances may differ among the various mechanisms related to the cerebral lesion burden, the interplay between cognitive and motor dysfunctions and the determination of different profiles of gait disturbance among the various subtypes of preclinical or clinical dementia may further contribute to early and differential diagnoses (11–14).

Atrial fibrillation (AF) is a common cardiac arrhythmia associated with a high vascular risk factor profile, cardiac comorbidities, frailty, reduced physical performance, and increased risk of stroke and cognitive decline (15, 16). Besides the occurrence of an acute stroke event, mechanisms such hypoperfusion, inflammation, and endothelial dysfunction may play a role in the association between AF and cognitive decline and may also represent possible common denominators of both vascular and degenerative underlying processes. Furthermore, preliminary data are emerging also on the association between AF and reduced mobility in older adults independently of comorbidities and frailty markers (17–19). Only one recent study by Marino and colleagues directly assessed the association between a reduced gait speed and the presence of cognitive

impairment in a population of elderly patients with AF (20). Their results confirmed such association independently from several demographic and clinical characteristics, and the authors concluded that physical changes in gait could be related to declines in the cognitive domains that regulate several gait elements as previously documented in literature on neurologic diseases.

The present study aims to assess in a cohort of elderly patients with a diagnosis of AF and ongoing anticoagulant therapy: (1) the association between motor and cognitive performances, and (2) the influence and potential mediating role of cerebral lesions burden.

## MATERIALS AND METHODS

The Strat-AF study (stratification of cerebral bleeding risk in AF) is an observational, prospective single-center hospital-based study aimed at improving the prediction of bleeding risk in AF patients under treatment with oral anticoagulants (OACs). Inclusion criteria were age  $\geq 65$  years, diagnosis of AF, ongoing OAC with vitamin K antagonists, or direct OACs, and no contraindications to MRI. Ethical approval was obtained by the Ethics Committee of Careggi University Hospital, and all participants gave written informed consent for inclusion before enrolment. Consecutive patients referring to Center of Thrombosis outpatient-clinic of the Careggi University Hospital of Florence and fulfilling inclusion criteria were invited to participate in the study. Clinico-radiological follow-up is still in progress. Study design and methodology have been previously described (21). At enrollment, data on demographic characteristics (age, sex, years of education), previous stroke events, and vascular risk factors and comorbidities (hypertension, diabetes, dyslipidemia, physical activity, smoking habits, alcohol consumption, peripheral arterial disease, ischemic heart disease, myocardial infarction, heart failure) were collected. Furthermore, according to the study protocol, at baseline evaluation all participants underwent a comprehensive cognitive and motor assessment and brain MRI.

### Cognitive and Motor Assessment

The neuropsychological battery included the Montreal cognitive assessment test (MoCA) as a global cognitive functioning test and 6-s level tests for the evaluation of the following domains: verbal



memory (Rey Auditory-Verbal Learning Test, short-story test), attention and executive functions (visual search test, Color Word Stroop), and language (semantic verbal fluency test, sentence construction test) (21). Neuropsychological tests' raw scores were corrected for demographics according to the Italian population normative data, and then used in the statistical analyses as continuous variables.

Motor performance assessment included an objective evaluation by means of the Short Physical Performance Battery (SPPB) and walking speed (22). The SPPB is a composite measure designed to assess three aspects of physical performance: standing balance (the ability to stand for up to 10 s with feet in side-by-side, semi-tandem, and tandem positions), gait (time to complete a 4-m walk), and sit-to-stand time (time to rise from a chair five times). Each task is scored out of four, with the scores from the three tests summed to give a total, with a maximum of 12 (best performance) and a minimum of 0 (worst performance).

Walking speed was measured on a flat surface, and patients were instructed to walk for 1 min at their usual speed. Walking speed (meters/seconds) for each patient was calculated.

## Neuroimaging Assessment

Brain MRI have been performed on a 1.5 T MRI (Ingenia, Philips Healthcare, Best, The Netherlands). The MRI protocol included the following sequences: sagittal T1-weighted spin-echo [repetition time (TR) = 547 ms; echo time (TE) = 12 ms; slice thickness = 5 mm; interslice spacing = 0.5 mm; matrix size = 320 × 250; field of view (FOV) = 23 cm × 23 cm; number of signals averaged (NSA) = 1], coronal T2-weighted fast spin-echo (TR = 3347 ms; TE = 110 ms; slice thickness = 5 mm; interslice spacing = 0.5 mm; matrix size = 512 × 322; FOV = 22 cm × 22 cm; NSA = 2); axial fluid-attenuated inversion recovery (FLAIR) [TR = 11,000 ms; TE = 125 ms; inversion time (TI) = 2800 ms; slice thickness = 5 mm; interslice spacing = 0.5 mm; matrix size = 384 × 204; FOV = 23 cm × 23 cm; NSA = 2]; axial gradient-echo T2\* (GRE) [TR = 534 ms; TE = 23 ms; flip angle (FA) = 18; slice thickness = 5 mm; interslice spacing = 0.5 mm; matrix size = 256 × 185; FOV = 23 cm × 23 cm; NSA = 1]; axial diffusion weighted imaging (DWI) (TR = 3891 ms; TE = 75 ms; slice thickness = 5 mm; interslice spacing = 0.5 mm; matrix size = 164 × 162; FOV = 23 cm × 23 cm; NSA = 2); gradient-echo 3D T1-weighted (TR = 7.5 ms; TE = 3.4 ms; TI = 950, slice thickness = 1 mm; matrix size = 256 × 241; FOV = 25.6 cm × 25.6 cm; NSA = 1) followed by multiplanar reconstruction (MPR) in axial, coronal, and sagittal planes. Cerebral lesion burden was visually assessed by a trained and experienced rater using validated scales.

Cerebrovascular lesion burden encompassed markers of small vessel disease (SVD) and large vessel disease.

- Non-lacunar infarcts were numerically rated on T1-weighted and FLAIR sequences.

SVD markers were selected and evaluated according to the STRIVE criteria (23), and included:

- White matter hyperintensities (WMH): rated on axial FLAIR sequences using the modified Fazekas scale (24), which defines three different grades of deep WMH severity: mild (single lesions <10 mm; areas of "grouped" lesions <20 mm in any diameter), moderate (single hyperintense lesions between 10 and 20 mm;

areas of "grouped" lesions ≥20 mm in any diameter; no more than "connecting bridges" between individual lesions), and severe (single lesions or confluent areas of hyperintensity ≥20 mm in any diameter).

- Cerebral microbleeds (CMB): rated on axial gradient-echo T2\* sequences according to the Microbleeds Anatomical Rating Scale (MARS) (25).

- Lacunar infarcts: numerically rated on T2 FLAIR sequences.

Further evaluation of cerebral lesion load, included:

- Global cortical atrophy (GCA): rated on axial T1 or FLAIR sequences using the 0–3 points Pasquier scale (26).

- Medial temporal atrophy (MTA): graded on coronal T1 or FLAIR sequences using the 0–4 points Scheltens visual scale (27).

## Statistical Analyses

Descriptive analyses (frequencies and percentages or means and standard deviations) were carried out to describe the total cohort in terms of demographics, vascular risk factors, comorbidities, history of stroke, and motor, cognitive, and neuroimaging characteristics. For analyses purposes, neuroimaging characteristics were dichotomized as follows: non-lacunar infarcts absent vs. ≥1; WMH absent-mild (Fazekas score 0–1) vs. moderate-severe (Fazekas score 2–3); cerebral microbleeds absent vs. ≥1; lacunar infarcts absent vs. ≥1; global cortical atrophy absent-mild (Pasquier score 0–1) vs. moderate-severe (Pasquier score 2–3); and mean left and right MTA Scheltens score 0–1 vs. 2–4.

Univariate analyses (Pearson's  $r$  or point-biserial  $r_{pb}$  correlations) were employed to evaluate the association between the performances in cognitive and motor tests, and demographics (age, sex, and education), vascular risk factors or comorbidities (hypertension, diabetes, dyslipidemia, physical activity, smoking habits, alcohol consumption, peripheral arterial disease, ischemic heart disease, myocardial infarction, heart failure), history of stroke, and neuroimaging characteristics. Results on the effects of demographics and vascular risk factors or comorbidities will be further used to decide for their introduction within multivariate models of analyses as potential confounders.

For all univariate analyses a conservative significance threshold of 0.01 was applied.

Independent multivariate linear regression models were used to evaluate the association between each cognitive test, considered as the dependent variable, and SPPB total score or walking speed as the main independent variable controlling for the influence of the cerebral lesions burden considered either as clinical history of stroke in Model 1 or as MRI markers (WMH, CMB, lacunar and non-lacunar infarcts, GCA, and MTA) in Model 2. All multivariate linear regressions used a full model, without any selection procedure for the included independent variables, and Bonferroni corrections for multiple comparisons were applied at the significance threshold of 0.05.

All analyses were done using the SPSS software version 25.

## RESULTS

From September 2017 to March 2019, out of the 194 subjects enrolled in the Strat-AF study, 170 (mean age  $77.7 \pm 6.8$

**TABLE 1** | Demographic, history of stroke, vascular risk factors, comorbidities, motor, cognitive, and neuroimaging characteristics of the Strat-AF study cohort (means and standard deviations or frequencies and percentages).

		Total cohort <i>n</i> = 170
Age (years)		77.7 ± 6.8
Sex (female)		60 (35%)
Education (years)		9.4 ± 4.3
History of stroke		38 (22%)
Hypertension		140 (82%)
Diabetes		22 (13%)
Dyslipidemia		87 (51%)
Physical activity		60 (35%)
Smoking habits		105 (62%)
Alcohol consumption		91 (53%)
Peripheral arterial disease		14 (8%)
Ischemic heart disease		18 (11%)
Myocardial infarction		15 (9%)
Heart failure		25 (15%)
CHA <sub>2</sub> DS <sub>2</sub> -VASc score		3.7 ± 1.5
Type of oral anticoagulant therapy	Vitamin K antagonists	52 (31%)
	Direct oral anticoagulants	118 (69%)
SPPB total score		9.5 ± 2.2
Walking speed		0.9 ± 0.2
MoCA		21.9 ± 3.9
Visual search		36.3 ± 7.4
Stroop (time to complete)		28.2 ± 28.7
RAVLT (immediate recall)		36.7 ± 8.5
RAVLT (delayed recall)		6.7 ± 2.6
Short story		14.2 ± 4.7
Sentence construction		19.5 ± 6.4
Semantic verbal fluency		42.4 ± 9.3
White matter hyperintensities	Moderate-severe	35 (21%)
Non-lacunar infarcts	≥ 1	53 (31%)
Lacunar infarcts	≥ 1	54 (32%)
Cerebral microbleeds	≥ 1	48 (28%)
Cortical atrophy	Moderate-severe	133 (78%)
Medial temporal atrophy	Mean ≥ 2	108 (64%)

SPPB, short physical performance battery; MoCA, montreal cognitive assessment, RAVLT, Rey auditory-verbal learning test.

years, 35% females) completed the baseline MRI protocol and were included in the present study. Demographic, vascular risk factors, comorbidities, motor, cognitive, and neuroimaging characteristics are shown in **Table 1**. Thirty-eight (22%) patients had history of stroke, the mean SPPB total score was  $9.5 \pm 2.19$ , mean walking speed  $0.9 \pm 0.21$ , and the mean MoCA score was  $21.9 \pm 3.9$ . Concerning the distributions of neuroimaging characteristics: a moderate to severe degree of WMH was present in the 21% of the total cohort, lacunar infarct in 32%, and CMB in 28%. A moderate to severe degree of cortical atrophy was observed in 78% of patients. Non-lacunar infarcts in 31%, and a mean MTA score  $\geq 2$  in 64%.

Concerning the influence of demographics on cognitive and motor performances, older age was significantly associated with a worse performance in both SPPB total score ( $r = -0.309$   $p = 0.001$ ) and walking speed ( $r = -0.409$   $p = 0.001$ ), and a lesser level of education was significantly associated with worse performances in MoCA ( $r = 0.200$   $p = 0.009$ ) and walking speed ( $r = 0.215$   $p = 0.005$ ). Compared to males, females had a statistically significant worse performance in MoCA ( $r_{pb} = -0.338$   $p = 0.001$ ), short story ( $r_{pb} = -0.329$   $p = 0.001$ ), and semantic verbal fluency ( $r_{pb} = -0.252$   $p = 0.001$ ), as well as in both motor indexes ( $r_{pb} = -0.245$   $p = 0.001$  for SPPB,  $r_{pb} = -0.345$   $p = 0.001$  for walking speed). All demographic variables were then introduced as independent variables in multivariate models of analysis.

Taking into account the effect of vascular risk factors and comorbidities on cognitive and motor performances, univariate analyses showed a significant association between heart failure and SPPB total score ( $r_{pb} = -0.201$   $p = 0.009$ ), and between physical activity and performances in MoCA ( $r_{pb} = 0.231$   $p = 0.003$ ), SPPB ( $r_{pb} = 0.278$   $p = 0.001$ ), and walking speed ( $r_{pb} = 0.349$   $p = 0.001$ ). Heart failure and physical activity were then introduced as independent variables in multivariate models of analysis.

**Table 2** shows the univariate associations between motor and cognitive performances. Both indexes of motor performance were significantly associated with MoCA, visual search, Stroop, short story, and semantic verbal fluency scores.

The influence of history of stroke on cognitive and motor performances, and its mediating role on their association, was further evaluated. In **Table 3**, the presence of history of stroke resulted significantly associated with a worse performance on MoCA, Stroop, and sentence construction tests, as well as with a reduced walking speed. Multivariate linear regression models on the association between cognitive tests and indexes of motor performance taking into account the effect of stroke history are shown in **Table 4** (Models 1). Even after controlling for history of stroke, both the motor indexes were significantly associated with MoCA, visual search, and semantic fluency scores in all adjusted models. The presence of stroke history was confirmed to be another statistically significant predictor of MoCA performance in both Models 1, while its associations with Stroop ( $\beta = 0.183$ ,  $p = 0.017$  for SPPB,  $\beta = 0.183$ ,  $p = 0.020$  for walking speed) and sentence construction ( $\beta = -0.184$ ,  $p = 0.020$  for SPPB,  $\beta = -0.176$ ,  $p = 0.028$  for walking speed) lost significance from a statistical point of view according to the correction for multiple comparisons.

**Table 3** shows the association between neuroimaging characteristics and measures of cognitive and motor performances by means of univariate correlational analyses. Among the neuroimaging characteristics, the presence of non-lacunar infarcts was significantly associated with MoCA scores and the presence of CMB with visual search test scores. In both cases, the statistical direction of the association indicated a worse cognitive performance in patients having at least one cerebral lesion.

Results from the independent multivariate linear regression models on the association between each cognitive test and

**TABLE 2 |** Association between cognitive and motor performances (univariate analyses: Pearson's *r*).

Cognitive domains	Cognitive measures	Short physical performance battery total score	Walking speed
Global cognitive functioning	Montreal cognitive assessment	<b>0.359*</b>	<b>0.372*</b>
Attention and executive functions	Visual search	<b>0.361*</b>	<b>0.322*</b>
	Stroop (time)	<b>−0.272*</b>	<b>−0.263*</b>
Memory	Rey Auditory-Verbal Learning Test (immediate recall)	0.172	0.132
	Rey Auditory-Verbal Learning Test (delayed recall)	0.038	0.063
	Short story	<b>0.263*</b>	<b>0.310*</b>
Language	Sentence construction	0.146	0.166
	Semantic verbal fluency	<b>0.311*</b>	<b>0.360*</b>

\*Statistically significant at  $p < 0.01$ . Bold values are statistically significant.

**TABLE 3 |** Cognitive and motor performances and their associations with history of stroke and neuroimaging characteristics (univariate analyses: Pearson's *r* and point-biserial  $r_{pb}$  correlations).

		History of stroke	WMH	Non-lacunar infarcts	Lacunar infarcts	CMB	GCA	MTA
		Present	Moderate-severe	≥1	≥1	≥1	Moderate-severe	Mean ≥ 2
Cognitive measures	MoCA	<b>−0.334*</b>	0.067	<b>−0.231*</b>	0.002	−0.046	0.052	0.027
	Visual search	−0.078	0.043	−0.065	0.032	<b>−0.239*</b>	−0.127	−0.022
	Stroop (time)	<b>0.222*</b>	−0.031	0.104	−0.057	0.024	0.025	0.091
	RAVLT (immediate recall)	−0.185	−0.019	−0.135	−0.015	−0.156	−0.028	0.004
	RAVLT (delayed recall)	−0.141	0.023	−0.046	0.086	0.048	0.096	0.023
	Short story	−0.147	0.157	−0.149	0.036	0.048	0.007	0.063
	Sentence construction	<b>−0.208*</b>	−0.013	−0.104	−0.057	0.044	−0.004	−0.143
	Semantic verbal fluency	−0.197	0.059	−0.190	0.064	−0.073	−0.007	−0.042
Motor indexes	SPPB total score	−0.177	−0.027	−0.141	0.024	−0.084	−0.117	−0.157
	Walking speed	<b>−0.236*</b>	−0.119	−0.192	−0.040	−0.033	−0.159	−0.143

\*Statistically significant at  $p < 0.01$ .

SPPB, short physical performance battery; MoCA, montreal cognitive assessment; RAVLT, Rey auditory-verbal learning test; WMH, white matter hyperintensities; CMB, cerebral microbleeds; GCA, global cortical atrophy; MTA, medial temporal atrophy. Bold values are statistically significant.

indexes of motor performance controlling for the effect of neuroimaging characteristics are shown in **Table 4** (Models 2). The associations of both motor indexes with MoCA, and visual search, and of walking speed with semantic fluency, were further confirmed to be statistically significant independently on the effect of neuroimaging characteristics. Furthermore, both motor indexes were significantly associated with short story. In multivariate models, the presence of CMB was confirmed to be another statistically significant predictor of visual search test performance in both Models 2, while the association between non-lacunar infarcts and MoCA remained as a trend but lost statistical significance according to the correction for multiple comparisons ( $\beta = -0.160$ ,  $p = 0.030$  for SPPB,  $\beta = -0.156$ ,  $p = 0.038$  for walking speed).

Finally, taking into account the influence of the other independent variables in multivariate models, sex was confirmed as another statistically significant predictor of MoCA and short-story tests only in Models 1 among demographics, while heart failure and physical activity were not statistically significant (**Table 4**).

## DISCUSSION

In this sample of hospital-based older adults with diagnosis of AF and ongoing anticoagulant therapy for the primary or secondary prevention of thromboembolism, we examined the relationship between mobility and cognition by the use of several objective measures of motor ability and high order cognitive functions. Our results showed a consistent association between motor and cognitive performances in our cohort. Specifically, motor abilities, herein evaluated both as a composite measure of physical performance and a gait speed measure, resulted as being associated with global cognitive functioning, attention, prose memory, and verbal fluency.

This evidence is in line with data from recent systematic reviews and meta-analyses of cross-sectional studies that support an association between mobility measures and cognitive assessments in healthy older adults (1, 7). Convergent evidence suggests that individuals with better mobility, mainly evaluated by means of gait speed, perform better on assessments of global cognition, executive function, processing speed, memory,

**TABLE 4 |** Association between the performances in cognitive tests and motor indexes adjusted for history of stroke (Model 1) or neuroimaging characteristics (Model 2), and demographics, heart failure, and physical activity (all models).

Cognitive measure (dependent)	Motor index (independent)	Model 1 <sup>#</sup>		Model 2 <sup>##</sup>	
		B standard	Other statistically significant independent variables	B standard	Other statistically significant independent variables
MoCA	SPPB total score	<b>0.256*</b>	Sex History of stroke	<b>0.276**</b>	
		<b>-0.206*</b>			
		<b>-0.262*</b>			
	Walking speed	<b>0.236*</b>	History of stroke	<b>0.272**</b>	
		<b>-0.257*</b>			
Visual search	SPPB total score	<b>0.350*</b>		<b>0.344**</b>	Cerebral microbleeds
	Walking speed	<b>0.313*</b>		<b>0.307**</b>	
				<b>-0.245**</b>	Cerebral microbleeds
Stroop (time to complete)	SPPB total score	-0.196		-0.212	
	Walking speed	-0.152		-0.199	
RAVLT (immediate recall)	SPPB total score	0.187		0.189	
	Walking speed	0.134		0.119	
RAVLT (delayed recall)	SPPB total score	0.034		0.051	
	Walking speed	0.057		0.077	
Short story	SPPB total score	0.197		<b>0.245**</b>	
		<b>-0.248*</b>	Sex		
	Walking speed	0.225		<b>0.273**</b>	
Sentence construction	SPPB total score	0.100		0.094	
	Walking speed	0.107		0.112	
Semantic verbal fluency	SPPB total score	<b>0.223*</b>		0.235	
	Walking speed	<b>0.261*</b>		<b>0.273**</b>	

<sup>#</sup>Multivariate independent models of linear regression adjusted for demographics (age, education, sex), heart failure, physical activity and history of stroke.

<sup>##</sup>Multivariate independent models of linear regression adjusted for demographics (age, education, sex), heart failure, physical activity, and neuroimaging characteristics (white matter hyperintensities; non-lacunar infarcts; lacunar infarcts; cerebral microbleeds; global cortical atrophy; medial temporal atrophy).

\*Statistically significant at  $p < 0.007$  (Bonferroni correction for multiple comparisons).

\*\*Statistically significant at  $p < 0.004$  (Bonferroni correction for multiple comparisons).

MoCA, montreal cognitive assessment; RAVLT, Rey auditory-verbal learning test; SPPB, short physical performance battery. Bold and italic values represent the statistically significant beta coefficients of the corresponding variables of the "Other statistically significant independent variables" column.

and language, thus reinforcing the hypothesis of a multifaceted influence of high-order cognitive abilities.

Among cognitive domains, attention and executive functions have received considerable interest in studies on the association between mobility and cognition (9, 10). The rationale of this interest relies on several potential factors, for example, the influence of psychomotor and processing speed on mobility, the attentional and executive demands associated with motor regulation, and the subcortical brain networks involvement in frontal lobes functions. Our results seemed to confirm a reliable association between mobility and cognitive performances related to attention and executive processes. Among the cognitive tests taken into consideration in the present study, those with the most consistent association with both mobility indexes were MoCA and visual search. MoCA is a screening test suggested by the National Institute for Neurological Disorders and Stroke and the Canadian Stroke Network (NINDS-CSN) to harmonize standards for the evaluation of vascular cognitive impairment, because it

includes several items assessing executive functions, attention and concentration (28). The visual search test is a simple timed selective digit cancellation task that involves focused and sustained attention together with the attentional control of the speed/accuracy trade-off.

Considering the specificity of our cohort, that is, elderly AF patients, our results were in line with those of the only study that showed a direct association between gait and cognition in this population (20). Marino and colleagues found that, among the 1,185 AF participants aged  $\geq 65$  years, those with low gait speed were significantly more likely to have cognitive impairment independently from several demographic and clinical characteristics. Also in our cohort, the association between motor and cognitive performances was confirmed to be independent of demographics, vascular risk factors, and comorbidities.

Furthermore, we introduced the potential effect of cerebral lesions burden within this association, and found its persistence independently of these factors.



One recent study by Conen and et al. (29) evaluated the relationships between cognitive function, assessed by MoCA, and vascular brain lesions in a large sample of patients with AF ( $N = 1,737$ , mean age  $73 \pm 8$  years). Their results showed a high burden of vascular brain lesions, mostly related to clinically silent infarcts. In our cohort, we found a comparable vascular lesion burden, taking into account also that actually our sample is 4 years older on average. Taking into account the impact of all different lesions types on cognition, Conen and colleagues found that only large infarcts were significantly associated with a lower MoCA performance. In line with this, also in our cohort we found that non-lacunar infarcts, or history of stroke, influenced MoCA performance.

Interestingly, in our cohort CMB seemed to consistently influence the performance on the visual search test. CMBs are recognized as MRI markers of SVD, and an increasing number of studies have linked their presence with cognitive decline (30, 31). Evidence suggest that CMB may play a role in vascular cognitive impairment, with preliminary data of an influence on tests sensitive to executive dysfunction, consistent with a possible effect of CMB on frontal-subcortical circuits. Results in our cohort seemed consistent with an influence of CMB on focused and sustained attention. Also, CMB prevalence within our sample seemed in line with rates reported in studies on patients with vascular cognitive impairment, and was slightly higher than the prevalence of 21% reported for the 1,490 adult AF participants of the CROMIS-2 study (31–34).

Limitations of our study need to be considered. The present study is based on a secondary analysis of the Strat-AF study, which is a single center study. The sample size imposes caution in the interpretation of our results that cannot be generalized to other populations. Moreover, the cross-sectional design of the analysis limits further interpretations of the direction of the association, precluding causal inferences regarding the relationship between gait and cognition. Longitudinal data collection is ongoing, and further prospective analysis will be conducted to elucidate the role of motor performance as potential predictor of cognitive impairment.

Another limitation is the neuroimaging assessment based on visual evaluations of brain MRI. Compared to the use of quantitative brain volumetric and morphometric measures, our approach might have reduced accuracy in the quantification of cerebral lesions burden. Also, CMB have been evaluated on traditional gradient recalled-echo (GRE) MRI sequences. The inclusion in the protocol of sequences with higher resolution, that is, the susceptibility-weighted imaging (SWI), would have increased the sensitivity in detecting CMB and probably would have reinforced the association with cognitive and motor performances. Finally, related to our limited sample size, we have used a dichotomic approach for the evaluation of cerebral lesions burden and this might have potentially underestimated their effect on clinical outcomes.

Recognized markers for neurodegeneration, specifically Alzheimer Disease, such as cerebrospinal fluid biomarkers (amyloid- $\beta$  and tau proteins concentrations) and positron emission tomography imaging (FDG and amyloid) are not available in our cohort (35). The only marker for neurodegeneration was MTA, and this was not associated with motor and cognitive performances. Of note, nearly two-thirds of our sample scored 2 or more on MTA. Despite the link between AF and cerebral volume loss remains unclear, possible hypotheses include mechanisms such as hypoperfusion, inflammation, and endothelial dysfunction, and thus a possible close interplay between vascular and neurodegenerative processes.

Last but not least, our approach to gait evaluation was based on qualitative measures, which on one side are feasible in clinical setting with minimal costs and time, on the other might be less sensitive than quantitative gait analysis (e.g., pace, rhythm, variability, asymmetry, and postural control).

In conclusion, our study has confirmed the existence of a direct and strong association between motor and cognitive performances in a population of elderly AF patients, also taking into account the effect and potential mediating role of cerebral lesion burden. The determinants and common mechanisms of this relationship remain unexplained, and further studies are needed to better characterize the association.

## DATA AVAILABILITY STATEMENT

The datasets presented in this article are not readily available because Data are not freely available. Requests to access the datasets should be directed to Anna Poggesi, [anna.poggesi@unifi.it](mailto:anna.poggesi@unifi.it).

## ETHICS STATEMENT

The studies involving human participants were reviewed and approved by Comitato Etico Area Vasta Centro—Careggi University Hospital. The patients/participants provided their written informed consent to participate in this study.

## AUTHOR CONTRIBUTIONS

AP, ES, and FG: study concept and design. FG, FU, CB, EC, SC, SDo, BF, SG, AM, DM, and VR: acquisition of data. AP, ES, FG, and FU: analysis and interpretation of data. AP, ES, and FG: preparation of the manuscript. EF, FC, SDi, BG, AG, CM, FP, GP, CS, and RM: critical revision of the manuscript. All authors contributed to the article and approved the submitted version.

## FUNDING

This research was funded by Tuscany region and Italian Ministry of Health under Grant Aired Research Call Bando Ricerca Finalizzata 2013 GR-2013-02355523.

## REFERENCES

- Demnitz N, Esser P, Dawes H, Valkanova V, Johansen-Berg H, Ebmeier KP, et al. A systematic review and meta-analysis of cross-sectional studies examining the relationship between mobility and cognition in healthy older adults. *Gait Posture*. (2016) 50:164–74. doi: 10.1016/j.gaitpost.2016.08.028
- Li KZH, Bherer L, Mirelman A, Maidan I, Hausdorff JM. Cognitive involvement in balance, gait and dual-tasking in aging: a focused review from a neuroscience of aging perspective. *Front Neurol*. (2018) 9:913. doi: 10.3389/fneur.2018.00913
- Montero-Odasso M, Annweiler C, Hachinski V, Islam A, Yang N, Vasudev A. Vascular burden predicts gait, mood, and executive function disturbances in older adults with mild cognitive impairment: results from the gait and brain study. *J Am Geriatr Soc*. (2012) 60:1988–90. doi: 10.1111/j.1532-5415.2012.04180.x
- Kikkert LHJ, Vuillerme N, van Campen JP, Hortobágyi T, Lamothe CJ. Walking ability to predict future cognitive decline in old adults: a scoping review. *Ageing Res Rev*. (2016) 27:1–14. doi: 10.1016/j.arr.2016.02.001
- Beauchet O, Annweiler C, Callisaya ML, De Cock AM, Helbostad JL, Kressig RW, et al. Poor gait performance and prediction of dementia: results from a meta-analysis. *J Am Med Dir Assoc*. (2016) 17:482–90. doi: 10.1016/j.jamda.2015.12.092
- Grande G, Triolo F, Nuara A, Welmer AK, Fratiglioni L, Vetrano DL. Measuring gait speed to better identify prodromal dementia. *Exp Gerontol*. (2019) 124:110625. doi: 10.1016/j.exger.2019.05.014
- Morris R, Lord S, Bunce J, Burn D, Rochester L. Gait and cognition: mapping the global and discrete relationships in ageing and neurodegenerative disease. *Neurosci Biobehav Rev*. (2016) 64:326–45. doi: 10.1016/j.neubiorev.2016.02.012
- Bayot M, Dujardin K, Tard C, Defebvre L, Bonnet CT, Allart E, et al. The interaction between cognition and motor control: a theoretical framework for dual-task interference effects on posture, gait initiation, gait and turning. *Neurophysiol Clin*. (2018) 48:361–75. doi: 10.1016/j.neucli.2018.10.003
- Yogev-Seligmann G, Hausdorff JM, Giladi N. The role of executive function and attention in gait. *Mov Disord*. (2008) 23:329–42. doi: 10.1002/mds.21720
- Wollacott M, Shumway-Cook A. Attention and the control of posture and gait: a review of an emerging area of research. *Gait Posture*. (2002) 16:1–14. doi: 10.1016/s0966-6362(01)00156-4
- Scherder E, Eggermont L, Swaab D, van Heuvelen M, Kamsma Y, de Greef M, et al. Gait in ageing and associated dementias; its relationship with cognition. *Neurosci Biobehav Rev*. (2007) 31:485–97. doi: 10.1016/j.neubiorev.2006.11.007
- Valkanova V, Ebmeier KP. What can gait tell us about dementia? Review of epidemiological and neuropsychological evidence. *Gait Posture*. (2017) 53:215–23. doi: 10.1016/j.gaitpost.2017.01.024
- McArdle R, Morris R, Wilson J, Galna B, Thomas AJ, Rochester L. What can quantitative gait analysis tell us about dementia and its subtypes? A structured review. *J Alzheimers Dis*. (2017) 60:1295–312. doi: 10.3233/JAD-170541
- Bahureksa L, Najafi B, Saleh A, Sabbagh M, Coon D, Mohler MJ, et al. The impact of mild cognitive impairment on gait and balance: a systematic review and meta-analysis of studies using instrumented assessment. *Gerontology*. (2017) 63:67–83. doi: 10.1159/000445831
- Staerk L, Sherer JA, Ko D, Benjamin EJ, Helm RH. Atrial fibrillation: epidemiology, pathophysiology, and clinical outcomes. *Circ Res*. (2017) 120:1501–17. doi: 10.1161/CIRCRESAHA.117.309732
- Poggesi A, Inzitari D, Pantoni L. Atrial fibrillation and cognition: epidemiological data and possible mechanisms. *Stroke*. (2015) 46:3316–21. doi: 10.1161/STROKEAHA.115.008225
- Donoghue OA, Jansen S, Dooley C, De Rooij S, Van Der Velde N, Kenny RA. Atrial fibrillation is associated with impaired mobility in community-dwelling older adults. *J Am Med Dir Assoc*. (2014) 15:929–33. doi: 10.1016/j.jamda.2014.08.005
- Koca M, Yavuz BB, Tuna Dogrul R, Çalişkan H, Sengül Ayçiçek G, Özsürekcı C, et al. Impact of atrial fibrillation on frailty and functionality in older adults. *Ir J Med Sci*. (2020) 198:917–24. doi: 10.1007/s11845-020-02190-x
- Welmer AK, Angleman S, Rydwick E, Fratiglioni L, Qiu C. Association of cardiovascular burden with mobility limitation among elderly people: a population-based study. *PLoS ONE*. (2013) 8:e65815. doi: 10.1371/journal.pone.0065815
- Marino FR, Lessard DM, Saczynski JS, McManus DD, Silverman-Lloyd LG, Benson CM, et al. Gait speed and mood, cognition, and quality of life in older adults with atrial fibrillation. *J Am Heart Assoc*. (2019) 8:e013212. doi: 10.1161/JAHA.119.013212
- Poggesi A, Barbato C, Galmozzi F, Camilleri E, Cesari F, Chiti S, et al. Role of biological markers for cerebral bleeding risk STRATification in patients with atrial fibrillation on oral anticoagulants for primary or secondary prevention of ischemic stroke (Strat-AF Study): study design and methodology. *Medicina*. (2019) 55:626. doi: 10.3390/medicina55100626
- Guralnik JM, Simonsick EM, Ferrucci L, Glynn RJ, Berkman LF, Blazer DG, et al. A short physical performance battery assessing lower extremity function: association with self-reported disability and prediction of mortality and nursing home admission. *J Gerontol*. (1994) 49:M85–94. doi: 10.1093/geronj/49.2.m85
- Wardlaw JM, Smith EE, Biessels GJ, Cordonnier C, Fazekas F, Frayne R, et al. Neuroimaging standards for research into small vessel disease and its contribution to ageing and neurodegeneration. *Lancet Neurol*. (2013) 12:822–38. doi: 10.1016/S1474-4422(13)70124-8
- Pantoni L, Basile AM, Pracucci G, Asplund K, Bogousslavsky J, Chabriat H, et al. Impact of age-related cerebral white matter changes on the transition to disability—the LADIS study: rationale, design and methodology. *Neuroepidemiology*. (2005) 24:51–62. doi: 10.1159/000081050
- Gregoire SM, Chaudhary UJ, Brown MM, Yousry TA, Kallis C, Jäger HR, et al. The microbleed anatomical rating scale (MARS): reliability of a tool to map brain microbleeds. *Neurology*. (2009) 73:1759–66. doi: 10.1212/WNL.0b013e3181c34a7
- Pasquier F, Leys D, Weerts JG, Mounier-Vehier F, Barkhof F, Scheltens P. Inter- and intraobserver reproducibility of cerebral atrophy assessment on MRI scans with hemispheric infarcts. *Eur Neurol*. (1996) 36:268–72. doi: 10.1159/000117270
- Scheltens P, Leys D, Barkhof F, Huglo D, Weinstein HC, Vermersch P, et al. Atrophy of medial temporal lobes on MRI in “probable” Alzheimer’s disease and normal ageing: diagnostic value and neuropsychological correlates. *J Neurol Neurosurg Psychiatry*. (1992) 55:967–72. doi: 10.1136/jnnp.55.10.967
- Hachinski V, Iadecola C, Petersen RC, Breteler MM, Nyenhuis DL, Black SE, et al. National institute of neurological disorders and stroke-canadian stroke network vascular cognitive impairment harmonization standards. *Stroke*. (2006) 37:2220–41. doi: 10.1161/01.STR.0000237236.88823.47
- Conen D, Rodondi N, Müller A, Beer JH, Ammann P, Moschovitis G, et al. Relationships of overt and silent brain lesions with cognitive function in patients with atrial fibrillation. *J Am Coll Cardiol*. (2019) 73:989–99. doi: 10.1016/j.jacc.2018.12.039
- Akoudad S, Wolters FJ, Viswanathan A, de Bruijn RF, van der Lugt A, Hofman A, et al. Association of cerebral microbleeds with cognitive decline and dementia. *JAMA Neurol*. (2016) 73:934–43. doi: 10.1001/jamaneurol.2016.1017
- Werring DJ, Gregoire SM, Cipolletti L. Cerebral microbleeds and vascular cognitive impairment. *J Neurol Sci*. (2010) 299:131–5. doi: 10.1016/j.jns.2010.08.034
- Valenti R, Del Bene A, Poggesi A, Ginestroni A, Salvadori E, Pracucci G, et al. Cerebral microbleeds in patients with mild cognitive impairment and small vessel disease: The Vascular Mild Cognitive Impairment (VMCI)-Tuscany study. *J Neurol Sci*. (2016) 368:195–202. doi: 10.1016/j.jns.2016.07.018
- Yates PA, Villemagne VL, Ellis KA, Desmond PM, Masters CL, Rowe CC. Cerebral microbleeds: a review of clinical, genetic, and neuroimaging associations. *Front Neurol*. (2014) 4:205. doi: 10.3389/fneur.2013.00205
- Wilson D, Ambler G, Shakeshaft C, Brown MM, Charidimou A, Al-Shahi Salman R, et al. Cerebral microbleeds and intracranial haemorrhage risk in patients anticoagulated for atrial fibrillation after acute ischaemic stroke or transient ischaemic attack (CROMIS-2): a multicentre observational cohort study. *Lancet Neurol*. (2018) 17:539–47. doi: 10.1016/S1474-4422(18)30145-5

35. Dubois B, Feldman HH, Jacova C, Dekosky ST, Barberger-Gateau P, Cummings J, et al. Research criteria for the diagnosis of alzheimer's disease: revising the NINCDS-ADRDA criteria. *Lancet Neurol.* (2007) 6:734–46. doi: 10.1016/S1474-4422(07)70178-3

**Conflict of Interest:** The authors declare that the research was conducted in the absence of any commercial or financial relationships that could be construed as a potential conflict of interest.

Copyright © 2020 Salvadori, Galmozzi, Uda, Barbato, Camilleri, Cesari, Chiti, Diciotti, Donnini, Formelli, Galora, Giusti, Gori, Marzi, Melone, Mistri, Pescini, Pracucci, Rinnoci, Sarti, Fainardi, Marcucci and Poggesi. This is an open-access article distributed under the terms of the Creative Commons Attribution License (CC BY). The use, distribution or reproduction in other forums is permitted, provided the original author(s) and the copyright owner(s) are credited and that the original publication in this journal is cited, in accordance with accepted academic practice. No use, distribution or reproduction is permitted which does not comply with these terms.



# Early Post-stroke Cognition: In-hospital Predictors and the Association With Functional Outcome

Richa Sharma<sup>1</sup>, Dania Mallick<sup>2</sup>, Rafael H. Llinas<sup>2</sup> and Elisabeth B. Marsh<sup>2\*</sup>

<sup>1</sup> Department of Neurology, Yale University School of Medicine, New Haven, CT, United States, <sup>2</sup> Department of Neurology, The Johns Hopkins School of Medicine, Baltimore, MD, United States

**Purpose:** To characterize and predict early post-stroke cognitive impairment by describing cognitive changes in stroke patients 4–8 weeks post-infarct, determining the relationship between cognitive ability and functional status at this early time point, and identifying the in-hospital risk factors associated with early dysfunction.

**Materials and Methods:** Data were collected for 214 patients with ischemic stroke and 39 non-stroke controls. Montreal Cognitive Assessment (MoCA) exams were administered at post-hospitalization clinic visits approximately 4–8 weeks after infarct. MoCA scores were compared for patients with: no stroke, minor stroke [NIH Stroke Scale (NIHSS) < 5], and major stroke. Ordinal logistic regression was performed to assess the relationship between MoCA score and functional status [modified Rankin Scale score (mRS)] at follow-up. Predictors of MoCA < 26 and < 19 (cutoffs for mild and severe cognitive impairment, respectively) at follow-up were identified by multivariable logistic regression using variables available during hospitalization.

**Results:** Post stroke cognitive impairment was common, with 66.8% of patients scoring < 26 on the MoCA and 22.9% < 19. The average total MoCA score at follow-up was 18.7 (SD 7.0) among major strokes, 23.6 (SD 4.8) among minor strokes, and 27.2 (SD 13.0) among non-strokes ( $p = <0.0001$ ). The follow-up MoCA score was associated with the follow-up mRS in adjusted analysis (OR 0.69; 95% C.I. 0.59–0.82). Among patients with no prior cognitive impairment ( $N = 201$ ), a lack of pre-stroke employment, admission NIHSS > 6, and left-sided infarct predicted a follow-up MoCA < 26 (c-statistic 0.75); while admission NIHSS > 6 and infarct volume > 17 cc predicted a MoCA < 19 (c-statistic 0.75) at follow-up.

**Conclusion:** Many patients experience early post-stroke cognitive dysfunction that significantly impacts function during a critical time period for decision-making regarding return to work and future independence. Dysfunction measured at 4–8 weeks can be predicted during the inpatient hospitalization. These high-risk individuals should be identified for targeted rehabilitation and counseling to improve longer-term post-stroke outcomes.

**Keywords:** stroke, recovery, cognition, rehabilitation, outcomes

## OPEN ACCESS

### Edited by:

Robert Zivadinov,  
University at Buffalo, United States

### Reviewed by:

Andy Lim,  
Monash Medical Centre, Australia  
Myzoon Ali,  
University of Glasgow,  
United Kingdom

### \*Correspondence:

Elisabeth B. Marsh  
ebmarsh@jhmi.edu

### Specialty section:

This article was submitted to  
Stroke,  
a section of the journal  
Frontiers in Neurology

**Received:** 02 October 2020

**Accepted:** 07 December 2020

**Published:** 23 December 2020

### Citation:

Sharma R, Mallick D, Llinas RH and Marsh EB (2020) Early Post-stroke Cognition: In-hospital Predictors and the Association With Functional Outcome. *Front. Neurol.* 11:613607. doi: 10.3389/fneur.2020.613607



## INTRODUCTION

There is a known link between ischemic stroke and long-term cognitive impairment. The prevalence of dementia in patients with a history of ischemic stroke is nearly thirty percent; 3.5–5.8 times higher than in patients without a stroke history (1). One follow-up study reported that over a quarter of stroke patients display delayed dementia, while additional studies using more formalized neuropsychological assessments such as the Montreal Cognitive Assessment (MoCA) or Mini-Mental Status Examination have reported rates of cognitive impairment ranging from 35 to 92% (2–4). Impairment has been reported to affect multiple cognitive domains (5), though a recent study evaluating those with transient ischemic attack and minor stroke found difficulty with executive function and psychomotor processing to be the most common cognitive deficits (6). Cognitive dysfunction in stroke patients can result in deficits such as impaired activities of daily living (ADLs) and instrumental activities of daily living (IADLs), lost wages, increased health care costs, loss of independence, and social isolation.

A recent retrospective study showed an association between MoCA scores documented acutely after stroke and functional outcome during rehabilitation (6). Our study takes the logical next step and addresses the ability of in-hospital variables to predict cognitive impairment and functional status once patients have been discharged home from the inpatient setting and are transitioning back to a “normal life.” These early months represent a critical time when patients and families make decisions regarding returning to work, living alone, and functioning independently. Prior studies have identified numerous factors associated with long-term cognitive impairment in stroke patients including: white matter disease (7), lower educational level, older age, female sex, recurrent stroke, and global cortical atrophy in patients with ischemic stroke and vascular cognitive impairment (8). But, the ability to predict cognitive dysfunction that may impact recovery, at the time of hospitalization, would potentially enable physicians to identify those at risk for early cognitive decline, before life-altering decisions are made impacting quality of life.

This study aims to: (1) assess cognition across multiple domains during the early phase of stroke recovery (first 1–6 months) among patients with major strokes, minor strokes, and non-stroke controls using a simple and efficient screen (the MoCA), (2) confirm the MoCA score at early follow-up is associated with concurrent functional status (modified Rankin Scale score), and (3) identify risk factors available during the stroke hospitalization predictive of early cognitive impairment at follow-up among those without a prior history of cognitive impairment.

## MATERIALS AND METHODS

This study was approved by our Institutional Review Board and was performed in accordance with STROBE criteria. Given the observational nature of the study and that data were collected as part of routine clinical care and stored in a HIPAA-approved clinical research database, informed consent was not required.

Any reasonable request for data sharing can be directed to the corresponding author.

## Study Population

A prospectively-collected series of patients presented to the Johns Hopkins Bayview Stroke Intervention Clinic (BASIC) in Baltimore, Maryland from January 2013 to August 2018 between 1 and 6 months after hospitalization for a symptomatic, acute ischemic stroke that was radiographically evident on noncontrast head computed tomography (CT) or magnetic resonance imaging (MRI). BASIC is a multidisciplinary stroke follow-up clinic that typically sees patients 4–8 weeks post-stroke. Patients are evaluated by a board-certified vascular neurologist and rehabilitation specialists (as needed). They undergo formal neurological evaluation along with assessment of mood, fatigue, cognition, and functional ability. Individuals were excluded from the study cohort if they were unable to participate in cognitive testing due to global aphasia, severe visual impairment, decreased level of alertness, or had intracranial hemorrhage on neuroimaging (CT or MRI). The MoCA patterns of these ischemic stroke patients were compared with a cohort of non-stroke patients with no prior history of neurodegenerative or psychiatric illness who presented to stroke clinic with diagnoses of transient ischemic attack, seizure, or migraine.

## Defining Cognitive Impairment

At their follow-up clinic visit, all patients underwent a basic neurological examination and were administered the MoCA, the validity of which has been demonstrated in stroke patients (9, 10). The total MoCA score along with scores for each domain of cognition (visuospatial/executive, naming, attention, language, abstraction, recall, and orientation) were recorded for each patient. “Any cognitive impairment” was defined as total a MoCA score of <26 (11). “Severe impairment” was defined as total MoCA scores of <19 (12). The MoCA was administered by trained clinic personnel who were blinded to the patient’s modified Rankin Scale score during the clinic visit.

## Covariates

Demographic, clinical, and radiologic covariates were collected including: demographics (age, sex, race, marital status, education, pre-stroke employment status, household income approximated by median income of the patient’s zip code); stroke characteristics (severity- admission National Institute of Health Stroke Scale (NIHSS) score, functional status- modified Rankin scale (mRS) score at baseline, stroke volume, lesion location, degree of chronic white matter disease, presence of cerebral microbleeds); and medical history [prior stroke, pre-existing history of cognitive impairment or dementia, vascular comorbidities, Charlson Comorbidity Index (13), anti-depressant use]. Modified Rankin Scale score was also documented at the stroke clinic follow-up appointment by the patient’s neurologist who was blinded to the patient’s clinic MoCA result.

## Neuroimaging

Masked review of available CT and MRI was performed to calculate stroke volume and other radiographic factors by a

board-certified vascular neurologist blinded to patient outcomes. The neuroimaging was obtained during hospital admission. The volume of a hypodensity on CT or diffusion restriction on MRI matching the vascular distribution of the clinical stroke was calculated by the ellipsoid ABC/2 method (14). On MRI, the T2 FLAIR sequence was also utilized to calculate the Cardiovascular Health Study (CHS) score to estimate the degree of white matter disease burden or leukoaraiosis using the CHS study library of templates (15). Studies were graded from 1 (barely detectable white matter changes) to 8 (extensive, confluent changes). Any evidence of large vessel infarct or lacunar infarct was excluded from this classification (16, 17). The presence of cerebral microhemorrhages by hemosiderin deposits were identified on gradient echo sequences as lesions  $\leq 10$  mm in diameter.

## Statistical Analysis

All statistical analyses were performed using SAS 9.4 (Cary, NC). Analysis of variance (ANOVA) testing was performed to compare total MoCA scores and domain-specific scores among patients with: no ischemic infarct, minor stroke (admission NIHSS  $\leq 4$ ), and major stroke (admission NIHSS  $> 4$ ). Additional comparisons across groups were performed using ANOVA testing for continuous variables and Pearson's Chi-square tests for categorical variables.

To assess the association between the follow-up total MoCA score obtained in clinic (the independent predictor of interest) as well as other factors, and functional status at that timepoint, we performed univariable and multivariable ordinal logistic regression analyses given the non-normal distribution of the variable, mRS. Variables significant in univariable analysis ( $p < 0.05$ ) were included in subsequent multivariable logistic regression analysis along with the MoCA score to adjust for potential confounders that may contribute to functional status at follow-up after stroke.

Further analyses were undertaken for the subgroup of patients with ischemic stroke and no prior history of cognitive impairment. Univariable logistic regressions were performed to predict two outcome measures: total MoCA score  $< 26$  and MoCA score  $< 19$ . We then created multivariable logistic regression models using variables significant in univariable analyses for each outcome if the  $p$ -value in univariable analysis was  $< 0.2$ . To prevent overfitting, variables were selected to be included in the final models by stepwise selection.

## RESULTS

### Characteristics of Ischemic Stroke Patients and Non-stroke Controls

Over the recruitment period, 253 patients presented to follow-up clinic and were eligible for enrollment: 214 ischemic stroke patients and 39 non-stroke controls. Differences between patients with major and minor stroke and non-stroke controls are displayed in **Table 1**. The non-stroke controls consisted of patients with the following diagnoses: migraine ( $N = 16$ ); transient ischemic attack ( $N = 10$ ); seizure ( $N = 7$ ); and post-concussive headache ( $N = 1$ ). Patients within the stroke cohort were significantly older, were less educated, had lower household

incomes, had higher baseline mRS scores, and had more vascular risk factors compared to the non-stroke cohort, but had similar degrees of white matter disease compared to controls. Those with major strokes were less likely to be employed at baseline than those with minor stroke or mimics. The mean time from symptom onset to clinic visit was 1.3 months for those with minor strokes and 1.2 months for patients with major strokes. Although stroke patients were only included if time from stroke to follow-up was  $\leq 6$  months,  $> 80\%$  of stroke patients were evaluated within 90 days of symptom onset. The mean volume of infarct was significantly higher among those with major (31.7 cc) vs. minor (9.8 cc) stroke, and patients with greater stroke severity were more likely to have suffered a cortical infarct. There was no difference in leukoaraiosis or microbleed burden among stroke patients by stroke severity.

Nearly two-thirds ( $n = 143$ , 66.8%) of patients with stroke had a MoCA score of  $< 26$  at follow-up; while 49 (22.9%) had a MoCA score of  $< 19$ . Numbers were highest in those with major stroke ( $n = 60$ , 82.2% for MoCA  $< 26$ ;  $n = 31$ , 42.5% for MoCA  $< 19$ ) compared to minor stroke ( $n = 83$ , 58.9% for MoCA  $< 26$ ;  $n = 18$ , 12.8% for MoCA  $< 19$ ). Cognitive impairment was also present in a portion of controls, but less common and less severe ( $n = 20$ , 51.3% MoCA  $< 26$ ;  $n = 2$ , 5.1% MoCA  $< 19$ ). The average total MoCA score was significantly lower for patients with major (mean 18.7, SD 7.0) and minor (mean 23.6, SD 4.8) strokes compared to non-stroke controls (mean 27.2, SD 13.0). Patients with no stroke performed significantly better across all cognitive domains with the exception of language compared to patients with minor stroke, who in turn performed better than patients with major stroke (**Figure 1**).

### Association Between the Follow-Up MoCA and Functional Status at That Timepoint

In univariable ordinal logistic regression analysis of patients with ischemic stroke, the MoCA score in clinic was significantly associated with follow-up mRS score (**Table 2**, OR 0.83; 95% C.I. 0.80–0.87). When adjusted for possible confounders including NIHSS score, demographic, clinical, and radiographic covariates, the follow-up MoCA score remained an independent and significant predictor of functional status at that follow-up timepoint (OR 0.69; 95% C.I. 0.59–0.82;  $c$ -statistic 0.93).

### Predictors of Follow-Up MoCA Scores

There were 201 ischemic stroke patients with no prior history of cognitive impairment in our cohort. Of these patients, 132 scored  $< 26$  (any cognitive impairment) and 41 scored  $< 19$  (severe impairment) on follow-up MoCA examination. Univariable regression analyses of factors predictive of a new diagnosis of mild cognitive impairment or MCI and severe impairment are displayed in **Table 3**. Continuous variables significant in univariable analyses were then dichotomized using their sample mean value (age  $> 65$ , baseline mRS  $> 2$ , Charlson Comorbidity Index  $> 3$ , stroke volume  $> 17$  cc, CHS score  $> 2$ , microbleed  $> 0$ ) with the exception of admission NIHSS, where a cut point of 6 was chosen based on previously published work (18). Multivariable logistic regression modeling with stepwise selection using the variables significant in univariable analyses

**TABLE 1** | Baseline demographic, clinical, and radiographic characteristics (*N* = 253).

Variable	Minor infarct ( <i>N</i> = 141)	Major infarct ( <i>N</i> = 73)	No infarct ( <i>N</i> = 39)	<i>P</i> -value
<b>Demographics</b>				
Age (mean years, SD)	63.2 (14.2)	64.7 (13.8)	57.6 (18.2)	0.047
Male sex ( <i>N</i> , %)	59 (41.8)	40 (54.8)	16 (41.0)	0.292
Caucasian race ( <i>N</i> , %)	112 (79.4)	33 (84.6)	33 (84.6)	0.144
Education >12th grade ( <i>N</i> , %)	72 (55.4)	32 (52.5)	34 (91.9)	<0.001
Household median income (mean, SD)	55,130.3 (18,630.7)	52,002.6 (17,930.8)	74,485.0 (30,225.6)	<0.001
Employed ( <i>N</i> , %)	52 (38.8)	12 (17.1)	14 (35.9)	0.006
Baseline mRS (mean)	1.2 (1.20)	2.3 (1.7)	0.8 (1.1)	<0.001
Lives alone ( <i>N</i> , %)	23 (16.4)	16 (21.9)	12 (30.8)	0.131
Time to follow-up (mean months, SD)	1.3 (4.9)	1.2 (2.4)	–	0.997
<b>Comorbidities</b>				
Diabetes ( <i>N</i> , %)	59 (41.8)	25 (34.3)	6 (15.4)	0.009
Hypertension ( <i>N</i> , %)	109 (77.3)	59 (80.8)	19 (48.7)	<0.001
Hyperlipidemia ( <i>N</i> , %)	112 (79.4)	52 (71.2)	22 (56.4)	0.014
Active smoker ( <i>N</i> , %)	51 (36.2)	35 (48.0)	13 (33.3)	0.178
Prior stroke ( <i>N</i> , %)	53 (37.9)	33 (45.2)	8 (20.5)	0.036
Prior dementia ( <i>N</i> , %)	6 (4.3)	7 (9.6)	2 (5.1)	0.286
Current use of anti-depressant ( <i>N</i> , %)	45 (31.9)	34 (46.6)	19 (48.7)	0.043
Charlson Comorbidity Index, mean (SD)	3.4 (2.6)	4.2 (2.6)	1.8 (2.5)	<0.001
<b>Clinical metrics</b>				
Admission NIHSS (mean, SD)	1.8 (1.3)	9.2 (4.8)	–	<0.001
Follow-up NIHSS (mean, SD)	1.3 (2.3)	2.7 (3.5)	–	<0.001
Follow-up mRS (mean, SD)	1.5 (1.3)	2.2 (1.4)	–	<0.001
Length of stay in days (mean, SD)	4.0 (4.3)	7.6 (6.9)	–	<0.001
<b>Radiographic characteristics</b>				
Stroke volume (mean cc, SD)	9.8 (21.1)	31.7 (54.6)	–	<0.001
Laterality, left ( <i>N</i> , %)	63 (48.8)	30 (42.3)	–	0.372
Cortical infarct ( <i>N</i> , %)	72 (51.4)	52 (71.2)	–	0.005
CHS score (mean, SD)	3.0 (1.8)	3.3 (2.0)	2.7 (1.8)	0.379
Microbleeds present ( <i>N</i> , %)	21 (23.9)	16 (36.4)	2 (12.5)	0.127

mRS, modified Rankin score; NIHSS, National Institutes of Health Stroke Severity; CMB, cerebral microbleed; CHS, Cardiovascular Health Study.

yielded 2 separate models predicting MoCA < 26 and MoCA < 19 (Table 4). Employment prior to stroke (OR 0.28; 95% C.I. 0.12–0.69), admission NIHSS > 6 (OR 4.48; 95% C.I. 1.15–17.47), and left-sided location of infarct (OR 2.85; 95% C.I. 1.17–6.95) were significant and independent predictors of MoCA < 26 with a model c-statistic of 0.75. MoCA < 19 was predicted by admission NIHSS > 6 (OR 7.00; 95% C.I. 2.53–19.40) and ischemic stroke volume > 17 cc (OR 3.60; 95% C.I. 1.24–10.47) with a model c-statistic of 0.75.

## DISCUSSION

This study characterizes impairment across multiple cognitive domains during the early phase of post-stroke recovery. In addition, it proves the logical assumption that cognitive status at follow-up is a significant, independent predictor for functional status at this timepoint. Finally, it identifies risk factors available during hospitalization that predict downstream cognitive dysfunction during the early phase of stroke recovery.

In our study, both the average and domain-specific MoCA scores were significantly lower in ischemic stroke patients vs. non-stroke controls. This finding suggests that the presence of any infarct is associated with at least some degree of early cognitive dysfunction. Nearly two-thirds of ischemic stroke patients with no prior history of cognitive impairment scored below normal on the MoCA (<26). While it is possible that some may have had subclinical dysfunction at baseline, this number is much higher than would have been expected, especially when considering that the average age of the cohort was <65 years. These results are particularly important given the significant relationship between MoCA scores and functional status at the post-stroke clinic visit, even after adjusting for multiple factors including NIHSS scale, emphasizing the impact of cognitive impairment on one's ability to remain independent after stroke. Though early, at 1–2 months post-infarct many patients and families are making decisions that impact the rest of their lives such as living alone or returning to work. Being able to identify those at risk to experience early cognitive dysfunction will allow for targeted rehabilitation focused on cognitive improvement and

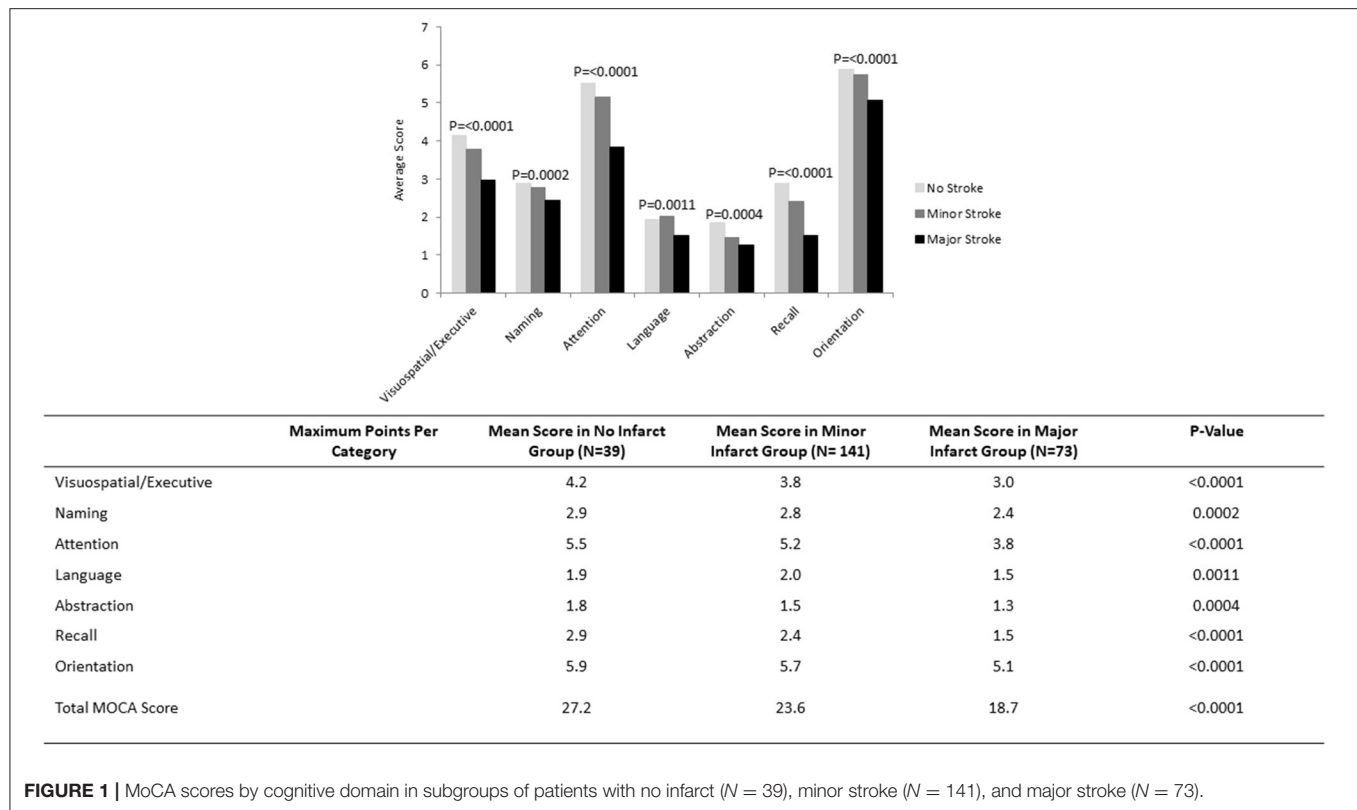


**FIGURE 1 |** MoCA scores by cognitive domain in subgroups of patients with no infarct ( $N = 39$ ), minor stroke ( $N = 141$ ), and major stroke ( $N = 73$ ).

allow for counseling regarding potential cognitive issues that may or may not resolve over time.

Additional variables improved our ability to predict the degree of cognitive dysfunction post-stroke. The likelihood of any cognitive impairment was predicted by employment status prior to stroke. This is probably a reflection of the individual's premorbid baseline. NIHSS scale at ischemic stroke presentation, infarct volume, and laterality of stroke were also important predictors, likely due to their measure of stroke severity.

Early post-stroke cognitive decline has been reported in the literature with varying trajectories for recovery (19). One prior study suggested rates of cognitive impairment during the initial months of stroke recovery can be as high as 57–67% (20). While this study did not specifically exclude those with pre-stroke cognitive impairment, a study evaluating patients without cognitive impairment prior to stroke found the prevalence of cognitive impairment remained high at 66.4% 2 months post-infarct (21). Collectively, these studies support our findings that early post-stroke cognitive dysfunction is common (22), illustrating the need for better characterization and prediction. Given that recovery from early dysfunction can be variable, chronic post-stroke dementia is typically not diagnosed until more than 6 months after infarct. However, as life-altering decisions are commonly made well before the 6-month time point, we argue it is important to identify early on those at highest risk.

Early cognitive dysfunction post-stroke is particularly important to identify given its association with overall functional

status. Classically, the mRS is considered a predominantly motor measure of function, with significant weight placed on ability to ambulate and perform physical activities of daily living. However, we have shown that cognitive status, in conjunction with NIHSS, persisted as an independent and significant predictor of functionality. Prior studies by Saver and Dong evaluated the relationship between the follow-up NIHSS and follow-up mRS as well as baseline MoCA with follow-up mRS, but not the follow-up MoCA with follow-up mRS (23, 24). The relationship between MoCA and mRS may be partly explained by the degree of cognitive function required to successfully care for oneself. Our findings also highlight the inability of the NIHSS to fully capture the range and degree of disability stroke patients suffer in the outpatient setting and suggest that the MoCA should be an important part of the follow-up clinical assessment.

The degree of morbidity attributable to cognitive impairment after a stroke in the follow-up setting provides a compelling justification for early stratification of risk for cognitive impairment after stroke. It is important to identify patients who may benefit from counseling about recovery prognosis as well as more in-depth early cognitive assessment and potential intervention. Patients and families may benefit from cognitive prognostication at the outset to prepare for how cognitive impairment may affect the ability to perform independently activities of daily living and impact the maintenance of overall health due to difficulty with medication and healthy lifestyle adherence. Although the evidence is currently limited, potential rehabilitation strategies that have therapeutic value



**TABLE 2 |** Unadjusted and adjusted associations between variables and modified Rankin Scale score at follow-up.

Variable	Unadjusted Odds Ratio (95% CI)	P-value	Adjusted Odds Ratio* (95% CI)	P-value
Follow-up MoCA	0.83 (0.80–0.87)	<0.001	0.69 (0.59–0.82)	<0.001
Follow-up NIHSS	1.29 (1.18–1.41)	<0.001	1.93 (1.40–2.67)	<0.001
Age	1.03 (1.01–1.04)	<0.001	0.95 (0.90–0.99)	0.033
Sex	1.12 (0.72–1.75)	0.623	0.37 (0.10–1.35)	0.133
Education	0.51 (0.31–0.82)	0.006	0.29 (0.09–0.97)	0.045
White race	1.13 (0.66–1.93)	0.660	9.33 (2.05–42.41)	0.004
Median household income < \$50,000	2.23 (1.40–3.56)	<0.001	0.85 (0.27–2.68)	0.780
Employment	0.29 (0.17–0.48)	<0.001	0.18 (0.05–0.71)	0.015
Lives alone	0.58 (0.33–1.03)	0.061	3.28 (0.67–16.08)	0.143
Hypertension	5.13 (2.94–8.96)	<0.001	8.04 (1.03–63.04)	0.047
Hyperlipidemia	1.74 (1.04–2.90)	0.035	0.38 (0.05–2.63)	0.324
Diabetes	1.31 (0.82–2.09)	0.255	1.14 (0.37–3.49)	0.817
Smoking	1.68 (1.06–2.66)	0.027	0.64 (0.21–1.99)	0.440
Prior stroke	2.35 (1.47–3.76)	<0.001	1.35 (0.47–3.89)	0.584
Prior dementia	2.75 (1.09–6.97)	0.033	1.05 (0.07–16.31)	0.972
Anti-depressant use	1.31 (0.83–2.08)	0.242	1.25 (0.41–3.79)	0.695
Charlson Comorbidity Index	1.18 (1.03–1.35)	0.015	1.09 (0.84–1.41)	0.539
Baseline mRS	2.19 (1.81–2.65)	<0.001	2.02 (1.25–3.26)	0.004
Infarct volume	1.01 (1.00–1.02)	0.002	1.04 (1.01–1.07)	0.014
Laterality, left	1.38 (0.86–2.21)	0.180	0.91 (0.34–2.48)	0.854
Cortical	0.91 (0.56–1.48)	0.712	0.11 (0.03–0.39)	<0.001
CHS score	1.18 (1.03–1.35)	0.015	0.83 (0.60–1.15)	0.261
CMB count	1.25 (1.08–1.45)	0.003	1.37 (1.10–1.70)	0.004

CI, confidence interval; MoCA, Montreal Cognitive Assessment; NIHSS, National Institutes of Health Stroke Severity; mRS, modified Rankin score; CHS, Cardiovascular Health Study; CMB, cerebral microbleed.

\*Adjusted for factors significant in univariable analysis ( $p < 0.05$ ): age, sex, race, education, household income, employment status prior to stroke, marital status, living alone, medical comorbidities, Charlson Comorbidity Index, follow-up NIHSS, baseline mRS, stroke volume, laterality of stroke, cortical location of stroke, CHS score, and CMB count.

include: kinematic analysis, memory enhancing tools, and even pharmacologic therapies.

Our study identified demographic, clinical, and radiographic characteristics associated with lower MoCA scores among those with no known pre-stroke cognitive impairment. The mechanism underlying cognitive impairment in stroke patients is yet to be fully elucidated. It has been hypothesized that a stroke may alter neuronal connectivity to the cortex, leading secondarily to cortical thinning and atrophy via myelin loss or axonal damage (25). In our study, we note that the radiographic size of the infarct was a significant predictor of MoCA < 19 but not MoCA < 26. This suggests a threshold capacity of the neuronal reserve that is able to compensate for injured cortex. It also suggests that mild cognitive impairment after stroke may occur regardless of final infarct volume (26), possibly due in part to other factors impacting cognitive reserve. As an example, severe small vessel disease has been identified as a predictor of post-stroke cognitive impairment in the literature and was significant in our univariable analyses, though not after controlling for infarct. Some studies suggest that patients with white matter disease are subject to neurodegeneration due to inflammation of the small blood vessels, and blood-brain barrier breakdown, resulting in the permeation of cytokines into perivascular space and neuronal tissue (27). Additional infarcts may cause further

white matter tract injury; however, the effect of leukoaraiosis can be dampened when adjusting for infarct or other variables related to baseline brain function. Accordingly, the CHANGE score (28) included age, education, and presence of chronic lacunar infarct as significant predictors of MOCA < 22 at 3–6 months after ischemic stroke. While age and education were not significant in our study, it is possible that in our population it was employment status that served a similar role to represent an individual's "pre-stroke baseline."

Interestingly, there were several factors that have been shown to be important predictors of post-stroke dementia that were not associated with early post-stroke cognitive decline. Depression was not a driving factor of impairment in our study, though has been reported to be an important predictor of post-stroke cognitive dysfunction (3). One possible explanation is that nearly half of our cohort was taking an antidepressant at the time of assessment. Additionally, vascular risk factors such as hypertension and diabetes have been found to significantly increase the risk of cognitive impairment after stroke in the long-term, but these were only statistically significant in our analysis in univariable analysis (29). This may illustrate their importance in brain function and long-term recovery, but the relatively greater importance of the presence of the infarct in the *early* disruption of cognition following stroke.

**TABLE 3 |** Univariable logistic regression analyses of the odds of at least mild cognitive impairment (MoCA < 26) and the odds of severe cognitive impairment (MoCA < 19) associated with each covariate in patients after ischemic stroke with no prior diagnosis of cognitive impairment ( $N = 201$ ).

Variable	Unadjusted odds ratio of any cognitive impairment ( $N = 132$ )	95% CI	P-value	Unadjusted odds ratio of severe cognitive impairment ( $N = 41$ )	95% CI	P-value
Age	1.04	1.01, 1.06	0.002	1.05	1.02, 1.08	<0.001
Sex	1.05	0.59, 1.89	0.862	1.16	0.59, 2.31	0.665
Caucasian race	0.58	0.28, 1.21	0.150	0.58	0.27, 1.24	0.161
Education	0.51	0.28, 0.98	0.043	0.77	0.36, 1.63	0.491
Median household income <\$50,000	1.26	0.68, 2.33	0.459	3.50	1.39, 8.81	0.008
Employment	0.51	0.27, 0.95	0.033	0.48	0.21, 1.12	0.091
Marital status	1.73	0.60, 5.02	0.313	0.67	0.20, 2.24	0.520
Living alone	0.67	0.32, 1.40	0.285	0.74	0.28, 1.91	0.531
Diabetes	1.04	0.58, 1.89	0.889	0.65	0.31, 1.34	0.238
Hypertension	1.93	0.97, 3.85	0.060	2.98	1.00, 8.89	0.050
Hyperlipidemia	0.91	0.45, 1.82	0.780	0.56	0.26, 1.20	0.135
Smoking	1.78	0.97, 3.28	0.065	1.93	0.97, 3.86	0.063
Prior stroke	2.21	1.20, 4.09	0.011	1.26	0.63, 2.52	0.518
Anti-depressant use	1.54	0.82, 2.89	0.176	1.22	0.60, 2.48	0.579
Charlson Comorbidity Index	1.25	1.09, 1.43	0.002	1.19	1.06, 1.35	0.004
Admission NIHSS	1.16	1.05, 1.27	0.003	1.18	1.09, 1.27	<0.001
Baseline mRS	1.54	1.20, 1.97	<0.001	1.66	1.26, 2.18	<0.001
Stroke volume	1.02	1.00, 1.03	0.028	1.01	1.00, 1.02	0.034
Laterality, left	2.08	1.12, 3.86	0.021	2.54	1.23, 5.24	0.012
Cortical	1.62	0.90, 2.91	0.110	2.84	1.30, 6.18	0.009
CHS score	1.42	1.15, 1.76	0.001	1.31	1.08, 1.58	0.006
CMB count	4.02	1.34, 12.03	0.013	1.12	0.97, 1.30	0.138

CI, confidence interval; NIHSS, National Institutes of Health Stroke Severity; mRS, modified Rankin score; CMB, cerebral microbleed; CHS, Cardiovascular Health Study.

This study is not without limitations. Our cohort was comprised of patients from a single Comprehensive Stroke Center where participants were predominantly Caucasian. In addition, the MoCA test is considered a brief screening tool for cognitive function and may not be the most sensitive metric to detect dysfunction. However, when compared with neuropsychological batteries in patients with strokes due to small vessel disease, there has been a high degree of accuracy in detecting cognitive impairment (28). In addition, the relative brevity may make it an ideal choice for a busy office setting. It is also important to note that given eligibility was predicated on being able to complete the MoCA, there is a possibility of selection bias. While patients with global aphasia were excluded, those with anterior or posterior aphasias may have language impairments that may confound their ability to perform well on the MoCA. Nevertheless, given the prevalence of aphasia as a presenting stroke symptom, including the performance of patients with incomplete aphasias adds to the generalizability of this study. Finally, we included patients with no history of pre-stroke cognitive impairment. These patients did not have formal neuropsychologic testing prior to the occurrence of ischemic stroke and may have had subclinical cognitive impairment, though this is less likely to have significantly biased results given the relatively young age of our cohort.

Despite these limitations, this study provides evidence that there are in-hospital metrics, readily available for all

**TABLE 4 |** Multivariable logistic regression models predicting MoCA < 26 (left) and MoCA < 19 (right) in patients after ischemic stroke without a diagnosis of cognitive impairment prior to the time of ischemic stroke presentation ( $N = 201$ ).

Predictors	MoCA < 26 ( $N = 132$ )		MoCA < 19 ( $N = 41$ )	
	Odds Ratio (95% CI)	P-value	Odds Ratio (95% CI)	P-value
Employment prior to stroke	0.28 (0.12, 0.69)	0.005	–	–
Admission NIHSS scale > 6	4.48 (1.15, 17.47)	0.031	7.00 (2.53, 19.4)	<0.001
Stroke volume > 17 cc	–	–	3.60 (1.24, 10.47)	0.019
Laterality of stroke (left)	2.85 (1.17, 6.95)	0.021	–	–

CI, confidence interval; NIHSS, National Institutes of Health Stroke Severity score. The c-statistic for predicting both MoCA < 26 and < 19 was 0.75.

patients, that can be used to predict cognitive impairment during the early phase of stroke recovery, and that this is important due to the strong association between cognition and overall function. Vulnerable patients may be identified at the time of discharge and provided with the necessary resources such as aggressive rehabilitation to potentially improve longer-term outcomes. Future studies are necessary

to validate our model in a larger, independent cohort of patients, and to determine whether early identification and aggressive treatment of at-risk individuals will reduce the rate of post-stroke dementia and improve longer-term post-stroke outcomes.

## CONCLUSION

Cognitive impairment, ranging from mild to severe, is common in the early months after ischemic stroke, and along with NIHSS contributes significantly to a patient's functional status at follow-up. Employment status prior to stroke, NIHSS at stroke presentation, infarct volume, and stroke laterality are strong predictors of dysfunction and may allow us to better identify and target at risk-individuals in the acute setting for aggressive rehabilitation.

## DATA AVAILABILITY STATEMENT

The raw data supporting the conclusions of this article will be made available by the authors, without undue reservation.

## REFERENCES

1. Principe M, Ferretti C, Casini AR, Santini M, Giubilei F, Culasso F. Stroke, disability, and dementia: results of a population survey. *Stroke*. (1997) 28:531–6. doi: 10.1161/01.STR.28.3.531
2. Nys GM, van Zandvoort MJ, de Kort PL, Jansen BP, de Haan EH, Kappelle LJ. Cognitive disorders in acute stroke: prevalence and clinical determinants. *Cerebrovasc Dis*. (2007) 23:408–16. doi: 10.1159/000101464
3. Jaillard A, Naegele B, Trabucco-Miguel S, LeBas JF, Hommel M. Hidden dysfunctioning in subacute stroke. *Stroke*. (2009) 40:2473–9. doi: 10.1161/STROKEAHA.108.541144
4. MacKenzie G, Gould L, Ireland S, LeBlanc K, Sahlas D. Detecting cognitive impairment in clients with mild stroke or transient ischemic attack attending a stroke prevention clinic. *Can J Neurosci Nurs*. (2011) 33:47–50.
5. Jokinen H, Melkas S, Ylikoski R, Pohjasvaara T, Kaste M, Erkinjuntti T, et al. Post-stroke cognitive impairment is common even after successful clinical recovery. *Eur J Neurol*. (2015) 22:1288–94. doi: 10.1111/ene.12743
6. Lim KB, Kim J, Lee HJ, Yoo J, You EC, Kang J. Correlation between montreal cognitive assessment and functional outcome in subacute stroke patients with cognitive dysfunction. *Ann Rehabil Med*. (2018) 42:26–34. doi: 10.5535/arm.2018.42.1.26
7. Salvadori E, Pasi M, Poggesi A, Chiti G, Inzitari D, Pantoni L. Predictive value of MoCA in the acute phase of stroke on the diagnosis of mid-term cognitive impairment. *J Neurol*. (2013) 260:2220–7. doi: 10.1007/s00415-013-6962-7
8. Chen X, Duan L, Han Y, Tian L, Dai Q, Wang S, et al. Predictors for vascular cognitive impairment in stroke patients. *BMC Neurol*. (2016) 16:115. doi: 10.1186/s12883-016-0638-8
9. Horstmann S, Rizos T, Rauch G, Arden C, Veltkamp R. Feasibility of the montreal cognitive assessment in acute stroke patients. *Eur J Neurol*. (2014) 21:1387–93. doi: 10.1111/ene.12505
10. Dong Y, Venketasubramanian N, Chan BP, Sharma VK, Slavin MJ, Collinson SL, et al. Brief screening tests during acute admission in patients with mild stroke are predictive of vascular cognitive impairment 3–6 months after stroke. *J Neurol Neurosurg Psychiatry*. (2012) 83:580–5. doi: 10.1136/jnnp-2011-302070
11. Nasreddine ZS, Phillips NA, Bédirian V, Charbonneau S, Whitehead V, Collin I, et al. The montreal cognitive assessment, MoCA: a brief screening tool for mild cognitive impairment. *J Am Geriatr Soc*. (2005) 53:695–9. doi: 10.1111/j.1532-5415.2005.53221.x

## ETHICS STATEMENT

The studies involving human participants were reviewed and approved by Johns Hopkins Hospital Institutional Review Board. Given the observational nature of the study, informed consent was not required.

## AUTHOR CONTRIBUTIONS

RS performed study design, data collection, data analysis, and manuscript writing. EM performed study design and manuscript writing. RL performed significant manuscript editing. DM performed data collection and manuscript editing. All authors contributed to the article and approved the submitted version.

## FUNDING

RS reports the following award disclosure: research support, NIH grant U10 NS086729. EM reports the following award disclosure: research support, AHA Innovative Project Grant 18IPA34170313.

12. Trzepacz PT, Hochstetler H, Wang S, Walker B, Saykin AJ, Alzheimer's Disease Neuroimaging Initiative. Relationship between the montreal cognitive assessment and mini-mental state examination for assessment of mild cognitive impairment in older adults. *BMC Geriatr*. (2015) 15:107. doi: 10.1186/s12877-015-0103-3
13. Charlson ME, Pompei P, Ales KL, MacKenzie CR. A new method of classifying prognostic comorbidity in longitudinal studies: development and validation. *J Chronic Dis*. (1987) 40:373–83. doi: 10.1016/0021-9681(87)90171-8
14. Broderick JP, Brott TG, Duldner JE, Tomsick T, Huster G. Volume of intracerebral hemorrhage. A powerful and easy-to-use predictor of 30-day mortality. *Stroke*. (1993) 24:987–93. doi: 10.1161/01.STR.24.7.987
15. Manolio TA, Kronmal RA, Burke GL, Poirier V, O'Leary DH, Gardin JM, et al. Magnetic resonance abnormalities and cardiovascular disease in older adults. The Cardiovascular Health Study. *Stroke*. (1994) 25:318–27. doi: 10.1161/01.STR.25.2.318
16. Yue NC, Arnold AM, Longstreth Jr. WT, Elster AD, Jungreis CA, O'Leary DH, et al. Sulcal, ventricular, and white matter changes at MR imaging in the aging brain: data from the cardiovascular health study. *Radiology*. (1997) 202:33–9. doi: 10.1148/radiology.202.1.8988189
17. Sudre CH, Anson BG, Davagnanam I, Schmitt A, Mendelson AF, Prados F, et al. Bullseye's representation of cerebral white matter hyperintensities. *J Neuroradiol*. (2018) 45:114–22. doi: 10.1016/j.neurad.2017.10.001
18. Adams HP, Davis PH, Leira EC, Chang KC, Bendixen BH, Clarke WR, et al. Baseline NIH Stroke Scale score strongly predicts outcome after stroke: a report of the Trial of Org 10172 in Acute Stroke Treatment (TOAST). *Neurology*. (1999) 53:126–31. doi: 10.1212/WNL.53.1.126
19. Mijajlović MD, Pavlović A, Brainin M, Heiss WD, Quinn TJ, Ihle-Hansen HB, et al. Post-stroke dementia - a comprehensive review. *BMC Med*. (2017) 15:11. doi: 10.1186/s12916-017-0779-7
20. Mellon L, Brewer L, Hall P, Horgan F, Williams D, Hickey A, et al. Cognitive impairment six months after ischaemic stroke: a profile from the ASPIRE-S study. *BMC Neurol*. (2015) 15:31. doi: 10.1186/s12883-015-0288-2
21. Nijse B, Visser-Meily JM, van Mierlo ML, Post MW, de Kort PL, van Heugten MC. Temporal evolution of poststroke cognitive impairment using the montreal cognitive assessment. *Stroke*. (2017) 48:98–104. doi: 10.1161/STROKEAHA.116.014168
22. Chaurasia RN, Sharma J, Pathak A, Mishra VN, Joshi D. Poststroke cognitive decline: a longitudinal study from a tertiary care center. *J Neurosci Rural Pract*. (2019) 10:459–64. doi: 10.1055/s-0039-1697872

23. Saver JL, Altman H. Relationship between neurologic deficit severity and final functional outcome shifts and strengthens during first hours after onset. *Stroke*. (2012) 43:1537–41. doi: 10.1161/STROKEAHA.111.636928
24. Dong Y, Slavin MJ, Chan BP, Venketasubramanian N, Sharma VK, Crawford JD, et al. Cognitive screening improves the predictive value of stroke severity scores for functional outcome 3–6 months after mild stroke and transient ischaemic attack: an observational study. *BMJ Open*. (2013) 3:e003105. doi: 10.1136/bmjopen-2013-003105
25. Duering M, Righart R, Csanadi E, Jouvent E, Hervé D, Chabriat H, et al. Incident subcortical infarcts induce focal thinning in connected cortical regions. *Neurology*. (2012) 79:2025–8. doi: 10.1212/WNL.0b013e3182749f39
26. Sachdev PS, Brodaty H, Valenzuela MJ, Lorentz L, Looi JC, Berman K, et al. Clinical determinants of dementia and mild cognitive impairment following ischaemic stroke: the Sydney Stroke Study. *Dement Geriatr Cogn Disord*. (2006) 21:275–83. doi: 10.1159/000091434
27. Te M, Zhao E, Zheng X, Sun Q, Qu C. Leukoaraiosis with mild cognitive impairment. *Neurol Res*. (2015) 37:410–4. doi: 10.1179/1743132815Y.0000000028
28. Chander RJ, Lam BY, Lin X, Ng AY, Wong AP, Mok VC, et al. Development and validation of a risk score (CHANGE) for cognitive impairment after ischemic stroke. *Sci Rep*. (2017) 7:12441. doi: 10.1038/s41598-017-12755-z
29. Béjot Y, Aboa-Eboulé C, Durier J, Rouaud O, Jacquin A, Ponavoy E, et al. Prevalence of early dementia after first-ever stroke: a 24-year population-based study. *Stroke*. (2011) 42:607–12. doi: 10.1161/STROKEAHA.110.595553

**Conflict of Interest:** The authors declare that the research was conducted in the absence of any commercial or financial relationships that could be construed as a potential conflict of interest.

Copyright © 2020 Sharma, Mallick, Llinas and Marsh. This is an open-access article distributed under the terms of the Creative Commons Attribution License (CC BY). The use, distribution or reproduction in other forums is permitted, provided the original author(s) and the copyright owner(s) are credited and that the original publication in this journal is cited, in accordance with accepted academic practice. No use, distribution or reproduction is permitted which does not comply with these terms.





# Cerebral Vessels: An Overview of Anatomy, Physiology, and Role in the Drainage of Fluids and Solutes

Nivedita Agarwal<sup>1,2,3\*</sup> and Roxana Octavia Carare<sup>3</sup>

<sup>1</sup> Hospital S. Maria del Carmine, Azienda Provinciale per i Servizi Sanitari, Rovereto, Italy, <sup>2</sup> Laboratory of Functional Neuroimaging, Center for Mind/Brain Sciences, University of Trento, Trento, Italy, <sup>3</sup> Faculty of Medicine, University of Southampton, Southampton, United Kingdom

## OPEN ACCESS

### Edited by:

Yulin Ge,  
New York University, United States

### Reviewed by:

Mariel Kozberg,  
Massachusetts General Hospital and  
Harvard Medical School,  
United States

Maxime Gauberti,  
INSERM U1237 Physiopathologie et  
imagerie des troubles Neurologiques  
(PhIND), France

### \*Correspondence:

Nivedita Agarwal  
nivedita.agarwal@apss.tn.it

### Specialty section:

This article was submitted to  
Stroke,  
a section of the journal  
Frontiers in Neurology

**Received:** 29 September 2020

**Accepted:** 30 November 2020

**Published:** 13 January 2021

### Citation:

Agarwal N and Carare RO (2021)  
Cerebral Vessels: An Overview of  
Anatomy, Physiology, and Role in the  
Drainage of Fluids and Solutes.  
Front. Neurol. 11:611485.  
doi: 10.3389/fneur.2020.611485

The cerebral vasculature is made up of highly specialized structures that assure constant brain perfusion necessary to meet the very high demand for oxygen and glucose by neurons and glial cells. A dense, redundant network of arteries is spread over the entire pial surface from which penetrating arteries dive into the cortex to reach the neurovascular units. Besides providing blood to the brain parenchyma, cerebral arteries are key in the drainage of interstitial fluid (ISF) and solutes such as amyloid-beta. This occurs along the basement membranes surrounding vascular smooth muscle cells, toward leptomeningeal arteries and deep cervical lymph nodes. The dense microvasculature is made up of fine capillaries. Capillary walls contain pericytes that have contractile properties and are lined by a highly specialized blood-brain barrier that regulates the entry of solutes and ions and maintains the integrity of the composition of ISF. They are also important for the production of ISF. Capillaries drain into venules that course centrifugally toward the cortex to reach cortical veins and empty into dural venous sinuses. The walls of the venous sinuses are also home to meningeal lymphatic vessels that support the drainage of cerebrospinal fluid, although such pathways are still poorly understood. Damage to macro- and microvasculature will compromise cerebral perfusion, hamper the highly synchronized movement of neurofluids, and affect the drainage of waste products leading to neuronal and glial degeneration. This review will present vascular anatomy, their role in fluid dynamics, and a summary of how their dysfunction can lead to neurodegeneration.

**Keywords:** cerebral vessel, glymphatic, intramural periarterial drainage, small vessel disease, neurodegeneration, perivascular space

## INTRODUCTION

Damage to cerebral vasculature and reduction in cerebral perfusion initiate a cascade of events that rapidly leads to disturbed cellular homeostasis and death of neurons and glial cells (1). The cerebral arterial network of vessels is unique in its anatomy, and its flow dynamics is inextricably intertwined with those of other fluids such as venous blood, cerebrospinal fluid (CSF), and the interstitial fluid (ISF) (2, 3). Emerging evidence regarding the role of cerebral vasculature in the drainage of solutes and fluids adds to the complexity of the overall interaction with neurofluids.

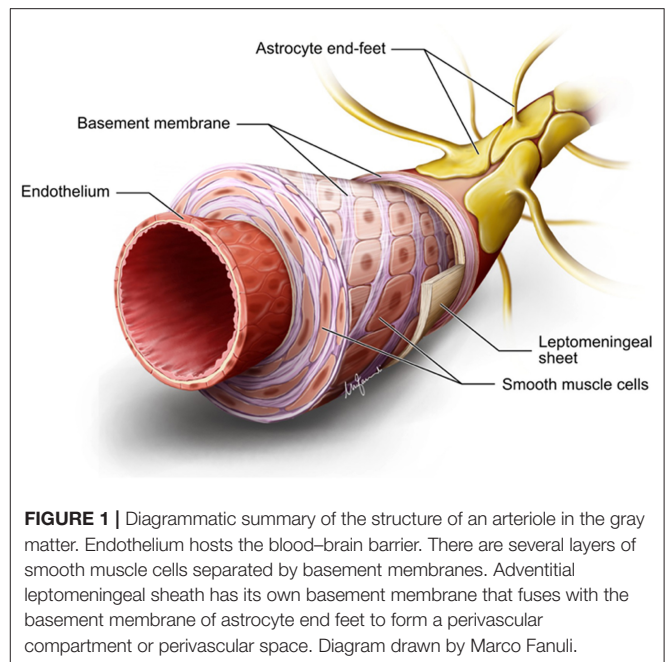
The arteries of the brain have a dual function: to supply oxygenated blood to neurons and glia and to drain ISF. Neurons and glial cells are constantly “at work,” even during rest, and this very

high demand for oxygen and glucose requires a steady supply of oxygenated blood. Histological and tracer studies reveal the intricate relationship of cortical arteries with meningeal sheaths and the constitution of the perivascular compartment and spaces that provide a pathway for inflow and outflow of ISF (4–6). Cerebral capillaries are considered important sites of CSF and ISF production and absorption. Capillaries drain into venules that are hierarchically organized and run centrifugally toward the cortex. All venous drainage occurs through dural venous sinuses that drain toward the neck veins. The walls of dural venous sinuses are also home to meningeal lymphatic vessels (7, 8), with a role in the drainage of CSF. In this review, a brief overview of the current evidence for the anatomy and function of vessels in the brain will be provided, followed by a summary of mechanisms of interaction of what we term “neurofluids”: blood, CSF, and ISF (2). A disruption of such mechanisms will trigger a series of pathological events such as microvascular injury, failure of ISF drainage, local deposition of amyloid-beta as cerebral amyloid angiopathy (CAA), focal ischemia, and demyelination.

## Arterial and Capillary Systems

The brain parenchyma is supplied by two internal carotid arteries (ICAs) and two vertebral arteries. The ICA enters the skull-base through the carotid canal, located in the petrous portion of the temporal lobe. It pierces through the dura mater at the level of the cavernous sinus and bifurcates within the subarachnoid space (SAS) into middle cerebral arteries and anterior cerebral arteries. The ICA carries ~80% of the total blood to the brain. The vertebral arteries enter the vertebral foramina at the level of C6; they exit out of C1 foramina, loop around the posterior arch of the atlas as they enter the foramen magna, and lies on the ventral surface of the brain stem to form the basilar artery (BA). The BA terminates into two posterior cerebral arteries. The anterior (ICA and its branches) and the posterior circulation (vertebral arteries and its branches) arteries come together at the base of the skull to form the circle of Willis that lies in the cisternal space (9).

A rich, anastomotic network of leptomeningeal arteries spreads over the pial surface from which numerous branches (arterioles) sprout out and pierce the glia limitans to dive into the cortex at approximately right angles to it. From a structural point of view, both pial arteries and penetrating arterioles lack an external elastic lamina, but leptomeningeal arteries retain an internal elastic lamina (10). The gray matter (GM) has a larger number of arterioles with respect to those in the white matter (WM) with a ratio of 8:1, which is proportionate to the elevated energy demand of the more cellular GM (11, 12). Penetrating arterioles are completely encased by a sheet of pia mater, which reflects off the cortical surface, separating them from the surrounding SAS and the brain parenchyma (4) (Figure 1). However, around the perivascular compartment of the arterioles in the WM, there are two such sheaths, creating a potential space for the accumulation of edematous fluid (13). At the capillary level, direct observations under the electron microscope in a variety of species reveal that the basement membrane of the pial sheath and the basement membranes of the astrocytes (glia limitans) fuse together to create a perivascular



compartment, or periarterial space, filled with an extracellular matrix (ECM), which is not continuous with the SAS (4, 14) and referred to as the “perivascular space” (PVS) (Figure 1). Indeed, PVSs, or more appropriately the periarterial spaces, are not visible within the cortical GM even under pathological conditions, whereas they are seen in the WM both in histological specimens and on neuroimaging (13, 15). Changes in the walls of capillaries and arterioles associated with aging, hypertension, or diabetes mellitus lead to small vessel disease (SVD) and vascular dementia (16, 17).

Pial surface arterial networks are richly innervated by sympathetic nerves from the superior cervical ganglion, sphenopalatine, otic, and trigeminal ganglia that release several neurotransmitters and neuromodulators such as a vasoactive intestinal peptide, nitric oxide synthase, acetylcholine, norepinephrine, and substance P (18). This innervation, also termed “extrinsic” innervation, ends in the precapillary segment and, more precisely, where the PVS terminates. The extrinsic innervation is primarily responsible for a prompt myogenic response to temporary pressure differences. According to Poiseuille’s law, a change in radius directly affects resistance to flow to the fourth power, thereby modulating blood flow instantly and efficaciously (19). Intraparenchymal arterioles are innervated by nerves arising from the nuclei of basal forebrain such as the locus coeruleus, nucleus basalis of Meynert, and raphe nuclei in the brain stem that release norepinephrine, acetylcholine, and 5-hydroxytryptamine as well as other neuropeptides either directly to the walls of capillaries or indirectly via local interneurons and astrocytes (18, 20). Such nerve endings are likely to control the intrinsic spontaneous contractile activity of vascular smooth muscle cells (VSMCs) in the tunica media, also termed “vasomotion.” Vasomotor

oscillations form the basis of ultra-slow 0.1-Hz wave activity in the microvasculature independent of neuronal activity (21, 22).

A dense capillary anastomotic network characterizes the GM and varies with its depth (23). Approximately 50–60% of total blood volume is within the capillaries (23). Capillary walls are made up of a single layer of endothelial cells, pericytes, and a basal lamina made up of collagen type IV, heparan sulfate proteoglycans, laminin, fibronectin, and other ECM proteins, in various proportions and with different isoforms depending on the type of vessel (24–26). The endothelial cells are bound together by tight junction proteins such as claudins and occludins, creating a highly regulated blood–brain barrier (BBB) that restricts transcellular flux of ions and hydrophilic solutes, shielding the internal parenchymal milieu from even the slightest fluctuations in the osmolarity of surrounding tissues and blood plasma (27, 28). The endothelium contains a spectrum of receptors essential for the entry and efflux of peptides, such as low-density lipoprotein related protein-1 or adenosine triphosphate-binding cassette transporters, which are essential for the efflux of soluble amyloid-beta from the brain parenchyma (29). The abluminal surface of the capillaries is continuous with astrocytic end feet (or glia limitans), containing aquaporin-4 (AQP-4) water channels.

## Venous System

The parenchymal microvasculature drains deoxygenated blood centrifugally from the ventricular ependymal surface toward the cortical pial surface, via medullary venules and veins arranged hierarchically and centrifugally from the ventricular ependymal wall toward the cortex (30). Large cortical bridging veins, such as the vein of Labbè and the Trolard vein, empty into the superficial dural venous sinuses (31). The superior sagittal sinus subdivides into right and left transverse sinus and continues directly via sigmoid sinuses into the internal jugular veins, extracranial neck vessels, and the intra- and extra-spinal venous plexi, conveying deoxygenated blood to the right atrium (32, 33). Deep internal veins form the inferior sagittal sinus, the vein of Galen, and the straight sinus to drain into the superior sagittal sinus posteriorly. Anterior venous drainage occurs through the cavernous sinus, sphenopetrosal sinuses, and sigmoid sinuses. Several anatomical variations exist, and veins can vary in number, size, symmetry across hemispheres, and their extracranial venous drainage patterns, adding to the complexity of the cerebral venous system. It is important to note that dural venous sinuses are valveless, making cephalad retrograde flow possible in cases of obstruction to downward flow (34).

Surrounding each parenchymal arteriole are eight venules (5). Venules typically have a larger lumen area and a thinner vessel wall with respect to arterioles (35). Exiting venules in the cortex are surrounded by an incomplete layer of pia mater (4). Paravenous spaces communicate with the SAS directly. The first reports of the presence of lymphatic vessels in the dura mater were reported in 1787, whereas histologic evidence of their existence was provided much later (36). More recently, lymphatic channels were described lining the dural venous sinuses that appear to be additional routes for the drainage of fluids and cells toward the deep cervical lymph nodes (7, 8). Lymphatic channels

are also found in the cribriform plate that drains fluids, cells, and solutes via nasal lymphatics toward the superficial cervical lymph nodes (37).

## Production and Drainage of Cerebrospinal Fluid and Interstitial Fluid

Our classic understanding of CSF fluid production and absorption is being challenged, as new evidence suggests that CSF production also occurs at other sites such as the capillary endothelial surface, as formulated by the Bulat–Klarica–Orešković hypothesis (38). Almost 80% of CSF is secreted by fenestrated capillaries in the choroid plexi at a rate of ~0.3–0.4 ml/min for a total production of 430–580 ml daily. CSF secretion across the blood–CSF barrier depends on hydrostatic and osmolarity gradients that exist between the plasma and the intraventricular CSF fluids. CSF comprises 99% water, some ions, and negligible quantities of proteins and glucose. Arachnoid granulations found in the dural venous sinuses are traditionally recognized to play a prime role in CSF reabsorption. However, the contemporary presence of the meninx *primitiva* and the lack of arachnoid granulations in the fetus suggests that there must be alternative routes for its absorption (37, 39).

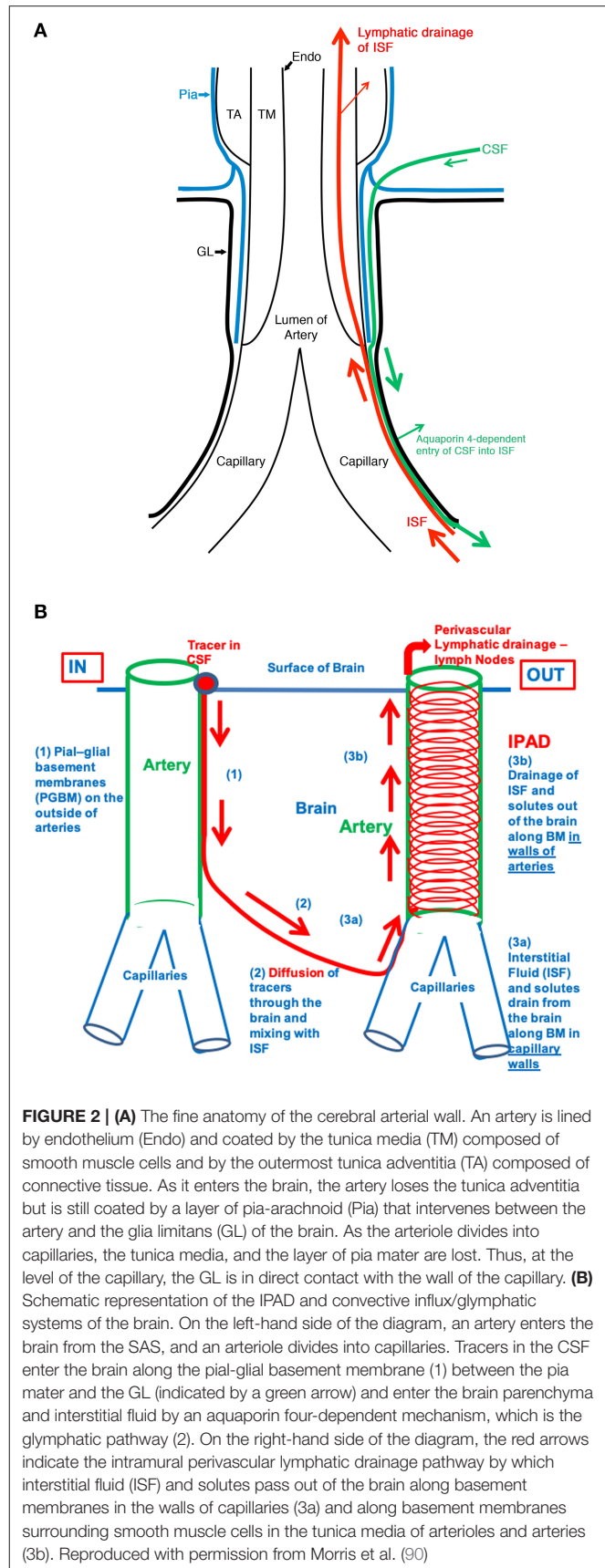
There are multiple sources of ISF production, such as filtration across the capillaries via the development of hydrostatic and osmotic pressures across the endothelium, secretion through choroid plexi, and cellular metabolism (40, 41). ISF fills the extracellular space (ECS) or interstitial space. This space contains an ECM made up of glycosaminoglycans, glycoproteins (e.g., laminins, collagen, chondroitin, fibronectin) and proteoglycans (e.g., hyaluronic acid, heparan sulfate). Such an environment determines a negatively charged ambient necessary for cellular communication, volume transmission, immunosurveillance, and a binding capacity for solutes to be transported around brain areas. ECS occupies ~15–20% of the total brain volume, and this volume can change in physiologic and pathologic conditions such as sleep, under anesthesia, and stroke (42–45). ISF is also the primary fluid medium for waste removal; however, the presence of BBB notably restricts the movement of proteins across the capillaries, which suggested that there must be alternative pathways. Bulk flow of ISF through the brain parenchyma was proposed as a route to flush out waste products and fluids toward the ventricular ependymal walls (46). In the past decade, multiple waste clearance pathways have been characterized in the brain: the glymphatic pathway, intramural periarterial drainage pathway (IPAD), flow along cranial nerves, and meningeal lymphatics along the dural venous sinuses (6, 39, 47), still extensively debated (48, 49). The glymphatic system proposes that CSF from the SAS recycles along the para-arterial spaces and enters the brain tissue via astrocytic AQP-4 water channels. CSF intermingles with ISF, which flows toward paravenous spaces via bulk flow, thus flushing out fluids and solutes from the brain (50, 51). However, diffusion rather than bulk flow may be the likely principal mechanism for flow with an unclear role for AQP-4 channels (40, 52–55). Also, the mechanism of unidirectional CSF flow along intraparenchymal para-arterial spaces remains debatable, as arterial pulsations alone do not determine such flow

(56). Furthermore, the glymphatic hypothesis does not explain why in CAA, the deposition of proteins occurs in the tunica media of arterioles and arteries, spreading to occupy the whole of the arterial wall and rarely involves veins (57–59).

On the other hand, tracer injection studies in animal brains have unequivocally demonstrated that one important route for ISF and solute removal is the IPAD. For decades, perivascular compartments have been considered to play a fundamental role in the removal of waste products (36, 60, 61). According to this mechanism, fluids and waste products flow within the basement membranes of arterioles and arteries in the opposite direction to arterial blood flow within their lumen and is primarily driven by vasomotion (62–65). The ultraslow frequency oscillation (<0.1 Hz) appears to be critical to the clearance of solutes. Electrophysiologically observed slow-wave oscillations characteristic of sleep are intricately associated with large CSF flow oscillations suggestive of vasomotion driven clearance of CSF and thereby of solutes and supportive of IPAD pathways of clearance (66).

## Neurofluid Physiology

To understand the interaction between the several space-competing compartments within the cranium, we must remind ourselves of the Monro–Kellie hypothesis, which remains a cardinal principle in the understanding of fluid movements (67). This hypothesis maintains that because the brain contents are enclosed in a non-expandable bony skull, the total brain volume must remain constant at all times to avoid a dangerous increase in ICP (68). However, with the recent discoveries of meningeal lymphatics and the understanding of mechanisms for brain waste clearance mechanisms, it has become necessary to revisit the original Monro–Kellie doctrine (69). With every systole, an increase in arterial pressure pumps ~700 ml of oxygenated blood, causing inflation of arteries, arterioles, and the microvascular bed (70). This expansion of vessels will squeeze ISF and CSF from the interstitium and promote flow. The creation of a pressure gradient between the cranial SAS and the spinal SAS will cause displacement of CSF toward the spinal SAS and facilitate venous outflow toward the extracranial neck vessels (3, 71). During diastole, as the elastic vessels relax, CSF flows back with little net forward displacement. Such pulsatile forces will also create a variable magnitude of brain tissue deformation, generating additional forces affecting blood flow, production, and absorption of ISF and CSF. The intrinsic viscoelasticity of the brain, or brain compliance, is the capacity of brain tissue to deform in conditions of intracranial pressure changes. Such mechanical and viscoelastic properties vary in different brain regions and depend on cellular morphology, capillary distribution, the compactness of white matter axons, their orientation, and ECM composition (72). These properties are different both at a macroscale (WM is stiffer than GM) and at a microscale (cortical GM is stiffer than hippocampal GM; WM in the corpus callosum is stiffer than WM in the corona radiata) (72). WM is three times stiffer than GM, accounting for differential response to compression load (73). Physiologic rheological properties of the brain can be measured *in vivo* by magnetic resonance elastography (74, 75). Thus, in





one magnetic resonance elastography study, the compression of internal jugular veins in the neck was shown to increase CSF pulsatility in the brain and increase stiffness within the brain parenchyma in accordance with the Monro–Kellie doctrine (75).

## Cerebrovascular Damage and Neurodegeneration

Our attention is drawn to the intricate coupling of arterial, venous, CSF, and brain parenchymal dynamics; damage to any one of them can initiate a cascade of events affecting clearance of waste products in the brain and lead thereby to neurodegeneration. Reduced cerebral perfusion is considered a potential link between vascular risk factors and the development of SVD, vascular dementia, and Alzheimer's disease (AD) (76). The most important risk factors are advancing age and hypertension, both of which will hamper cerebral blood flow by directly damaging arterial walls and the microvasculature. Patients with SVD and AD often present with increased arterial stiffness, altered BBB permeability, VSMC loss, multiple fenestrations in the internal elastic lamina, remodeled arterial wall basement membranes, pericyte degeneration, increased intercapillary distance, reduced capillary density, increased arteriolar tortuosity, and swelling of astrocyte end feet, ultimately reducing the capacity for an optimal exchange of substances across the capillary endothelium (77–80). The inefficient transfer of pulsatile energy from the arterial bed toward the capillaries and the venous walls will disrupt hydrostatic forces. Arterial vasomotion will also be affected in several ways: direct arterial wall damage, deposition of amyloid-beta, and loss of cholinergic innervation of VSMCs. The geometry of ECS changes with age and disease, as free water within the parenchyma increases and toxic solutes such as amyloid-beta deposit within the extracellular space (81). In this scenario, the glymphatic/convective influx as well as IPAD will be hampered.

As the density of capillaries is lower in the white matter than in the gray matter and capillary basement membranes are the entry portals for IPAD by which ISF and solutes drain from brain tissue, the shortage of capillaries in the white matter may be a factor in a reduced capacity for IPAD in the white matter (82). Obstruction of CSF drainage from the cerebral ventricles results in dilatation of the ventricular system and the accumulation of fluid in the periventricular white matter in the acute stages of hydrocephalus

with the slowly progressive destruction of white matter fibers and gliosis, suggesting that the capacity for IPAD is lower in the white matter compared with the gray matter (83).

Damage to veins, venules, and capillaries can also characterize other subtypes of SVD, such as perivenous collagenosis (84). This is characterized by concentric thickening of venular walls and pathological deposition of collagen resulting in leukoaraiosis or white matter hyperintensities on magnetic resonance imaging. Occlusion of venules and veins causes hypoperfusion and ischemia and affects the drainage of CSF via meningeal lymphatics (85).

There are several, albeit nonspecific, magnetic resonance imaging biomarkers such as dilated PVS, white matter hyperintensity, cerebral microbleeds, and superficial siderosis that characterize SVD, AD, and CAA that are an expression of impaired clearance of proteins and fluids, focal ischemia, and deposition of amyloid-beta within the walls of capillaries and neurodegeneration (82, 86–89). Neural tissue can become stiffer via several processes such as Wallerian degeneration, axonal atrophy, loss of oligodendroglial cells, microglial activation, neuroinflammation, and microvascular damage, resulting in a range of microstructural changes from increased tissue water content to progressive gliosis and loss of volume.

There is substantial evidence that fluid movements in the brain are related such that damage to one compartment can lead to several events leading to neuroglial vascular compromise (Figure 2). In particular, the morphological damage to macro/microvasculature or their dysfunction will most likely compromise the movement of fluids, with impact on the perfusion of the brain and the drainage of CSF, ISF, altering the homeostasis of the brain, which in turn leads to neuronal cell loss and dementia.

## AUTHOR CONTRIBUTIONS

NA wrote the manuscript. RC edited the manuscript. All authors contributed to the article and approved the submitted version.

## ACKNOWLEDGMENTS

The authors thank the Stroke Association of the United Kingdom for financial support.

## REFERENCES

- Iadecola C, Nedergaard M. Glial regulation of the cerebral microvasculature. *Nat Neurosci.* (2007) 10:1369–76. doi: 10.1038/nn2003
- Agarwal N, Contarino C, Toro EF. Neurofluids: a holistic approach to their physiology, interactive dynamics and clinical implications for neurological diseases. *Veins Lymphat.* (2019) 8:49–58. doi: 10.4081/vl.2019.8470
- Beggs CB. Cerebral venous outflow and cerebrospinal fluid dynamics. *Veins Lymphat.* (2014) 3:1–8. doi: 10.4081/vl.2014.1867
- Zhang ET, Inman CBE, Weller RO. Interrelationships of the pia mater and the perivascular (Virchow-Robin) spaces in the human cerebrum. *J Anat.* (1990) 170:111–23.
- Marín-Padilla M. The human brain intracerebral microvascular system: development and structure. *Neuroanat.* (2012) 6:38. doi: 10.3389/fnana.2012.00038
- Carare RO, Bernardes-Silva M, Newman TA, Page AM, Nicoll JAR, Perry VH, et al. Solutes, but not cells, drain from the brain parenchyma along basement membranes of capillaries and arteries: significance for cerebral amyloid angiopathy and neuroimmunology. *Neuropathol Appl Neurobiol.* (2008) 34:131–44. doi: 10.1111/j.1365-2990.2007.00926.x
- Louveau A, Smirnov I, Keyes TJ, Eccles JD, Rouhani SJ, Peske JD, et al. Structural and functional features of central nervous system lymphatic vessels. *Nature.* (2015) 523:337–41. doi: 10.1038/nature14432

8. Aspelund A, Antila S, Proulx ST, Karlsen TV, Karaman S, Detmar M, et al. A dural lymphatic vascular system that drains brain interstitial fluid and macromolecules. *J Exp Med.* (2015) 212:991–9. doi: 10.1084/jem.20142290
9. Agarwal N, Port JD. *Neuroimaging: Anatomy Meets Function.* Switzerland: Springer International (2017).
10. Hill MA, Nourian Z, Ho IL, Clifford PS, Martinez-Lemus L, Meininger GA. Small artery elastin distribution and architecture—focus on three dimensional organization. *Microcirculation.* (2016) 23:614–20. doi: 10.1111/micc.12294
11. Blinder P, Tsai PS, Kaufhold JP, Knutsen PM, Suhl H, Kleinfeld D. The cortical angiome: an interconnected vascular network with noncolumnar patterns of blood flow. *Nat Neurosci.* (2013) 16:889–97. doi: 10.1038/nn.3426
12. Tsai PS, Kaufhold JP, Blinder P, Friedman B, Drew PJ, Karten HJ, et al. Correlations of neuronal and microvascular densities in murine cortex revealed by direct counting and colocalization of nuclei and vessels. *J Neurosci.* (2009) 29:14553–70. doi: 10.1523/JNEUROSCI.3287-09.2009
13. MacGregor Sharp M, Bulters D, Brandner S, Holton J, Verma A, Werring DJ, et al. The fine anatomy of the perivascular compartment in the human brain: relevance to dilated perivascular spaces in cerebral amyloid angiopathy. *Neuropathol Appl Neurobiol.* (2018) 45:305–8. doi: 10.1111/nan.12480
14. Hutchings M, Weller RO. Anatomical relationships of the pia mater to cerebral blood vessels in man. *J Neurosurg.* (1986) 65:316–25. doi: 10.3171/jns.1986.65.3.0316
15. Wardlaw JM, Smith EE, Biessels GJ, Cordonnier C, Fazekas F, Frayne R, et al. Neuroimaging standards for research into small vessel disease and its contribution to ageing and neurodegeneration. *Lancet Neurol.* (2013) 12:822–38. doi: 10.1016/S1474-4422(13)70124-8
16. Hase Y, Polvikoski TM, Firbank MJ, Craggs LJJ, Hawthorne E, Platten C, et al. Small vessel disease pathological changes in neurodegenerative and vascular dementias concomitant with autonomic dysfunction. *Brain Pathol.* (2020) 30:191–202. doi: 10.1111/bpa.12769
17. Horsburgh K, Wardlaw JM, Van Agtmael T, Allan SM, Ashford MLJ, Bath PM, et al. Small vessels, dementia and chronic diseases - molecular mechanisms and pathophysiology. *Clin Sci.* (2018) 132:851–68. doi: 10.1042/CS20171620
18. Hamel E. Perivascular nerves and the regulation of cerebrovascular tone. *J Appl Physiol.* (2006) 100:1059–64. doi: 10.1152/jappphysiol.00954.2005
19. Fantini S, Sassaroli A, Tgavalekos KT, Kornbluth J. Cerebral blood flow and autoregulation: current measurement techniques and prospects for noninvasive optical methods. *Neurophotonics.* (2016) 3:031411. doi: 10.1117/1.NPH.3.3.031411
20. Toussay X, Basu K, Lacoste B, Hamel E. Locus coeruleus stimulation recruits a broad cortical neuronal network and increases cortical perfusion. *J Neurosci.* (2013) 33:3390–401. doi: 10.1523/JNEUROSCI.3346-12.2013
21. Rayshubskiy A, Wojtasiewicz TJ, Mikell CB, Bouchard MB, Timerman D, Youngerman BE, et al. Direct, intraoperative observation of ~0.1Hz hemodynamic oscillations in awake human cortex: implications for fMRI. *Neuroimage.* (2014) 87:323–31. doi: 10.1016/j.neuroimage.2013.10.044
22. Zanatta P, Toffolo GM, Sartori E, Bet A, Baldanzi F, Agarwal N, et al. The human brain pacemaker: synchronized infra-slow neurovascular coupling in patients undergoing non-pulsatile cardiopulmonary bypass. *Neuroimage.* (2013) 72:10–9. doi: 10.1016/j.neuroimage.2013.01.033
23. Gould IG, Tsai P, Kleinfeld D, Linninger A. The capillary bed offers the largest hemodynamic resistance to the cortical blood supply. *J Cereb Blood Flow Metab.* (2016) 37:52–68. doi: 10.1177/0271678X16671146
24. Di Russo J, Hannocks MJ, Luik AL, Song J, Zhang X, Yousif L, et al. Vascular laminins in physiology and pathology. *Matrix Biol.* (2017) 57–8:140–8. doi: 10.1016/j.matbio.2016.06.008
25. Yousif LF, Di Russo J, Sorokin L. Laminin isoforms in endothelial and perivascular basement membranes. *Cell Adhes Migr.* (2013) 7:101–10. doi: 10.4161/cam.22680
26. Abbott NJ, Rönnbäck L, Hansson E. Astrocyte-endothelial interactions at the blood-brain barrier. *Nat Rev Neurosci.* (2006) 7:41–53. doi: 10.1038/nrn1824
27. Searson PC. The blood-brain barrier: an engineering perspective. *Neuroeng.* (2013) 6:7. doi: 10.3389/fneng.2013.00007
28. Hannocks MJ, Pizzo ME, Huppert J, Deshpande T, Abbott NJ, Thorne RG, et al. Molecular characterization of perivascular drainage pathways in the murine brain. *J Cereb Blood Flow Metab.* (2018) 38:669–86. doi: 10.1177/0271678X17749689
29. Bell RD, Sagare AP, Friedman AE, Bedi GS, Holtzman DM, Deane R, et al. Transport pathways for clearance of human Alzheimer's amyloid  $\beta$ -peptide and apolipoproteins E and J in the mouse central nervous system. *J Cereb Blood Flow Metab.* (2007) 27:909–18. doi: 10.1038/sj.cbfm.9600419
30. Taoka T, Fukusumi A, Miyasaka T, Kawai H, Nakane T, Kichikawa K, et al. Structure of the medullary veins of the cerebral hemisphere and related disorders. *Radiographics.* (2017) 37:281–97. doi: 10.1148/rg.2017160061
31. Schmidek H, Auer LM, Kapp JP. The cerebral venous system. *Neurosurgery.* (1985) 17:663–78. doi: 10.1227/00006123-198510000-00024
32. Batson O. The function of the vertebral veins and their role in the spread of metastases. *Clin Orthop Rel Res.* (1995) 112:138–49. doi: 10.1097/0000658-194007000-00016
33. Pearce JMS. The craniocervical venous system. *Eur Neurol.* (2006) 56:136–8. doi: 10.1159/000095706
34. Kiliç T, Akakin A. Anatomy of cerebral veins and sinuses. *Front Neurol Neurosci.* (2008) 23:4–15. doi: 10.1159/000111256
35. MacGregor Sharp M, Criswell TP, Dobson H, Finucane C, Verma A, Carare RO. Solving an old dogma: is it an arteriole or a venule? *Front Aging Neurosci.* (2019) 11:289. doi: 10.3389/fnagi.2019.00289
36. Földi M, Gellért A, Kozma M, Poberai M, Zoltán OT, Csanda E. New contributions to the anatomical connections of the brain and the lymphatic system. *Acta Anat.* (1966) 64:498–505. doi: 10.1159/000142849
37. Weller RO, Sharp MM, Christodoulides M, Carare RO, Møllgård K. The meninges as barriers and facilitators for the movement of fluid, cells and pathogens related to the rodent and human CNS. *Acta Neuropathol.* (2018) 135:363–85. doi: 10.1007/s00401-018-1809-z
38. Orešković D, Radoš M, Klarica M. New concepts of cerebrospinal fluid physiology and development of hydrocephalus. *Pediatr Neurosurg.* (2016) 52:417–25. doi: 10.1159/000452169
39. Ahn JH, Cho H, Kim J-H, Kim SH, Ham J-S, Park I, et al. Meningeal lymphatic vessels at the skull base drain cerebrospinal fluid. *Nature.* (2019) 572:1–29. doi: 10.1038/s41586-019-1419-5
40. Abbott NJ. Evidence for bulk flow of brain interstitial fluid: significance for physiology and pathology. *Neurochem Int.* (2004) 45:545–52. doi: 10.1016/j.neuint.2003.11.006
41. Brinker T, Stopa E, Morrison J, Klinge P. A new look at cerebrospinal fluid circulation. *Fluids Barriers CNS.* (2014) 11:10. doi: 10.1186/2045-8118-11-10
42. Syková E, Nicholson C. Diffusion in brain extracellular space. *Physiol Rev.* (2008) 88:1277–340. doi: 10.1152/physrev.00027.2007
43. Hablitz LM, Vinitzky HS, Sun Q, Stæger FF, Sigurdsson B, Mortensen KN, et al. Increased glymphatic influx is correlated with high EEG delta power and low heart rate in mice under anesthesia. *Sci Adv.* (2019) 5:eav5447. doi: 10.1126/sciadv.aav5447
44. Hauglund NL, Pavan C, Nedergaard M. Cleaning the sleeping brain – the potential restorative function of the glymphatic system. *Curr Opin Physiol.* (2020) 15:1–6. doi: 10.1016/j.cophys.2019.10.020
45. Xie L, Kang H, Xu Q, Chen MJ, Liao Y, Thiyagarajan M, et al. Sleep drives metabolite clearance from the adult brain. *Science* (80-). (2013) 342:373–7. doi: 10.1126/science.1241224
46. Cserr HF. Role of secretion and bulk flow of brain interstitial fluid in brain volume regulation. *Ann N Y Acad Sci.* (1988) 529:9–20. doi: 10.1111/j.1749-6632.1988.tb51415.x
47. Iliff JJ, Wang M, Liao Y, Plogg BA, Peng W, Gundersen GA, et al. A paravascular pathway facilitates CSF flow through the brain parenchyma and the clearance of interstitial solutes, including amyloid  $\beta$ . *Sci Transl Med.* (2012) 4:147ra111. doi: 10.1126/scitranslmed.3003748
48. Hladky SB, Barrand MA. Elimination of substances from the brain parenchyma: efflux via perivascular pathways and via the blood-brain barrier. *Fluids Barriers CNS.* (2018) 15:1–73. doi: 10.1186/s12987-018-0113-6
49. Tarasoff-Conway JM, Carare RO, Osorio RS, Glodzik L, Butler T, Fieremans E, et al. Clearance systems in the brain—implications for Alzheimer disease. *Nat Rev Neurol.* (2015) 11:457–70. doi: 10.1038/nrneurol.2015.119
50. Iliff JJ, Wang M, Zeppenfeld DM, Venkataraman A, Plog BA, Liao Y, et al. Cerebral arterial pulsation drives paravascular CSF-interstitial fluid exchange in the murine brain. *J Neurosci.* (2013) 33:18190–9. doi: 10.1523/JNEUROSCI.1592-13.2013

51. Benveniste H, Lee H, Volkow ND. The glymphatic pathway: waste removal from the CNS via cerebrospinal fluid transport. *Neurosci.* (2016) 23:454–65. doi: 10.1177/1073858417691030
52. Asgari M, De Zélicourt D, Kurtcuoglu V. Glymphatic solute transport does not require bulk flow. *Sci Rep.* (2016) 6:38635. doi: 10.1038/srep38635
53. Ray LA, Heys JJ. Fluid flow and mass transport in brain tissue. *Fluids.* (2019) 4:133–96. doi: 10.3390/fluids4040196
54. Martinac AD, Bilston LE. Computational modelling of fluid and solute transport in the brain. *Biomech Model Mechanobiol.* (2020) 19:781–800. doi: 10.1007/s10237-019-01253-y
55. Faghili MM, Sharp MK. Is bulk flow plausible in perivascular, paravascular and paravenous channels? *Fluids Barriers CNS.* (2018) 15:1–10. doi: 10.1186/s12987-018-0103-8
56. Jin BJ, Smith AJ, Verkman AS. Spatial model of convective solute transport in brain extracellular space does not support a “glymphatic” mechanism. *J Gen Physiol.* (2016) 148:489–501. doi: 10.1085/jgp.201611684
57. Attems J, Jellinger KA, Thal DR, Van Nostrand W. Review: sporadic cerebral amyloid angiopathy. *Neuropathol Appl Neurobiol.* (2011) 37:75–93. doi: 10.1111/j.1365-2990.2010.01137.x
58. Carare RO, Hawkes CA, Jeffrey M, Kalaria RN, Weller RO. Review: cerebral amyloid angiopathy, prion angiopathy, CADASIL and the spectrum of protein elimination failure angiopathies (PEFA) in neurodegenerative disease with a focus on therapy. *Neuropathol Appl Neurobiol.* (2013) 39:593–611. doi: 10.1111/nan.12042
59. Keable A, Fenna K, Yuen HM, Johnston DA, Smyth NR, Smith C, et al. Deposition of amyloid  $\beta$  in the walls of human leptomeningeal arteries in relation to perivascular drainage pathways in cerebral amyloid angiopathy. *Biochim Biophys Acta.* (2016) 1862:1037–46. doi: 10.1016/j.bbdis.2015.08.024
60. Casley Smith JR, Foldi Borcsok E, Foldi M. The prelymphatic pathways of the brain as revealed by cervical lymphatic obstruction and the passage of particles. *Br J Exp Pathol.* (1976) 57:179–88.
61. Weller RO, Kida S, Zhang ET. Pathways of fluid drainage from the brain—morphological aspects and immunological significance in rat and man. *Brain Pathol.* (1992) 2:277–84. doi: 10.1111/j.1750-3639.1992.tb00704.x
62. Diem AK, Tan M, Bressloff NW, Hawkes C, Morris AWJ, Weller RO, et al. A simulation model of periaxonal clearance of amyloid- $\beta$  from the brain. *Front Aging Neurosci.* (2016) 8:18. doi: 10.3389/fnagi.2016.00018
63. Sharp MK, Diem AK, Weller RO, Carare RO. Peristalsis with oscillating flow resistance: a mechanism for periaxonal clearance of amyloid beta from the brain. *Ann Biomed Eng.* (2015) 44:1–13. doi: 10.1007/s10439-015-1457-6
64. Carare RO, Aldea R, Bulters D, Alzetani A, Birch AA, Richardson G, et al. Vasomotion drives periaxonal drainage of A $\beta$  from the brain. *Neuron.* (2020) 105:400–1. doi: 10.1016/j.neuron.2020.01.011
65. van Veluw SJ, Hou SS, Calvo-Rodriguez M, Arbel-Ornath M, Snyder AC, Frosch MP, et al. Vasomotion as a driving force for paravascular clearance in the awake mouse brain. *Neuron.* (2020) 105:549–61.e5. doi: 10.1016/j.neuron.2019.10.033
66. Fultz NE, Bonmassar G, Setsompop K, Stickgold RA, Rosen BR, Polimeni JR, et al. Coupled electrophysiological, hemodynamic, and cerebrospinal fluid oscillations in human sleep. *Science (80-).* (2019) 366:628–31. doi: 10.1126/science.aax5440
67. Kellie G. An account of the appearances observed in the dissection of two of three individuals presumed to have perished in the storm of the 3d, and whose bodies were discovered in the vicinity of Leith on the morning of the 4th, November 1821 : with some reflectio. *Trans Med Chir Soc Edinb.* (1824) 1:84–122.
68. Mokri B. The monro-kellie hypothesis: applications in CSF volume depletion. *Neurology.* (2001) 56:1746–8. doi: 10.1212/WNL.56.12.1746
69. Wilson MH. Monro-Kellie 2.0: the dynamic vascular and venous pathophysiological components of intracranial pressure. *J Cereb Blood Flow Metab.* (2016) 36:1338–50. doi: 10.1177/0271678X16648711
70. Linninger AA, Tangen K, Hsu C-Y, Frim D. Cerebrospinal fluid mechanics and its coupling to cerebrovascular dynamics. *Annu Rev Fluid Mech.* (2016) 48:219–57. doi: 10.1146/annurev-fluid-122414-034321
71. Greitz D, Wirestam R, Franck A, Nordell B, Thomsen C, Ståhlberg F. Pulsatile brain movement and associated hydrodynamics studied by magnetic resonance phase imaging. The monro-kellie doctrine revisited. *Neuroradiology.* (1992) 34:370–80. doi: 10.1007/BF00596493
72. Lee SJ, King MA, Sun J, Xie HK, Subhash G, Sarntinoranont M. Measurement of viscoelastic properties in multiple anatomical regions of acute rat brain tissue slices. *J Mech Behav Biomed Mater.* (2014) 29:213–24. doi: 10.1016/j.jmbbm.2013.08.026
73. Budday S, Nay R, De Rooij R, Steinmann P, Wyrobek T, Ovaert TC, et al. Mechanical properties of gray and white matter brain tissue by indentation. *J Mech Behav Biomed Mater.* (2015) 46:318–30. doi: 10.1016/j.jmbbm.2015.02.024
74. Kruse SA, Rose GH, Glaser KJ, Manduca A, Felmlee JP, Jack CR, et al. Magnetic resonance elastography of the brain. *Neuroimage.* (2008) 39:231–7. doi: 10.1016/j.neuroimage.2007.08.030
75. Hatt A, Cheng S, Tan K, Sinkus R, Bilston LE. MR elastography can be used to measure brain stiffness changes as a result of altered cranial venous drainage during jugular compression. *AJNR Am J Neuroradiol.* (2015) 36:1971–7. doi: 10.3174/ajnr.A4361
76. Sweeney MD, Kisler K, Montagne A, Toga AW, Zlokovic BV. The role of brain vasculature in neurodegenerative disorders. *Nat Neurosci.* (2018) 21:1318–31. doi: 10.1038/s41593-018-0234-x
77. Kalaria RN, Pax AB. Increased collagen content of cerebral microvessels in Alzheimer's disease. *Brain Res.* (1995) 705:349–52. doi: 10.1016/0006-8993(95)01250-8
78. Vanherle L, Matuskova H, Don-Doncow N, Uhl FE, Meissner A. Improving cerebrovascular function to increase neuronal recovery in neurodegeneration associated to cardiovascular disease. *Front Cell Dev Biol.* (2020) 8:1–8. doi: 10.3389/fcell.2020.00053
79. Wolters FJ, Zonneveld HI, Hofman A, Van Der Lugt A, Koudstaal PJ, Vernooij MW, et al. Cerebral perfusion and the risk of dementia: a population-based study. *Circulation.* (2017) 136:719–28. doi: 10.1161/CIRCULATIONAHA.117.027448
80. Montagne A, Barnes SR, Sweeney MD, Halliday MR, Sagare AP, Zhao Z, et al. Blood-brain barrier breakdown in the aging human hippocampus. *Neuron.* (2015) 85:296–302. doi: 10.1016/j.neuron.2014.12.032
81. Dumont M, Roy M, Jodoin PM, Morency FC, Houde JC, Xie Z, et al. Free water in white matter differentiates MCI and AD from control subjects. *Front Aging Neurosci.* (2019) 11:270. doi: 10.3389/fnagi.2019.00270
82. Sharp MM, Saito S, Keable A, Gatherer M, Aldea R, Agarwal N, et al. Demonstrating a reduced capacity for removal of fluid from cerebral white matter and hypoxia in areas of white matter hyperintensity associated with age and dementia. *Acta Neuropathol Commun.* (2020) 1:1–14. doi: 10.1186/s40478-020-01009-1
83. Weller RO, Wisniewski H, Shulman K, Terry RD. Experimental hydrocephalus in young dogs: histological and ultrastructural study of the brain tissue damage. *J Neuropathol Exp Neurol.* (1971) 30:613–26. doi: 10.1097/00005072-197110000-00006
84. Moody DM, Brown WR, Challa VR, Anderson RL. Periventricular venous collagenosis: association with leukoaraiosis. *Radiology.* (1995) 194:469–76. doi: 10.1148/radiology.194.2.7824728
85. Nan D, Cheng Y, Feng L, Zhao M, Ma D, Feng J. Potential mechanism of venous system for leukoaraiosis: from post-mortem to in vivo research. *Neurodegener Dis.* (2020) 130021:101–8. doi: 10.1159/000505157
86. Banerjee G, Kim HJ, Fox Z, Jäger HR, Wilson D, Charidimou A, et al. MRI-visible perivascular space location is associated with alzheimer's disease independently of amyloid burden. *Brain.* (2017) 140:1107–16. doi: 10.1093/brain/awx003
87. Hurford R, Charidimou A, Fox Z, Cipolletti L, Jager R, Werring DJ. MRI-visible perivascular spaces: relationship to cognition and small vessel disease MRI markers in ischaemic stroke and TIA. *J Neurol Neurosurg Psychiatry.* (2014) 85:522–5. doi: 10.1136/jnnp-2013-305815
88. Brown R, Benveniste H, Black SE, Charpak S, Dichgans M, Joutel A, et al. Understanding the role of the perivascular space in cerebral

- small vessel disease. *Cardiovasc Res.* (2018) 114:1462–73. doi: 10.1093/cvr/cvy113
89. Francis F, Ballerini L, Wardlaw JM. Perivascular spaces and their associations with risk factors, clinical disorders and neuroimaging features: a systematic review and meta-analysis. *Int J Stroke.* (2019) 14:359–71. doi: 10.1177/1747493019830321
90. Morris A, Carare RO, Schreiber S, Hawkes CA. The cerebrovascular basement membrane: role in the clearance of  $\beta$ -amyloid and cerebral amyloid angiopathy. *Front Aging Neurosci.* (2014) 6:251. doi: 10.3389/fnagi.2014.00251

**Conflict of Interest:** The authors declare that the research was conducted in the absence of any commercial or financial relationships that could be construed as a potential conflict of interest.

Copyright © 2021 Agarwal and Carare. This is an open-access article distributed under the terms of the Creative Commons Attribution License (CC BY). The use, distribution or reproduction in other forums is permitted, provided the original author(s) and the copyright owner(s) are credited and that the original publication in this journal is cited, in accordance with accepted academic practice. No use, distribution or reproduction is permitted which does not comply with these terms.





# Comparison of Longitudinal Changes of Cerebral Small Vessel Disease Markers and Cognitive Function Between Subcortical Vascular Mild Cognitive Impairment With and Without *NOTCH3* Variant: A 5-Year Follow-Up Study

Cindy W. Yoon<sup>1</sup>, Young-Eun Kim<sup>2</sup>, Hee Jin Kim<sup>3</sup>, Chang-Seok Ki<sup>4</sup>, Hyejoo Lee<sup>3</sup>,  
Joung-Ho Rha<sup>1</sup>, Duk L. Na<sup>3</sup> and Sang Won Seo<sup>3\*</sup>

<sup>1</sup> Department of Neurology, Inha University School of Medicine, Incheon, South Korea, <sup>2</sup> Department of Laboratory Medicine, Hanyang University College of Medicine, Seoul, South Korea, <sup>3</sup> Department of Neurology, Samsung Medical Center, Sungkyunkwan University School of Medicine, Seoul, South Korea, <sup>4</sup> Genome Research Center, Green Cross Genome, Yong-in, South Korea

## OPEN ACCESS

### Edited by:

Mark Haacke,  
Wayne State University, United States

### Reviewed by:

Michele Romoli,  
University of Perugia, Italy  
Yeo Jin Kim,  
Hallym University, South Korea

### \*Correspondence:

Sang Won Seo  
sangwonseo@empal.com

### Specialty section:

This article was submitted to  
Stroke,  
a section of the journal  
Frontiers in Neurology

Received: 23 July 2020

Accepted: 05 February 2021

Published: 25 February 2021

### Citation:

Yoon CW, Kim Y-E, Kim HJ, Ki C-S,  
Lee H, Rha J-H, Na DL and Seo SW  
(2021) Comparison of Longitudinal  
Changes of Cerebral Small Vessel  
Disease Markers and Cognitive  
Function Between Subcortical  
Vascular Mild Cognitive Impairment  
With and Without *NOTCH3* Variant: A  
5-Year Follow-Up Study.  
Front. Neurol. 12:586366.  
doi: 10.3389/fneur.2021.586366

No study yet has compared the longitudinal course and prognosis between subcortical vascular cognitive impairment patients with and without genetic component. In this study, we compared the longitudinal changes in cerebral small vessel disease markers and cognitive function between subcortical vascular mild cognitive impairment (svMCI) patients with and without *NOTCH3* variant [*NOTCH3*(+) svMCI vs. *NOTCH3*(-) svMCI]. We prospectively recruited patients with svMCI and screened for *NOTCH3* variants by sequence analysis for mutational hotspots in the *NOTCH3* gene. Patients were annually followed-up for 5 years through clinical interviews, neuropsychological tests, and brain magnetic resonance imaging. Among 63 svMCI patients, 9 (14.3%) had either known mutations or possible pathogenic variants. The linear mixed effect models showed that the *NOTCH3*(+) svMCI group had much greater increases in the lacune and cerebral microbleed counts than the *NOTCH3*(-) svMCI group. However, there were no significant differences between the two groups regarding dementia conversion rate and neuropsychological score changes over 5 years.

**Keywords:** *NOTCH3*, CADASIL, lacune, cerebral microbleed, subcortical vascular cognitive impairment

## INTRODUCTION

Cerebral autosomal dominant arteriopathy with subcortical infarcts and leukoencephalopathy (CADASIL) is an autosomal dominant disorder of cerebral small vessels caused by mutations in the *NOTCH3* gene on chromosome 19 (1). CADASIL is characterized by cerebral small vessel disease (CSVD) and cognitive impairment, and is therefore considered as a genetic form of subcortical vascular cognitive impairment (SVCI). On the other hand, sporadic SVCI is mostly caused by vascular risk factors. Advanced age, hypertension (HTN), diabetes mellitus (DM), and other

vascular risk factors can lead to CSVD characterized by white matter hyperintensities (WMHs), lacunes, and cerebral microbleeds (CMBs) on magnetic resonance imaging (MRI) (2).

Typically, patients with CADASIL are young at onset and have no vascular risk factors (3). However, we previously reported that approximately 13% of consecutive patients with SVCI had *NOTCH3* variants, although they were of advanced age and frequently had a history of HTN (4). In our previous cross-sectional studies, these atypical SVCI patients with *NOTCH3* variant have shown no significant differences in clinical and imaging features compared to patients without *NOTCH3* variant (4, 5). However, cross-sectional comparison, a snapshot of a single moment in time, has interpretative limitations.

To our best knowledge, no study yet has compared the longitudinal course and prognosis between SVCI patients with and without genetic component. Therefore, in this study, we compared the longitudinal changes in CSVD markers and cognitive function in subcortical vascular mild cognitive impairment (svMCI) patients with [*NOTCH3*(+) svMCI] and without [*NOTCH3*(-) svMCI] *NOTCH3* variant for a better understanding of the impact of *NOTCH3* variant.

## MATERIALS AND METHODS

### Participants

We prospectively recruited 72 patients with svMCI between September 2008 and September 2011 at Samsung Medical Center in Seoul, Korea. All recruited patients met the modified Petersen's criteria for MCI as previously described (6) and had evidence of significant ischemia on their MRI scans, seen as a cap or band  $\geq 10$  mm and a deep white matter lesion  $\geq 25$  mm (modified from Fazekas ischemia criteria) (7, 8). Of the 72 svMCI patients, nine were excluded because they or their caregivers chose not to participate in the study. After a complete description of the study, written informed consent was obtained from each patient (or legally authorized representatives). The Institutional Review Board of Samsung Medical Center approved the study protocol. This study was planned and conducted in accordance with the Declaration of Helsinki. This study has been registered in the Korean Clinical Trial Registry (registration number: KCT0005516).

### Molecular Genetic Analysis

Genetic analysis was performed according to the protocols previously described (4). Peripheral blood specimens were collected after obtaining informed consent. Genomic DNA was extracted using the Wizard Genomic DNA purification kit according to the manufacturer's instructions. Mutational hotspots of the *NOTCH3* gene including exons 2–6, 8, 11, 18, 19, and 22 were sequenced. All tested exons and their exon-intron boundaries in the *NOTCH3* gene were amplified by polymerase chain reaction, as described previously (9). Cycle sequencing was performed using a BigDye Terminator Cycle Sequencing Ready Reaction kit on an ABI 3130xl Genetic Analyzer (Applied Biosystems). The nucleotides of *NOTCH3* complementary DNA were numbered according to a reference sequence (GenBank accession number: NM\_000435.2). Sorting

Intolerant From Tolerant (10) and Polymorphism Phenotyping (PolyPhen-2 v2.1) (11) servers were used to predict the effect of non-synonymous variants of unknown significance (VUS) on protein structure, function, phenotype, sequence conservation, and/or protein structure. In addition, 358 age- and sex-matched healthy Korean controls were screened for novel VUS in the *NOTCH3* gene using matrix-assisted laser desorption/ionization time-of-flight mass spectrometry, as described previously (12). Written informed consent was obtained from all participants including healthy controls.

Among 63 svMCI patients, nine (14.3%) had either known mutations or variants of unknown significance (VUS). Three known mutations were found in six patients: p.R544C ( $n = 4$ ), p.R587C ( $n = 1$ ), and p.V237M ( $n = 1$ ). In addition, four VUS were identified in three patients: three missense variants (p.P572L, p.S947I, and p.R1175W) and one frameshift variant (p.Glu990Argfs\*282). Two VUS (p.P572L and p.R1175W) were found in one patient. A control study of 716 chromosomes identified one variant (p.R1175W) (**Supplementary Table 1**). This variant might be a polymorphism rather than a pathogenic variant. These results were included in our previous report (4).

### MRI Techniques

T1, T2, 3-dimensional fluid-attenuated inversion recovery (FLAIR), and T2 Fast Field Echo-MR images were acquired using the same 3.0T MRI scanner (Philips 3.0T Achieva).

### Assessment of Lacunes and CMBs on MRI

Lacunes were defined as small lesions ( $\leq 15$  and  $\geq 3$  mm in diameter) with low signal on T1-weighted images, high signal on T2-weighted images, and a perilesional halo on 80 axial slices from FLAIR images.

CMBs were defined as lesions  $\leq 10$  mm in diameter by using the criteria proposed by Greenberg et al. (13) on 20 axial slices of T2\*gradient echo-MR images. CMBs were counted in four lobar regions (frontal, temporal, parietal, and occipital) and deep brain regions. The lobar regions were defined as regions  $\leq 10$  mm from the brain surface.

### Neuropsychological Testing

All patients underwent neuropsychological testing using the Seoul Neuropsychological Screening Battery (14, 15).

### Pittsburgh Compound B-positron Emission Tomography ([ $^{11}$ C]-PiB)-PET

All patients underwent a standardized [ $^{11}$ C]-PiB-PET scan at the Samsung or Asan Medical Center on a Discovery STE PET/CT scanner (GE Medical Systems, Milwaukee, WI, USA) to minimize any variance due to scanner differences. The detailed radiochemistry profiles, scanning protocol, and data analysis method were described in a previous study (8). Briefly, we calculated the PiB-uptake ratio of each voxel using the cerebellum as a reference region in the analysis. The global cortical PiB-uptake ratio was determined by combining the bilateral frontal, parietal, and temporal cortices, and the posterior cingulate gyrus. Patients were considered PiB-positive if their global PiB uptake

ratio was more than 2 standard deviations (PiB retention ratio  $\geq 1.5$ ) from the mean of the normal controls.

## Follow-Up Evaluations

All patients underwent clinical interviews, a neurological examination, neuropsychological tests, brain MRI, and PiB-PET imaging at baseline. Patients were annually evaluated for 5 years through clinical interviews, neuropsychological tests, and brain MRI.

Completeness of follow-up was 63/63 (100%) at 1 year, 60/63 (95.2%) at 2 years, 55/63 (87.3%) at 3 years, 51/63 (81.0%) at 4 years, and 43/63 (68.3%) at 5 years; 7/9 (77.8%) among *NOTCH3*(+) svMCI and 36/54 (66.7%) among *NOTCH3*(-) svMCI (Supplementary Figure 1). The comparison between patients with and without complete 5-year follow-up is shown in Supplementary Table 2. There were no significant differences between the two groups except for the female ratio. The female ratio was higher in patients with complete 5-year follow-up than in those without complete follow-up.

## Statistical Analysis

To analyze the baseline differences between svMCI patients with and without *NOTCH3* variant, we used the Chi-square test or Fisher's exact test for categorical variables, and the Mann-Whitney U-test or Student *t*-test for continuous variables.

We used the linear mixed-effects model to estimate changes in CSVD markers and cognitive measures over the follow-up period. In the linear mixed-effects model, the interactions between the presence of *NOTCH3* variant and time interval (presence of *NOTCH3* variant  $\times$  time) were explored to determine the influence of the presence of *NOTCH3* variant on the rate of change in CSVD markers. We controlled for age, HTN, baseline number of lacunes or CMBs, and time interval from baseline tests. To determine the trend of changes in each group, linear mixed-model analyses were separately performed in each group using age, HTN, and baseline number of lacunes or CMBs as covariates, and time interval from baseline evaluation as a predictor.

Longitudinal changes of cognitive scores in two svMCI groups were compared with linear mixed-effect models using the presence of *NOTCH3* variant and time interval (presence of *NOTCH3* variant  $\times$  time) as a predictor; age, sex, education, and time interval from baseline tests were used as covariates. Because multiple cognitive scores were used for comparison, correction for multiple comparisons was performed by false discovery rate correction.

Cox regression models were used to compare the risks of progression to dementia between *NOTCH3*(+) and *NOTCH3*(-) svMCI groups after controlling for age, sex, education, and PiB positivity. Patients who did not progress to dementia were treated as censored observations from the time of their final follow-up visit.

**TABLE 1 |** Baseline characteristics of patients with subcortical vascular mild cognitive impairment (svMCI), with and without *NOTCH3* variant.

	<i>NOTCH3</i> (+) svMCI	<i>NOTCH3</i> (-) svMCI	<i>p</i> -value
<b>Number</b>	9	54	
<b>Demographics</b>			
Baseline age, mean $\pm$ SD (years)	70.3 $\pm$ 10.5	72.8 $\pm$ 6.3	0.519
Sex, female, <i>N</i> (%)	4 (44.4)	33 (61.1)	0.469
Education, mean $\pm$ SD (years)	8.4 $\pm$ 6.0	9.1 $\pm$ 6.3	0.610
<b>Vascular risk factor, <i>N</i> (%)</b>			
Hypertension	8 (88.9)	41 (75.9)	0.670
Diabetes mellitus	1 (11.1)	14 (25.9)	0.673
Hyperlipidemia	4 (44.4)	15 (27.8)	0.434
APOE4 carrier, <i>N</i> (%)	1 (11.1)	12 (22.2)	0.671
<b>Imaging markers</b>			
Number of lacunes, median (IQR)	8 (3–12)	3 (1–7)	0.095
Number of CMBs, median (IQR)	4 (1–16)	0 (0–5)	0.135
PiB positive (SUVR $\geq 1.5$ ), <i>N</i> (%)	1 (11.1)	18 (33.3)	0.253
PiB SUVR, median (IQR)	1.25 (1.18–1.40)	1.35 (1.25–1.59)	0.147
<b>General cognition</b>			
MMSE, mean $\pm$ SD	25.8 $\pm$ 5.3	26.0 $\pm$ 3.0	0.488
CDR-SOB, median (IQR)	1 (0.5–1.5)	1 (0.5–1.5)	0.739
<b>Geriatric depression scale</b> , mean $\pm$ SD	10.3 $\pm$ 5.6	12.9 $\pm$ 5.8	0.222
<b>Follow-up duration</b> , mean $\pm$ SD	55.7 $\pm$ 11.6	52.5 $\pm$ 15.9	0.844
<b>Dementia conversion</b> , <i>N</i> (%)	1 (11.1)	12 (22.2)	0.671

SD, Standard deviation; IQR, Interquartile range; CMB, Cerebral microbleed; SUVR, Standardized uptake value ratio; MMSE, Mini-Mental State Examination; CDR-SOB, Clinical Dementia Rating Scale Sum of Boxes.

## RESULTS

### Baseline Characteristics and Longitudinal Follow-Up

Baseline characteristics of the subjects are shown in Table 1. There were no significant differences between the two groups with respect to age, sex ratio, education years, and prevalence of vascular risk factors. No significant group differences were seen in the baseline number of lacunes and CMBs, PiB SUVR, and mini-mental state exam (MMSE) and clinical dementia rating scale sum of boxes (CDR-SOB) scores.

The mean (standard deviation) duration of follow-up were 55.7 (11.6) months in nine *NOTCH3*(+) svMCI patients and 52.5 (15.9) months in 54 *NOTCH3*(-) svMCI patients. Thirteen of 63 patients (20.6%) showed conversion to dementia on follow-up: 1/9 (11.1%) among the *NOTCH3*(+) svMCI group and 12/54 (22.2%) among the *NOTCH3*(-) svMCI group. The time to dementia diagnosis was 11 months in one *NOTCH3*(+) svMCI patient. The mean (range) time to dementia diagnosis was 31.1 (11–54) months in 12 *NOTCH3*(-) svMCI patients.

### The Impact of *NOTCH3* Variant on Longitudinal Changes of CSVD Markers

Linear mixed-effect model analysis separately performed in each svMCI group showed that there were increases in

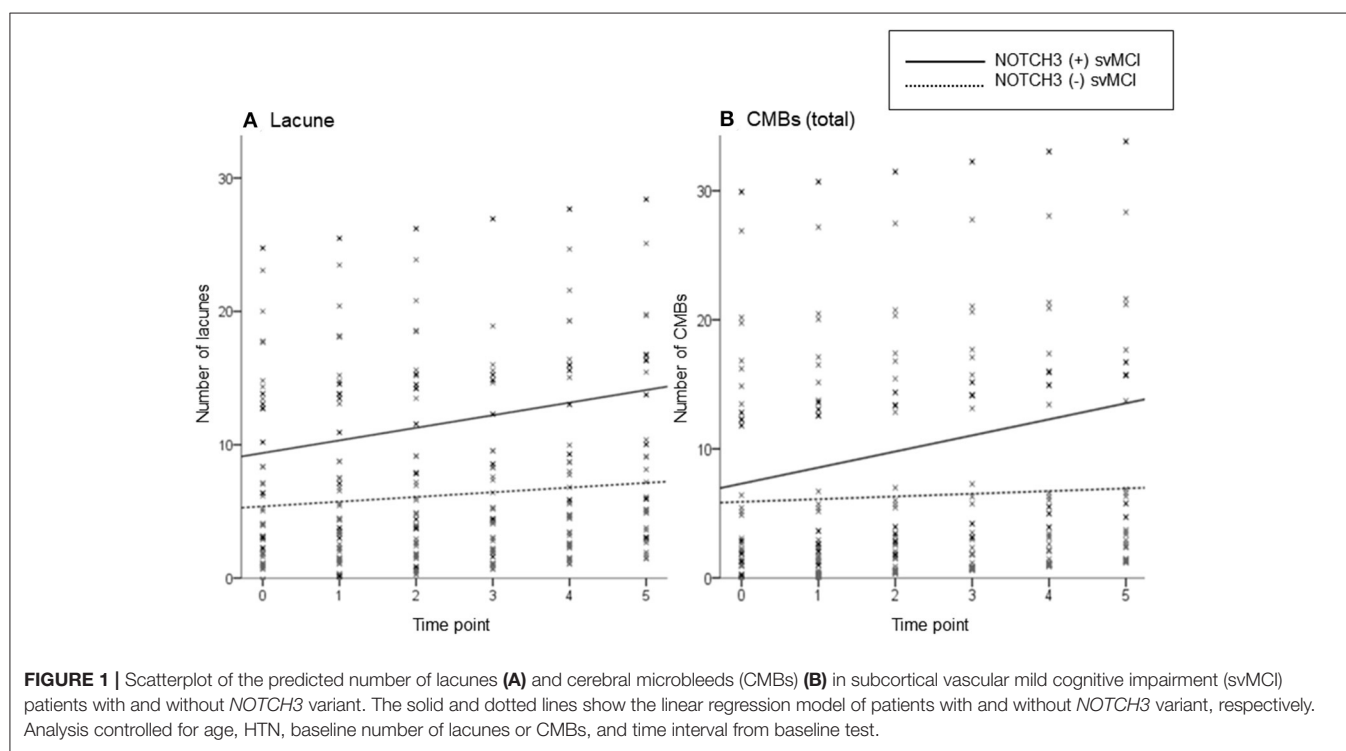
**TABLE 2 |** Comparison of longitudinal changes in the number of lacunes and cerebral microbleeds in patients with subcortical vascular mild cognitive impairment (svMCI), with and without *NOTCH3* variant.

	<i>NOTCH3</i> (+) svMCI*		<i>NOTCH3</i> (-) svMCI*		<i>NOTCH3</i> (+) svMCI vs. <i>NOTCH3</i> (-) svMCI (reference) <sup>†</sup>	
	<i>B</i> (SE)	<i>p</i>	<i>B</i> (SE)	<i>p</i>	<i>B</i> (SE)	<i>p</i>
<b>Lacunes (Total)</b>	0.83 (0.21)	<0.001	0.37 (0.06)	< 0.001	0.32 (0.15)	0.034
<b>CMBs</b>						
Total	1.24 (0.30)	<0.001	0.28 (0.09)	0.002	0.48 (0.22)	0.037
Deep	0.70 (0.24)	0.008	0.19 (0.07)	0.009	0.49 (0.18)	0.007
Lobar	0.11 (0.12)	0.336	0.13 (0.06)	0.031	0.01 (0.15)	0.961

SE, Standard error; CMBs, Cerebral microbleeds.

\*Results of linear mixed models separately performed in *NOTCH3*(+) or *NOTCH3*(-) svMCI group using age, HTN, and baseline number of lacunes (or CMBs) as covariates, and time interval from baseline evaluation as a predictor.

<sup>†</sup>Results of linear mixed models using age, HTN, baseline number of lacunes (or CMBs), and time interval from baseline tests as covariates, and the interaction between the presence of *NOTCH3* mutation and time interval as a predictor.



lacune and CMB counts in both svMCI groups according to the time interval from baseline evaluation (Table 2). The linear mixed-effect models that tested the interactive effect of *NOTCH3* variant and time showed that the *NOTCH3*(+) svMCI group had much greater increases in lacune and CMB (total and deep) counts than *NOTCH3*(-) svMCI group after controlling for age, HTN, and baseline number of lacunes or CMBs (Table 2). Figure 1 shows the estimated effect of *NOTCH3* variant on the longitudinal changes of the number of lacunes and CMBs over a 5-year follow-up period.

## The Impact of *NOTCH3* Variant on Longitudinal Cognitive Changes

In the linear mixed-effect model that tested the interactive effect of *NOTCH3* variant and time on changes of neuropsychological test scores, no neuropsychological tests showed significant differences in longitudinal change according to the presence of *NOTCH3* variant (Table 3).

Cox regression model showed that dementia risk was not significantly different between *NOTCH3*(+) and *NOTCH3*(-) svMCI patients after controlling for age, sex, education, and



**TABLE 3 |** Comparison of longitudinal changes in neuropsychological test scores between subcortical vascular mild cognitive impairment (svMCI) patients with and without *NOTCH3* variant.

Neuropsychological test	<i>NOTCH3</i> (+) svMCI vs. <i>NOTCH3</i> (-) svMCI (reference)*	
	<i>B</i> (SE)	<i>p</i>
Digit span forward	−0.06 (0.09)	1.000
Digit span backward	−0.05 (0.07)	0.916
Calculation	0.05 (0.16)	0.908
K-BNT	0.40 (0.55)	0.842
RCFT copy	0.27 (0.41)	0.773
SVLT immediate recall	0.38 (0.32)	0.711
SVLT delayed recall	0.10 (0.16)	0.681
SVLT recognition	0.40 (0.20)	0.387
RCFT immediate recall	−0.06 (0.41)	0.943
RCFT delayed recall	−0.25 (0.36)	0.792
RCFT recognition	−0.36 (0.16)	0.576
COWAT animal	0.03 (0.29)	0.909
COWAT supermarket	0.30 (0.32)	0.928
COWAT phonemic	−0.63 (0.46)	0.783
Stroop color reading	0.96 (1.49)	0.720
MMSE	0.41 (0.30)	0.634
CDR sum of boxes	−0.27 (0.18)	0.750
Geriatric depression scale	−0.34 (0.54)	0.637

SE, standard error; K-BNT, Korean version of Boston Naming Test; RCFT, Rey–Osterrieth Figure Test; SVLT, Seoul Verbal Learning Test; COWAT, Controlled Oral Word Association Test; MMSE, Mini-mental Status Examination; CDR, Clinical Dementia Rating.

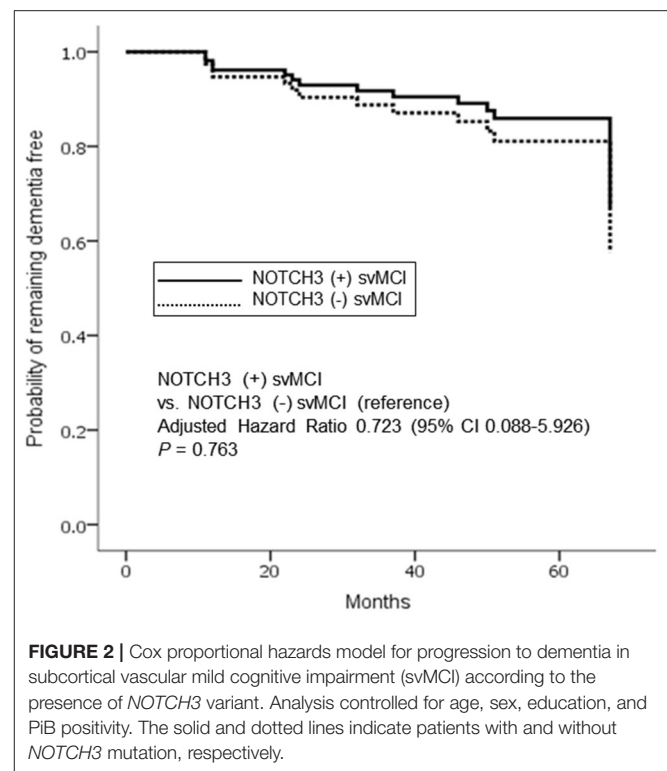
\*Results of linear mixed models using age, sex, education, and time interval from baseline tests as covariates, and the interaction between the presence of *NOTCH3* mutation and time interval as a predictor. *P*-values are corrected for multiple comparisons using false discovery rate correction.

PiB positivity ( $p = 0.763$ ; adjusted hazard ratio, 0.723; 95% confidence interval, 0.088–5.926) (Figure 2).

## DISCUSSION

In this prospective study, we compared the longitudinal course of svMCI patients according to the presence of *NOTCH3* variant in a well-defined svMCI cohort based on standardized imaging protocols, detailed clinical evaluation, and genetic analysis. Regarding the longitudinal changes of CSVD markers, *NOTCH3*(+) svMCI patients showed much greater increase in lacune and CMB counts than the *NOTCH3*(-) svMCI patients. However, there were no significant differences between the two groups regarding longitudinal cognitive changes including dementia conversion rate and neuropsychological score changes over 5 years. We believe this is the first study to compare the longitudinal changes of CSVD markers and cognition between SVCI patients with and without *NOTCH3* variant.

Our major finding was that the rate of increase in lacune and CMB counts was much greater in patients with *NOTCH3* variant than in those without *NOTCH3* variant. Because previous longitudinal studies have suggested that the baseline burden of CSVD is associated with the rate of change in CSVD markers (16, 17), we adjusted for baseline lacune and CMB counts. We



also controlled for age and HTN as well-known risk factors for progression of CSVD. The presence of *NOTCH3* variant still remained an independent predictor for change in lacune and CMB counts.

Mutations in the *NOTCH3* gene cause degeneration of smooth muscle cells in the tunica media and thickening of the walls of cerebral small vessels (18, 19). Lacunes in CADASIL are caused by reduced microvascular perfusion due to small arteriopathy affected by *NOTCH3* mutation. Considering the similar burden of conventional vascular risk factors and additional damage to cerebral small vessels by *NOTCH3* mutation, it is understandable that *NOTCH3*(+) svMCI patients in our study showed a markedly greater increase in lacune count than *NOTCH3*(-) svMCI patients.

Both total and deep CMBs tended to increase much faster in *NOTCH3*(+) than *NOTCH3*(-) patients; however, this association was not found in lobar CMBs. In previous CADASIL studies, the distribution of CMBs is predominantly in deep location including the bilateral thalami and basal ganglia and less commonly at the gray–white junction (20–22). *NOTCH3* mutations cause arteriopathy affecting the small cerebral (deep) and leptomeningeal (superficial) penetrating arteries (23), and CMBs might result from vascular leakage of these fragile small vessels (24). Although superficial small perforating arteries associated with lobar CMBs might be also affected by *NOTCH3* mutation, the majority are thought to be deep small perforating arteries responsible for deep CMBs.

Lacunes and CMBs have been associated with cognitive impairment and decline in many previous cross-sectional (25–28) and longitudinal studies (29–32). A previous 7-year follow-up

study investigating longitudinal associations between radiologic changes and cognitive decline in CADASIL patients have also shown that cognitive decline might be associated with increases in lacune and CMB counts (33). However, unexpectedly, despite a much greater increase in lacune and CMB counts in *NOTCH3*(+) svMCI patients than *NOTCH3*(-) svMCI patients, there were no significant differences in dementia conversion rate or neuropsychological score changes over 5 years between the two groups. This is likely because of similar baseline CSVD burden and inadequate differences in radiological changes to make a significant difference to cognitive decline between the two groups. Baseline CSVD burden including the number of lacunes or CMBs has been a significant predictor of cognitive decline in previous longitudinal studies (29–32). In our study, both svMCI groups with and without *NOTCH3* variant had relatively severe CSVD burden at baseline with a similar degree between the two groups. It is also possible that a much longer follow-up is required to demonstrate significant differences in cognitive decline between the two groups. Another possible explanation is because of amyloid burden. In our study, *NOTCH3*(-) svMCI group tended to have more amyloid burden than *NOTCH3*(+) svMCI group, although it was not statistically significant. In previous studies from our group, higher amyloid uptake in svMCI was associated with more severe cognitive impairment and faster cognitive decline (34, 35). A relatively small number of *NOTCH3*(+) patients could have also attributed to these negative findings.

The strengths of our study are its prospective setting, standardized imaging protocols, and detailed clinical evaluation during follow-up. However, our results should be interpreted with caution because our *NOTCH3*(+) patients were not representative of the typical CADASIL patients (4). This was a single-center study examining a small cohort of patients and the sample size of the *NOTCH3*(+) svMCI group was particularly small. The rate of follow-up loss at 5 years was relatively high. Finally, the possibility of polymorphisms rather than pathogenic variants remains in three VUS, although these VUS were not found in 716 control chromosomes. Thus, we performed additional analyses excluding three patients with VUS and obtained similar results (Supplementary Tables 3, 4).

## CONCLUSION

*NOTCH3*(+) svMCI group had much greater increases in the lacune and cerebral microbleed counts than the *NOTCH3*(-) svMCI group. However, there were no significant differences between the two groups regarding dementia conversion rate and neuropsychological score changes over 5 years.

## REFERENCES

1. Joutel A, Corpechot C, Ducros A, Vahedi K, Chabriat H, Mouton P, et al. Notch3 mutations in CADASIL, a hereditary adult-onset condition causing stroke and dementia. *Nature*. (1996) 383:707. doi: 10.1038/383707a0

## DATA AVAILABILITY STATEMENT

The datasets generated for this study will be made available on request to the corresponding author.

## ETHICS STATEMENT

The studies involving human participants were reviewed and approved by The Institutional Review Board of Samsung Medical Center. The patients/participants provided their written informed consent to participate in this study.

## AUTHOR CONTRIBUTIONS

CY: conceptualization of the study, methodology, formal analysis, and writing - original draft. Y-EK and C-SK: methodology, validation, and formal analysis. HK: methodology and data curation. HL: methodology and formal analysis. J-HR: methodology, writing - review and editing. DN: conceptualization of the study, methodology, investigation, and supervision. SS: conceptualization of the study, methodology, formal analysis, writing-review and editing, supervision, and funding acquisition. All authors contributed to the article and approved the submitted version.

## FUNDING

This research was supported by the Brain Research Program through the National Research Foundation of Korea (NRF) funded by the Ministry of Science, ICT & Future Planning (2016M3C7A1913844), the grant funded by Research of Korea Centers for Disease Control and Prevention (2018-ER6203-02), the NRF grant funded by the Korea government (MSIT) (NRF-2019R1A5A2027340), and the grant of the Korea Health Technology R&D Project through the Korea Health Industry Development Institute (KHIDI), funded by the Ministry of Health & Welfare and Ministry of science and ICT, Republic of Korea (HU20C0111).

## ACKNOWLEDGMENTS

A preliminary version of this paper was presented at the 6th congress of the European Academy of Neurology (36).

## SUPPLEMENTARY MATERIAL

The Supplementary Material for this article can be found online at: <https://www.frontiersin.org/articles/10.3389/fneur.2021.586366/full#supplementary-material>

2. Pantoni L. Cerebral small vessel disease: from pathogenesis and clinical characteristics to therapeutic challenges. *Lancet Neurol*. (2010) 9:689–701. doi: 10.1016/S1474-4422(10)70104-6
3. Chabriat H, Joutel A, Dichgans M, Tournier-Lasserre E, Boussier M-G. Cadasil. *Lancet Neurol*. (2009) 8:643–53. doi: 10.1016/S1474-4422(09)70127-9

4. Yoon CW, Kim Y-E, Seo SW, Ki C-S, Choi SH, Kim J-W, et al. NOTCH3 variants in patients with subcortical vascular cognitive impairment: a comparison with typical CADASIL patients. *Neurobiol Aging*. (2015) 36:2443.e1–7. doi: 10.1016/j.neurobiolaging.2015.04.009
5. Kim KW, Kwon H, Kim Y-E, Yoon CW, Kim YJ, Kim YB, et al. Multimodal imaging analyses in patients with genetic and sporadic forms of small vessel disease. *Sci Rep*. (2019) 9:787 doi: 10.1038/s41598-018-36580-0
6. Seo SW, Cho SS, Park A, Chin J, Na DL. Subcortical vascular versus amnesic mild cognitive impairment: comparison of cerebral glucose metabolism. *J Neuroimaging*. (2009) 19:213–9. doi: 10.1111/j.1552-6569.2008.00292.x
7. Fazekas F, Chawluk JB, Alavi A, Hurtig HI, Zimmerman RA. MR signal abnormalities at 1.5 T in Alzheimer's dementia and normal aging. *Am J Roentgenol*. (1987) 149:351–6. doi: 10.2214/ajr.149.2.351
8. Lee J, Kim S, Kim G, Seo S, Park H, Oh S, et al. Identification of pure subcortical vascular dementia using 11C-Pittsburgh compound B. *Neurology*. (2011) 77:18–25. doi: 10.1212/WNL.0b013e318221acee
9. Kim Y-E, Yoon CW, Seo SW, Ki C-S, Kim YB, Kim J-W, et al. Spectrum of NOTCH3 mutations in Korean patients with clinically suspicious cerebral autosomal dominant arteriopathy with subcortical infarcts and leukoencephalopathy. *Neurobiol Aging*. (2014) 35:726.e1–6. doi: 10.1016/j.neurobiolaging.2013.09.004
10. Ng PC, Henikoff S. Predicting deleterious amino acid substitutions. *Genome Res*. (2001) 11:863–74. doi: 10.1101/gr.176601
11. Ramensky V, Bork P, Sunyaev S. Human non-synonymous SNPs: server and survey. *Nucleic Acids Res*. (2002) 30:3894–900. doi: 10.1093/nar/gkf493
12. Song M-J, Lee S-T, Lee M-K, Ji Y, Kim J-W, Ki C-S. Estimation of carrier frequencies of six autosomal-recessive Mendelian disorders in the Korean population. *J Hum Genet*. (2012) 57:139. doi: 10.1038/jhg.2011.144
13. Greenberg SM, Vernooij MW, Cordonnier C, Viswanathan A, Salman RA-S, Warach S, et al. Cerebral microbleeds: a guide to detection and interpretation. *Lancet Neurol*. (2009) 8:165–74. doi: 10.1016/S1474-4422(09)70013-4
14. Kang Y. *Samsung Neuropsychological Screening Battery*. Current Research in Dementia. Seoul: The Korean Dementia Association (1998). p. 99–107.
15. Kang SH, Park YH, Lee D, Kim JP, Chin J, Ahn Y, et al. The cortical neuroanatomy related to specific neuropsychological deficits in Alzheimer's continuum. *Dementia Neurocogn Disord*. (2019) 18:77–95. doi: 10.12779/dnd.2019.18.3.77
16. Lee S-H, Lee S-T, Kim BJ, Park H-K, Kim C-K, Jung K-H, et al. Dynamic temporal change of cerebral microbleeds: long-term follow-up MRI study. *PLoS ONE*. (2011) 6:e25930. doi: 10.1371/journal.pone.0025930
17. Sachdev P, Wen W, Chen X, Brodaty H. Progression of white matter hyperintensities in elderly individuals over 3 years. *Neurology*. (2007) 68:214–22. doi: 10.1212/01.wnl.0000251302.55202.73
18. Miao Q, Paloneva T, Tuominen S, Pöyhönen M, Tuisku S, Viitanen M, et al. Fibrosis and stenosis of the long penetrating cerebral arteries: the cause of the white matter pathology in cerebral autosomal dominant arteriopathy with subcortical infarcts and leukoencephalopathy. *Brain Pathol*. (2004) 14:358–64. doi: 10.1111/j.1750-3639.2004.tb00078.x
19. Okeda R, Arima K, Kawai M. Arterial changes in cerebral autosomal dominant arteriopathy with subcortical infarcts and leukoencephalopathy (CADASIL) in relation to pathogenesis of diffuse myelin loss of cerebral white matter: examination of cerebral medullary arteries by reconstruction of serial sections of an autopsy case. *Stroke*. (2002) 33:2565–9. doi: 10.1161/01.STR.0000032620.91848.1C
20. Oberstein SL, Van den Boom R, Van Buchem M, Van Houwelingen H, Bakker E, Vollebregt E, et al. Cerebral microbleeds in CADASIL. *Neurology*. (2001) 57:1066–70. doi: 10.1212/WNL.57.6.1066
21. Lee JS, Kang C-h, Park SQ, Choi HA, Sim K-B. Clinical significance of cerebral microbleeds locations in CADASIL with R544C NOTCH3 mutation. *PLoS ONE*. (2015) 10:e0118163. doi: 10.1371/journal.pone.0118163
22. Schrag M, Greer DM. Clinical associations of cerebral microbleeds on magnetic resonance neuroimaging. *J Stroke Cerebrovasc Dis*. (2014) 23:2489–97. doi: 10.1016/j.jstrokecerebrovasdis.2014.07.006
23. Kalimo H, Ruchoux MM, Viitanen M, Kalaria RN. CADASIL: a common form of hereditary arteriopathy causing brain infarcts and dementia. *Brain Pathol*. (2002) 12:371–84. doi: 10.1111/j.1750-3639.2002.tb00451.x
24. Braun H, Schreiber S. Microbleeds in cerebral small vessel disease. *Lancet Neurol*. (2013) 12:735–6. doi: 10.1016/S1474-4422(13)70148-0
25. Poels MM, Ikram MA, van der Lugt A, Hofman A, Niessen WJ, Krestin GP, et al. Cerebral microbleeds are associated with worse cognitive function: the Rotterdam Scan Study. *Neurology*. (2012) 78:326–33. doi: 10.1212/WNL.0b013e3182452928
26. Yakushiji Y, Noguchi T, Hara M, Nishihara M, Eriguchi M, Nanri Y, et al. Distributional impact of brain microbleeds on global cognitive function in adults without neurological disorder. *Stroke*. (2012) 43:1800–5. doi: 10.1161/STROKEAHA.111.647065
27. Gold G, Kövari E, Herrmann FR, Canuto A, Hof PR, Michel J-P, et al. Cognitive consequences of thalamic, basal ganglia, and deep white matter lacunes in brain aging and dementia. *Stroke*. (2005) 36:1184–8. doi: 10.1161/01.STR.0000166052.89772.b5
28. Benjamin P, Lawrence AJ, Lambert C, Patel B, Chung AW, MacKinnon AD, et al. Strategic lacunes and their relationship to cognitive impairment in cerebral small vessel disease. *Neuroimage Clin*. (2014) 4:828–37. doi: 10.1016/j.nicl.2014.05.009
29. Akoudad S, Wolters FJ, Viswanathan A, de Bruijn RF, van der Lugt A, Hofman A, et al. Association of cerebral microbleeds with cognitive decline and dementia. *JAMA Neurol*. (2016) 73:934–43. doi: 10.1001/jamaneurol.2016.1017
30. Benjamin P, Trippier S, Lawrence AJ, Lambert C, Zeestraten E, Williams OA, et al. Lacunar infarcts, but not perivascular spaces, are predictors of cognitive decline in cerebral small-vessel disease. *Stroke*. (2018) 49:586–93. doi: 10.1161/STROKEAHA.117.017526
31. Jokinen H, Gouw A, Madureira S, Ylikoski R, Van Straaten E, Van Der Flier W, et al. Incident lacunes influence cognitive decline: the LADIS study. *Neurology*. (2011) 76:1872–8. doi: 10.1212/WNL.0b013e31821d752f
32. Gregoire S, Smith K, Jäger H, Benjamin H, Kallis C, Brown M, et al. Cerebral microbleeds and long-term cognitive outcome: longitudinal cohort study of stroke clinic patients. *Cerebrovasc Dis*. (2012) 33:430–5. doi: 10.1159/000336237
33. Liem M, Oberstein SL, Haan J, Van der Neut I, Ferrari M, Van Buchem M, et al. MRI correlates of cognitive decline in CADASIL: a 7-year follow-up study. *Neurology*. (2009) 72:143–8. doi: 10.1212/01.wnl.0000339038.65508.96
34. Lee MJ, Seo SW, Na DL, Kim C, Park JH, Kim GH, et al. Synergistic effects of ischemia and  $\beta$ -amyloid burden on cognitive decline in patients with subcortical vascular mild cognitive impairment. *JAMA Psychiatry*. (2014) 71:412–22. doi: 10.1001/jamapsychiatry.2013.4506
35. Kim HJ, Yang JJ, Kwon H, Kim C, Lee JM, Chun P, et al. Relative impact of amyloid- $\beta$ , lacunes, and downstream imaging markers on cognitive trajectories. *Brain*. (2016) 139:2516–27. doi: 10.1093/brain/aww148
36. Yoon CW, Seo SW. [EPR3032]: comparison of longitudinal changes of cerebral small vessel disease markers and cognitive function between subcortical vascular mild cognitive impairment with and without NOTCH3 variant: a 5-year follow-up study. *Eur J Neurol*. (2020) 27:434. doi: 10.1111/ene.14307

**Conflict of Interest:** The authors declare that the research was conducted in the absence of any commercial or financial relationships that could be construed as a potential conflict of interest.

Copyright © 2021 Yoon, Kim, Kim, Ki, Lee, Rha, Na and Seo. This is an open-access article distributed under the terms of the Creative Commons Attribution License (CC BY). The use, distribution or reproduction in other forums is permitted, provided the original author(s) and the copyright owner(s) are credited and that the original publication in this journal is cited, in accordance with accepted academic practice. No use, distribution or reproduction is permitted which does not comply with these terms.



# Screening for Cognitive Impairment After Stroke: Validation of the Chinese Version of the Quick Mild Cognitive Impairment Screen

Yangfan Xu<sup>1†</sup>, Lingrong Yi<sup>2†</sup>, Yangyang Lin<sup>1</sup>, Suiying Peng<sup>1</sup>, Weiming Wang<sup>1</sup>, Wujian Lin<sup>1</sup>, Peize Chen<sup>1</sup>, Weichao Zhang<sup>1</sup>, Yujie Deng<sup>1</sup>, Suimin Guo<sup>3</sup>, Le Shi<sup>1</sup>, Yuling Wang<sup>1\*</sup>, D. William Molloy<sup>4,5‡</sup> and Rónán O'Caoimh<sup>4,5,6\*‡</sup>

<sup>1</sup> Department of Rehabilitation Medicine, The Sixth Affiliated Hospital, Sun Yat-sen University, Guangzhou, China,

<sup>2</sup> Department of Rehabilitation Medicine, The Second Affiliated Hospital, Chongqing Medical University, Chongqing, China,

<sup>3</sup> Center for Child Health and Mental Health, Shenzhen Children's Hospital, Shenzhen, China, <sup>4</sup> Centre for Gerontology and Rehabilitation, University College Cork, St Finbarr's Hospital, Cork, Ireland, <sup>5</sup> Department of Geriatric Medicine, Mercy University Hospital, Cork, Ireland, <sup>6</sup> Clinical Sciences Institute, National University of Ireland Galway, Galway, Ireland

## OPEN ACCESS

### Edited by:

Robert Zivadinov,  
University at Buffalo, United States

### Reviewed by:

Jelle Demeestere,  
University Hospitals Leuven, Belgium  
Dejan Jakimovski,  
Buffalo Neuroimaging Analysis Center,  
United States

### \*Correspondence:

Yuling Wang  
wangyul@mail.sysu.edu.cn  
Rónán O'Caoimh  
rocaoinmh@hotmail.com

<sup>†</sup>These authors share first authorship

<sup>‡</sup>These authors share  
senior authorship

### Specialty section:

This article was submitted to  
Stroke,  
a section of the journal  
Frontiers in Neurology

**Received:** 30 September 2020

**Accepted:** 11 February 2021

**Published:** 05 March 2021

### Citation:

Xu Y, Yi L, Lin Y, Peng S, Wang W, Lin W, Chen P, Zhang W, Deng Y, Guo S, Shi L, Wang Y, Molloy DW and O'Caoimh R (2021) Screening for Cognitive Impairment After Stroke: Validation of the Chinese Version of the Quick Mild Cognitive Impairment Screen. *Front. Neurol.* 12:608188. doi: 10.3389/fneur.2021.608188

**Background:** Screening for post-stroke cognitive impairment (PSCI) is necessary because stroke increases the incidence of and accelerates premorbid cognitive decline. The Quick Mild Cognitive Impairment (*Qmci*) screen is a short, reliable and accurate cognitive screening instrument but is not yet validated in PSCI. We compared the diagnostic accuracy of a Chinese version of the *Qmci* screen (*Qmci*-CN) compared with the widely-used Chinese versions of the Montreal Cognitive Assessment (MoCA-CN) and Mini-Mental State Examination (MMSE-CN).

**Methods:** We recruited 34 patients who had recovered from a stroke in rehabilitation unit clinics in 2 university hospitals in China: 11 with post-stroke dementia (PSD), 15 with post-stroke cognitive impairment no dementia (PSCIND), and 8 with normal cognition (NC). Classification was made based on clinician assessment supported by a neuropsychological battery, independent of the screening test scores. The *Qmci*-CN, MoCA-CN, and MMSE-CN screens were administered randomly by a trained rater, blind to the diagnosis.

**Results:** The mean age of the sample was  $63 \pm 13$  years and 61.8% were male. The *Qmci*-CN had statistically similar diagnostic accuracy in differentiating PSD from NC, an area under the curve (AUC) of 0.94 compared to 0.99 for the MoCA-CN ( $p = 0.237$ ) and 0.99 for the MMSE-CN ( $p = 0.293$ ). The *Qmci*-CN (AUC 0.91), MoCA-CN (AUC 0.94), and MMSE-CN (AUC 0.79) also had statistically similar accuracy in separating PSD from PSCIND. The MoCA-CN more accurately distinguished between PSCIND and normal cognition than the *Qmci*-CN ( $p = 0.015$ ). Compared to the MoCA-CN, the administration times of the *Qmci*-CN (329s vs. 611s, respectively,  $p < 0.0001$ ) and MMSE-CN (280 vs. 611s, respectively,  $p < 0.0001$ ) were significantly shorter.

**Conclusion:** The *Qmci*-CN is accurate in identifying PSD and separating PSD from PSCIND in patients post-stroke following rehabilitation and is comparable to the widely-used MoCA-CN, albeit with a significantly shorter administration time.



The *Qmci*-CN had relatively poor accuracy in identifying PSCIND from NC and hence may lack accuracy for certain subgroups. However, given the small sample size, the study is under-powered to show superiority of one instrument over another. Further study is needed to confirm these findings in a larger sample size and in other settings (countries and languages).

**Keywords:** cognition screen, mild cognitive impairment, post-stroke dementia, China, stroke, *Qmci*-CN

## INTRODUCTION

Post-stroke cognitive impairment (PSCI) is increasingly prevalent among community-dwelling older adults, due to the increasing incidence and the decreasing mortality associated with stroke (1, 2). This trend is also evident in China (3). According to the degree of cognitive decline and impairment in activities of daily living (ADL), patients with PSCI can be divided into 2 groups: post-stroke cognitive impairment no dementia (PSCIND), those with slight cognitive impairment with or without subtle impairment in instrumental ADL (IADL) and those with established post-stroke dementia (PSD) with definite impairment in basic ADL (BADL) (4). PSCI is common in China, affecting ~80% of stroke survivors of which PSCIND and PSD represent around 49% and 32% of cases, respectively (5). Once established cognition may decline rapidly (6). Despite this, care usually focuses on post-stroke physical disability with less attention paid to cognitive decline (7–9). PSCI has a significant impact on independence and on the potential to return to work after stroke (10). Given these points, international guidelines recommend cognitive screening for those at risk of PSCI (4, 11).

As yet, no single screening and assessment tool is recommended, although tools should be selected according to the population being evaluated, the stage of progression based on functional status, the preferences of patients and families, as well as the resources available (4). Studies show that both the Montreal Cognitive Assessment (MoCA) and Mini Mental State Examination (MMSE) are both widely-used to detect cognitive impairment after stroke, though in a recent systematic review comparing the accuracy and utility of instruments, the MoCA was shown to be the most valid and clinically feasible to identify PSCI (12). The Chinese version of the MoCA (MoCA-CN) shows high sensitivity and specificity for PSCI (13) as well as other types of vascular cognitive impairment (14), although the Chinese version of MMSE (MMSE-CN) remains the most widely-used screening instrument in China (4).

The Quick mild cognitive impairment (*Qmci*) screen is a new, short cognitive screening instrument originally designed to identify mild cognitive impairment (MCI), which is highly accurate in differentiating between normal cognitive function, subjective cognitive disorders, MCI and early dementia (15, 16). The *Qmci* screen is more accurate than MMSE in detecting early cognitive changes (17–19) and when compared to the MoCA, it has similar accuracy and better specificity but a shorter administration time (20–22). The Chinese version of the *Qmci* (*Qmci*-CN) has recently been validated in a Chinese general rehabilitation outpatient clinic sample (23). To date, the *Qmci*

screen has not been examined in patients post-stroke. Given this point, the aim of this research was to investigate the diagnostic accuracy of the *Qmci*-CN in detecting cognitive impairment by comparing it to Chinese versions of the standardized MMSE (MMSE-CN) and MoCA (MoCA-CN) in patients recovering from stroke attending Chinese rehabilitation unit clinics.

## METHODS

### Participants

Consecutive participants were recruited by therapists from rehabilitation clinics in two hospitals in Guangzhou, China between August 2017 and April 2018. All patients were aged over 18 years of age and had a stroke diagnosed by a neurologist confirmed with brain imaging (CT or MRI). Only patients consented by their attending doctor participated. The study excluded patients who were unable to communicate verbally in Chinese or had communication problems that could influence the performance of cognitive testing such as severe dysphasia, apraxia, visual impairment, hearing loss, or altered consciousness. Patients with known dementia prior to the stroke or those with existing neurological, psychiatric disorders or other comorbidities that potentially affect cognitive function, e.g., Parkinson's disease were also excluded. Further, patients who couldn't read and write, those with a recent history of alcohol or drug abuse and those who declined to participate were excluded. All those included signed informed written consent. This study received ethical approval from The Six Affiliated Hospital of Sun Yat-sen University, reference number 2019ZSLYEC-110.

### The *Qmci*-CN

The *Qmci* screen has 6 subtests covering 5 cognitive domains (16). The first subtest examines orientation to place and time. The second, five-word registration, examines attention and working memory. The third, a clock drawing test, examines visuospatial/executive function and attention. The fourth subtest is delayed recall examining episodic memory (5-word recall). The next subtest is categorical verbal fluency tests semantic memory and language (e.g., naming of animals in 1 min). The final subtest is logical memory, immediate verbal recall of a short story, which also examines episodic memory. Each subtest is time-limited with an administration time of ~5 min for the *Qmci* screen (16). The total possible score is 100 points with higher scores suggesting normal cognition. The optimal cut-off score for cognitive impairment (MCI and dementia vs. normal controls) for the *Qmci* screen (original English language version) is  $\leq 62/100$  (20). However, the optimal cut-off for the Chinese

version (Qmci-CN) is lower at  $\leq 55/100$  (23). This difference is considered to be multi-factorial but most likely relates to the small sample of Chinese patients included in the single validation study to date (23).

## Data Collection

Patients' characteristics including their age, sex, educational level, and other demographic and clinical information were collected. The Qmci-CN, MoCA-CN, and MMSE-CN were administered in random order by a trained rater, who was blind to the diagnosis. The interval between administration of the scales was  $\sim 5$  min. Following screening, patients were administered a battery of neuropsychologist tests and the Lawton Instrumental Activities of Daily Living (IADL) scale (24) scale to support a clinician to make a diagnosis and classify patients into those with normal cognition, PSCIND, and PSD. The diagnostic classification was made independent of the results of the cognitive screening instruments. The following neuropsychological tests were used to assess cognitive function: (1) The Auditory Verbal Learning Test–H tested memory including immediate and delayed recall (25); (2) The Rey-Osterrieth Complex Figure Test (RCFT) was used to examine the visuospatial function domain (26, 27); (3) Animal Fluency Test was used to assess language (27); (4) and the Chinese modified version of the Trail Making Test (TMT-A, TMT-B) was used to examine executive function (28). The caregiver burden inventory was also administered to the family or nurse of the patient to assess carer strain (29). These widely-used scales were chosen as they have good reliability and validity. PSCIND was diagnosed among those with decline in at least 1 cognitive domain (memory, visuospatial function, language and executive function) but normal or subtle functional IADL decline related to cognitive decline rather than stroke-related (4). PSD was diagnosed if at least 2 out of 4 cognitive function domains were impaired on the neuropsychologist tests with ADL impairment attributable to cognitive decline rather than stroke-related physical disability.

## Statistical Analyses

Statistical analyses were performed with SPSS 20.0 and MEDCALC® 19.2.0. The Chi-squared ( $\chi^2$ ) test was used to investigate differences between categorical variables among groups. Normality was tested with Shapiro-Wilk test. If variables were normally distributed, then Levene's test for homogeneity of variance was performed. Variables with homogeneity of variance, were compared using a student *t*-test or one-way analysis of variance (ANOVA) for differences between three or more groups (NC, PSCIND and PSD). If data weren't normally distributed, the Kruskal-Wallis H test was used to test for differences between the 3 diagnostic groups. Significance was set a level of 0.05. Receiver operating characteristic (ROC) curve analysis was used to assess diagnostic accuracy based on the area under the curve (AUC). ROC curves were compared using the DeLong method (30). Accuracy was excellent if AUC results were between 0.90 and 1.0, good if they were between 0.8 and 0.9, fair if between 0.7 and 0.8, poor between 0.6 and 0.7, and where values were found to be between 0.50 and 0.60 they were regarded as a fail. The optimal cut-off for each test was determined from Youden's

Index ( $J = \text{sensitivity} + \text{specificity} - 1$ ). We estimated sample size using a precision-based calculation. Here as the expected prevalence of cognitive impairment (PSD or PSCIND) was  $\sim 70\%$  based on existing studies (5) and the sensitivity and specificity of the Qmci-CN for detecting cognitive impairment is  $\sim 85\%$  [based on existing studies of the instrument (15)], it was estimated that between 70 and 164 patients would be required at a precision of 0.1 (10%) at a significance of 0.05 ( $\alpha$ ).

## RESULTS

In all, 230 patients with stroke were screened for the study, 125 patients with stroke were excluded as they met exclusion criteria, while 54 declined to participate. Hence, 51 patients with stroke were recruited. Among these, 17 patients did not complete the full assessment. Of the final sample of 34 patients included, 8 had normal cognition (NC), 15 were classified as having PSCIND and 11 patients were diagnosed with PSD. Patient characteristics are presented in **Table 1**. In all, 13 (38.2%) participants were female. The mean age of the total sample was 63 years, with a standard deviation (SD) of 13 years. The mean ( $\pm$ SD) age of those in the NC, PSCIND, and PSD group were 58 ( $\pm 13$ ), 65 ( $\pm 11$ ), and 65 ( $\pm 16$ ) years, respectively. The mean ( $\pm$ SD) number of years in education of all participants was 13( $\pm 4$ ) years, with a mean of 14( $\pm 5$ ), 13( $\pm 3$ ), and 10( $\pm 5$ ) among the NC, PSCIND and PSD groups, respectively. There were no statistically significant differences in age ( $p = 0.338$ ), sex ( $p = 0.254$ ), or educational level ( $p = 0.306$ ) between the 3 diagnostic groups. The interval between presentation with stroke and the assessment varied from 2 weeks up to 13 years.

## Cognitive Test Scoring and Administration

The median scores and administration times for each diagnostic group with their interquartile range (IQR) including comparisons between all 3 diagnostic groups and pair-wise comparisons are presented in **Table 2**. We found statistically significant differences in total median test scores between all 2 diagnostic groups (NC, PSCIND, and PSD) ( $p < 0.01$ ). Analyses showed that all 3 diagnostic groups were different from each other, and higher tests scores related with higher level of cognitive ability. While the MoCA showed a clear gradient in median scores from NC to PSCIND and PSD (decreasing from 27 to 22 to 13), the Qmci-CN had similar median scores for NC and PSCIND. The MMSE-CN had similar values for PSCIND and PSD. Comparisons between administration times for the cognitive screens are presented in **Table 3**. The median ( $\pm$  IQR) administration time for the Qmci-CN was  $328.50 \pm 50.25$  s vs.  $610.87 \pm 116.75$  for the MoCA-CN, a statistically significant difference ( $p < 0.0001$ ). The median administration time for the MMSE-CN was  $280.17 \pm 43.75$ , which was also shorter than the MoCA-CN ( $p < 0.0001$ ). Examining administration times by diagnostic classification group showed that there were no significant differences for either the Qmci-CN ( $p = 0.144$ ), MoCA-CN ( $p = 0.333$ ), or MMSE-CN ( $p = 0.173$ ). A moderate gradient effect was seen with the Qmci-CN ( $r = 0.52$ ,  $p = 0.771$ ); those with better cognition had higher scores, albeit these were not statistically significantly shorter.

**TABLE 1 |** Characteristics of the participants included in total ( $n = 34$ ) and according to diagnosis classification.

Characteristics	All ( $n = 34$ ) N (%) or Mean $\pm$ SD [Range]	NC ( $n = 8$ ) N (%) or Mean $\pm$ SD [Range]	PSCIND ( $n = 15$ ) N (%) or Mean $\pm$ SD [Range]	PSD ( $n = 11$ ) N (%) or Mean $\pm$ SD [Range]	$P = x$
<b>Gender</b>					
Female	13 (38.2%)	1 (12.5%)	5 (33.3%)	6 (54.5%)	0.254
Male	21 (61.8%)	7 (87.5%)	9 (60%)	5 (45.5%)	
Age (years)	63.38 $\pm$ 13.07 [31–85]	57.75 $\pm$ 12.78 [31–71]	65.4 $\pm$ 11.12 [45–79]	64.73 $\pm$ 15.58 [43–85]	0.338
Education (years)	12.56 $\pm$ 4.25 [0–19]	14.25 $\pm$ 4.56 [6–19]	13 $\pm$ 3.29 [6–17]	10.74 $\pm$ 4.86 [0–19]	0.306
<b>Living arrangements</b>					
Living with family	26 (76.5%)	8 (100%)	12 (80%)	8 (90.9%)	0.188
Living with a formal carer	6 (17.6%)	0 (0%)	3 (20%)	2 (18.2%)	
Living alone	2 (5.9%)	0 (0%)	0 (0%)	1 (9.1%)	
<b>Work intensity</b>					
Low	11 (32.4%)	3 (37.5%)	6 (40%)	1 (9.1%)	0.110
Medium	5 (14.7%)	3 (37.5%)	6 (40%)	7 (63.6%)	
High	5 (14.7%)	2 (25%)	2 (13.3%)	1 (9.1%)	
Other (none, volunteer or not provided)	13 (38.2%)	0 (0%)	1 (6.7%)	2 (18.2%)	
Hypertension (proportion with)	20 (58.8%)	4 (50%)	12 (80%)	10 (90.0%)	0.021*
Hyperglycaemia (proportion with)	13 (38.2%)	3 (37.5%)	5 (33.3%)	4 (36.4%)	0.204
Hyperlipemia (proportion with)	9 (26.5%)	1 (12.5%)	8 (53.3%)	1 (9.1%)	0.034*
Dyssomnia (proportion with)	7 (20.6%)	2 (25%)	4 (26.7%)	1 (9.1%)	0.202

NC, normal cognitive; PSCIND, post-stroke cognitive impairment no dementia; PSD, post-stroke dementia; SD, standard deviation.

\*Statistically significant ( $p < 0.05$ ).

**TABLE 2 |** Test scores and administration times for the Chinese versions of the quick mild cognitive impairment screen (Qmci-CN), montreal cognitive assessment (MoCA-CN) and mini mental state examination (MMSE-CN) by diagnostic group.

Cognitive test (score/ administration time)	Total sample ( $n = 34$ )	NC ( $n = 8$ )	PSCIND ( $n = 15$ )	PSD ( $n = 11$ )	Kruskal– Wallis H-test comparing all 3 groups ( $P = x$ )	NC vs. PSCIND ( $P = x$ )	NC vs. Post-stroke CI (PSCIND & PSD) ( $P = x$ )	PSCIND vs. PSD ( $P = x$ )
Qmci-CN scores (median $\pm$ IQR)	55.50 $\pm$ 14.25 [0–69]	57.50 $\pm$ 8.25 [48–66]	57.00 $\pm$ 7.00 [47–69]	37.00 $\pm$ 35.00 [4–57]	$P < 0.001^*$	$P = 0.548$	$P = 0.074$	$P < 0.001^*$
MoCA-CN scores (median $\pm$ IQR)	22.00 $\pm$ 8.50 [1–30]	27.00 $\pm$ 5.50 [22–30]	22.00 $\pm$ 3.00 [15–27]	13.00 $\pm$ 9.00 [1–22]	$P < 0.001^*$	$P = 0.007^*$	$P < 0.001^*$	$P < 0.001^*$
MMSE-CN scores (median $\pm$ IQR)	25.00 $\pm$ 3.79 [0–30]	27.00 $\pm$ 1.00 [25–29]	24.00 $\pm$ 3.71 [23–30]	23.00 $\pm$ 17.00 [0–25]	$P = 0.001^*$	$P = 0.040$	$P = 0.003^*$	$P = 0.011$
Qmci-CN time (s) (median $\pm$ IQR)	328.50 $\pm$ 50.25 [150–408]	273.00 $\pm$ 91.00 [230–382]	331.00 $\pm$ 41.00 [298–406]	335.00 $\pm$ 45.00 [150–408]	$P = 0.144$	$P = 0.034$	$P = 0.082$	$P = 0.878$
MoCA-CN time (s) (median $\pm$ IQR)	610.87 $\pm$ 116.75 [176–1023]	580.50 $\pm$ 154.65 [357–633]	617.00 $\pm$ 186.00 [454–791]	610.87 $\pm$ 286.00 [176–1023]	$P = 0.333$	$P = 0.076$	$P = 0.110$	$P = 1.000$
MMSE-CN time(s) (median $\pm$ IQR)	280.17 $\pm$ 43.75 [178–510]	255.00 $\pm$ 59.38 [178–326]	280.17 $\pm$ 15.00 [193–329]	280.17 $\pm$ 70.00 [182–510]	$P = 0.173$	$P = 0.076$	$P = 0.110$	$P = 0.799$

CI, cognitive impairment; IQR, interquartile range; NC, normal cognition; PSCIND, post-stroke cognitive impairment no dementia; PSD, post-stroke dementia. \*Statistically significant ( $p < 0.01$ ).

**TABLE 3 |** ANOVA *Post-hoc* pair-wise analysis comparing administration times for the Qmci-CN screen, MoCA-CN, and MMSE-CN.

Variable	Group 1	Group 2	Mean difference	Std. error	P-value	95% Confidence interval	
						Lower bound	Upper bound
Time taken	Qmci-CN	MoCA-CN	-291.753	30.567	<0.0001	-368.33	-215.18
	Qmci-CN	MMSE-CN	38.951	18.562	0.123	-7.48	85.38
	MoCA-CN	MMSE-CN	330.704	33.434	<0.0001	247.84	413.57

MMSE-CN, mini mental state examination; MoCA-CN, montreal cognitive assessment; Qmci-CN, quick mild cognitive impairment screen.

**TABLE 4 |** Area Under the Curve (AUC) values and optimal cut-offs for the Chinese versions of the quick mild cognitive impairment (Qmci-CN) screen, montreal cognitive assessment (MoCA-CN), and mini mental state examination (MMSE-CN).

Diagnostic classification	Cognitive screen	AUC [95% CI]	Optimal cut-off point (youden index)	Sensitivity and specificity [%]
PSCIND vs. NC	Qmci-CN	0.583 [0.336–0.831]	≤55.5	Sensitivity = 88%, Specificity = 53%
	MoCA-CN	0.842 [0.672–1.000]	≤26	Sensitivity = 63%, Specificity = 7%
	MMSE-CN	0.763 [0.561–0.964]	≤26.5	Sensitivity = 88%, Specificity = 27%
PSD vs. NC	Qmci-CN	0.938 [0.833–1.000]	≤47	Sensitivity = 100%, Specificity = 18%
	MoCA-CN	0.994 [0.972–1.000]	≤19.5	Sensitivity = 100%, Specificity = 9%
	MMSE-CN	0.983 [0.935–1.000]	≤26	Sensitivity = 88%, Specificity = 0%
PSD vs. PSCIND	Qmci-CN	0.909 [0.783–1.000]	≤46.5	Sensitivity = 100%, Specificity = 18%
	MoCA-CN	0.936 [0.839–1.000]	≤18.5	Sensitivity = 93%, Specificity = 9%
	MMSE-CN	0.791 [0.613–0.969]	≤21	Sensitivity = 100%, Specificity = 55%
Post stroke CI (PSCIND/PSD) vs. NC	Qmci-CN	0.733 [0.558–0.909]	≤55.5	Sensitivity = 88%, Specificity = 39%
	MoCA-CN	0.906 [0.800–1.000]	≤21.5	Sensitivity = 100%, Specificity = 39%
	MMSE-CN	0.856 [0.727–0.984]	≤26.5	Sensitivity = 88%, Specificity = 15%
PSD vs. Post stroke CI (NC/PSCIND)	Qmci-CN	0.919 [0.808–1.000]	≤46.5	Sensitivity = 100%, Specificity = 18%
	MoCA-CN	0.957 [0.889–1.000]	≤18.5	Sensitivity = 96%, Specificity = 9%
	MMSE-CN	0.858 [0.730–0.985]	≤23.64	Sensitivity = 74%, Specificity = 27%

CI, cognitive impairment; NC, normal cognition; PSCIND, post-stroke cognitive impairment no dementia; PSD, post stroke dementia.

## Screening for Post-stroke Cognitive Impairment (PSCIND and PSD)

Measures of diagnostic accuracy including optimal cut-offs for each instrument are presented in **Table 4**. Cross cross-tabulated results are provided as **Supplementary Material**. Comparisons between instruments are presented in **Table 5**. ROC curve analyses showed that the Qmci-CN, MoCA-CN and MMSE-CN had similar accuracy in separating PSD from NC; the MoCA-CN (AUC 0.994) had slightly higher accuracy but this was not

statistically greater than the Qmci-CN (AUC 0.938) or MMSE-CN (AUC 0.983). At their optimal cut-offs, all 3 tests showed excellent sensitivity but poor specificity for the ability to separate PSD from NC. The Qmci-CN had an optimal cut-off score of ≤47 vs. ≤19.5 for the MoCA-CN and ≤26 for the MMSE-CN. The results also showed that the Qmci-CN, MMSE-CN, and MoCA-CN had statistically similar accuracy in separating PSCIND from PSD. The Qmci-CN had an AUC of 0.906 compared to an AUC of 0.936 for the MoCA-CN and an AUC of 0.791 for the MMSE-CN.



**TABLE 5 |** Pair-wise comparisons between the diagnostic accuracy of the Chinese versions of the quick mild cognitive impairment (*Qmci*-CN) screen, montreal cognitive assessment (MoCA-CN) and mini mental state examination (MMSE-CN).

Diagnostic classification	Comparison group (area under the curve)		Z-statistic	P-value
PSCIND vs. NC	<i>Qmci</i> -CN	MoCA-CN	2.442	0.015*
	(0.583)	(0.842)		
	<i>Qmci</i> -CN	MMSE-CN	1.457	0.145
	(0.583)	(0.763)		
	MoCA-CN	MMSE-CN	0.747	0.455
	(0.842)	(0.763)		
PSD vs. NC	<i>Qmci</i> -CN	MoCA-CN	0.517	0.237
	(0.938)	(0.994)		
	<i>Qmci</i> -CN	MMSE-CN	1.818	0.293
	(0.938)	(0.983)		
	MoCA-CN	MMSE-CN	1.866	0.406
	(0.994)	(0.983)		
PSD vs. PSCIND	<i>Qmci</i> -CN	MoCA-CN	0.517	0.605
	(0.909)	(0.936)		
	<i>Qmci</i> -CN	MMSE-CN	1.818	0.069
	(0.909)	(0.791)		
	MoCA-CN	MMSE-CN	1.866	0.062
	(0.936)	(0.791)		
Post stroke CI (PSCIND/PSD) vs. NC	<i>Qmci</i> -CN	MoCA-CN	2.489	0.013*
	(0.733)	(0.906)		
	<i>Qmci</i> -CN	MMSE-CN	1.594	0.111
	(0.733)	(0.856)		
	MoCA-CN	MMSE-CN	0.842	0.400
	(0.906)	(0.856)		
PSD vs. NC/PSCIND	<i>Qmci</i> -CN	MoCA-CN	0.795	0.426
	(0.919)	(0.957)		
	<i>Qmci</i> -CN	MMSE-CN	1.216	0.224
	(0.919)	(0.858)		
	MoCA-CN	MMSE-CN	1.821	0.069
	(0.957)	(0.858)		

CI, cognitive impairment; NC, normal cognition; PSCIND, post-stroke cognitive impairment no dementia; PSD, post-stroke dementia.

\*Statistically Significant.

ROC analysis showed that the *Qmci*-CN had an AUC of 0.733 compared with AUCs of 0.906 and 0.856 for the MoCA-CN and MMSE-CN, respectively, in separating PSCI (either PSCIND/PSD) from NC. The *Qmci*-CN was less accurate than the MoCA-CN ( $p = 0.013$ ) but was similar to the MMSE-CN ( $p = 0.11$ ) in differentiating PSCI (either PSCIND/PSD) from NC. The *Qmci*-CN was also less accurate in its ability to distinguish PSCIND from NC (AUC 0.583) compared with the MoCA-CN (AUC of 0.842), ( $p = 0.015$ ). ROC curves are presented in **Figure 1**.

## DISCUSSION

This study compared the diagnostic accuracy of the newly-developed *Qmci*-CN for its ability to screen for PSCI with

the widely-used MoCA-CN and MMSE-CN in a rehabilitation population in China. This is, to our knowledge, the first study validating the *Qmci* screen in a post-stroke population in any language. The results showed that all three of these scales are equally able to differentiate PSD from NC and PSD from PSCIND. The *Qmci*-CN had excellent accuracy (AUC > 0.90) in separating both diagnostic groups but poor accuracy in distinguishing PSCIND from NC. While the MoCA-CN was significantly more accurate in separating post-stroke CI (either PSCIND or PSD) from normal and in turn PSCIND from NC than the *Qmci*-CN, it had a statistically significantly longer median administration time. The MoCA-CN took almost twice as long to score. This is a consistent finding in studies comparing the two instruments (15). It also had similar accuracy to the MMSE-CN but again longer administration times. The *Qmci*-CN and MMSE-CN had similar administration times in this study.

These results are different from previous research examining the diagnostic accuracy of other language versions of the *Qmci*, especially the English version, which show that the *Qmci* screen is more accurate in discriminating MCI (equivalent of PSCIND) from both normal controls and dementia than the MoCA and the MMSE (17–20). These studies also generally show that the MMSE is less accurate than both the MoCA and *Qmci* screen (15). The reasons for why this study differs from others is most likely related to its very small sample size. Sample size calculations based on previous studies suggest that this study was not powered adequately to show superiority of one test over the other. The sample size in some of the diagnostic groups, particularly the NC group ( $N = 8$ ), is too small to interpret the findings reliably. Further, those included in this study were a different cohort with all patients recovering from an acute stroke. These may have cognitive impairment in multiple other cognitive domains, while retaining memory (31). The *Qmci*-CN is better able to detect amnesic type cognitive impairment (32) compared with other short screens as it is more heavily weighted toward memory. This said, the goal of this study was not to show superiority of the *Qmci*-CN but to examine its utility and psychometric properties in patients post-stroke compared with more-commonly used screening tests.

This study also examines the optimal cut-off points for the 3 instruments to identify NC, PSCIND, and PSD. At the established cut-off for cognitive impairment ( $\leq 26$ ) rather than post-stroke cognitive impairment ( $\leq 22$ ) (33), the MoCA had excellent sensitivity but poor specificity. While the MMSE may lack sensitivity for single domain cognitive impairment (33), using the optimal cut-off points identified using Youden's Index, this study found that the MMSE had a similarly high sensitivity but low specificity. The optimal cut-off point for the *Qmci*-CN in separating PSCIND from NC was  $\leq 55.5$  compared with  $\leq 47$  to differentiate PSD from normal. While lower than the results in Irish (20) and Canadian (34) cohorts in patients attending memory clinics, these are more similar to results in Turkey ( $< 53$  for separating MCI from normal cognition) (22, 35) and recently in Greece ( $< 51$  for separating MCI from normal cognition) (36). Possible reasons for this difference might include the background of participants including their educational level, albeit the sample included here had a similar median number

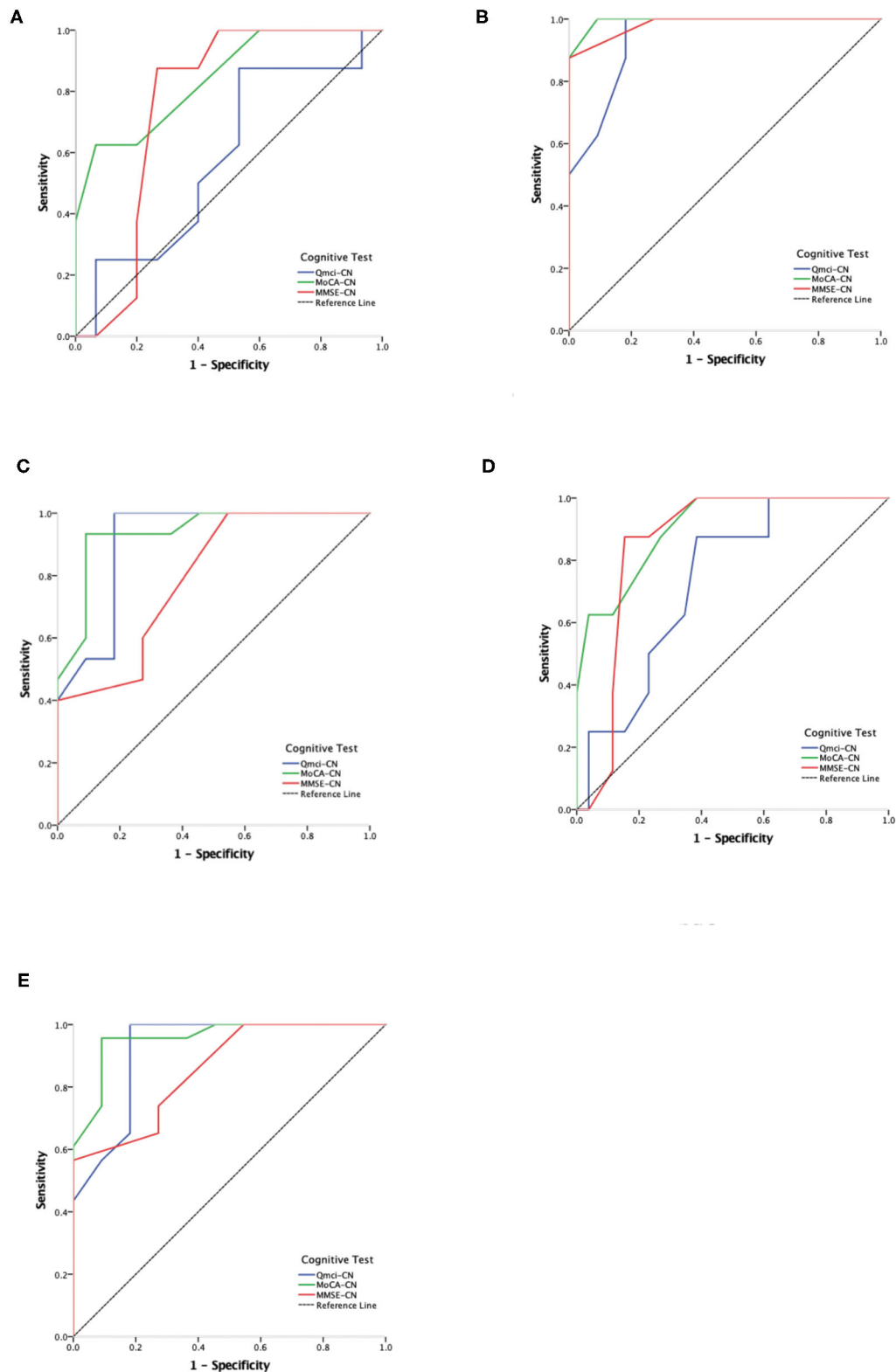


**FIGURE 1 |** Receiver Operating Characteristic (ROC) curve analysis comparing the Chinese versions of the Quick Mild Cognitive Impairment (Qmci-CN) screen, Montreal Cognitive Assessment (MoCA-CN) and Mini Mental State Examination (MMSE-CN) in separating normal cognition (NC), post-stroke cognitive impairment no dementia (PSCIND) and post-stroke dementia (PSD). **(A)** NC vs. PSCIND; **(B)** NC vs. PSD; **(C)** PSCIND vs. PSD; **(D)** NC vs. PSCIND/PSD; **(E)** PSD vs. NC/PSCIND.

of years in education to those in North America and Western Europe and higher than those in Turkey and Greece. Again the setting may have influenced the cut-offs as all patients here were recruited from rehabilitation clinics having had a recent acute stroke. This may have influenced the performance of patients in testing across several cognitive domains resulting in lower total scores, irrespective of diagnostic classification. However, given that this is a small sample, care should be taken when interpreting and applying these cut-offs. The authors caution that normative data are required to develop accurate cut-off scores for the *Qmci*-CN and to determine if these are comparable with the English language version of the *Qmci* screen.

## LIMITATIONS

This study has a number of limitations as follows. First, the definitions of PSCI in the literature and in clinical practice are variable, differing from study to study (37). In our research, we defined PSCI as a post-stroke neuropsychological syndrome with any cognitive impairment, which develops following a stroke event, including the subgroups of PSD and PSCIND. This definition does not suggest any particular underlying neuropathological process. Other definitions include time limits on the onset of cognitive decline, though we did not apply this. This is a limitation. For example, a national Korean study examining the epidemiology of vascular cognitive defined PSD as any major cognitive impairment evident more than 3 months after a stroke (38). Others suggest the final diagnosis of PSD should be delayed until at least 6 months as stroke commonly results in delirium or transient reductions in cognition that do not persist. Hence, making the diagnosis too early may result in a higher prevalence of PSCI than would be expected (39). Here no time interval was pre-specified and we recruited patients having completed a stroke at least 2 weeks but up to 13 years after the event. Hence, to ensure homogeneity and comparability, further study applying pre-specified time-based definitions of PSCI are therefore needed. Second, as the diagnostic criteria for PSCI incorporates ADL function and many patients with stroke have related physical impairment, it can be difficult to assess whether the changes in ADLs are truly related to cognitive impairment (37). This may increase the heterogeneity among the 3 groups and is a potential confounder. Thirdly, as patients were all recruited from the department of rehabilitation medicine, most of these may have completed cognitive assessment before, with either the MoCA-CN and the MMSE-CN, potentially creating learning effects and introducing bias. This said, none of the patients would have been tested with the *Qmci*-CN while inpatients. Finally, the sample here is small and likely prone to selection bias, reducing the generalisability of the results and under-powering the study to show superiority of one screening instrument over another based on our sample size calculation, increasing the chance of type II errors. Only those who received rehabilitation were available and included, potentially reducing the generalisability of the findings. Hence, further studies examining these instruments in a broader sample of

patients post-stroke including those who did not receive formal rehabilitation or were unlikely to benefit from rehabilitation should be recruited. As the sample size was small, recruitment in multiple sites over a longer period of time is also needed to increase the reliability, generalisability and ability to confirm superiority of one instrument over another.

## CONCLUSION

In conclusion, the *Qmci*-CN was accurate in screening for PSD in a post-stroke rehabilitation clinic and had excellent accuracy in separating PSD from PSCIND and PSD from NC. The administration time of the *Qmci*-CN was significantly lower than the MoCA-CN, suggesting it is a reasonable alternative in busy clinics. However, the *Qmci*-CN had poor accuracy in separating PSCIND from NC and PSCI from NC, suggesting it may lack accuracy for certain subgroups even if its administration time is shorter. The MoCA-CN and MMSE-CN both had similar accuracy in PSCI, which given the shorter administration time of the MMSE-CN suggests that it may be the better instrument to use in this setting. However, because this was a small study, under-powered to show superiority of one instrument over another, with several limitations, further study is now needed before recommending the routine use of the *Qmci*-CN in order to confirm these findings by recruiting a larger sample size and externally validating the *Qmci*-CN in other samples and populations.

## DATA AVAILABILITY STATEMENT

The raw data supporting the conclusions of this article will be made available by the authors, without undue reservation.

## ETHICS STATEMENT

The studies involving human participants were reviewed and approved by this study received ethical approval from The Sixth Affiliated Hospital of Sun Yat-sen University, reference number 2019ZSLYEC-110. The patients/participants provided their written informed consent to participate in this study.

## AUTHOR CONTRIBUTIONS

YX and LY: design, concept, data collection, analysis, writing, and revising manuscript. YW: design, concept, and supervision. YL, SP, WW, WL, PC, WZ, YD, SG, and LS: concept and data collection. YX and LY: statistical analysis and supervision of statistics. DM: design and concept. RO'C: design, concept, analysis, writing, and revising manuscript. All authors contributed to the article and approved the submitted version.

## FUNDING

The work described in this manuscript was fully supported by a grant from the Guangzhou Municipal Technological Major Tackling Plan Modern Industrial Technology Project of

China (Grant No. 201802010039), the Guangdong Hopson-Pearl River Education Development Foundation (Grant No. H20190116202012724) and two grants from the National Natural Science Foundation of China (Grant Nos. 81601981 and 81472155).

## REFERENCES

- Feigin VL, Lawes CM, Bennett DA, Barker-Collo SL, Parag V. Worldwide stroke incidence and early case fatality reported in 56 population-based studies: a systematic review. *Lancet Neurol.* (2009) 8:355–69. doi: 10.1016/S1474-4422(09)70025-0
- Pendlebury ST, Rothwell PM. Prevalence, incidence, and factors associated with pre-stroke and post-stroke dementia: a systematic review and meta-analysis. *Lancet Neurol.* (2009) 8:1006–18. doi: 10.1016/S1474-4422(09)70236-4
- Liu M, Wu B, Wang WZ, Lee LM, Zhang SH, Kong LZ. Stroke in China: epidemiology, prevention, and management strategies. *Lancet Neurol.* (2007) 6:456–64. doi: 10.1016/S1474-4422(07)70004-2
- Chinese Stroke Association. Post-stroke cognitive impairment management expert committee. Expert consensus on Post-stroke cognitive impairment management. *Chin J Stroke.* (2017) 12:519–31. doi: 10.3969/j.issn.1673-5765.2017.06.011
- Qu Y, Zhuo L, Li N, Hu Y, Chen W, Zhou Y, et al. Prevalence of post-stroke cognitive impairment in China: a community-based, cross-sectional study. *PLoS ONE.* (2015) 10:e0122864. doi: 10.1371/journal.pone.0122864
- Levine DA, Galecki AT, Langa KM, Unverzagt FW, Kabeto MU, Giordani B, et al. Trajectory of cognitive decline after incident stroke. *JAMA.* (2015) 314:41–51. doi: 10.1001/jama.2015.6968
- Lees R, Fearon P, Harrison JK, Broomfield NM, Quinn TJ. Cognitive and mood assessment in stroke research: focused review of contemporary studies. *Stroke.* (2012) 43:1678–80. doi: 10.1161/STROKEAHA.112.653303
- McKevitt C, Fudge N, Redfern J, Sheldenkar A, Crichton S, Rudd AR, et al. Self-Reported long-term needs after stroke. *Stroke.* (2011) 42:1398–403. doi: 10.1161/STROKEAHA.110.598839
- Pollock A, St George B, Fenton M, Firkins L. Top ten research priorities relating to life after stroke. *Lancet Neurol.* (2012) 11:209. doi: 10.1016/S1474-4422(12)70029-7
- Fride Y, Adamit T, Maier A, Ben Assayag E, Bornstein NM, Korczyn AD, et al. What are the correlates of cognition and participation to return to work after first ever mild stroke? *Top Stroke Rehabil.* (2015) 22:317–25. doi: 10.1179/1074935714Z.00000000013
- Go AS, Mozaffarian D, Roger VL, Benjamin EJ, Berry JD, et al. Heart disease and stroke statistics—2013 update: a report from the American heart association. *Circulation.* (2012) 127:e6–245. doi: 10.1161/CIR.0b013e31828124ad
- Burton L, Tyson S. Screening for cognitive impairment after stroke: a systematic review of psychometric properties and clinical utility. *J Rehabil Med.* (2015) 47:193–203. doi: 10.2340/16501977-1930
- Chen KL, Xu Y, Chu AQ, Ding D, Liang XN, Nasreddine ZS, et al. Validation of the Chinese version of montreal cognitive assessment basic for screening mild cognitive impairment. *J Am Geriatr Soc.* (2016) 64:e285–90. doi: 10.1111/jgs.14530
- GhafariMZZA, Miptah HN, O'Caioimh R. Cognitive screening instruments to identify vascular cognitive impairment: a systematic review. *Int J Geriatr Psychiatry.* (2019) 34:1114–27. doi: 10.1002/gps.5136
- O'Caioimh R, Molloy DW. The quick mild cognitive impairment screen (Qmci). In: Larner AJ, editor. *Cognitive Screening Instruments*. Cham: Springer. doi: 10.1007/978-3-319-44775-9\_12
- O'Caioimh R, Gao Y, Gallagher PF, Eustace J, McGlade C, Molloy DW. Which part of the quick mild cognitive impairment screen (Qmci) discriminates between normal cognition, mild cognitive impairment and dementia? *Age Ageing.* (2013) 42:324–30. doi: 10.1093/ageing/af044
- O'Caioimh R, Gao Y, McGlade C, Healy L, Gallagher P, Timmons S, et al. Comparison of the quick mild cognitive impairment (Qmci) screen and the SMMSE in screening for mild cognitive impairment. *Age Ageing.* (2012) 41:624–9. doi: 10.1093/ageing/afs059
- Bunt S, O'Caioimh R, Krijnen WP, Molloy DW, Goodijk GP, van der Schans CP, et al. Validation of the dutch version of the quick mild cognitive impairment screen (Qmci-D). *BMC Geriatr.* (2015) 15:115. doi: 10.1186/s12877-015-0113-1
- Clarnette R, Goh M, Bharadwaj S, Ryan J, Ellis S, Svendrovski A, et al. Screening for cognitive impairment in an Australian aged care assessment team as part of comprehensive geriatric assessment. *Aging Neuropsychol Cogn.* (2019) 26:336–47. doi: 10.1080/13825585.2018.1439447
- O'Caioimh R, Timmons S, Molloy DW. Screening for mild cognitive impairment: comparison of “MCI specific” screening instruments. *J Alz Dis.* (2016) 51:619–29. doi: 10.3233/JAD-150881
- Clarnette R, O'Caioimh R, Antony DN, Svendrovski A, Molloy DW. Comparison of the quick mild cognitive impairment (Qmci) screen to the montreal cognitive assessment (MoCa) in an Australian geriatrics clinic. *Int J Geriatr Psychiatry.* (2016) 32:643–9. doi: 10.1002/gps.4505
- Yavuz BB, Varan HD, O'Caioimh R, Kizilarslanoglu MC, Kilic MK, Molloy DW, et al. Validation of the turkish version of the quick mild cognitive impairment screen. *Am J Alzheimer's Dis Other Dement.* (2017) 32:145–56. doi: 10.1177/1533317517691122
- Xu Y, Lin Y, Yi L, Li Z, Li X, Yu Y, et al. Screening for cognitive frailty using short cognitive screening instruments: comparison of the Chinese versions of the MoCA and Qmci screen. *Front Psychol.* (2020) 11:558. doi: 10.3389/fpsyg.2020.00558
- Wen-Jia J, Jing S, Jing-Nian NI. Activities of daily living rating for differentiating mild cognitive impairment and dementia. *Chin J Gerontol.* (2014) 34:865–8. doi: 10.3969/j.issn.1005-9202.2014.04.001
- Qinjie LI, Ya M, Yuan Z, Geriatrics DO. Auditory verbal learning test-huashan version in the diagnosis of amnesic mild cognitive impairment. *Geriatr Health Care.* (2016) 16:282–285. doi: 10.3969/j.issn.1008-8296.2016.05.06
- Guo QH, Lv CZ, Hong Z. Application of rey-osterrieth complex figure test in Chinese normal old people. *Chin J Clin Psychol.* (2000) 8:205–8. doi: 10.16128/j.cnki.1005-3611.2000.04.003
- Yan Z, Jun-Chao LU, Qi-Hao G. Rey-osterriche complex figure test used to identify mild alzheimer's disease. *Chin J Clin Neurosci.* (2006) 14:501–4. doi: 10.3969/j.issn.1008-0678.2006.05.010
- Guo QH, Yuan J, Hong Z. Application of eight executive tests in participants at shanghai communities. *Chin J Behav Med Sci.* (2007) 16:628–31. doi: 10.3760/CMA.J.ISSN.1005-8559.2007.07.022
- Chou KR, Jiann-Chyun L, Chu H. The reliability and validity of the Chinese version of the caregiver burden inventory. *Nurs Res.* (2002) 51:324–31. doi: 10.1097/00006199-200209000-00009
- DeLong ER, DeLong DM, Clarke-Pearson DL. Comparing the areas under two or more correlated receiver operating characteristic curves: a nonparametric approach. *Biometrics.* (1988) 44:837–45. doi: 10.2307/2531595
- Erkinjuntti T, Gauthier S. Diagnosing vascular cognitive impairment and dementia: concepts and controversies. In: Wahlund L-O, editor. *Vascular Cognitive Impairment in Clinical Practice*. Cambridge University Press. (2009). p. 3–10. doi: 10.1017/CBO9780511575976.002
- Glynn K, Coen R, Lawlor BA. Is the quick mild cognitive impairment screen (QMCI) more accurate at detecting mild cognitive impairment than existing short cognitive screening tests? A systematic review of the current literature. *Int J Geriatr Psychiatry.* (2019) 34:1739–46. doi: 10.1002/gps.5201
- Lees R, Selvarajah J, Fenton C, Pendlebury ST, Langhorne P, Stott DJ, et al. Test accuracy of cognitive screening tests for diagnosis of dementia and multidomain cognitive impairment in stroke. *Stroke.* (2014) 45:3008–18. doi: 10.1161/STROKEAHA.114.005842

## SUPPLEMENTARY MATERIAL

The Supplementary Material for this article can be found online at: <https://www.frontiersin.org/articles/10.3389/fneur.2021.608188/full#supplementary-material>



34. O'Caoimh R, Gao Y, Gallagher P, Eustace J, Molloy DW. Comparing approaches to optimize cut-off scores for short cognitive screening instruments in mild cognitive impairment and dementia. *J Alzheimers Dis.* (2017) 57:123–33. doi: 10.3233/JAD-161204
35. Varan HD, Kizilarlanoglu MC, Balci C, Deniz O, Cotelis S, Dogrul RT, et al. Comparison of the accuracy of short cognitive screens among adults with cognitive complaints in Turkey. *Alzheimer Dis Assoc Disord.* (2020) 34:350–6. doi: 10.1097/WAD.0000000000000391
36. Messinis L, O'Donovan MR, Molloy DW, Mougias A, Nasios AG, Papathanasopoulos P, et al. Comparison of the Greek version of the quick mild cognitive impairment screen and standardised mini-mental state examination. *Arch Clin Neuropsychol.* (2020). doi: 10.1093/arclin/acia062. [Epub ahead of print].
37. Ritchie CW, Terrera G, Quinn TJ. Dementia trials and dementia tribulations: methodological and analytical challenges in dementia research. *Alzheimer Res Ther.* (2015) 7:31. doi: 10.1186/s13195-015-0113-6
38. Yu KH, Cho SJ, Oh MS, Jung S, Lee JH, Shin JH, et al. Cognitive impairment evaluated with vascular cognitive impairment harmonization standards in a multicenter prospective stroke cohort in Korea. *Stroke.* (2013) 44:786–8. doi: 10.1161/STROKEAHA.112.668343
39. Ihle-Hansen H, Thommessen B, Bruun Wyller T, Engedal K, Øksengård AR, Stenset V, et al. Incidence and Subtypes of MCI and dementia 1 year after first-ever stroke in patients without pre-existing cognitive impairment. *Dement Geriatr Cogn Disord.* (2011) 32:401–7. doi: 10.1159/000335361

**Conflict of Interest:** DM and RO'C are co-copyright holders of the Qmci screen. DM, RO'C, and YX are copyright holders of the translation into Chinese, the Qmci-CN screen.

The remaining authors declare that the research was conducted in the absence of any commercial or financial relationships that could be construed as a potential conflict of interest.

Copyright © 2021 Xu, Yi, Lin, Peng, Wang, Lin, Chen, Zhang, Deng, Guo, Shi, Wang, Molloy and O'Caoimh. This is an open-access article distributed under the terms of the Creative Commons Attribution License (CC BY). The use, distribution or reproduction in other forums is permitted, provided the original author(s) and the copyright owner(s) are credited and that the original publication in this journal is cited, in accordance with accepted academic practice. No use, distribution or reproduction is permitted which does not comply with these terms.



# An Overview of Venous Abnormalities Related to the Development of Lesions in Multiple Sclerosis

E. Mark Haacke<sup>1\*</sup>, Yulin Ge<sup>2</sup>, Sean K. Sethi<sup>1</sup>, Sagar Buch<sup>1</sup> and Paolo Zamboni<sup>3</sup>

<sup>1</sup> Department of Radiology, Wayne State University, Detroit, MI, United States, <sup>2</sup> Department of Radiology, Center for Biomedical Imaging, NYU Grossman School of Medicine, New York, NY, United States, <sup>3</sup> Vascular Diseases Center, University of Ferrara, Ferrara, Italy

## OPEN ACCESS

### Edited by:

Deqiang Qiu,  
Emory University, United States

### Reviewed by:

Salem Hannoun,  
American University of  
Beirut, Lebanon  
Bo Gao,  
Affiliated Hospital of Guizhou Medical  
University, China  
Gabriel Gonzalez-Escamilla,  
Johannes Gutenberg University  
Mainz, Germany

### \*Correspondence:

E. Mark Haacke  
nmrimaging@aol.com

### Specialty section:

This article was submitted to  
Applied Neuroimaging,  
a section of the journal  
Frontiers in Neurology

**Received:** 12 May 2020

**Accepted:** 26 March 2021

**Published:** 26 April 2021

### Citation:

Haacke EM, Ge Y, Sethi SK, Buch S  
and Zamboni P (2021) An Overview of  
Venous Abnormalities Related to the  
Development of Lesions in Multiple  
Sclerosis. *Front. Neurol.* 12:561458.  
doi: 10.3389/fneur.2021.561458

The etiology of multiple sclerosis (MS) is currently understood to be autoimmune. However, there is a long history and growing evidence for disrupted vasculature and flow within the disease pathology. A broad review of the literature related to vascular effects in MS revealed a suggestive role for abnormal flow in the medullary vein system. Evidence for venous involvement in multiple sclerosis dates back to the early pathological work by Charcot and Bourneville, in the mid-nineteenth century. Pioneering work by Adams in the 1980s demonstrated vasculitis within the walls of veins and venules proximal to active MS lesions. And more recently, magnetic resonance imaging (MRI) has been used to show manifestations of the central vein as a precursor to the development of new MS lesions, and high-resolution MRI using Ferumoxytol has been used to reveal the microvasculature that has previously only been demonstrated in cadaver brains. Both approaches may shed new light into the structural changes occurring in MS lesions. The material covered in this review shows that multiple pathophysiological events may occur sequentially, in parallel, or in a vicious circle which include: endothelial damage, venous collagenosis and fibrin deposition, loss of vessel compliance, venous hypertension, perfusion reduction followed by ischemia, medullary vein dilation and local vascular remodeling. We come to the conclusion that a potential source of MS lesions is due to locally disrupted flow which in turn leads to remodeling of the medullary veins followed by endothelial damage with the subsequent escape of glial cells, cytokines, etc. These ultimately lead to the cascade of inflammatory and demyelinating events which ensue in the course of the disease.

**Keywords:** multiple sclerosis, susceptibility weighted imaging, MS lesion development, USPIO-enhanced magnetic resonance imaging, vascular abnormalities

## INTRODUCTION

Multiple sclerosis (MS) is usually described as an inflammatory, demyelinating, autoimmune disease (1). Conventionally, it is thought that the autoimmune processes may lead to a breakdown of the capillary and venous wall with increased perivascular inflammatory cells and other detrimental factors which attack the myelin sheath and lead to neurodegeneration (2). In this overview, we will review the literature focusing on the changes in the venous vasculature and inflammation, which are likely to be the earliest processes in the development of the disease. This review will lead us to the chicken and egg question as to whether there is venous damage

that precedes the inflammatory response or inflammation that leads to vasculitis followed by an autoimmune response and then demyelination.

In general, for this review, the PubMed ([www.ncbi.nlm.nih.gov/pubmed/](http://www.ncbi.nlm.nih.gov/pubmed/)) database was used and the search terms were (venous pathology) AND (MS OR multiple sclerosis) with a date range of 1940–present, which resulted in 900+ papers. Out of these 900+ papers, roughly 200 were reviewed in detail. This review process led us to many collateral papers that might link key pieces of information on the topics of vascular remodeling, venous collagenosis, abnormal venous flow, perfusion, endothelial dysfunction and vascular endothelial growth factors. The focus in most of these papers was on clinical studies involving human subjects, but studies on animal models were also considered if the results were directly related to the hypotheses drawn from the human subjects. The primary aim of this review was to provide an overview to non-clinical and clinical readers alike, particularly for biomedical researchers who would like study vascular involvement in MS. For an in-depth discussion of the topics covered, the readers should refer to the original publications.

These papers included some systematic reviews that provided current knowledge of the available evidence of venous vascular damage as it relates to the pathology of MS, including some very recent publications. Three comprehensive recent reviews cover the history of the vascular aspects of MS (3–5). These reviews show that there has been evidence dating back to the works of Cruveilhier, Rindfleisch [originator of the central vein observation] (6), Ribbert (7), and Charcot (8) and Bourneville and Guérard (9) in the mid-nineteenth century regarding the presence of venous abnormalities in MS. The outline of this review considers the role of: 1) inflammation and its relationship to vasculitis; 2) collagenosis and vessel narrowing; 3) ischemia; 4) infarction and abnormal venous flow; 5) abnormal bulk dural sinus flow; 6) abnormal perfusion; 7) fibrin deposition; 8) vascular abnormalities preceding vasculitis; 9) medullary vein flow; 10) central veins; 11) dilated medullary veins; 12) endothelial dysfunction; 13) medullary vein density; 14) microvascular remodeling; 15) early vascular changes as a marker for new lesions; 16) advanced microvascular magnetic resonance imaging (MRI) using ultra-small superparamagnetic iron oxides (USPIO); and 17) imaging indications of venous abnormalities. All these points help us in understanding the putative timeline of events in the pathophysiology of MS related to these venous vascular effects. Although the source of the progression of MS is currently not clear, we deduce that it may be related to abnormal flow causing the subsequent events of vasculitis, leading to a cascade of increased local blood pressure due to lumen narrowing, inflammation, extravasation of cytokines, microglial cells, peptides, etc., that promotes both demyelination and further reduction of vascular compliance, eventually leading to cell death and atrophy; or can be caused by the endothelial dysfunction due to early increase in pro-inflammatory cytokines leading to vasodilation and vascular remodeling that is typical to MS, followed by chronic hypoperfusion in the later degenerative stage of the lesion. This comprehensive overview of vascular effects in MS should open the door to study venous abnormalities

and abnormal venous flow and their temporal relationship to the development of MS lesions using a variety of *in vivo* imaging methods.

The early pathological understanding evidenced throughout this work suggests a major role for the veins in MS, however, the temporal evolution still remains unclear: “Does poor flow generate the endothelial response and vessel wall inflammation or does the abnormal flow lead to ischemia and vessel wall breakdown including inflammation and vasculitis?” In both cases, there will be an extravasation of auto-immune invoking products that follow these processes. As we progress through the different forms of evidence, the role of abnormal flow will occur again and again as a potential source initiating the inflammatory response. After this, the usual cascade of damaging events to the tissue and demyelination will occur.

## Inflammation and Vascular Damage

Early cadaver brain studies of MS patients showed that the veins and venules in or at a distance from active lesions frequently exhibited an inflammatory lymphocytic reaction essentially located only in the vessel wall (10). When confined to the venous wall, these inflammatory changes can be regarded as a form of local venous vasculitis or cerebral venulitis. In this work, they showed that the cerebral venular wall in multiple sclerosis is the site of lymphocytic infiltration that may, at first, particularly in grossly normal white matter, be confined to the vessel wall alone (10). As the inflammatory process proceeds, the cellular infiltrate appears to spread to the perivascular space and even into plaque tissue. This may occur without any obvious surrounding demyelination (11). Venous walls then undergo focal intimal hyperplasia, intimal organization and collagenous thickening. Such features suggest a mild expression of subacute or chronic endovenulitis of the cerebral veins. Chronic inflammation can also lead to hemorrhage, increased permeability of the vessel wall and vasculitis. In the absence of other pathology, it is reasonable to assume that the scarring results from early inflammatory changes. The pathogenic mechanisms that cause the cerebral venulitis in multiple sclerosis could be the deposition or penetration into the venous wall of some circulating factor from the blood, a specific lesion of the venous wall or the release of a substance from the damaged brain, such as a lysosomal enzyme or thromboplastin (10). Adams further showed that in some active acute cases of multiple sclerosis the venous walls themselves are heavily infiltrated with inflammatory cells, but without infiltration of the adventitia and perivascular tissues (12). Chronic plaques often contain venous walls thickened by collagen, whereas active inflamed lesions exhibit a more fibrinous exudate (10). Although these processes are non-specific, they do indicate that the venous wall is implicated in the inflammatory process, and is thereby damaged and thickened, partly analogous to the thickening in endarteritis obliterans in arteries passing through foci of chronic inflammation. Nevertheless, it could be held that the venous wall is merely acting as a conduit for inflammatory cells but, if so, it should return to normality after subsidence of inflammation as, in fact, it does in MS. These works show that the venous wall is affected during the process of developing MS. Some have gone so far as to hypothesize that one

of the fundamental components of MS is a form of auto-immune vasculopathy (5).

## Venous Collagenosis

Another major effect seen in the vasculature of MS and other diseases is collagenosis, a process that affects connective tissue and is often associated with fibrinoid necrosis or vasculitis. In their work on stroke, Black et al. comment on the role of arteriolar tortuosity, reduced vessel density and occlusive venous collagenosis (gradual thickening of the vessel wall from collagen build up) which causes venous insufficiency and vasogenic edema (13). The key markers and evidence for this are activated microglia, oligodendroglial apoptosis, clasmotodendritic astrocytosis, and upregulated hypoxia-markers. Gao et al. proposed that venous collagenosis dilates the veins and causes venous insufficiency with consequent vessel leakage, i.e., vasogenic edema (14). Moody noted that the blood-brain barrier (BBB) is abnormally breached in conditions such as hypertension, intra-arterial injections of hyperosmolar solutions, exposure to inflammatory mediators (cytokines), activation of leukocytes, hypercapnia, and ischemia (15). With serious injury to the BBB, large amounts of plasma proteins can escape into the brain tissue, resulting in vasogenic edema. Brown et al. show that collagenosis of the veins could prevent exchange between the surrounding CSF and the venous blood that may act as a drainage for waste products of the brain (16). Further, stiff arteries may not provide the needed pulsatility to drive the CSF and again reduce macromolecular transport to the CSF from the brain and eventually to the venous blood (17). These effects may affect the function of what is referred to today as the glymphatic system (18).

Moody et al. proposed that periventricular venous collagenosis (PVC) could lead to venous wall thickening of the periventricular and subependymal veins, luminal narrowing and eventually vessel occlusion (19). They also associated this with leukoaraiosis in elderly individuals when there was no evidence of small arterial disease. They believed this lack of flow could lead to: reduced perfusion pressure, increase in associated venous pressure, chronic cerebral edema, disordered venous flow, BBB breakdown, ischemia infarct and hemorrhage (19, 20). The development of leukoaraiosis may be slow when PVC is present because of the presence of collateral flow and alternate pathways in these areas (although such pathways are not endless). They also note that the obstruction of flow might interfere with the “paravascular” channels and the exchange of extracellular fluid to the systemic circulation. Further, the collagenic venous thickening is likely to impede resorption of the CSF and extracellular fluid. They note that the thicker wall might prevent rupture and venous collapse when there is increased ventricular cerebrospinal fluid pressure or vigorous pulsations. This can lead to increases in transmural pressure preventing the usual flow of metabolic wastes into the venous system (21). Houck et al. focus on the role of medullary venule collagenosis and associated vasogenic edema in white matter hyperintensities (WMH) and Alzheimer’s disease (AD) (22). They studied 682 older adults without dementia and found an increase in diameter of the internal cerebral veins and

basal veins of Rosenthal were associated with greater total WMH volume in different regions of the brain. Keith et al. showed in a cadaver brain study of dementia and healthy controls (HCs) that collagenosis of venules best predicted WMH volumes (20). They note clearing of interstitial solutes such as beta-amyloid occurs via the glymphatic system associated with the perivascular spaces. Therefore, if venous dilation affects paravascular spaces, the glymphatic system could be disrupted.

Despite the fact that these papers are referring to stroke, hypertension and dementia, the findings for the early role of the medullary venous system are clear, their flow and perhaps function have been compromised.

## The Role of Venous Ischemia

Yan et al. discussed the role of WMH in general in other diseases excluding MS but we can learn from this data too; there may well be some hints of the mechanisms including dilated veins (23). Increased levels of WMH are associated with an increased risk for dementia and stroke. There is often reduced blood flow in these regions with BBB damage (24, 25). Cerebral venous collagenosis (VC) may cause “venous ischemia by increasing vascular resistance and compromising interstitial fluid circulation, with consequent vessel leakage, i.e., vasogenic edema, and lead to non-necrotic hyperintensities on MRI (13, 19).” The resulting reduced venous outflow and venous hypertension may lead to dilation of deep medullary veins (DMV) (26). WMH could be induced by stenosis or occlusion of deep cerebral veins (26). In addition, retrograde venous hypertension could lead to decreased cerebral blood flow (CBF), venous ischemia and hypoxia (27). Willinsky et al. and Van Den Berg et al. also note that there can be partially reversible WMHs in patients with arteriovenous malformations (28, 29) and that venous ischemia was more likely to be a cause of WMHs.

Keith et al. (20) used cadaver brains to stain for venous wall thickening and occlusion caused by collagenosis. Although they found higher venous collagenosis for smaller veins 150  $\mu\text{m}$  and less, VC in larger veins ( $>200 \mu\text{m}$ ) correlated with higher WMH scores. They also found VC was frequent in patients with periventricular infarcts identified on imaging in both AD and non-AD patients. The etiology of WMH remains unclear although there is an association with cerebrovascular disease and hypertension potentially leading to ischemia. Their previous work also suggested that venous insufficiency and vasogenic edema may be factors in the development of WMH (13) and may be present in cerebral autosomal dominant arteriopathy with subcortical infarcts and leukoencephalopathy (CADASIL) as well (30). Small vein collagenosis and white matter pallor was more prevalent in the presence of arteriosclerosis. *They assume white matter pallor represents myelin loss.* In summary, periventricular venous infarction accounts for 22% of ischemic stroke in adults and 75% of subcortical lesions in perinatal stroke.

These works continue to develop the concept that the veins can play a major role in ischemia and lead to white matter hyperintensities.



## Cerebral Venous Infarction

Schaller and Graf show that when cerebrovascular occlusion (CVO) is present, the local pressure increases leading to: a dilated venous and capillary bed, the development of interstitial edema, increased CSF production, decreased CSF absorption and rupture of venous structures (hematoma) (26). If promptly diagnosed, CVO is reversible and this can avoid venous infarction. They note the following: (a) an increase in venous and capillary pressure leads to diapedesis of erythrocytes by BBB disruption; (b) dilatation of venules can occur with no arterial effects; (c) reduced CBF leads to an acute energy drop, dysfunction of the membrane-bound  $\text{Na}^+ - \text{K}^+ - \text{ATPase}$  pump, intracellular entry of water, cytotoxic edema and cell lysis. These phenomena can be considered as a disruption of the shift of interstitial fluid from the capillary bed toward the ventricle. The key is that despite the immediate metabolically disturbed state after CVO, the effects may be reversible, which is certainly true in MS as long as adequate perfusion has been maintained during the stressed conditions. This is likely made possible by venous anastomosis acting as the collateral pathways. The other thing to remember is that venous flow can change direction since there are no valves in the veins. Therefore, subsequent dilation of the veins and recruitment of (or remodeling of) neighboring outflow territories may temporarily compensate for changes in pressure. If pressure increases beyond some limit, this could cause BBB disruption and alter the fluid exchange between cerebral intra- and extravascular compartments, causing cytotoxic and vasogenic edema. This protective nature of alternate venous pathways has been shown in rat studies of venous occlusion (31). Increased pressure and tissue swelling can also cause collapse of the capillaries.

This work shows that under abnormal flow conditions, veins can be damaged, dilate and restrict blood flow disrupting the BBB and fluid exchange in the lymphatic system.

## Dural Sinus Flow Effects, Abnormal CSF Flow, and Increases in Venous Pressure

Several authors have shown a combination of intraluminal obstacles and/or external compression, hampering the venous outflow at the extracranial level, particularly in the internal jugular veins (IJVs) (32–37). According to fluid dynamic simulations using a mathematical model based on human vascular structure, these dural sinus flow abnormalities can lead to an increased pressure in intracranial veins (38, 39). They show that when both IJVs are obstructed, there can be a rise in pressure of up to 13 mm Hg (38). This might explain the dilation of the cerebral venules and medullary veins assessed by Gaitán et al. (40), in consequence of the increased transmural pressure at that level. It has been shown in a rat model that an embolus in the external jugular can produce large venous pressure changes in the superior sagittal sinus and subsequently a loss of CBF and accumulation of nicotinamide adenine dinucleotide (NADH) in cortical structures indicating ischemic damage (31).

CSF is ultrafiltrated from the high-pressure capillary bed of the choroid plexus into the subarachnoid space. From the subarachnoid space, CSF is driven into the Virchow-Robin spaces

by a combination of arterial pulsatility, respiration, and pressure gradients. When blood reaches the low pressure system of the cerebral venules, water is reabsorbed into the venous system from the interstitial fluid and CSF (41). CSF absorption is linked with a gradient of pressure between the brain parenchyma and the venules, constituting the so called G-lymphatic system (42–44). When IJV obstruction occurs, the increased venous pressure is propagated to the intracranial sinuses and venules. The effects of higher pressure in the cerebral venous system are, therefore, significant for any fluid exchange, because either the G-lymphatic fluid absorption or the CSF passage into the dural sinuses is based on a favorable pressure gradient (43, 44). In case of extracranial venous obstruction, the increase in pressure at the venular level can affect the absorption of peptides, triggering the inflammatory process (44), and affect the passage of macromolecules (17). One also observes in MS that the ventricles are enlarged relative to controls as are the perivascular spaces close to venules (45). Magnano et al. showed that CIS patients had net reduced CSF flow and that their conversion to clinically definite MS in the following year was related to this decreased CSF flow (46). The perivenous spaces in the brain parenchyma are increasingly recognized for their role in leukocyte trafficking as well as for their potential to modulate immune responses and, therefore, might be considered biomarker of inflammation. Finally, increases of macromolecular concentrations in the perivascular spaces caused by impaired transport across the venous wall could lead to edema (17).

These papers demonstrate that changes in flow whether microscopic or macroscopic that affect the venous system upstream can cause pressure changes leading to further exacerbations of abnormal flow.

## Changes in Perfusion of MS Lesions and Normal Appearing White Matter (NAWM)

A number of studies have shown that there is a general reduction of perfusion in chronic lesions in MS and in NAWM as well (47–52). One paper notes a reduced CBF by about 25% and increased mean transit time (MTT) of 3 to 4 s in MS lesions (52). The trend of lower CBF and cerebral blood volume (CBV) in NAWM became worse in primary progressive MS (PP-MS) and Expanded Disability Status Scale (EDSS) was significantly correlated with the periventricular CBF and CBV as well as the frontal CBV (53). Reduced CBV was found to correlate with working and secondary verbal memory for clinically isolated syndrome (CIS) patients (54). Another paper showed reduced CBF in NAWM and decreased NAA/Cr in the centrum semiovale and increased PCr/ $\beta$ -ATP (51). Law et al. has also shown a decreased cerebral blood flow and a prolonged mean transit time in periventricular regions of NAWM (55). Dynamic susceptibility contrast perfusion may also be used to view microvascular changes in non-enhancing lesions (56). These flow reductions in lesions and NAWM may lead to a state of hypoxia in the tissue. Generally, worse flow is associated with progression of the disease and more severe physical disabilities (57).

On the other hand, in the acute stage, there is evidence of increased CBV (58), CBF (47, 50, 59), and reduced MTT,

the latter being associated with higher disease severity and with the presence of disease 1 year later in newly diagnosed MS patients (60). Another paper compared high-inflammatory and low-inflammatory patients and found that the former had significantly higher CBV and CBF values (59). Interestingly, CIS patients have also been shown to have increased CBV (61, 62). Ge et al. also show that lesions with low CBF and low CBV (basically chronic lesions) do not show enhancing lesions with gadolinium (56). An excellent review of all the literature related to MRI perfusion imaging is given in Laganà et al. (57) and on the role of chronic inflammation and imaging inflammation is given by Matthews (63).

One of the more interesting findings are the changes in blood flow and blood volume preceding the formation of acute lesions (45, 59). These effects appear to remain for several weeks even after BBB breakdown has ceased. The increase in CBF and CBV suggests a possible dramatic change in the local vasculature preceding the inflammatory stage.

The take home message from this section is that reduced perfusion can lead to loss of brain function even in CIS. Especially suggestive is the finding that blood flow changes can precede lesion formation. We propose that the odd increases in blood flow may be caused by vascular remodeling and the subsequent increase in local venous blood volume.

### Fibrin, Flow Disruption, and Ischemia

Wakefield et al. studied the role of vascular injury in MS (64). Damage to the veins causes vascular endothelial cell activation, vasculitis, vascular occlusion including class II antigen expression and fibrin deposition (usually a sign of active lesions) possibly in that order making the antigen expression an early event in the evolution of vascular injury. These changes can occur prior to cerebral parenchymal reaction and demyelination and suggest that ischemia could be an early component in the evolution of multiple sclerosis. They also note that these vascular effects were present in many thin walled vessels, including both veins and capillaries, while other vessels were occluded by reticulated fibrin thrombus. When fibrin was present, the walls of these vessels appeared widened by inflammatory infiltrate and edema. For more advanced cases, reactive astroglial cells were present around the damaged vessels. In some cases, groups of vessels were apparently obliterated and the vascular origin of the associated lesions was confirmed by collagen type IV immunostaining. Fibrin is also associated with vessel wall infiltrated by inflammatory cells, and may progress to occlusive venous thrombosis (hemorrhage was frequently seen in relation to these damaged vessels). In some experimental allergic encephalomyelitis models, fibrin formation appears to be a prerequisite for the development of clinical disease where they show disease activity began only with the appearance of fibrin in this model (65).

So, what role does focal cerebral ischemia play in the pathological and clinical features of multiple sclerosis? The preservation of axon cylinders is a recognized feature of hypoxia and is seen in leukoencephalopathy (66). Some evidence for ischemia exists from MRI where it has been shown that there is an increase in lactate (67). They note that shunting of blood from poorly perfused lesions could produce an acute

symptomatic deterioration and in turn the restoration of blood flow could produce a rapid clinical improvement. This could explain the coming and going of MS lesions over time and only those lesions with chronically dysfunctional flow may become permanent. In conclusion, they propose that “focal endothelial cell activation which progresses to occlusive vascular inflammation is a precursor of both cellular infiltration of vessels and demyelination.” And they close with this comment: “Advanced vascular injury is associated with infiltration of the vessel wall by inflammatory cells and reactive changes in the neuropil. We propose that activation of the cerebral endothelium is a primary event in multiple sclerosis; that induction of procoagulant activity in endothelial cells is a feature of acute multiple sclerosis; and that demyelination may have an ischemic basis in this disease.”

The two papers by Wakefield and Ginsberg begin to strengthen this picture of ischemia, abnormal flow, fibrin deposition, and the shunting of blood from poorly perfused regions leading to acute symptomatic degeneration. The comment that a return of normal flow could lead to resolution of the inflammation and disappearance of the lesion is reminiscent of what is seen in relapsing remitting MS.

### Evidence That Vascular Abnormalities Precede Vasculitis and Inflammation

It is well-known that patients with retinal vasculitis can go on and develop MS. Retinal vasculitis has four main abnormal immunological findings: 1) macular edema; 2) periphlebitis and perivascular sheathing; 3) capillary closure and/or leakage; and 4) venous occlusion and new vessel formation (68). In periphlebitis retinæ there is sheathing and hemorrhage in veins in the retina (69). Also, patients with retinal vascular abnormalities in optic neuritis have a high probability to develop MS (70) and the overall risk of being diagnosed as clinically definite is 28%. These authors note that both the brain and the retina have continuous endothelial tight junctions which are permeable to a variety of molecules (70): “We therefore suggest that the sheathing of retinal vessels that we observed ophthalmoscopically is the visible clinical sign of the perivascular lymphocytic infiltration and accompanying edema which characterizes the lesions of MS.” and more interestingly they comment: “The occurrence of perivenular abnormalities in a region free of myelin and oligodendrocytes provides evidence that the vascular changes in MS can occur independently of contiguous demyelination and may be the primary event in the formation of a new lesion.”

This long-standing evidence of the relationship of poor flow with retinal vasculitis is indicative that poor flow can and does appear in some cases as a precursor to inflammation.

### Medullary Veins

The medullary veins of the brain play a key role in draining the blood from white matter. A number of diseases are associated with the medullary veins including hemorrhagic disorders, inflammatory changes that spread along the veins, and neoplasms within the veins (71). The first two may be related to metabolic changes associated with venous wall damage and are implicated

in MS. It is well-known that there are pathological changes of veins in plaques that include: lymphocyte cuffs, intramural fibrinoid deposition, collagenized vessel walls, and perivenous iron deposition (12). On the arterial side, Nonaka et al. note that the presence of anastomoses among the terminal branches of the deep white matter protects against ischemic infarction (72). This type of anastomosis is likely present in the DMV as well. Okudera et al. studied the zones of convergence of the medullary veins (73). There were four zones of convergence: the superficial, candelabra, palmate and subependymal. Several zones are related to venous crossings of the fibers of the corona radiata and optic radiations. The arcuate veins may link to the cortical veins and these can be called sub-cortical veins. The deep medullary and superficial medullary veins can be connected by anastomotic veins. The longitudinal caudate vein of Schlesinger is also referred to as an ependymal vein when running beside the lateral ventricles (74). He notes that there are medullary veins around the fourth ventricle too. The superficial and deep medullary vein territories represent the watershed zone between the cortex (pial) and deep white matter (ependymal drainage). When the balance of drainage is disrupted between these two systems, the veins now responsible for the larger than normal flow will dilate. Finally, Willinsky noted that venous congestion may lead to rerouting into dilated transosseous venous channels or retrograde flow (28).

The structure of the medullary vein system could well explain the location of both the periventricular and zone 2 lesions by the candelabra medullary veins as well as the presence of transmedullary veins related to the gray matter. The medullary veins of course pervade all the tissue and a breakdown of the drainage system could have drastic consequences despite the fact that the venous system offers multiple anastomotic connections.

## Central Vein Sign (CVS)

As mentioned earlier, Rindfleisch had already noted the presence of a central vein in the mid-1800s (6). It was not until mid-1900 that this became more evident in Dow and Berglund's work (75). A major recent focus has been on the presence of a central vein in MS lesions especially in Dawson fingers and sometimes in smaller lesions as well (76, 77). This sign has been used to differentiate other white matter diseases that are often part of the differential diagnosis from MS, sometimes quite successfully (76). The presence of abnormal veins is a possible explanation of the widely held hypothesis that the formation of an MS lesion depends on the entry of inflammatory cells from the systemic circulation into the brain parenchyma possibly from a disrupted endothelium of the veins. However, not all lesions show major veins, although with the help of the Microvascular *in-vivo* Contrast Revealed Origins (MICRO) imaging approach, where a USPIO agent, Ferumoxytol, is administered and high-resolution susceptibility weighted imaging (SWI) images are acquired, we can visualize any vascularity within the MS lesions (Figures 1–3). One immediate question is: "Are there, in fact, veins present, but they just can't be seen?" Some evidence for this exists. One case study has shown that a central vein became visible only after the use of a Gadolinium contrast agent. One

explanation for not always seeing a CVS is that reduced metabolic function of adjacent tissue leads to a loss of visibility of the medullary vein. Several authors have suggested the use of contrast to further enhance the visibility of the veins (77, 80). This can be understood as a T2\*-T1 coupling for improved signal loss in SWI (81).

An early study by Broman used trypan blue staining of the MS plaques and found only veins were stained. The staining correlated with the degree of demyelination and in some cases an obvious correlation between the course and branches of the veins and the shape and extension of the plaques. He found that there were central veins in every plaque (82) and that there was some degree of correlation with blue staining and demyelination. Fog (83) stated that MS lesions typically were developed around small veins. This work also noted that 2/3 of plaques evaluated followed the veins along a classic Dawson finger profile. More interestingly, the course and size of the veins determined the shape, course and dimension of the plaques. Further evidence of the vascular mechanical effect comes from Allen's observations, who noticed the wide vascular beds around veins and the central widening of the venous tree that testifies an intermittent increase in cerebral pressure (84). This is similar to Schelling's findings (85).

In an effort to establish a standard radiological definition of the CVS to improve diagnosis of MS, Tallantyre et al. introduced the "40% rule" which assesses the number of MS lesions with CVS as a fraction of the total number of lesions. A 40% cut-off threshold was able to discriminate MS from healthy subjects (86). Sati et al. used the 40% CVS rule to separate MS lesions from other types of lesions with a small number of cases (87). Mistry et al. found 45% CVS was a good separator for MS vs. other diseases such as microangiopathy even at 3T (88). Samaraweera et al. used a high resolution segmented echo planar imaging (SEPI) sequence with echo train length (ETL) = 15 and with 0.55 mm isotropic resolution in 4 min 14 s (89). In this method, the long echoes and high CSF signal help visualize the lesions better. They also showed a much smaller fraction of CVS with patients with small vessel disease (SVD). We can use an iron-based contrast agent to enhance the visibility of CVS with a practical scanning time, or a longer TR, longer TE and lower flip angle non-invasively to try to enhance this contrast [this is particularly true for 7T (90)]. Maggi et al. studied the prevalence of CVS in MS vs. systemic autoimmune diseases and primary angiitis of the cerebral nervous system (91). Using a threshold of 50% for the perivenular lesions, all other vasculitis like diseases were ruled out. Behcet's disease had the highest perivenular lesion load of all vasculitis diseases. All of these studies have very strong predictive value in terms of differentiating MS from other diseases and further implicate the venous role in MS.

Clearly, the medullary veins are a major presence in MS lesions. However, this could be even more evident if much higher resolution imaging could be used where more "micro" level venous abnormalities could be seen. This is in fact demonstrated later in this paper under section Imaging the Microvasculature Using a USPIO Contrast Agent.



## Evidence of Dilated Veins

The behavior of the medullary veins is complicated. For example, in stroke and restricted retrograde venous hypertension, DMV could dilate or appear dilated in SWI due to the increased levels of deoxyhemoglobin. Actually physical increases are also possible if there is a source of stenosis downstream that could lead to mechanical effects such as pulsating blood and enlargement of the perivenous spaces because of this (85). These flow disturbances could lead to deleterious effects on the vessel wall allowing lymphocytes etc. to escape. Eventually, upon tissue death, the veins may also atrophy or become so constricted due to collagenosis that the effective blood volume is decreased in chronic lesions (58). Yan et al. used SWI to evaluate the volume of DMVs in patients with WMHs and HCs (23). The volumes of DMV on SWI may make it possible to monitor the severity and progression of disease associated with WMHs and to evaluate response to therapy. This venulopathy causes dilatation of upstream venule beds. Further, they found a correlation of DMV volumes with the number of lacunes as did another more recent study by Zhang et al. (92). This apparent increase in DMV could be caused by increased cerebral metabolism or reduced flow. It has been shown in subjects with large WMH volumes that there is reduced CMRO<sub>2</sub> (93, 94). Black et al. proposed that venous collagenosis could dilate the veins and damage the myelin and axons with the consequent leakage of potentially toxic substances (13). It has been shown that the DMV were not only diminished in density (95), but also shortened and sometimes dilated and for early patients can appear longer (96). Adams noted that chronic plaques showed thick-walled vessels and little lymphocytic infiltration (12). Usually, less blood flow would lead to an increase in the visibility of veins in SWI under normal tissue functioning. However, if the tissue is not functioning at capacity, then there will be less deoxyhemoglobin and there will be a loss of visibility in SWI.

Gaitán et al. showed that the veins found inside MS lesions were smaller than the veins outside MS lesions (40). They also found that the veins located around and outside lesions in people with MS were larger than the veins in people without MS. They proposed that compression within the active lesions by the perivascular cuffing or hardening of the vascular wall (like necrosis) causes reduced vascular compliance in chronic lesions. They also suggest these enlarged extralesional veins could be due to: ex vacuo dilatation due to overall brain volume loss or an apparent increase from T2\* blooming artifact caused by an increase in the amount of deoxyhemoglobin in the blood. Assuming that arterial blood in MS is normally oxygenated, the results would suggest that early in MS there is a diffuse increase in cerebral metabolism, perhaps associated with inflammation, which results in greater oxygen extraction from blood. Patankar et al. show dilated Virchow-Robin spaces (VRS) as representative of white matter abnormalities in patients with subcortical vascular dementia (97). They found more WMH and higher VRS scores in ischemic vascular dementia patients compared with subjects with Alzheimer's disease or healthy controls. Murray et al. show that periventricular lesions had the largest loss of oligodendrocytes and increased levels of microglia (98). They suggest that age related loss of myelin basic protein

and small vessel density may lead to vacuolation of WM and accumulation of interstitial fluid.

In the Ganesh and Stahnisch review (4), they note that Schelling suggested mechanical effects leading to "retrograde dilatation of cerebral veins, releasing various immunological phenomena" such as those observed in MS (85). Talbert similarly hypothesized that excessive venous hypertension could stretch the venous wall sufficiently to separate the tight junctions between endothelial cells, allowing colloids and other materials to pass through the exposed porous basement membranes (99). The resulting changes in osmotic pressure could disrupt the internal transport systems of axons and dendrites, leading to their disintegration, triggering the inflammatory processes as in MS. This process might be indistinguishable from those of autoimmune disease forms, which have likewise marked the waxing and waning of experimental autoimmune encephalomyelitis animal models for the study of MS (100).

Dilated veins may be another interesting marker of abnormal flow and MS lesions. As discussed in sections Imaging the Microvasculature Using a USPIO Contrast Agent and Venous Abnormalities Seen With MICRO Imaging and as shown in **Figures 1–3**, the dilated veins and abnormal venous remodeling can by itself serve as a lesion defining marker.

## Endothelial Dysfunction

The dysfunction of the vessel endothelial cells has been proposed to cause alterations of the blood vessel architecture. These changes could lead to both enlargement and narrowing of the vessel lumen, along with vessel stiffening (101). As mentioned earlier, the MS progression and demyelinated lesions have been correlated with increased CBV and vasodilation, which could be caused by the increased endothelial cell proliferation and high levels of vascular endothelial growth factor (VEGF) and VEGF receptors (102) that are associated with the MS population compared to normal controls (103, 104). VEGF production is known to be promoted by several pro-inflammatory cytokines such as interleukin (IL)-1 $\beta$ , IL-1 $\alpha$ , and IL-18 (105). In response to increased VEGF, there is an increase in the expression of the endothelial cell adhesion molecules, including the vascular cell adhesion molecules (VCAM) and vascular growth factors; creating a cascade of inflammation and angiogenesis, which promotes the vascular remodeling that is typical to MS. This may result in endothelial junction disorganization, increased iron deposition and immune cell extravasation, which culminates in the loss of neural and glial cells (106, 107). Over time, the chronic MS lesions have been shown to have reduced perfusion due to the reduced axonal activity, lower K<sup>+</sup> release in the periaxonal and perivascular space and reduced astrocyte metabolism (104, 108). Hence, in summary, the pro-inflammatory cytokines could cause endothelial dysfunction and an increase in vascular endothelial growth factor and its receptors at early inflammatory stages of the lesion. This can promote the increase in production of vascular adhesion molecules that eventually lead to expediting the loop of inflammation with the increased angiogenesis and/or vascular remodeling. An increase in the production of angiogenic endothelial cells could be due to an endogenous attempt to overcome the chronic hypoperfusion of demyelinating lesions at



a late degenerative phase (109, 110) which is linked with the loss of neural and glial cells over time (111).

### Loss of Medullary Vein Density (MVD)

There is also evidence that there is a loss of MVD when comparing relapsing remitting MS (RRMS) to secondary progressive MS (SPMS) to PPMS (95). It has been shown that the MVD decreases supposedly due to poor neuronal function and oxygen extraction and, therefore, leads to reduced levels of deoxyhemoglobin and loss of visibility of the veins in SWI. Another reason could be that the veins are too small to be seen with the current resolution. Zeng et al. also found intracerebral venous (ICV) measure of the MVD is highest in CIS and progressively worsens in patients with a longer disease duration (96). They also noted that the periventricular penetrating veins were well-defined in active lesions and ill-defined in non-active lesions. Zhang et al. also present a scoring system for the DMV and find that as the disease progresses the MVD decreases (92). Sinnecker et al. found venous density decreased with increasing lesion count and this loss of medullary veins was already present in CIS to some degree (112).

Although it is not yet clear if this loss of visibility is a marker for continued loss of flow or tissue atrophy, it is yet another marker in the importance of the venous system, especially in the progression of MS.

### Developmental Venous Anomalies (DVAs)

DVAs contain veins that are dilated, twisted and follow a chaotic pattern. They are often referred to as Caput Medusa and sometimes they take on the look of the spokes of a wheel. Here we will focus on evidence of spontaneous vascular remodeling and refer to these as atypical DVAs. This finding may indicate a more serious effect on the surrounding tissue compared to the usual congenital DVAs. Kroll et al. note that devastating venous infarctions after ligation of a DVA confirms that it serves as the only draining route for its corresponding brain segment (113). They also suggest that those DVAs with increased flow (and associated venous congestion likely due to a local venous stenosis) and effects on the surrounding parenchyma should be considered as atypical DVAs (which are more at risk for complications such as hemorrhage or thrombosis). The authors suggest flow may provide a better means for diagnosing an increased risk of associated complications.

Several papers have reported signal intensity abnormalities in and around the tissue in which the DVA is embedded (26, 114) and particularly seen with FLuid Attenuation Inversion Recovery (FLAIR) (115), although Sahin et al. found contrast enhancement and perfusion in the tissue around the DVA in the basal ganglia (116). Umino et al. found 25% of DVAs showed high signal WMH on FLAIR suggesting significant underlying WM disease (117). There was a significant correlation between patient age and the size of WMH abnormalities (117); the age dependence being likely due to time after onset. Linscott et al. showed that deep venous DVAs were more predictive of signal abnormalities (118). Okudera et al. proposed they arose from aplasia, hypoplasia, or occlusion of some part of the medullary venous system or from a pial vein prior to opening to a dural sinus (and these authors

also note it could be from chronic venous hypertension caused by anomalous venous drainage) (73). The presence of the bright signals may be from edema, demyelination or gliosis related to abnormal flow from the venous stenosis (117). They ask the key question: "How does a DVA change or grow in time?" Their cross-sectional results suggest that the size increases with age and, hence, they may grow in time. Could the increased resistance to venous outflow lead to leukoaraiosis and collagenous thickening of the venous wall thereby leading to chronic local ischemia and tissue edema? Santucci et al. found non-hemorrhagic signal changes in 12.5% of cases and an association with age (114). Both research teams found one of their patients who met their criteria had MS (114, 117). A very recent study showed nearly 30% of MS patients showed DVAs compared to a control group of headache patients with only 14% of cases (119). More recently using post-contrast T1 weighted imaging and FLAIR, Kruczek et al. confirmed that DVAs are more common in CIS and early-onset MS groups compared to controls, however, prevalence of DVA was not related to other imaging markers, or conversion from CIS to clinically definite MS (120). They found roughly 29% of lesions were DVAs and 21/25 cases had at least one DVA. Nevertheless, the authors note the lack of sensitivity of the sequences they used and recommended the use of other sequences such as SWI (120).

Several groups used perfusion weighted imaging (PWI) and showed many DVAs had increased CBF, CBV, MTT, and Tmax (121–123). Iv et al. postulate that DVAs with intrinsic arterial spin labeling (ASL) signal or signal in draining veins may be associated with arteriovenous shunting (transitional lesions) (123). Kroll et al. used computer tomography (CT) perfusion and found increased CBV, CBF and MTT in the vicinity of the DVA (113). They suggest two types of DVAs: a benign type and one that can lead to tissue damage through ischemia and venous congestion (113). These can be referred to as typical (uncomplicated) and atypical DVAs, respectively. Stenoses, dystrophic calcifications, and cavernous venous malformations are all considered atypical and cavernous malformations (CM) are also considered to be the leading cause of intracerebral hemorrhage. This altered flow pattern seen in PWI may represent venous congestion caused by stenosis of the main draining vein, likely the core etiology in the development of symptomatic DVAs. These atypical DVA may also serve as risk factors for future hemorrhage. Hong et al. suggested that the angioarchitecture of rapidly curving, narrowing and tortuous veins could be risk factors for the formation of cavernous malformations. If two or more of these factors are present, then the risk is much higher. San Millán Ruíz et al. studied the drainage territories of DVAs and their associated parenchymal abnormalities (124). They suggest that outflow obstruction, thickening of venous walls and convergence may lead to the development of venous hypertension in DVA. Stenoses and venous hypertension can lead to demyelination, degenerative alterations of nerve cells, gliosis and leukomalacia around DVAs. Although the medullary veins in the periventricular white matter are ubiquitous, the key finding is that the white matter abnormalities appear to develop along the veins and that they often define the lesion shape as we also see with the micro DVAs (125).

Typical DVAs are usually large venous structural and flow anomalies. Atypical DVAs may be far more serious and in the case of MS, evidence is mounting that they are related to the remodeling alluded to in the above sections and several examples of which are clearly shown in MICRO imaging of MS lesions as discussed in sections Imaging the Microvasculature Using a USPIO Contrast Agent and Venous Abnormalities Seen With MICRO Imaging.

## Vascular Changes as a Pre-Cursor to the Formation of Acute Lesions

Guttman et al. performed an 8 week longitudinal study and found that a stenosis of the vein could be observed on SWI at the time of enhancement on post-gadolinium T1-weighted images, suggesting that vein narrowing may be occurring before BBB disruption (126). There may also be some evidence that intralésional vein stenosis is reversible and consistent with focal hypercellularity in the context of T-cell aggregation during MS plaque formation. In our recent microvascular imaging work, we are seeing local partial inflammation along the outside of the veins that has not yet extended to the entire length of the vein. Finally, another recent study shows that there are changes in the local blood volume in the brain that serve as a pre-cursor to future lesion development before inflammation is seen (127). They provide strong evidence for the role of venous changes pre-plaque development, showing higher venous volumes 1 year before plaque detection and the corresponding NAWM regions (127). Interestingly, they also show that venous volumes are higher even in established plaques and NAWM. Wuerfel et al. assessed around 15 days before MS plaque formation leads to a significant decreased perfusion in the same area. In addition, Holland et al. (48) showed that plaques disappear when brain perfusion is good, and this demonstrates the possibility of myelin repair on behalf of the oligodendrocyte when the oxygen level is adequate (45). It seems that low perfusion is a necessary element for either plaque formation or lesion dissemination.

This recent MRI work presents more direct evidence in MS patients that flow abnormalities occur prior to an inflammatory response. Based on the above material, this vascular effect may well be from abnormal flow in the medullary veins.

## Imaging the Microvasculature Using a USPIO Contrast Agent

We recently introduced a new approach to image vessels as small as 50 to 100 microns in size. This approach makes it possible to study microvascular disease only matched before using cadaver brain studies. We use Ferumoxytol with a dose of 4 mg/kg to increase the susceptibility of the veins and add susceptibility to the arteries so that all vessels are visible with SWI (see **Figure 1**). The increased susceptibility induces a major signal loss for the small vessels that are less than a voxel in size (128, 129). By using a resolution of 220 microns we can see vessels smaller than 100 microns at 3T, demonstrating the pitchfork (candelabra) behavior of the vessels that matches with the illustrations from the earlier cadaver brain work (**Figure 2**). USPIO contrast agents

have been used before to study MS. These studies showed that more lesions could be found with USPIOs than with gadolinium and postulated that the lesions seen only with USPIO were representative of local macrophage activity otherwise invisible to normal imaging (130–132).

MICRO imaging has been used to visualize the microvascular (predominantly venous) abnormalities in MS lesions. The hypothesis was that using MICRO imaging it will be possible to see the complete venous vascular tree and, hence, be able to study the MS lesions for the presence of vascular abnormalities much better than has ever been done before *in vivo*. MICRO imaging has the potential to study the microvasculature of MS lesions and to follow vascular changes longitudinally over time similar to previous studies (133) to determine which comes first: abnormal vessel structure and flow or inflammation that then affects the vessel wall (129, 134, 135). Or, perhaps both contain some level of guilt and they create a destructive feedback loop exacerbating the disease. The ability to visualize the microvasculature of MS lesions could provide novel information in the development and progression of MS lesions (135).

## Venous Abnormalities Seen With Micro Imaging

Although the presence of Ferumoxytol increases visibility for both arterial and venous vascular network, there is a much higher probability of a vein being present inside the MS lesions as opposed to an artery. Most of the MS plaques are distributed in the WM (136–138) and the arterial blood in the WM is supplied through arterial branches arising from the cerebral arteries, which are roughly 100  $\mu\text{m}$  in size making them very difficult to visualize, especially once they branch into much smaller arterioles and capillaries (72). On the other hand, the medullary veins, subependymal veins and other subcortical WM veins have their primary confluence located in the periventricular region, where the WM lesion occurrence is the highest (138, 139) making them much larger, at  $\sim 300 \mu\text{m}$  in size, than the arterial network in the same region (72). Additionally, the venous blood volume is roughly four times that of the arterial vasculature (140–146), leaving little signal to arise from the arteries. Nevertheless, there is still a need to confirm whether the vascular anomalies have only venous origins. Hence, the pre-contrast SWI data should be used to confirm that these vascular anomalies are part of the venous network.

We have seen a number of key venous vascular abnormalities in our MICRO imaging data even for just the first five patients scanned (see **Figure 3**) including:

**a) Angiomas:** Several small/micro-angiomas have been observed in the 5 cases we have done to date. The extent of the angioma predicts the region of inflammation seen in the FLAIR data (**Figure 3A**). The presence of these small DVAs or venous anomalies is not inconsistent with the fact that it is just those lesions with higher CBV that tend to show as acute lesions (47, 58).

**b) Micro-angiomas:** We also observed several lesion-centric angiomas-like vessel behavior, where fewer ( $\sim 3$ – $4$  vessels), much smaller (1 voxel-wide visibility) veins show a hint of

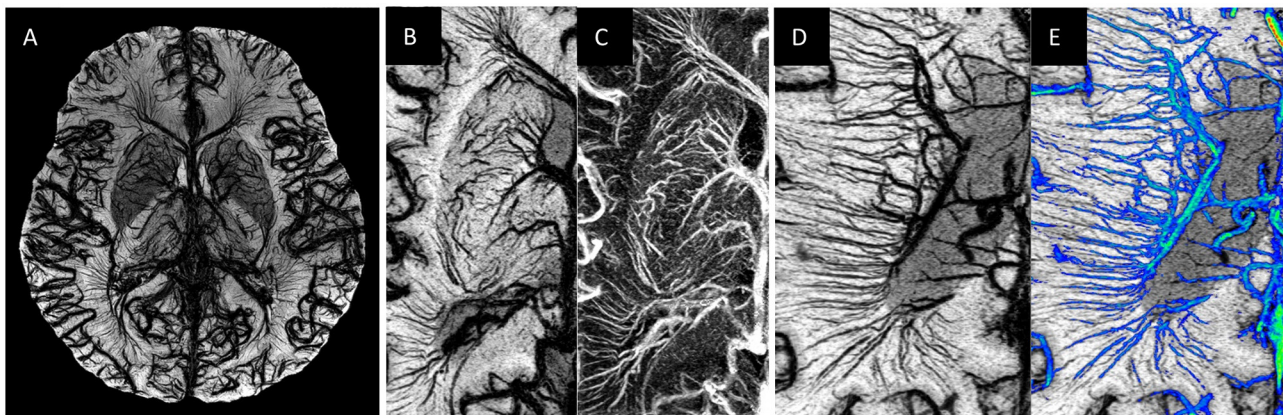


**FIGURE 1 |** Examples of MICRO imaging: **(A)** whole brain; **(B,C)** locally in the basal ganglia (image **B** is the SWI and image **C** image is the susceptibility map) and **(D,E)** the medullary veins. For part **(D)** the Frangi vesselness mask (78) was used to separate the veins (image **E**, shown in blue) from the background tissue from which one can calculate a medullary vein density (MVD).

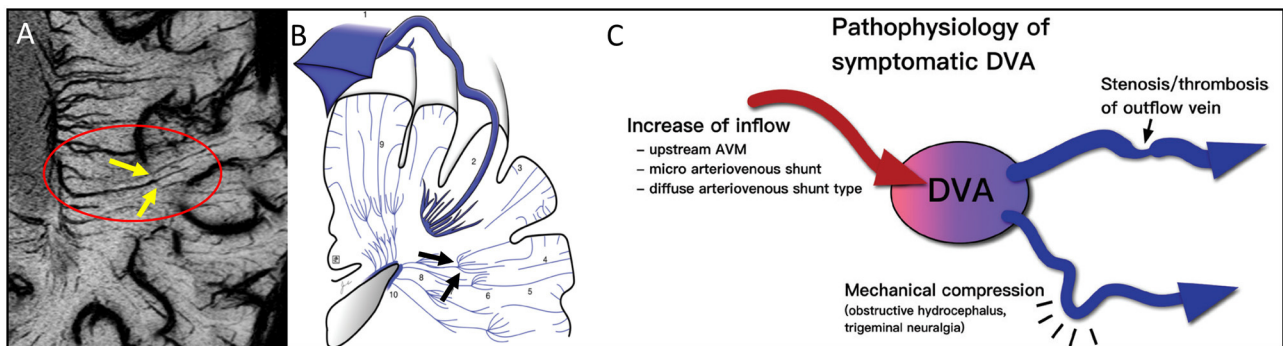


**FIGURE 2 |** Note the clear example of the pitchfork (candelabra) seen with MICRO imaging **(A)**, yellow arrows within red oval) that matches the sketch (79) from the cadaver brain work of Okudera (73) (black arrows in **B**). The idea of remodeling of the venous vasculature and recruiting anastomoses between medullary veins is not new. It is thought that these can occur for reasons of blocked flow and subsequent increases of inflow initially. This concept fits the results illustrated by the MICRO imaging data shown in **Figure 3**. The atypical DVA can have significant effects on the local flow and multiple clinical consequences **(C)**. Illustration taken from Aoki and Srivatanakul (79). This diagram shows that there can be increases in inflow, decreases in venous flow and mechanical compression as part of the pathophysiology of DVAs. **(B, C)** reproduced/adapted from Neurologia medico-chirurgica (NMC) under CC-BY license.

an irregular, spoke-like vascular pattern that we expect from an angioma (**Figure 3B**). We termed this category as “micro-angiomas,” which were visible due to the high-resolution post-contrast SWI data.

**c) Engorged/dilated vessels:** We note that not only is the CVS often present but using MICRO imaging we can see that veins can be locally dilated and it is exactly in this region where FLAIR lesions appear (**Figure 3C**). The SWI data must be minimum intensity projected (mIP) over a few neighboring slices to increase the visualization along the axis of the vein and to confirm the abrupt changes in its diameter.

**d) Small ovoid lesions:** Similarly, we observed local WMHs that only partially encapsulate the vein, unlike the usual CVS (**Figure 3D**). These were smaller in size (<3 mm in length) than the other WMHs and, due to their smaller size, are generally not considered during MS lesion classification (76).

These local WMH suggest collagenous thickening of the vessel wall and, as Lumsden notes, these lesions may enlarge and coalesce into a larger plaque over time (147). In fact, an early paper at 7T already showed evidence of small lesions that appeared along the veins but there was no enhancement when gadolinium was used (56).

**e) Perpendicular vessel connections:** In one subject, a medullary vein perpendicular to the usual venous drainage pathway was present perhaps due to local obstructed flow (again a form of vascular remodeling). Interestingly, these cases were located at the boundary of what appears to be the corona radiata, identified by a reduction in intensity from medial-to-lateral direction in the WM on FLAIR and SWI-FLAIR images (**Figure 3E**).

These various abnormalities are possible manifestations of poor flow and venous remodeling, all consistent with the previous



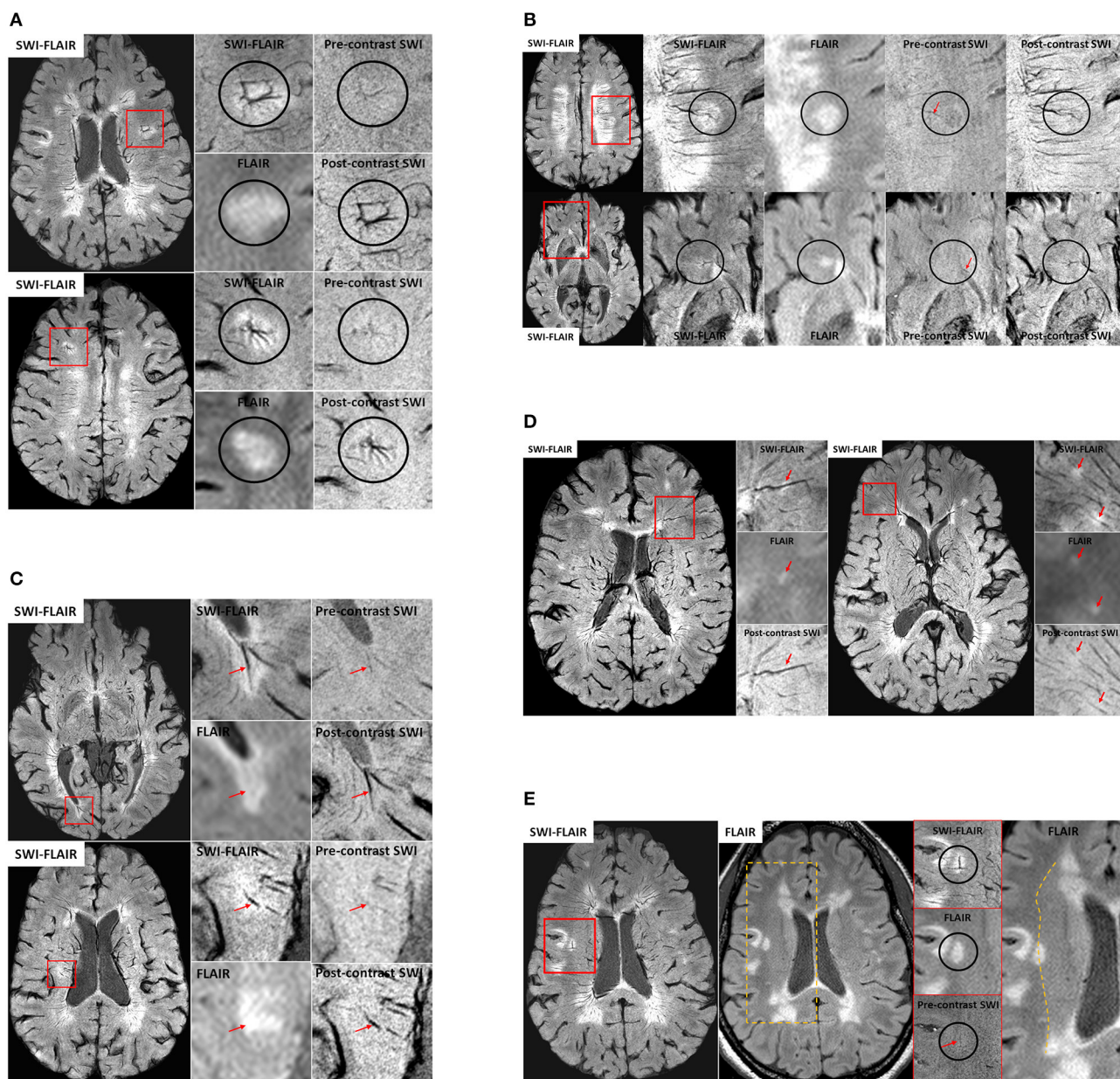
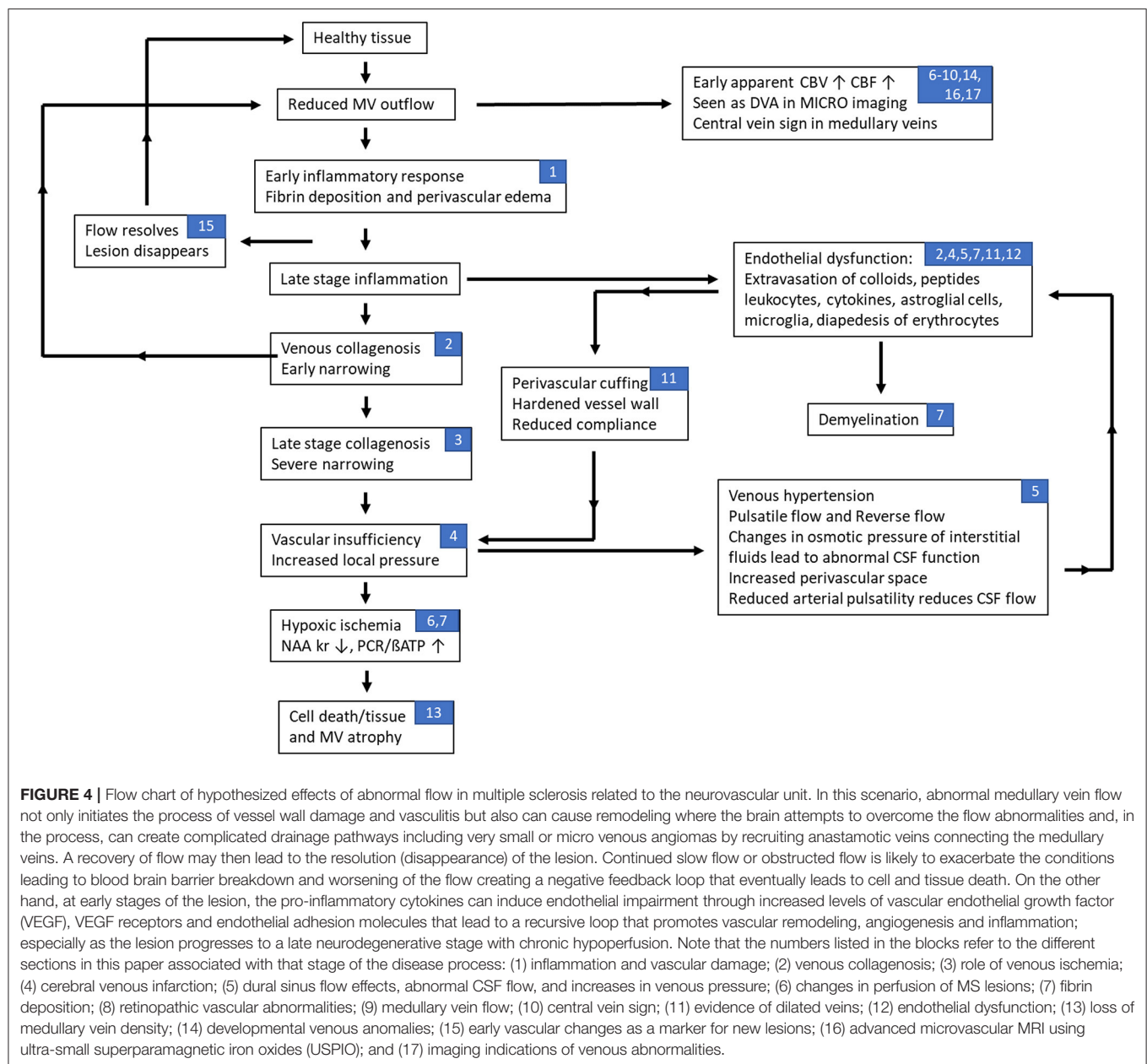


**FIGURE 3 |** (A) Examples of venous angioma like abnormalities in MS lesions from two patients. The small vessels joining the lesion-centric junction are not visible in conventional imaging and hence these DVAs have gone unrecognized in the past. Only the primary draining veins were slightly visible on the pre-contrast SWI data, confirming their venous origin. (B) Two different examples of micro-angiomas in MS lesions. Unlike the cases for larger angiomas, the pre-contrast SWI does not show any hints of these smaller vessels seen on the post-contrast SWI or SWI-FLAIR data, except for the primary vein (red arrows) that is draining the lesion-centric spoke-like small vessels. (C) Two different veins exhibiting dilation with the MS plaques. SWI-FLAIR data clearly shows the abrupt change in the vein diameter within the lesion. If these are active lesions, the inflammation may continue to develop around these vessels over time. In these cases, there may not be any further gadolinium enhancement as the lesion grows due to reduction of the vessel size or the complete blockage due to collagenosis. (D) Small ovoid WMHs (red arrows) located along the vessel wall of the small vessels as confirmed on SWI-FLAIR, FLAIR and post-contrast SWI data. (E) An example case showing a potential anastomotic vein. Once again, the pre-contrast SWI data was used to confirm the venous origin (red arrow) of this lesion-centric anomaly. The medial-to-lateral change in WM intensity on the FLAIR data (dotted line on the right-most image) is suggestive of the presence of the corona radiata layer in the WM and note that the anastomotic vein is abutting at this junction.





sections, all perhaps indicative of microvascular effects in the developing MS lesions.

## SUMMARY OF THE PUTATIVE TIMELINE OF EVENTS IN MS

The various materials introduced above include inflammation, vasculitis, abnormal flow, fibrin and collagen deposition leading to further reduced flow and perivascular medullary vein involvement. Recent imaging evidence provides the foundation stones for building a potential timeline for events that may represent some aspects of the pathophysiology of multiple sclerosis. Although the key source of MS is unknown, we

make the assumption that it is, in fact, initially related to abnormal flow and the cascade of events that would follow including vasculitis, inflammation, demyelination, ischemia and eventual tissue death. Based on all these works, we present our interpretation of the timeline of events in **Figure 4**. In this scenario, abnormal medullary vein flow not only initiates the process of vessel wall damage and vasculitis but also can cause vascular remodeling where the brain attempts to overcome the flow abnormalities and, in the process, can create complicated drainage pathways including very small or micro venous angiomas by recruiting anastomotic veins connecting the medullary veins. Sosa et al. show that the abnormal flow can initiate an endothelial response which in turn can cascade into further vascular damage and flow obstruction eventually

leading to an hypoxic ischemic situation which in the case of chronic inflammation finally leads to the destruction of the tissue (148). They also note that the anterior and posterior horns are particularly vulnerable because they are at the watershed zone of the anterior and middle cerebral arteries (148). Using an animal model, Desai et al. note that lesions tended to form specifically in areas of hypoxia and that by reducing the level of hypoxia lesions were less likely to form (149). These observations are complementary to the discussion in Caprio et al. in their review of cardiovascular risk factors related to MS (3). They consider the roles of smoking, hypertension, diabetes, vitamin D, etc. They also note that there are elevated levels of endothelin-1, a potent vasoconstrictor, in the plasma of MS patients. They conclude that endothelial cell adhesion molecules, pro-inflammatory cytokines, vascular growth factors and other molecules could contribute to vascular remodeling that is typical of MS, which can be exacerbated during chronic hypoperfusion in later stages of the lesion progression.

## FUTURE POSSIBILITIES AND OTHER CONSIDERATIONS

Subjects diagnosed with radiologically isolated syndrome (RIS) can be described as asymptomatic individuals with incidental radiologic abnormalities suggestive of MS and we have focused on the studies that cover the pathogenesis for the subjects that have already clinical signs related to the MS. Nevertheless, there have been studies that show that in subjects with RIS, around one-third of all subjects developed neurological symptoms within 5 years (150). Another recent study examined the occurrence of CVS in RIS subjects and found the number of CVS in RIS much higher (75%) than the 40% rule in the MS subjects reflecting a higher rate of perivenous inflammatory demyelination (151). This reduction in CVS from 75% in RIS to 40–50% in MS could suggest that, for the subjects that do evolve to symptomatic MS, the venous collagenosis developed over time due to the surrounding inflammation and this led to venous wall thickening, luminal narrowing and vessel occlusion. However, their subject size was small ( $n = 20$ ) and the prospective follow-up study has not been published yet to confirm how many showed neurological symptoms similar to MS. We would need a larger population to definitively conclude that venous process.

A key question to resolve in the future with a longitudinal study would be: “Are the small lesions that appear around the normal appearing vessels representative of the development of future lesions?” With the help of longitudinal MICRO data, we could further elucidate whether the abnormal vessel behavior, within or surrounding the lesion, act as a potential source initiating the inflammatory response. Finally, the automatic separation of venous and arterial components of the microvasculature for MICRO imaging is an important challenge to address. This will then allow us to separate the effects of arterial or venous network on the demyelination over time. One could potentially achieve this by acquiring SWI at multiple timepoints with increasing Ferumoxytol concentration levels to elucidate the difference in temporal signal changes for arterial and venous blood pools.

## CONCLUSION

All this evidence of venous vascular abnormalities in MS leads to a critical hypothesis as to one potential cause of MS: “*Local disrupted venous flow leads to remodeling of the medullary veins followed by a breakdown of the endothelium with the subsequent escape of glial cells, cytokines, etc. that in turn lead to the autoimmune demyelinating process and subsequent tissue death and atrophy.*” There are several key features in MS that can be understood in the context of this review. Whether or not venous flow disruption occurs first, the pathological course of MS is consistent with the continual feedback loop of constantly reducing blood flow over time. This is consistent with all findings in the literature. There are multiple mechanisms by which demyelination could occur at the cellular level but the source likely remains the extravasation of various cells and how they might precipitate demyelination. Abnormal flow is also consistent with generating an endothelial response in the form of inflammation first. This then leads again to the conventional wisdom on how the endothelium responds to inflammation. However, in the scenario outlined here, we show the effects of continued flow reduction because of processes such as fibrin deposition and collagenosis. This can then create a feedback loop as shown in **Figure 4** where vascular insufficiency leads to venous hypertension and other flow effects that then lead to a breakdown of the BBB. Further, the return to normal flow may, in fact, predict why lesions can recover as the usual nutrients and conditions required for endothelial health return to normal as well. In summary, this comprehensive overview of vascular effects in MS should open the door to study abnormal flow and its temporal relationship to the development of MS lesions using a variety of *in vivo* imaging methods. We encourage further research to study the microvasculature in MS as it relates to lesion formation and the development of chronic lesions.

## AUTHOR CONTRIBUTIONS

EH wrote the first draft of the manuscript. EH, YG, SS, SB, and PZ prepared, critically discussed the review, and edited the manuscript. All authors contributed to the article and approved the submitted version.

## FUNDING

This work was supported in part by a grant from the National Institute of Child Health and Human Development (grant number: R21 HD094424 02) to YG; by a grant from the National Institute of Neurological Disorders and Stroke (grant number: R01 NS108491) to YG and EH; and also, by a grant from the National Institute on Aging (grant number: R56 AG060822 01A1) for EH.

## ACKNOWLEDGMENTS

We would like to acknowledge Pavan Jella and Karthikeyan Subramanian for their assistance with image collection and post-processing. We would like to thank the Office of the Vice President for Research for its support of the MR Research Center.

## REFERENCES

- Compston A, Coles A. Multiple sclerosis. *Lancet*. (2008) 372:1502–17. doi: 10.1016/S0140-6736(08)61620-7
- Frischer JM, Bramow S, Dal-Bianco A, Lucchinetti CF, Rauschka H, Schmidbauer M, et al. The relation between inflammation and neurodegeneration in multiple sclerosis brains. *Brain*. (2009) 132:1175–89. doi: 10.1093/brain/awp070
- Caprio MG, Giugliano A, Ragucci M, Mancini M. Vascular disease in patients with multiple sclerosis: a review. *J Vasc Med Surg*. (2016) 4:1–12. doi: 10.4172/2329-6925.1000259
- Ganesh A, Stahnisch FW. The gray degeneration of the brain and spinal cord: a story of the once favored diagnosis with subsequent vessel-based etiopathological studies in multiple sclerosis. *J Nerv Ment Dis*. (2019) 207:505–14. doi: 10.1097/NMD.0000000000001002
- Kapadia A, Dmytriw AA. Multiple sclerosis is a systemic venous vasculopathy: a single unifying mechanism. *Med Hypotheses*. (2020) 140:1–5. doi: 10.1016/j.mehy.2020.109645
- Rindfleisch E. Histologisches Detail zu der grauen degeneration Von Gehirn und Rückenmark (Zugleich ein Beitrag zu der Lehre von der Entstehung und Verwandlung der Zelle). *Arch Pathol Anat Physiol Klin Med*. (1863) 26:474–83. doi: 10.1007/BF01878008
- Ribbert H. Ueber multiple sclerose des Gehirns und Rückenmarks. *Arch Pathol Anat Physiol Klin Med*. (1882) 90:243–60. doi: 10.1007/BF01931359
- Charcot JM. Histologie de la sclérose en plaques (leçon recueillie par Bournville). *Gaz Hop Civ*. (1868) 1051:140.
- Bourneville DM, Guérard L. *De la Sclérose en Plaques Disséminées*. Paris: Delahaye (1869).
- Adams CWM, Poston RN, Buk SJ, Sidhu YS, Vipond H. Inflammatory vasculitis in multiple sclerosis. *J Neurol Sci*. (1985) 69:269–83. doi: 10.1016/0022-510X(85)90139-X
- Adams CWM. The onset and progression of the lesion in multiple sclerosis. *J Neurol Sci*. (1975) 25:165–82. doi: 10.1016/0022-510X(75)90138-0
- Adams CWM. Perivascular iron deposition and other vascular damage in multiple sclerosis. *J Neurol Neurosurg Psychiatry*. (1988) 51:260–5. doi: 10.1136/jnnp.51.2.260
- Black S, Gao F, Bilbao J. Understanding white matter disease: imaging-pathological correlations in vascular cognitive impairment. *Stroke*. (2009) 40:48–52. doi: 10.1161/STROKEAHA.108.537704
- Gao F, van Gaal S, Levy-Cooperman N, Ramirez J, Scott CJM, Bilbao J, et al. P2-010: does variable progression of incidental white matter hyperintensities in Alzheimer's disease relate to venous insufficiency? *Alzheimer's Dement*. (2008) 4:T368–9. doi: 10.1016/j.jalz.2008.05.1090
- Moody DM. The blood-brain barrier and blood-cerebral spinal fluid barrier. *Semin Cardiothorac Vasc Anesth*. (2006) 10:128–31. doi: 10.1177/1089253206288992
- Brown WR, Moody DM, Challa VR, Thore CR, Anstrom JA. Venous collagenosis and arteriolar tortuosity in leukoaraiosis. *J Neurol Sci*. (2002) 203–4:159–63. doi: 10.1016/S.0022-510X(02)00283-6
- Krishnamurthy S, Li J, Shen Y, Duncan TM, Jenrow KA, Haacke ME. Normal macromolecular clearance out of the ventricles is delayed in hydrocephalus. *Brain Res*. (2018) 1678:337–55. doi: 10.1016/j.brainres.2017.10.013
- Jessen NA, Munk ASE, Lundgaard I, Nedergaard M. The glymphatic system: a beginner's guide. *Neurochem Res*. (2015) 40:2583–99. doi: 10.1007/s11064-015-1581-6
- Moody DM, Brown WR, Challa VR, Anderson RL. Periventricular venous collagenosis: association with leukoaraiosis. *Radiology*. (1995) 194:469–76. doi: 10.1148/radiology.194.2.7824728
- Keith J, Gao FQ, Noor R, Kiss A, Balasubramaniam G, Au K, et al. Collagenosis of the deep medullary veins: an underrecognized pathologic correlate of white matter hyperintensities and periventricular infarction? *J Neuropathol Exp Neurol*. (2017) 76:299–312. doi: 10.1093/jnen/nlx009
- Franceschi C. The unsolved puzzle of multiple sclerosis and venous function. *J Neurol Neurosurg Psychiatry*. (2009) 80:358. doi: 10.1136/jnnp.2008.168179
- Houck AL, Gutierrez J, Gao F, Igwe KC, Colon JM, Black SE, et al. Increased diameters of the internal cerebral veins and the basal veins of Rosenthal are associated with white matter hyperintensity volume. *Am J Neuroradiol*. (2019) 40:1712–8. doi: 10.3174/ajnr.A6213
- Yan S, Wan J, Zhang X, Tong L, Zhao S, Sun J, et al. Increased visibility of deep medullary veins in leukoaraiosis: a 3-T MRI study. *Front Aging Neurosci*. (2014) 6:144. doi: 10.3389/fnagi.2014.00144
- Akiguchi I, Tomimoto H, Suenaga T, Wakita H, Budka H. Blood-brain barrier dysfunction in Binswanger's disease; an immunohistochemical study. *Acta Neuropathol*. (1997) 95:78–84. doi: 10.1007/s004010050768
- Brickman AM, Zahra A, Muraskin J, Steffener J, Holland CM, Habeck C, et al. Reduction in cerebral blood flow in areas appearing as white matter hyperintensities on magnetic resonance imaging. *Psychiatry Res Neuroimaging*. (2009) 172:117–20. doi: 10.1016/j.psychres.2008.11.006
- Schaller B, Graf R. Cerebral venous infarction: the pathophysiological concept. *Cerebrovasc Dis*. (2004) 18:179–88. doi: 10.1159/000079939
- Bederson JB, Wiestler OD, Brüstle O, Roth P, Frick R, Yaşargil MG. Intracranial venous hypertension and the effects of venous outflow obstruction in a rat model of arteriovenous fistula. *Neurosurgery*. (1991) 29:341–50. doi: 10.1097/00006123-199109000-00002
- Willinsky RA, Goyal M, TerBrugge K, Montanera W. Tortuous, engorged pial veins in intracranial dural arteriovenous fistulas: correlations with presentation, location, and MR findings in 122 patients. *Am J Neuroradiol*. (1999) 20:1031–6.
- Van Den Berg R, Buis DR, Lagerwaard FJ, Lycklama A, Nijeholt GJ, Vandertop WP. Extensive white matter changes after stereotactic radiosurgery for brain arteriovenous malformations: a prognostic sign for obliteration? *Neurosurgery*. (2008) 63:1064–9. doi: 10.1227/01.NEU.0000330413.73983.02
- De Guio F, Vignaud A, Ropele S, Duering M, Duchesnay E, Chabriat H, et al. Loss of venous integrity in cerebral small vessel disease: a 7-T MRI study in cerebral autosomal-dominant arteriopathy with subcortical infarcts and leukoencephalopathy (CADASIL). *Stroke*. (2014) 45:2124–6. doi: 10.1161/STROKEAHA.114.005726
- Kurokawa Y, Hashi K, Okuyama T, Ueda T. Regional ischemia in cerebral venous hypertension due to embolic occlusion of the superior sagittal sinus in the rat. *Surg Neurol*. (1990) 34:390–5. doi: 10.1016/0090-3019(90)90242-H
- Zamboni P, Galeotti R, Menegatti E, Malagoni AM, Tacconi G, Dall'ara S, et al. Chronic cerebrospinal venous insufficiency in patients with multiple sclerosis. *J Neurol Neurosurg Psychiatry*. (2009) 80:392–9. doi: 10.1136/jnnp.2008.157164
- Zivadinov R, Marr K, Cutter G, Ramanathan M, Benedict RHB, Kennedy C, et al. Prevalence, sensitivity, and specificity of chronic cerebrospinal venous insufficiency in MS. *Neurology*. (2011) 77:138–44. doi: 10.1212/WNL.0b013e318212a901
- Trifan G, Sethi S, Elias S, Hewett J, Feng W, Haacke EM. Magnetic resonance imaging signatures of vascular pathology in multiple sclerosis. *Neurol Res*. (2012) 34:780–92. doi: 10.1179/1743132812Y.0000000078
- Veroux P, Giaquinta A, Perricone D, Lupo L, Gentile F, Virgilio C, et al. Internal jugular veins outflow in patients with multiple sclerosis: a catheter venography study. *J Vasc Interv Radiol*. (2013) 24:1790–7. doi: 10.1016/j.jvir.2013.08.024
- Lee BB, Baumgartner I, Berlien P, Bianchini G, Burrows P, Głowiczki P, et al. Diagnosis and treatment of venous malformations. consensus document of the International Union of Phlebology (IUP): updated 2013. *Int Angiol*. (2015) 34:97–149. Retrieved from: <https://www.minervamedica.it/en/journals/international-angiology/>
- Zhou D, Ding J, Asmaro K, Pan L, Ya J, Yang Q, et al. Clinical characteristics and neuroimaging findings in internal jugular venous outflow disturbance. *Thromb Haemost*. (2019) 119:308–18. doi: 10.1055/s-0038-1676815
- Gadda G, Taibi A, Sisini F, Gambaccini M, Zamboni P, Ursino M. A new hemodynamic model for the study of cerebral venous outflow. *Am J Physiol Hear Circ Physiol*. (2015) 308:H217–31. doi: 10.1152/ajpheart.00469.2014
- Toro E, Muller L, Cristini M, Menegatti E, Zamboni P. Impact of jugular vein valve function on cerebral venous haemodynamics. *Curr Neurovasc Res*. (2015) 12:384–97. doi: 10.2174/1567202612666150807112357
- Gaitán MI, De Alwis MP, Sati P, Nair G, Reich DS. Multiple sclerosis shrinks intraslesional, and enlarges extraslesional, brain parenchymal veins. *Neurology*. (2013) 80:145–51. doi: 10.1212/WNL.0b013e31827b916f
- Orešković D, Klarica M. The formation of cerebrospinal fluid: nearly a hundred years of interpretations and misinterpretations. *Brain Res Rev*. (2010) 64:241–62. doi: 10.1016/j.brainresrev.2010.04.006

42. Klose U, Strik C, Kiefer C, Grodd W. Detection of a relation between respiration and CSF pulsation with an echoplanar technique. *J Magn Reson Imaging*. (2000) 11:438–44. doi: 10.1002/(SICI)1522-2586(200004)11:4<438::AID-JMRI12>3.0.CO;2-O
43. Iliff JJ, Nedergaard M. Is there a cerebral lymphatic system? *Stroke*. (2013) 44:S93–5. doi: 10.1161/STROKEAHA.112.678698
44. Zamboni P. The contribution of extra cranial venous drainage to neuro-inflammation in multiple sclerosis. *Neuroinflammation*. (2018) 2018:579–99. doi: 10.1016/B978-0-12-811709-5.00036-3
45. Wuelfel J, Bellmann-Strobl J, Brunecker P, Aktas O, McFarland H, Villringer A, et al. Changes in cerebral perfusion precede plaque formation in multiple sclerosis: a longitudinal perfusion MRI study. *Brain*. (2004) 127:111–9. doi: 10.1093/brain/awh007
46. Magnano C, Schirda C, Weinstock-Guttman B, Wack DS, Lindzen E, Hojnacki D, et al. Cine cerebrospinal fluid imaging in multiple sclerosis. *J Magn Reson Imaging*. (2012) 36:825–34. doi: 10.1002/jmri.23730
47. Ge Y, Law M, Johnson G, Herbert J, Babb JS, Mannon LJ, et al. Dynamic susceptibility contrast perfusion MR imaging of multiple sclerosis lesions: characterizing hemodynamic impairment and inflammatory activity. *Am J Neuroradiol*. (2005) 26:1539–47. Retrieved from: <http://ajnr.org>
48. Holland CM, Charil A, Csapo I, Liptak Z, Ichise M, Khoury SJ, et al. The relationship between normal cerebral perfusion patterns and white matter lesion distribution in 1,249 patients with multiple sclerosis. *J Neuroimaging*. (2012) 22:129–36. doi: 10.1111/j.1552-6569.2011.00585.x
49. Francis PL, Jakubovic R, O'Connor P, Zhang L, Eilaghi A, Lee L, et al. Robust perfusion deficits in cognitively impaired patients with secondary-progressive Multiple Sclerosis. *Am J Neuroradiol*. (2013) 34:62–7. doi: 10.3174/ajnr.A3148
50. Peruzzo D, Castellaro M, Calabrese M, Veronese E, Rinaldi F, Bernardi V, et al. Heterogeneity of cortical lesions in multiple sclerosis: an MRI perfusion study. *J Cereb Blood Flow Metab*. (2013) 33:457–63. doi: 10.1038/jcbfm.2012.192
51. Steen C, D'haeseleer M, Hoogduin JM, Fierens Y, Cambron M, Mostert JP, et al. Cerebral white matter blood flow and energy metabolism in multiple sclerosis. *Mult Scler J*. (2013) 19:1282–9. doi: 10.1177/1352458513477228
52. Sowa P, Bjørnerud A, Nygaard GO, Damangir S, Spulber G, Celius EG, et al. Reduced perfusion in white matter lesions in multiple sclerosis. *Eur J Radiol*. (2015) 84:2605–12. doi: 10.1016/j.ejrad.2015.09.007
53. Adhya S, Johnson G, Herbert J, Jaggi H, Babb JS, Grossman RI, et al. Pattern of hemodynamic impairment in multiple sclerosis: dynamic susceptibility contrast perfusion MR imaging at 3.0 T. *Neuroimage*. (2006) 33:1029–35. doi: 10.1016/j.neuroimage.2006.08.008
54. Papadaki EZ, Simos PG, Panou T, Mastorodemos VC, Maris TG, Karantanias AH, et al. Hemodynamic evidence linking cognitive deficits in clinically isolated syndrome to regional brain inflammation. *Eur J Neurol*. (2014) 21:499–505. doi: 10.1111/ene.12338
55. Law M, Saindane AM, Ge Y, Babb JS, Johnson G, Mannon LJ, et al. Microvascular abnormality in relapsing-remitting multiple sclerosis: perfusion MR imaging findings in normal-appearing white matter. *Radiology*. (2004) 231:645–52. doi: 10.1148/radiol.2313030996
56. Ge Y, Zohrabian VM, Grossman RI. Seven-tesla magnetic resonance imaging: new vision of microvascular abnormalities in multiple sclerosis. *Arch Neurol*. (2008) 65:812–6. doi: 10.1001/archneur.65.6.812
57. Lagana M, Pelizzari L, Baglio F. Relationship between MRI perfusion and clinical severity in multiple sclerosis. *Neural Regen Res*. (2020) 15:646–52. doi: 10.4103/1673-5374.266906
58. Haacke EM, Li M, Juvvigitun F. Tissue similarity maps (TSMs): a new means of mapping vascular behavior and calculating relative blood volume in perfusion weighted imaging. *Magn Reson Imaging*. (2013) 31:481–9. doi: 10.1016/j.mri.2012.10.005
59. Bester M, Forkert ND, Stellmann JP, Aly L, Drabik A, Young KL, et al. Increased perfusion in normal appearing white matter in high inflammatory multiple sclerosis patients. *PLoS ONE*. (2015) 10:e0142464. doi: 10.1371/journal.pone.0142464
60. Sowa P, Nygaard GO, Bjørnerud A, Celius EG, Harbo HF, Beyer MK. Magnetic resonance imaging perfusion is associated with disease severity and activity in multiple sclerosis. *Neuroradiology*. (2017) 59:655–64. doi: 10.1007/s00234-017-1849-4
61. Papadaki EZ, Mastorodemos VC, Amanakis EZ, Tsekouras KC, Papadakis AE, Tsavalas ND, et al. White matter and deep gray matter hemodynamic changes in multiple sclerosis patients with clinically isolated syndrome. *Magn Reson Med*. (2012) 68:1932–42. doi: 10.1002/mrm.24194
62. Papadaki EZ, Simos PG, Mastorodemos VC, Panou T, Maris TG, Karantanias AH, et al. Regional MRI perfusion measures predict motor/executive function in patients with clinically isolated syndrome. *Behav Neurol*. (2014) 2014:1–8. doi: 10.1155/2014/252419
63. Matthews PM. Chronic inflammation in multiple sclerosis — seeing what was always there. *Nat Rev Neurol*. (2019) 15:582–93. doi: 10.1038/s41582-019-0240-y
64. Wakefield AJ, More LJ, Difford J, McLaughlin JE. Immunohistochemical study of vascular injury in acute multiple sclerosis. *J Clin Pathol*. (1994) 47:129–33. doi: 10.1136/jcp.47.2.129
65. Paterson PY. Experimental allergic encephalomyelitis: role of fibrin deposition in immunopathogenesis of inflammation in rats. *Fed Proc*. (1976) 35:2428–34.
66. Ginsberg MD, Hedley-Whyte ET, Richardson EP. Hypoxic-Ischemic Leukoencephalopathy in Man. *Arch Neurol*. (1976) 33:5–14. doi: 10.1001/archneur.1976.00500010007002
67. Graham EM, Stanford MR, Sanders MD, Kasp E, Dumonde DC. A point prevalence study of 150 patients with idiopathic retinal vasculitis: 1. Diagnostic value of ophthalmological features. *Br J Ophthalmol*. (1989) 73:714–21. doi: 10.1136/bjo.73.9.714
68. Kasp E, Graham EM, Stanford MR, Sanders MD, Dumonde DC. A point prevalence study of 150 patients with idiopathic retinal vasculitis: 2. Clinical relevance of antiretinal autoimmunity and circulating immune complexes. *Br J Ophthalmol*. (1989) 73:722–30. doi: 10.1136/bjo.73.9.722
69. Mark Haacke EB, Beggs C, Habib C. The role of venous abnormalities in neurological disease. *Rev Recent Clin Trials*. (2012) 7:100–16. doi: 10.2174/157488712800100305
70. Lightman S, McDonald WI, Bird AC, Francis DA, Hoskins A, Batchelor JR, et al. Retinal venous sheathing in optic neuritis: its significance for the pathogenesis of multiple sclerosis. *Brain*. (1987) 110:405–14. doi: 10.1093/brain/110.2.405
71. Taoka T, Fukusumi A, Miyasaka T, Kawai H, Nakane T, Kichikawa K, et al. Structure of the medullary veins of the cerebral hemisphere and related disorders. *Radiographics*. (2017) 37:281–97. doi: 10.1148/rg.2017160061
72. Nonaka H, Akima M, Hatori T, Nagayama T, Zhang Z, Ihara F. Microvasculature of the human cerebral white matter: arteries of the deep white matter. *Neuropathology*. (2003) 23:111–8. doi: 10.1046/j.1440-1789.2003.00486.x
73. Okudera T, Huang YP, Fukusumi A, Nakamura Y, Hatazawa J, Uemura K. Micro-angiographical studies of the medullary venous system of the cerebral hemisphere. *Neuropathology*. (1999) 19:93–111. doi: 10.1046/j.1440-1789.1999.00215.x
74. Lee C, Pennington MA, Kenney CM. MR evaluation of developmental venous anomalies: medullary venous anatomy of venous angiomas. *Am J Neuroradiol*. (1996) 17:61–70.
75. Dow RS, Berglund G. Vascular pattern of lesions of multiple sclerosis. *Arch Neurol Psychiatry*. (1942) 47:1–18. doi: 10.1001/archneurpsyc.1942.02290010011001
76. Sati P, Oh J, Todd Constable R, Evangelou N, Guttmann CRG, Henry RG, et al. The central vein sign and its clinical evaluation for the diagnosis of multiple sclerosis: a consensus statement from the North American Imaging in Multiple Sclerosis Cooperative. *Nat Rev Neurol*. (2016) 12:714–22. doi: 10.1038/nrneurol.2016.166
77. Tan IL, Van Schijndel RA, Pouwels PJW, Van Walderveen MAA, Reichenbach JR, Manoliu RA, et al. MR venography of multiple sclerosis. *Am J Neuroradiol*. (2000) 21:1039–42. Retrieved from: <http://ajnr.org>
78. Frangi AF, Niessen WJ, Vincken KL, Viergever MA. Multiscale vessel enhancement filtering. *Lecture Notes Comp Sci*. (1998) 1496:130–7.
79. Aoki R, Srivatanakul K. Developmental venous anomaly: benign or not benign. *Neurol Med Chir*. (2016) 56:534–43. doi: 10.2176/nmc.ra.2016-0030
80. Maggi P, Mazzoni L, N., Moretti M., Grammatico M., Chiti S., and Massacesi L. (2015). SWI enhances vein detection using gadolinium in multiple sclerosis. *Acta Radiol. Open* 4:2047981614560938. doi: 10.1177/2047981614560938



81. Lin W, Mukherjee P, An H, Yu Y, Wang Y, Vo K, et al. Improving high-resolution MR bold venographic imaging using a T1 reducing contrast agent. *J Magn Reson Imaging*. (1999) 10:118–23.
82. Broman T. Blood-brain barrier damage in multiple sclerosis supravital test-observations. *Acta Neurol Scand Suppl*. (1964) 40:21–4. doi: 10.1111/j.1600-0404.1964.tb04718.x
83. Fog T. On the vessel-plaque relationships in the brain in multiple sclerosis. *Acta Neurol Scand*. (1964) 40:9–15. doi: 10.1111/j.1600-0404.1964.tb04716.x
84. Allen IV. The pathology of multiple sclerosis - fact, fiction and hypothesis. *Neuropathol Appl Neurobiol*. (1981) 7:169–82. doi: 10.1111/j.1365-2990.1981.tb00087.x
85. Schelling F. Damaging venous reflux into the skull or spine: relevance to multiple sclerosis. *Med Hypotheses*. (1986) 21:141–8. doi: 10.1016/0306-9877(86)90003-4
86. Tallantyre EC, Dixon JE, Donaldson I, Owens T, Morgan PS, Morris PG, et al. Ultra-high-field imaging distinguishes MS lesions from asymptomatic white matter lesions. *Neurology*. (2011) 76:534–9. doi: 10.1212/WNL.0b013e31820b7630
87. Sati P, George IC, Shea CD, Gaitán MI, Reich DS. FLAIR\*: a combined MR contrast technique for visualizing white matter lesions and parenchymal veins. *Radiology*. (2012) 265:926–32. doi: 10.1148/radiol.12120208
88. Mistry N, Abdel-Fahim R, Samaraweera A, Mougín O, Tallantyre E, Tench C, et al. Imaging central veins in brain lesions with 3-T T2\*-weighted magnetic resonance imaging differentiates multiple sclerosis from microangiopathic brain lesions. *Mult Scler*. (2016) 22:1289–96. doi: 10.1177/1352458515616700
89. Samaraweera APR, Clarke MA, Whitehead A, Falah Y, Driver ID, Dineen RA, et al. The central vein sign in multiple sclerosis lesions is present irrespective of the T2\* sequence at 3 T. *J Neuroimaging*. (2017) 27:114–21. doi: 10.1111/jon.12367
90. Kilsdonk ID, Wattjes MP, Lopez-Soriano A, Kuijter JPA, De Jong MC, De Graaf WL, et al. Improved differentiation between MS and vascular brain lesions using FLAIR\* at 7 Tesla. *Eur Radiol*. (2014) 24:841–9. doi: 10.1007/s00330-013-3080-y
91. Maggi P, Absinta M, Grammatico M, Vuolo L, Emmi G, Carlucci G, et al. Central vein sign differentiates Multiple Sclerosis from central nervous system inflammatory vasculopathies. *Ann Neurol*. (2018) 83:283–94. doi: 10.1002/ana.25146
92. Zhang R, Zhou Y, Yan S, Zhong G, Liu C, Jiaerken Y, et al. A brain region-based deep medullary veins visual score on susceptibility weighted imaging. *Front Aging Neurosci*. (2017) 9:269. doi: 10.3389/fnagi.2017.00269
93. Decarli C, Maisog J, Murphy DGM, Teichberg D, Rapoport SI, Horwitz B. Method for quantification of brain, ventricular, and subarachnoid csf volumes from mr images. *J Comput Assist Tomogr*. (1992) 16:274–84. doi: 10.1097/00004728-199203000-00018
94. O'Sullivan M, Lythgoe DJ, Pereira AC, Summers PE, Jarosz JM, Williams SCR, et al. Patterns of cerebral blood flow reduction in patients with ischemic leukoaraiosis. *Neurology*. (2002) 59:321–6. doi: 10.1212/WNL.59.3.321
95. Ge Y, Zohrabian VM, Osa EO, Xu J, Jaggi H, Herbert J, et al. Diminished visibility of cerebral venous vasculature in multiple sclerosis by susceptibility-weighted imaging at 3.0 tesla. *J Magn. Reson. Imaging*. (2009) 29:1190–4. doi: 10.1002/jmri.21758
96. Zeng C, Chen X, Li Y, Ouyang Y, Lv F, Rumzan R, et al. Cerebral vein changes in relapsing-remitting multiple sclerosis demonstrated by three-dimensional enhanced T2\*-weighted angiography at 3.0 T. *Eur Radiol*. (2013) 23:869–78. doi: 10.1007/s00330-012-2637-5
97. Patankar TF, Mitra D, Varma A, Snowden J, Neary D, Jackson A. Dilatation of the Virchow-Robin space is a sensitive indicator of cerebral microvascular disease: study in elderly patients with dementia. *Am J Neuroradiol*. (2005) 26:1512–20. Retrieved from: <http://ajnr.org>
98. Murray ME, Vemuri P, Preboske GM, Murphy MC, Schweitzer KJ, Parisi JE, et al. A quantitative postmortem MRI design sensitive to white matter hyperintensity differences and their relationship with underlying pathology. *J Neuropathol Exp Neurol*. (2012) 71:1113–22. doi: 10.1097/NEN.0b013e318277387e
99. Talbert DG. Raised venous pressure as a factor in multiple sclerosis. *Med Hypotheses*. (2008) 70:1112–7. doi: 10.1016/j.mehy.2007.10.009
100. Croxford AL, Kurschus FC, Waisman A. Mouse models for multiple sclerosis: historical facts and future implications. *Biochim Biophys Acta Mol Basis Dis*. (2011) 1812:177–83. doi: 10.1016/j.bbadis.2010.06.010
101. Wardlaw JM, Smith C, Dichgans M. Mechanisms of sporadic cerebral small vessel disease: insights from neuroimaging. *Lancet Neurol*. (2013) 12:483–97. doi: 10.1016/S1474-4422(13)70060-7
102. Seabrook TJ, Littlewood-Evans A, Brinkmann V, Pöllinger B, Schnell C, Hiestand PC. Angiogenesis is present in experimental autoimmune encephalomyelitis and pro-angiogenic factors are increased in multiple sclerosis lesions. *J Neuroinflammation*. (2010) 7:95. doi: 10.1186/1742-2094-7-95
103. Roscoe WA, Welsh ME, Carter DE, Karlik SJ. VEGF and angiogenesis in acute and chronic MOG(35-55) peptide induced EAE. *J Neuroimmunol*. (2009) 209:6–15. doi: 10.1016/j.jneuroim.2009.01.009
104. Girolamo F, Coppola C, Ribatti D, Trojano M. Angiogenesis in multiple sclerosis and experimental autoimmune encephalomyelitis. *Acta Neuropathol Commun*. (2014) 2:84. doi: 10.1186/s40478-014-0084-z
105. Cho ML, Jung YO, Moon YM, Min SY, Yoon CH, Lee SH, et al. Interleukin-18 induces the production of vascular endothelial growth factor. (VEGF) in rheumatoid arthritis synovial fibroblasts via AP-1-dependent pathways. *Immunol Lett*. (2006) 103:159–66. doi: 10.1016/j.imlet.2005.10.020
106. Williams R, Rohr AM, Wang WT, Choi IY, Lee P, Berman NEJ, et al. Iron deposition is independent of cellular inflammation in a cerebral model of multiple sclerosis. *BMC Neurosci*. (2011) 12:59. doi: 10.1186/1471-2202-12-59
107. Zivadinov R, Weinstock-Guttman B, Pirko I. Iron deposition and inflammation in multiple sclerosis. Which one comes first? *BMC Neurosci*. (2011) 12:60. doi: 10.1186/1471-2202-12-60
108. De Keyser J, Steen C, Mostert JP, Koch MW. Hypoperfusion of the cerebral white matter in multiple sclerosis: possible mechanisms and pathophysiological significance. *J Cereb Blood Flow Metab*. (2008) 28:1645–51. doi: 10.1038/jcbfm.2008.72
109. Graumann U, Reynolds R, Steck AJ, Schaeren-Wiemers N. Molecular changes in normal appearing white matter in multiple sclerosis are characteristic of neuroprotective mechanisms against hypoxic insult. *Brain Pathol*. (2003) 13:554–73. doi: 10.1111/j.1750-3639.2003.tb00485.x
110. Holley JE, Newcombe J, Whatmore JL, Gutowski NJ. Increased blood vessel density and endothelial cell proliferation in multiple sclerosis cerebral white matter. *Neurosci Lett*. (2010) 470:65–70. doi: 10.1016/j.neulet.2009.12.059
111. Lucchinetti C, Bruck W. The pathology of primary progressive multiple sclerosis. *Mult Scler*. (2004) 10:S23–30. doi: 10.1191/1352458504ms1027oa
112. Sinnecker T, Bozin I, Dörr J, Pfueller CF, Harms L, Niendorf T, et al. Periventricular venous density in multiple sclerosis is inversely associated with T2 lesion count: a 7 tesla MRI study. *Mult Scler J*. (2013) 19:316–25. doi: 10.1177/1352458512451941
113. Kroll H, Soares BP, Saloner D, Dillon WP, Wintermark M. Imagerie tomodesitométrique de perfusion des angiomes veineux: aspects typiques et atypiques. *J Neuroradiol*. (2010) 37:239–42. doi: 10.1016/j.neurad.2009.09.002
114. Santucci GM, Leach JL, Ying J, Leach SD, Tomsick TA. Brain parenchymal signal abnormalities associated with developmental venous anomalies: detailed MR imaging assessment. *Am J Neuroradiol*. (2008) 29:1317–23. doi: 10.3174/ajnr.A1090
115. Rogers DM, Shah LM, Wiggins RH. The central vein: FLAIR signal abnormalities associated with developmental venous anomalies in patients with multiple sclerosis. *Am J Neuroradiol*. (2018) 39:2007–13. doi: 10.3174/ajnr.A5819
116. Sahin N, Solak A, Genc B, Bilgic N. Atypical developmental venous anomaly associated with contrast enhancement and hyperperfusion in the surrounding basal ganglia. *Quant Imaging Med Surg*. (2015) 5:472–5. doi: 10.3978/j.issn.2223-4292.2014.09.02
117. Umino M, Maeda M, Matsushima N, Matsuura K, Yamada T, Sakuma H. High-signal-intensity abnormalities evaluated by 3D fluid-attenuated inversion recovery imaging within the drainage territory of developmental venous anomalies identified by susceptibility-weighted imaging at 3 T. *Jpn J Radiol*. (2014) 32:397–404. doi: 10.1007/s11604-014-0322-0
118. Linscott LL, Leach JL, Zhang B, Jones BV. Brain parenchymal signal abnormalities associated with developmental venous anomalies in children and young adults. *Am J Neuroradiol*. (2014) 35:1600–7. doi: 10.3174/ajnr.A3960
119. Halicioglu S, Turkoglu SA. Role of developmental venous anomalies in etiopathogenesis of demyelinating diseases. *Int J Neurosci*. (2019) 129:245–51. doi: 10.1080/00207454.2018.1527330

120. Kruczek P, Bellenberg B, Lutz T, Schneider R, Ahlborn C, Gold R, et al. Developmental venous anomalies are more common in patients with multiple sclerosis and clinically isolated syndrome: coincidence or relevant? *Clin Neuroradiol.* (2021) 31:225–34. doi: 10.1007/s00062-019-00869-y
121. Hong YJ, Chung TS, Suh SH, Park CH, Tomar G, Seo KD, et al. The angioarchitectural factors of the cerebral developmental venous anomaly; Can they be the causes of concurrent sporadic cavernous malformation? *Neuroradiology.* (2010) 52:883–91. doi: 10.1007/s00234-009-0640-6
122. Sharma A, Zipfel GJ, Hildebolt C, Derdeyn CP. Hemodynamic effects of developmental venous anomalies with and without cavernous malformations. *Am J Neuroradiol.* (2013) 34:1746–51. doi: 10.3174/ajnr.A3516
123. Iv M, Fischbein NJ, Zaharchuk G. Association of developmental venous anomalies with perfusion abnormalities on arterial spin labeling and bolus perfusion-weighted imaging. *J Neuroimaging.* (2015) 25:243–50. doi: 10.1111/jon.12119
124. San Millán Ruiz D, Delavelle J, Yilmaz H, Gailloud P, Piovan E, Bertramello A, et al. Parenchymal abnormalities associated with developmental venous anomalies. *Neuroradiology.* (2007) 49:987–95. doi: 10.1007/s00234-007-0279-0
125. Haacke EM, Chen Y, Utriainen D, Wu B, Wang Y, Xia S, et al. STRategically Acquired Gradient Echo (STAGE) imaging, part III: technical advances and clinical applications of a rapid multi-contrast multi-parametric brain imaging method. *Magn Reson Imaging.* (2020) 65:15–26. doi: 10.1016/j.mri.2019.09.006
126. Guttmann CRG, Rousset M, Roch JA, Hannoun S, Durand-Dubief F, Belaroussi B, et al. Multiple sclerosis lesion formation and early evolution revisited: a weekly high-resolution magnetic resonance imaging study. *Mult Scler.* (2016) 22:761–9. doi: 10.1177/1352458515600247
127. Dal-Bianco A, Hametner S, Grabner G, Scherthaner M, Kronnerwetter C, Reitner A, et al. Veins in plaques of multiple sclerosis patients – a longitudinal magnetic resonance imaging study at 7 Tesla –. *Eur Radiol.* (2015) 25:2913–20. doi: 10.1007/s00330-015-3719-y
128. Liu S, Brisset JC, Hu J, Haacke EM, Ge Y. Susceptibility weighted imaging and quantitative susceptibility mapping of the cerebral vasculature using ferumoxytol. *J Magn Reson Imaging.* (2018) 47:621–33. doi: 10.1002/jmri.25809
129. Shen Y, Hu J, Eteer K, Chen Y, Buch S, Alhourani H, et al. Detecting sub-voxel microvasculature with USPIO-enhanced susceptibility-weighted MRI at 7 T. *Magn Reson Imaging.* (2020) 67:90–100. doi: 10.1016/j.mri.2019.12.010
130. Dousset V, Brochet B, Deloire MSA, Lagoarde L, Barroso B, Caille JM, et al. MR imaging of relapsing multiple sclerosis patients using ultra-small-particle iron oxide and compared with gadolinium. *Am J Neuroradiol.* (2006) 27:1000–5. Retrieved from: <http://ajnr.org>
131. Vellinga MM, Vrenken H, Hulst HE, Polman CH, Uitdehaag BMJ, Pouwels PJW, et al. Use of ultrasmall superparamagnetic particles of iron oxide (USPIO)-enhanced mri to demonstrate diffuse inflammation in the normal-appearing white matter (NAWM) of multiple sclerosis (MS) patients: an exploratory study. *J Magn Reson Imaging.* (2009) 29:774–9. doi: 10.1002/jmri.21678
132. Tourdias T, Roggerone S, Filippi M, Kanagaki M, Rovaris M, Miller DH, et al. Assessment of disease activity in multiple sclerosis phenotypes with combined gadolinium- and superparamagnetic iron oxide-enhanced MR imaging. *Radiology.* (2012) 264:225–33. doi: 10.1148/radiol.12111416
133. Dal-Bianco A, Grabner G, Kronnerwetter C, Weber M, Höftberger R, Berger T, et al. Slow expansion of multiple sclerosis iron rim lesions: pathology and 7 T magnetic resonance imaging. *Acta Neuropathol.* (2017) 133:25–42. doi: 10.1007/s00401-016-1636-z
134. Buch S, Wang Y, Park MG, Jella PK, Hu J, Chen Y, et al. Subvoxel vascular imaging of the midbrain using USPIO-Enhanced MRI. *Neuroimage.* (2020) 220:117106. doi: 10.1016/j.neuroimage.2020.117106
135. Buch S, Subramanian K, Jella PK, Chen Y, Wu Z, Shah K, et al. Revealing vascular abnormalities and measuring small vessel density in multiple sclerosis lesions using USPIO. *NeuroImage Clin.* (2021) 29:1–16. doi: 10.1016/j.nicl.2020.102525
136. Brownell B, Hughes JT. The distribution of plaques in the cerebrum in multiple sclerosis. *J Neurol Neurosurg Psychiatry.* (1962) 25:315–20. doi: 10.1136/jnnp.25.4.315
137. McDonald WI, Compston A, Edan G, Goodkin D, Hartung HP, Lublin FD, et al. Recommended diagnostic criteria for multiple sclerosis: guidelines from the International Panel on the Diagnosis of Multiple Sclerosis. *Ann Neurol.* (2001) 50:121–7. doi: 10.1002/ana.1032
138. Vellinga MM, Geurts JJG, Rostrup E, Uitdehaag BMJ, Polman CH, Barkhof F, et al. Clinical correlations of brain lesion distribution in multiple sclerosis. *J Magn Reson Imaging.* (2009) 29:768–73. doi: 10.1002/jmri.21679
139. Charil A, Zijdenbos AP, Taylor J, Boelman C, Worsley KJ, Evans AC, et al. Statistical mapping analysis of lesion location and neurological disability in multiple sclerosis: application to 452 patient data sets. *Neuroimage.* (2003) 19:532–44. doi: 10.1016/S1053-8119(03)00117-4
140. Poser CM. *Arterial Behavior and Blood Circulation in the Brain.* New York, NY: Plenum Press (1987).
141. McCormick PW, Stewart M, Goetting MG, Balakrishnan G. Regional cerebrovascular oxygen saturation measured by optical spectroscopy in humans. *Stroke.* (1991) 22:596–602. doi: 10.1161/01.STR.22.5.596
142. Pollard V, Prough DS, Eric DeMelo A, Deyo DJ, Uchida T, Stoddart HF. Validation in volunteers of a near-infrared spectroscope for monitoring brain oxygenation in vivo. *Anesth Analg.* (1996) 82:269–77. doi: 10.1213/00000539-199602000-00010
143. Van Zijl PCM, Eleff SM, Ulatowski JA, Oja JME, Ulug AM, Traystman RJ, et al. Quantitative assessment of blood flow, blood volume and blood oxygenation effects in functional magnetic resonance imaging. *Nat Med.* (1998) 4:159–67. doi: 10.1038/nm0298-159
144. An H, Lin W. Cerebral venous and arterial blood volumes can be estimated separately in humans using magnetic resonance imaging. *Magn Reson Med.* (2002) 48:583–8. doi: 10.1002/mrm.10257
145. An H, Lin W. Cerebral oxygen extraction fraction and cerebral venous blood volume measurements using MRI: effects of magnetic field variation. *Magn Reson Med.* (2002) 47:958–66. doi: 10.1002/mrm.10148
146. Hua J, Liu P, Kim T, Donahue M, Rane S, Chen JJ, et al. MRI techniques to measure arterial and venous cerebral blood volume. *Neuroimage.* (2019) 187:17–31. doi: 10.1016/j.neuroimage.2018.02.027
147. Bo L, Evangelou N, Tallantyre E. The neuropathology of progressive multiple sclerosis. *Progr Multip Scler.* (2013) 51–70. doi: 10.1007/978-1-4471-2395-8\_4
148. Sosa SM, Smith KJ. Understanding a role for hypoxia in lesion formation and location in the deep and periventricular white matter in small vessel disease and multiple sclerosis. *Clin Sci.* (2017) 131:2503–24. doi: 10.1042/CS20170981
149. Desai RA, Davies AL, Tachrount M, Kasti M, Laulund F, Golay X, et al. Cause and prevention of demyelination in a model multiple sclerosis lesion. *Ann Neurol.* (2016) 79:591–604. doi: 10.1002/ana.24607
150. Okuda DT, Siva A, Kantarci O, Inglese M, Katz I, Tutuncu M, et al. Radiologically isolated syndrome: 5-year risk for an initial clinical event. *PLoS ONE.* (2014) 9:e90509. doi: 10.1371/journal.pone.0090509
151. Suthiphosuwat S, Sati P, Guenette M, Montalban X, Reich DS, Bharatha A, et al. The central vein sign in radiologically isolated syndrome. *Am J Neuroradiol.* (2019) 40:776–83. doi: 10.3174/ajnr.A6045

**Conflict of Interest:** EH and SS are employed by SpinTech, Inc. and MR Innovations, Inc.

The remaining authors declare that the research was conducted in the absence of any commercial or financial relationships that could be construed as a potential conflict of interest.

Copyright © 2021 Haacke, Ge, Sethi, Buch and Zamboni. This is an open-access article distributed under the terms of the Creative Commons Attribution License (CC BY). The use, distribution or reproduction in other forums is permitted, provided the original author(s) and the copyright owner(s) are credited and that the original publication in this journal is cited, in accordance with accepted academic practice. No use, distribution or reproduction is permitted which does not comply with these terms.



# Severity of Lesions Involving the Cortical Cholinergic Pathways May Be Associated With Cognitive Impairment in Subacute Ischemic Stroke

Huo-Hua Zhong<sup>1†</sup>, Jian-feng Qu<sup>1†</sup>, Wei-Min Xiao<sup>1\*</sup>, Yang-kun Chen<sup>1\*</sup>, Yong-lin Liu<sup>1</sup>, Zhi-qiang Wu<sup>1</sup>, Dong-hai Qiu<sup>1</sup> and Wen-cong Liang<sup>2</sup>

<sup>1</sup> Department of Neurology, Dongguan People's Hospital, Dongguan, China, <sup>2</sup> Graduate School, Guangdong Medical University, Dongguan, China

## OPEN ACCESS

### Edited by:

Meiyun Wang,  
Henan Provincial People's Hospital,  
China

### Reviewed by:

Dafin F. Muresanu,  
Iuliu Hațieganu University of Medicine  
and Pharmacy, Romania  
Sheila Gillard Crewther,  
La Trobe University, Australia

### \*Correspondence:

Yang-kun Chen  
cykun78@163.com  
Wei-Min Xiao  
xwm1115@126.com

<sup>†</sup>These authors have contributed  
equally to this work

### Specialty section:

This article was submitted to  
Stroke,  
a section of the journal  
Frontiers in Neurology

**Received:** 15 September 2020

**Accepted:** 04 May 2021

**Published:** 08 June 2021

### Citation:

Zhong H-H, Qu J-f, Xiao W-M,  
Chen Y-k, Liu Y-l, Wu Z-q, Qiu D-h  
and Liang W-c (2021) Severity of  
Lesions Involving the Cortical  
Cholinergic Pathways May Be  
Associated With Cognitive Impairment  
in Subacute Ischemic Stroke.  
Front. Neurol. 12:606897.  
doi: 10.3389/fneur.2021.606897

**Purpose:** Impairment of cortical cholinergic pathways (CCP) is an important risk factor for chronic vascular cognitive impairment. However, this phenomenon has rarely been studied in post-stroke cognitive impairment (PSCI). We investigated the relationship between PSCI and CCP lesions assessed by structural magnetic resonance imaging (MRI).

**Patients and methods:** We prospectively enrolled 103 patients within 7 days of ischemic stroke onset. CCP was measured by the cholinergic pathways hyperintensities scale (CHIPS), which semiquantitatively grades MR lesions strategically located on the CCP identified in human brains. We also measured other MRI parameters, including the location and volumes of acute infarcts, cerebral microbleeds, medial temporal lobe atrophy, and white matter lesions. Neuropsychological assessments were performed using the 60-min modified vascular dementia battery (VDB) at 3 months after the index stroke, and PSCI was defined according to VDB as well as ADL.

**Results:** Of all 103 patients, 69 men (67.0%) and 34 women (33.0%) with a mean age of  $57.22 \pm 12.95$  years, 55 patients (53.4%) were judged to have PSCI at 3 months, including 43 (41.7%) patients with PSCI-no dementia and 12 (11.7%) patients with poststroke dementia. According to the VDB assessment, the most commonly impaired cognitive domain was visuomotor speed (27.2%) followed by verbal memory (25.2%). Univariate analysis showed that patients with PSCI were older; had higher informant questionnaire on cognitive decline in the elderly (IQCODE) scores; had more frequent previous stroke history and atrial fibrillation; and had higher CHIPS scores, more severe white matter lesions, and medial temporal lobe atrophy. PSCI patients also had higher depression scores at 3 months. In the multivariate regression analysis, age, IQCODE score, CHIPS score, and Hamilton depression rating scale score were independent predictors of PSCI. Ordinal regression analysis for risk factors of poor functional outcomes revealed that IQCODE scores and cognitive function status were related to mRS score at 3 months after stroke.

**Conclusion:** In patients with early subacute ischemic stroke, the severity of lesions involving the CCP may be associated with cognitive impairment at 3 months.

**Clinical Trial Registration:** Chinese Clinical Trial Registry, identifier: ChiCTR1800014982.

**Keywords:** stroke, cortical cholinergic pathways, brain MRI, cognitive impairment, white matter lesions

## INTRODUCTION

Poststroke cognitive impairment (PSCI), which includes PSCI-no dementia (PSCI-ND) and poststroke dementia (PSD), is one of the most common outcomes of acute ischemic stroke, occurring in  $\geq 80\%$  of survivors (1, 2). It has a negative effect on functional outcomes (1, 3) and predicts the recurrence of vascular events (4). However, the precise pathological mechanisms of PSCI remain unclear.

Acetylcholine (ACh) functions as an excitatory neuromodulator of the cerebral cortex and participates in nearly all aspects of cortical function, and its reduction may be closely related to the occurrence of PSCI (5). ACh is mainly located in the axons of cholinergic neurons, which is the synthesis of choline and acetyl-CoA in one step by choline acetyltransferase (ChAT). ACh depends on the vesicle ACh transporter (VACHT) to be transported and stored in synaptic vesicles. During an action potential, under the mediation of  $\text{Ca}^{2+}$ , ACh vesicles fuse with the presynaptic membrane, and the vesicles rupture. ACh enters the synaptic cleft and binds to the ACh receptors of the presynaptic and postsynaptic membranes, thereby causing physiological effects. The release of ACh is regulated by many factors. Activation of noradrenergic  $\alpha 1$  receptors may increase cortical ACh release, and glutamate can excite basal forebrain cholinergic neurons and increase cortical high-affinity bile alkali uptake and ACh release (6–8). There are two types of ACh receptors: muscarinic acetylcholine receptors (mAChRs) and nicotinic acetylcholine receptors (nAChRs), located in the presynaptic and postsynaptic membranes in the brain, playing important roles in regulating the release of glutamate,  $\gamma$ -aminobutyric acid, dopamine, norepinephrine, and other neurotransmitters related to cognitive function (9, 10). ChAT is the most specific marker for cholinergic neurons. The cortical cholinergic pathway (CCP) was discovered through brain ChAT immunohistochemical staining and magnetic resonance imaging (MRI) overlay analysis technology (11). The CCP is one of the major cholinergic structural connections in the brain. It includes the diagonal band of Broca, the medial septal nuclei, and the nucleus basalis of Meynert (nbM) and projecting fibers from these cells (12). Severe neurofibrillary degeneration of cholinergic cell bodies in the nucleus basalis and correspondingly severe denervation of neocortical cholinergic projections was reported in a patient with Alzheimer's disease (AD) (13). Damage to cholinergic fibers and a decrease in cholinergic neurotransmitters may be involved in cognitive impairment.

The CCP represents fibers that project from the nbM to the cortex and amygdala and also branch into the medial and lateral pathways (11, 14, 15). In 2005, Bocti et al. developed

the cholinergic pathways hyperintensities scale (CHIPS) based on immunohistochemical research to measure CCP (16). Lim et al. first established a case-control study of patients with acute ischemic stroke, using a modified version of CHIPS to evaluate the MRI data and reported that disruption of the cholinergic pathways and major hubs of large-scale neural networks might contribute to newly developed dementia after acute ischemic stroke (17). However, the sample in this previous study was relatively small, and the potential relationship between CCP involvement and PSCI in patients with acute or early subacute ischemic stroke was not studied in detail. Hence, we conducted the present study to explore the relationship between the degree of CCP involvement and PSCI in patients with early subacute ischemic stroke.

## METHODS

### Patients

The study was conducted in Division I, Department of Neurology, Dongguan People's Hospital (Dongguan, China) between September 1, 2018, and July 31, 2019. The inclusion criteria for the study were (1) age  $> 18$  years, (2) first or recurrent early subacute ischemic stroke occurring within 7 days before admission (the ischemic stroke diagnosis was made in accordance the American Heart Association Stroke Council criteria) (18), and (3) that a complete brain MRI examination had been performed. The exclusion criteria were (1) transient ischemic attack, cerebral hemorrhage, epidural or subdural hematoma, or subarachnoid hemorrhage; (2) prestroke cognitive impairment, which was assessed using the informant questionnaire on cognitive decline in the elderly (IQCODE) in hospital (19); (3) coexisting conditions (beside stroke) that affect cognitive function (e.g., major depression or anxiety, chronic alcoholism, previously diagnosed psychiatric conditions, epilepsy, severe traumatic brain injury, Parkinson's disease, multiple sclerosis); (4) lack of complete clinical or MRI data; (5) death during hospitalization; (6) severe stroke indicated by a National Institutes of Health stroke scale (NIHSS) score  $\geq 15$  points at discharge; (7) patients with severe comorbidities (e.g., liver, kidney, heart, or respiratory failure or malignant tumors); (8) severe hearing disabilities, sight disabilities, or language disorders at discharge according to physical examination; and (9) refusal by patients or their relatives to provide informed consent.

### Collection of Demographic Data

Demographic and clinical variables (i.e., age, sex, years of education, onset time, vascular risk factors, history of stroke, and neurological deficit status assessed using the NIHSS)



were collected. Preexisting cognitive status was evaluated using the IQCODE within 3 days after admission. The IQCODE questionnaire consists of 16 items that assess impairment in the patient over the previous 10 years. The IQCODE score ranges from 16 (marked improvement in all items) to 80 (marked worsening in all items). A total score >51 points is considered to indicate a preexisting cognitive impairment (19).

## MRI Assessments

Brain MRI scanning, including T1-, T2-, diffusion-, and susceptibility-weighted imaging sequences were performed on each participant using a 3.0-T system (Sonata; Siemens Medical, Erlangen, Germany) within 7 days after admission. Diffusion-weighted image spin-echo echo-planar imaging (repetition time [TR]/echo time [TE]/excitation: 2,162/76/1; matrix: 128×128; field of view (FOV): 230 mm; slice thickness/gap: 6 mm/1 mm; echo-planar imaging factor: 47; acquisition time: 25.9 s) with three orthogonally applied gradients was used with a *b* value of 0 and 1,000. Axial spin echo T1 (TR/TE/excitation: 488/15/1; FOV: 230 mm, slice thickness/gap: 6 mm/1 mm; matrix: 256 × 256; time of acquisition: 1 min 24.8 s) and turbo spin echo T2 (TR/TE/excitation: 3,992/110/2; turbo factor: 15; FOV: 230 mm; slice thickness/gap: 6 mm/1 mm; matrix: 512 × 512, time of acquisition: 1 min 55.8 s) images were also captured.

A neurologist (JFQ) measured the MRI variables as follows:

**(1) Assessment of lesions involving the CCP.** Lesions involving the CCP were assessed using CHIPS (16), which was developed based on immunohistochemical tracings of the cholinergic pathways in humans, superimposed onto a structural MRI image (11). Measurement zones within four index slices of white matter regions were demarcated on axial T2-weighted images of the lateral ventricles and the third ventricle. Slices: (A) low external capsule layer (four separate zones: bilateral anterior and posterior zones), (B) high external capsule layer (six separate zones: bilateral anterior, posterior, and cingulate gyrus zones), (C) corona radiata (six separate zones: bilateral anterior, posterior, and cingulate gyrus zones), and (D) semioval center (four separate zones: bilateral anterior and posterior zones). The severity of white matter hyperintensities (WMHs) in each zone was scored as (1) normal (0 points), (2) <50% of the region involved (1 point), and (3) ≥50% of the region involved (2 points). Severity scores were weighted according to the distribution density of cholinergic fibers. The weighting coefficients were as follows: 4 for slice A, 3 for slice B, 2 for slice C, and 1 for slice D. The score for each region was obtained by adding all points from the measurements of small zones and multiplying them by the weighting coefficient. The maximum score per hemisphere was 50, and the total maximum score per scan when combining scores for all four regions was 100. The CHIPS total score showed a good correlation with lesion volume within the cholinergic pathways (Spearman's  $\rho = 0.87$ ,  $p < 0.0001$ ). Higher CHIPS scores suggest more severe CCP impairment (16). Lesions involving the CCP included acute infarction, old infarction, or WMHs (Figure 1) (20).

**(2) Acute infarcts.** Acute infarcts were defined as regions of restricted water diffusion identified on diffusion-weighted imaging with *b* values of 1,000 together with hypointensity on

the corresponding apparent diffusion coefficient map. The sites of acute infarcts were divided into cortical regions (frontal, temporal, parietal, and occipital lobes), subcortical regions (white matter, basal ganglia, and thalamus), and infratentorial regions (i.e., brainstem and cerebellum). The contours of an acute infarct on diffusion-weighted imaging were manually outlined. The total volume was subsequently calculated by multiplying the total area by the sum of the slice thickness and the gap.

**(3) White matter lesions (WMLs).** The severity of WMLs, including deep white matter hyperintensities (DWMH) and periventricular hyperintensities (PVH), were scored using fluid-attenuated inversion recovery images with the Fazekas scale (range 0–3) (21).

**(4) Medial temporal lobe atrophy (MTLA).** MTLA was assessed using the Scheltens' scale (22) in which coronal MRI sections are used to judge the severity of MTLA based on standard images (range from 0 to 4, no atrophy to severe atrophy).

**(5) Cerebral microbleeds.** These were defined as small (2–10 mm) hypointense lesions with a clear margin in susceptibility-weighted imaging. Symmetric basal ganglia calcification and flow void artifacts of the pial blood vessels were excluded.

## Cognitive and Psychological Assessments

Neuropsychological assessments were performed at 3 months through a face-to-face interview with patients after the index stroke by a trained neurologist (HHZ), who was blinded to all clinical data. We did not assess cognitive impairment in the acute phase because, in acute stroke, assessment of cognitive function is not reliable because of cognitive status being unstable, and the severity of disease can preclude lengthy neuropsychological testing (23, 24). We did not assess the cognitive function used by the Montréal Cognitive Assessment because it is commonly used as a screening tool rather than a diagnostic criteria (25, 26). We used a more comprehensive neuropsychological battery that was a modified version of the vascular dementia battery (VDB) (27, 28), which comprises the following seven cognitive domains: (1) executive functions [frontal assessment battery (29, 30); trail-making test, parts A and B]; (2) attention (digit span: forward and backward) (31), visual memory span (forward and backward) (32) and the auditory detection test (28); (3) language (modified Boston naming test) (33) and verbal fluency (34) (animal and food categories); (4) verbal memory (immediate and delayed word list recall, delayed word list recognition, and immediate and delayed story recall) (35). For this, the tester needs to clearly read 12 related vocabularies or a story to the testee, learn it three times, and then the tester needs to recall the vocabulary or story in real time and then recall the vocabulary or story they just learned 20 min later. During the delayed word list recognition, according to the content just learned, the testee needs to recognize the order of the vocabulary. Next is (5) visual memory (immediate picture recall, delayed picture recall, and delayed picture recognition) (32), visual reproduction I and II and delayed recognition from the Wechsler memory scale III (WMS-III) (32); (6) visuoconstruction [clock drawing test (35), Wechsler adult intelligence scale III [WAIS-III] block design (31) and visual reproduction (copy) from WMS-III (32)];

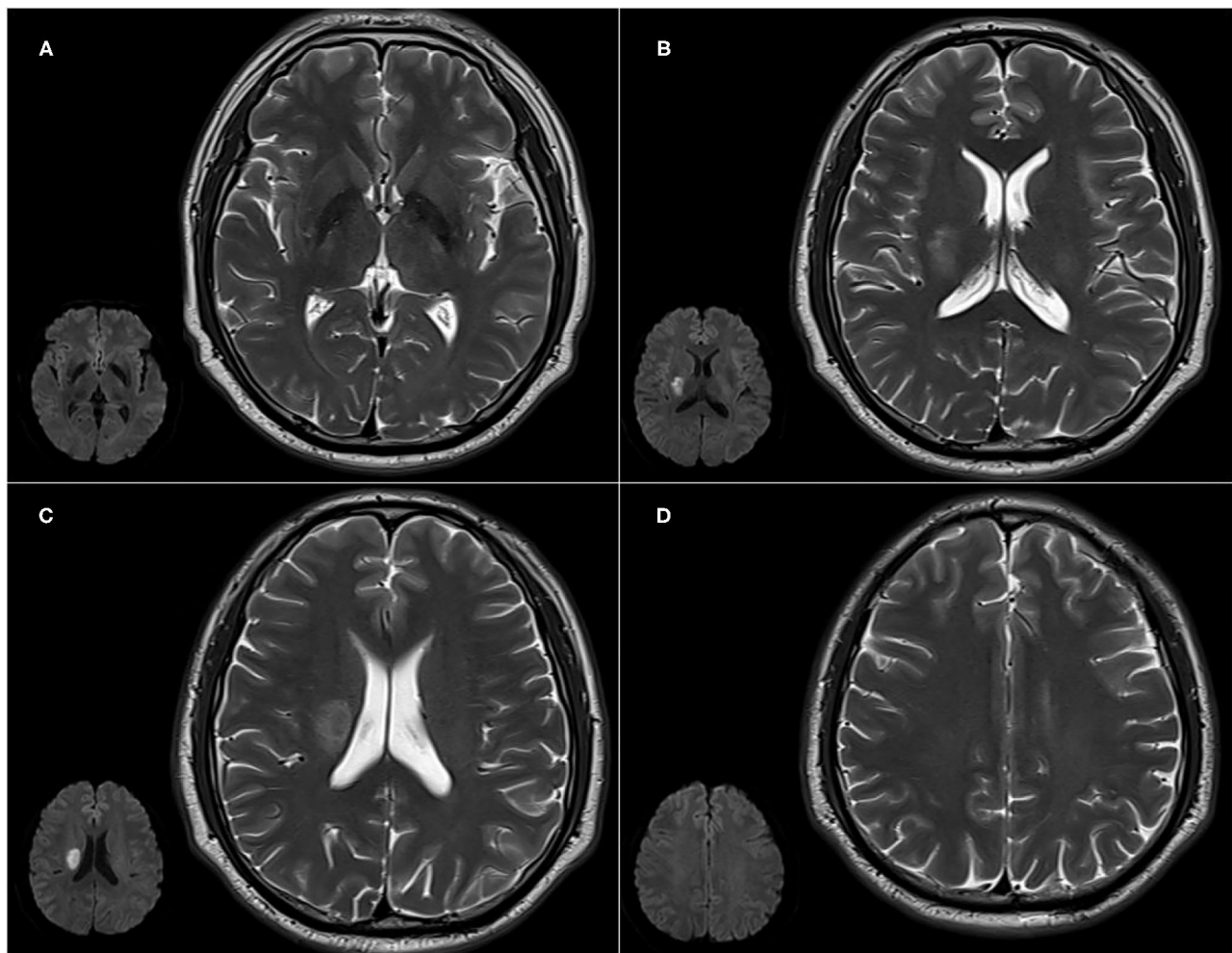


**FIGURE 1 |** Cholinergic Pathways Hyperintensities Scale (CHIPS) scores from representative patients with both early subacute ischemic stroke and white matter lesions (WMLs). Slices: **(A)** low external capsule layer (bilateral posterior zones score are 1 each, bilateral anterior zones score 0); **(B)** high external capsule layer (bilateral posterior zones score 1 each, bilateral anterior and cingulate gyrus zones score 0); **(C)** corona radiata (right posterior zone score 1, bilateral anterior and cingulate gyrus zones score 0); and **(D)** the semioval center (bilateral anterior and posterior zones score 0).

(7) visuomotor speed [symbol digit modalities test (36), digit cancellation test, and the maze task (28)]. The testee can see the content of the test. In the symbol digit modalities test, he or she needs to simulate different symbols corresponding to different numbers that have been specified, fill in the corresponding numbers in the space below the symbols, and record the number filled in by the tester in 120 s. In the digit cancellation test, the subject needs to cross out the number to be canceled as much as possible within 90 s. The maze task is to calculate the time it takes for the testee to successfully find the exit route of the maze. Apart from the executive domain, impairment of individual cognitive domains was identified if at least 50% of the subtests were below the cutoff points. The cutoff points were derived from a Chinese sample (33) (**Supplementary Table 1**). The criteria for impairment in any of the seven cognitive components were adjusted for the education level of each patient (28). PSCI refers to a series of syndromes meeting the diagnostic

criteria of cognitive impairment within 6 months after an index stroke according to the Diagnostic and Statistical Manual of Mental Disorders (Fifth Edition) criteria (37). We defined PSCI as impairment in at least one cognitive domain; PSCI-ND was defined as impairment in at least one cognitive domain but with normal daily abilities, which were assessed using the Lawton activities of daily living (ADL) scale (38). Cases with simultaneous impairment in at least two cognitive domains and IADL were considered to have PSD. Additionally, we also assessed the anxiety and depression statuses of patients, which were measured using the Hamilton anxiety rating scale (HAMA) and the Hamilton depression rating scale (HAMD), respectively.

### Functional Dependence and Disability Assessment at 3 Months

The functional dependence assessment at 3 months used the ADL scale. The ADL, which includes the instrumental ADL

(IADL) and basic ADL (BADL) scales, examines the current functional level of a patient and can identify improvement or deterioration over time. The eight domains of function measured with the IADL scale include the ability to use a telephone, shopping, food preparation, housekeeping, laundry, mode of transportation, responsibility for own medications, and ability to handle finances. The total IADL score is calculated by summing up the points obtained for each item. The maximum IADL score is 32. The BADL scale features six additional questions that measure different levels of toilet activity, feeding, dressing, grooming, and physical activities. The total ADL score is calculated by summing the IADL and BADL scores together. The lowest possible ADL score is 14 points, which indicates that the patient's abilities are completely normal. If the score is >14 points, there is a reduced function, and the highest possible score is 56 points. The severity of disability was measured with the modified Rankin scale (mRS). We defined a poor disability outcome as mRS > 2 points. Death and recurrence of stroke during the follow-up period were also recorded.

## Statistical Analysis

All statistical analyses were conducted using the SPSS Version 24.0 (IBM Corp., Armonk, NY, USA) software. Descriptive data are presented as proportions, means, or medians as appropriate. A univariate analysis was performed to compare putative risk factors between patients with and without PSCI. In the logistic regression analysis, we used a backward elimination procedure. The PSCI served as a dependent variable. Subsequently, risk factors with a value of  $P < 0.05$  were analyzed with a multivariate logistic regression analysis using a backward stepwise selection strategy. Correlation analyses were conducted to test collinearity between candidate independent variables. If the correlation coefficient between any of these putative risk factors was  $\geq 0.50$ , then variables with a smaller  $P$ -value were entered into the logistic regression. As age and prestroke cognitive status were important risk factors for PSCI, we set up two models, respectively. Model 1 included age, and model 2 included IQCODE score with the rest of the putative factors held constant. The odds ratio of any independent risk factor was interpreted as the risk of non-remission of PSCI, when all other risk factors were held constant. For the analysis of the association between cognitive status and mRS, we constructed an ordinal regression model (dependent variable: mRS grading), adjusted for age education level, IQCODE, NIHSS score at admission, and PVH. The level of statistical significance was set at  $P < 0.05$  (two-sided).

## RESULTS

During the study period, 279 Chinese patients were consecutively screened, and 103 patients were included in the analysis. The patient selection process is shown in **Figure 2**.

Compared with the excluded patients, the study population was younger ( $57.22 \pm 12.95$  years vs.  $65.74 \pm 13.51$  years;  $P < 0.001$ ) and had lower NIHSS scores and IQCODE scores (2 [1–4] vs. 4 [2–8.5],  $P = 0.003$ ; 49 [48–49] vs. 50 [48–53.75],  $P < 0.001$ , respectively); however, there was no significant difference in sex (69 men [67.0%] vs. 117 women [66.5%];  $P = 0.930$ ), respectively.

The baseline characteristics of the recruited patients are summarized in **Table 1**. The study sample comprised 69 men (67.0%) and 34 women (33.0%) with a mean age of  $57.22 \pm 12.95$  years. The IADL score is 8 (8–9) and the mRS score was 1 (0–2) at 3 months.

Of the 103 patients who completed the modified VDB assessment at 3 months and according to the modified VDB assessment, 48 patients had no impaired cognitive domain. The distribution of numbers of impaired cognitive domains were: one (20 patients), two (18 patients), three (seven patients), four (six patients), five (one patient), six (three patients), and all seven domains (one patient). The most commonly impaired cognitive domain was visuomotor speed with impairment found in 28 (27.2%) cases, followed by verbal memory impairment in 26 (25.2%) cases. Visual memory was least commonly impaired with only nine (8.7%) cases exhibiting visual memory impairment (**Supplementary Figure 1**). By definition, a total of 55 patients had PSCI, of which 43 (41.7%) were PSCI-ND and 12 (11.7%) were PSD patients. The comparisons of CHIPS scores in terms of each cognitive domain impairment or not are shown in **Supplementary Table 4**. It reveals that, except for the visual memory, CHIPS scores were significantly higher in patients with impairment in all other cognitive domains (**Figure 3**).

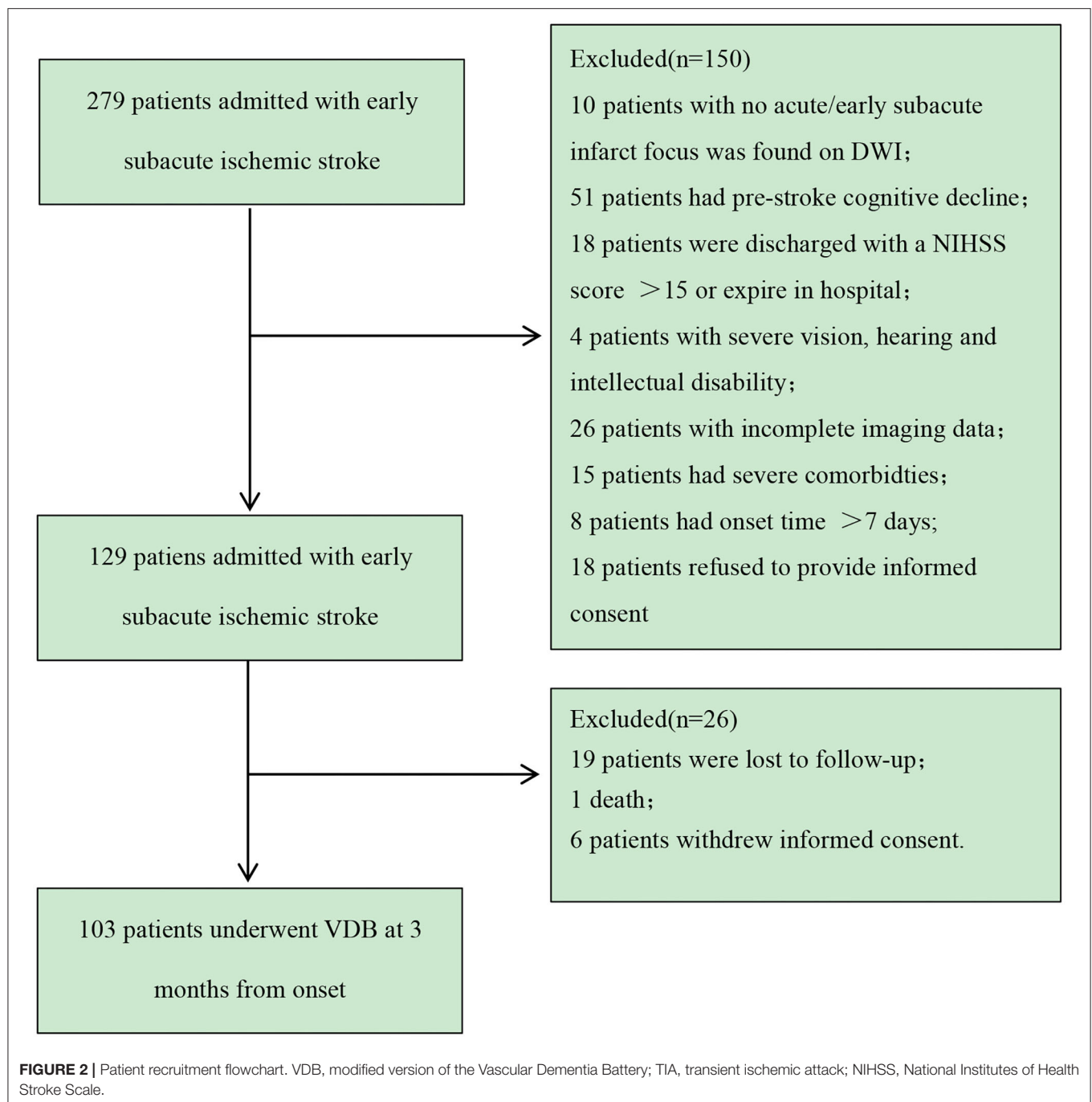
## Univariate Analysis of PSCI

The univariate analysis reveals that patients with PSCI were older, had higher IQCODE scores, had more frequent previous stroke history and atrial fibrillation, had higher CHIPS scores, and had more severe WMLs and MTLA. Additionally, patients with PSCI had higher HAMD scores at 3 months (**Table 1**). Furthermore, PSCI patients had severer impairment in each zone of the CCP in comparison to those with non-PSCI (**Supplementary Table 2**).

## Multivariate Logistic Regression Analysis of PSCI

The independent variables with values of  $P < 0.05$  in the univariate analysis results (**Table 1**) were subjected to Spearman's correlation analysis to check the colinearity, including age, IQCODE score, ischemic stroke history, atrial fibrillation history, infratentorial acute infarction, total CHIPS score, PVH, DWMH, MTLA, and HAMD. Age was significantly correlated with IQCODE score, PVH score, and MTLA score (correlation coefficient  $r = 0.566, 0.509$ , and  $0.549$ , respectively). Additionally, PVH score was significantly correlated with DWMH score, CHIPS score, and MTLA score ( $r = 0.675, 0.586$ , and  $0.557$ , respectively), and CHIPS score was also significantly correlated with DWMH score and MTLA score ( $r = 0.713$  and  $0.529$ , respectively). There were no significant correlations between any other independent variables (the correlation coefficients were all  $< 0.5$ ). Because both age and IQCODE score are important factors affecting PSCI, we set up two models to analyze them. Model 1 included age, and model 2 included IQCODE score with the rest of the factors held constant; history of ischemic stroke, history of atrial fibrillation, acute infratentorial infarction, CHIPS score, and HAMD score served as independent variables.

The logistic regression of model 1 revealed that age, CHIPS score, and HAMD score were independent risk factors for PSCI



at 3 months, whereas model 2 revealed that IQCODE, CHIPS, and HAMD scores were independent risk factors for PSCI at 3 months (**Table 2**). Compared with model 2, the predictive probability of model 1 was greater (80.6 vs. 74.8%), and the model fit was higher (Cox and Snell  $R^2 = 0.377$  vs. 0.309; Nagelkerke  $R^2 = 0.504$  vs. 0.413).

As the history of stroke was an important risk factor for PSCI, we conducted another regression model in patients without stroke history (**Supplementary Table 3**). The analysis revealed that, despite adjusting for the previous stroke, higher CHIPS scores were also associated with PSCI at 3 months.

Ordinal regression analysis revealed that more severe cognitive dysfunction was significantly associated with higher mRS, adjusted for age, education level, IQCODE, NIHSS score at admission, and PVH (**Table 3**).

## DISCUSSION

In this longitudinal observational study, we assessed the associations between PSCI and lesions involving the CCP in Chinese patients with early subacute ischemic stroke. Our main finding was that a higher CHIPS score was associated with



**TABLE 1 |** Comparisons of demographic, clinical, and imaging characteristics between patients with normal cognition and those with PSCI.

	Whole sample <i>n</i> = 103	Normal <i>n</i> = 48	PSCI <i>n</i> = 55	<i>t/z/χ</i> <sup>2</sup>	<i>P</i> -value
Age (years) <sup>a</sup>	57.22 ± 12.95	51.33 ± 13.24	62.36 ± 10.31	−4.667	<0.001
Male <sup>b</sup>	69 (67.0%)	36 (75.0%)	33 (60.0%)	2.608	0.106
Education level <sup>b</sup>				86.878	0.619
Illiteracy (<1 year)	6 (5.8%)	1 (2.1%)	5 (9.1%)		
Primary (1–6 years)	51 (49.5%)	18 (37.5%)	33 (60.0%)		
Secondary (7–12 years)	38 (36.9%)	23 (47.9%)	15 (27.3%)		
University (>12 years)	8 (7.8%)	6 (12.5%)	2 (3.6%)		
IQCODE score <sup>c</sup>	49 (48–49)	48 (48–48)	49 (49–50)	−5.630	<0.001
Smoking history (≥6 months) <sup>b</sup>	37 (35.9%)	19 (51.4%)	18 (48.6%)	0.523	0.469
Hypertension <sup>b</sup>	64 (62.1%)	26 (40.6%)	38 (59.4%)	2.427	0.119
Diabetes mellitus <sup>b</sup>	31 (20.1%)	11 (22.9%)	20 (36.4%)	2.203	0.138
Ischemic stroke history <sup>b</sup>	14 (13.6%)	3 (6.3%)	11 (20.0%)	4.126	0.042
Atrial fibrillation <sup>b</sup>	11 (10.7%)	1 (2.1%)	10 (18.2%)	6.964	0.008
NIHSS score at admission <sup>c</sup>	2 (1–4)	2 (1.5–4)	3 (2–4)	−1.208	0.227
i.v. thrombolysis <sup>b</sup>	16 (15.5%)	7 (14.6%)	9 (16.4%)	0.062	0.803
Stroke subtype <sup>b</sup>				8.343	0.072
Large artery	31 (30.1%)	12 (25.0%)	19 (34.5%)		
Cardioembolism	12 (11.7%)	2 (4.2%)	10 (18.2%)		
Small artery	37 (35.9%)	21 (43.8%)	16 (29.1%)		
Other etiologies	7 (6.8%)	5 (10.4%)	2 (3.6%)		
Unknown etiologies	16 (15.5%)	8 (16.7%)	8 (14.5%)		
<b>Location of acute infarction</b>					
Cortical region <sup>b</sup>	47 (45.6%)	18 (37.5%)	29 (52.7%)	2.396	0.122
Subcortical region <sup>b</sup>	72 (69.9%)	31 (64.6%)	41 (74.5%)	1.209	0.272
Infratentorial <sup>b</sup>	29 (28.2%)	18 (37.5%)	11 (20.0%)	3.880	0.049
Infarct volume <sup>c</sup>	1.37 (0.52–8.14)	1.20 (0.38–11.10)	3.74 (0.67–11.93)	−1.690	0.091
Total CHIPS score <sup>c</sup>	16 (4–36)	8 (2.5–18.5)	27 (10–44.5)	−3.611	<0.001
PVH <sup>c</sup>	1 (0–2)	1 (0–1)	2 (1–2)	−2.997	0.003
DWMH <sup>c</sup>	1 (0–1)	0 (0–1)	1 (1–2)	−2.769	0.006
MTLA <sup>c</sup>	1 (0–4)	0 (0–2)	2 (1–4)	−3.596	<0.001
Presence of CMBs <sup>b</sup>	38 (36.9%)	15 (31.3%)	23 (41.8%)	1.130	0.288
HAMA <sup>c</sup>	7 (5–10)	7 (5–10)	9 (5–12.75)	−1.714	0.087
HAMD <sup>c</sup>	8 (5–12)	8 (5–10)	9.5 (6–14)	−2.514	0.012
ADL <sup>c</sup>	14 (14–16)	14 (14–14)	14 (14–19)	−2.802	0.005
IADL <sup>c</sup>	8 (8–9)	8 (8–8)	8 (8–12)	−2.633	0.008
BADL <sup>c</sup>	6 (6–6)	6 (6–6)	6 (6–7)	−3.201	0.001
mRS <sup>c</sup>	1 (0–2)	1 (0–1)	1 (0–2)	−2.075	0.007

<sup>a</sup>Mean (SD), *t*-test.<sup>b</sup>*n* (%), chi-squared test.<sup>c</sup>*M*(*Qu*-*QL*), Mann–Whitney *U*-test.

PSCI, post-stroke cognitive impairment; IQCODE, Informant Questionnaire on Cognitive Decline in the Elderly; NIHSS, National Institutes of Health Stroke Scale; i.v., intravenous; CHIPS, Cholinergic Pathways Hyperintensities Scale; PVH, periventricular hyperintensity; DWMH, deep white matter hyperintensity; MTLA, medial temporal lobe atrophy; CMBs, cerebral microbleeds; HAMA, Hamilton Anxiety Rating Scale; HAMD, Hamilton Depression Rating Scale; ADL, Lawton Activities of Daily Living; IADL, Instrumental Activities of Daily Living; BADL, Basic Activities of Daily Living; mRS, modified Rankin Scale.

the presence of PSCI at 3 months after stroke adjusted for possible confounders, indicating CCP lesions might play a role in PSCI.

In the present study, the incidence of PSCI at 3 months after a mild-to-moderate index stroke was 53.4%. This finding was similar to the results of several previous studies (2, 39). Differences in the reported incidence of PSCI may be attributed to different definitions of PSCI, use of different assessment tools,

different sample sizes, the healthcare institutions in which the patients were treated, and different therapeutic management.

Our findings suggest that severe lesions involving the CCP may be associated with cognitive impairment at 3 months after an ischemic stroke. The reduction of certain neural matrices in the cholinergic pathway or the disruption of information transmission on this pathway may lead to a disruption of the neural network connections, potentially contributing to

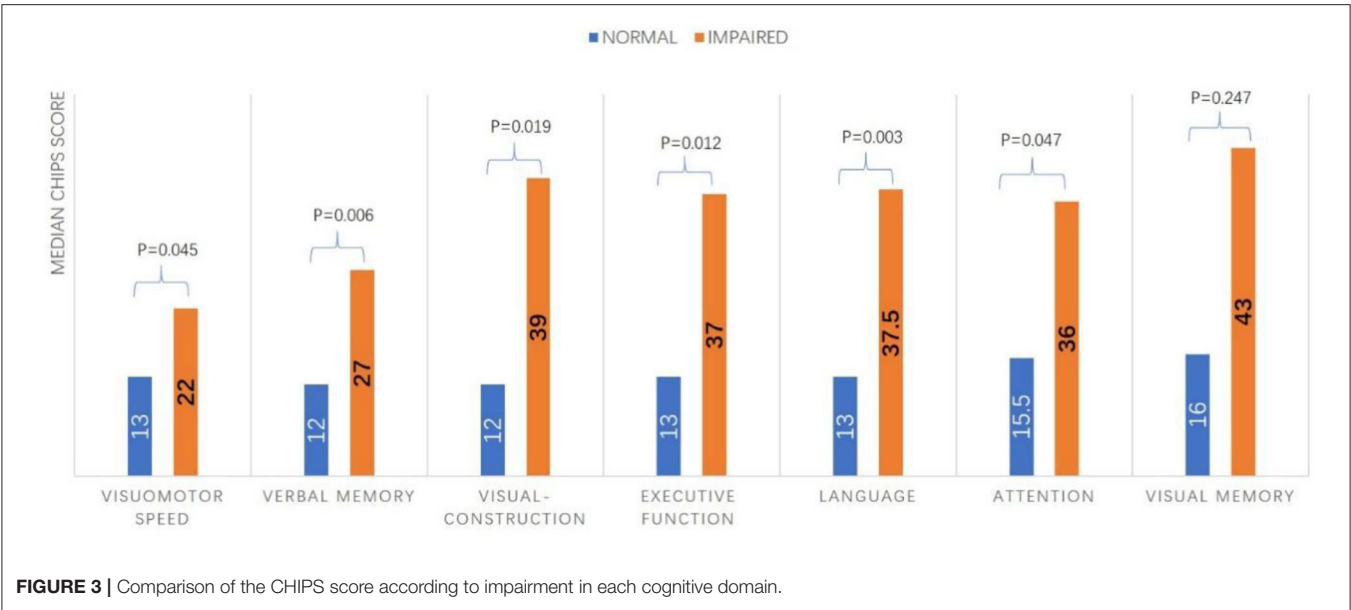


**TABLE 2 |** Multivariate logistic regression of risk factors for PSCI.

		B	OR (95% CI)	P-value
Model 1	Age (years)	0.078	1.081 (1.032–1.132)	0.001
	Ischemic stroke history	−0.117	0.890 (0.178–4.443)	0.887
	Atrial fibrillation	1.570	4.805 (0.540–42.735)	0.159
	Acute infratentorial infarction	−0.844	0.430 (0.141–1.313)	0.138
	Total CHIPS score	0.034	1.034 (1.006–1.063)	0.016
	HAMD	0.148	1.160 (1.047–1.284)	0.004
Model 2	IQCODE score	1.405	4.074(2.064–8.041)	<0.001
	Ischemic stroke history	−0.151	0.860 (0.160–4.615)	0.860
	Atrial fibrillation	1.417	4.378 (0.445–43.025)	0.205
	Acute infratentorial infarction	−0.437	0.646 (0.199–2.094)	0.467
	Total CHIPS score	0.037	1.038 (1.009–1.067)	0.009
	HAMD	0.115	1.122 (1.011–1.246)	0.030

OR, odds ratio; CI, confidence interval; CHIPS, Cholinergic Pathways Hyperintensities Scale; HAMD, Hamilton Depression Rating Scale; IQCODE, Informant Questionnaire on Cognitive Decline in the Elderly.

newly developed PSD (17). The lesions measured in CCP using the CHIPS included WMH lesions on T2-weighted MRI, which might have been caused by chronic and acute vascular damage. All these lesions involving the CCP may affect information transmission in the central acetylcholinergic system, thereby affecting cognitive and modulate attentional functions. Additionally, some studies suggest that the pathogenesis of PSCI may include the coexistence of neurodegenerative pathology and cerebrovascular damage in patients after stroke, which mutually promote and may contribute to cognitive impairment (11, 39–41). Furthermore, several studies demonstrate that PSCI development and a poor functional prognosis after stroke are not only the result of acute ischemic stroke lesions; the adaptive capacity of the brain (including brain reserve and cognitive reserve capacities) before stroke also plays a vital role (42). CHIPS not only measures lesions on the CCP caused by old-/new-onset

infarction, but also by aging or disease-related changes in the white matter leading to a disruption of cholinergic fibers by strategically located WMHs (20). It is, therefore, reasonable to take new-onset acute infarction, old infarction, and WMHs into consideration when calculating the CHIPS score.

As previously reported in other studies, we found that age and IQCODE score were important risk factors for PSCI (43, 44). Previous studies indirectly suggest that PSCI is closely related to brain cognitive function reserve before stroke. The present results indicate that higher depressive scores may be associated with PSCI. Several other studies reported similar results, depressive status was closely associated with cognitive impairment in stroke patients (1, 41) because lesion damage can induce inflammation, and circulating cytokines and immune responses may promote depression and cognitive impairment (45).

**TABLE 3 |** Ordinal regression analysis of mRS at 3 months\*.

	Estimate	95% C.I.	P-value
Age	−0.010	−0.051–0.031	0.636
IQCODE score	0.133	−0.376–0.643	0.608
Education level	0.387	−0.217–0.990	0.209
NIHSS score at admission	0.165	0.047–0.284	0.006
PVH	0.301	−0.164–0.767	0.204
Cognitive status	1.176	0.431–1.920	0.002

IQCODE, Informant Questionnaire on Cognitive Decline in the Elderly; NIHSS, National Institutes of Health Stroke Scale; PVH, periventricular hyperintensity.

\*Cognitive status includes normal cognitive function, PSCI-ND and PSD.

Our study did not distinguish the impact of left and right hemisphere damage on cognitive function or CCP. As required by most studies, the VDB test requires that the patient does not have significant aphasia. Therefore, patients with severe language impairment most likely caused by left-hemispheric infarction had been excluded, resulting in a potentially selected bias. Previous research also shows that the transmission of cholinergic signals in the brain is network transmission not just limited to the unilateral cerebral hemisphere (15). Thus, it is not reliable to assess the impact of left or right hemisphere lesions on CCP and cognitive outcomes.

According to **Table 2**, the current results indicate that severe lesions of CCP may be correlated with PSCI in patients with recurrent or first-ever stroke. Many previous studies show that people with multiple strokes are substantially more likely to have PSCI than people with the first stroke. According to **Supplementary Table 3**, involving a regression model that did not include patients with previous stroke also suggest that higher CHIPS scores were associated with PSCI. These results indicate that CCP is a major risk factor for PSCI not only in patients with first-ever stroke but also those with multiple strokes.

The current findings also reveal that PSCI was associated with more severe disability at 3 months, which suggests that it is important to screen for and treat PSCI after stroke. However, in the current study, the NIHSS scores of the included patients were lower, and most patients had mild mRS scores at 3 months after stroke, potentially generating a statistical offset.

As a strength of the present study, we collected relatively detailed clinical, imaging, and follow-up data from early subacute ischemic stroke patients using a prospective research method. The second strength was the use of comprehensive MRI assessments, including acute cerebral infarction assessment and preexisting abnormalities assessments, which include CMBs, MTLA, and WMLs. Third, when the promotion of advanced MRI is limited, we can use the CHIPS score, the semiquantitative MR score, to assess the degree of CCP damage, which has been rarely investigated in acute ischemic stroke. However, this study was also characterized by several limitations: (1) The rate of loss to follow-up in the present study was relatively high, and the sample size was relatively small. (2) The IQCODE is a global assessment of cognitive impairment prestroke; it is inadequate for rigorous assessment of specific cognitive domains. Therefore, residual

confounding of prestroke cognitive function remains possible. (3) Although we have excluded obvious visual and auditory impairments, neurological diseases and previous psychiatric history based on medical records and physical examinations, we did not conduct a detailed evaluation of these conditions, which might affect the results of the cognitive assessment. (4) NIHSS, mRS, and ADL scores at 3 months for most patients were low, and patients with severe stroke were excluded, potentially limiting the generalizability of the current findings. (5) MRI with a slice thickness/gap of 6 mm/1 mm cannot accurately measure the degree of CCP lesions, which means that we may have missed small lesions in the CCP. (6) We only used semiquantitative measurement tools to assess MRI features. These tools cannot accurately distinguish and measure cholinergic nerve pathways and other related nerve pathway fibers (e.g., glutaminergic and other neurotransmitter pathways), nor can they evaluate certain measurements that may predict cognitive function, such as cortical thickness or hippocampal volume.

In conclusion, the incidence of PSCI in the present study population was 53.4%. The severity of lesions involving the CCP may be associated with cognitive impairment at 3 months after stroke. Additionally, cognitive function status is closely related to prognostic outcome and can affect stroke survivors' quality of life.

## DATA AVAILABILITY STATEMENT

The original contributions presented in the study are included in the article/**Supplementary Material**, further inquiries can be directed to the corresponding author/s.

## ETHICS STATEMENT

The study protocol was approved by the Ethics Committee of Dongguan People's Hospital (no. KYKT2018-006).

## AUTHOR CONTRIBUTIONS

J-fQ, H-HZ, W-MX, and Y-kC are the principal investigator that designed the study, carried out the quantitative analysis, and drafted the article. Y-IL and W-cL collected the data. Z-qW and D-hQ reviewed and edited the manuscript. All authors have read and approved the final manuscript.

## ACKNOWLEDGMENTS

We would like to acknowledge all authors who contributed to this article. We thank Benjamin Knight, MSc., from Liwen Bianji, Edanz Editing China ([www.liwenbianji.cn/ac](http://www.liwenbianji.cn/ac)), for editing the English text of a draft of this manuscript.

## SUPPLEMENTARY MATERIAL

The Supplementary Material for this article can be found online at: <https://www.frontiersin.org/articles/10.3389/fneur.2021.606897/full#supplementary-material>

## REFERENCES

- Jokinen H, Melkas S, Ylikoski R, Pohjasvaara T, Kaste M, Erkinjuntti T, et al. Post-stroke cognitive impairment is common even after successful clinical recovery. *Eur J Neurol*. (2015) 22:1288–94. doi: 10.1111/ene.12743
- Barbay M, Taillia H, Nedelec-Ciceri C, Bompairé F, Bonnin C, Varvat J, et al. Prevalence of poststroke neurocognitive disorders using national institute of neurological disorders and stroke-Canadian Stroke Network, VASCOG Criteria (Vascular Behavioral and Cognitive Disorders), and optimized criteria of cognitive deficit. *Stroke*. (2018) 49:1141–7. doi: 10.1161/STROKEAHA.117.018889
- Oksala NK, Jokinen H, Melkas S, Oksala A, Pohjasvaara T, Hietanen M, et al. Cognitive impairment predicts poststroke death in long-term follow-up. *J Neurol Neurosurg Psychiatry*. (2009) 80:1230–5. doi: 10.1136/jnnp.2009.174573
- Lee M, Saver JL, Hong KS, Wu YL, Liu HC, Rao NM, et al. Cognitive impairment and risk of future stroke: a systematic review and meta-analysis. *Cmaj*. (2014) 186:536–46. doi: 10.1503/cmaj.140147
- Francis PT. Glutamatergic approaches to the treatment of cognitive and behavioural symptoms of Alzheimer's disease. *Neurodegener Dis*. (2008) 5:241–3. doi: 10.1159/000113713
- Lamour Y, Dutar P, Rascol O, Jobert A. Basal forebrain neurons projecting to the rat frontoparietal cortex: electrophysiological and pharmacological properties. *Brain Res*. (1986) 362:122–31. doi: 10.1016/0006-8993(86)91405-8
- Wenk GL. Pharmacological manipulations of the substantia innominata-cortical cholinergic pathway. *Neurosci Lett*. (1984) 51:99–103. doi: 10.1016/0304-3940(84)90269-6
- Kurosawa M, Sato A, Sato Y. Stimulation of the nucleus basalis of Meynert increases acetylcholine release in the cerebral cortex in rats. *Neurosci Lett*. (1989) 98:45–50. doi: 10.1016/0304-3940(89)90371-6
- Brown DA. Muscarinic acetylcholine receptors (mAChRs) in the nervous system: some functions and mechanisms. *J Mol Neurosci*. (2010) 41:340–6. doi: 10.1007/s12031-010-9377-2
- Dajas-Bailador F, Wonnacott S. Nicotinic acetylcholine receptors and the regulation of neuronal signalling. *Trends Pharmacol Sci*. (2004) 25:317–24. doi: 10.1016/j.tips.2004.04.006
- Selden NR, Gitelman DR, Salamon-Murayama N, Parrish TB, Mesulam MM. Trajectories of cholinergic pathways within the cerebral hemispheres of the human brain. *Brain*. (1998) 121:2249–57. doi: 10.1093/brain/121.12.2249
- Mesulam MM. The cholinergic innervation of the human cerebral cortex. *Prog Brain Res*. (2004) 145:67–78. doi: 10.1016/S0079-6123(03)45004-8
- Riascos D, Nicholas A, Samaekia R, Yukhananov R, Mesulam MM, Bigio EH, et al. Alterations of Ca<sup>2+</sup>-responsive proteins within cholinergic neurons in aging and Alzheimer's disease. *Neurobiol Aging*. (2014) 35:1325–33. doi: 10.1016/j.neurobiolaging.2013.12.017
- Bloem B, Schoppink L, Rotaru DC, Faiz A, Hendriks P, Mansvelder HD, et al. Topographic mapping between basal forebrain cholinergic neurons and the medial prefrontal cortex in mice. *J Neurosci*. (2014) 34:16234–46. doi: 10.1523/JNEUROSCI.3011-14.2014
- Chandler D, Waterhouse BD. Evidence for broad versus segregated projections from cholinergic and noradrenergic nuclei to functionally and anatomically discrete subregions of prefrontal cortex. *Front Behav Neurosci*. (2012) 6:20. doi: 10.3389/fnbeh.2012.00020
- Bocti C, Swartz RH, Gao FQ, Sahlas DJ, Behl P, Black SE. A new visual rating scale to assess strategic white matter hyperintensities within cholinergic pathways in dementia. *Stroke*. (2005) 36:2126–31. doi: 10.1161/01.STR.0000183615.07936.b6
- Lim JS, Kim N, Jang MU, Han MK, Kim S, Baek MJ, et al. Cortical hubs and subcortical cholinergic pathways as neural substrates of poststroke dementia. *Stroke*. (2014) 45:1069–76. doi: 10.1161/STROKEAHA.113.004156
- Furie KL, Jayaraman MV. 2018 guidelines for the early management of patients with acute ischemic stroke. *Stroke*. (2018) 49:509–10. doi: 10.1161/STROKEAHA.118.020176
- Harrison JK, Fearon P, Noel-Storr AH, McShane R, Stott DJ, Quinn TJ. Informant Questionnaire on Cognitive Decline in the Elderly (IQCODE) for the diagnosis of dementia within a secondary care setting. *Cochrane Database Syst Rev*. (2015) 3:CD010772. doi: 10.1002/14651858.CD010772.pub2
- Qu JF, Chen YK, Luo GP, Zhao JH, Zhong HH, Yin HP. Severe lesions involving cortical cholinergic pathways predict poorer functional outcome in acute ischemic stroke. *Stroke*. (2018) 49:2983–9. doi: 10.1161/STROKEAHA.118.023196
- Fazekas F, Chawluk JB, Alavi A, Hurtig HI, Zimmerman RA. MR signal abnormalities at 1.5 T in Alzheimer's dementia and normal aging. *Am J Roentgenol*. (1987) 149:351–6. doi: 10.2214/ajr.149.2.351
- Scheltens P, Leys D, Barkhof F, Huglo D, Weinstein HC, Vermersch P, et al. Atrophy of medial temporal lobes on MRI in "probable" Alzheimer's disease and normal ageing: diagnostic value and neuropsychological correlates. *J Neurol Neurosurg Psychiatry*. (1992) 55:967–72. doi: 10.1136/jnnp.55.10.967
- Pendlebury ST, Klaus SP, Thomson RJ, Mehta Z, Wharton RM, Rothwell PM. Methodological factors in determining risk of dementia after transient ischemic attack and stroke: (III) applicability of cognitive tests. *Stroke*. (2015) 46:3067–73. doi: 10.1161/STROKEAHA.115.010290
- Mijajlović MD, Pavlović A, Brainin M, Heiss WD, Quinn TJ, Ihle-Hansen HB, et al. Post-stroke dementia - a comprehensive review. *BMC Med*. (2017) 15:11. doi: 10.1186/s12916-017-0779-7
- Nasreddine ZS, Phillips NA, Bédirian V, Charbonneau S, Whitehead V, Collin I, et al. The Montreal Cognitive Assessment, MoCA: a brief screening tool for mild cognitive impairment. *J Am Geriatr Soc*. (2005) 53:695–9. doi: 10.1111/j.1532-5415.2005.53221.x
- Godefroy O, Yaïche H, Taillia H, Bompairé F, Nédélec-Ciceri C, Bonnin C, et al. Who should undergo a comprehensive cognitive assessment after a stroke? A cognitive risk score. *Neurology*. (2018) 91:e1979–87. doi: 10.1212/WNL.0000000000006544
- Tang WK, Chen YK, Lu JY, Wong A, Mok V, Chu WC, et al. Absence of cerebral microbleeds predicts reversion of vascular 'cognitive impairment no dementia' in stroke. *Int J Stroke*. (2011) 6:498–505. doi: 10.1111/j.1747-4949.2011.00682.x
- Tham W, Auchus AP, Thong M, Goh ML, Chang HM, Wong MC, et al. Progression of cognitive impairment after stroke: 1-year results from a longitudinal study of Singaporean stroke patients. *J Neurol Sci*. (2002) 203–204:49–52. doi: 10.1016/S0022-510X(02)00260-5
- Mok VC, Wong A, Yim P, Fu M, Lam WW, Hui AC, et al. The validity and reliability of Chinese frontal assessment battery in evaluating executive dysfunction among Chinese patients with small subcortical infarct. *Alzheimer Dis Assoc Disord*. (2004) 18:68–74. doi: 10.1097/01.wad.0000126617.54783.7
- Royall DR. The FAB: a frontal assessment battery at bedside. *Neurology*. (2001) 57:565. doi: 10.1212/WNL.57.3.565
- Wechsler D. *Wechsler Adult Intelligence Scale, 3rd version*. New York, NY: The Psychological Corporation (1997). doi: 10.1037/t49755-000
- Wechsler D. *Wechsler Memory Scale, 3rd version*. San Antonio: The Psychological Corporation (1997).
- Cheung RW, Cheung MC, Chan AS. Confrontation naming in Chinese patients with left, right or bilateral brain damage. *J Int Neuropsychol Soc*. (2004) 10:46–53. doi: 10.1017/S1355617704101069
- Chiu HF, Chan CK, Lam LC, Ng KO, Li SW, Wong M, et al. The modified Fuld Verbal Fluency Test: a validation study in Hong Kong. *J Gerontol B Psychol Sci Soc Sci*. (1997) 52:P247–50. doi: 10.1093/geronb/52B.5.P247
- Sunderland T, Hill JL, Mellow AM, Lawlor BA, Gundersheimer J, Newhouse PA, et al. Clock drawing in Alzheimer's disease. A novel measure of dementia severity. *J Am Geriatr Soc*. (1989) 37:725–9. doi: 10.1111/j.1532-5415.1989.tb02233.x
- Smith A. *Symbol Digit Modalities Test*. Los Angeles: Western Psychological Services (1991).
- American Psychiatric Association. *Diagnostic and Statistical Manual of Mental Disorders*. Arlington, VA: American Psychiatric Publishing (2013). doi: 10.1176/appi.books.9780890425596
- Lawton MP, Brody EM. Assessment of older people: self-maintaining and instrumental activities of daily living. *Gerontologist*. (1969) 9:179–86. doi: 10.1093/geront/9.3\_Part\_1.179
- Picciotto MR, Higley MJ, Mineur YS. Acetylcholine as a neuromodulator: cholinergic signaling shapes nervous system function and behavior. *Neuron*. (2012) 76:116–29. doi: 10.1016/j.neuron.2012.08.036
- Micheau J, Marighetto A. Acetylcholine and memory: a long, complex and chaotic but still living relationship. *Behav Brain Res*. (2011) 221:424–9. doi: 10.1016/j.bbr.2010.11.052



41. Hasselmo ME, Sarter M. Modes and models of forebrain cholinergic neuromodulation of cognition. *Neuropsychopharmacology*. (2011) 36:52–73. doi: 10.1038/npp.2010.104
42. Mok VC, Lam BY, Wong A, Ko H, Markus HS, Wong LK. Early-onset and delayed-onset poststroke dementia - revisiting the mechanisms. *Nat Rev Neurol*. (2017) 13:148–59. doi: 10.1038/nrneurol.2017.16
43. Akinyemi RO, Allan L, Owolabi MO, Akinyemi JO, Ogbale G, Ajani A, et al. Profile and determinants of vascular cognitive impairment in African stroke survivors: the CogFAST Nigeria Study. *J Neurol Sci*. (2014) 346:241–9. doi: 10.1016/j.jns.2014.08.042
44. Kovalenko EA, Bogolepova AN, Katunin DA. The role of pre-stroke cognitive disorders in the formation of post-stroke cognitive impairment. *Zh Nevrol Psikhiatr Im S S Korsakova*. (2017) 117:19–24. doi: 10.17116/jnevro201711712219-24
45. Pessoa Rocha N, Reis HJ, Vanden Berghe P, Cirillo C. Depression and cognitive impairment in Parkinson's disease: a role for inflammation and immunomodulation? *Neuroimmunomodulation*. (2014) 21:88–94. doi: 10.1159/000356531

**Conflict of Interest:** The authors declare that the research was conducted in the absence of any commercial or financial relationships that could be construed as a potential conflict of interest.

Copyright © 2021 Zhong, Qu, Xiao, Chen, Liu, Wu, Qiu and Liang. This is an open-access article distributed under the terms of the Creative Commons Attribution License (CC BY). The use, distribution or reproduction in other forums is permitted, provided the original author(s) and the copyright owner(s) are credited and that the original publication in this journal is cited, in accordance with accepted academic practice. No use, distribution or reproduction is permitted which does not comply with these terms.



# All Central Nervous System Neuro- and Vascular-Communication Channels Are Surrounded With Cerebrospinal Fluid

Lara M. Fahmy<sup>1†</sup>, Yongsheng Chen<sup>2†</sup>, Stephanie Xuan<sup>3</sup>, E. Mark Haacke<sup>3</sup>, Jiani Hu<sup>3\*</sup> and Quan Jiang<sup>4\*</sup>

<sup>1</sup> Department of Psychiatry and Behavioral Neurosciences, Wayne State University, Detroit, MI, United States, <sup>2</sup> Department of Neurology, Wayne State University, Detroit, MI, United States, <sup>3</sup> Department of Radiology, Wayne State University, Detroit, MI, United States, <sup>4</sup> Department of Neurology, Henry Ford Health System, Detroit, MI, United States

## OPEN ACCESS

### Edited by:

Achim Gass,  
University of Heidelberg, Germany

### Reviewed by:

Nobutaka Hattori,  
Juntendo University, Japan  
Erik Nicolaas Theodorus Petrus  
Bakker,  
University of Amsterdam, Netherlands

### \*Correspondence:

Jiani Hu  
jhu@med.wayne.edu  
Quan Jiang  
qjiang1@hfhs.org

<sup>†</sup>These authors have contributed  
equally to this work and share first  
authorship

### Specialty section:

This article was submitted to  
Applied Neuroimaging,  
a section of the journal  
Frontiers in Neurology

**Received:** 06 October 2020

**Accepted:** 29 April 2021

**Published:** 17 June 2021

### Citation:

Fahmy LM, Chen Y, Xuan S,  
Haacke EM, Hu J and Jiang Q (2021)  
All Central Nervous System Neuro-  
and Vascular-Communication  
Channels Are Surrounded With  
Cerebrospinal Fluid.  
Front. Neurol. 12:614636.  
doi: 10.3389/fneur.2021.614636

**Background:** Recent emerging evidence has highlighted the potential critical role of cerebrospinal fluid (CSF) in cerebral waste clearance and immunomodulation. It is already very well-established that the central nervous system (CNS) is completely submerged in CSF on a macro-level; but to what extent is this true on a micro-level? Specifically, within the peri-neural and peri-vascular spaces within the CNS parenchyma. Therefore, the objective of this study was to use magnetic resonance imaging (MRI) to simultaneously map the presence of CSF within all peri-neural (cranial and spinal nerves) and peri-vascular spaces *in vivo* in humans. Four MRI protocols each with five participants were used to image the CSF in the brain and spinal cord. Our findings indicated that all CNS neuro- and vascular-communication channels are surrounded with CSF. In other words, all peri-neural spaces surrounding the cranial and spinal nerves as well as all peri-vascular spaces surrounding MRI-visible vasculature were filled with CSF. These findings suggest that anatomically, substance exchange between the brain parenchyma and outside tissues including lymphatic ones can only occur through CSF pathways and/or vascular pathways, warranting further investigation into its implications in cerebral waste clearance and immunity.

**Keywords:** cerebrospinal fluid, central nervous system, glymphatic clearance, cerebral waste clearance, magnetic resonance imaging

## INTRODUCTION

The critical involvement of cerebrospinal fluid (CSF) in metabolic cerebral waste clearance (CWC) has gained a lot of momentum lately. Our traditional understanding of CSF circulation is that it is produced by the choroid plexus and circulates through the ventricles and subarachnoid spaces, exiting directly into the dural venous sinuses via arachnoid granulations/villi (1–5). Recent studies have expanded upon this traditional understanding and demonstrated that CSF penetrates and interacts with the brain parenchyma through a defined pathway with the purpose of CWC; this has been coined the glymphatic pathway (6). A significant portion of the subarachnoid CSF penetrates the brain parenchyma through para-arterial routes, facilitated by aquaporin-4 protein water channels (AQP4) on astrocytic end-feet (7–12). CSF then mixes

with the interstitial fluid, and together, they are cleared debatably though para-venous routes with any associated solutes; once again, facilitated by AQP4 (8, 13–15). Dysfunctions of this glymphatic pathway have been associated with a broad range of neurological diseases including, but not limited to, Alzheimer's disease, stroke, traumatic brain injury, multiple sclerosis, diabetes, and chronic traumatic encephalopathy; begging the question of its involvement in virtually all neurodegenerative diseases (8–10, 12, 14, 16–19). Therefore, it has become apparent that gaining a complete and accurate understanding of CSF physiology is an essential prerequisite to understanding the pathophysiology underlying this broad range of neurological disease.

In light of the importance of CSF physiology, researchers have focused their attention on investigating CWC CSF outflow pathways, out of the central nervous system (CNS). The traditional outflow pathway via the arachnoid granulations/villi is becoming increasingly unpopular due to the lack of physiological evidence to support it (20, 21). This traditional pathway was primarily based on a study published over a 100 years ago, performed under non-physiologically high CSF pressure in human cadaver brain (22). More recently, the lymphatics have been identified as a major outflow pathway via peri-neural spaces (23, 24). Several studies have demonstrated the presence of CSF tracer within the sheaths surrounding cranial and spinal nerves; with the spotlight focused on the olfactory nerve (CN I) peri-neural space depositing into the nasal submucosa lymphatics (23–29). CSF within these peri-neural spaces exits the cranial cavity and vertebral column along the cranial and spinal nerves, respectively. At this point, CSF within the peri-neural spaces is proposed to be absorbed into the surrounding interstitial space/epidural tissue, and/or directly into the surrounding regional lymphatic vessels outside the CNS (26, 28, 30–34). Furthermore, the recently established meningeal lymphatic vessels are proposed to serve as another lymphatic-associated outflow pathway; However, the exact mechanism remains unclear (11, 35–37).

Although our understanding of CSF physiology remains relatively rudimentary and is still very much under investigation, one concept has become increasingly apparent: all CNS neuro- and vascular-communication channels are surrounded with CSF. It is already very well-established that the CNS is completely submerged in CSF on a macro-level; but now we know that this is true even on a micro-level, specifically within the peri-neural and peri-vascular spaces within the CNS parenchyma. Most studies have asynchronously investigated these spaces and these investigations have been mainly conducted in animals and human cadavers. Moreover, although CSF-filled peri-vascular spaces in several brain regions have been illustrated in several studies, to our knowledge, there is no systematic study focusing on whether all cerebral vasculature (with the exception of capillaries) are surrounded with CSF, and this can only be revealed using *in vivo* imaging methods. Therefore, the objective of this study was to use magnetic resonance imaging (MRI) to simultaneously map the presence of CSF within all peri-neural (cranial and spinal nerves) and peri-vascular spaces *in vivo* in humans.

## METHOD

To prove the concept, we designed four types of experiments each with five healthy participants (ages 23–59 years; three males and two females). Each protocol was tailored to a specific area of investigation and anatomical structures, such as cranial nerves and their corresponding perineural spaces, cerebral vasculature and their corresponding perivascular spaces, and different segments of the spinal cord. The study was approved by local Institutional Review Board. Written consent was obtained prior to each MRI experiment. Various sequences were used to image CSF in the brain and spinal cord at 3T (Verio, Siemens Healthineers, Erlangen, Germany).

The first experiment employed a 3D T2-weighted (T2W) “Sampling Perfection with Application optimized Contrasts using different flip angle Evolution” (T2W-SPACE) sequence to image the CSF and cranial nerves with hyperintense CSF signal and hypointense signal for cranial nerves and blood vessels (38). This sequence yields a high nerve-to-CSF contrast and a high spatial resolution within a practical scanning time period. By optimizing timing parameters, uniform signal intensity of gray matter and white matter was acquired with repetition time (TR)/echo time (TE) = 1,000/132 ms. Imaging resolution was  $0.5 \times 0.5 \times 0.8 \text{ mm}^3$ . With a parallel imaging accelerating factor of 2, the scanning time was 5 min for 114 axial slices covering the brain. All diameters were measured on the best shown slice using the standard software provided with the MRI scanner. We have reported the diameters as mean( $\pm$ SE), as well as the diameter ratio of the cranial nerve diameter over the total diameter (cranial nerve diameter + corresponding peri-neural space diameter), for all 12 cranial nerves in healthy humans (Figures 1, 2).

For the second experiment, in order to image CSF in peri-vascular spaces and to demonstrate that all MRI-visible cerebral blood vessels were surrounded by CSF, we used high-resolution “STrategically Acquired Gradient Echo” (STAGE) imaging to simultaneously obtain bright-blood and dark-blood images (39–41). The STAGE imaging included a proton density weighted (PDW) scan and a T1-weighted (T1W) scan. Both images were fully flow compensated with bright blood signal. By subtracting the PDW from the inverted T1W image, one could obtain a synthetic T2W dark-blood image (sT2W) presenting bright-CSF and uniform gray matter and white matter intensities. The high-resolution STAGE data were acquired in the sagittal plane with a scan matrix of  $2,048 \times 832$  leading to a resolution of  $0.1 \times 0.2 \times 2.0 \text{ mm}^3$ . Scan time was 17 min. The STAGE method simultaneously yielded naturally co-registered dark-blood (sT2W) and bright-blood (T1W) which were used to visualize the blood vessels and perivascular spaces in the order of  $100 \mu\text{m}$ . In addition, to acquire a pure CSF image with suppressed blood signals, we used a 3D turbo-spin echo (TSE) sequence with TR/TE = 2,000/345 ms and an isotropic voxel size of 0.5 mm. With such a long echo time, the images were heavily T2-weighted such that all tissues other than CSF (very long T2) were suppressed. Given the long TR/TE and high-resolution 3D sampling scheme, the sequence took half an hour covering the central half of the brain in the sagittal plane.

The third experiment was performed on the cervical spinal cord at the C4/C5 level. A 2D T2\* weighted spoiled gradient echo sequence (Multiple Echo Data Image Combination, MEDIC) was used to acquire images with hyperintense CSF and blood vessels, and hypointense nerves. This sequence is one of the clinical sequences for cervical protocol. Imaging parameters were: TR = 587 ms, TE = 17 ms, flip angle = 30°, in-plane resolution =  $0.5 \times 0.5 \text{ mm}^2$ , slice thickness = 3 mm, scanning time = 3 min.

The fourth and final experiment was for imaging the lumbar spinal nerves at L3/L4 level. A regular T2W-TSE sequence was used with the following imaging parameters: TR = 5,490 ms, TE = 87 ms, in-plane resolution =  $0.6 \times 0.6 \text{ mm}^2$ , slice thickness = 4 mm, scanning time = 2 min. This sequence, with sub-millimeter in-plane resolution, provided high nerve-to-CSF contrast. The 12 pairs of cranial nerves and spinal nerves were labeled by experienced neuroradiologist on images from the first, third and fourth experiments.

## RESULTS

All MRI data were first visually evaluated to label nerves and vessels on representative images. Representative images of the first experiment are shown in **Figures 1, 2**. Images in **Figure 3** are from the third and fourth experiments. The results of the second experiment are shown in **Figure 4**.

### The CNS Neuro-Communication Channels Are Surrounded With CSF

The CNS neuro-communication channels consist of 12 pairs of cranial nerves and 31 pairs of spinal nerves. Images from the first experiment were used to visualize all 12 pairs of the cranial nerves (**Figures 1, 2**). As illustrated, the cranial nerves were hypointense, while the peri-neural spaces surrounding the cranial nerves were hyperintense, indicating the presence of CSF within these spaces. We qualitatively observed that the peri-neural spaces had a slightly higher signal intensity than other CSF compartments. This is consistent with an array of previous studies which has already taken a closer look at the peri-neural spaces and its fluid contents, indicating that the peri-neural spaces are filled with a mixture of CSF and interstitial fluid (ISF) (24, 26–29, 42–51).

**Figure 1A** shows an axial view of a pair of hypointense CN I, encased in hyperintense CSF-filled perineural space, on either side of a bony projection inferior to the frontal lobe, the crista galli. The mean diameter for CN I was  $4.3(\pm 0.8) \text{ mm}$  and the mean total diameter (CN I + corresponding peri-neural space) was  $6.0(\pm 0.6) \text{ mm}$ , with a diameter ratio (CN I diameter over total diameter) of 0.7 (**Table 1**). **Figure 1B** shows an axial view of a pair of hypointense optic nerves (CN II), encased in hyperintense CSF-filled perineural space, emerging from the optic chiasm. The mean diameter for CN II was  $3.2(\pm 0.5) \text{ mm}$  and the mean total diameter (CN II + corresponding peri-neural space) was  $5.0(\pm 0.5) \text{ mm}$ , with a diameter ratio (CN II diameter over total diameter) of 0.6 (**Table 1**). **Figure 1C** shows an axial view of a pair of hypointense oculomotor nerves (CN III), surrounded with hyperintense CSF-filled perineural space, emerging from the midbrain. The mean diameter for CN

III was  $1.9(\pm 0.5) \text{ mm}$  and the mean total diameter (CN III + corresponding peri-neural space) was  $2.6(\pm 0.4) \text{ mm}$ , with a diameter ratio (CN III diameter over total diameter) of 0.7 (**Table 1**). **Figures 1D,E** show axial views of a pair of hypointense trochlear nerves (CN IV), surrounded with hyperintense CSF-filled perineural space, emerging from the midbrain. The mean diameter for CN IV was  $0.9(\pm 0.3) \text{ mm}$  and the mean total diameter (CN IV + corresponding peri-neural space) was  $1.4(\pm 0.5) \text{ mm}$ , with a diameter ratio (CN IV diameter over total diameter) of 0.6 (**Table 1**). **Figure 1F** shows an axial view of a pair of hypointense trigeminal nerves (CN V), encased in hyperintense CSF-filled perineural space, emerging from the pons. The mean diameter for CN V was  $4.6(\pm 0.4) \text{ mm}$  and the mean total diameter (CN V + corresponding peri-neural space) was  $5.7(\pm 0.4) \text{ mm}$ , with a diameter ratio (CN V diameter over total diameter) of 0.8 (**Table 1**).

**Figure 2A** shows an axial view of a pair of hypointense abducens nerves (CN VI), surrounded with hyperintense CSF-filled perineural space, emerging from the pons. The mean diameter for CN VI was  $1.1(\pm 0.1) \text{ mm}$  and the mean total diameter (CN VI + corresponding peri-neural space) was  $1.9(\pm 0.2) \text{ mm}$ , with a diameter ratio (CN VI diameter over total diameter) of 0.6 (**Table 1**). **Figure 2B** shows an axial view of a pair of hypointense facial nerves (CN VII), surrounded with hyperintense CSF-filled perineural space, emerging from the pons. The mean diameter for CN VII was  $1.0(\pm 0.2) \text{ mm}$  and the mean total diameter (CN VII + corresponding peri-neural space) was  $1.6(\pm 0.1) \text{ mm}$ , with a diameter ratio (CN VII diameter over total diameter) of 0.6 (**Table 1**). **Figure 2C** shows an axial view of a pair of hypointense vestibulocochlear nerves (CN VIII), surrounded with hyperintense CSF-filled perineural space, emerging from the pons. The mean diameter for CN VIII was  $1.1(\pm 0.3) \text{ mm}$  and the mean total diameter (CN VIII + corresponding peri-neural space) was  $1.7(\pm 0.2) \text{ mm}$ , with a diameter ratio (CN VIII diameter over total diameter) of 0.6 (**Table 1**). **Figure 2D** shows an axial view of a pair of hypointense glossopharyngeal nerves (CN IX), surrounded with hyperintense CSF-filled perineural space, emerging from the medulla. The mean diameter for CN IX was  $1.2(\pm 0.1) \text{ mm}$  and the mean total diameter (CN IX + corresponding peri-neural space) was  $1.9(\pm 0.3) \text{ mm}$ , with a diameter ratio (CN IX diameter over total diameter) of 0.6 (**Table 1**). **Figure 2E** shows an axial view of a pair of hypointense vagus nerves (CN X), encased in hyperintense CSF-filled perineural space, emerging from the medulla. The mean diameter for CN X was  $1.4(\pm 0.2) \text{ mm}$  and the mean total diameter (CN X + corresponding peri-neural space) was  $1.9(\pm 0.3) \text{ mm}$ , with a diameter ratio (CN X diameter over total diameter) of 0.7 (**Table 1**). **Figure 2F** shows an axial view of a pair of hypointense accessory nerves (CN XI), encased in hyperintense CSF-filled perineural space, emerging from the medulla. The mean diameter for CN XI was  $1.1(\pm 0.1) \text{ mm}$  and the mean total diameter (CN XI + corresponding peri-neural space) was  $1.7(\pm 0.2) \text{ mm}$ , with a diameter ratio (CN XI diameter over total diameter) of 0.6 (**Table 1**). **Figures 2G,H** show axial views of a pair of hypointense hypoglossal nerves (CN XII), encased in hyperintense CSF-filled perineural space, emerging from the medulla. The mean diameter for CN XII was  $0.9(\pm 0.2) \text{ mm}$ .



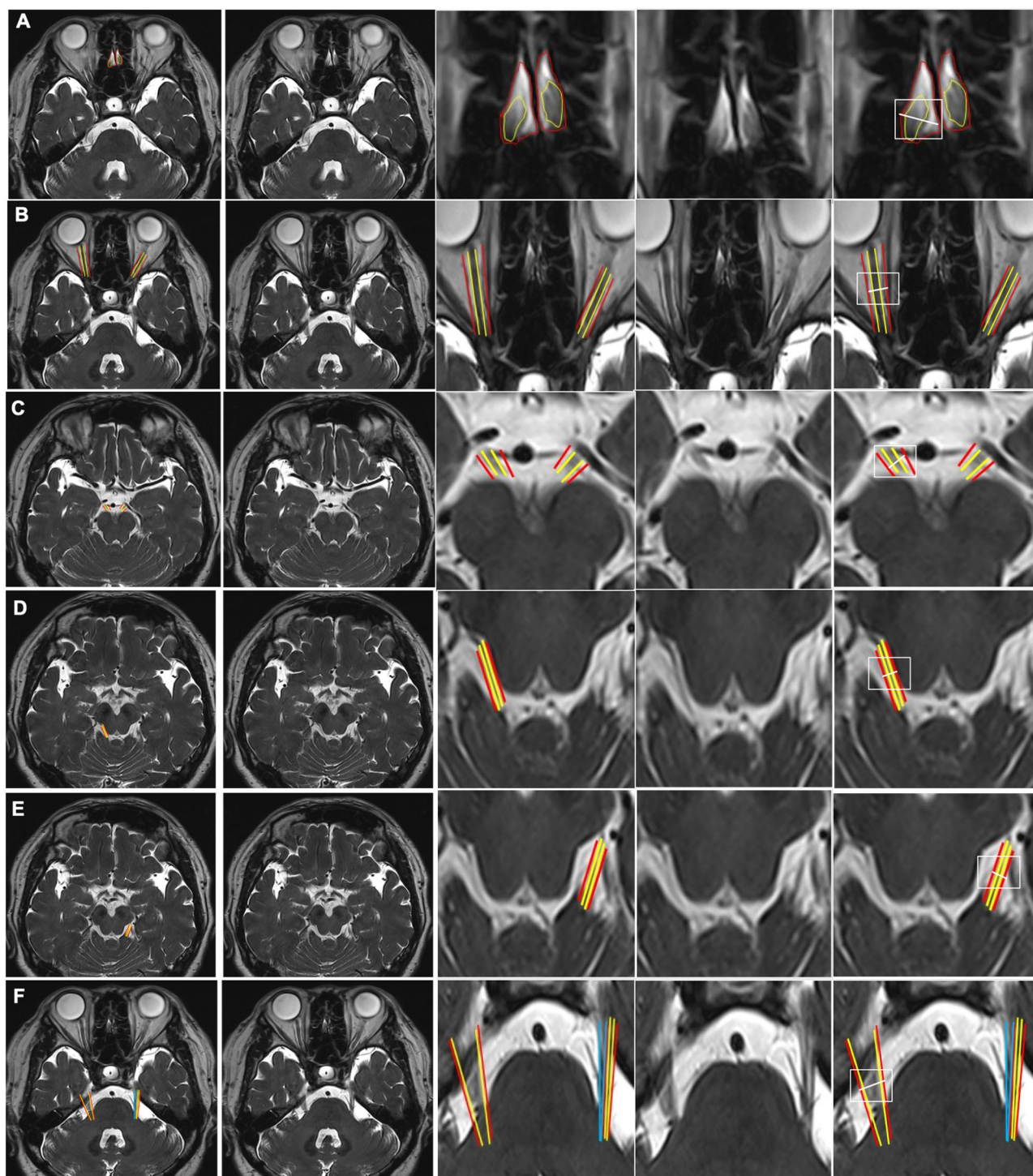


**FIGURE 1** | CSF-filled peri-neural spaces surrounding the first five cranial nerves (CN I-CN V). **(A)** Olfactory nerves (CN I), (two original images, two corresponding magnified images and measurement location); **(B)** Optic nerves (CN II) (two original images, two corresponding magnified images and measurement location); **(C)** Oculomotor nerves (CN III) (two original images, two corresponding magnified images and measurement location); **(D)** Right trochlear nerve (CN IV) (two original images, two corresponding magnified images and measurement location); **(E)** Left CN IV (two original images, two corresponding magnified images and measurement location); and **(F)** Trigeminal nerves (CN V) (two original images, two corresponding magnified images and measurement location). Space within the yellow lines: respective nerve (hypointense signal). Space between the red and yellow lines: peri-neural space (hyperintense signal). Space between the blue lines: CN V (hypointense signal). White line: measurement location. All images were generated from the first experiment as described in the method section.

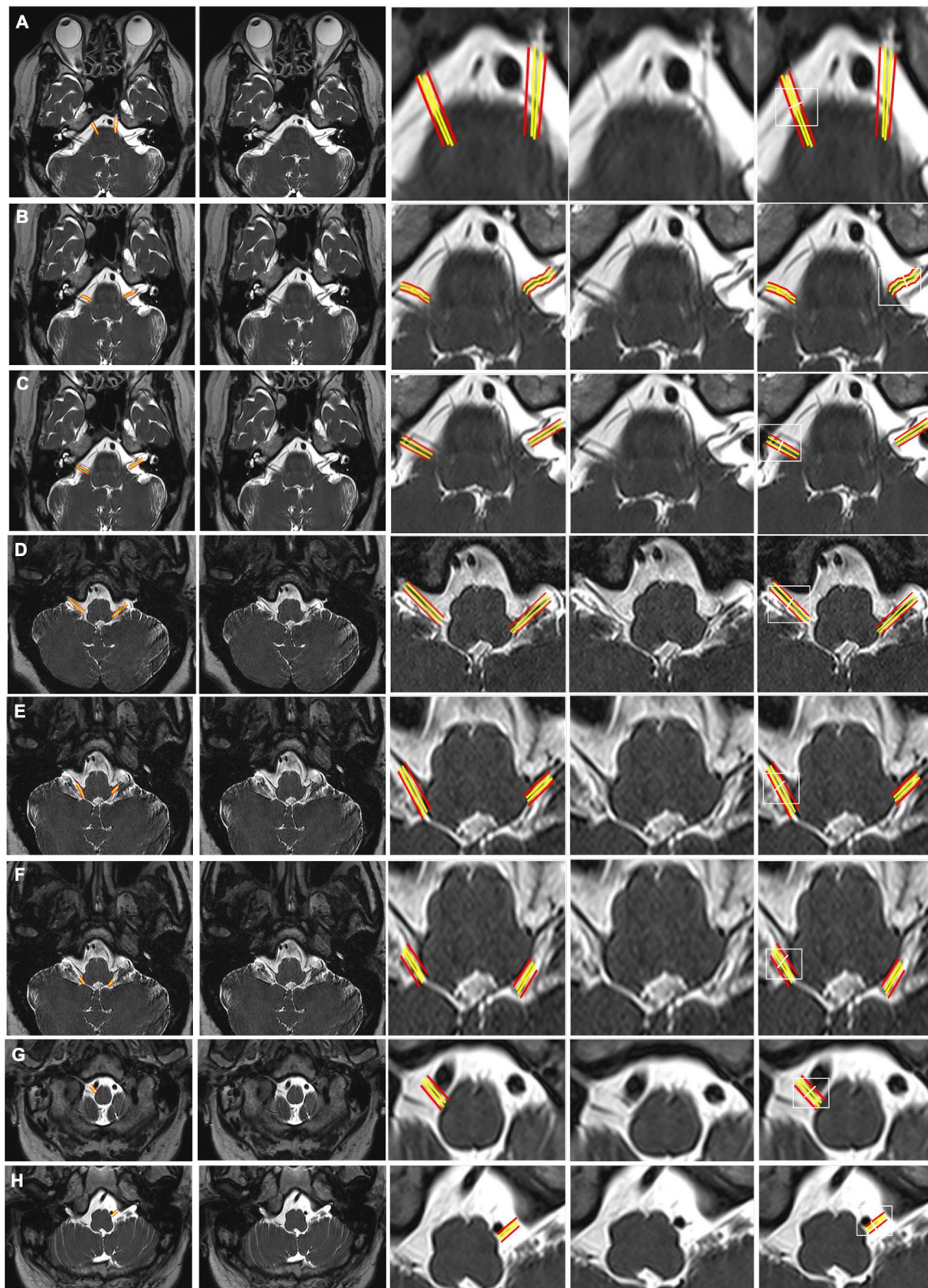


**FIGURE 2 |** CSF-filled peri-neural spaces surrounding the cranial nerves 6–12 (CN VI–CN XII). **(A)** Abducens nerves (CN VI) (two original images, two corresponding magnified images and measurement location); **(B)** Facial nerves (CN VII) (two original images, two corresponding magnified images and measurement location); **(C)** Vestibulocochlear nerves (CN VIII) (two original images, two corresponding magnified images and measurement location); **(D)** Glossopharyngeal nerves (CN IX) (two  
(Continued)



**FIGURE 2** | original images, two corresponding magnified images and measurement location); **(E)** Vagus nerves (CN X) (two original images, two corresponding magnified images and measurement location); **(F)** Accessory nerves (CN IX) (two original images, two corresponding magnified images and measurement location); **(G)** Right hypoglossal nerve (CN XII) (two original images, two corresponding magnified images and measurement location); and **(H)** Left CN XII (two original images, two corresponding magnified images and measurement location). Space between the red and yellow lines: peri-neural space (hyperintense signal). White line: location to measure the diameters of cranial nerves and corresponding peri-neural spaces. All images were generated from the first experiment as described in the method section.

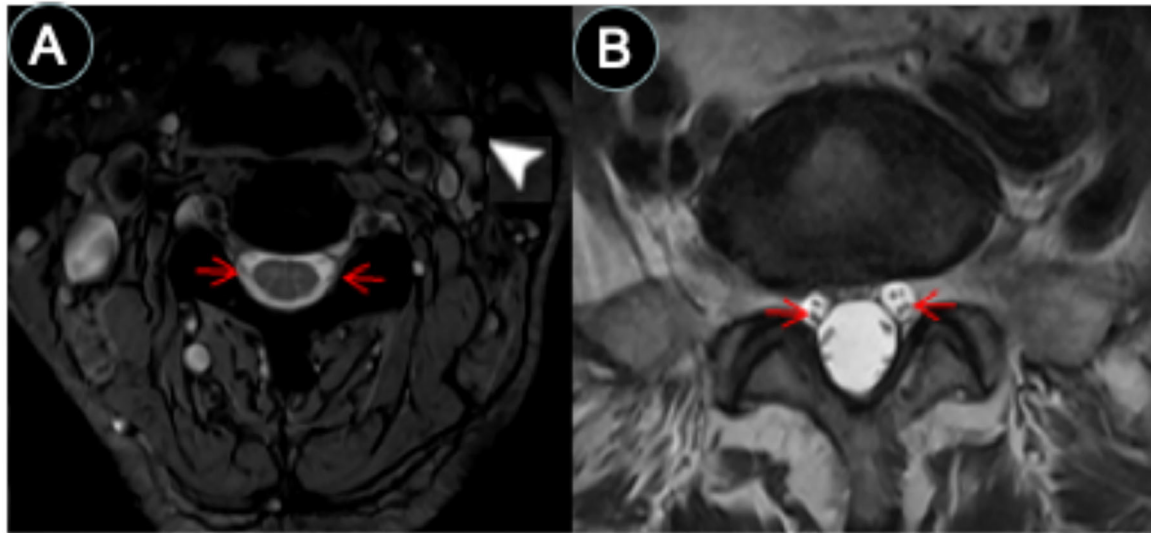


**FIGURE 3** | CSF-filled peri-neural spaces surrounding spinal nerves. **(A)** Cervical spinal nerves (brachial plexus). Cervical nerves four are pointed with red arrows (hypointense signal), and the space surrounding the nerves is the CSF-filled peri-neural space (hyperintense signal). Multiple lymph nodes are detected from MRI (white arrowhead). **(B)** Lumbar spinal nerves (red arrows, hypointense signal) surrounded with CSF-filled peri-neural space (hyperintense signal). Images were generated from the third and the fourth experiments as described in the method section.

mm and the mean total diameter (CN XII + corresponding peri-neural space) was  $1.3(\pm 0.1)$  mm, with a diameter ratio (CN XII diameter over total diameter) of 0.7 (**Table 1**).

The spinal nerves were visualized on the images from the third and fourth experiments (**Figure 3**). Similarly, the spinal nerves were hypointense, while the peri-neural spaces surrounding the spinal nerves were hyperintense, indicating the presence of CSF. **Figure 3A** shows an axial view of a pair of hypointense cervical spinal nerves emerging from the spinal cord at the level of C4/C5, surrounded with hyperintense CSF-filled perineural space. **Figure 3B** shows an axial view of a pair of hypointense lumbar spinal nerves emerging from the spinal cord at the level of L3/L4, encased in hyperintense CSF-filled perineural space.

## The CNS Vascular-Communication Channels Are Surrounded With CSF

The high-resolution (in the order of  $100\ \mu\text{m}$ ) sT2W (**Figure 4A**, bright CSF and dark blood) and T1W (**Figure 4B**, bright blood and dark CSF) derived from STAGE imaging demonstrated that all MRI-visible vasculature were surrounded with CSF. By comparing these two images, we found that all MRI-visible vasculature were indeed surrounded by CSF. Moreover, in order to further confirm these findings, we used a T2W-TSE image acquired with a very long echo

time ( $TE = 345\ \text{ms}$  at 3T) to generate “pure” CSF images, with bright CSF and dark blood (**Figures 4C,D**). Once again, all MRI-visible vasculature were indeed surrounded with CSF.

## DISCUSSION

To our knowledge, this is the first study to simultaneously and systematically verify that all 12 pairs of cranial nerves, all MRI-visible vasculature and spinal nerves are surrounded with CSF *in vivo* in humans; as opposed to previous studies that have asynchronously investigated this, mainly in animals and human cadavers. Our findings indicate that all brain parenchyma and spinal cord communication channels, both neuro- and vascular-communication channels, are encased in CSF. The diameter ratios, nerve diameter over total diameter (nerve diameter + corresponding peri-neural space), ranged from 0.6–0.8. It logically follows that CSF must play a critical role in substance exchange between the brain parenchyma/spinal cord and its communication channels as well as its surrounding environment/tissue—a role that has been historically underestimated and understudied. Our findings are consistent with previous literature that have asynchronously investigated CSF-filled peri-neural spaces, mostly in the context

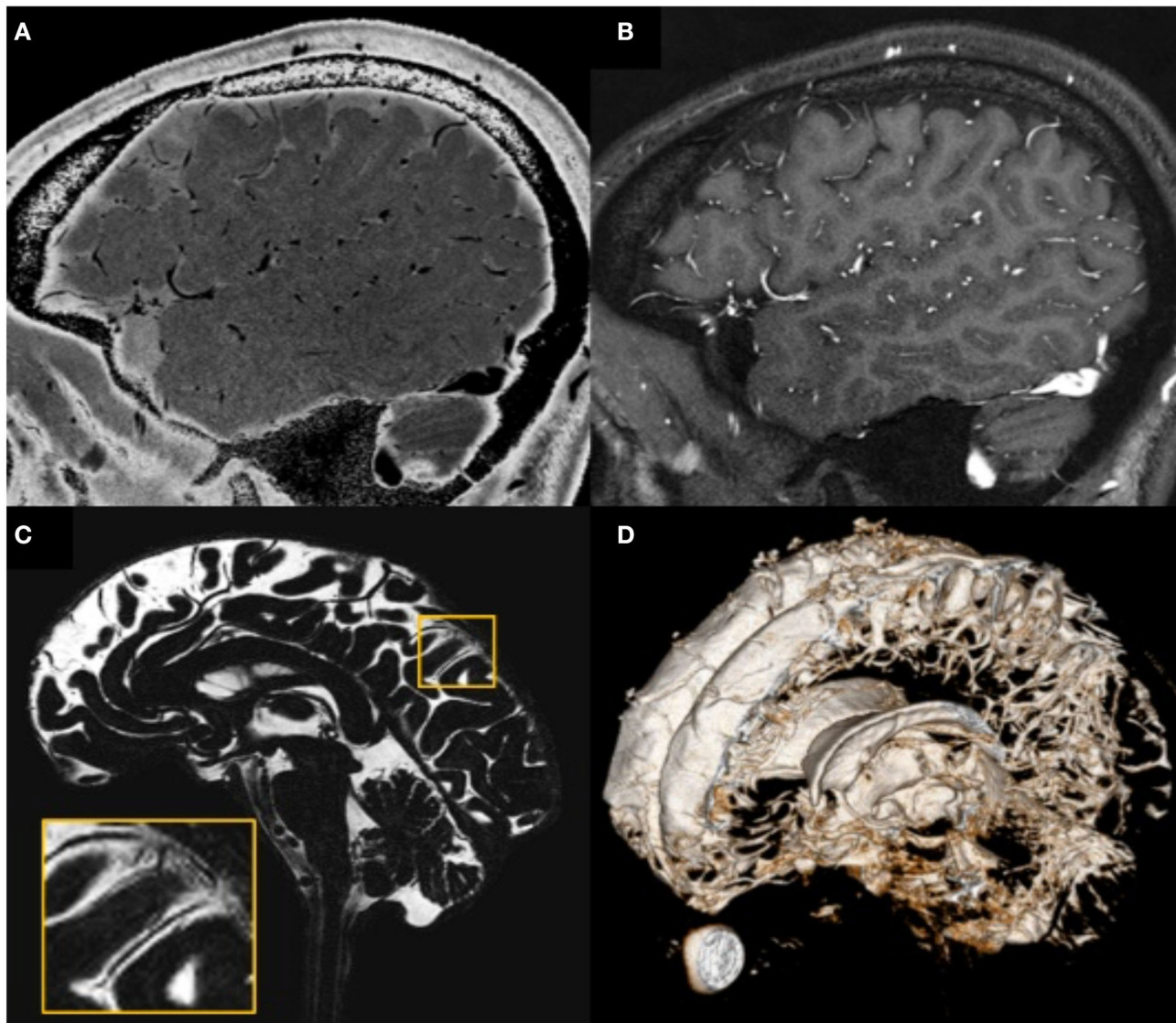


**FIGURE 4 |** Illustration showing that all MRI-visible vasculature were surrounded by CSF. **(A)** sT2W image with bright CSF and dark blood; **(B)** T1W with bright blood signal but dark CSF signal; **(C)** CSF-only images, acquired by T2-TSE sequence with TE = 345 ms at 3T; **(D)** a 3D rendering of the CSF-only images. **(A)** and **(B)** were results from the high-resolution STAGE scans. The enlarged image in **(C)** shows several MRI-visible vasculature (dark curves) surrounded by bright CSF. Images were generated from the second experiment as described in the method section.

of CWC lymphatic-associated CSF outflow pathways, as well as peri-vascular spaces (2, 7, 8, 52, 53).

Our findings indicated that CN I is surrounded with a CSF-filled peri-neural space, with a diameter ratio of 0.7. This is consistent with several studies that have focused on investigating the peri-neural spaces surrounding CN I. In 1958, Svane-Knudsen et al. observed that an iron solution injected in the CSF of guinea pigs made its way to the peri-neural spaces of CN I and the nasal interstitium (43). Bradbury et al. found that a radio-labeled intra-parenchymal tracer injection in rabbits drained via peri-vascular spaces and peri-neural spaces surrounding the CN I, allowing passage into the nasal submucosa and lymphatics (45). Similar findings were observed in a study

conducted by Pile-Spellman et al. in cats and rabbits, where radiolabeled colloid tracer injected in the ventricles made its way into the nasal submucosa and eventually into the cervical lymph nodes (46). A series of experiments conducted by Mollanji et al. identified the peri-neural spaces surrounding CN I as a major lymphatic-associated CSF outflow pathway in sheep; and demonstrated that blockage of the cribriform plate increased intracranial pressure and CSF outflow resistance, and decreased CSF transport (48–50). Moreover, in a series of experiments conducted by Johnston et al. in sheep, pigs, rabbits, mice, rats, monkeys and human cadavers, demonstrated that a silicone compound CSF tracer made its way into an extensive network of lymphatic vessels present in the nasal submucosa via peri-neural



**TABLE 1** | Diameter measurements and diameter ratios for all 12 cranial nerves.

Cranial nerve	Nerve diameter, mm mean( $\pm$ SE)	Total diameter (nerve + corresponding peri-neural space), mm mean( $\pm$ SE)	Ratio (nerve diameter over total diameter)
CN I	4.3( $\pm$ 0.8)	6.0( $\pm$ 0.6)	0.7
CN II	3.2( $\pm$ 0.5)	5.0( $\pm$ 0.5)	0.6
CN III	1.9( $\pm$ 0.5)	2.6( $\pm$ 0.4)	0.7
CN IV	0.9( $\pm$ 0.3)	1.4( $\pm$ 0.5)	0.6
CN V	4.6( $\pm$ 0.4)	5.7( $\pm$ 0.4)	0.8
CN VI	1.1( $\pm$ 0.1)	1.9( $\pm$ 0.2)	0.6
CN VII	1.0( $\pm$ 0.2)	1.6( $\pm$ 0.1)	0.6
CN VIII	1.1( $\pm$ 0.3)	1.7( $\pm$ 0.2)	0.6
CN IX	1.2( $\pm$ 0.1)	1.9( $\pm$ 0.3)	0.6
CN X	1.4( $\pm$ 0.2)	1.9( $\pm$ 0.3)	0.7
CN XI	1.1( $\pm$ 0.1)	1.7( $\pm$ 0.2)	0.6
CN XII	0.9( $\pm$ 0.2)	1.3( $\pm$ 0.1)	0.7

Measurement locations are indicated in **Figures 1, 2**. We have reported the diameters as mean( $\pm$ SE), as well as a diameter ratio of the nerve diameter over the total diameter (nerve diameter + corresponding peri-neural space diameter), for all 12 cranial nerves in five healthy human volunteers.

spaces surrounding CN I (28). More recent studies have been consistently confirming these findings (24, 29, 51). Furthermore, and interestingly, Czerniawska et al. found evidence of retrograde transport of a gold tracer injected in rabbit nasal mucosa back into the CSF (44). However, to the best of our knowledge, none of these studies have reported a quantitative diameter ratio for CN I.

Our findings also indicated that, in addition to CN I, the other 11 cranial nerves are also surrounded with CSF-filled peri-neural spaces, with diameter ratios ranging from 0.6–0.8. The peri-neural spaces of other cranial nerves have been studied to a lesser extent. In 1972, Arnold et al., using mice, rats, guinea pigs and rabbits, reported that the peri-neural spaces along CNV III played a role in CSF drainage into the perilymphatic spaces of the inner ear, following ink and thorotrast CSF cisterna magna tracer injection. Moreover, Kida et al. observed CSF tracer deposition along the peri-neural spaces of CN II, in addition to CN I and CN III, following an injection of india ink CSF cisterna magna tracer in rats (26). Similar findings (for CN I, CN II and CNV III) were observed in an experiment conducted by Boulton et al. in sheep injected with radiolabeled CSF tracer (47). Furthermore, Zakharov et al. identified the peri-neural spaces along CN V, CNV II, CN IX, CN X, CN XII and spinal nerves as contributors to the lymphatic-associated CSF outflow pathway in sheep, following a silicone compound CSF cisterna magna injection (27). A couple of other studies have also identified the spinal nerves as contributors to the lymphatic-associated CSF outflow pathway (29, 42). More recently, Ma et al. identified the peri-neural spaces along CN XI, in addition to CN I, CN II, CN V, CN VII, CN IX and CN X, as contributors to the lymphatic-associated CSF outflow pathway in rats, following a near-infrared CSF lateral ventricle injection (24). To our knowledge, the peri-neural

spaces along the CN III, the CN IV and CN VI have not been previously identified as CSF-filled and potentially contributing to lymphatic-associated CSF outflow pathways. Moreover, to our knowledge, none of these previous studies have reported quantitative diameter ratios for the cranial nerves. Unlike the diameter ratios of peri-vascular spaces, which have been previously reported mainly in animal studies (8), the diameter ratios of peri-neural spaces have simply passed under the radar. The utility of these diameter ratios can be investigated in neurodegenerative diseases such as Alzheimer's disease. In other words, future studies can focus on investigating the association between these diameter ratio changes and neurodegenerative diseases; since enlarged peri-vascular spaces have been reported with neurodegenerative diseases (17, 54, 55).

Our findings drive home the point that CSF lays between every cranial/spinal nerve and its surroundings (i.e., brain parenchyma and/or peripheral lymphatics), in the peri-neural spaces. Therefore, CSF must play a critical role in regulating the communication between the cranial nerves and their surroundings. One such type of communication regulation is with the lymphatic system. In fact, the interaction of CSF with the lymphatic system is only beginning to be understood. There is a growing body of evidence to suggest that CSF tracer eventually makes it into the deep cervical lymph nodes (24, 36, 37). Historically, the CNS is considered an immune-privileged site and therefore it was believed that antigens in the CNS did not communicate with the immune system (56–58). However, about 14–47% of radiolabeled tracers make their way into the lymphatic system, following CSF or intra-parenchymal injections (59). Therefore, antigens are transported to the immune system and can induce an immune response (56–58). Louveau et al. further demonstrated a decrease in the inflammatory response of brain-reactive T cells in a multiple sclerosis mouse model, following meningeal lymphatic vessel ablation (37). Anatomically-speaking, there is no direct interaction between the lymphatic system and CNS, and any interaction can only be accomplished through the CSF. Therefore, this begs the question of the role of CSF in immunomodulation, and together with our findings, the magnitude of this role.

Our findings also drive home the point that all MRI-visible vasculature is surrounded with CSF-filled peri-vascular spaces. Therefore, CSF must play a critical role in regulating the communication between the blood and the brain parenchyma, as well as CWC at large. In 1985, Rennels et al. introduced the idea of a fluid circulation system throughout the CNS via peri-vascular spaces (7). But it was not until 2012 that Iliff et al. solidified our understanding of this CSF circulation system via peri-vascular spaces within the brain parenchyma (labeled the glymphatic pathway); and demonstrated its critical role in amyloid beta (A $\beta$ ) clearance (8). Further investigations have indicated that the diameter ratios between the peri-arterial spaces and their corresponding arterial vessels are larger than the diameter ratios between the peri-venous spaces and their corresponding venous spaces (60). As mentioned earlier, dysfunctions of this glymphatic pathway have been associated with a broad range of neurological diseases including, but not limited to, Alzheimer's disease, stroke, traumatic brain injury, multiple sclerosis, diabetes, and

chronic traumatic encephalopathy; begging the question of its involvement in virtually all neurodegenerative diseases (8–10, 12, 14, 16–19). Therefore, disruptions to CWC can either initiate or/and aggravate the pathophysiology of an array of neurological diseases.

Starting 6 years ago, gadolinium-based contrast agent (GCA) residual deposition in the brain parenchyma with chronic administration has been documented (61, 62). GCA is a widely used contrast agent in clinical MRI. It does not cross the BBB and is renally eliminated from the human body; and thus, considered safe for clinical use. Therefore, the residual deposition of IV-administered GCA in individuals with an intact BBB and normal renal function raised a lot of questions. How does the IV-administered GCA enter and deposit in the brain parenchyma? Currently, the mainstream theory is through the CSF via the glymphatic pathway. Based on several studies, it is hypothesized that the IV-administered GCA enters the CSF compartment through the choroid plexus, cranial nerve endings and/or peri-vascular spaces surrounding vessels; from here it re-circulates and enters the brain parenchyma via peri-arterial routes—a portion gets deposited in the brain parenchyma, while the remaining portion gets carried away via peri-venous routes, eventually draining into the lymphatics (63–66). CSF involvement was further confirmed by Öner et al. in a study investigating individuals with chronic intrathecal administration of GCA who had never undergone IV-administration of GCA; similar GCA deposition patterns were observed (67). GCA deposition via CSF is an example of how CSF-filled peri-vascular and peri-neural spaces play a critical and major role in substance deposition and re-circulation. Long-term effects of GCA deposition are unknown and require further investigation.

There are several major strengths to our study. First, to our knowledge, it is the first study to systematically and simultaneously verify that CSF surrounds all cranial (including CN III, CN IV and CN VI which have not been previously investigated), all MRI-visible vasculature and spinal nerves. Second, our study was performed *in vivo* in humans. Third, our study utilized MRI which is minimally invasive and therefore caused minimal disruption to the biological system. In the past, most MRI studies of the peri-neural and peri-vascular spaces have been mainly conducted in animals (64, 68).

On the other hand, the major limitation of our study is that we did not investigate the underlying mechanisms of how CSF made it into or out of these peri-vascular and peri-neural spaces. Although this has been a topic-of-interest as of late, and several strides have been made to address this topic, the latest of which has been the establishment of the glymphatic pathway, the CSF efflux mechanisms remain unclear. One current question of interest is: “What is the underlying pathway/mechanism by which CSF drains into the meningeal lymphatics, and how is this pathway/mechanism related to CSF-filled peri-vascular and peri-neural spaces?” Another major limitation is that we did not investigate if and how CSF communicates with the CNS neuro- and vascular-communication channels themselves (i.e., the vasculature and nerves that it surrounds), nor a quantitative morphometric measurement of the arterial and venous blood

vessels and their corresponding peri-vascular spaces. There is growing evidence to suggest that CSF in peri-vascular spaces might be involved in the direct transport of cerebral waste into the parenchymal vasculature, perhaps through transcellular mechanisms (29, 69, 70). However, given the pathophysiological variations, the systematic measurement of blood vessels and their corresponding peri-vascular space across multiple regions of the brain are complex and also warrant further investigation. Another major limitation is our small sample size of healthy human volunteers. Therefore, future investigations with larger sample sizes are warranted; perhaps even these investigations should be extended to beyond healthy individuals, i.e., patients with neurodegenerative diseases such as Alzheimer’s disease. Finally, the measured size of cranial nerves and their relative perineural spaces may suffer from partial volume effects which is a common issue with MRI.

In conclusion, our findings indicate that all CNS neuro- and vascular-communication channels are surrounded with CSF. In other words, all peri-neural spaces surrounding the cranial and spinal nerves as well as all peri-vascular spaces surrounding MRI-visible vasculature were filled with CSF. These findings highlight the extent to which CSF infiltrates the parenchyma and its importance, therefore, warranting further investigation into its potential implications.

## DATA AVAILABILITY STATEMENT

The raw data supporting the conclusions of this article will be made available by the authors, without undue reservation.

## ETHICS STATEMENT

The studies involving human participants were reviewed and approved by Wayne State University Institutional Review Board. The patients/participants provided their written informed consent to participate in this study.

## AUTHOR CONTRIBUTIONS

LF participated in conceptualization, data acquisition, data analysis, manuscript writing, and manuscript editing. YC participated in conceptualization, investigation, data acquisition, data analysis, manuscript writing, and manuscript editing. SX participated in data acquisition, data analysis, and manuscript editing. EH participated in methodology, data analysis, and manuscript editing. JH participated in conceptualization, methodology, data analysis, and manuscript editing. QJ participated in conceptualization, methodology, data analysis, and manuscript editing. All authors contributed to the article and approved the submitted version.

## FUNDING

This work was supported by the following NIH grants: R01-NS108491, RF1-AG057494, and R01-NS108463.

## REFERENCES

- McAllister JP II, Chovan P. Neonatal hydrocephalus. Mechanisms and consequences. *Neurosurg Clin N Am.* (1998) 9:73–93. doi: 10.1016/S1042-3680(18)30281-X
- Pollay M. The function and structure of the cerebrospinal fluid outflow system. *Cerebrospinal Fluid Res.* (2010) 7:9. doi: 10.1186/1743-8454-7-9
- Wright BL, Lai JT, Sinclair AJ. Cerebrospinal fluid and lumbar puncture: a practical review. *J Neurol.* (2012) 259:1530–45. doi: 10.1007/s00415-012-6413-x
- Bakker EN, Bacskaï BJ, Arbel-Ornath M, Aldea R, Bedussi B, Morris AW, et al. Lymphatic clearance of the brain: perivascular, paravascular and significance for neurodegenerative diseases. *Cell Mol Neurobiol.* (2016) 36:181–94. doi: 10.1007/s10571-015-0273-8
- Javed K, Reddy V, Lui F. *Neuroanatomy, Choroid Plexus*. Treasure Island (FL): StatPearls (2020).
- Wang, JJ, Iliff M, Liao Y, Chen MJ, Shinseki MS, Venkataraman A, et al. Cognitive deficits and delayed neuronal loss in a mouse model of multiple microinfarcts. *J Neurosci.* (2012) 32:17948–60. doi: 10.1523/JNEUROSCI.1860-12.2012
- Rennels ML, Gregory TF, Blaumanis OR, Fujimoto K., Grady PA. Evidence for a 'paravascular' fluid circulation in the mammalian central nervous system, provided by the rapid distribution of tracer protein throughout the brain from the subarachnoid space. *Brain Res.* (1985) 326:47–63. doi: 10.1016/0006-8993(85)91383-6
- Iliff JJ, Wang M, Liao Y, Plogg BA, Peng W, Gundersen GA, et al. A paravascular pathway facilitates CSF flow through the brain parenchyma and the clearance of interstitial solutes, including amyloid beta. *Sci Transl Med.* (2012) 4:147ra111. doi: 10.1126/scitranslmed.3003748
- Rangroo Thrane, AS, Thrane V, Plog BA, Thiyagarajan M, Iliff JJ, Deane R et al. Paravascular microcirculation facilitates rapid lipid transport and astrocyte signaling in the brain. *Sci Rep.* (2013) 3:2582. doi: 10.1038/srep02582
- Jessen NA, Munk AS, Lundgaard I, Nedergaard M. The lymphatic system: a beginner's guide. *Neurochem Res.* (2015) 40:2583–99. doi: 10.1007/s11064-015-1581-6
- Louveau A, Smirnov I, Keyes TJ, Eccles JD, Rouhani SJ, Peske JD, et al. Structural and functional features of central nervous system lymphatic vessels. *Nature.* (2015) 523:337–41. doi: 10.1038/nature14432
- Plog BA, Dashnaw ML, Hitomi E, Peng W, Liao Y, Lou N, et al. Biomarkers of traumatic injury are transported from brain to blood via the glymphatic system. *J Neurosci.* (2015) 35:518–26. doi: 10.1523/JNEUROSCI.3742-14.2015
- Carare RO, Bernardes-Silva M, Newman TA, Page AM, Nicoll JA, Perry VH, et al. Solutes, but not cells, drain from the brain parenchyma along basement membranes of capillaries and arteries: significance for cerebral amyloid angiopathy and neuroimmunology. *Neuropathol Appl Neurobiol.* (2008) 34:131–44. doi: 10.1111/j.1365-2990.2007.00926.x
- Arbel-Ornath M, Hudry E, Eikermann-Haerter K, Hou S, Gregory JL, Zhao L, et al. Interstitial fluid drainage is impaired in ischemic stroke and Alzheimer's disease mouse models. *Acta Neuropathol.* (2013) 126:353–64. doi: 10.1007/s00401-013-1145-2
- Albargothy NJ, Johnston DA, MacGregor-Sharp M, Weller RO, Verma A, Hawkes CA, et al. Convective influx/glymphatic system: tracers injected into the CSF enter and leave the brain along separate periaxonal basement membrane pathways. *Acta Neuropathol.* (2018) 136:139–52. doi: 10.1007/s00401-018-1862-7
- Louveau A, Da Mesquita S, Kipnis J. Lymphatics in neurological disorders: a neuro-lympho-vascular component of multiple sclerosis and Alzheimer's disease? *Neuron.* (2016) 91:957–73. doi: 10.1016/j.neuron.2016.08.027
- Jiang Q, Zhang L, Ding G, Davoodi-Bojd E, Li Q, Li L, et al. Impairment of the glymphatic system after diabetes. *J Cereb Blood Flow Metab.* (2017) 37:1326–37. doi: 10.1177/0271678X16654702
- Mestre H, Tithof J, Du T, Song W, Peng W, Sweeney AM, et al. Flow of cerebrospinal fluid is driven by arterial pulsations and is reduced in hypertension. *Nat Commun.* (2018) 9:4878. doi: 10.1038/s41467-018-07318-3
- Mestre H, Du T, Sweeney AM, Liu G, Samson AJ, Peng W, et al. Cerebrospinal fluid influx drives acute ischemic tissue swelling. *Science.* (2020) 367:6483. doi: 10.1126/science.aax7171
- McComb JG. Recent research into the nature of cerebrospinal fluid formation and absorption. *J Neurosurg.* (1983) 59:369–83. doi: 10.3171/jns.1983.59.3.0369
- Zakharov A, Papaiconomou C, Johnston M. Lymphatic vessels gain access to cerebrospinal fluid through unique association with olfactory nerves. *Lymphat Res Biol.* (2004) 2:139–46. doi: 10.1089/lrb.2004.2.139
- Weed LH. Studies on Cerebro-Spinal Fluid. No. III: The pathways of escape from the Subarachnoid Spaces with particular reference to the Arachnoid Villi. *J Med Res.* (1914) 31:51–91.
- Koh L, Zakharov A, Johnston M. Integration of the subarachnoid space and lymphatics: is it time to embrace a new concept of cerebrospinal fluid absorption? *Cerebrospinal Fluid Res.* (2005) 2:6. doi: 10.1186/1743-8454-2-6
- Ma, BV, Ineichen Q, Detmar M, Proulx ST. Outflow of cerebrospinal fluid is predominantly through lymphatic vessels and is reduced in aged mice. *Nat Commun.* (2017) 8:1434. doi: 10.1038/s41467-017-01484-6
- Bradbury MW, Westrop RJ. Factors influencing exit of substances from cerebrospinal fluid into deep cervical lymph of the rabbit. *J Physiol.* (1983) 339:519–34. doi: 10.1113/jphysiol.1983.sp014731
- Kida S, Pantazis A, Weller RO. CSF drains directly from the subarachnoid space into nasal lymphatics in the rat. Anatomy, histology and immunological significance. *Neuropathol Appl Neurobiol.* (1993) 19:480–8. doi: 10.1111/j.1365-2990.1993.tb00476.x
- Zakharov A, Papaiconomou C, Djenic J, Midha R, Johnston M. Lymphatic cerebrospinal fluid absorption pathways in neonatal sheep revealed by subarachnoid injection of Microfil. *Neuropathol Appl Neurobiol.* (2003) 29:563–73. doi: 10.1046/j.0305-1846.2003.00508.x
- Johnston M, Zakharov A, Papaiconomou C, Salmasi G, Armstrong D. Evidence of connections between cerebrospinal fluid and nasal lymphatic vessels in humans, non-human primates and other mammalian species. *Cerebrospinal Fluid Res.* (2004) 1:2. doi: 10.1186/1743-8454-1-2
- Krishnamurthy S, Li J, Shen Y, Duncan TM, Jenrow KA, Haacke EM. Normal macromolecular clearance out of the ventricles is delayed in hydrocephalus. *Brain Res.* (2018) 1678:337–55. doi: 10.1016/j.brainres.2017.10.013
- Shen JY, Kelly DE, Hyman S, McComb JG. Intraorbital cerebrospinal fluid outflow and the posterior uveal compartment of the hamster eye. *Cell Tissue Res.* (1985) 240:77–87. doi: 10.1007/BF00217560
- Erlich SS, McComb JG, Hyman S, Weiss MH. Ultrastructural morphology of the olfactory pathway for cerebrospinal fluid drainage in the rabbit. *J Neurosurg.* (1986) 64:466–73. doi: 10.3171/jns.1986.64.3.0466
- Erlich SS, McComb JG, Hyman S, Weiss MH. Ultrastructure of the orbital pathway for cerebrospinal fluid drainage in rabbits. *J Neurosurg.* (1989) 70:926–31. doi: 10.3171/jns.1989.70.6.0926
- Zakharov A, Papaiconomou C, Koh L, Djenic J, Bozanovic-Sosic R, Johnston M. Integrating the roles of extracranial lymphatics and intracranial veins in cerebrospinal fluid absorption in sheep. *Microvasc Res.* (2004) 67:96–104. doi: 10.1016/j.mvr.2003.08.004
- Ludemann W, Berens von Rautenfeld D, Samii M, Brinker T. Ultrastructure of the cerebrospinal fluid outflow along the optic nerve into the lymphatic system. *Childs Nerv Syst.* (2005) 21:96–103. doi: 10.1007/s00381-004-1040-1
- Aspelund A, Antila S, Proulx ST, Karlens TV, Karaman S, Detmar M, et al. A dural lymphatic vascular system that drains brain interstitial fluid and macromolecules. *J Exp Med.* (2015) 212:991–9. doi: 10.1084/jem.20142290
- Da Mesquita S, Louveau A, Vaccari A, Smirnov I, Cornelison RC, Kingsmore KM, et al. Functional aspects of meningeal lymphatics in ageing and Alzheimer's disease. *Nature.* (2018) 560:185–91. doi: 10.1038/s41586-018-0368-8
- Louveau A, Herz J, Alme MN, Salvador AF, Dong MQ, Viar KE, et al. CNS lymphatic drainage and neuroinflammation are regulated by meningeal lymphatic vasculature. *Nat Neurosci.* (2018) 21:1380–91. doi: 10.1038/s41593-018-0227-9
- Mugler JP III, Bao S, Mulkern RV, Guttman CR, Robertson RL, Jolesz FA, et al. Optimized single-slab three-dimensional spin-echo MR imaging of the brain. *Radiology.* (2000) 216:891–9. doi: 10.1148/radiology.216.3.r00au46891
- Chen Y, Liu S, Wang Y, Kang Y, Haacke EM. STategically Acquired Gradient Echo (STAGE) imaging, part I: Creating enhanced T1 contrast and standardized susceptibility weighted imaging and quantitative susceptibility mapping. *Magn Reson Imaging.* (2018) 46:130–9. doi: 10.1016/j.mri.2017.10.005

40. Wang Y, Chen Y, Wu D, Wang Y, Sethi SK, Yang G, et al. STrategically Acquired Gradient Echo (STAGE) imaging, part II: Correcting for RF inhomogeneities in estimating T1 and proton density. *Magn Reson Imaging*. (2018) 46:140–50. doi: 10.1016/j.mri.2017.10.006
41. Haacke EM, Chen Y, Utriainen D, Wu B, Wang Y, Xia S, et al. STrategically Acquired Gradient Echo (STAGE) imaging, part III: Technical advances and clinical applications of a rapid multi-contrast multi-parametric brain imaging method. *Magn Reson Imaging*. (2020) 65:15–26. doi: 10.1016/j.mri.2019.09.006
42. Brierley JB, Field EJ. The connexions of the spinal sub-arachnoid space with the lymphatic system. *J Anat*. (1948) 82:153–66.
43. Svane-Knudsen V. Resorption of the cerebro-spinal fluid in guinea-pig; an experimental study. *Acta Otolaryngol*. (1958) 49:240–51. doi: 10.3109/00016485809134752
44. Czerniawska A. Experimental investigations on the penetration of <sup>198</sup>Au from nasal mucous membrane into cerebrospinal fluid. *Acta Otolaryngol*. (1970) 70:58–61. doi: 10.3109/00016487009181859
45. Bradbury MW, Cserr HF, Westrop RJ. Drainage of cerebral interstitial fluid into deep cervical lymph of the rabbit. *Am J Physiol*. (1981) 240:F329–36. doi: 10.1152/ajprenal.1981.240.4.F329
46. Pile-Spellman JM, McKusick KA, Strauss HW, Cooney J, Taveras JM. Experimental in vivo imaging of the cranial perineural lymphatic pathway. *AJNR Am J Neuroradiol*. (1984) 5:539–45.
47. Boulton M, Young A, Hay J, Armstrong D, Flessner M, Schwartz M. Drainage of CSF through lymphatic pathways and arachnoid villi in sheep: measurement of <sup>125</sup>I-albumin clearance. *Neuropathol Appl Neurobiol*. (1996) 22:325–33. doi: 10.1111/j.1365-2990.1996.tb01111.x
48. Mollanji R, Bozanovic-Sosic R, Silver I, Li B, Kim C, Midha R. Intracranial pressure accommodation is impaired by blocking pathways leading to extracranial lymphatics. *Am J Physiol Regul Integr Comp Physiol*. (2001) 280:R1573–81. doi: 10.1152/ajpregu.2001.280.5.R1573
49. Mollanji R, Papaiconomou C, Boulton M, Midha R, Johnston M. Comparison of cerebrospinal fluid transport in fetal and adult sheep. *Am J Physiol Regul Integr Comp Physiol*. (2001) 281:R1215–23. doi: 10.1152/ajpregu.2001.281.4.R1215
50. Mollanji R, Bozanovic-Sosic R, Zakharov A, Makarian L, Johnston MG. Blocking cerebrospinal fluid absorption through the cribriform plate increases resting intracranial pressure. *Am J Physiol Regul Integr Comp Physiol*. (2002) 282:R1593–9. doi: 10.1152/ajpregu.00695.2001
51. Liu H, Ni Z, Chen Y, Wang D, Qi Y, Zhang Q, et al. Olfactory route for cerebrospinal fluid drainage into the cervical lymphatic system in a rabbit experimental model. *Neural Regen Res*. (2012) 7:766–71. doi: 10.3969/j.issn.1673-5374.2012.10.009
52. Sakka L, Coll G, Chazal J. Anatomy and physiology of cerebrospinal fluid. *Eur Ann Otorhinolaryngol Head Neck Dis*. (2011) 128:309–16. doi: 10.1016/j.anorl.2011.03.002
53. Chen L, Elias G, Yostos MP, Stimec B, Fasel J, Murphy K. Pathways of cerebrospinal fluid outflow: a deeper understanding of resorption. *Neuroradiology*. (2015) 57:139–47. doi: 10.1007/s00234-014-1461-9
54. Doubal FN, MacLulich AM, Ferguson KJ, Dennis MS, Wardlaw JM. Enlarged perivascular spaces on MRI are a feature of cerebral small vessel disease. *Stroke*. (2010) 41:450–4. doi: 10.1161/STROKEAHA.109.564914
55. Wardlaw JM, Smith C, Dichgans M. Mechanisms of sporadic cerebral small vessel disease: insights from neuroimaging. *Lancet Neurol*. (2013) 12:483–97. doi: 10.1016/S1474-4422(13)70060-7
56. Ferguson TA, Griffith TS. A vision of cell death: insights into immune privilege. *Immunol Rev*. (1997) 156:167–84. doi: 10.1111/j.1600-065X.1997.tb00967.x
57. Streilein JW, Ksander BR, Taylor AW. Immune deviation in relation to ocular immune privilege. *J Immunol*. (1997) 158:3557–60.
58. Streilein JW, Takeuchi M, Taylor AW. Immune privilege, T-cell tolerance, and tissue-restricted autoimmunity. *Hum Immunol*. (1997) 52:138–43. doi: 10.1016/S0198-8859(96)00288-1
59. Cserr HF, Harling-Berg CJ, Knopf PM. Drainage of brain extracellular fluid into blood and deep cervical lymph and its immunological significance. *Brain Pathol*. (1992) 2:269–76. doi: 10.1111/j.1750-3639.1992.tb00703.x
60. Jochems ACC, Blair GW, Stringer MS, Thrippleton MJ, Clancy U, Chappell FM, et al. Relationship between venules and perivascular spaces in sporadic small vessel diseases. *Stroke*. (2020) 51:1503–6. doi: 10.1161/STROKEAHA.120.029163
61. Pulicino R, Radon M, Biswas S, Bhojak M, Das K. A review of the current evidence on gadolinium deposition in the brain. *Clin Neuroradiol*. (2018) 28:159–69. doi: 10.1007/s00062-018-0678-0
62. Taoka T, Naganawa S. Gadolinium-based contrast media, cerebrospinal fluid and the glymphatic system: possible mechanisms for the deposition of gadolinium in the brain. *Magn Reson Med Sci*. (2018) 17:111–9. doi: 10.2463/mrms.rev.2017-0116
63. Aoki YJ, Wu I, Silva AC, Lynch RM, Koretsky AP. In vivo detection of neuroarchitecture in the rodent brain using manganese-enhanced MRI. *Neuroimage*. (2004) 22:1046–59. doi: 10.1016/j.neuroimage.2004.03.031
64. Iliff JJ, Lee H, Yu M, Feng T, Logan J, Nedergaard M, et al. Brain-wide pathway for waste clearance captured by contrast-enhanced MRI. *J Clin Invest*. (2013) 123:1299–309. doi: 10.1172/JCI67677
65. Jost G, Frenzel T, Lohrke J, Lenhard DC, Naganawa S, Pietsch H. Penetration and distribution of gadolinium-based contrast agents into the cerebrospinal fluid in healthy rats: a potential pathway of entry into the brain tissue. *Eur Radiol*. (2017) 27:2877–85. doi: 10.1007/s00330-016-4654-2
66. Naganawa S, Kawai H, Taoka T, Sone M. Improved HYDROPS: imaging of endolymphatic hydrops after intravenous administration of gadolinium. *Magn Reson Med Sci*. (2017) 16:357–61. doi: 10.2463/mrms.tn.2016-0126
67. Oner AY, Barutcu B, Aykol S, Tali ET. Intrathecal contrast-enhanced magnetic resonance imaging-related brain signal changes: residual gadolinium deposition? *Invest Radiol*. (2017) 52:195–7. doi: 10.1097/RLI.0000000000000327
68. Lee H, Xie L, Yu M, Kang H, Feng T, Deane R, et al. The effect of body posture on brain glymphatic transport. *J Neurosci*. (2015) 35:11034–44. doi: 10.1523/JNEUROSCI.1625-15.2015
69. Weller RO, Massey A, Newman TA, Hutchings M, Kuo YM, Roher AE. Cerebral amyloid angiopathy: amyloid beta accumulates in putative interstitial fluid drainage pathways in Alzheimer's disease. *Am J Pathol*. (1998) 153:725–33. doi: 10.1016/S0002-9440(10)65616-7
70. Da Mesquita S, Fu Z, Kipnis J. The meningeal lymphatic system: a new player in neurophysiology. *Neuron*. (2018) 100:375–88. doi: 10.1016/j.neuron.2018.09.022

**Conflict of Interest:** The authors declare that the research was conducted in the absence of any commercial or financial relationships that could be construed as a potential conflict of interest.

Copyright © 2021 Fahmy, Chen, Xuan, Haacke, Hu and Jiang. This is an open-access article distributed under the terms of the Creative Commons Attribution License (CC BY). The use, distribution or reproduction in other forums is permitted, provided the original author(s) and the copyright owner(s) are credited and that the original publication in this journal is cited, in accordance with accepted academic practice. No use, distribution or reproduction is permitted which does not comply with these terms.





# Spatial Navigation Is Impaired in Elderly Patients With Cerebral Small Vessel Disease

Hóngyi Zhao<sup>1,2†</sup>, Liyi Chi<sup>3†</sup>, Yanhai Zhang<sup>4</sup>, Yonghua Huang<sup>1\*</sup> and Hongyan Tian<sup>5</sup>

<sup>1</sup> Department of Neurology, Chinese PLA General Hospital, Beijing, China, <sup>2</sup> Department of Neurology, NO 984 Hospital of PLA, Beijing, China, <sup>3</sup> Department of Neurology, First Affiliated Hospital of Air Force Military Medical University, Xi'an, China, <sup>4</sup> Department of Geriatrics, First Affiliated Hospital of Air Force Military Medical University, Xi'an, China, <sup>5</sup> Department of Cardiology, The First Affiliated Hospital of Xi'an Jiaotong University, Xi'an, China

## OPEN ACCESS

### Edited by:

Yulin Ge,  
New York University, United States

### Reviewed by:

Alessandra Rufa,  
University of Siena, Italy  
Cristina Fernandez-Baizan,  
University of Oviedo, Spain

### \*Correspondence:

Yonghua Huang  
huangyonghua2017@126.com

<sup>†</sup>These authors have contributed  
equally to this work and share first  
authorship

### Specialty section:

This article was submitted to  
Stroke,  
a section of the journal  
Frontiers in Neurology

**Received:** 21 September 2020

**Accepted:** 28 June 2021

**Published:** 08 September 2021

### Citation:

Zhao H, Chi L, Zhang Y, Huang Y and  
Tian H (2021) Spatial Navigation Is  
Impaired in Elderly Patients With  
Cerebral Small Vessel Disease.  
Front. Neurol. 12:608797.  
doi: 10.3389/fneur.2021.608797

Cerebral small vessel disease (SVD) refers to a heterogeneous group of pathological processes that result from damage to the small penetrating vessels in the brain. Spatial navigation, one of the most fundamental behaviors, has lately attracted considerable clinical interest. This study aimed to determine whether spatial navigation performance is impaired in elderly SVD patients. In total, 18 elderly patients with severe SVD, 40 elderly patients with non-severe SVD, and 41 age-matched healthy volunteers were classified according to the Fazekas scale. Spatial navigation was evaluated by Amunet (a computer-based analogy of Morris water maze software), and a mini-mental scale evaluation (MMSE), animal category verbal fluency test (VFT), clock drawing test (CDT), and trail making test (TMT) -B were also applied. Compared to healthy controls, severe SVD, rather than non-severe SVD patients, exhibited significantly worse performance on “allocentric + egocentric” ( $41.74 \pm 29.10$  vs.  $31.50 \pm 16.47$  vs.  $29.21 \pm 19.03$ ;  $p = 0.031$ ). Furthermore, the different abilities of spatial navigation among groups reached a statistical level on allocentric subtests ( $46.93 \pm 31.27$  vs.  $43.69 \pm 23.95$  vs.  $28.56 \pm 16.38$ ;  $p = 0.003$ ), but not on egocentric subtest ( $56.16 \pm 39.85$  vs.  $56.00 \pm 28.81$  vs.  $43.06 \pm 25.07$ ;  $p = 0.105$ ). The linear regression analysis revealed that allocentric navigation deficit was significantly correlated with TMT-B ( $p = 0.000$ , standardized  $\beta = 0.342$ ) and VFT ( $p = 0.016$ , standardized  $\beta = -0.873$ ) performance in elderly SVD patients. These results elucidated that spatial navigation ability could be a manifestation of cognitive deficits in elderly patients with SVD.

**Keywords:** aging, cognitive function, spatial navigation, executive function, small vessel disease

## INTRODUCTION

Spatial navigation is the process that determines and maintains a trajectory between different points within local environments (1). The success of the navigation process can be influenced by two codependent strategies: egocentric and allocentric navigation strategies (2). The former requires the moving agent to visualize and gauge self-to-object relationships from a body-centered viewpoint, while the latter requires the agent to visualize and map out object-to-object relationships from a disembodied or environment-centered viewpoint (3). Previous functional and structural MRI findings revealed that egocentric navigation might be related to occipital and parietal place area (1), whereas allocentric navigation might be associated more with the hippocampal and prefrontal region (3). Empirically, patients suffering from different types of brain lesions tend to have worse

spatial navigation performance. For example, elderly patients with mild cognitive impairment (MCI) and Alzheimer's disease (AD) have a high risk of getting lost behavior (4). Nowadays, several studies have reported that spatial navigation could be modified into a sensitive tool for the preclinical screening of Alzheimer's disease (AD) and dementia (5).

Cerebral small vessel disease (SVD) is a syndrome that involves diseases of the small vessels in the brain, such as white matter hyperintensity lesions, Lacunar Infarctions (LI), etc (6). SVD has received increasing attention in cerebrovascular practice because it is a major cause of vascular dementia and cognitive impairment. The disruption of crucial subcortical connections in the frontal and other lobes, as well as basal ganglia area, following multiple pathophysiological changes such as chronic hypoperfusion, impaired cerebrovascular reactivity, and blood–brain barrier (BBB) leakage, is the core mechanism through which SVD affects cognition (7, 8). As distinguishable from the primary pathological features (cognitive dysfunction) of AD, SVD patients often showed impairments in attention, episodic memory, naming, mental flexibility, and psychomotor speed (6). Although some researchers found that LI was associated with spatial navigation deficits (9), whether the patients with white matter hyperintensities (one of the imaging markers of SVD in MRI) showed spatial navigation abnormalities is still unclear. Besides, we have hypothesized whether the spatial navigation disability in SVD patients was associated with a certain aspect of cognitive decline. In this study, we sought to identify the spatial navigation characteristics of SVD patients by using both egocentric and allocentric strategies and the changes in cognitive function in elderly patients with varying degrees of SVD.

## METHODS

### Subjects

From June 1, 2019, to December 31, 2019, a total of 18 and 40 elderly patients with high (severe group) and low (non-severe group) SVD burden, respectively, and 41 age-matched healthy volunteers (control group) were enrolled into this study. All subjects provided written informed consent, and the study protocol was approved by the ethics committee of the Seventh Medical Center of PLA General Hospital. After screening by a 3-Tesla MRI scanner, they were classified based on the Fazekas scale as shown in **Supplementary Material 1**. The severity of white matter hyperintensities was ranked as follows: grade 0 (no lesion), grade 1 (punctate lesion), grade 2 (early confluent lesion), and grade 3 (confluent lesion). According to the Fazekas scale, the severe group, non-severe group, and control group were defined as grade 2–3, grade 1, and grade 0, respectively. All participants were right-handed, at least 65 years old, and had ordinary visual acuity and other visual capacities. Patients were excluded from the study if they had an intracerebral hemorrhage, major psychiatric disorders, non-vascular dementia, multisystem diseases, taken psychotropic drugs, MRI contraindication, and other causes of leukoencephalopathy (e.g., demyelination, genetic, and immune factors). Basic demographic data, such as age, gender, identity, and educational status, were collected from all participants.

## Neuropsychological Assessment

All subjects were asked to complete a series of neuropsychological tests, including clock drawing test (CDT; reflecting visuospatial function), mini-mental scale evaluation (MMSE; reflecting global cognitive level), trail making test (TMT-B; reflecting cognitive flexibility), and category verbal fluency test (VFT; reflecting semantic memory).

### Spatial Navigation Tests

The Amunet test (a computer-based analogy of Morris water maze software, NeuroScios GmbH, Austria) was used to evaluate the impairment of spatial navigation, which involves both egocentric and allocentric spatial reference systems (9). For the egocentric subtest, subjects were required to navigate a target goal by using the starting position, in the absence of distal orientation cues. For the allocentric subtest, subjects could orientate in a virtual environment using two distal cues, where the starting position was not related to the goal position. In addition, the “allocentric + egocentric” subtest was conducted, which involved the navigation of the goal using both starting position and distal orientation cues (10). Eight trials from each subtest were then used to average the index. Spatial navigational ability was evaluated by measuring the distance between the participants' choice and the correct goal location, which could also be applied as a measure of navigational accuracy.

### Statistical Analysis

The statistical differences in demographic characteristics, CDT, MMSE, TMT-B, VFT, and spatial navigation ability (e.g., “allocentric + egocentric” subtest, egocentric subtest, and allocentric subtest) between the three groups were compared using analysis of variance (ANOVA), with adjustment for age and educational level as covariates. Further comparison of the adjusted means was carried out using a least-squares difference (LSD) test if necessary. A linear regression model (after adjusting for age, sex, and educational level) was used to determine the relationship between spatial navigation impairment and each domain of the cognitive function. All results were presented as mean  $\pm$  standard deviation, and a  $p$ -value of less than 0.05 was deemed statistically significant. All statistical tests were conducted using the statistical software package SPSS version 22.0 (IBM Corp., Armonk, New York, USA).

## RESULTS

There were no significant differences among severe SVD, non-severe SVD, and control groups with regards to age, gender, and education level. The MMSE score was decreased in the severe SVD group ( $24.89 \pm 5.70$ ) compared to non-severe SVD and control groups ( $26.88 \pm 3.55$  and  $27.28 \pm 2.04$ , respectively), but no statistically significant difference was observed ( $p = 0.133$ ). Similarly, the VFT ( $16.34 \pm 6.00$  vs.  $16.10 \pm 7.28$  vs.  $14.06 \pm 6.98$ ) and CDT ( $9.78 \pm 1.39$  vs.  $9.70 \pm 1.58$  vs.  $8.83 \pm 1.66$ ) scores were also not significantly different among the three groups ( $p = 0.462$  and  $p = 0.076$ , respectively). On the contrary, the TMT-B score was significantly lower ( $89.30 \pm 28.98$  seconds;  $p = 0.035$ ) in the severe SVD group compared to the non-severe and control

**TABLE 1** | Clinical and demographic characteristics and index of spatial navigation performance of the participants.

	Severe SVD individuals (N = 18)	Non-severe SVD (N = 40)	Healthy (N = 41)	P value
Men, %	55.56%	72.50%	78.05%	0.213
Age, years	71.28 (7.82)	70.75 (7.78)	73.76 (6.77)	0.169
Education, years	12.67 (3.66)	13.05 (3.25)	12.75 (3.55)	0.898
MMSE, score	24.89 (5.71)	26.88 (3.55)	27.24 (4.19)	0.147
VFT, words	14.06 (6.98)	16.10 (7.28)	16.34 (6.01)	0.462
CDT, score	8.83 (1.65)	9.70 (1.59)	9.78 (1.39)	0.076
TMT-B, seconds	65.70 (18.97)	74.00 (20.47)	89.30 (28.98)	0.035 <sup>#</sup>
Allocentric+egocentric navigation	41.74 (29.10)	31.50 (16.47)	29.21 (19.03)	0.003 <sup>#&amp;</sup>
Egocentric navigation	56.16 (39.85)	56.00 (28.82)	43.06 (25.07)	0.105
Allocentric navigation	46.93 (31.27)	43.69 (23.95)	28.56 (16.38)	0.031 <sup>#</sup>

Mean (Standard Deviation). <sup>#</sup>*P* < 0.05 severe SVD relative to non-severe SVD. <sup>#</sup>*P* < 0.05 severe SVD relative to healthy individuals. <sup>&</sup>*P* < 0.05 non-severe SVD relative to healthy individuals.

groups ( $74.00 \pm 20.47$  seconds and  $65.70 \pm 18.97$  seconds). Further details were in **Table 1**.

During the allocentric+egocentric subtest, the subjects in severe SVD ( $41.74 \pm 29.10$ ), rather than non-severe SVD ( $31.50 \pm 16.47$ ) groups, performed worse than those in the control group ( $29.21 \pm 19.03$ ; *p* = 0.031). For the egocentric subtest, the performances among the three groups were not significantly different ( $56.16 \pm 39.85$  vs.  $56.00 \pm 28.81$  vs.  $43.06 \pm 25.07$ ; *p* = 0.105). However, for the allocentric subtest, neither the subjects in the severe SVD group ( $46.93 \pm 31.27$ ; *p* = 0.004) nor the subjects in the non-severe SVD group ( $43.69 \pm 23.95$ ; *p* = 0.005) performed as well as healthy individuals ( $28.56 \pm 16.38$ ). These details are shown in **Table 1**.

Furthermore, the relationship between cognitive task score and spatial navigation ability of elderly SVD patients was determined using linear regression analysis. After adjusting for age, gender, and education level, the average total error in the allocentric subtest was positively associated with TMT-B (*p* = 0.000, standardized  $\beta$  = 0.342), and negatively associated with VFT (*p* = 0.016, standardized  $\beta$  = -0.873). However, the average total errors in “allocentric + egocentric” and egocentric subtests were not significantly associated with the performance indices of neuropsychological tests conducted in this study. More details can be found in **Table 2**.

## DISCUSSION

In this work, the spatial navigation performance of SVD patients was shown to be poorer compared to healthy individuals, as reflected in “allocentric + egocentric” (for severe SVD patients only) and allocentric (for both severe and non-severe SVD patients) subtests, rather than egocentric subtest. Moreover, elderly patients with SVD exhibited cognitive deficits, such as mental flexibility, in comparison with healthy controls. Besides, the spatial navigation ability of elderly SVD patients during the

allocentric subtest was associated with TMT-B and VFT performance. However, similar trends were not observed in these patients during “allocentric + egocentric” and egocentric subtests.

Spatial navigation is an essential human behavior that involves a multitude of cognitive processes interacting with one another (11). This kind of brand-new assessment is becoming more and more popular in clinical researches because it has fewer cultural, educational, and verbal biases compared to the existing cognitive tests (1). Different aspects of spatial navigation abnormalities have been reported in patients with neuropsychiatric disorders, including AD, persistent postural perceptual dizziness, traumatic brain injury, etc (5, 12, 13). Our results indicated that elderly patients with severe SVD exhibited poorer spatial navigation in both allocentric+egocentric subtest and allocentric subtest compared to healthy elderly subjects, indicating that severe SVD patients may encounter the problem of wayfinding in their daily life.

Although both allocentric and egocentric navigation strategies can be combined to attain optimum cognitive functioning, several studies (9, 14, 15) reported that a specific aspect of spatial navigation strategy dysfunction might imply the underlying pathophysiological processes. For example, autism spectrum disorder patients showed particularly difficulties in allocentric navigation, leaving egocentric navigation intact (14); LI patients performed worse than healthy control subjects during egocentric subtest (9); and AD patients exhibited significant both allocentric and egocentric navigation impairments relative to control individuals (15). In this study, elderly patients with SVD performed significantly worse on allocentric and “allocentric + egocentric” subtests, rather than egocentric subtests, when compared to healthy elderly subjects. This may be explained by the fact that disease burden disproportionately affects the network between the prefrontal cortex, hippocampus, and retrosplenial cortex (3, 16).

**TABLE 2 |** Association between the index of spatial navigation performance and neuropsychological assessment data in aged SVD patients.

	Allocentric + egocentric navigation		Egocentric navigation		Allocentric navigation	
	Standardized $\beta$ value	P value	Standardized $\beta$ value	P value	Standardized $\beta$ value	P value
<b>VFT, words</b>						
Model 1	−0.386	0.254 <sup>#</sup>	−0.342	0.504	−0.869	0.015 <sup>*</sup>
Model 2	−0.394	0.244 <sup>#</sup>	−0.386	0.433	−0.873	0.016 <sup>*</sup>
<b>CDT, score</b>						
Model 1	−1.063	0.464	−0.465	0.833	0.412	0.785
Model 2	−1.129	0.435	−0.688	0.745	0.419	0.784
<b>TMT-B, seconds</b>						
Model 1	0.042	0.585	0.277	0.021	0.335	0.000 <sup>#</sup>
Model 2	0.019	0.809	0.224	0.057	0.342	0.000 <sup>#</sup>

Data are standardized  $\beta$  values, except for P value. Model 1 represents the relation between the index of spatial navigation performance and neuropsychological assessment data without adjustment; Model 2 represents the relation between the index of spatial navigation performance and neuropsychological assessment data adjusted for age, gender and education. <sup>\*</sup>P < 0.05, <sup>#</sup>P < 0.01.

The relationship between spatial navigation and cognitive impairment has been explored recently. Laczo et al. (17) found that spatial navigation was not, or marginally, associated with most cognitive functions (attention, working memory, executive functions, verbal memory, and language learning) in mild cognitive impairment patients and healthy individuals. On the contrary, Brown et al. (18) proposed a significant association between spatial navigation, episodic memory, and executive functions. In the present study, we found a close relationship between allocentric spatial navigation and executive function/cognitive flexibility as well as semantic memory. However, similar trends were not observed for “allocentric + egocentric” or egocentric spatial navigation. The discrepancy between these studies could be explained by the distinct choice of cognitive assessment and distinct groups of individuals recruited. For example, Parizkova et al. (19) discovered that patients suffering from AD preferred more obviously egocentric strategies to allocentric strategies relative to healthy controls. Our findings illustrated that allocentric navigation strategy and executive function/cognitive flexibility might share the same functional brain area in aged SVD patients and the elderly.

Several limitations of this study need to be pointed out. First, the sample size was not large. Second, there is a lack of comprehensive assessment protocol, especially for Trail Making Test-A, as spatial navigation can potentially be affected by poor attention, cognitive flexibility, and psychomotor speed. Therefore, future research should encompass more study subjects and neuropsychological tests to address these shortcomings.

In summary, SVD patients showed spatial navigation deficits, especially on the allocentric navigation subtest. The allocentric navigation impairment was associated with TMT-B and VFT, rather than CDT performance, which are representations of cognitive flexibility and semantic memory, respectively. Furthermore, spatial navigation might serve as a promising tool to reflect a cognitive decline in elderly patients with SVD.

## DATA AVAILABILITY STATEMENT

The raw data supporting the conclusions of this article will be made available by the authors, without undue reservation.

## ETHICS STATEMENT

The studies involving human participants were reviewed and approved by the ethics committee of the Seventh Medical Center of PLA General Hospital. The patients/participants provided their written informed consent to participate in this study.

## AUTHOR CONTRIBUTIONS

YH and HT carried out the study concept and design. LC and HZ handled the acquisition of data. YZ carried out the analysis and interpretation of data. LC and HZ performed the drafting of the manuscript. All authors contributed to the article and approved the submitted version.

## FUNDING

This work was supported by the Wu Jieping Foundation (Grant No. 320.6750.18456) and Foundation CJ17J01.

## ACKNOWLEDGMENTS

We thank Ph.D. Manfred Windisch and colleagues from NeuroScios GmbH for the supply of software and method assistance. We have cited them in references 6 and 13. We also thank Ms. Qiuju Bai for her technical support. We would like to express their gratitude to EditSprings (<https://www.editsprings.com/>) for the expert linguistic services provided.

## SUPPLEMENTARY MATERIAL

The Supplementary Material for this article can be found online at: <https://www.frontiersin.org/articles/10.3389/fneur.2021.608797/full#supplementary-material>



## REFERENCES

- Coughlan G, Laczó J, Hort J, Minihane AM, Hornberger M. Spatial navigation deficits-overlooked cognitive marker for preclinical Alzheimer disease? *Nat Rev Neurol*. (2018) 14:496–506. doi: 10.1038/s41582-018-0031-x
- Boccia M, Nemmi F, Guariglia C. Neuropsychology of environmental navigation in humans: review and Meta-analysis of fMRI studies in healthy participants. *Neuropsychol Rev*. (2014) 24:236–51. doi: 10.1007/s11065-014-9247-8
- Zhong JY, Moffat SD. Extrahippocampal contributions to age-related changes in spatial navigation ability. *Front Hum Neurosci*. (2018) 12:272. doi: 10.3389/fnhum.2018.00272
- Yatawara C, Ng KP, Lim L, Chander R, Zhou J, Kandiah N. Cerebrovascular disease is a risk for getting lost behavior in prodromal dementia. *Am J Alzheimers Dis Other Dement*. (2019) 34:344–52. doi: 10.1177/1533317519852864
- Allison SL, Rodebaugh TL, Chiharu J, Fagan AM, Morris JC, Head D. Developing a spatial navigation screening tool sensitive to the preclinical Alzheimer Disease Continuum. *Arch Clin Neuropsychol*. (2019) 34:1138–55. doi: 10.1093/arclin/acz019
- Zhào H, Wei W, Do EY-L, Huang Y. Assessing performance on digital Clock Drawing Test in aged patients with cerebral small vessel disease. *Front Neurol*. (2019) 10:1259. doi: 10.3389/fneur.2019.01259
- Biesbroek JM, Weaver NA, Biessels GJ. Lesion location and cognitive impact of cerebral small vessel disease. *Clin Sci*. (2017) 131:715–28. doi: 10.1042/CS20160452
- Joutel A, Chabriat H. Pathogenesis of white matter changes in cerebral small vessel diseases: beyond vessel-intrinsic mechanisms. *Clin Sci*. (2017) 131:635–51. doi: 10.1042/CS20160380
- Wu Y, Wu W, Liu Q, He W, Ding H, Nedelska Z, et al. Presence of lacunar infarctions is associated with the spatial navigation impairment in patients with mild cognitive impairment: a DTI study. *Oncotarget*. (2016) 7:78310–9. doi: 10.18632/oncotarget.13409
- Laczo J, Andel R, Vyhnaek M, Vlcek K, Nedelska Z, Matoska V, et al. APOE and spatial navigation in amnesic MCI: Results from a computer-based test. *Neuropsychol*. (2014) 28:676–84. doi: 10.1037/neu0000072
- Lester AW, Moffat SD, Wiener JM, Barnes CA, Wolbers T. The aging navigational system. *Neuron*. (2017) 95:1019–35. doi: 10.1016/j.neuron.2017.06.037
- Skelton RW, Ross SP, Nerad L, Livingstone SA. Human spatial navigation deficits after traumatic brain injury shown in the arena maze, a virtual Morris water maze. *Brain Inj*. (2006) 20:189–203. doi: 10.1080/02699050500456410
- Breinbauer HA, Contreras MD, Lira JP, Guevara C, Castillo L, Ruëdinger K, et al. Spatial navigation is distinctively impaired in persistent postural perceptual dizziness. *Front Neurol*. (2020) 10:1361. doi: 10.3389/fneur.2019.01361
- Ring M, Gaigg SB, Altgassen M, Barr P, Bowler DM. Allocentric versus egocentric spatial memory in adults with autism spectrum disorder. *J Autism Dev Disord*. (2018) 48:2101–11. doi: 10.1007/s10803-018-3465-5
- Zanco M, Plácido, J, Marinho V, Ferreira JV, de Oliveira F, Monteiro-Junior R, et al. Spatial navigation in the elderly with Alzheimer's Disease: a cross-sectional study. *J Alzheimer Dis*. (2018) 66:1683–94. doi: 10.3233/JAD-180819
- Irving S, Schöberl F, Pradhan C, Brendel M, Bartenstein P, Dieterich M, et al. A novel real-space navigation paradigm reveals age- and gender-dependent changes of navigational strategies and hippocampal activation. *J Neurol*. (2018) 265:113–26. doi: 10.1007/s00415-018-8987-4
- Laczo J, Andel R, Nedelska Z, Vyhnaek M, Vlcek K, Crutch S, et al. Exploring the contribution of spatial navigation to cognitive functioning in older adults. *Neurobiol Aging*. (2017) 51:67–70. doi: 10.1016/j.neurobiolaging.2016.12.003
- Brown T, Chrastil ER. Editorial: spatial navigation: memory mechanisms and executive function interactions. *Front Hum Neurosci*. (2019) 13:202. doi: 10.3389/fnhum.2019.00202
- Parizkova M, Lerch O, Moffat SD, Andel R, Mazancova AF, Nedelska Z, et al. The effect of Alzheimer's disease on spatial navigation strategies. *Neurobiol Aging*. (2018) 64:107–15. doi: 10.1016/j.neurobiolaging.2017.12.019

**Conflict of Interest:** The authors declare that the research was conducted in the absence of any commercial or financial relationships that could be construed as a potential conflict of interest.

**Publisher's Note:** All claims expressed in this article are solely those of the authors and do not necessarily represent those of their affiliated organizations, or those of the publisher, the editors and the reviewers. Any product that may be evaluated in this article, or claim that may be made by its manufacturer, is not guaranteed or endorsed by the publisher.

Copyright © 2021 Zhào, Chi, Zhang, Huang and Tian. This is an open-access article distributed under the terms of the Creative Commons Attribution License (CC BY). The use, distribution or reproduction in other forums is permitted, provided the original author(s) and the copyright owner(s) are credited and that the original publication in this journal is cited, in accordance with accepted academic practice. No use, distribution or reproduction is permitted which does not comply with these terms.

# Advantages of publishing in Frontiers



## OPEN ACCESS

Articles are free to read  
for greatest visibility  
and readership



## FAST PUBLICATION

Around 90 days  
from submission  
to decision



## HIGH QUALITY PEER-REVIEW

Rigorous, collaborative,  
and constructive  
peer-review



## TRANSPARENT PEER-REVIEW

Editors and reviewers  
acknowledged by name  
on published articles

## Frontiers

Avenue du Tribunal-Fédéral 34  
1005 Lausanne | Switzerland

Visit us: [www.frontiersin.org](http://www.frontiersin.org)

Contact us: [frontiersin.org/about/contact](http://frontiersin.org/about/contact)



## REPRODUCIBILITY OF RESEARCH

Support open data  
and methods to enhance  
research reproducibility



## DIGITAL PUBLISHING

Articles designed  
for optimal readership  
across devices



## FOLLOW US

@frontiersin



## IMPACT METRICS

Advanced article metrics  
track visibility across  
digital media



## EXTENSIVE PROMOTION

Marketing  
and promotion  
of impactful research



## LOOP RESEARCH NETWORK

Our network  
increases your  
article's readership